University of South Wales
2059577

Bound by Abbey
Bookbinding Co.,
Cardiff, South Wales
Tel:(01222) 395882

The Development of a Novel Air Bearing Device for Aerodynamic Flow Control

Ali M. Al-Obidy Al-Shihry, B.Sc., M.Sc

King Saud University, Riyadh, Saudi Arabia

A submission presented in partial fulfillment of the requirements of

the University of Glamorgan

for the Degree of Doctor of Philosophy

Department of Mechanical and Manufacturing Engineering

July 1997

أولم يروا إلى الطير فوقهم صافات ويقبضن

ما يمسكهن إلا الرحمن إنه بكل شيء بصير

(سورة تبارك)

Do they not see the birds above them, spreading out their wings and folding them in? None upholds them except the Most Beneficent (Allah). Verily, he is the All-Seer of every thing.

Holy Qura'an

Declaration

This work has not previously been accepted in substance for any degree and is not being concurrently submitted in candidature for ~~any~~ degree.

Signed ..... 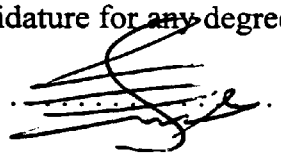 .....(candidate)

Date 1/10/97

Statement 1

This thesis is the result of my own investigation, except where otherwise stated. Other sources are acknowledged by giving explicit references. A bibliography is appended.

Signed ..... 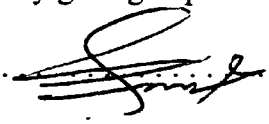 ..... (candidate)

Date .....1./.10./.97.....

Signed ..... (supervisor)

Date .....

Signed ..... (supervisor)

Date .....

Statement 2

I hereby give consent for my thesis, if accepted, to be available for photocopying and for inter-library loan, and for the title and summary to be made available to outside organizations

Signed .....  ..... (candidate)

Date .....1./.10./.97.....

To

my father

my mother,

my wife

for their encouragement, patience and love !

Acknowledgments

All my thanks are due to Allah for giving me the ability and guidance to undertake this work.

I wish, also, to express my deep gratitude and sincere thanks to my supervisors Dr. T.M.A. Maksoud and Prof. J. Ward for their valuable advice and encouragement during their supervision of this project.

I wish also to thank all technical and secretarial staff of the Department of Mechanical and Manufacturing Engineering for their kindness and support during this research.

I wish to express my thanks and admiration to my wife and children who have always been a source of inspiration, encouragement and support with their kind patience throughout my study. Their sacrifice will not be forgotten, and I find nothing is enough to reward them but a sincere Dua'a.

With their tremendous encouragement and very valuable advice, my father, Mohammed Sa'ad and my brother Abdullah greatly assisted in making this study a matter of fact. I wish to express all my gratitude and thanks to them, and all of my relatives and friends.

I am also greatly indebted to Dr. Mohammed Diya and all the staff in the Saudi Cultural Bureau, London and in the College of Technology, Riyadh, Saudi Arabia for their continuous advice and help.

Abstract

Since the first flight of the Wright brothers, there has been considerable effort devoted to improving wing performance. Many techniques have been developed to reduce drag and improve the lift of aerofoil. This research introduces a new novel method, a so-called "air bearing device" (ABD) which provides both drag reduction and enhancement of lift.

The basic principle of this technique is to introduce a groove in the solid upper surface and an air stream is injected into one side of the groove and then removed from the other side. The direction of this secondary flow is essentially parallel to the main flow and all the injected fluid is completely removed from the suction side. This flow is thus similar to an "air roller". The benefits of the device depend on the injection velocity and the geometry of the ABD groove. Optimizing the shape of the ABD constitutes a wide area for future research. The performance of the ABD was studied both theoretically and experimentally.

This device is considered to enhance the main flow in two ways. Firstly it appears to 'energize' the main flow by injecting some kinetic energy to the "weak" fluid particles near the wall. Secondly the pressure drop associated with the high speed of the flow inside the ABD is assumed to 'absorb' some of the adverse pressure resistance. The boundary layer thickness of the main flow is then reduced and, consequently, the main flow will be more capable of resisting separation. The source of the injected/sucked flow inside the ABD may be an external supply (an auxiliary fan) or may be taken from the higher/lower pressure regions around the aerofoil. One of the main objectives of the present study is to investigate theoretically the design aspects and the parameters that affect the ABD performance. The other objective is to investigate experimentally the effect of the device. Due to limitations in the experimental facility, it was not possible to examine experimentally all the theoretical cases. It should be noted however that optimization of the performance of the ABD was not the intention in this study.

The results obtained from this investigation were extremely promising and it can be concluded that:

- The geometry of the ABD can effect the performance and will need to be optimized in future work.
- When the "rolling" velocity in the ABD exceeds the main stream flow speed, improvements in lift and drag are obtained.
- The improvements in drag and lift greatly exceed the penalty of the power consumption needed to operate the ABD.
- The increase in lift and decrease in drag occur simultaneously and up to 30% improvements were achieved.

Optimization of the performance of the ABD is a very wide area of research due to large number of parameters and strong interactions existing between them. Since the concept of the ABD is new the project was aimed at clarifying the general behavior of the device at this stage.

نبذة مختصرة

منذ أول محاولة طيران في العصر الحديث قام بها الأخوان رايت، بذلت جهود هائلة لتحسين أداء أجنحة الطائرات. إذ تم تطوير عدة تقنيات لتقليل مقاومة الأجنحة للهواء وتحسين قوة رفعها . ويتم في هذا البحث تقديم طريقة مبتكرة جديدة تسمى (أداة تحميل هوائية ABD) والتي تقلل المقاومة وتحسن قوة الرفع في آن واحد .

إن المبدأ الرئيسي لهذا الأبتكار هو أن يتم عمل مجرى صغير بشكل هندسي مدروس على امتداد السطح العلوي من جناح الطائرة وفي هذا المجرى يتم إدخال تيار من الهواء من أحد جانبيه وسحبه كله من الجانب الآخر؛ ويكون اتجاه الهواء داخل المجرى موازيا لمجرى الهواء الرئيسي فوق الجناح. وبهذا الترتيب يشكل التيار داخل المجرى ما يشبه "الدوار الهوائي" . وتعتمد فائدة هذه الأداة ABD على سرعة التيار داخل المجرى وعلى شكله الهندسي ولذلك يشكل موضوع تحسين أداءها مجالا بحثيا واسعا . ولقد تم في هذا البحث دراسة أداء الـABD نظريا (باستخدام المحاكاة بالحاسب الآلي) وعمليا على نموذج جناح مصغر.

إن هذه الأداة ABD تعزز سريان الهواء على سطح الجناح لسببين: الأول لأنها تزود الهواء فوق الجناح بطاقة حركية تستفيد منها الجزيئات البطيئة المجاورة للسطح والتي فقدت جزءا من طاقتها نتيجة للاحتكاك بسطح الجناح. الثاني: يساعد انخفاض الضغط المصاحب للتيار السريع داخل مجرى الـABD على امتصاص جزء من الضغط المرتد (المتزايد) فوق الجناح. وينتج من ذلك أيضا ان يقل سمك الطبقة الجدارية (Boundary Layer) التي تنتج في الهواء الرئيسي نتيجة الاحتكاك وبذلك يكون سريان الهواء على الجناح أقدر على تفادي مشكلة الإنفصال وهي مشكلة تهدد جميع الأجنحة.

يمكن توفير الهواء المطلوب لتشغيل أداة الـABD من مصدر خارجي (مضخة إضافية مثلا) أو باستغلال فروقات الضغط على الجناح.

إن أحد الأهداف الرئيسية لهذا البحث هو الدراسة النظرية التفصيلية للإعتبارات التصميمية وللعوامل التي تؤثر في أداء هذه الأداة المبتكرة ABD. والهدف الرئيسي الآخر هو إجراء دراسة معملية لأثر هذه الأداة على عمل الجناح. ونظرا لأن الدراسة المعملية عادة ما تتطلب إمكانات كبيرة فلم يمكن إختبار جميع الحالات التي تمت دراستها نظريا (باستخدام المحاكاة بالحاسب الآلي) . ويجدر التنبيه على كل حال أن (تحسين أداء الـ ABD) لم يكن هدفا مقصودا في هذا البحث بقدر ما كان الهدف دراسة قدرة هذه الأداة –التي تبتكر لأول مرة– على تحسين أداء الجناح ذاته.

لقد كانت النتائج التي تم الحصول عليها نظريا ومعمليا واعدة جدا حيث يمكن تلخيصها فيما يلي:

◆ إن الشكل الهندسي للـ ABD يؤثر كثيرا في كفائتها ولذلك يحتاج مزيدا من الدراسة مستقبلا لمعرفة أفضل شكل.

◆ حالما تزيد سرعة التيار الهوائي داخل مجرى الـABD عن سرعة التيار الرئيسي تبدأ الأداة ABD بتحسين قوة الرفع وتقليل المقاومة.

◆ إن الفائدة الناتجة عن تحسين أداء الجناح بواسطة الـABD تربو على الطاقة الإضافية المطلوبة لتشغيلها .

◆ إن هذه التقنية تتميز عن غيرها بقدرتها على تحقيق زيادة قوة الرفع وتقليل قوة المقاومة في آن واحد، وقد أمكن الحصول على تحسين بنسبة كبيرة تصل إلى ٣٠٪.

إن دراسة التصميم الأمثل لأداة الـABD تشكل مجال بحث واسع جدا لكثرة العوامل الهندسية التي تدخل في تصميمها ولقوة الترابط والتداخل بين تلك العوامل. ولأن هذا البحث هو أول دراسة علمية لهذا الإبتكار فقد إقتصر البحث في هذه المرحلة على دراسة (الأداء العام) لهذه الأداة.

Nomenclature

C	Chord length of the aerofoil
C_d	Drag coefficient
C_f	Local skin friction coefficient
$C_{f,0}$	Skin friction coefficient at the wall
C_i	Flow rate coefficient inside ABD
C_l	Lift coefficient
C_q	Suction coefficient, v_0/U_∞
H	Height of the ABD
h	Relative height of the ABD base
k	Thermal Conductivity
L_s	Distance from the leading edge to the ABD
M	Molecular weight
M_∞	Mach number
m_{fr}	Mass flow rate inside the ABD
p	Local static pressure
P_j	Injection pressure
P_{op}	Operating pressure
P_∞	Free stream pressure
P^*_{inj}	Power required for injection
P^*_{suc}	Power required for suction
P^*_{total}	Total power to drive the ABD
R	Radius of the ABD-base
R_0	Universal gas constant
Re	Reynolds number
Re_δ	Reynolds number based on boundary layer thickness, δ
Re_θ	Reynolds number based on boundary layer displacement thickness, θ
Re_c	Reynolds number based on chord length
Re_{crit}	Critical Reynolds number
S	Width of the ABD
T	Instantaneous temperature
T_∞	Free stream temperature
$T_{u\infty}$	Turbulence intensity in x-direction
$T_{v\infty}$	Turbulence intensity in y-direction
T_0	Temperature of the fluid at the wall

u, v, w	Instantaneous Velocity component in x, y and z directions, respectively
$\bar{u}, \bar{v}, \bar{w}$	Mean Velocity component in x, y and z directions, respectively
U_∞	Free stream velocity
U_j	Injection speed
v_0	Suction/Injection velocity ($v_0 < 0$ suction, $v_0 > 0$ injection)
x, y, z	Distance along x, y, z axis in Cartesian coordinate

Greek Letters

γ	Kinematic Viscosity
μ	Dynamic viscosity
τ	Shear stress
τ_0	Shear stress at the wall
α	Angle of incidence of an aerofoil
ρ	Density of the fluid
ρ_w	Density of the injected fluid
ρ_∞	Density of the main stream flow
η	Flap angle of incidence
δ	Boundary layer thickness
δ_1	Displacement thickness
δ_2	Momentum thickness

Superscripts

$'$	Denotes fluctuating components

Subscripts

$0, w$	Denotes the value at the wall
∞	Denotes the value at free stream region
inj	Injection
suc	Suction
$crit$	Critical condition

Table of contents

Chapter One

Introduction and Literature Review

Chapter one

Introduction and Literature Review

1.1 Introduction

The existence of a viscous boundary layer in flow over the surfaces of aerodynamic and hydrodynamic devices leads to a number of undesirable effects such as friction forces and displacement effects. Lift devices are mainly used to produce lift force, usually perpendicular to the main stream flow, while the drag force tends to retard the forward motion of the body. A schematic diagram of these two forces and their directions is shown in Figure 1-1. Inevitably, viscous effects, compressibility effects, and the finite span of the lift surface all ensure that drag is also produced. Apart from the induced (vortex) drag, the dominant drag force on immersed bodies is mainly due to the shear stresses set up within the boundary layer. If the drag forces exceed a certain limit, the flow will depart from the surface of the body causing "flow separation".

Over curved bodies, where a positive pressure gradient exists, flow separation may occur if the adverse pressure is high enough to bring the slope of the velocity profile $(\partial u/\partial y)_{wall}$ down to zero. Figure 1-2 shows the successive profile shapes in the stream wise direction of the flow over a curved body; (Houghton and Carruthers, 1982). The separation process over a curved body thus depends on the severity of the positive pressure gradient, Reynolds number, the flow structure (laminar or turbulent) and the surface roughness of the body. Laminar flow is less able to withstand a positive pressure gradient than turbulent flow. Separation of the flow over an aerofoil results in increasing the thickness of the wake flow, with a consequent reduction in the pressure rise, which should occur near the trailing edge. As the separation point advances towards the leading edge, the pressure drag increases substantially and the lift force is accordingly reduced. This will take the aerofoil towards a "stall" condition.

In the range of Reynolds number (based on the chord of the aerofoil), $Re_c > 10^6$, which is typical for large aircraft, boundary layer transition to turbulence usually takes place ahead of the theoretical laminar separation point. This kind of lift surface often experiences a trailing edge stall at relatively high angles of attack, (McMasters and Henderson, 1980).

For the range of $Re_c < 10^4$ (typical of insects and small model aeroplanes) the boundary layer around the lift surface is always laminar. Stalling in this case is caused by an abrupt separation of the laminar flow near the leading edge as the angle of attack is increased above modest values; (Carmichael, 1981).

In the range of $10^4 \leq Re_c \leq 10^6$, a substantial improvement in lift to drag ratio of an aerofoil takes place. "This is the Reynolds number regime where we find man and nature together in flight; large soaring birds, large radio-controlled model aircraft, human powered aircraft and remoted piloted vehicles (RPVs) used for military scientific and sampling, monitoring, and surveillance", (Carmichael, 1981). In this range of Reynolds numbers very complex phenomena take place within a short distance on the upper surface of an aerofoil particularly at high angles of incidence. The boundary layer remains laminar at the onset of pressure recovery where the high local curvature may initiate a laminar separation. Under certain conditions, the separation laminar layer may undergo transition to turbulence. Subsequent reattachment of the separated region may take place because of the increased entrainment associated with the turbulent flow. In this way a bubble of fluid is trapped under the separated shear layer between the separation and reattachment points. This bubble either remains small (when the Reynolds number based on the displacement thickness of the boundary layer, $Re_\theta < 400$) and consequently the effect is confined to a negligible reduction in the peak suction value, or this bubble enlarges (when $Re_\theta > 550$) to cover almost the entire chord length. In this latter condition the value of the peak suction is greatly affected and "stall" is almost unavoidable, (Houghton and Carruthers, 1982).

The maximum lift to drag ratio improves dramatically in this range of Reynolds numbers as can be seen in Figure 1-3; (McMasters and Henderson, 1980), and as a result substantial improvements can be achieved in the performance of the lift devices. Controlling the boundary layer flow by means of artificial techniques is historically

aimed at providing this improvement and a range of methods have been developed. The purpose of these methods is to affect the whole flow in a desired direction by influencing the structure or the characteristics of the boundary layer. The improvement is obtained by increasing the ratio of C_l/C_d and the lift device is then made to operate in the upper range of the curve in Figure 1-3.

Accordingly, the main goals of aerodynamics research are usually focused on drag reduction and enhancement of lift. In order to study the different methods available in literature, they can be classified into:

* Separation / reattachment control,
* Transition delay/ advancement
* Drag reduction.

These techniques are considered separately in this review. However, there are clear interrelations between these objectives so that satisfying one of them may lead to the loss of another. This point will be further discussed in later sections.

(Gad-el-hak, 1990) attempted to present a unified view of the above methods and in the following sections this unified view is established through detailed study of the governing equations of the flow. The references (Bushnell, 1983), (Gad-el-hak, 1989) and (Bushnell, 1994) may be consulted for more details. The following sections of this chapter will describe the techniques that are used in controlling the flow. Some of these techniques are under practical usage today, while the others have demonstrated promise in laboratory tests but are not yet used practically. Each section gives a brief explanation of the technique and the amount of improvement it provides. The related term(s) in the governing equations affected by the technique are described as are the interrelations with other techniques, the practicality and feasibility of the technique, and the practical applications.

This chapter then concludes with a description of the scope of the current study and the techniques that were investigated in the project.

1.2 The Governing Equations

Three dimensional, steady, incompressible, isothermal flow with constant viscosity is governed by the continuity equation as well as the Navier-Stokes momentum equations; (Schlichting, 1979) so that:

$$\frac{\partial u}{\partial x}+\frac{\partial v}{\partial y}+\frac{\partial w}{\partial z}=0 \tag{1-1}$$

$$u\frac{\partial u}{\partial x}+v\frac{\partial u}{\partial y}+w\frac{\partial u}{\partial z}=-\frac{1}{\rho}\frac{\partial p}{\partial x}+\mu\left(\frac{\partial^2 u}{\partial x^2}+\frac{\partial^2 u}{\partial y^2}+\frac{\partial^2 u}{\partial z^2}\right) \tag{1-2}$$

$$u\frac{\partial v}{\partial x}+v\frac{\partial v}{\partial y}+w\frac{\partial v}{\partial z}=-\frac{1}{\rho}\frac{\partial p}{\partial y}+\mu\left(\frac{\partial^2 v}{\partial x^2}+\frac{\partial^2 v}{\partial y^2}+\frac{\partial^2 v}{\partial z^2}\right) \tag{1-3}$$

$$u\frac{\partial w}{\partial x}+v\frac{\partial w}{\partial y}+w\frac{\partial w}{\partial z}=-\frac{1}{\rho}\frac{\partial p}{\partial z}+\mu\left(\frac{\partial^2 w}{\partial x^2}+\frac{\partial^2 w}{\partial y^2}+\frac{\partial^2 w}{\partial z^2}\right) \tag{1-4}$$

Applying these equations to the flow over a rigid surface over which $u=w=0$ and the viscosity varies with space and time as a result of surface heating/cooling, leads to the following equations

$$v_w\left[\frac{\partial u}{\partial y}\right]_0+\frac{1}{\rho}\left[\frac{\partial p}{\partial x}\right]_0-\left[\frac{\partial \gamma}{\partial y}\right]_0\left[\frac{\partial u}{\partial y}\right]_0=\left[\gamma\frac{\partial^2 u}{\partial y^2}\right]_0 \tag{1-5}$$

$$0+\frac{1}{\rho}\left[\frac{\partial p}{\partial y}\right]_0-0=\left[\gamma\frac{\partial^2 v}{\partial y^2}\right]_0 \tag{1-6}$$

$$v_w\left[\frac{\partial w}{\partial y}\right]_0+\frac{1}{\rho}\left[\frac{\partial p}{\partial z}\right]_0-\left[\frac{\partial \gamma}{\partial y}\right]_0\left[\frac{\partial w}{\partial y}\right]_0=\left[\gamma\frac{\partial^2 w}{\partial y^2}\right]_0 \tag{1-7}$$

While the equation for the mean stream wise momentum of the turbulent flow can be written according to (Gad-el-hak, 1990) as follows:

$$v_w\left[\frac{\partial \bar{u}}{\partial y}\right]_0 + \frac{1}{\rho}\left[\frac{dp}{dx}\right]_0 - \frac{d\gamma}{dT}\left[\frac{\partial \bar{T}}{\partial y}\frac{\partial \bar{u}}{\partial y}\right]_0 + \left[\frac{\partial \overline{u'v'}}{\partial y}\right]_0 = \left[\gamma \frac{\partial^2 \bar{u}}{\partial y^2}\right]_0 \qquad (1\text{-}8)$$

Where v_0 is the suction or injection speed; $v_0 < 0$ for suction, $v_0 > 0$ for discharge, u′ and v′are the instantaneous velocities, and $[\ ]_0$ denotes the quantity at the wall.

The above equations indicate that the instantaneous flux of span wise vorticity $(\partial u/\partial y)_0$ and stream wise vorticity $(\partial w/\partial y)_0$ at the wall could be affected by suction / injection, by stream wise or span wise pressure gradient, and changes in viscosity in the normal direction. The terms in the above equations form the base for discussing the techniques used to control the flow towards achieving the goals mentioned earlier. Each technique affects one or more terms in these equations and can lead to achieving and/or losing one or more of the desirable goals. Looking at the techniques to control flow in the light of these equations helps in establishing a unified view of the different techniques as well as clarifying the interrelations between them.

1.3 Separation Control Techniques

Fluid particles in a boundary layer are slowed down by wall friction. The decelerated fluid particles in this boundary layer do not, in all cases, remain in a thin layer which adheres to the body along the whole wetted length of the wall. The retardation of those particles may be increased, for example due to the presence of an adverse pressure gradient, to the extent that it will increase the thickness of the boundary layer and affect the external flow outside of it. If the external potential flow is sufficiently retarded the momentum of these particles will be consumed by both the wall shear and the pressure gradient. Thus at a particular location, the flow stream departs away from the bounding surface causing the surface streamline nearest to the wall to leave the body, and the flow is then said to separate. In the separation region, the thickness of the rotational-flow layer next to the wall is increased, as well as the normal component of the velocity, and therefore the approximations of the boundary layer equations are no longer valid. The performance of lift devices is influenced by separation because it is associated with large losses of the energy of the flow. These losses are due to the increase in the pressure (form) drag and decrease in the lift resulting in the separation region.

Figure 1-4 shows the gradient $(\partial u/\partial y)_0>0$ upstream of separation, $(\partial u/\partial y)_0=0$ at separation, and $(\partial u/\partial y)_0<0$ in the reverse flow after separation. The velocity profile at separation must then have a positive curvature at the wall. Since $(\partial^2 u/\partial y^2)_0>0$ is a necessary condition for a steady, two dimensional boundary layer to separate, the opposite, i.e. a negative curvature of the velocity profile at the wall (Figure 1-4a) is a sufficient condition for the boundary layer flow to remain attached.

The above discussion indicates that there are several possible methods of control to delay separation. The object of all of these methods is to keep $(\partial^2 u/\partial y^2)_0$ as negative as possible. The following sections present the most important methods used to control separation through affecting the terms in the left hand side of equation (1-8) in such a way to keep $(\partial^2 u/\partial y^2)_0$ as negative as possible.

1.3.1 Separation Control Through Suction[1]

A suction technique was used as early as 1904 when Prandtl applied suction through a span wise slot on one side of a circular cylinder. This experiment was the first step towards using suction as a separation control technique. Later on, suction has also been used as a transition control technique. However, the characteristics of suction are different in these two cases as will be seen later.

As a separation control technique, the effect of suction is to give the velocity at the wall v_0 a negative value, and hence to give the first term in the left hand side of equation (1-8) a negative value. This will make it more likely that $(\partial^2 u/\partial y^2)_0<0$ so that flow separation is inhibited. Suction removes decelerated fluid particles from the boundary layer before they have a chance to cause separation. In Figure 1-5, sucked air is taken through the slot, and a new boundary layer which is capable of overcoming the adverse pressure gradient is allowed to form in the region behind this slot. Separation can be completely prevented if a suitable slot is provided under favourable conditions (Schlichting, 1979). Alternatively, suction can be applied continuously over the surface starting at a certain distance from the leading edge. This can be achieved using a porous material or a perforated surface. Braslow et al. (1990), discussed the benefits of using perforated surfaces instead of multiple slots including ease of manufacture, a greater

[1] Suction techniques will be discussed in detail because of their close relationship to the present study.

tolerance to two-dimensional disturbances and local blockages, easier maintenance, a closer approach to ideal continuous suction, and increased tolerance to off-design conditions. They made useful suggestions regarding the manufacture of perforated wing surfaces and the layout of the ducting system, and highlighted the difficulties as well as the benefits of using the alternative of multiple slots.

The amount of suction required to prevent separation has been studied both theoretically using the momentum-integral equations and experimentally.

For two dimensional, incompressible flow with suction the momentum integral equation can be written as:

$$\frac{d}{dx}(u^2\delta_2) + \delta_1 u\frac{du}{dx} - v_0 u = \frac{\tau_0}{\rho} \qquad (1\text{-}9)$$

where δ_1 and δ_2 are the displacement thickness and momentum thickness respectively.

The additional term ($v_0\, u$) in the above equation is due to suction at the wall. This term means that shear stress increases with suction; but because δ_1 and δ_2 (in the first two terms) decrease substantially with suction the sum of the terms in the left hand side decreases.

Prandtl used this equation and made a simple estimation of the required suction which is just sufficient to prevent separation. He found that, for a body with an arbitrary shape:

$$v_0 = -2.18\sqrt{\nu\left(-\frac{du}{dx}\right)}$$

The value of $\frac{du}{dx}$ depends on the geometry of the wall over which the fluid flows.

Applying these equations to the case of a circular cylinder gives a value of suction coefficient, C_q, equal to:

$$C_q = 4.36\,\mathrm{Re}^{-0.5}$$

where C_q=v_0/U_∞, and for the case of a symmetrical Joukowski aerofoil with a chord-length Reynolds number, Re, is found to be; (Pfenninger and Bacon, 1965):

$$C_q = 1.12Re^{-0.5}$$

It can be seen from the above equations that the magnitudes of C_q are so small that the flow at the wall still satisfies the simplifying conditions which form the basis of boundary layer theory. Thus it is possible to neglect the loss of mass (or sink effect) on the external potential flow, and the external flow may be assumed to remain unaffected by suction applied to the surface of the body.

Delaying or preventing flow separation minimises drag and also helps to overcome the problem of stall due to a massive separation which usually starts at the trailing edge and progresses towards the leading edge. The lift devices will then be capable of operation over an extended range of angles of attack.

Of particular interest is the application of substantial suction on laminar-flow aerofoils[2]. In general, the maximum thickness of these aerofoils is located very close to the trailing edge. Therefore the resulting large wake thickness can be reduced by carefully situated suction slots which prevent separation at points where the section thickness starts rapidly to decrease. This type of aerofoil is also called a Griffith aerofoil; See Figure 1-6.

It is worth mentioning that the use of suction as a means of separation control is a very well established technique, (Gad-el-hak, 1989). The extensive and detailed research work undertaken on this technique has allowed a wide range of practical application, (Braslow et al. 1990). In Figure 1-7, the effect of suction in a real flight test is obvious from the shape of the tufts.

1.3.1.1 Disadvantages of Suction

The suction technique requires an external source of power to operate and/or maintain the suction flow which is a disadvantage common to all active techniques. The net benefit from using suction should thus be greater than the penalty of the extra power required to operate it, and also outweigh the other disadvantages; e.g. costs of manufacturing, maintenance, and operation.

[2] The design principles of these aerofoils will be discussed in section (1.4.2) Natural Laminar Flow (NLF)

In fact, however, using suction as a separation control method creates less problems than the other uses of suction, as will be seen later. This is due to the relative simplicity of manufacturing the suction slots or perforated surfaces. The remaining part of the problem is providing the source of power to suck in the air. This is still an active area of research although this technique has proved highly efficient and economical.

1.3.2 Injection / Blowing

Separation of the boundary layer can also be inhibited or prevented by supplying additional energy to the particles of the fluid which are being retarded near the surface. This can be accomplished through injection of a high-momentum stream of fluid into the boundary layer so that the thickness is reduced. By using a tangential injection technique; the term v_0 in equation (1-8) becomes zero over the surface (even at the tangential injection points), and due to enhancement of the momentum of the flow just over the surface, $(\partial u/\partial y)_0$ will have a large positive value. The first term in equation (1-8) is thus zero whilst the third (-ve) term is increased and this will translate to large negative values of $(\partial^2 u/\partial y^2)_0$ and therefore enable the flow to resist separation. The principle has been adopted in the design of "slotted wings" in which high momentum air is taken from the pressure side of the wing and then injected at a certain point in the suction side, see Figure 1-8. The blowing (or injection) technique has been used in the design of high lift wing sections since the early decades of this century, (Abbott and von Doenhoff, 1959). Three types of wing section use this technique namely:-

(1) Slotted flap wings (Figure 1-9)

(2) Leading-edge slat wings (Figure 1-10)

(3) Wings with a backward-opening blowing slot (Figure 1-11)

These arrangements have made it possible to restrict separation to large angles of incidence, and to achieve greatly enhanced lift. Figure 1-12 shows the effectiveness of injection technique in providing a large increase in lift. The characteristics for the slot formed by the flap near the trailing edge are, in principle, the same as those at a forward slat. However, the slot shape must be designed carefully in order to prevent the jet from dissolving into vortices at a short distance behind the exit section (Schlichting, 1979).

The gain in lift achieved by this method can be estimated by comparing the pressure distributions of an airfoil with and without injection . In Figure 1-13, the effect of injection in delaying the separation is shown together with the corresponding changes in pressure distribution and boundary layer velocity profile. It is important to note that the principle of blowing (or injection) for separation control is completely different than the principle when it is used as a transition control tool.[3]

Although direct energy expenditure is not required in this technique, the blowing intensity is limited by the pressure difference obtainable over the body itself. However, due to the effectiveness and practicality of the technique, it is employed in most civil transport aircraft nowadays.

1.3.3 Heating/Cooling

Flow separation can also be inhibited through transferring heat from the wall into a liquid (i.e. heating of a liquids) or transferring heat from a gas into the wall (i.e. cooling of the gas flows). In both cases the viscosity will decrease near the wall leading to higher local Reynolds numbers and consequently a fuller velocity profile near the wall.

For cooling of gases, $(\partial T/\partial y)_0 > 0$ so that $(\partial \gamma/\partial T)_0 > 0$; while in the case of liquids heating $(\partial T/\partial y)_0 < 0$ and $(\partial \gamma/\partial T)_0 < 0$. Both cases ensure that the 3rd term in equation (1-8) is negative in value with a consequent delay in separation. Although this method of control has been successfully applied to delay transition (see section 1.4.3), its use to prevent separation has been demonstrated only for higher speed gaseous flows, (Gad-el-hak, 1989). It also has obvious practical limitations.

1.3.4 Transverse Grooves

The methods stated so far to control the boundary layer separation are active methods which usually require auxiliary power. Consequently so-called passive methods which do not require additional power are also used to control separation.

One of these passive methods is the use of transverse grooves over the surface perpendicular to the flow. When the fluid flows over the grooves, the associated drag of the flow is found to be reduced, and the flow resists separation over larger distances. Howard and Goodman, (1985), conducted tests for several arrangements of transverse

[3] See section (1.5.2.1) Reduction of Near Wall Momentum (Injection)

grooves over bluff bodies subject to Reynolds numbers from 20,000 to 200,000 based on the body diameter. By definition, bluff bodies have a low fitness ratio, defined as the chord-to-thickness ratio of the body, (i.e. of the order of 3 or less). The presence of grooves was found to reduce the drag to levels equivalent to a streamlined body having a 67% greater fitness ratio. Reductions in drag of up to 33% were reported for some cases using V-shaped grooves. In another study using transverse and longitudinal grooves, Howard and Goodman, (1987), concluded that "these studies showed that both types of grooves were beneficial in reducing the base drag on a body at zero angle of yaw."

Using transverse grooves to control the flow, albeit through a different approach, is a part of the present research since this technique was applied to an aerofoil surface. It will thus be discussed in more detail in the following chapters.

1.3.5 Other Techniques

(Chang, 1976) reviewed several other passive and active methods which have been used to delay separation in both low and high speed flows. Among the methods discussed are boundary layer fences to prevent separation at the tips of swept-back wings, placing an array of vortex generators on the body to raise the turbulence level and to enhance fluid momentum and energy in the neighbourhood of the wall (Kalugin et al. 1982), geometric design to avoid shock-induced separation, machining a series of lateral grooves in the surface of the body upstream of separation, using of a rippled trailing edge, stream wise corrugations, or the use of a screen to divert the flow and to increase the velocity gradient at the surface. Among the other active methods are periodic forcing of the velocity field via an oscillating wire or flap, oscillatory surface heating, sound and vibration techniques; see for example (Bandyopadhyay, 1986). A moving surfaces technique (MST) was studied by (Arain, 1991) and (Modi et al. 1994) who concluded that locating a rolling cylinder in the surface of the aerofoil can largely enhance the flow and control the separation.

1.4 Transition Control Techniques

Many advantages can be achieved by delaying laminar-to-turbulent transition in a boundary layer. The skin friction drag in the laminar flow case can be as much as an

order of magnitude less than that in the turbulent condition depending on the Reynolds number of the flow.

Another advantage of a laminar boundary layer is that it is thinner than a turbulent layer which means that the pressure drag associated with the laminar boundary layer is considerably smaller. Flow-induced noise results from the pressure fluctuations in the turbulent boundary layer and, hence, is virtually eliminated in the laminar case. Reducing boundary layer noise is important for many applications such as military submarines.

"Transition is an extremely complex phenomenon, and we know very little about it. Although significant progress has been made in recent years, we still do not know what causes transition in Reynolds pipe flow", (Malik, 1990).

Whilst many techniques can be used to delay transition, they can be classified into three main types: (1) inhibiting or eliminating the so-called Tollmien-Shlichting waves which are forms of instability in the flow. This will lead to higher transition Reynolds numbers. The growth of these linear disturbances in the flow can be minimised using any, or a combination, of the so-called stability modifiers which alter the shape of the velocity profile. These include increasing the extent of the region of favourable pressure gradient, wall transpiration, wall motion, and surface heating/cooling. (2) Reducing forcing disturbances which "trigger" transition in laminar flow. This can be achieved by using smooth surfaces, reducing the free-stream turbulence and any radiated sound, minimising body vibration, and ensuring particulate-free incoming flow, or, in the case of a contaminated environment, using a particle-defence mechanism. (3) Preventing the instability associated with a cross-flow as in the case of a swept wing. Minimising the sweep on lift surfaces helps in this case.

1.4.1 Delaying Transition by Application of Suction

It has been found that withdrawing small amounts of fluid at the surface can greatly alter the stability characteristics of the boundary layer so that laminar flow is maintained well beyond the normal transition limit. Suction provides another important advantage in that it inhibits the growth of the boundary layer thickness so that the critical Reynolds

number, $Re_{\delta crit}$, (which is based on the thickness of the boundary layer) may never be reached.

For steady incompressible flow over a flat plate with suction, the von Kàrmàn integral equation can be written as:

$$\frac{C_f}{2} = \frac{d\delta_2}{dx} + \frac{v_0}{U_\infty} \qquad (1\text{-}10)$$

where C_f is the skin friction coefficient. Although it is possible to obtain any desired reduction in the boundary layer thickness using uniform suction over the surface, provided that enough fluid is sucked away, the goal is to accomplish transition delay with the minimum suction flow rate. The second term in the right hand side of equation (1-10) is the suction coefficient C_q and "although withdrawing the fluid through the wall leads to a decrease in the rate of growth of the momentum thickness of the boundary layer, C_f increases directly with C_q" (Gad-el-hak, 1990). However, fluid withdrawn from the surface has to come from outside the boundary layer where the stream wise momentum per unit mass is relatively high. In fact, suction can be used to maintain a laminar boundary layer not only due to considerable reduction of the boundary layer thickness but also due to a large increase in the stability of the velocity profile. Schlichting, (1979) showed that $Re_{\delta crit}$ =520 for a flat plate without suction and can be increased with suction to $Re_{\delta crit}$ =70,000 ,i.e. more than 130 times, which provides clear evidence demonstrating the high stabilising effect of suction.

Although Prandtl (1904) used suction to prevent flow separation from the surface of a cylinder as mentioned earlier, the first experimental demonstration that boundary layer transition can be delayed by withdrawing near-wall fluid did not take place until about five decades later, (see Jones and Head, 1951). The concept of laminar flow control (LFC) is a technology that dates back to the 1930's, when early application of stability theory for laminar boundary layers was investigated. Stabilisation by means of a pressure gradient became known as natural laminar flow (NLF).

Pfenninger and Bacon, (1965), successfully carried out a series of relaminarization experiments and found it necessary to ingest the entire flow in the boundary layer up to (1.5 δ) to capture all the "sub layer" fluctuating vorticity. International research on

stabilisation by suction started in the 1950's and by the end of the decade it was used in real flight tests carried out in the USA. The first flight test used a suction glove on an F-94 aircraft with an unswept wing (Groth et al. 1957). In 1966 further flight tests with a swept LFC wing were carried out on a WB-66 aircraft (Harris and Henfer, 1987; and White et al. 1966). The drag was reduced by 20% as compared to the no suction case. "These flight experiments removed any doubt that extensive laminar flow (up to Reynolds number as high as 4.7×10^{7}) could be achieved in flight", (Wagner et al. 1989). Despite the success of these flight tests with suction, "unresolved concerns prevented serious consideration of LFC as a design option in the airframe industry.", (Wagner and Fischer, 1984). In the past, a principal concern was the practicality (using the technology available at that time) of producing a wing surface sufficiently smooth and wave-free to meet the laminar flow criteria. Maintaining the wing surface quality in normal service was a further problem. The practical use of suction as an LFC technique is still beset by difficulties. Thus insects can stick to the leading edge during flight at low level (mainly during take off and landing) and may partially block some of the suction holes and also increase the turbulence intensity of the main flow so that the prescribed amount of suction would be insufficient to maintain the laminar situation. Icing can also block part of the suction slots or part of any porous surface.

Consequently in recent years, new approaches have been established. Wagner et al., (1989), and Wagner and Fischer, (1984), summarised the new approaches which were undertaken in a NASA programme entitled "Air Craft Energy Efficiency, ACEE". The main themes of current research in this area of transition delay involve:

(1) Combining LFC techniques with NLF ones to produce so called Hybrid Laminar Flow wings, HLFC.

(2) Using new materials and fabrication methods such as (i)using an electronic beam-perforated method to produce finely spaced perforations of 0.0635 mm (0.0025 inch) diameter; and (ii) fabricating a wave-free surface which is only recently available due to advancement in high-technology processes.

(3) Integrating the suction system with other devices; for example (i) incorporating suction in the high lift device used as a shield against insects; (ii) the slots at the

leading edge which dispense the cleaning/anti-icing fluid during climb out are used as a suction holes at cruise condition.

With these new approaches, significant progress has been made in the development of LFC, NLF and HLFC wings so that laminar flow can be maintained over up to 60% of the chord on normally swept wings. Wagner and Fischer, (1984) and (Wagner et al. 1989) evaluated the benefits of attaching suction arrangements to an aircraft designed to carry 400 passengers some 6500 nautical miles. "The LFC aircraft would have a gross takeoff weight 8.5% lower than the "turbulent-flow" aircraft and burn 21.7% less fuel. The LFC plane would cost $1.9 million more, but its fuel saving will cover this difference in the first six months of its operation. Thereafter, the annual fuel saving would be nearly $4 million per aircraft".

1.4.2 Natural Laminar Flow (NLF)

Transition from laminar to turbulent flow can be delayed by designing the body in such a way that a favourable pressure gradient is maintained over most of the surface. This idea is usually applied in the so called "Laminar aerofoils" in which the point of maximum thickness occurs far away from the leading edge. The location of the point of transition in the boundary layer is strongly influenced by the pressure gradient in the external stream. With a decrease in this pressure gradient, transition occurs at much higher boundary layer Reynolds numbers so that the stability of the boundary layer flow is enhanced by a decrease in pressure. This fact can be understood by referring to equation (1-8) where the pressure gradient term has a negative value i.e. ($dp/dx < 0$).[4]

It can be assumed as an approximation that at medium Reynolds number ($Re=10^6$ to 10^7) the point of instability coincides with the point of minimum pressure and that transition follows shortly afterwards, (Schlichting, 1979). As a result, transition moves forward on the suction side with increasing angle of incidence whilst simultaneously moving backwards on the pressure side.

With laminar flow aerofoils, the fluid is maintained in a laminar condition over most of the surface. However, the adverse pressure gradient after the maximum thickness is so severe that the flow tends to separate rapidly before reaching the trailing edge.

[4] See section (1.6) Interrelation Between the Techniques

Therefore, it is advantageous to apply suction in this region to control the separation[5] and, hence, to have a thinner-wake flow. The recent success of the Voyager's nine-day, un-refuelled flight around the world was due -in part- to wing design employing natural laminar flow over approximately half of the chord length, (Cebeci, 1989).

Factors that limit the use of NLF aerofoils include cross-flow instabilities, leading edge contamination on swept wings, adhesion of insects, the high Reynolds numbers which occur at lower cruise altitudes and performance degradation at high angles of attack due to the necessarily small leading edge radius. Despite these obstacles, the potential benefits particularly when coupled with the feasibility of using associated techniques like suction[6] has resulted in great interest in NLF. Designing a "fastenerless" composite aircraft is a current area of research, see (van Rijin, 1996). In his review, Braslow et al., (1990), stated that "...recent research indicates that (1) modern construction techniques are capable of providing the required surface tolerances; (2) practical means are available for maintenance of sufficiently smooth surfaces during routine flight operations; (3) practical suction systems are available when needed for large scale, high-sweep configurations; (4) hybrid LFC appears possible for medium sized aircraft with moderate sweep; and (5) maintenance of appreciable natural laminar flow may be a design option for medium-sized aircraft with wing sweeps up to approximately 20°."

1.4.3 Heating/Cooling

Changing the temperature of the surface by heating or cooling can affect the stability of the flow. The viscosity increases with temperature for gases but decreases with temperature for liquids, so that different effects are experienced for the two fluids.

(1) By changing temperature the velocity gradient near the wall increases and the velocity profile becomes fuller and more stable. This is clear from equation (1-8), where the third term will be negative either in the case of cooling gases where ($dT/dy > 0$) or in the case of heating liquids (where $d\gamma/dT < 0$).

(2) The critical Reynolds number is increased by a decrease in viscosity; and consequently the flow becomes more stable and any unstable waves have a reduced rate

[5] See section (1.3.1) Separation Control Through Suction

[6] See section (1.4) Transition Control Techniques

of amplification. Accordingly, a substantial delay in transition is feasible with a surface that is only a few degrees hotter (in water) or colder (in air) than the free stream.

The use of heating or cooling of the surface as a transition control technique has been known since (Linke, 1942) who noticed that drag over a flat plate placed in a wind tunnel was increased substantially when the plate was heated. Since then, this subject has been studied extensively both experimentally and theoretically. It has been found for example, that the critical Reynolds number (based on the distance from the leading edge) increased from 10^5 to 10^7 when the wall of a flat plate has a temperature 70% lower than the absolute ambient air temperature. Also if the wall is cooled to $0.95T_\infty$ (Kelvin) the critical Reynolds number will be doubled (Reshotko, 1979a). Dougherty and Fisher, (1980) reported that the critical Reynolds number varies approximately as $(T_0)^{-7}$ where T_0 is the absolute wall temperature difference.

This method of controlling transition is not practical for aircraft except possibly in the case of the vehicles which use a cryogenic-fuel such as liquid hydrogen or liquid methane. The fuel can then be used to cool the major aerodynamic surfaces. The weight of the fuel saved is well in excess of the weight of the cooling system; (Reshotko, 1979b).

On the other hand, the use of this technique in under water vehicles can be extremely effective and more practical. In a typical low-speed situation, surface heating of $1°C$ above water temperature has approximately the same effect on the curvature of the velocity profile at the wall as a surface cooling of $20°C$ in air, or alternatively a suction coefficient of 0.0003, (Liepmann et al. 1982). For a heated body of revolution the critical Reynolds number can be increased from 4.5×10^6 to 3.6×10^8 if the surface of the body has an excess temperature of $25°C$ (Lauchle and Gurney, 1984).

The source of heat when applying this technique can be the rejected heat from the propulsion systems. The major obstacle for practical implementation of this technique is the presence of suspended particles in the flow which can decrease the efficiency of the technique dramatically; and therefore "practical-defence" mechanisms must be sought before using these methods in a contaminated environment, (Gad-el-hak, 1990).

1.4.4 Other Techniques

Transition control can in principle be achieved through other various techniques which are generally applicable in a laboratory but difficult to implement practically. Among these is wave superposition which helps to suppress disturbances in the flow. This technique can result in a doubling of the transition Reynolds number. The technique has been applied by means of wall heating/cooling, plate vibration, or periodic suction/injection, (Gad-el-hak and Blackwelder, 1989). Another technique to control transition is the use of "compliant walls". Gad-el-hak, (1986) investigated experimentally the response of elastic and viscoelastic surfaces to a turbulent boundary layer in water. Carpenter, (1990) reviewed this area of research and concluded that this technique could be a promising method of transition control in water. "Nevertheless, much remains to be done before compliant walls can be used technologically for transition control", (Carpenter, 1990 and Gad-el-hak, 1996).

1.5 Drag Reduction Techniques

The third range of techniques for controlling the flow focuses on reducing the drag of aerodynamic or hydrodynamic devices. The total drag of a body immersed in a fluid in motion consists of four components: (1) skin friction (equal to the sum -or integration- of the stream wise components of shear stress over the surface), (2) the pressure drag, equal to the stream wise component of the sum of all normal forces. Streamlining of immersed bodies, however, leads to minimum pressure drag, so that the overall drag is largely due to skin friction with additional contributions due to the displacement effect of the boundary layer, (3) wave resistance in supersonic flows, and (4) drag induced by lift in finite bodies. In the work of (Lock, 1986), each of these components were calculated theoretically and compared with experimental results. In separated flows, pressure drag is much larger than that due to skin friction.

Reducing vehicle drag can result in savings in fuel or an increase in speed for the same fuel consumption. In pipe flow reducing drag results in reduced pumping power, improved throughput, or reduced size and cost. As an example of the importance of drag reduction, more than 70,000 tonnes of fuel are carried aloft for the 2212 aircraft taking-off each day from airports throughout the UK, (Jones et. al., 1996); while the annual fuel bill for all commercial airlines in the USA is about $10 billions. At subsonic cruising

speed, half of the total drag of conventional takeoff and landing aircraft is due to skin friction. Hence, a reduction in skin friction drag of 20% translates into annual fuel saving of $1.0 billion; (Henfer, 1988). More information about the significance of research on drag reduction can be found in (Henfer, 1986) and (Coustiex et al. 1993).

Form or pressure drag can be reduced by a range of passive and active techniques which lead to a reduction in the wake momentum deficit (i.e. wake recovery is enhanced). A splitter plate at the trailing edge can disrupt the process of vortex formation and lead to instability and drag reduction. Another technique is to apply continuous or a pulsating base bleed, as in (Wood, 1967), to modify the flow in the separated region. Williams and Amato, (1989) showed that this technique is very effective when the bleed pulsates at twice the Kàrmàn vortex shedding frequency even with a net mass addition equal to zero.

Wave resistance can be reduced by changes in geometrical design. Swept wings enable a subsonic aircraft to fly at higher Mach numbers without experiencing a sudden increase in drag.

Induced drag of an aircraft wing is about 25% of the total aeroplane drag at subsonic cruising speeds. Amongst the techniques to reduce this type of drag is to increase the aspect ratio of the wing as much as possible since it has been found that induced drag is inversely proportional to the aspect ratio. Installing end plates or other vortex diffusers can also be used to further reduce the induced drag. Harris and Henfer, (1987).

Most current research concentrates on reducing skin friction drag and because of its importance it "justifies the study of unusual or high-risk approaches on an exploratory basis" (Bushnell, 1983).

The equation defining the skin-friction coefficient of a Newtonian fluid can be written as:

$$C_f = \frac{2\tau_0}{\rho U_\infty^2} = \frac{2\gamma}{U_\infty^2}\left[\frac{\partial u}{\partial y}\right]_0 \qquad (1\text{-}11)$$

Where γ is the kinematic viscosity.

This equation shows that to obtain small values of C_f, the slope of the velocity profile $(\partial u/\partial y)_0$ should be kept small. Referring to equation (1-8), this means that $(\partial^2 u/\partial y^2)_0$ should have as positive a value as possible[7]. This can be accomplished by applying several techniques and some of these will be discussed in relation to both laminar and turbulent flow.

1.5.1 Reduction of Skin Friction in Laminar Flow

Skin friction drag for laminar flow is small compared to that in turbulent flow, (it can be as much as an order of magnitude less), and hence most of the proposed techniques have focused on turbulent skin friction. Thus for laminar flow applications the priority is to maintain this type of flow over most of the surface. However, normal fluid injection has been tried as a means of reducing skin friction in laminar flow.

Normal Injection through holes can reduce laminar skin friction substantially as is clear from equation (1-8). This technique was applied by (Bushnell and Waston, 1975) who reported a reduction in skin friction of up to 80% for a blowing parameter $(\rho_0 v_0/\rho_\infty v_\infty)$ of around 3, see Figure 1-14. "Of course, it is possible to reduce the skin friction to zero by this approach but only on the expense of lift and of pressure drag" (Cebeci, 1990).

Application of an adverse pressure gradient, $(\partial p/\partial x)_0 > 0$, and wall heating in air $(\partial T/\partial y)_0 < 0$ and $(\partial \gamma/\partial T)_0 > 0$; or cooling in water $(\partial T/\partial y)_0 > 0$ and $(\partial \gamma/\partial T)_0 < 0$ have also been suggested to reduce skin friction in laminar boundary layer flows; (Bandyopadhyay, 1986).

It should be noted that all these techniques will, in general, lead to reduced skin friction but will promote separation. The adverse effect of separation must be carefully considered when deciding how far to go in attempting to reduce C_f, i.e. skin friction drag.

1.5.2 Turbulent Drag Reduction

Turbulent drag reduction (TDR) has received great attention in recent years. Most aerodynamic devices work at high Reynolds numbers, $>(10^7)$, as already noted in section 1.5, skin friction drag may constitute half, or more, of the total drag. LFC

[7]. This contradicts with the objective of separation control methods reported in previous sections; and this conflict will be discussed in further details in a later section.

techniques are applicable up to Reynolds numbers of 2.5×10^7 , (Bushnell, 1983), so that turbulent drag reduction is still very important even after the application of LFC. The research into drag reduction in turbulent flow may be classified into the following four main areas.

1.5.2.1 Reduction of Near Wall Momentum (Injection)

Fluid injection has traditionally been used to either control boundary layer separation or to reduce skin friction or viscous drag. As a separation control technique, it has been discussed in section (1.3.2).

It is well known in addition that injection can produce large reductions in skin friction. Injection was used for film cooling long before it was applied as a drag reduction technique, (Aubrey et al. 1970). Therefore, the literature for using injection for film cooling is extensive and goes back to late 1950's; whereas much less data is available for the use of injection as a drag reduction technique, (Henfer and Bushnell, 1990). Beckwith and Bushnell, (1971), calculated numerically the effectiveness of slot injection and discussed the effect of various parameters affecting the performance of the process. Henfer and Bushnell, (1990), also studied this problem and concluded that "slot injection can consistently provide large, local skin friction reductions which are predictable with present-day-numerical technology."

Typical arrangements for injection are shown in Figure 1-15 for normal injection and in Figure 1-16 for tangential slot injection. However, " limited information indicates that, on a per mass basis, tangential injection is somewhat more effective for turbulent drag reduction"; (Bushnell, 1994). If the injected fluid has higher specific momentum than that of free stream, the local skin friction is increased and the slow moving particles within the boundary layer are energised and become more able to "survive" without separation[8]. When the jet momentum is greater than the free-stream momentum, the flow configuration is often referred to as a "wall jet". On the other hand, when the specific momentum of the injected fluid is less than the momentum of the mean stream, the local skin friction is reduced; and this arrangement is referred to as a "wall wake" according to (Bushnell, 1983). The amount of drag reduction from slot injection is predictable and significant. The cost of collecting and discharging the injected air can be

[8] See section (1.3.2) Injection / Blowing

a severe penalty and has ,in fact, been the main reason that the injection technique has not historically been considered attractive for drag-reduction. In low speed flows, the slot velocity, U_j (Figure 1-16) must be less than the main stream velocity, U_∞ in order to reduce skin friction. In this case, the local skin friction is lowest near the slot and increases downstream, approaching the no-slot values. The rate of mixing between the injected and boundary layer flows determines the exact distribution of skin friction downstream of the slot. The main parameters affecting the amount of skin friction reduction include:

- The injected fluid velocity.
- The lip thickness.
- The characteristics of the injected flow (laminar, turbulent, its velocity profile).
- The boundary layer thickness relative to the location of the slot.
- The composition of the injectant.
- The Reynolds number of the main flow.
- Stream and slot flow turbulence levels.
- The pressure gradient in the main flow (e.g. flat plate or curved bodies)
- The three-dimensionality of the flow (e.g. the use of discrete holes or slots)
- The injection range (i.e. the distance between two adjacent injection locations)

It is difficult to obtain empirical correlations because of the large number of parameters.

In fact, the effects of most of these parameters on skin friction reduction have never been experimentally determined, (Henfer and Bushnell, 1990). In Figure 1-17, skin friction distributions are shown for subsonic flows downstream of a tangential slot injection for several slot-to-free stream velocity ratios. As can be seen, smaller injection velocities yield lower initial drag levels and, as a result of the increased mean shear/mixing rate away from the wall, more rapid recovery to the "undisturbed" skin friction levels occurs.

Skin friction reduction can be determined in various ways but direct measurement of surface shear using force balances is the most reliable, (Henfer and Bushnell, 1990). The technique can be designed to include the net-effect of the injection process. The

thickness of the injection slot lip has a very important effect on performance. In general, the finite thickness of the slot lip can produce von Kàrmàn vortex shedding with consequent alterations to the mixing process. The base drag of the slot is an extremely important factor which can reduce the efficiency of this technique and, therefore, it must be known accurately to evaluate the feasibility of using injection for drag reduction. To reduce the base drag penalty, a device which increases mixing in the vicinity of the slot should be used. On the other hand, to improve the length of the low drag region downstream of the slot, it is necessary to retard mixing between the injected and the external boundary layer flows. These two approaches are obviously in opposition to each other, and careful study of the balance between them should be performed in order to obtain optimal drag reduction.

Multiple-slot injection can be used to enhance the effect of this technique. However, the favourable drag reduction obtained must be weighed against the cost of acquiring the slot injection air. For closely spaced slots, each downstream slot actually provides less drag reduction per unit volume of injected air than the proceeding one. This suggests that separate slots spaced far apart are more efficient drag reducers. An alternative means of improving the efficiency of multiple slots, is to vary the injection flow rate for each slot to obtain maximum efficiency on an injection mass-flow basis. This subject was studied by (Howard et al. 1975).

When the external flow is supersonic, additional parameters must be considered and in particular the ratio of the slot static pressure p_j to the free stream static pressure p_∞. It has been found that if the air is injected at a lower pressure, ($p_j < p_\infty$), the mixing region will be shorter than in the low speed case; whilst if $p_j > p_\infty$, the mixing region will be greater than in the low speed case, see for example (Parthasrathy and Zakkay, 1970).

The source of injected air, when this technique is applied to conventional aircraft, can be either by bleeding engine air, using the air from base suction on a truncated fuselage, or using the fuselage boundary layer air ingested into an engine. Alternatively this technique can be combined with other flow-control schemes using suction[9]. Detailed

[9] see section (1.3.1) Separation Control Through Suction, and section (1.4.1) Delaying transition by application of suction.

discussion of each of these sources as well as practical suggestions for improving slot injection efficiency can be found in (Henfer and Bushnell, 1990).

1.5.2.2 Geometrical Modifications (Riblets)

The idea of riblets was originally proposed in 1976 by R. L. Ash who suggested that small flow-aligned fences can modify the near-wall structure of the turbulent boundary layer and reduce skin friction (Walsh, 1983) . The first results of the NASA Langley Research Centre work on riblets were reported by (Walsh and Weinstein, 1978). A riblet is the name given at Langley for a longitudinally grooved surface used to reduce skin friction in turbulent flow. Despite the fact that a drag reduction up to 8% can be obtained by riblets, the mechanisms contributing to the positive effects are still under investigation. Vukoslavceic et al. (1991) and (Wilkinson and Lazos, 1987) tried to study the characteristics of the flow inside the riblets and reported a change in the magnitude of the turbulence intensity. In his comprehensive review, Walsh, (1990), summarised the development of riblets. In addition, he discussed how the parameters of the riblet geometry affect drag reduction. In an attempt to "clarify the phenomena that underlay the reduction of turbulent drag by such surfaces", Luchini et al., (1991), carried out a numerical study for different shapes and sizes of grooves. Bechert and Hoppe, (1990) studied the effect of riblets on the cross flow and lateral fluctuations near the surface. "Nevertheless, it is still not clear how riblets actually reduce friction drag, and there is no general agreement between researchers even about the influence of riblets on flows over flat surfaces", (Baron and Quadrio, 1993).

In general, riblets may be v-shaped grooves, see for example (Quass et al. 1981) and (Konovalov et al. 1992); or small rectangular cross sectional grooves, see for example (Lazos and Wilkinson, 1988). The dimensions of these grooves depends on the characteristics of the flow. As a general guide, the riblets should have dimensions smaller than the low-speed streaks in the near-wall region of the boundary layer. However, "from an overall drag performance view point, the optimum riblet appears to be a v-shaped groove with h/s=0.3~0.5", (Walsh, 1990). The 3M company manufacture symmetric v-groove riblets with h/s=1.0 with a physical dimension in the range of 0.0152~0.152 mm (0.0006~0.006-inches).

Riblets appear to reduce the turbulence intensity of the flow, see (Johansoen, 1986), with consequent reduction in Reynolds stresses as reported by (Walsh, 1980). Although the turbulence intensity is reduced, the riblets have no effect on the mechanics of the stream wise fluctuations. They thus have little effect on burst frequencies, (Walsh, 1990). Khan, (1986), studied numerically the effect of riblets on both turbulent and laminar flows and reported good agreement with experimental data for both types of flows. A comprehensive review of the experimental research on riblets can be found in (Wallace and Balint, 1988), and experimental data is still the most reliable method for assessing the effect of on drag, (Bushnell, 1994).

Walsh and Lindemann, (1984), found that the efficiency of riblets in providing drag reduction is virtually unchanged for angles of flow incidence up to 15°, but concluded that over flow angles (of 25-30°) , there is a substantial reduction in this effect.

"The effect of riblets on laminar flows are less clear, and their effects on transition or separation can only be guessed", as reported by (Walsh, 1990) who also concluded that the skin friction reductions in laminar flow reported by some researchers may lie within the measurement accuracy of the experiments. Accordingly, if riblets are to be used over an aerofoil, the characteristics of the flow should be known so that optimal benefits can be obtained. However, riblets can undoubtedly reduce turbulent skin friction for external flows, and reductions of approximately of 6% have been reported by (McLean et al. 1987) and (Walsh et al. 1988) in actual flight tests. Lashkov et al. (1992) used riblets on a curved surface inside a jet and reported an improvement in its efficiency. Konovalov et al. (1992) reported up to 8% reduction in drag over axisymmetric bodies and riblets are now being used in the latest Boeing 777; see the photograph in Figure 1-18.

Combining riblets with other drag reduction techniques has also been extensively studied. Walsh and Lindemann, (1984) evaluated the drag reduction performance of a combination of riblets and large eddy break-up devices (LEBUs). It was found that overall the reduction in skin friction drag were approximately additive, (Coustols et al. 1987). Reidy and Anderson, (1988), Baron and Quadrio, (1993), and Anderson et al. (1993), among other researchers, tested the effects of combining the addition of polymers to liquids (mainly water) and riblets for both external and internal flows. It was found that, in some cases, the overall drag reduction was greater than the sum of

reductions for the two individual techniques. It is believed that the use of this combination for drag reduction is sensitive to the type of polymer used, its concentration, and its molecular weight; (Beauchamp, 1988).

1.5.2.3 Introduction of Foreign Substances into the Flow

This method is used only for liquids and the two main techniques mentioned under this title involves: (1) polymer addition and (2) micro bubbles. In the former a small quantity of polymer is added to a solvent such as water. This technique has been studied since the 1940's. Toms, (1977) has reviewed the work on drag reduction by the addition of polymers and concluded that as discovered earlier in 1946 the rate of turbulent flow through a pipe can be increased at constant pressure with an increase in polymer concentration. The results are clear evidence of a lowering of the wall shear stress. "More than 1000 papers have been written on this topic since then, and very large drag reductions (up to 80%) have been achieved", (Bandyopadhyay, 1986). Hoyt, (1990), and Kane, (1990), also reviewed the research on this technique and suggested that it may be used effectively in reducing drag for pipe-flows.

The "micro bubbles" technique involves the injection of bubbles of up to 50μm in diameter through a porous wall into the boundary layer. Again very high drag reductions (up to 80%) have been measured, see for example (Madavan et al. 1984). Perkins and Reece, (1963) used a purpose-designed cavity for the injection of the air into the nose of an underwater vehicle. Drag reductions of up to 18% were reported for short high-speed vehicles (about 6m long) while this technique failed to improve the drag of long vehicles (about 30m long).

Merkle and Deutsch, (1990), reviewed the work done on this technique and reported that it is most effective at high speeds; while for very low speed conditions buoyancy becomes so dominant that micro bubble injection is ineffective. The effect of the method of injecting the air, the bubble size, air-flow rate and other parameters were presented in this review. Fontaine and Deutsch, (1992), reported that the type of injected gas has no significant effect on drag reduction; so that the use of air on underwater vehicles is preferred due to its availability.

1.5.2.4 Other Techniques

In addition to the methods discussed in the previous sections, many other techniques have been studied for turbulent drag-reduction (TDR).

Among the most promising of these methods is the use of Large Eddy Break-up Devices (LEBUs) which constitutes probably the most exciting single recent development in turbulent drag reduction, (Bushnell, 1983). In this method, devices are installed, as in Figure 1-19, to alter or break-up the large vortices that form at the convoluted outer edge of the turbulent boundary layer, see for example (Henfer et al. 1979), (Anders and Watson, 1985) and (Bandyopadhyay, 1985). These devices consist of one or more splitter plates placed in tandem in the outer part of boundary layer. In low Reynolds number flows, (with a local boundary layer thickness δ), very thin elements of 0.01δ thickness and δ chord length are used. In higher Reynolds number flows, the use of thin, tapered plates of an aerofoil shape have resulted in reductions in skin friction of up to 40%, (Anders and Watson, 1985). The net drag reduction obtained from these devices can be as much as 20%, (Corke et al. 1979). A review of the work done on this technique can be found in (Anders, 1990) who concluded that "the economic benefits of this practical, passive drag reduction technique provide a strong motivation for continued research."

Another method to reduce turbulent boundary layer drag is the application of massive suction. In this method, the whole turbulent boundary layer is "*swallowed*", leaving a relaminarized boundary flow to be re-established. The problem arising after that is how to *maintain* the new laminar boundary layer beyond the suction location. An ideal application of this technique may be at some distance after the cockpit of an aircraft where no geometry changes are found over the rest of the fuselage; (Bushnell, 1994); see Figure 1-20. In fact, reducing the flow over the fuselage to the laminar case could translate into a large saving in operating cost since the turbulent drag over the fuselage is an important part of the total drag of an aircraft. Another method to reduce the turbulent drag over the fuselage is to combine injection at the beginning of fuselage and suction at its end as suggested by (Cary et al. 1977). This was thought to keep the base flow attached, reduce the base drag and enable the fuselage to be truncated instead of having relatively long boat tail leading to a reduction in structural weight. This arrangement is shown in Figure 1-21.

Introducing curvature to the surface over which the fluid flows can change the turbulent stresses; (Smits et al. 1979). This idea can be applied successfully to two dimensional and axisymmetric bodies; and it usually referred to as the convex curvature technique. A good review has been presented by (Bandyopadhyay, 1990) who "combined" the different applications which were done over the years and "remained scattered in the literature in a fragmented manner". As a conclusion of this review it was pointed out that "an optimised implementation has not yet been achieved, and improvements may be possible".

Among other methods is the use of interactive, or non-interactive wall motion, see for example (Cary et al. 1979) and (Wilkinson, 1990). Thomas, (1990), assessed this technique and suggested some possible practical applications such as in the nozzle of low-disturbance wind tunnels "where the operating conditions are well defined and reasonably constant". Hill, (1994), proposed the idea of a "smart surface" over which an array of sensors and actuators could be arranged and interconnected. He reported a reduction of up to 15% in skin friction from this numerical study.

Reducing vortex drag was attempted by (Wikoff et al. 1987) and (Hackett, 1980). Large drag reduction was reported in both researches.

Introducing corrugations to the trailing edge of thick bodies was found to cause "significant improvements" in drag reduction; (Whitehead et al. 1982). This may be useful in turbine blades which need to have thick trailing edges for cooling purposes.

The application of surface coatings has been studied in an actual flight test by (Kreitinger and Middleton, 1981). Drag resistance was found to vary by ±0.2% depending on the surface coating material. These coatings, however, must provide satisfactory corrosion protection if they are to be used in place of accepted corrosion protection paints or treatments.

Further details can be obtained from (Bandyopadhyay, 1986), (Gad-el-hak, 1989), (Gad-el-hak, 1990) and (Bushnell, 1994).

1.6 Interrelations Between the Techniques

Aerodynamic flow control is aimed at improving the performance of lift surfaces and all the methods discussed in the previous sections are ultimately aimed at achieving this.

Thus the desired goals of external flow control include: separation/reattachment control, lift enhancement, laminar to turbulent transition delay, and drag reduction. These objectives are interrelated and achieving a beneficial effect in one aspect may very well adversely affect another.

As an example, if the boundary layer becomes turbulent, its resistance to separation is enhanced, and more lift can be obtained at increased angle of incidence. On the other hand, the skin friction drag for a laminar boundary layer can be as much as an order of magnitude lower than that for a turbulent layer. Thus if transition can be delayed, lower skin friction is achieved. However, the laminar boundary layer can only support a very small adverse pressure gradient without separation, and subsequent loss of lift and a consequent increase in drag occurs.

Another example is that in liquid flows heating is recommended to enhance the stability of the flow, but skin friction drag will be simultaneously increased. Also an adverse pressure gradient can be used to minimise skin friction, but it promotes transition and separation.

These examples point to potential conflicts since trying to achieve a particular benefit may adversely affect another area. An ideal method of control that is simple, inexpensive to construct and to operate, and does not have any adverse disadvantages does not exist. Therefore there must be a compromise to achieve a particular design feature. Figure 1-22, taken from (Gad-el-hak, 1990), and Figure 1-23 are schematic representations of the interrelationships between different flow control goals and techniques. In Figure 1-22, the main parameters that are affected by any flow control process are transition, separation, reattachment, drag and lift and any change in these five parameters will affect the others either in a favourable way (rounded edge rectangles are used for advantages) or in an unfavourable way (represented by rectangles). In Figure 1-23, the main techniques are listed in the middle of the diagram, and arrows point out the resulting advantage(s) from using the technique and the resulting disadvantage(s). Only the *active* techniques are listed in this figure but interrelationships also exist for the passive techniques.

1.7 Scope of Present Work

The main objective of the present project was to create an "air roller bearing" on the top of an aerofoil section. Initially it was hoped to achieve this by the introduction of transverse grooves on the suction side of the aerofoil. To enhance the "rolling" action of the fluid inside the grooves, two further developments were carried out. The first development involved the introduction of a "backward" suction inside the grooves. The second development was introducing both injection and suction simultaneously into the groove. The later development proved to be the most effective method of creating the "roller" air bearing. This air bearing was restricted to a single groove and the technique was patented and termed an "Air Bearing Device, (ABD)". This method is original and the current thesis presents the first reported use of the device.

The ABD proved to be an efficient flow control technique as will be described later in the thesis.

1.7.1 Principle of the ABD

The main purpose of the ABD is to introduce a groove in the solid surface perpendicular to the main stream flow direction as in Figure 1-24. Another fluid stream (with the same fluid as the main flow) is injected through one side of the groove and then "sucked" away from the other side. The direction of this secondary flow inside the ABD should be essentially parallel to the main flow and the injected fluid should be completely sucked away in the suction. Consequently:

$$\textit{The injection flow rate} = \textit{The suction flow rate}$$

The geometry of this groove can be varied although the simplest form is a rectangular groove with a flat-base. Optimising the shape of the ABD would require a wide ranging programme of research and is largely outside the scope of this thesis. The curvature of the base, the design of the inlet and outlet, the location of the device (relative to the leading edge) and the flow characteristics inside the ABD are all important parameters in determining the performance of the device. These parameters are shown in Figure 1-25, and their effects are inter-related so that a very large research study is necessary in order to fully understand the behaviour of the device.

This device, however, is thought to enhance the main flow in two ways. Firstly it is thought to "energise" the main flow by importing additional kinetic energy to the slowly moving fluid particles near the wall. Secondly the pressure drop associated with the high speed of the flow inside the ABD is assumed to "absorb" some of the adverse pressure resistance. The boundary layer thickness of the main flow is then reduced and, consequently, this flow will be more capable of resisting separation.

The source of the injected/sucked flow inside the ABD may be from an external supply (an auxiliary fan) or may be taken from the higher/lower pressure regions around the aerofoil. This, again, could be subject of further research.

1.8 Layout of the Thesis

This introductory Chapter has presented a review of the most important approaches to flow control as well as their feasibility, applicability and interrelation with each other.

Chapter Two presents details of the theoretical modelling which was undertaken to study the problem of the roller air bearing induced by the presence of transverse grooves and the further development of the system to the ABD.

Chapter Three presents details of the experimental facilities used in this study.

The experimental results are presented in **Chapter Four**, whilst the results of the theoretical study are presented in **Chapter five.**

In **Chapter Six,** some suggestions for further studies and recommendations are also introduced.

Figures

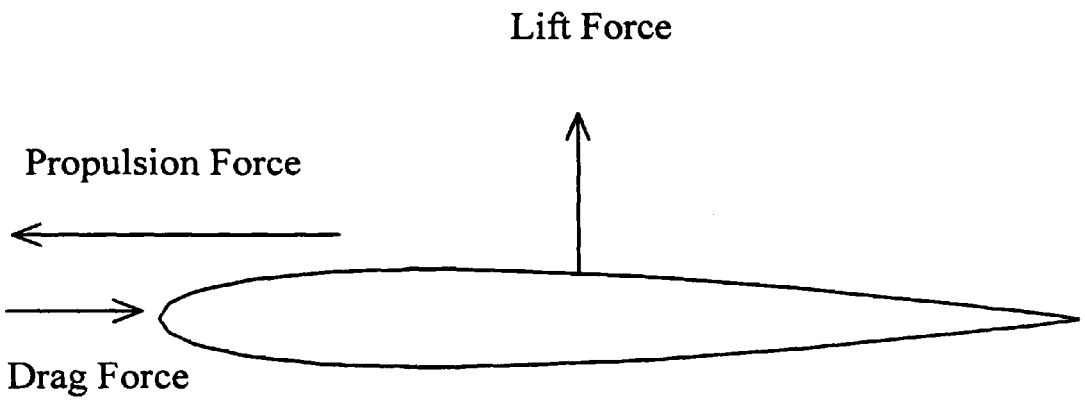

Figure 1-1: Forces acting upon a lift device

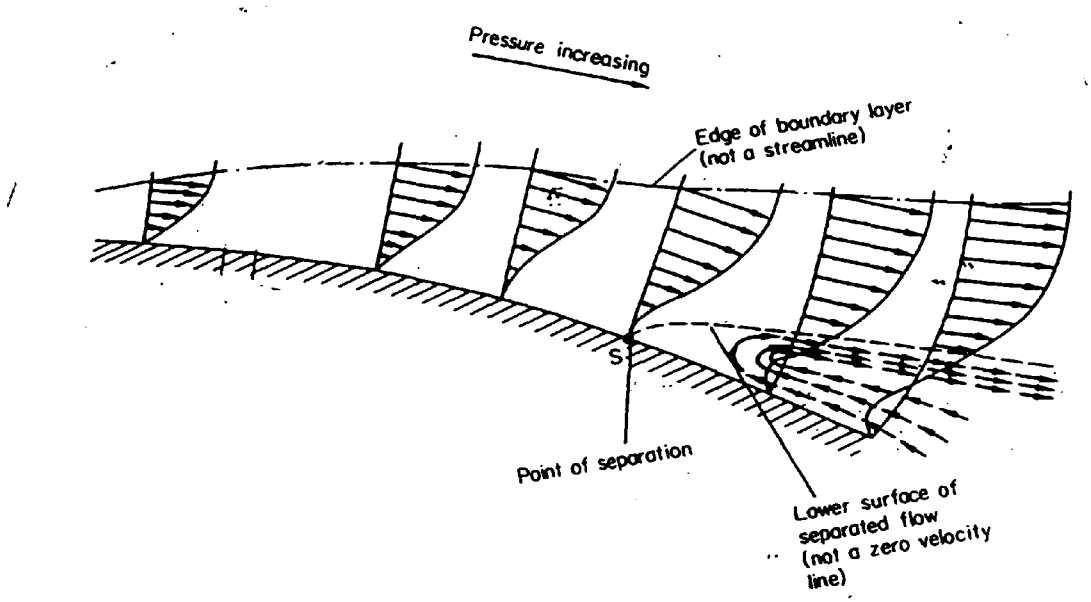

Figure 1-2: Flow separation over a curved body

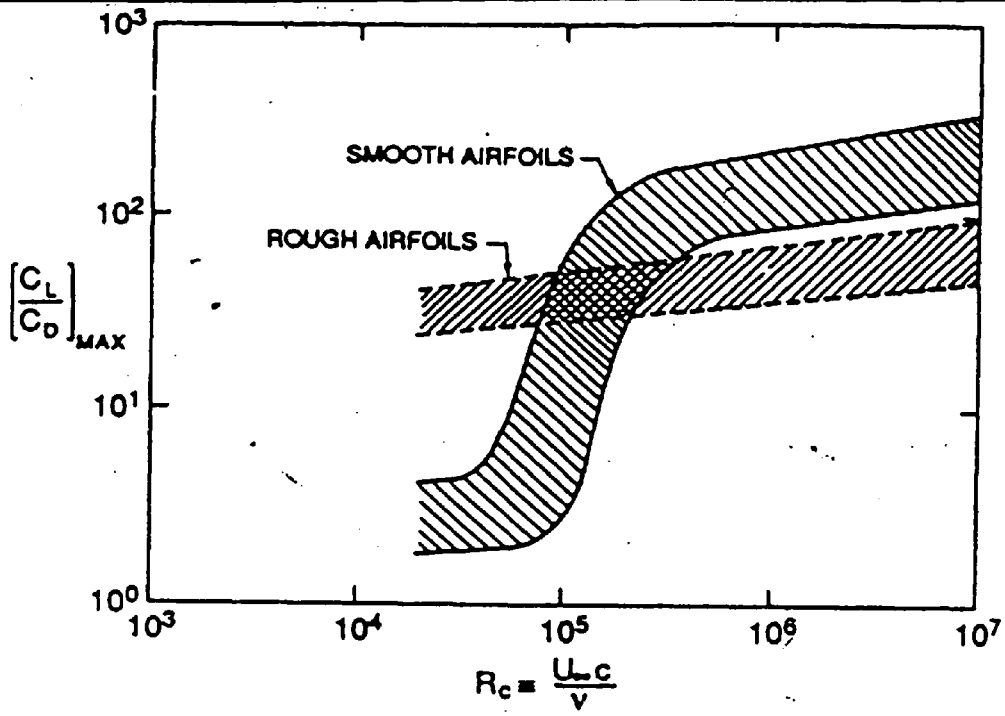

Figure 1-3 Aerofoil Performance as a function of chord Reynolds number, (McMasters and Henderson, 1980)

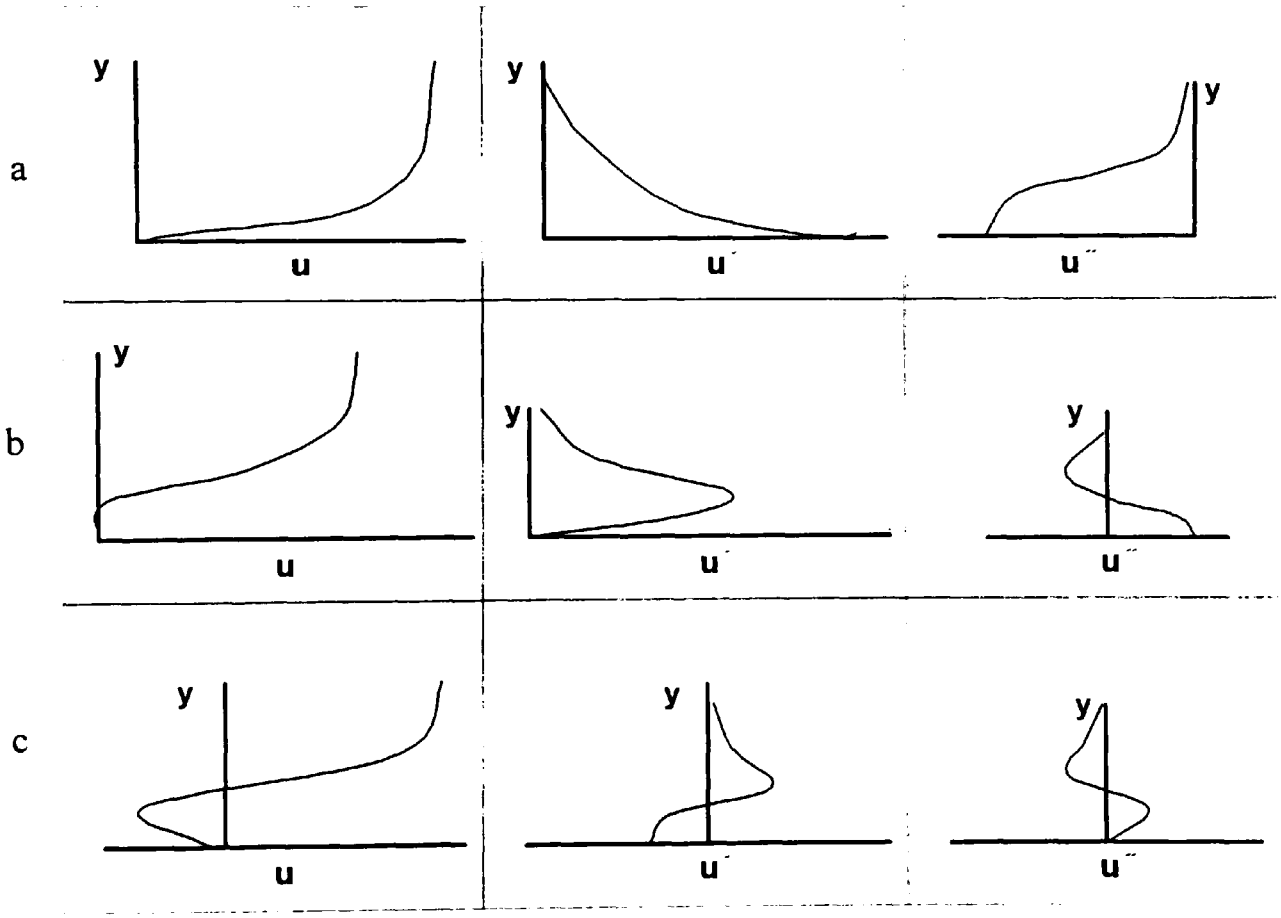

Figure 1-4: Velocity profiles and first and second derivatives.

(a) upstream of separation, (b) at the separation point and (c) after separation (reverse flow).

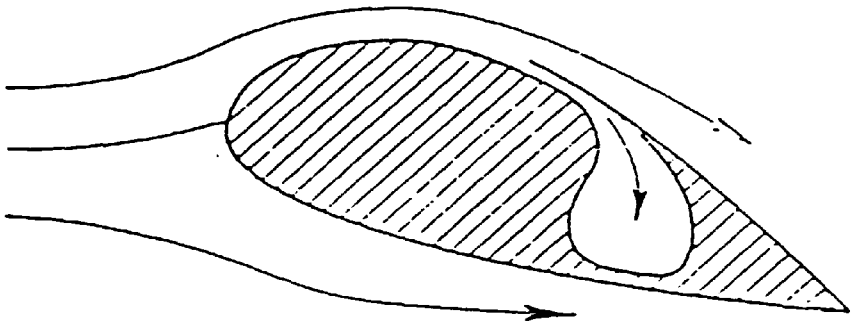

Figure 1-5: Boundary layer control through suction.

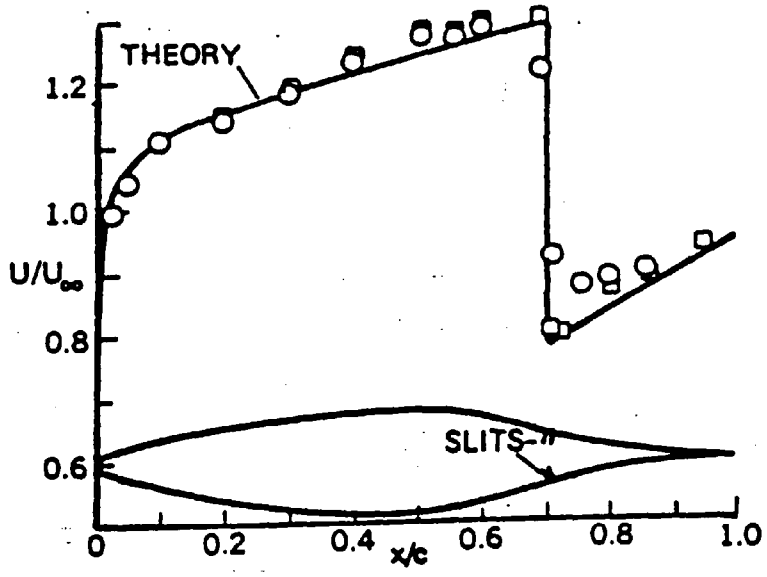

Figure 1-6: Laminar Flow (NLF) Aerofoil,, (Cebeci, 1989).

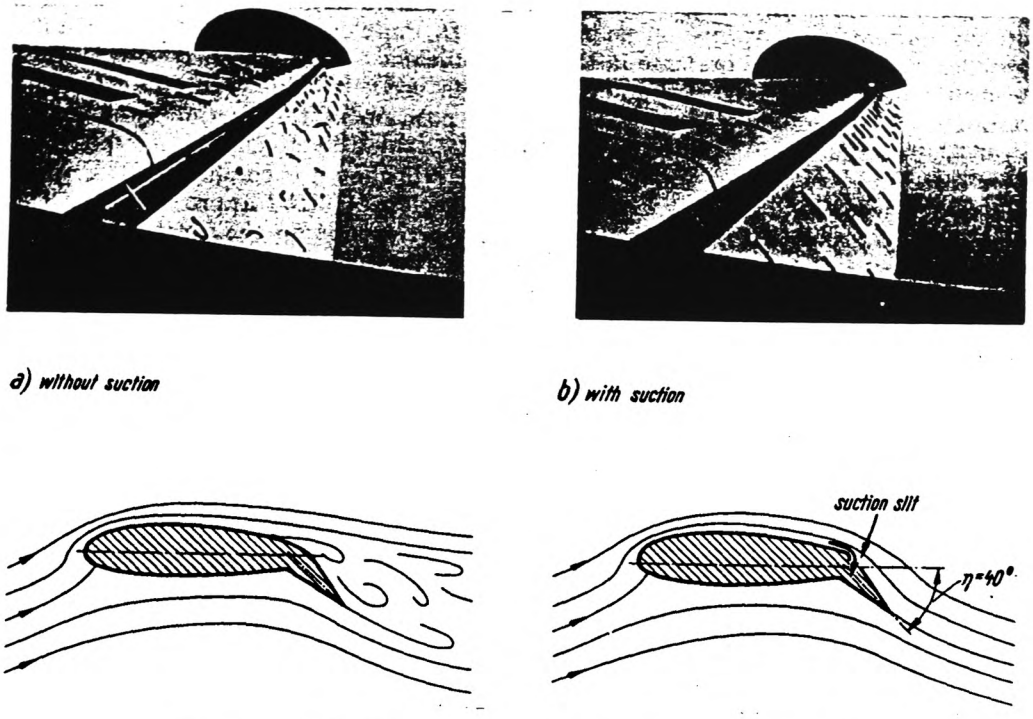

Figure 1-7: Flow about the wing of aeroplane.

The flap is in the down position. Suction keeps the tufts attached to the flap. (Schlichting, 1979).

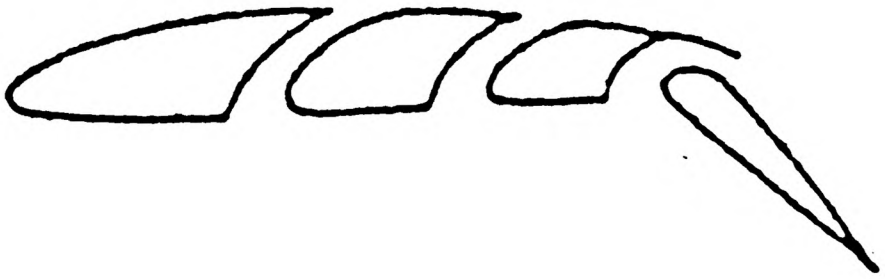

Figure 1-8: Slotted aerofoils with flaps

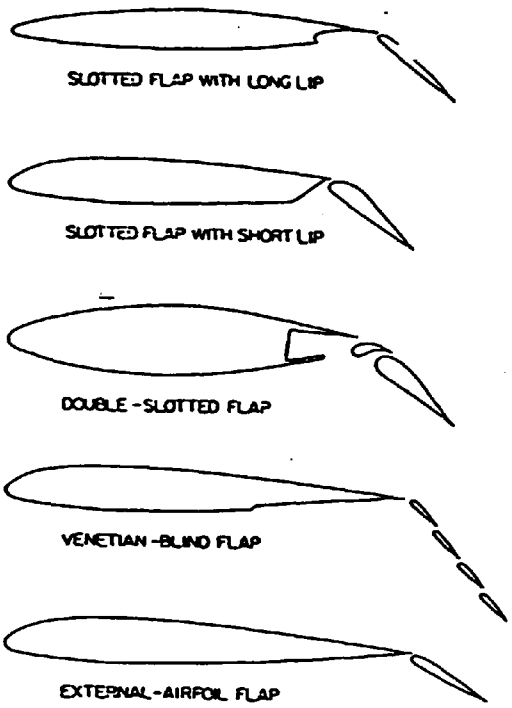

Figure 1-9: Several types of slotted flaps.

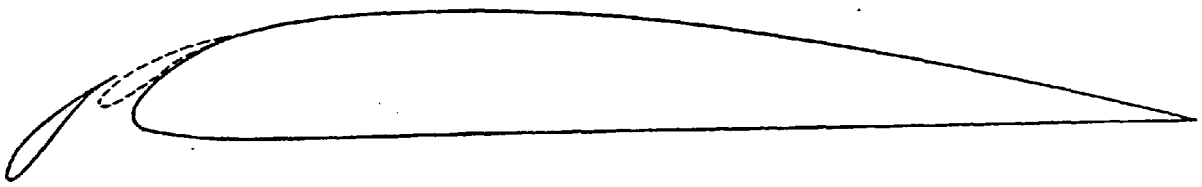

Figure 1-10: Special retractable slat on a wing section

(Abbott and von Doenhoff, 1959)

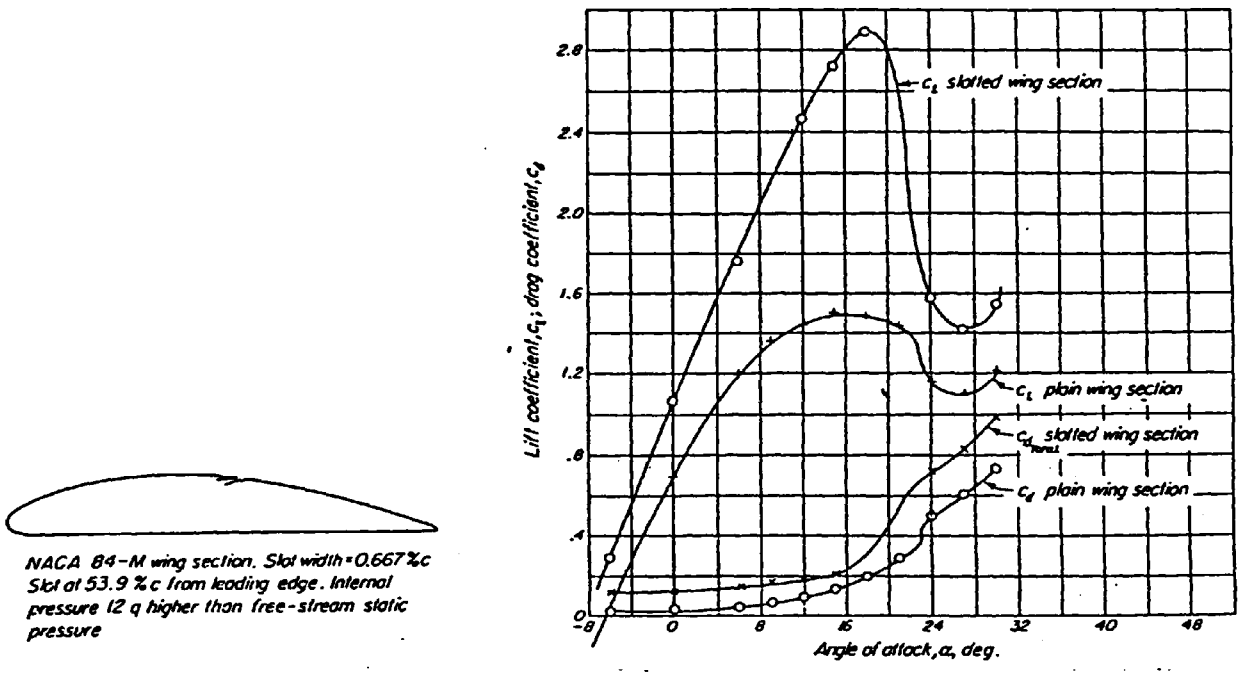

Figure 1-11: Effect of boundary layer control by means of backward-opening slot, (Schlichting, 1979)

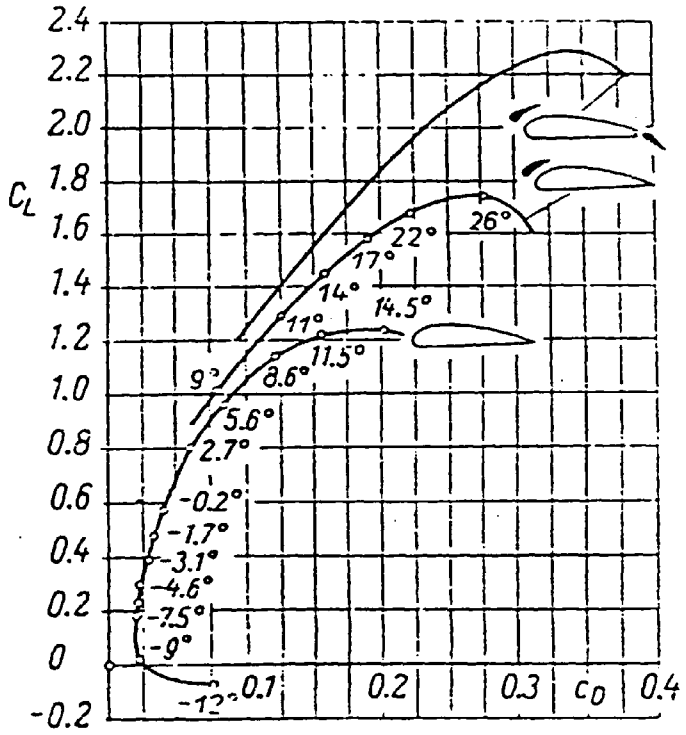

Figure 1-12: Effect of using a forward slat and flaps on the performance of the wing at different angles of incidence.

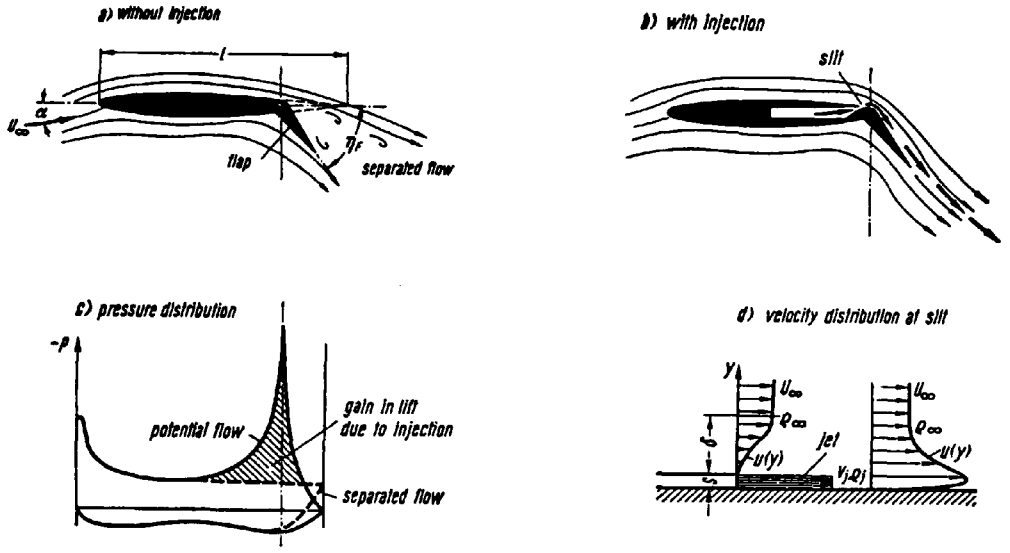

Figure 1-13: Flat wing with injection through a slit at the nose of the flap for the purpose of increasing maximum lift.

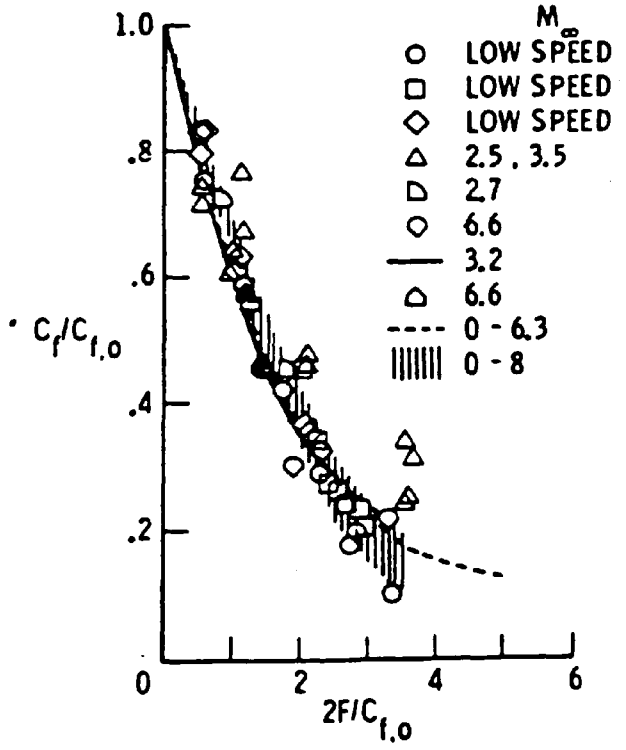

C_{f0}: Coefficient of skin friction of the flat plate without injection

C_f: Local Coefficient of skin friction

M_∞: Mach Number

F: Blowing Parameter ($\rho_w v_w / \rho_\infty v_\infty$)

Figure 1-14: Influence of surface normal injection on skin friction, (Cebeci, 1990).

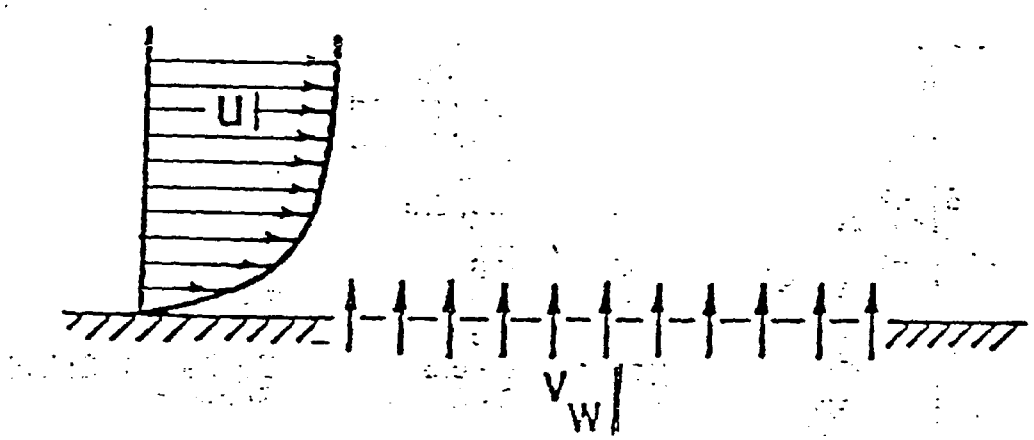

Figure 1-15: Schematic diagram of normal injection into low speed flows,

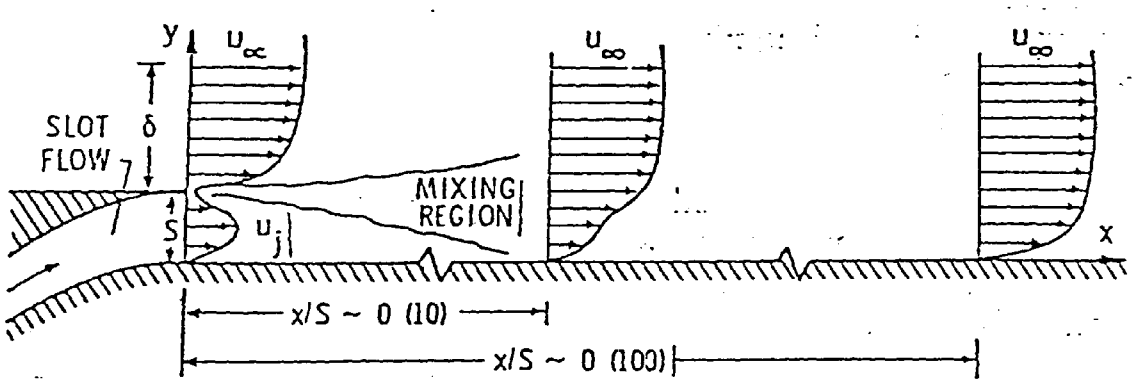

Figure 1-16: Schematic diagram of tangential injection into low speed flows, (Henfer and Bushnell, 1990).

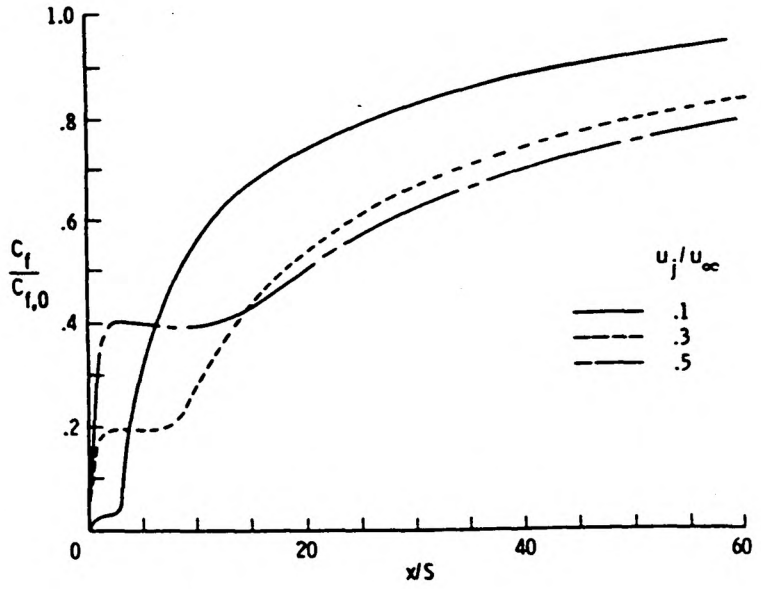

$C_{f,0}$: Coefficient of skin friction of the flat plate without injection

C_f: Local Coefficient of skin friction

U_j: Injection Speed

S Distance along the surface

Figure 1-17 Predicted effect of slot velocity ratio on local skin friction at subsonic velocities, (Bushnell, 1983).

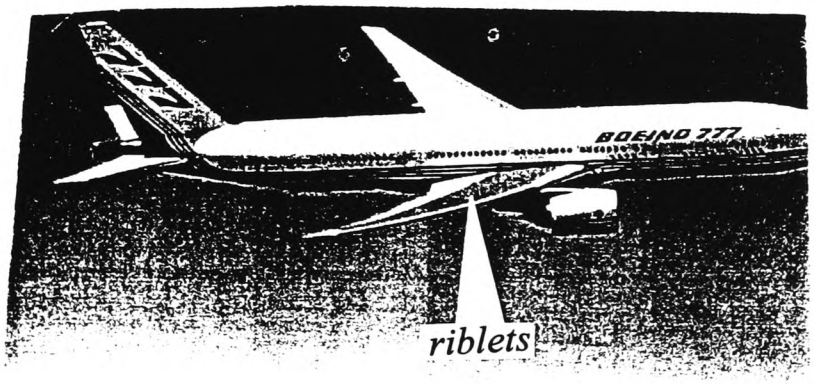

Figure 1-18 The new Boing 777 with riblets on its wings.

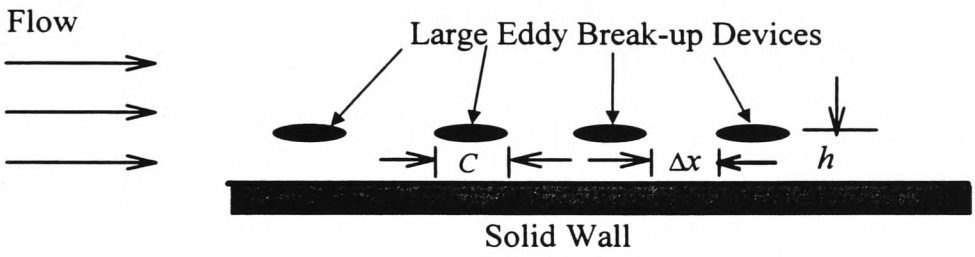

Figure 1-19 Large-eddy break-up devices for turbulence control and viscous drag reduction.

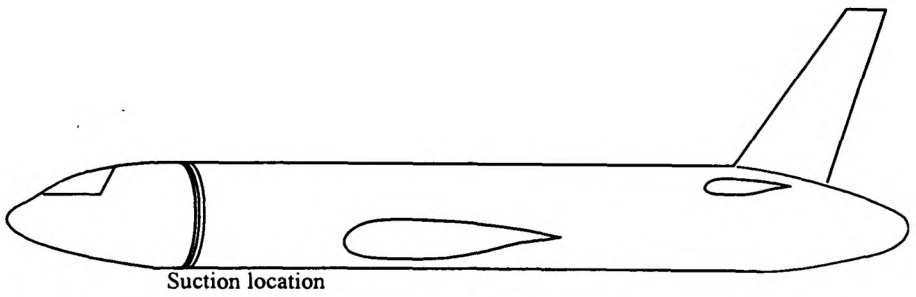

Figure 1-20 Application of suction a short distance after the cockpit to re-laminarize the flow over a fuselage of an aeroplane.

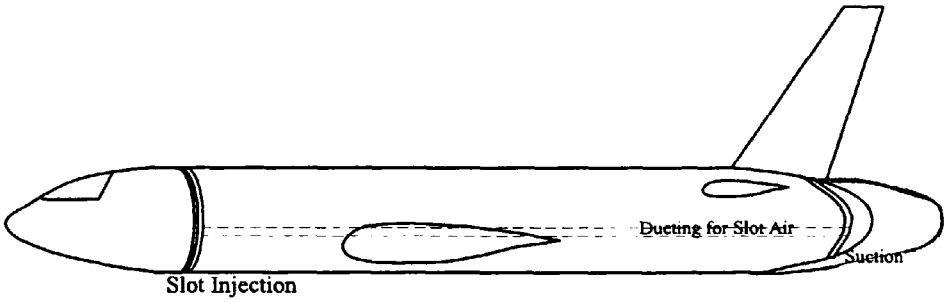

Figure 1-21 Arrangement of combining injection and suction over a fuselage of an aeroplane, (Cary et al. 1977).

This is to reduce turbulent drag and base drag of a truncated fuselage

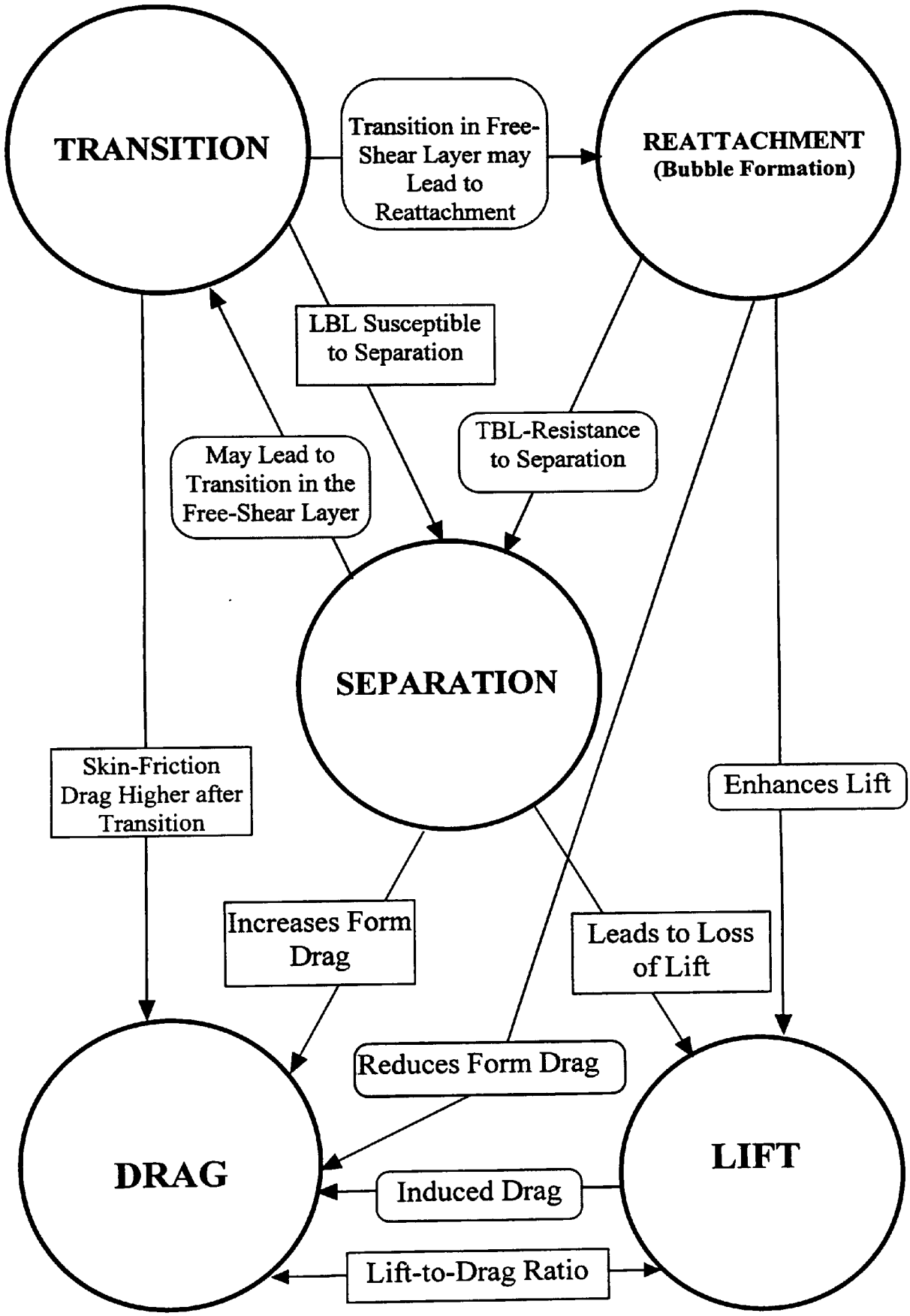

Figure 1-22 Interrelation between flow control goals, (Gad-el-hak, 1990)

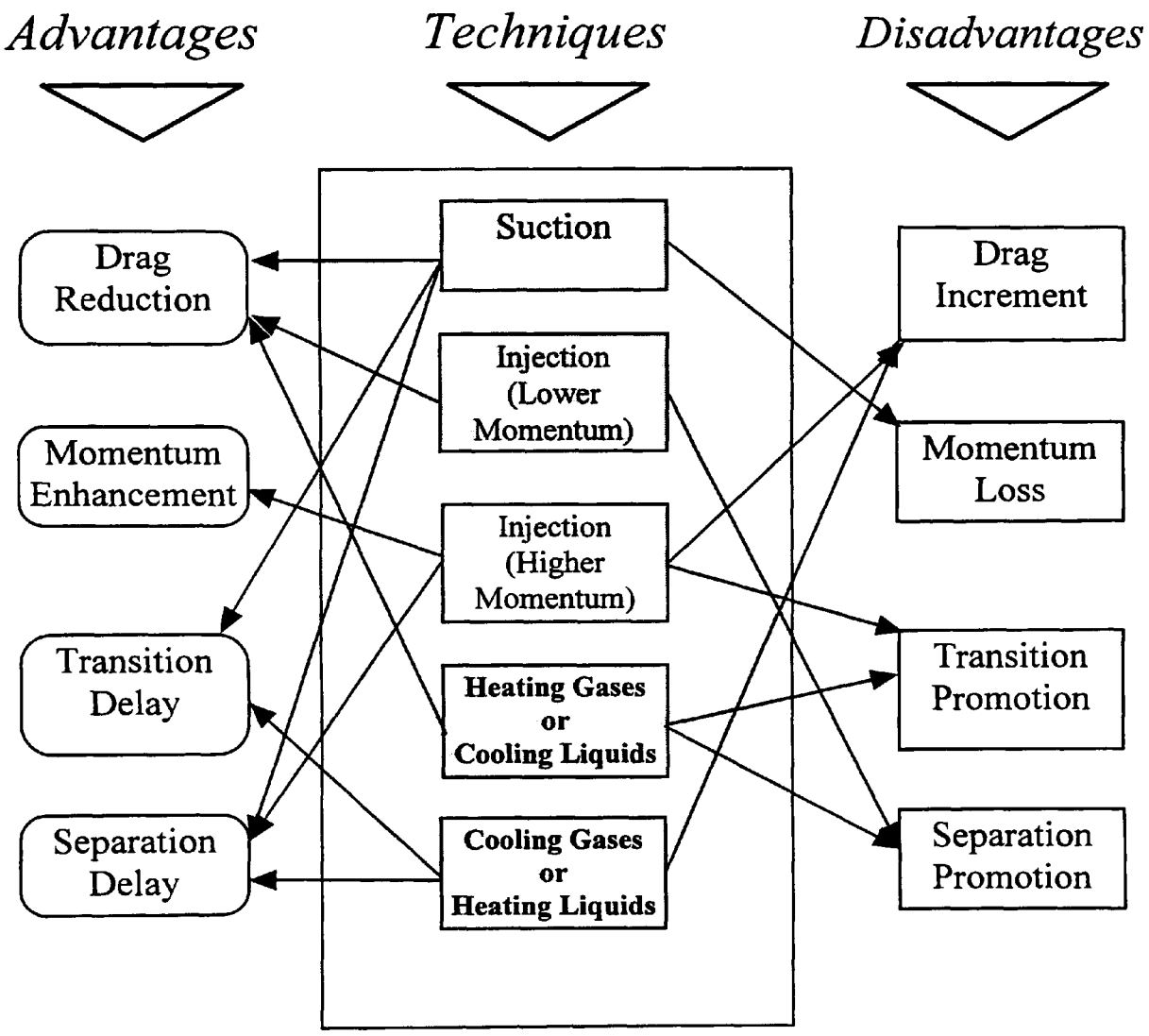

Figure 1-23 Interrelation between the effects of some flow-control techniques

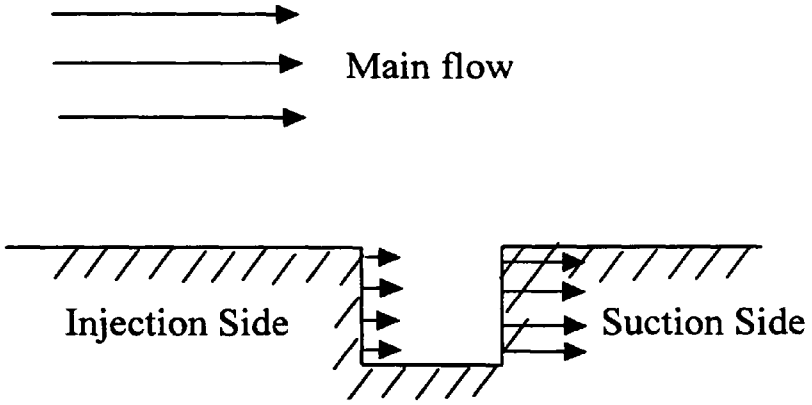

Figure 1-24: Layout of the ABD.

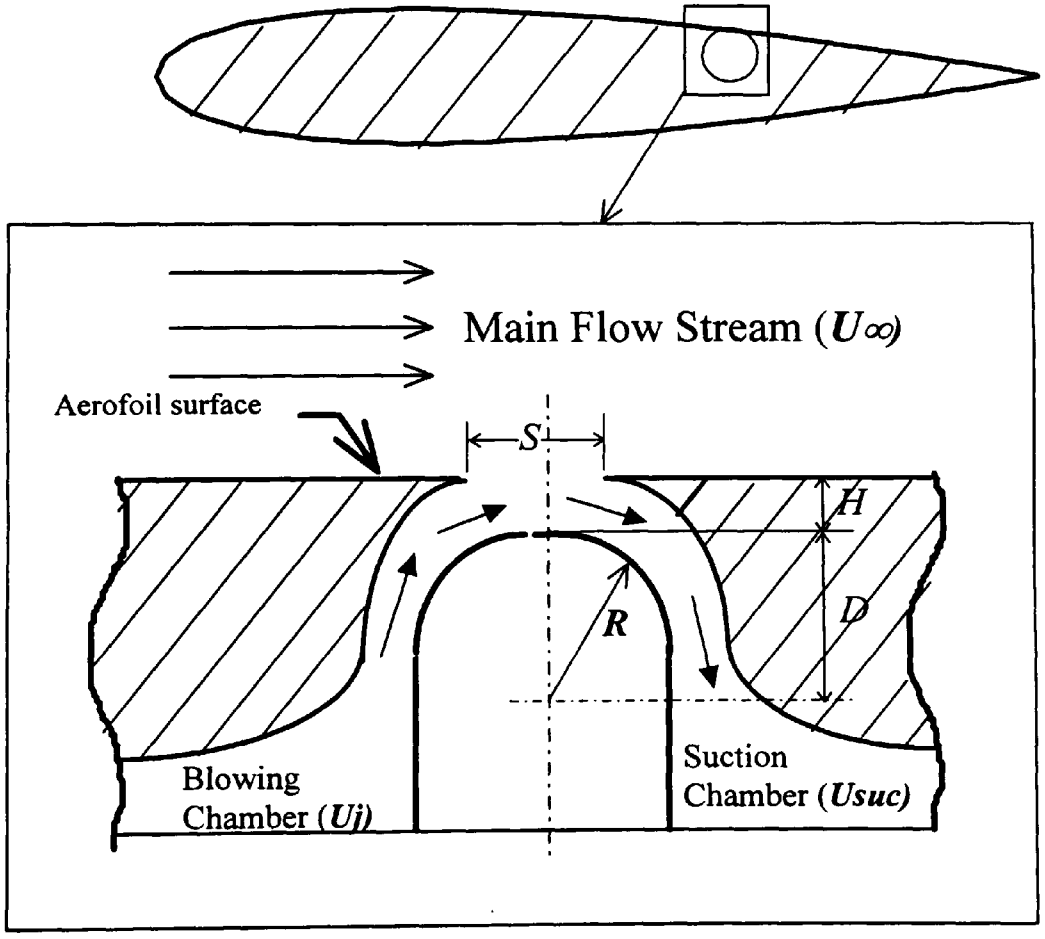

Figure 1-25 Schematic Diagram for the Idea of Roller Air Bearing Device on the Top Surface of the Airfoil

Chapter Two

Computational Modelling of the Problem

2.1 Introduction
2.2 Governing Equations
2.3 Turbulence Models
2.4 Numerical Solution of the Governing Equations
2.5 Modelling of the Present Problem

Chapter Two

Computational Modelling of the Problem

2.1 Introduction

Mathematical solution of the flow field is increasingly becoming a very efficient tool to simulate and predict flow problems of practical interest. These solutions often provide results more economically, quickly and correctly than is possible by other means (for example, experiments on actual systems or models.) In order to achieve correct results, the computational model should simulate the flow in all important respects (geometry, boundary conditions, physical properties of the fluid, turbulence, etc.) and provide a means by which the governing equations may be solved. Significant progress has been achieved in mathematical techniques that yield correct predictions of the flow patterns over aerodynamic devices. As computers became more powerful, it has been possible for aerodynamicists to do calculations and experimental analysis which were not previously possible. Computational Fluid Dynamics, (CFD), is now often favoured by the aviation industry as a substitute for expensive "real" experiments. In a presentation of the history of CFD, (Rubbert, 1994) summarised the main steps associated with the development of the technique. First came the panel methods (based on a surface distribution of singularity elements) for linear flows, and 2-D boundary layers, then 3-D boundary layer methods, transonic small disturbances and full potential methods, Euler and various means of modelling the Navier Stokes equations, see (Al-Shihry, 1989; El-Seif et al. 1990). Direct numerical simulation of turbulence and transition then followed, see (Vandam and Hafiz, 1989). Each of these steps in their time were leading edge challenges; Figure 2-1 shows those stages. "Only later did the confidence, reliability, and automation of those codes develop to the point where they could be accepted as standard computational procedures for regular use in the aeroplane design process", (Rubbert, 1994).

The commercial code, FLUENT, which was designed to model fluid flow, heat transfer and chemical reactions was used in the present study. It incorporates up-to-date modelling techniques and a wide range of physical models for simulating fluid flow problems. The computer code solves the governing conservation equations which dictate the properties of the flow throughout the computational domain. The equations in question are those governing the transport of mass, momentum, enthalpy, and chemical species. The differential equations are expressed in finite difference form, and solved numerically over a discrete grid node arrangement. Closure and completeness of the governing equation set are achieved by means of models of the physical processes taking place within the calculation domain.

In this chapter, the governing equations for fluid flow problems are presented and the approaches used to solve them numerically are discussed. Turbulence modelling is briefly presented as well as the boundary conditions associated with fluid flow problems. The second part of this chapter presents details of the modelling process of the problem considered in the current study.

2.2 Governing Equations

The similarity between the differential equations that govern the flow, (i.e. mass, momentum, energy, and chemical species conservation equations), and their diffusional relations allows them all to be put in the common tensor-form. Thus for any quantity ϕ, (Patankar, 1980):

$$\underbrace{\frac{\partial}{\partial t}(\rho\phi)}_{Accumluation} + \underbrace{\frac{\partial}{\partial x_i}\left(\rho u_i \phi\right)}_{Convection} = \underbrace{D\phi}_{Diffusion} + \underbrace{S_\phi}_{Source} \qquad (2\text{-}1)$$

In words, equation (2-1) can be written as follows:

Rate of increase of ϕ of the fluid element	+	Net rate of flow of ϕ out of the fluid element	=	Rate of increase of ϕ due to diffusion	+	Rate of increase of ϕ due to sources

In the present study there is no phase-change or chemical reaction in the processes under investigation, and hence the equation of species conservation will not be considered.

The remaining set of equations are the continuity, momentum (Navier Stokes) equations and the energy equation.

2.2.1 Mass Conservation (Continuity) Equation

$$\frac{\partial}{\partial x_i}(\rho u_i) = -\frac{\partial \rho}{\partial t} + S_m \tag{2-2}$$

Equation (2-2) means that the net rate of inflow of mass into a unit volume equals the rate of increase in density. The source term S_m is the mass added to the continuous phase from any dispersed second phase (e.g. due to vaporisation of liquid droplets). S_m equals zero for single-phase flow.

2.2.2 Momentum Conservation Equation

Conservation of momentum in the i^{th} direction is described by the following equation:

$$\frac{\partial}{\partial x_i}(\rho u_i u_j) = \frac{\partial p}{\partial x_i} + \frac{\partial \tau_{ij}}{\partial x_i} - \frac{\partial \rho u_i}{\partial t} + \rho g_i + F_i \tag{2-3}$$

where p is the static pressure, g_i is the i-directional gravitational acceleration force, F_i is the external body force in the i-direction (e.g. arising from any interaction with a dispersed phase), and τ_{ij} is the stress tensor given by:

$$\tau_{ij} = \left[\mu\left(\frac{\partial u_i}{\partial x_j} + \frac{\partial u_j}{\partial x_i}\right)\right] - \frac{2}{3}\mu\frac{\partial u_l}{\partial x_l} \tag{2-4}$$

where μ is the molecular viscosity and the second term on the right hand side is summed over all three directions. Equation (2-3) means that the rate of increase of i-direction momentum per unit volume equals the net rate of inflow of the i-direction momentum into a unit volume plus the net force on that unit volume.

2.2.3 Energy Conservation Equation

Conservation of energy can be solved in terms of the conservation of the static enthalpy, h, which is defined as:

$$h = \int_{T_{ref}}^{T} C_p dT \tag{2-5}$$

Where T_{ref} is a reference temperature and C_p is the specific heat at constant pressure. The energy conservation equation can be written as:

$$\frac{\partial}{\partial x_i}(\rho u_i h) = \frac{\partial}{\partial x_i}\left(k \frac{\partial T}{\partial x_i}\right) - \frac{\partial}{\partial t}(\rho h) + \frac{\partial p}{\partial t} + u_i \frac{\partial p}{\partial x_i} + \tau_{ij} \frac{\partial u_i}{\partial x_j} + S_h \tag{2-6}$$

Where T is the temperature, τ_{ij} is the viscous stress tensor defined in equation (2-4), and k is the mixture thermal conductivity. S_h is a source term that includes sources of enthalpy due to chemical reaction, radiation, and exchange of heat with a second phase.

In the case of conduction of heat in solid wall regions, the energy equation can be solved in the following simplified form:

$$\frac{\partial}{\partial x_i}(\rho u_w h_w) = \frac{\partial}{\partial x_i}\left(k_w \frac{\partial T_w}{\partial x_i}\right) + S_{h,w} \tag{2-7}$$

where the subscript w refers to wall properties and $S_{h,w}$ is the volumetric heat rate, and

$$h_w = C_p\left(T_w - T_{ref}\right) \tag{2-8}$$

The flows in the present project were isothermal and any surfaces were regarded as adiabatic, i.e. the net heat exchange is equal to zero. Thus the energy equation was not used. However, the energy equations mentioned above would be necessary when applying CFD techniques to turbine blades or when predicting the effect of heating/cooling on drag reduction or delay of transition as discussed in Chapter(1).

2.2.4 Equation of State for the Density

The density of the gas can be computed via the ideal gas law as:

$$\rho = \frac{P_{op} + p'}{R_0 \cdot T \cdot \frac{1}{M}} \tag{2-9}$$

Where P_{op} is the operating pressure and P' is the local static pressure (defined relative to P_{op}), M is the molecular weight of the gas, and R_0 is the universal gas constant. Equation (2-9) describes the general, "compressed", form of the gas law. If the fluid under consideration is incompressible, the term P' can be omitted from equation (2-9). If the

problem deals with a mixture of gases, the molecular weight should be replaced with a mean mixture molecular weight which may be calculated from the mass fraction m_j and the molecular weight of species j, M_j. In such a case,

$$\rho = \frac{\left(p_{op} + p'\right)\cdot}{R_0 \cdot T \cdot \sum \frac{m_j}{M_j}} \tag{2-10}$$

2.3 Turbulence Models

Equations (2-1), (2-2), (2-3), (2-4)) and (2-6) are the instantaneous governing equations in time-dependent form. They are exact for not only laminar but also turbulent flows. It is well known that they are too complex to be readily solved analytically because they are non-linear and turbulence in addition is three-dimensional and takes place over tiny spatial distances and very short time steps. However, for engineering applications the prediction of the instantaneous structure in the turbulent flow field generally does not need to be considered so that the interest is in the mean flow properties. By applying the so-called "Reynolds averaging" to the scalar quantities in the above instantaneous equations, these can be resolved into their mean and fluctuating components respectively as follows:

$$\begin{aligned} u_i &= \overline{u}_i + u_i' \\ \rho_i &= \overline{\rho}_i + \rho_i' \\ p_i &= \overline{p}_i + p_i' \\ \phi_i &= \overline{\phi}_i + \phi_i' \end{aligned} \tag{2-11}$$

where the bars over the symbols are the time-averaged values and the primed-letters are the fluctuating components.

Introducing the definitions of equation (2-11) into the generic transport equation for a conserved scalar quantity (2-1) results in

$$\frac{\partial}{\partial t}\left(\overline{\rho}\overline{\phi}\right) + \frac{\partial}{\partial x_i}\left(\overline{\rho}\overline{u}_i\overline{\phi}\right) = -\frac{\partial}{\partial x_i}\left(\overline{\rho u_i'\phi'}\right) + \overline{D\phi} + \overline{S_\phi} \tag{2-12}$$

The terms in equations (2-12) are similar to those in the equation (2-1) except that each quantity in (2-12) is represented by a time averaged value and a new term containing the correlation term ($\overline{u_i'\phi'}$) now appears in the right hand side. Physically, this correlation represents the transport or "diffusion" of ϕ due to turbulent fluctuations.

By definition $\bar{\phi}'_i=0$, but not ($\overline{u_i'\phi'}$). The second order product of the fluctuations, ($\overline{u_i'\phi'}$), are known as " Reynolds stress" terms. It is the main task of a turbulence model to provide expressions or "closures" that allow the evaluation of these correlations in terms of the mean values of the flow parameters. In other words, the system of equations has new "unknowns", therefore it needs new "equations" to complete the system; a turbulence model provides these equations.

A variety of turbulence models have been proposed in order to represent the flow characteristics. The main justification for these models is that they are based on a hypothesis which has been verified by experiments. Due to the complexity of the turbulence process it has not been possible to develop a turbulence model analytically. "It is not very likely that science will even achieve a complete understanding of the mechanism of turbulence because of its extremely complicated nature", (Schlichting, 1979).

The Eddy Viscosity Concept

Boussinesq (Kaname Sato, 1994) introduced for the first time the concept of mixing coefficient by which he related the Reynolds stresses in turbulent flow to the mean velocity. The mixing coefficient, μ_t which is often called "apparent", or "virtual" or "eddy" viscosity, is defined by:

$$\tau_t = \rho\mu_t \frac{d\bar{u}}{dy} \qquad (2\text{-}13)$$

where, μ_t corresponds to the viscosity, μ, in laminar flow.

Accordingly, the Reynolds stresses were presented as:

$$-\rho\overline{u_i'u_j'} = \mu_t\left(\frac{\partial \bar{u}_i}{\partial x_j} + \frac{\partial \bar{u}_j}{\partial x_i}\right) \tag{2-14}$$

Although μ_t, the eddy viscosity, is analogous to the fluid molecular viscosity, it should be recognised that it is not a property of the fluid, but instead, can be considered as a property of the local state of turbulence.

2.3.1 Turbulence Model Classification

The Prandtl mixing length theory was the first turbulence model to be proposed in the published literature. This model, initially proposed by Prandtl in 1925, is usually known as the mixing-length hypothesis, see for example, (Galbraith and Head, 1975), and can be expressed as:

$$\mu_t = \rho l_m^2 \left|\frac{\partial u}{\partial y}\right| \tag{2-15}$$

where l_m is the mixing-length derived from experimental data. In many cases it is possible to establish a simple relation between the mixing-length and a characteristic length of the flow; (Galbraith and Head, 1975). The model has been adopted for two-dimensional, thin shear layers (Rodi, 1979) but is not suitable when convective, diffusive transport of turbulence, or history effects are important, (Patankar, 1980).

The model was extended to the Kolmogrov-Prandtl expression, (Kaname Sato, 1994), so that:

$$\mu_t = \rho\kappa^{\frac{1}{2}} l_m \tag{2-16}$$

where κ is the kinetic energy of the turbulence defined as:

$$\kappa = \frac{1}{2}\sum u_i'^2 = \frac{1}{2}\left(u_1'^2 + u_2'^2 + u_3'^2\right) \tag{2-17}$$

The local kinetic energy of turbulence, κ, can be determined from a transport equation for κ, equation (2.22) which is discussed later.

The next development in the turbulence model is that the length scale, l_m, can be expressed as:

$$l_m = C_\mu \frac{\kappa^{\frac{3}{2}}}{\varepsilon} \tag{2-18}$$

Where C_μ is an empirical constant and ε is the rate of dissipation of turbulence energy (obtained from the solution of transport equation).

The well known κ-ε model is derived from this concept and gives good results for many simple flows with moderate turbulence levels. Convergence is usually excellent (Kaname Sato, 1994).

2.3.2 The κ-ε Turbulence Model

The κ-ε turbulence model is an eddy-viscosity model in which the Reynolds stresses are assumed to be proportional to the mean velocity gradients, with the constant of proportionality being the turbulent eddy viscosity, μ_t.

In this model, equation (2-14) is modified to be in the following form, (Hinze, 1975):

$$\rho\overline{u_i'u_j'} = \rho\frac{2}{3}\kappa\delta_{ij} + \mu_t\left(\frac{\partial u_i}{\partial x_j} + \frac{\partial u_j}{\partial x_i}\right) - \frac{2}{3}\mu_t\frac{\partial u_l}{\partial x_l} \tag{2-19}$$

Equation (2-19) for Reynolds stresses is analogous to that describing the shear stresses that arise in laminar flow, equation (2-4), with the turbulent viscosity playing the same role as the molecular viscosity μ. This analogy indicates that the laminar momentum equation, i.e. equation (2-3) is used in turbulent flow except that μ is replaced by the effective viscosity μ_{eff} where:

$$\mu_{eff} = \mu + \mu_t \tag{2-20}$$

The κ-ε model assumes that μ_t is proportional to the product of length scale l_m defined in equation (2-18) and velocity scale $\sqrt{\kappa}$. Hence;

$$\mu_t = \rho C_\mu \frac{\kappa^2}{\varepsilon} \tag{2-21}$$

The values of κ and ε required in equation (2-21) can be obtained from the solution of following conservation equations:

$$\frac{\partial}{\partial t}(\rho\kappa)+\frac{\partial}{\partial x_i}(\rho u_i\kappa)=\frac{\partial}{\partial x_i}\left(\frac{\mu}{\sigma_\kappa}\frac{\partial\kappa}{\partial x_i}\right)+G_k+\rho\varepsilon \qquad (2\text{-}22)$$

$$\frac{\partial}{\partial t}(\rho\varepsilon)+\frac{\partial}{\partial x_i}(\rho u_i\varepsilon)=\frac{\partial}{\partial x_i}\left(\frac{\mu}{\sigma_\varepsilon}\frac{\partial\varepsilon}{\partial x_i}\right)+C_{1\varepsilon}\frac{\varepsilon}{\kappa}G_\kappa-C_{2\varepsilon}\rho\frac{\varepsilon^2}{\kappa} \qquad (2\text{-}23)$$

Where $C_{1\varepsilon}$ and $C_{2\varepsilon}$ are empirical constants, σ_κ and σ_ε are "Prandtl" numbers governing the diffusion of κ and ε, and G_κ is the rate of production of turbulent kinetic energy:

$$G_\kappa=\mu_t\left(\frac{\partial u_i}{\partial x_j}+\frac{\partial u_j}{\partial x_i}\right)\frac{\partial u_i}{\partial x_i} \qquad (2\text{-}24)$$

2.3.3 The Reynolds Stress Model (RSM)

The major limitation of the κ-ε model is that μ_t is isotropic. This implies that viscosity and length scales are the same in all directions. In the case of complex flows, such as highly swirling flows, the velocity length scales can vary significantly with direction. Using a κ-ε model in such flows is inadequate and considerable errors may occur. In order to avoid this problem, the Reynolds stresses should be computed individually. This is achieved in the RSM.

The calculation of Reynolds stresses $\overline{u_i'u_j'}$ in this turbulence model is made through the solution of transport equations for the individual stresses. These transport equations are derived from the momentum equations and have the following form:

$$\frac{\partial}{\partial t}\left(\overline{u_i'u_j'}\right)+\bar{u}_\kappa\frac{\partial\left(\overline{u_i'u_j'}\right)}{\partial x_\kappa}=\frac{\partial}{\partial x_\kappa}\left(\frac{\mu_t}{\sigma_k}\frac{\partial\left(\overline{u_i'u_j'}\right)}{\partial x_\kappa}\right)+P_{ij}+\phi_{ij}-\varepsilon_{ij} \qquad (2\text{-}25)$$

where P_{ij} is the stress production rate defined as:

$$P_{ij}=-\left(\overline{u_i'u_k'}\frac{\partial u_j}{\partial x_k}+\overline{u_j'u_k'}\frac{\partial u_i}{\partial x_k}\right) \qquad (2\text{-}26)$$

and ϕ_{ij} is a source/sink due to the pressure/strain correlation and is expressed as:

$$\phi_{ij}=-C_3\frac{\varepsilon}{\kappa}\left(\overline{u_i'u_j'}-\frac{2}{3}\delta\kappa\right)-C_4\left(P_{ij}-\frac{1}{3}\delta_{ij}P_{ij}\right) \qquad (2\text{-}27)$$

and ε_{ij} is the viscous dissipation modelled as :

$$\varepsilon_{ij} = \frac{2}{3}\delta_{ij}\varepsilon \qquad (2\text{-}28)$$

and ε is the isotropic dissipation rate obtained from equation (2-23).

The empirical constants appearing in the above equations for the κ-ε and RSM models normally have the following values, (Fluent, 1994):

Constant	Value
C_μ	0.09
σ_k	1.0
σ_ε	1.3
$C_{1\varepsilon}$	1.44
$C_{2\varepsilon}$	1.92
C_3	1.5
C_4	0.4

2.3.4 Boundary Conditions

Solution of the equations presented in the previous sections requires knowledge of the conditions on the boundaries of the flow domain. By providing these boundary conditions the system of equations is said to be "closed" and is ready for solution using the procedures presented in the next section.

(1) "Inlet" boundary condition

This is the boundary at which the flow enters (or is withdrawn) at a known velocity, composition (for multi phase flow applications), and temperature. In turbulent flows, the κ and ε values are also defined. It is possible to specify κ and ε directly or indirectly by calculating the values from inputs of the turbulence intensity and the characteristic length.

As an alternative to specifying the inlet velocity, the inlet pressure can be given. In this case, the velocity is calculated from the inlet pressure (which is treated as total pressure) by solving a loss-free momentum balance (e.g. Bernoulli's equation). When an inlet boundary is used as an exit boundary, the boundary pressure is treated as the static

pressure of the existing flow, and all scalar quantities and the flow angle are obtained from the upstream flow conditions.

It is possible to specify the inlet boundary condition using a particular profile (e.g. a distribution derived from experimental data), or as a uniform value.

(2) "Outlet" boundary condition

The flow at this boundary corresponds to fully developed and/or supersonic flow conditions, and in subsonic flow the normal velocities at the outlet are adjusted to satisfy an overall mass balance for the computational domain. All values at this boundary are extrapolated from the adjacent cells from the interior domain.

(3) "Symmetry" boundary condition

At this boundary, all the variables have a zero normal gradient, except for the normal velocity component which vanishes.

(4) "Cyclic" boundary condition

This boundary condition can be very useful when a flow field solution is to be transferred from one boundary to another at the opposite side of the solution domain. This type of boundary condition provides a high flexibility in designing the grid mesh of a problem as will be seen in the next section (2.6.2).

2.3.5 Near-Wall Boundary Condition

It is necessary to describe the near-wall pressure gradient and shear stress at the wall in order to solve the momentum equation (2-3). It can be assumed that the pressure gradient at the wall is zero and therefore the only remaining parameter is the shear stress at the wall. In laminar flows, it is possible to use the following equation:

$$\tau_w = \mu \left.\frac{\partial u}{\partial y}\right|_w \approx \mu \frac{\Delta u}{\Delta y} \qquad (2\text{-}29)$$

where u is the velocity component parallel to the wall and y is the co-ordinate normal to the wall. Δy and Δu are determined using the values stored in the computational cells adjusted to the wall.

In turbulent flows, the treatment of the wall boundary conditions is divided into two regions: the laminar sub layer, where $y^+ \leq 11.63$, and equation (2-29) is valid. The other region, i.e. the turbulent region starts from $y^+ > 11.63$, and the following log-law of the wall is used to compute the shear stress:

$$u^+ = \frac{1}{\kappa_v} \ln(Ey^+) \tag{2-30}$$

where $u^+ = \frac{u}{u_\tau}$, the frictional velocity $(u_\tau) = \sqrt{\tau_w/\rho}$, u is the fluid velocity at a point in the log-law layer, κ_v is the von-Karman constant, E is the "roughness parameter", and E=9.8 for a smooth wall. y^+ is the dimensionless distance from the wall and generally:

$$y^+ = \rho u_\tau \frac{y}{\mu} \tag{2-31}$$

y^+ can be computed from the following equation provided that the turbulent boundary layer is in an equilibrium condition (turbulence production equals its dissipation):

$$y^+ = \frac{C_\mu^{\frac{1}{4}} \rho \kappa^{\frac{1}{2}} y}{\mu} \tag{2-32}$$

where κ is the near-wall kinetic energy which is computed from the full transport equation (2-22) assuming zero gradient for κ at the wall.

The near-wall value for ε is computed as follows

$$\varepsilon_p = \frac{C_\mu^{\frac{3}{4}} \kappa^{\frac{3}{2}}}{\kappa_v \Delta y} \tag{2-33}$$

2.4 Numerical Solution of the Governing Equations

2.4.1 Introduction

There are three distinct techniques for numerical solution namely: finite difference, finite element and spectral methods, (Versteeg and Malalasekera, 1995). The numerical solution of flow problems involves:

- Approximation of the unknown flow variables by means of simple functions.
- Discretization of the governing equations by converting them into algebraic equations using approximations of the unknowns.
- Solution of the algebraic equations.

These three steps are employed in the numerical solution using CFD codes and can also require:

- Definition of the geometry of the problem: i.e. the physical and computational domain.
- Grid generation
- Definition of the fluid properties and the physical and the chemical phenomena to be modelled.
- Specification of the boundary condition for the problem
- Presentation of the results of the calculation including:
  - Display of the geometry and grids.
  - Display of the contours and vectors of the flow variables.
  - Alpha-numerical data.
  - Hard copy output in a professional manner.

"However, the main differences between the three separate streams are associated with the way in which the flow variables are approximated and with the discretization procedures." (Versteeg and Malalasekera, 1995).

The finite volume method is considered as a special finite difference formulation and is well established, and is a thoroughly validated general purpose CFD technique, (Smith, 1985).

2.4.2 The Control Volume Technique

In the control volume technique the computational domain is divided into a discrete control volumes called cells as in Figure 2-2, and the differential equations are then integrated over each control volume. Using a divergence theorem and finite difference approximations, these equations are converted into a set of algebraic equations which

can be solved numerically. The resulting equations conserve the quantities on a control-volume basis.

The equations are written for a control volume bounded by the grid lines I-1th, Ith, J-1th, Jth lines using one of the differencing schemes. Stability, convergence, and the accuracy of the solution are all affected by the type of differencing scheme used.

An extensive review can be found in (Roache, 1982) (who reviewed more than 1100 papers) and more recently (Fletcher, 1991). (Versteeg and Malalasekera, 1995) present a thorough discussion and assessment of each of these schemes.

The SIMPLE (Semi-Implicit Method for Pressure-Linked Equations) algorithm is used to calculate the pressure and velocity through an iterative procedure from the coupled equations of motion.

2.4.3 Interactive Solution Procedure

It is well known that the equations of motion are coupled and non-linear. The velocity and pressure fields can thus be related to each other via the SIMPLE algorithm as mentioned above. The non-linearity of the equations results in the need to use iterative solution procedures. In each iteration the equations are linearized by using values of the non-linear terms from the previous iterations. Initial estimations or "guesses" are used for the first iteration. These terms are then calculated and updated for use in the next iteration. This iterative solution is continued until satisfactory convergence of all quantities is achieved for all grid points.

A typical iterative procedure involves the following steps:

1) The momentum equations are solved with a "guessed" pressure (or values from a previous cycle), P^*, to obtain intermediate velocity fields, u_1^*, u_2^*, u_3^*.
2) The finite difference form of the pressure equation P' is solved using a Tridiagonal Matrix Algorithm, TDMA, in order to obtain the pressure correction. The pressure field is therefore corrected by adding P' to P^*.
3) The velocity components are updated using the new values of the pressure.

4) If the flow is turbulent the κ and ε equations (or Reynolds stress transport equations) are solved using the updated velocity in order to obtain the distribution of the effective viscosity and/or Reynolds Stresses.

5) The equations governing any other property (e.g. enthalpy, species conservation and radiation) are then solved using the most recent values of the other variables.

6) The corrected pressure field is taken as the new estimated pressures for the next iteration and the whole process is repeated until the residuals in any of the finite difference equations are small (usually less than 10^{-3})

The iteration procedures are carried out in two stages. *Firstly* the equations are solved simultaneously along a ***J***-line, Figure 2-3, using a TDMA where the primitive variables are calculated along the ***J***-line. This stage is called *sweeping*. *Secondly* The solution is performed at the next "***J***" line (i.e. advancing from line ***J*** to line ***J+1***). This is called *marching*. Usually, sweeping takes place along the y-direction (perpendicular to the flow direction) and marching takes place in the x-direction (parallel to the main flow direction)

The grid size affects the accuracy of the solution. In general, fine grids give greater accuracy, and vice versa. Therefore, grid refinement is the main tool in the hands of the CFD user for the improvement of the accuracy of a simulation, (Versteeg and Malalasekera, 1995). However, there are practical limitations to grid refinement owing to the limited size of available computer memory and to restrictions on computer time. Coarse meshes can be used first to get an initial estimate of the overall features of the solution. The grids can then be refined in stages until no significant differences in the predictions occur between successive grid refinement stages. The solution is then termed "grid independent".

Grids are not necessarily uniform throughout the domain of calculation. Fine grids must be used in areas where there are high rates of change in the flow properties; while coarse grids can be used elsewhere. This type of arrangement is widely used in CFD problems and has the advantage of achieving high accuracy with a minimum calculation time.

The size ratio between any two adjacent cells must be kept within a certain range in order to safeguard the accuracy and stability of the solution. Normally the condition which should be satisfied is:

$$0.7 \leq \frac{\Delta y_{I+1}}{\Delta y_I} \leq 1.3 \tag{2-34}$$

Since the grids can be non uniform, the cell aspect ration, $(\Delta x_i/\Delta y_j)_{i\neq j}$, should not be exceed 10. In regions of complex multidimensional flows it is preferred that this ratio should be kept close to 1.0.

Convergence of the solution is affected by many parameters such as the grid size, the interpolation method used in the discretization of the equations, marching and sweeping techniques, and the complexity of the flow problem.

Due to the non-linear nature of the equations to be solved, convergence can be achieved by underrelaxation which reduces the change in each variable produced during each iteration. In simple form, the new value of the variable ϕ_p at node P depends upon old value, $\phi_{p,old}$, the computed change in ϕ_p, $\Delta\phi_p$, and the underrelaxation factor β as follows:

$$\phi_p = \phi_{p,old} + \beta\Delta\phi_p$$

where the value of β should be between 0 and 1.

Optimised convergence is then required for every individual problem in order to get the fastest solution. A poor choice of one or more of the parameters leads not only to slow convergence but sometimes the solution diverges rapidly with subsequent failure. When the residuals for one or more iterations remain nearly constant over a large number of iterations (or the solution tends to diverge) then additional approaches should be used to "restart" and/or speed up convergence. These approaches include: increasing the number of sweep cycles, changing the sweep direction, smoothing the grid spacing and adjusting the values of the underrelaxation factors.

2.4.4 Body Fitted co-ordinates

Computational fluid dynamics methods based on Cartesian or cylindrical co-ordinate systems have certain limitations when applied to irregular geometries. Practical boundary geometries can be complex and often irregular and they can only be approximated in Cartesian or cylindrical co-ordinate systems by treating surfaces in a stepwise manner as illustrated in Figures 2-4 and 2-5. In order to model a cylindrical surface using a Cartesian co-ordinate system, the cylindrical system may be represented by a step approximation and cells inside the solid part of the cylinder are blocked in the calculation. This has considerable disadvantages since the approximate boundary description is tedious to setup and introduces errors, especially if the wall shear stress needs to be calculated to a great deal of accuracy (as is the case in the present study). The other disadvantage of Cartesian/cylindrical co-ordinate systems is the waste of computer storage and resources due to (1) blocking of the cells in solid regions and (2) the introduction of a fine mesh in regions of particular interest can result in unnecessary refinement in another region of minimal interest.

Methods based on body-fitted grid or non-orthogonal grid systems have been developed to overcome the aforementioned limitations and are used increasingly in present-day CFD procedures.

The geometrical flexibility offered by body-fitted grid techniques is useful in the modelling of practical problems involving irregular geometries because (1) all geometry details can be *accurately* incorporated and (2) the grid properties can be controlled to capture flow details in regions of interest.

It is worth mentioning that all tests in the present study were simulated in body fitted co-ordinates which were adapted to the geometry under consideration.

2.5 Modelling of the Present Problem

As illustrated previously a computational modelling process usually involves five main steps:

1) Geometry setup

2) Grid generation

3) Case setup

4) Calculation process

5) Presentation of the results

In the first step, the geometry of the problem is defined by prescribing walls, inlets, outlets and all the boundaries of the problem. This process may be carried out using the CFD package itself or by an external computer aided design (CAD) package and imported to the CFD code. Usually the geometry can be modelled to a high accuracy. In the second step, grid generation, a computational domain is defined by a mapping process which assigns a grid distribution along all boundaries of the geometry, and the interpolation process which creates the grid inside the domain. In this step, it is important to determine the critical region(s) of the problem and, consequently, to choose the appropriate grid size and distribution.

In the third step, the case setup, the fluid characteristics, the inlet boundary conditions, the type of problem, and the solution parameters are all prescribed. The calculation process, i.e. the iterative solution to solve the governing equations in their algebraic form is undertaken in step 4. Finally the results are stored in ASCII files to be manipulated using specially designed FORTRAN programs while other results can be presented using some of the facilities in the package itself.

2.5.1 Modelling of the ABD in a Flat Plate

Initially a flat plate problem was modelled essentially to demonstrate the performance of the air bearing device (ABD)[1]. Several cases of a flat plate fitted with the ABD were studied and different parameters of the ABD were tested. The geometry of the flat plate problem is shown in Figure 2-6. The location of the ABD (L_s) was changed as well as the other parameters. Table (2-1) shows the different cases. Body fitted co-ordinates were used and the grids were condensed at the viscous layer and around the ABD to give a correct description of the high rate of change of the flow parameters in these critical regions. The overall computational domain was divided into 60×30 cells.

The inlet boundary condition was defined by prescribing the inlet velocity and a pressure reference point at an arbitrary location. The upper boundary was defined as having a symmetry condition. The velocity of the main flow stream was uniform and

[1] The principles and characteristics of the ABD were discussed in Chapter (1).

fixed at 40 m/sec which is the maximum speed of the wind tunnel. This is to achieve consistency in the free-stream flow characteristics between the two cases of the flat plate and the aerofoil.

The inlet to the ABD (injection side) and the outlet (suction side) were both fixed by inlet boundary conditions so that the velocity at the outlet boundary was always negative. Specifying an inlet boundary condition for the suction side results in "full control" of the out-flow from the ABD. If an outlet boundary condition had been chosen then the suction flow speed could not be controlled because the outflow rate would be solely determined by the pressure difference around the suction side. All the inlet boundary conditions were given a uniform velocity in the x-direction (i.e. parallel to the flat plate) and a turbulence intensity of 3% (i.e. similar to the value in the wind tunnel) was also specified. The length of the flat plate is taken as the characteristic length. Using the properties of the air at 20°C (i.e. the average temperature in the laboratory) the corresponding Reynolds number at the trailing edge of the flat plate was equal to 4×10^5. The under relaxation factors were given the following values:

Parameter	First 50 Iterations	Rest of the Iterations
Velocities	0.4	0.6
Pressure	0.5	0.5
κ	0.3	0.4
ε	0.3	0.4
Effective viscosity	0.3	0.4

This arrangement resulted in convergence after 200 iterations instead of 500 iterations when the default values of the package were used.

The results of the calculations were presented as follows:

- Velocity profiles at the trailing edge and at any location on the flat plate,
- Pressure distributions over a flat plate,
- Stream function contours, and
- Filled contours of pressure, u-velocity, κ and ε.

The velocity profile data was outputted as an ASCII data and imported to a FORTRAN program to calculate the drag.

The results of the calculations for flow over a flat plate are presented in Chapter (5).

Since the flat plate is a straight forward simple problem, only numerical modelling was studied. The agreement achieved between the numerical and experimental cases on the aerofoil sections suggests that similar agreement would be obtained in the case of a flat plate.

2.5.2 Modelling of a Smooth Aerofoil

Two main problems were encountered when attempting to model a smooth aerofoil . Firstly modelling the dead region inside the aerofoil and secondly maintaining the continuity of the modelled region at the trailing edge. The first problem was tackled by using the O-type grid scheme[2]. In this scheme the closed region is modelled inside the main flow stream. The second problem was tackled by choosing appropriate values for the interpolation factors of the grids at the outlet boundary. This method when applied with O-type grids can improve the distribution of the grid lines around the discontinued curve at the trailing edge.

The following steps were used to model the aerofoil:

- Creating the aerofoil-surface curve by prescribing the locations of points on it according to Table (2-2). This table presents the co-ordinates of points on both the upper and lower surfaces of the NACA standard aerofoil simulated in the current project.
- The computational domain can be defined as in Figure 2-7 based on the physical domain, Figure 2-8,
- Creating the boundaries and then assigning the boundary conditions at these boundaries.
- Grids were generated in two steps: mapping all the curves in the geometry and creating grids inside the domain using an interpolation method. The interpolation factors used at the boundaries are listed in Table (2-3).

The effect of prescribing the interpolation factors along the boundaries is to control the distribution of the mesh points to achieve a reasonable spacing at certain locations.

[2] see Appendix A for details of the O-Grid type

- Constructing the grid mesh using a 4-point interpolation process throughout the domain.
- Verifying that the grids are correctly defined, that the ratio between any two adjacent cells is within an acceptable range, and that there is no overlap between adjacent sections of the mesh.

The resulting grid mesh is illustrated in Figure 2-9. Figure 2-10 shows an expanded view of the grids around the trailing edge of the aerofoil.

The grids were condensed in the critical regions, namely the viscous region and the area after the trailing edge while coarse grids were used in the free stream regions. The computational domain was divided overall into 150×26 cells. In order to check the dependency of the solution on the grid size two other cases were tested. In these cases the grids were doubled in the x-direction then in the y-direction and the results were compared with each other. The solutions were found to be virtually identical and therefore the simulation can be considered as grid independent. This is an important condition in validation of the numerical solution. (Roache, 1982), and (Versteeg and Malalasekera, 1995).

The cases for different angles of incidence were treated individually following the same procedures. Each case has its own particular characteristics regarding grid distribution and interpolation factors; but they all use the same mesh size and the same grid type (i.e. O-type).

The inlet boundary was prescribed by fixing the main stream velocity at an uniform value of 40m/s, and the turbulence intensity at 3%. The pressure reference points were prescribed as well. The relative pressures are calculated from the total pressures using the value at this reference point. These values were chosen to represent the measured values in the wind tunnel. A symmetry-boundary condition type was chosen for both the upper and the lower boundaries. The aerofoil chord Reynolds number (Re_c) was accordingly equal to 4×10^5.

Under-relaxation factors were again adopted to achieve more rapid convergence. The following values were used which made the solution converge after some 500 iterations, while the default values of the package needed some 900 iterations.

Parameter	First 50 Iterations	Rest of Iterations
Velocities	0.45	0.6
Pressure	0.45	0.55
κ	0.4	0.5
ε	0.3	0.4
Effective viscosity	0.4	0.45

The following output data were obtained from the solution of the flow over a smooth aerofoil:

- The velocity profiles at any point on the two surfaces of the aerofoil and in the wake region.
- The pressure distributions over the aerofoil .
- Contours of the flow parameters such as:
  - Stream function
  - u & v velocities
  - Pressure distribution
  - Turbulence intensity
- Integrated values such as:
  - X- and Y-shear stress
  - Reynolds stresses

Many of these parameters were stored in text files and processed by FORTRAN programs in order to calculate and/or plot the appropriate variables. As an example, the CFD simulation give the pressure values at the top and bottom surfaces of the aerofoil in points with different x-locations. Consequently, to calculate the pressure difference accurately it was necessary to interpolate between these values. The computer program which is used to perform this interpolation was written and is listed in Appendix B.

The lift coefficient, C_l, was calculated by interpolating the pressure difference over an aerofoil as follows (Houghton and Carruthers, 1982).

$$C_l = \frac{\int_0^c \Delta p dx}{\frac{1}{2}\rho U_\infty^2} \qquad (2\text{-}35)$$

Where Δp is the pressure difference between the two surfaces of the aerofoil.

The drag coefficient, C_d, can be calculated (per unit span) from the following equation, (Schlichting, 1979), :

$$C_D = \frac{\int_0^c \rho u(U_\infty - u)dy}{\frac{1}{2}\rho U_\infty^2 C} \qquad (2\text{-}36)$$

where u is the velocity in the wake far away from the trailing edge of the aerofoil (i.e. at a location where the local static pressure is equal to p_∞).

In practice (either in a wind tunnel or in real flight) it is inconvenient -or impossible- to arrange for measurement this far away from the aerofoil or wing section. (Jones, 1936), developed a method which allows measurements to be made relatively close behind the immersed body. In this method, C_d can be calculated as follows:

$$C_D = 2\int_{Wake} \sqrt{\frac{H_1 - p_1}{H_\infty - p_\infty}}\left(1 - \sqrt{\frac{H_1 - p_\infty}{H_\infty - p_\infty}}\right)d\left(\frac{y}{c}\right) \qquad (2\text{-}37)$$

where H_∞ and p_∞ are the total and static pressure, respectively, at the free stream flow and H_1 and p_1 are, respectively, the total and static pressure at a plane close downstream of the aerofoil. If a series of values of the quantity:

$$\sqrt{\frac{H_1 - p_1}{H_\infty - p_\infty}}\left(1 - \sqrt{\frac{H_1 - p_\infty}{H_\infty - p_\infty}}\right)$$

are plotted against the variable (y/c), a closed area will be obtained because the integral becomes zero at each edge of the wake. The magnitude of this area will be the value of this integral, so that the drag coefficient, C_d, is given directly by twice the area under the curve.

This method is still used effectively in aerodynamic research to assess the characteristics of both aerofoils and wings. Thus (McLean et al. 1987) used it to assess the effect of riblets on a real flight test.

2.5.3 Modelling of the Aerofoil with Grooves

The modelling process for the aerofoil with grooves went through the same procedures and techniques as these used for the smooth aerofoil.

The main difference is that the top surface is grooved and hence these grooves should be represented. Three cases were tested. In the first case the grooves were only positioned on the front half of the top surface, while in the second case the rear half was grooved. All the top surface was grooved in the third case. The grooves were of square shape with a side length T_g where:

$$T_g = \text{Width of the groove / Chord length of the aerofoil} = 0.009$$

This value was taken to be the same as in the experiments. It was possible to represent the geometry of the grooves accurately as in Figure 2-11.

Since the size of the grooves is very small, the ratio between the grid size and the groove size is high (i.e. of the order of unity) unless a very large number of grid points is chosen near the grooves. The use of such a high number of node points was beyond the capacity of the computer resources. As a result the grids were not distributed correctly inside and around the grooves. Consequently the computational domain did not completely represent the real physical domain. Figures 2-12 and 2-13 show the mapping of the grooved surface where the grooves were represented incompletely.

However, the calculation was undertaken with this nodal representation and the results are presented in (Maksoud and Al-Shihry, 1994) and (George, 1995). The results of this calculation can thus only provide a general guide to the characteristics of an aerofoil but are unlikely to yield accurate quantitative predictions of the "real" simulation. Fortunately, the experimental work undertaken with this technique did not suffer from this difficulty since it was possible to accurately construct the grooved surface. Thus the experiments provide appropriate data on the effect of introducing grooves into the top surface of the aerofoil.

2.5.4 Modelling of the Aerofoil with the Air Bearing Device

In general, modelling of the aerofoil fitted with the ABD is similar to modelling of the smooth aerofoil. However, introducing the ABD to the top surface of an aerofoil needs two additional main steps:

the ABD was chosen to be sufficient to represent the flow details inside the device. Figures 2-15 through 2-17 show the mesh of the aerofoil with the ABD. It is clear from this figure that the grids were condensed at the near wall region as well as at the other critical regions such as near the ABD, and around the trailing edge.

These steps were repeated for all the different geometries of the ABD and also repeated at each angle of incidence. The injection/suction flows were always introduced perpendicular to the inlet/outlet faces of the device. This involved specifying the co-ordinates of each modelled point of the ABD. Table (2-4) shows the different values of the injection/suction speeds at different angles. The use of a twin ABDs over an aerofoil was also simulated. Table (2-5) shows the values of different parameters used in this case.

The effect of changing the five main parameters of the ABD, namely L_s, S, H, h, and C_i was studied numerically and the values which were investigated are shown in Table (2-6).

The rest of the modelling procedures are the same as discussed in section (2.6.2), modelling of a smooth aerofoil.

Case	L_s/C	S/C	H/C
ft-01	0.7	0.05	0.04
ft-02	0.8	↓	↓
ft-03	0.9	↓	↓
ft-04	0.8	0.04	↓
ft-05	↓	0.03	↓
ft-06	↓	0.04	0.05
ft-07	↓	0.04	0.06

Table (2-1) Parameters for the case of flat plate problem. Cases were repeated for C_i=1, 1.5, 2.0, and 2.5.

x/C Chord	y/C Upper Surface	y/C Lower Surface
0	0	0
0.05	-0.05924	-0.05924
0.1	-0.07805	-0.07805
0.15	-0.08909	-0.08909
0.2	-0.09563	-0.09563
0.25	-0.09902	-0.09902
0.3	-0.10003	-0.10003
0.35	-0.09914	-0.09914
0.4	-0.09672	-0.09672
0.45	-0.09301	-0.09301
0.5	-0.08823	-0.08823
0.55	-0.08254	-0.08254
0.6	-0.07606	-0.07606
0.65	-0.06887	-0.06887
0.7	-0.06107	-0.06107
0.75	-0.05267	-0.05267
0.8	-0.04372	-0.04372
0.85	-0.03421	-0.03421
0.9	-0.02413	-0.02413
0.95	-0.01344	-0.01344
1	-0.0021	-0.0021

Table(2-2) Co-ordinate of NACA0012 aerofoil, (Thibert, 1979)

Curve	*No. of interpolation points*	*Relative distance*	*Weight factor*
Lower	2	0.0	3.0
Line1	2	0.0	7.0
Line2	2	1.0	7.0
Out	3	0.0	5.0

Table (2-3) Example of Interpolation Factor Used in Grid Mapping Process

Angle	U_i m/s	C_i U_i/U_∞	Point P_s		Point P_{slow}		u_{ix} m/s	u_{iy} m/s
			x, m	y, m	x, m	y,m		
Cases AB4-10, AB4-20, AB4-30								
4	40	1	0.087	0.011	0.086	0.006	39.135	8.2718
	60	1.5	↓	↓	↓	↓	58.703	12.407
	80	2	↓	↓	↓	↓	78.270	16.543
	100	2.5	↓	↓	↓	↓	97.838	20.679
Cases AB4-40,AB4-50, AB4-60								
4	40	1	0.062	0.015	0.061	0.01	39.79	4.0642
	60	1.5	↓	↓	↓	↓	59.689	6.096
	80	2	↓	↓	↓	↓	79.58	8.1284
	100	2.5	↓	↓	↓	↓	99.482	10.161
Cases AB8-10,AB8-20, AB8-30								
8	40	1	0.0876	0.005	0.087	0.0005	39.063	8.608
	60	1.5	↓	↓	↓	↓	58.594	12.912
	80	2	↓	↓	↓	↓	78.125	17.216
	100	2.5	↓	↓	↓	↓	97.657	21.520
Cases AB8-40,AB8-50, AB8-60								
8	40	1	0.063	0.010	0.062	0.005	39.414	6.824
	60	1.5	↓	↓	↓	↓	59.120	10.236
	80	2	↓	↓	↓	↓	78.827	13.648
	100	2.5	↓	↓	↓	↓	98.534	17.060

Table(2-4) Cases Studied in the CFD Simulation - Single ABD

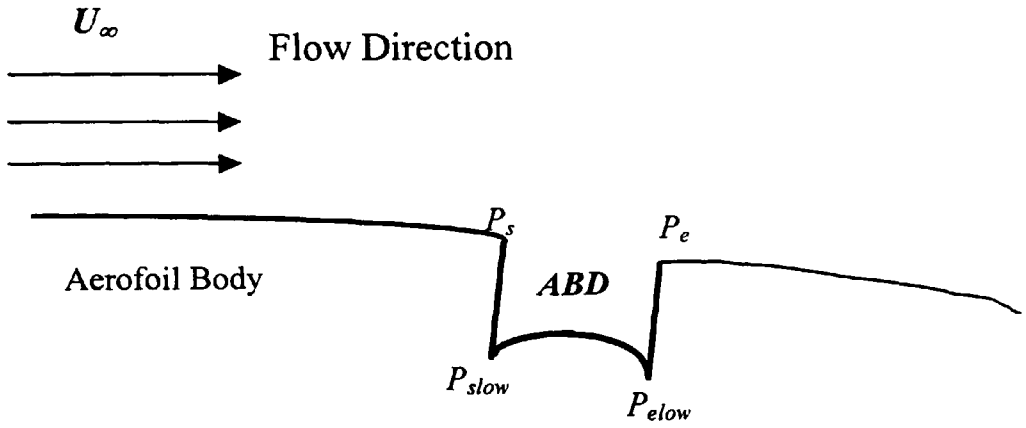

Angle	U_i m/s	C_i U_i/U_∞	*Point* P_s		*Point* P_{slow}		u_{ix} m/s	u_{iy} m/s
			x, m	y, m	x, m	y,m		
Cases AB12-10, AB12-20, AB12-30								
12	40	1	0.088	-0.0006	0.086	-0.005	38.378	11.275
	60	1.5	↓	↓	↓	↓	57.567	16.913
	80	2	↓	↓	↓	↓	76.756	22.550
	100	2.5	↓	↓	↓	↓	95.945	28.188
Cases AB12-40, AB12-50, AB12-60								
12	40	1	0.063	0.006	0.062	0.001	38.840	9.562
	60	1.5	↓	↓	↓	↓	58.260	14.344
	80	2	↓	↓	↓	↓	77.680	19.125
	100	2.5	↓	↓	↓	↓	97.100	23.906
Cases AB14-10, AB14-20, AB14-30								
14	40	1	0.08771	-0.0036	0.08613	-0.0083	37.9477	12.648
	60	1.5	↓	↓	↓	↓	56.9216	18.972
	80	2	↓	↓	↓	↓	75.8955	25.296
	100	2.5	↓	↓	↓	↓	94.8693	31.620
Cases AB14-40, AB14-50, AB14-60								
14	40	1	0.064	0.004	0.062	-0.0008	38.483	10.912
	60	1.5	↓	↓	↓	↓	57.724	16.368
	80	2	↓	↓	↓	↓	76.966	21.824
	100	2.5	↓	↓	↓	↓	96.207	27.280

Table(2-4) Cases Studied in the CFD Simulation - Single ABD (continued..)

Angle	U_i m/s	C_i U_i/U_∞	*Point* P_s		*Point* P_{slow}		u_{ix} m/s	u_{iy} m/s
			x, m	y, m	x, m	y,m		
Case TW12-10 Front								
4	40	1	0.037	0.012	0.036	0.007	38.769	9.849
	60	1.5	↓	↓	↓	↓	58.153	14.773
	80	2	↓	↓	↓	↓	77.537	19.697
	100	2.5	↓	↓	↓	↓	96.922	24.621
Cases TW12-30 Rear								
4	40	1	0.088	-0.001	0.086	-0.005	37.605	13.632
	60	1.5	↓	↓	↓	↓	56.408	20.449
	80	2	↓	↓	↓	↓	75.211	27.265
	100	2.5	↓	↓	↓	↓	94.013	34.081
Case TW14-10 Front								
8	40	1	0.038	0.011	0.036	0.006	38.402	11.193
	60	1.5	↓	↓	↓	↓	57.603	16.789
	80	2	↓	↓	↓	↓	76.804	22.386
	100	2.5	↓	↓	↓	↓	96.005	27.982
Cases TW14-30 Rear								
8	40	1	0.064	0.004	0.062	-0.001	38.483	10.912
	60	1.5					57.724	16.368
	80	2					76.966	21.824
	100	2.5					96.207	27.280

Table(2-5) Cases Studied in the CFD Simulation - Twin ABDs

Angle	U_i	C_i	*Point* P_s		*Point* P_{slow}		u_{ix}	u_{iy}
	m/s	U_i/U_∞	*x, m*	*y, m*	*x, m*	*y,m*	*m/s*	*m/s*
Cases TW16-30 Front								
12	40	1	0.038	0.009	0.036	0.005	37.990	12.521
	60	1.5	↓	↓	↓	↓	56.985	18.781
	80	2	↓	↓	↓	↓	75.980	25.041
	100	2.5	↓	↓	↓	↓	94.975	31.302
Cases TW16-30 Rear								
12	40	1	0.088	-0.007	0.086	-0.011	36.582	16.178
	60	1.5	↓	↓	↓	↓	54.874	24.267
	80	2	↓	↓	↓	↓	73.165	32.356
	100	2.5	↓	↓	↓	↓	91.456	40.445

Table (2-5) Cases Studied in the CFD Simulation - Twin ABDs (continued)

Geometry	File Name	U_∞	C_l	S (cm)	L_s(cm)	H(cm)	h(cm)
10	AB*-10	40	1	0.6	8.7	0.5	0
	AB*-13		1.5				
	AB*-15		2				
	AB*-16		2.5				
20	AB*-20		1	0.8			
	AB*-23		1.5				
	AB*-25		2				
	AB*-26		2.5				
30	AB*-30		1	1.0			
	AB*-33		1.5				
	AB*-35		2				
	AB*-36		2.5				
40	AB*-40		1	0.6	6.2		
	AB*-43		1.5				
	AB*-45		2				
	AB*-46		2.5				
50	AB*-50		1	0.8			
	AB*-53		1.5				
	AB*-55		2				
	AB*-56		2.5				
60	AB*-60		1	1.0			
	AB*-63		1.5				
	AB*-65		2				
	AB*-66		2.5				
80	AB*-80		1.5	0.6	8.7		0.1
81	AB*-81						0.2
82	AB*-82						0.3
83	AB*-83					0.4	0
84	AB*-84					0.3	0
85	AB*-85					0.2	0

Table(2-6) ABD Parameters for Different Modelled Cases

Repeated at angles 4°,8°,12°,14°,16°

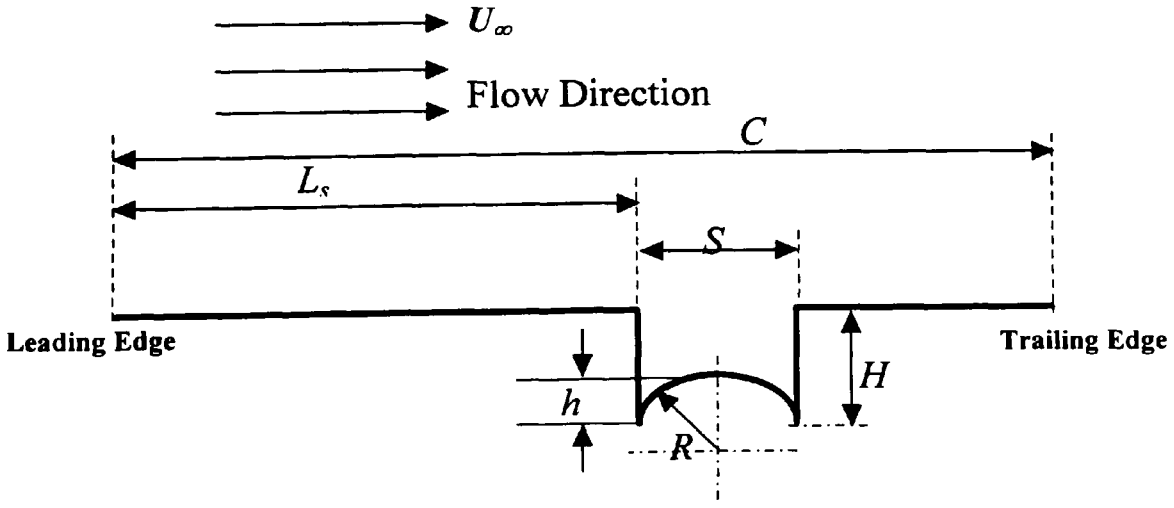

Figures

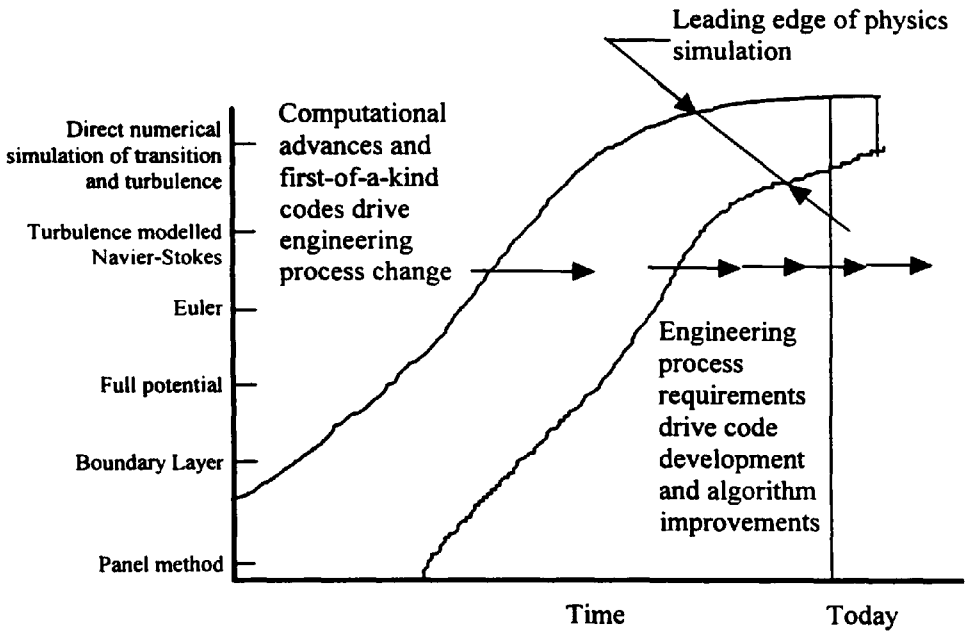

Figure 2-1 History of CFD, Crossing the Leading Edge

From (Rubbert, 1994)

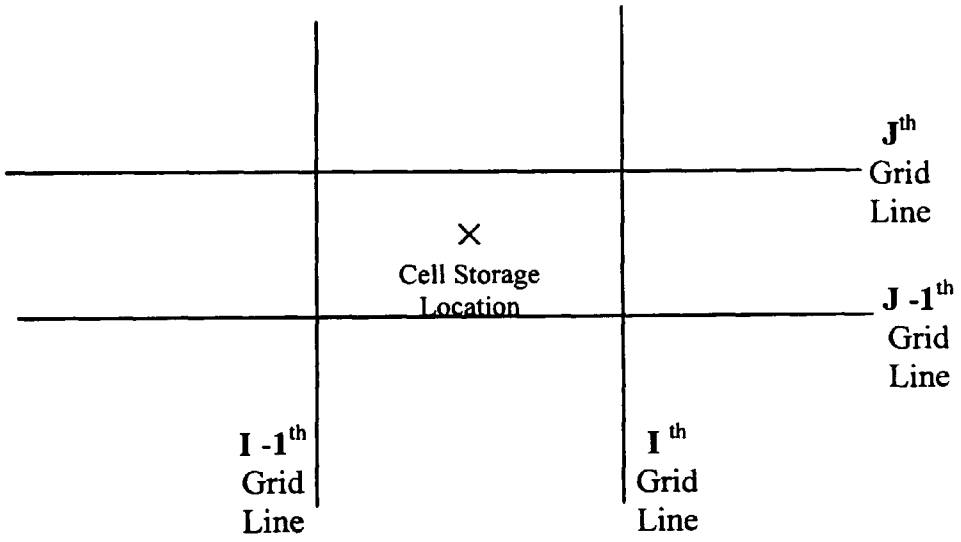

Figure 2-2 Control Volume Identification.

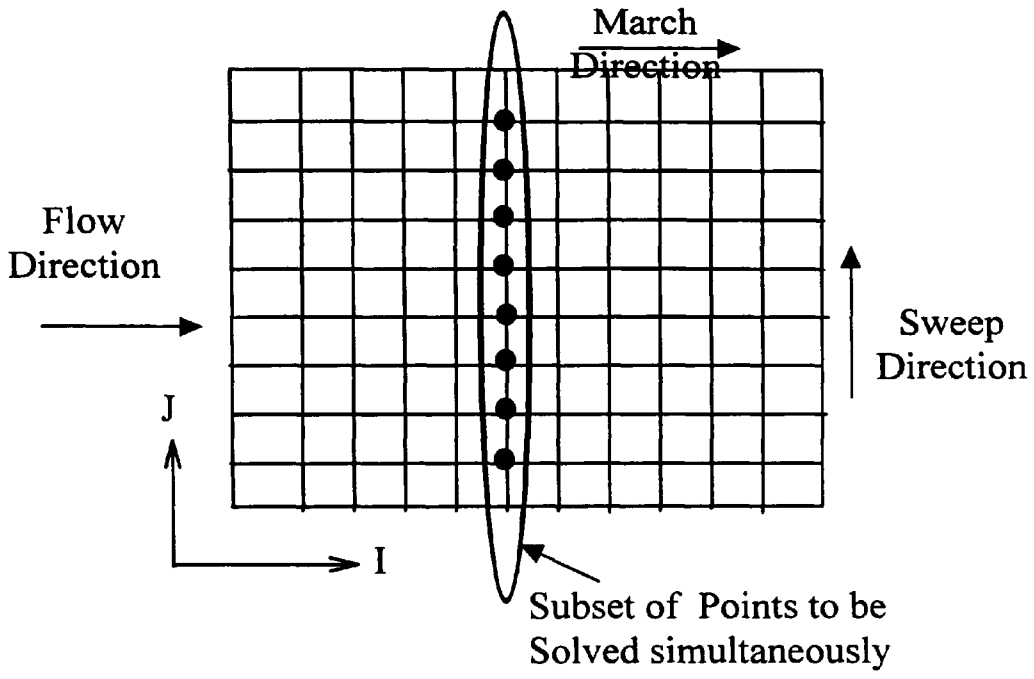

Figure 2-3 Sweeping and Marching Procedures

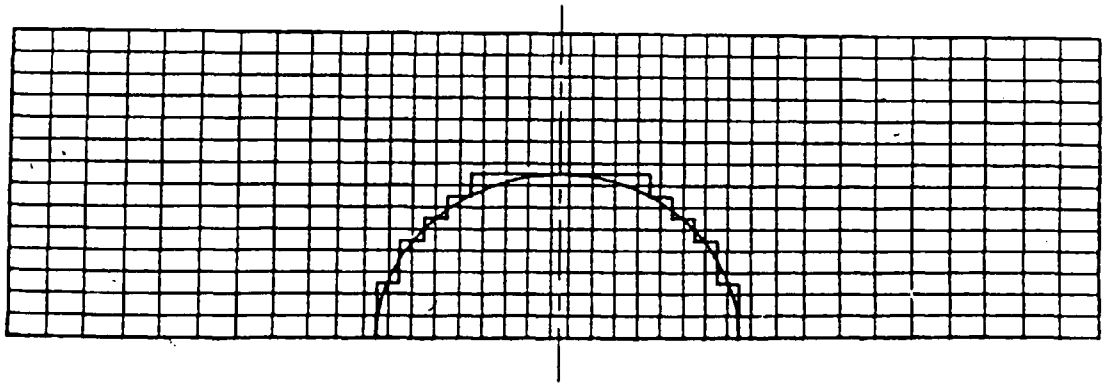

Figure 2-4a Grids in Cartesian Co-ordinate

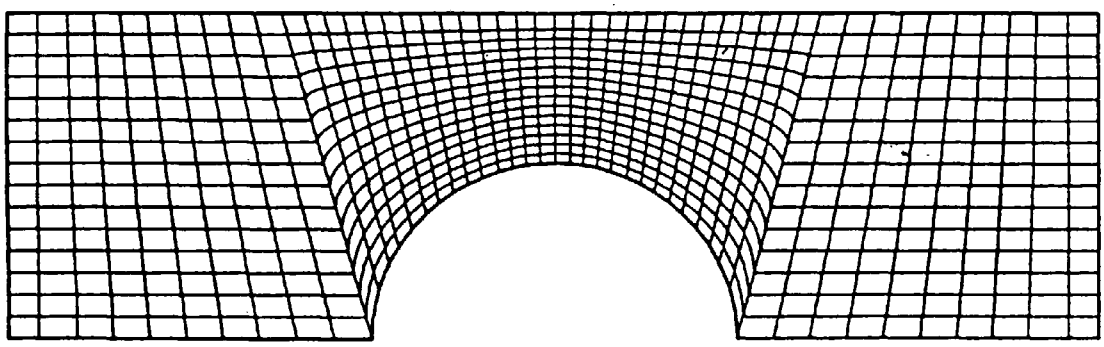

Figure 2-4b Grids in Body Fitted Co-ordinates (Continued...)

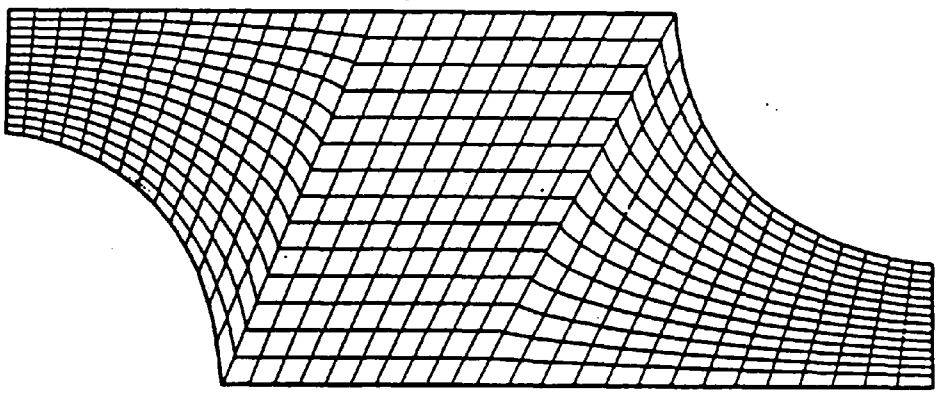

Figure 2-5 Flexibility of the Body Fitted Co-ordinates

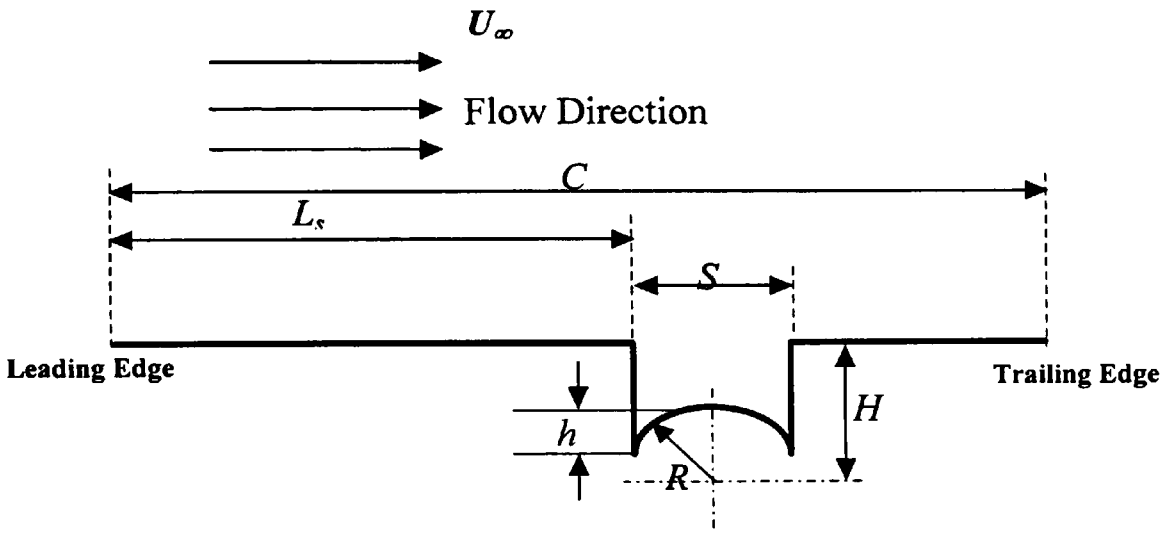

Figure 2-6 Geometry of the Flat Plate Problem

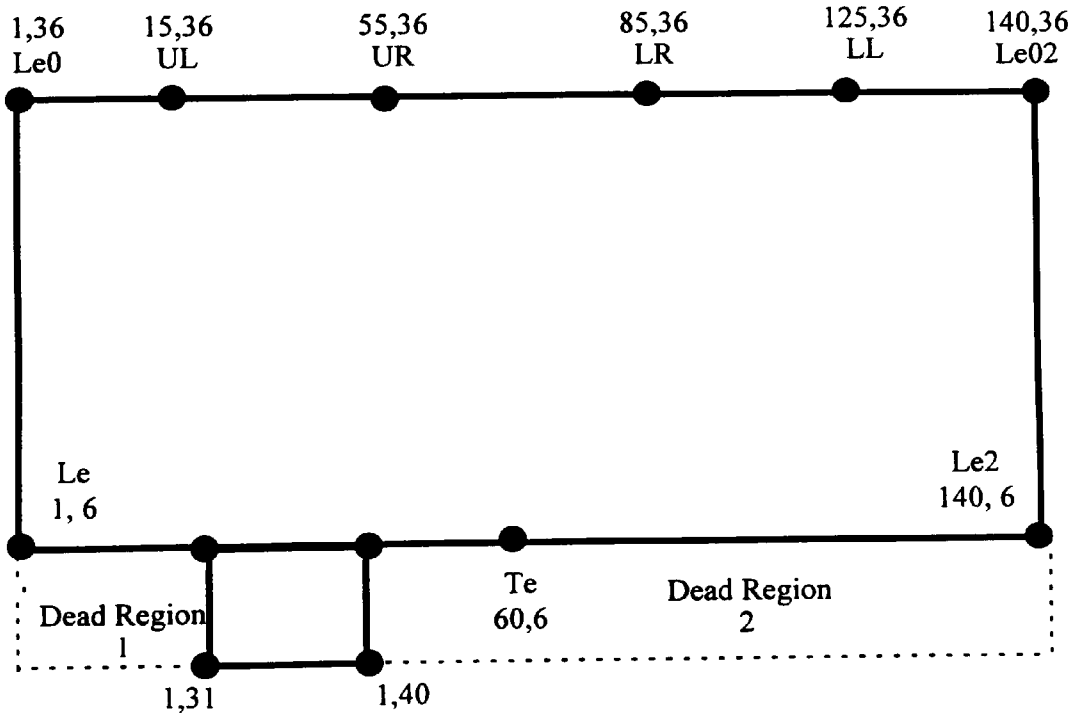

Figure 2-7 Computational Domain of the Aerofoil Problem

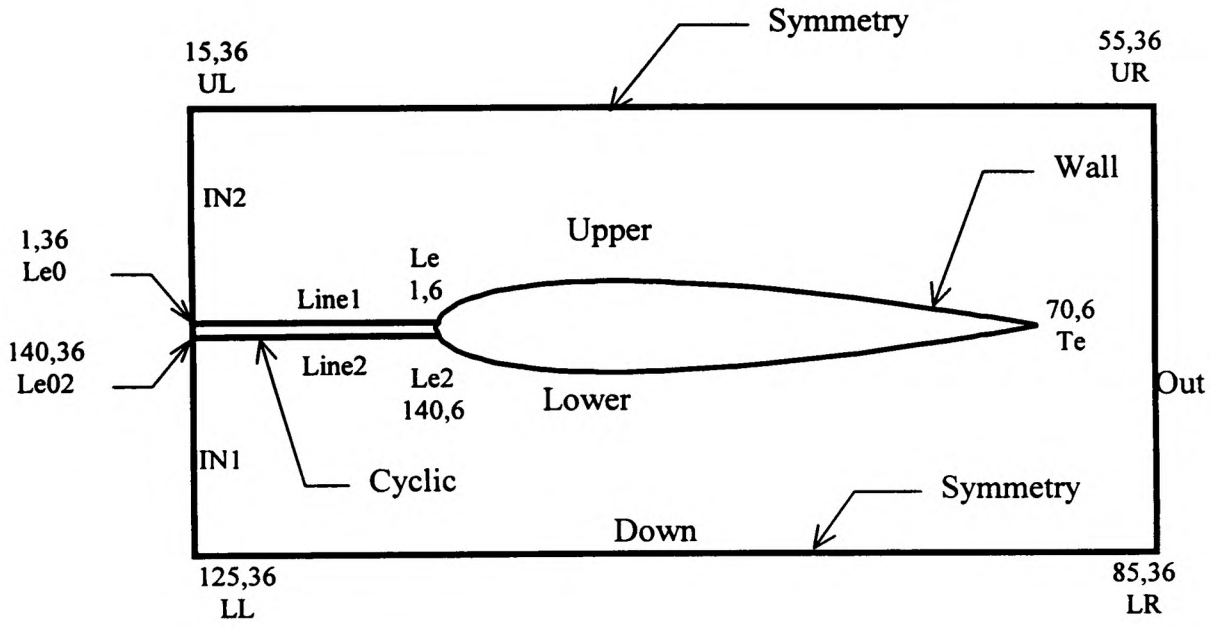

Figure 2-8 Physical Domain of the Aerofoil Problem

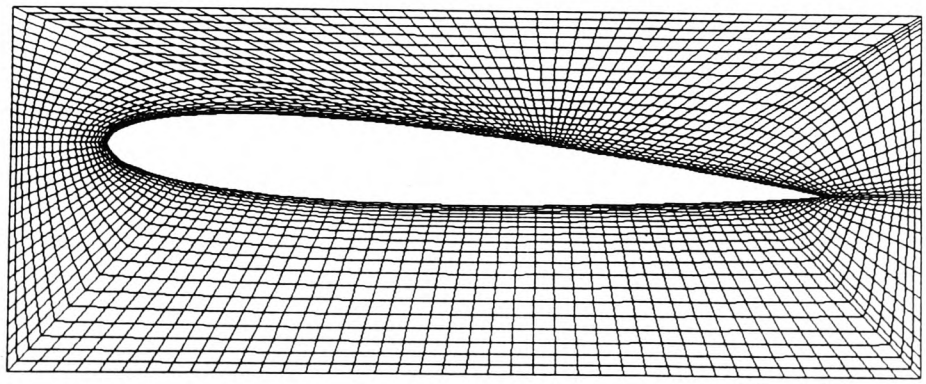

Figure 2-9 Grid distribution around an aerofoil

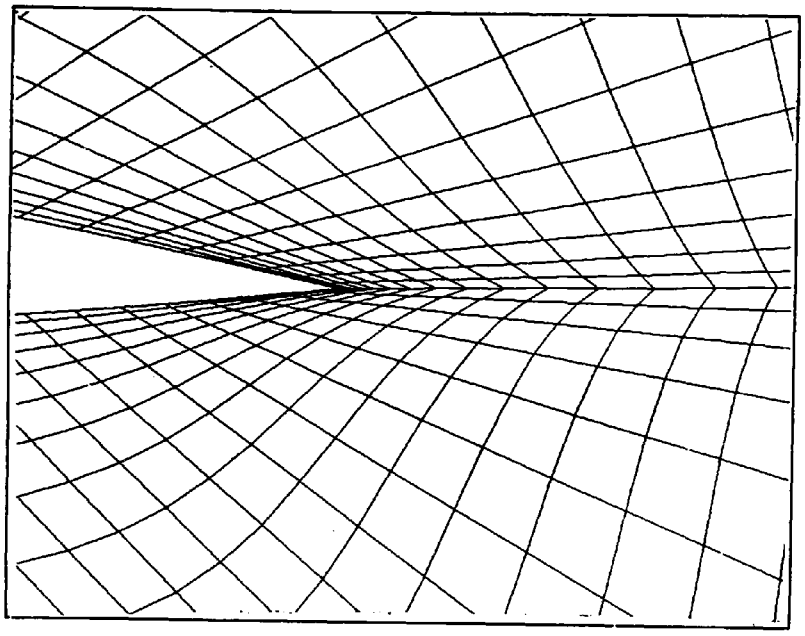

Figure 2-10 Expanded view of grids around trailing edge

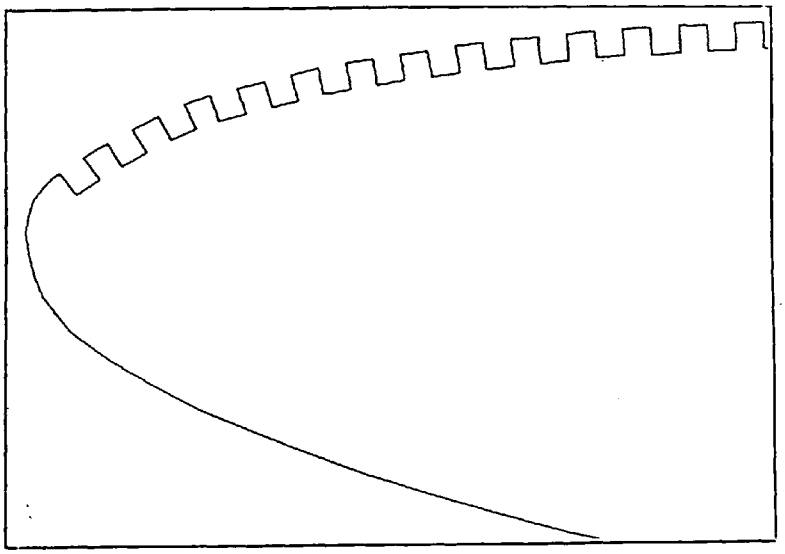

Figure 2-11 Geometry of grooves over an aerofoil

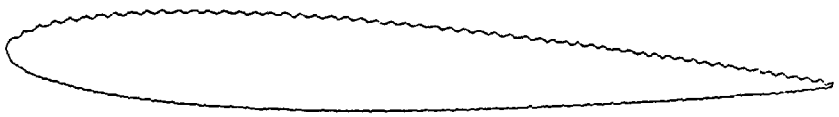

Figure 2-12 Grooves were incompletely represented

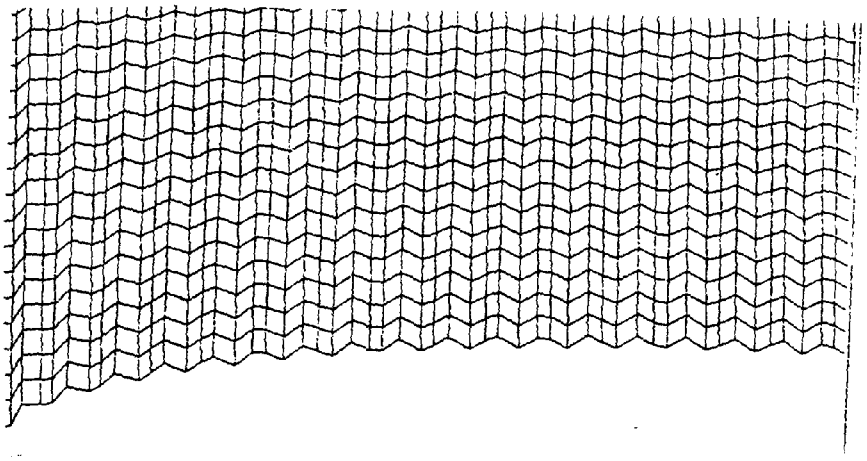

Figure 2-13 Grid distribution over the grooved aerofoil

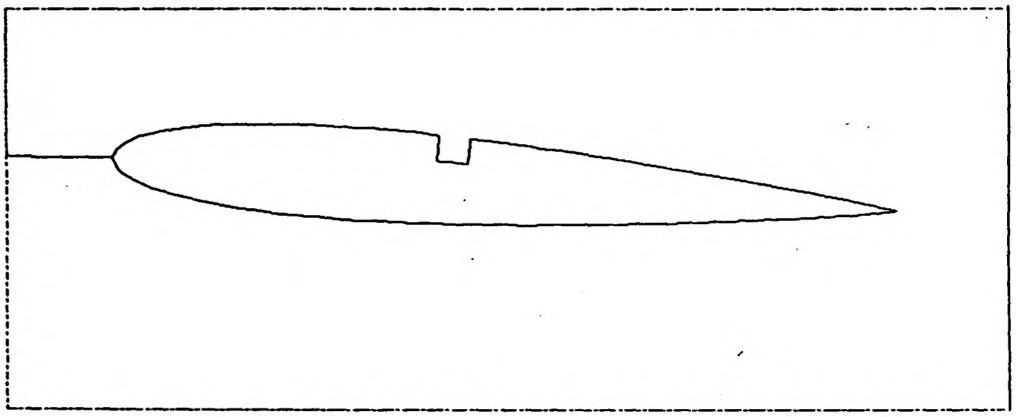

Figure 2-14 Geometry of an aerofoil with ABD

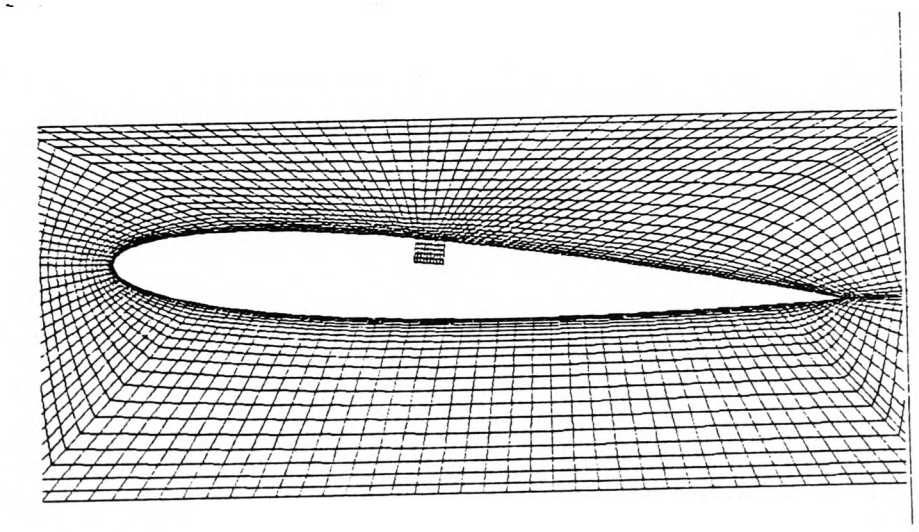

Figure 2-15 Grid distribution over an aerofoil with ABD

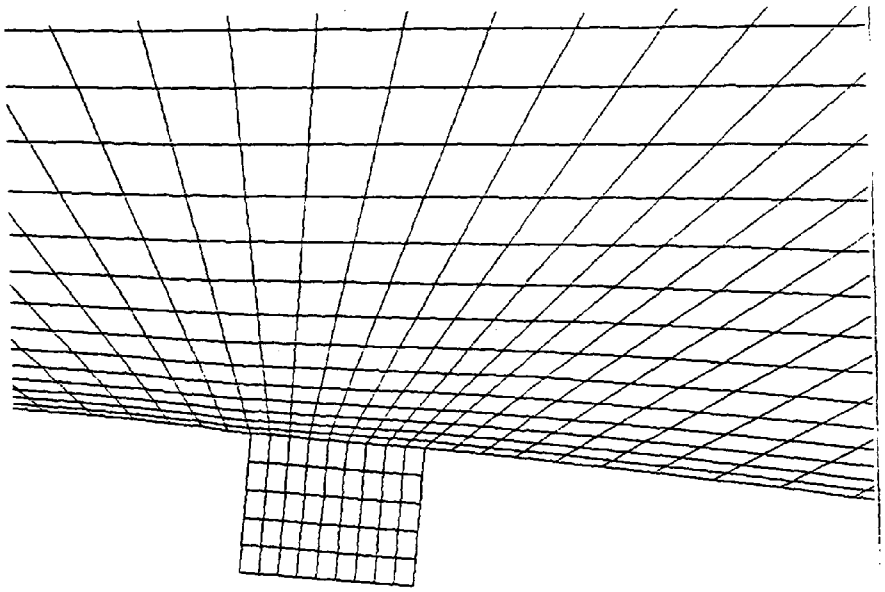

Figure 2-16 Expanded view of gird distribution inside the ABD

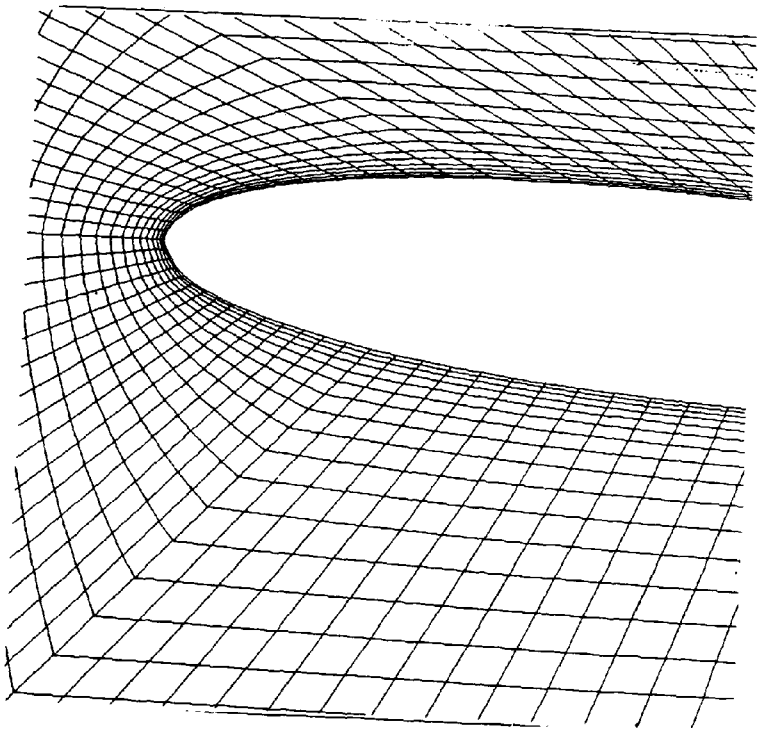

Figure 2-17 Expanded view of gird distribution around the trailing edge

Chapter Three

Experimental Techniques

3.1 Introduction
3.2 The Apparatus Used in the Present Study
3.3 The Present Experimental Technique

Chapter Three

Experimental Techniques

This chapter describes the laboratory facilities which were used in the present study. The specifications and limitations of the facilities as well as the modifications which were undertaken are all presented. The experimental phases of the project are also discussed as well as the main details of the experimental programme. Potential sources of error in the experimental results are finally described in the last section of this chapter.

3.1 Introduction

In aerodynamics research, wind tunnel testing is the major source of design data for new aircraft projects. Despite the progress which has been achieved in computers and CFD methods, experimental testing in wind tunnels remains the main tool to study the new designs. "In the late 1960's it became more and more obvious that although rapid progress was observed in computerised fluid dynamics experimental aerodynamics should not stop developing", (Bouis et al. 1994).

Experimental modelling of large aerodynamic devices can be undertaken through careful simulation of both the body and the fluid environment. Thus obtaining the large Reynolds numbers, and perhaps Mach numbers to simulate the cases of large aerodynamic devices (such as large transport aircraft) is always a challenging task.

Generally, there are two possible ways to improve the experimental simulation inside the wind tunnel. The first one is to enlarge the dimensions of the wind tunnel test section and to use larger wind tunnel models. This option is not cost-effective beyond certain limits due to limitations on power consumption and cost. The second possibility is to change the thermodynamic conditions. Pressurising the wind tunnel enhances linearly the Reynolds number. This approach is limited by considerations of model

strength. However, if the temperature is decreased at constant pressure the viscosity and the velocity of sound decreases and the density increases. The overall effect of cooling is that the Reynolds number increases rapidly whilst the model loads remain the same. Also the power required to drive the wind tunnel decreases. Therefore, the concept of a "cryogenic" temperature pressurised wind tunnel was introduced. In the early 1970s the cryogenic concept was extensively investigated. Among the largest wind tunnels in the world is the National Transonic Facility (NTF) which was built in 1975 in the USA and the European Transonic Wind Tunnel (ETW) which was completed at 1993. The aerodynamic circuit and some characteristics of the ETW are presented in Figure 3-1, (Bouis et al. 1994).

Recently, (Ewald et al. 1994) introduced the concept of a standard design of low speed wind tunnels of different sizes. The aim of this concept was to "provide universities, research facilities and industrial companies with the opportunity to acquire a wind tunnel with a proper quality at reduced cost".

The relative magnitude of the longitudinal and transverse fluctuations of velocity is a very important variable in wind-tunnel measurements; it determines the degree to which measurements performed on a model can be applied to the full scale structure as well as how measurements performed in different tunnels can be compared with each other. It is well known that transition from laminar to turbulent flow strongly depends on the magnitude of the oscillating velocity components, Figure 3-2. The whole development of the turbulent boundary layer and the location of the separation point as well as the rate of heat transfer depend on the intensity of turbulence in the free stream. The magnitude of the turbulence intensity in a given wind tunnel can be reduced substantially by putting screens, grids or honeycombs. This, of course, will lead to a pressure loss in the wind tunnel. It has been found that for a given pressure loss the reduction in turbulence intensity is greater when large numbers of screens of small resistance is chosen in preference to a single screen of large resistance; (Schlichting, 1979).

It is necessary to design wind tunnels with low turbulence intensity if model measurements are to be applicable to the design of full-scale aircraft. The model should be supported inside the tunnel so that the aerodynamic the forces exerted upon the model can be readily transmitted to the measuring systems.

Blockage of the test section, caused by the presence of the model inside the section, should be within an acceptable limits in order to give a correct simulation to the free-stream case. Minimising the effect of blockage of the test section can be accomplished either by the use small-scale models or by using a perforated- or slotted-wall test section. Interference from the test-section walls usually affects the results obtained from the experiments made in the wind tunnels. Some corrections to those results are normally used, see (Thibert, 1979).

The flow characteristics over a model are usually determined by undertaking one or more of the following measurements:

- Instantaneous velocities can be measured directly using either a constant temperature anemometer, (CTA), with single, cross, or triple hot wire(s) and film probes, see for example (Korner and Redeker, 1994), or Laser Doppler Anemometry, (LDA), which has also became an important tool for measuring velocities and the size of particles in the flow, see (Dantec, 1995). Alternatively, indirect measurement of the flow speed can be obtained through pressure measurements. In this latter method both mean and instantaneous values can be determined. Flow turbulence can then be inferred from the instantaneous velocities.
- The pressures over the surface of the model or in its wake can be measured using either liquid-filled manometers (with an accuracy up to 0.002mm of water), (Smith and Murphy, 1955) and (Ower and Pankhurst, 1965), or pressure transducers, (Neubert, 1963). Measuring the pressure over the surface of a model, using these very accurate micro-manometers, is one of the most reliable and accurate methods of measuring the flow mean-speeds and pressure distribution. Pressure transducers are usually categorised as high response instruments. This means that they can measure rapid fluctuations in pressure with frequencies up to 600KHz.
- The lift and drag forces exerted on the model can be measured directly through the reaction of supporting balance systems. A three-component balance is normally used for 2-D flows while the six-component balance is appropriate for 3-D flow models or half span models. These balances usually use strain gauges to measure the forces and can be connected through suitable acquisition devices to a computer system. The accuracy and reliability of balance systems as well as

details of the calibration, (especially if they are to be used over a large temperature range), has been extensively studied and greatly improved. Thus (Ewald, 1994) proposed an advanced force testing technology for cryogenic and conventional wind tunnels. (Dress, 1989) studied magnetic suspension in which the model is completely supported inside the test section using magnetic fields from the sides of the test section. The main benefit of this technique is that it avoids interference by the supports in the flow. This method is the only way to eliminate completely this interference. "Many other advantages will accrue, such as (1) elimination of model modifications to accommodate the string, (2) ease of model movement for dynamic testing, (3) fast, efficient testing at any attitude, and (4) improvement in productivity due to elimination of strings and struts.", (Dress, 1989).

Flow visualisation is a very useful method of determining the qualitative characteristics of the flow around the model inside the test section. Many methods of flow visualisation are in common use such as smoke injection, surface tracing methods, tufts, and the use of a Laser Sheet. Flow visualisation, either in wind tunnel or in real flight experiments, provides information about the location of separation and reattachment, the location of transition from the laminar to the turbulent state and the existence of cross or reverse flows.

3.2 The Apparatus Used in the Present Study

3.2.1 The Wind Tunnel

The experiments undertaken in the present project were conducted in the 300 ×300 mm test section of a PLINT TE54 low speed, open wind tunnel; Figure 3-3. The maximum air speed in this tunnel is 40 m/s and the velocity profile is essentially uniform, see Figure 3-4. The turbulence intensity of the flow inside the wind tunnel was measured using hot wire anemometry and is shown in Figures 3-5 and 3-6. The value of this parameter is approximately 4% and this is a high level for this type of work. This high value results because there is no means of reducing the turbulence intensity by screens or honeycomb meshes. Control of the air speed is performed through a choking device downstream of the working section.

It is thought, however, that the tests performed in the present study at relatively low Reynolds numbers is applicable for flows at high Reynolds numbers provided that the

incompressibility assumptions are still valid. The most important parameter which will be increased in incompressible flows of high Reynolds number is the turbulence intensity and since the value used in the present experiments is relatively high, the results obtained are most likely applicable in high-Reynolds-number flows. On the other hand, the proposed technique may be used in many applications where the Reynolds number is relatively small. This will be discussed in Chapter 6.

A purpose designed test section was constructed from transparent perspex for the purpose of the present study. In this test section, one of the side walls contained a sliding holder which holds a hot wire probe or pitot tube. By sliding this holder vertically, the probe or pitot tube can be moved into any location along a vertical line in the flow. By moving the position of the slider mechanism parallel to the direction of the flow in the side wall of the section holder (i.e. replacing it at another section), the hot wire or pitot sensors can be located at any desired location in the test section. The slider holder was manufactured with a high accuracy so as to provide a flat and smooth side wall. Checks were carried out to ensure that the vertical movement of the holder does not affect the flatness of the wall.

A purpose made traversing mechanism was designed to move the slider vertically. This traversing mechanism can be moved horizontally parallel to the flow. The accuracy of the vertical movement was estimated to be 0.1 mm and this precise movement is important when acquiring data in the critical regions of the flow where high velocity gradients exist. This traversing system was controlled by a computer program which was specifically written for this purpose. This program is capable of performing the following tasks:

- Moving the traversing system through a user-defined range and step-length and acquiring the instantaneous velocities of the flow from cross hot wires at every step.
- Calculating the relevant flow-variables such as T_∞, RMS velocities, ...etc.
- Creating output text-files for further usage.

This program is listed in Appendix C. The model aerofoil was supported by a three component balance system located on the other side of the wind tunnel, see Figure 3-7. This balance was upgraded to measure the fore and aft lift and drag forces.

Special load cells were used to perform the measurements. The total lift force on the aerofoil was calculated from the sum of the fore and aft lift forces.

The model aerofoils were manufactured from resin material and were cast in a specially-made die. The cast models have an identical geometry so that comparison between different models was possible. The aerofoil section used in this study was the symmetrical NACA0012, with a 150 mm chord length and 18 mm maximum thickness located at 30% chord. The small dimensions of the aerofoil model presented a significant challenge when the geometry was modified to incorporate grooves or the ABD. This is one of the important limitations of the present facilities. Despite these difficulties careful design and construction ensured that the proposed geometry modifications were successfully carried out.

The model to wall clearances at either end of the model were kept to a minimum (less than 2 mm) so as to avoid leakage paths around the aerofoil. A flexible silicon sealant was attached to both ends of the model to fill the clearances. Checks were carried out to ensure that the sealant did not obstruct the motion of the aerofoil within the working section so that the lift and drag forces were correctly transferred to the balance system.

Small tufts were put over the surface of the aerofoil to check visually that no cross-flow resulted from the small clearance and/or the presence of the sealant. The two-dimensionality of the flow was verified before every test.

The experimental measurements were undertaken using four techniques as discussed in the following sections. Combining these methods is thought to provide sufficient information about the flow but other important techniques such as Laser Doppler Anemometry (LDA) and Laser flow visualisation could be used for further study.

3.2.2 Hot Wire Anemometry

Velocities and turbulence parameters were measured at various locations around the aerofoil model using a X-hot wire probe with data acquisition through a Dantec-56C01 CTA multi-channel system. The X-probe was fixed to face the flow with angles α_A=45°, and α_B=135°, see Figure 3-8.The velocity components and turbulence intensity were calculated from the instantaneous readings from the following equations, according to (Klatt, 1969):

Mean Velocities:

$$\frac{\bar{u}}{\bar{u}_\infty} \approx \frac{1}{2}\left\{\left[\frac{\bar{E}_A^{\,2}-\bar{E}_{0A}^{\,2}}{\bar{E}_{A\infty}^{\,2}-\bar{E}_{0A}^{\,2}}\right]^{\frac{1}{n_A}}+\left[\frac{\bar{E}_B^{\,2}-\bar{E}_{0B}^{\,2}}{\bar{E}_{B\infty}^{\,2}-\bar{E}_{0B}^{\,2}}\right]^{\frac{1}{n_B}}\right\}+\frac{\sin(\alpha_A+\alpha_B)}{2}\left\{\left[\frac{\bar{E}_A^{\,2}-\bar{E}_{0A}^{\,2}}{\bar{E}_{A\infty}^{\,2}-\bar{E}_{0A}^{\,2}}\right]^{\frac{1}{n_A}}-\left[\frac{\bar{E}_B^{\,2}-\bar{E}_{0B}^{\,2}}{\bar{E}_{B\infty}^{\,2}-\bar{E}_{0B}^{\,2}}\right]^{\frac{1}{n_B}}\right\}$$

(3-1)

$$\frac{\bar{v}}{\bar{u}_\infty} \approx \frac{1+\cos(\alpha_A-\alpha_B)}{2}\left\{\left[\frac{\bar{E}_A^{\,2}-\bar{E}_{0A}^{\,2}}{\bar{E}_{A\infty}^{\,2}-\bar{E}_{0A}^{\,2}}\right]^{\frac{1}{n_A}}+\left[\frac{\bar{E}_B^{\,2}-\bar{E}_{0B}^{\,2}}{\bar{E}_{B\infty}^{\,2}-\bar{E}_{0B}^{\,2}}\right]^{\frac{1}{n_B}}\right\}$$

(3-2)

Turbulence Intensity

$$T_{u\infty}=\left\{H_A^{\,2}\overline{e_A'^{\,2}}+H_AH_B\frac{K^2_{AB}-1}{K^2_{AB}+1}(\overline{e_A'^{\,2}}+\overline{e_B'^{\,2}})+H_B^{\,2}\overline{e_B'^{\,2}}+2\sin(\alpha_A+\alpha_B)(H_A^{\,2}\overline{e_A'^{\,2}}-H_B^{\,2}\overline{e_B'^{\,2}})\right\}^{\frac{1}{2}}$$

(3-3)

$$T_{v\infty}=(1+\cos(\alpha_A-\alpha_B)\left\{H_A^{\,2}\overline{e_A'^{\,2}}-H_AH_B\frac{K^2_{AB}-1}{K^2_{AB}+1}(\overline{e_A'^{\,2}}+\overline{e_B'^{\,2}})+H_B^{\,2}\overline{e_B'^{\,2}}\right\}^{\frac{1}{2}} \quad (3\text{-}4)$$

Shear Stress

$$\frac{\overline{u'v'}}{\bar{u}_\infty^{\,2}}=(1+\cos(\alpha_A-\alpha_B)\left\{H_A^{\,2}\overline{e_A'^{\,2}}-H_B^{\,2}\overline{e_B'^{\,2}}\right\}+\sin(\alpha_A+\alpha_B)T^2_{v\infty} \quad (3\text{-}5)$$

Where

$$K_{AB}=\sqrt{\frac{\overline{(e_A'+e_B')^2}}{(e_A'-e_B')^2}}, \qquad H_A=\frac{\bar{E}_A}{n_A(E_A^{\,2}-\bar{E}_{0A}^{\,2})}\left\{\left[\frac{\bar{E}_A^{\,2}-\bar{E}_{0A}^{\,2}}{\bar{E}_{A\infty}^{\,2}-\bar{E}_{0A}^{\,2}}\right]^{\frac{1}{n_A}}\right\}, \quad \text{and}$$

$$H_B=\frac{\bar{E}_B}{n_B(E_B^{\,2}-\bar{E}_{0B}^{\,2})}\left\{\left[\frac{\bar{E}_B^{\,2}-\bar{E}_{0B}^{\,2}}{\bar{E}_{B\infty}^{\,2}-\bar{E}_{0B}^{\,2}}\right]^{\frac{1}{n_B}}\right\}$$

The readings were taken at frequencies up to 40 kHz. The hot wire measurements were recorded in the wake of the aerofoil to describe the wake flow and the wake decay re-

gion. They were also used to describe the flow upstream and in locations over the top surface of the model aerofoil.

Prediction of drag from the wake velocity profile was made using the Jones method, see equation (2-39), in the last chapter. In this method it is possible to use the values of the wake velocity at a position close to the trailing edge of an aerofoil. This method is extensively used in both wind tunnels and real flight experiments. The wake velocity profile can also be used to estimate the lift force as suggested by (Zaman et al. 1993). This method was not used in the present study because lift and drag forces were obtained more accurately by direct measurement or from pressure measurements. It should be clear, however, that the accurate measurement of the wake velocities is important especially for comparison with CFD data.

3.2.3 Direct Measurements of Lift and Drag Using the Balance System

Direct measurement of the aerodynamic forces using a balance system is usually used to assess the two-dimensional character of the flow and consequently verify that the two-dimensional formulation of the problem is correct and valid. Another benefit of using the direct measurement is that it provides net values of the measured drag and the lift forces. This feature can be useful in assessing the accuracy of indirect methods of calculation (e.g. calculating the drag from the velocity profile in the wake of the model.)

In some applications direct measurement is the only reliable technique especially when the changes in the flow variables are small so that measurements cannot be undertaken accurately. The use of riblets, (Walsh, 1990), and air injection as a drag reduction technique are examples where this occurs; (Henfer and Bushnell, 1990).

The balance system used in the present study measures three-components of force. The aerofoil model was mounted with its span wise axis perpendicular to the supporting platform. The three forces were measured directly by load cells and the readings were recorded by means of a purpose designed computer program. To facilitate the supply piping for the ABD and for the pressure-distribution tappings the free end of the aerofoil was fitted with a circular disc as shown in Figure 3-9. The disc can be rotated inside a rectangular slider. The height of this slider was made longer than the height of the test section and the system can slide vertically to compensate for the eccentricity of the rotating disc and to ensure that the aerofoil is free to move due to the effect of lift and drag

forces. The pipes connected to the aerofoil were made from very soft, light and flexible material, and attached to the slider in such away that the aerofoil loading was virtually unaffected.

To avoid interference from vibrations transmitted from the fan and the frame of the wind tunnel on the readings, the frequencies of those vibrations were measured and then isolated using a filter designed for this purpose. Figure 3-10 shows the readings before and after filtering the vibrations. The drag forces measured from integrating the values of the wake velocity behind an aerofoil is reasonably agreed with the values obtained from the direct measurements.

3.2.4 Pressure Distribution

Traditionally, measurements of the pressure distribution over the surface are frequently used to determine the performance of an aerofoil. Lift, drag and pitching moment coefficient can be directly, and accurately, estimated from the pressure distribution over an aerofoil. However, some properties of the flow such as the turbulence level and the characteristics of the boundary layer over the aerofoil surface cannot be determined directly from the pressure distribution. Thus in order to have a complete picture of the flow field, more than one method of measurement should be used.

The design and installation of the pressure tappings and the connecting tubes inside the aerofoil was difficult due to the small size of the model. Another difficulty was that the air bearing device occupied part of the aerofoil top and bottom surfaces[1]; and consequently tappings in this area were lost. Fortunately, the significant changes in the pressure distribution were located far from the ABD, i.e. they occurred near to the leading edge, so that the difficulty in measuring pressure over the area occupied by the ABD is unlikely to result in significant errors in measuring the overall pressure distribution over the aerofoil. Any errors were reduced by measuring the pressure as close as possible to the ABD device. Similar arrangements were used by (Modi et al. 1994) where they faced problems near the leading edge area. Figure 3-11 shows the 14 tappings distributed over the surface which were used to yield detailed information about the surface loading. Connecting pipes for pressure tappings were removed out through the interior

[1] This difficulty is only present in this study due to the small dimensions of the aerofoil. If the ABD was fitted to larger aerofoil section (or a real wing of an aircraft), no such problems would arise. The ABD in a real situation will occupy only a very small volume of the wing.

of the aerofoil. It is worth mentioning that the lift force measured from integrating the pressure values over the aerofoil was compared with the values obtained from the direct measurements and found to be in good agreement.

3.2.5 Flow Visualisation

Flow visualisation provides qualitative information of the flow around a model. Two methods were used in the present study to visualise the flow. Tufts, which were distributed over the top surface of the aerofoil model were found to be useful to obtain information regarding separation and the occurrence of cross flow.

The second method was to use smoke injection around the model to illustrate the flow patterns with the ABD fitted to the aerofoil. Typical patterns from these visualisation methods are shown in Figures 3-12 and 3-13, (Nakayama, 1988). The flow patterns from this visualisation were recorded on video for further analysis.

3.3 The Present Experimental Technique

3.3.1 Casting of the Aerofoil Model

Figure 3-14 shows the die which was used in casting the aerofoil models. The carefully chosen resin material used in casting was rigid and easily machinable. Casting also had the advantage of relatively simple installation of the ABD and it was easy to machine the grooves. Additionally, a cast model is cheaper and requires less production time.

Transverse grooves were machined over the top surface of the aerofoil in four arrangements:

- front half grooves,
- rear half grooves,
- full-surface grooves,
- full-surface grooves with suction holes over the front-half, see Figure 3-15.

Ideally, the suction holes should be located in the backward face of each groove; see Figure 3-15 since this arrangement was thought to enhance the circulation inside the groove as well as providing the benefits of a suction technique. Since it was difficult to machine the suction holes in the backward side of the grooves, the holes were installed

in the bottom of these grooves. Consequently, this led to lower enhancement of the circulation. Piping for the suction holes was also inserted during the casting process.

3.3.2 The Air Bearing Device ABD

Due to its relatively complex geometry, it was difficult to machine the ABD directly in the top surface of the aerofoil. Consequently, the device comprising the suction and injection chambers and an appropriate connection was machined separately from aluminium and mounted in the aerofoil as shown in Figures 3-16 and 3-18.

The design of the ABD should meet the following objective. It is vital that the injected and suction air flows should be uniform over the span of the aerofoil. This is necessary to produce a homogenous air roller-bearing action. The pressure difference between the two sides of the chamber was found to increase with an increase in the injection speed. At high injection speeds a negative pressure was experienced at both the inlet and suction sides of the chamber.

Achieving an uniform flow represented a major challenge in the design of the ABD. The problems were addressed by a numerical simulation of the ABD using Fluent to determine the proper design and shape of the injection and suction chambers. Several practical models for these chambers were simulated and tested. Initially, a telescopic-pipe with holes distributed along the length, see Figure 3-19, was tried and while a relatively good distribution of air was obtained a local increase in velocity was observed near the points at which the diameter changed. The next modification involved a slotted telescopic pipe which provided an improved distribution. Unfortunately, the uniformity of the flow from the slotted telescopic pipe was highly sensitive to the change in thickness of the slot. Any small change in slot thickness, e.g. during the casting process, leads to non-uniform distribution. Consequently, the final modification involved a tapered-cross section inlet chamber with a large number of holes, see Figure 3-20, and this was found to be the best among all the alternatives tested. During this procedure a hot wire traverse was employed to check the uniformity of the flow.

After casting, the model fitted with the ABD was tested to verify that:

- The injection flow rate equals the suction flow rate,

- There is a uniform distribution of the flow inside the ABD throughout the span wise direction,
- The injected flow is not entrained into the main flow.

These tests were conducted using hot wire measurements of the velocity around the ABD and using tufts over the top surface of the aerofoil. A photograph of the assembled aerofoil with the ABD Model-2 is shown in Figure 3-21.

It is worth mentioning that operating the ABD with no main-stream flow creates little movement of the air over the top surface.

A D-32, blower/vacuum fan with a capacity of 730 litres/min supplied by Utile Engineering Co. Ltd. was used to provide the suction and injection flows. The piping system is illustrated in Figure 3-22, where the injected/sucked flows were controlled via gate valves and flow meters with a range of 0~100 litres/sec.

3.3.3 Experimental Programme

The experimental programme involved the following phases:

1. Calibration of the hot wire probes, Constant Temperature Anemometry (CTA), and load cells. The calibration of the wire probes was repeated every time the probes were changed.
2. Testing the smooth-aerofoil case to compare it with published data for the characteristics of a NACA0012 aerofoil section. These data were used as a reference for the rest of the experiments.
3. Testing the five cases of the grooved aerofoil with variable amounts of suction.
4. Testing the aerofoil with the ABD fitted on its top surface. The two cases tested are illustrated in Figures 3-16, 3-17 and 3-18.

Each experiment involved in the following measurements:

1. Lift and drag forces using the three component balance.
2. Velocities throughout the wake region using hot wire Anemometry and pitot tube traverses.
3. Pressure distributions over the aerofoil.
4. Flow visualisation using tufts over the top surface of the aerofoil.

These experiments were undertaken over a range of angles of incidence from -2° to 14° at 2° intervals. The free stream speed of the wind tunnel was 30 m/s. All data were stored in computer files where further manipulation was carried out using appropriate programs.

3.3.4 Sources of Error

The experimental programme undertaken in this study was designed to provide adequate and reliable information. Despite the fact that every effort was made to achieve accurate results, and the results obtained compared well with published data, there are sources which can affect the accuracy of the measurements. The main sources, and the steps which were taken to minimise the effects are as follows:

- The vibration of the wind tunnel frame can affect the readings of the force balance and the hot wire probe holder. Whilst performing these tests in a vibration-free test section can minimise this source of inaccuracy, this was not possible. Consequently, the effect of vibrations was minimised in this study by measuring the frequencies and filtering them as discussed in section (3.2.3)
- Friction between the model and its supports can affect the transfer of the forces exerted on the aerofoil to the load cells. Alternative arrangements for supporting the model can reduce this source of error. Different support arrangements are described in the published literature. Thus performing the tests on 3-D or half-span models can produce friction-free results. However, in the present tests care was taken as described earlier to minimise frictional effects by providing suitable clearances. Moreover, the effect of friction was also minimised since it exists for both the smooth construction and the aerofoils with the ABD so that the effect should be substantially "cancelled out" when the results of the two cases are compared.
- The distribution of the injected and sucked air inside the ABD is important to create homogenous momentum enhancement to the main free stream flow across the span wise direction. Using an accurately-machined slot instead of large number of holes should improve the distribution. This will require more specialised manufacturing facilities than were available for the present work. These should be readily available on an industrial scale, however.

- Performing the tests in a less disturbed main flow (i.e. in a low turbulence wind tunnel) would reduce the effects of high turbulence levels such as vibration and instability in the flow. In addition, using a perforated- or slotted-wall test section would reduce the effect of blockage of the wind tunnel test section especially at higher angles of attack. Again due to the largely comparative nature of the present study the effects are not likely to be serious.

Overall, despite these potential sources of error, the results obtained from the experimental programme should be adequate in studying the benefits of using the ABD as a flow-control technique.

Figures

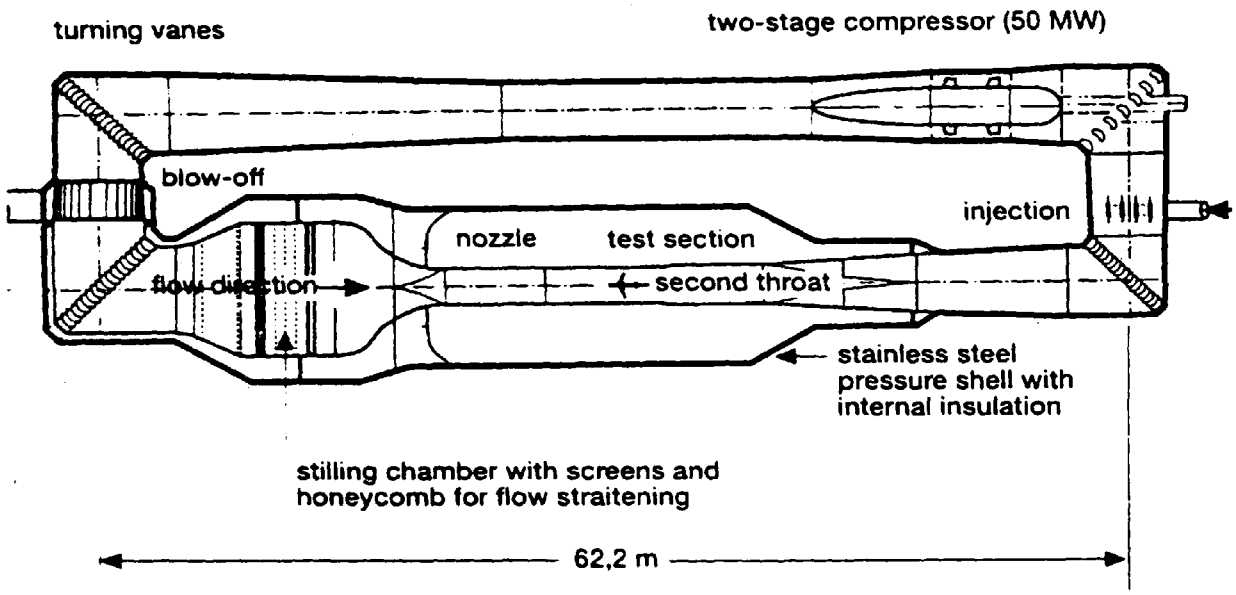

Figure 3-1 ETW Circuit and Characteristics

(Bouis et al. 1994)

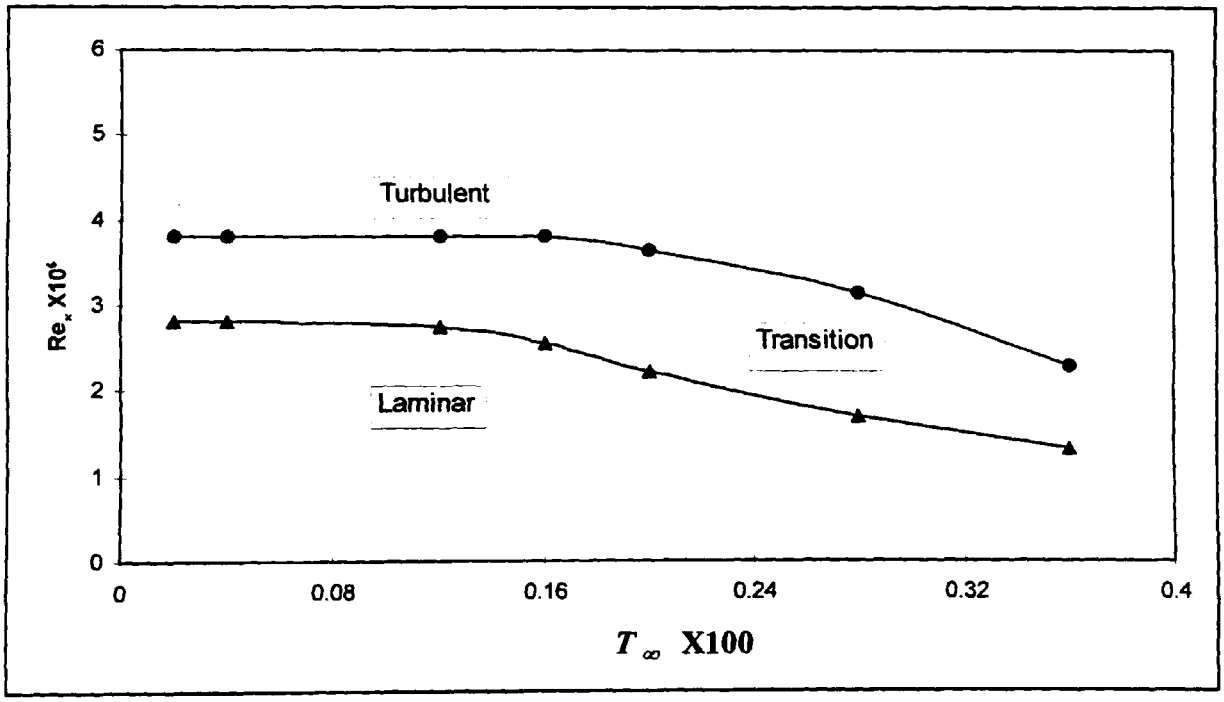

Figure 3-2 Influence of Turbulence Intensity on Critical Reynolds Number on a Flat Plate at Zero Incidence, (Schlichting, 1979).

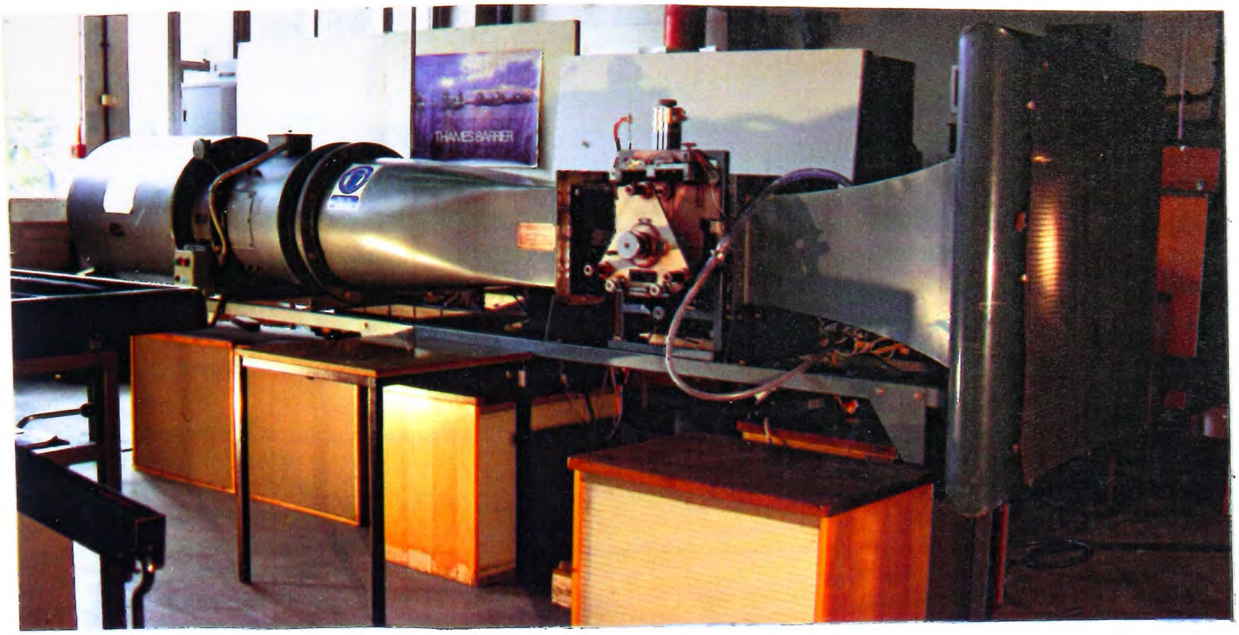

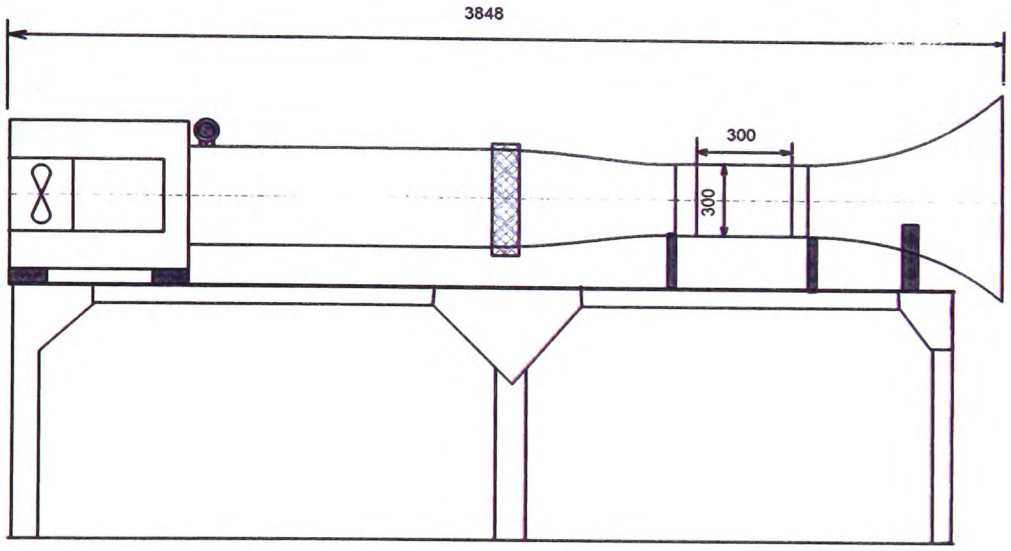

Figure 3-3 PLINT-TE54 Low Speed Wind Tunnel

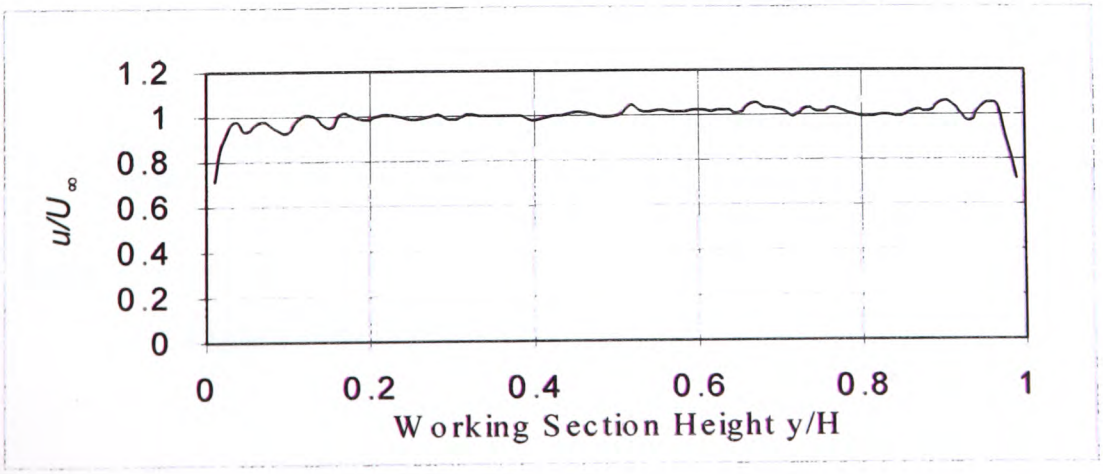

Figure 3-4 Velocity Profile Along the Height of the Test Section

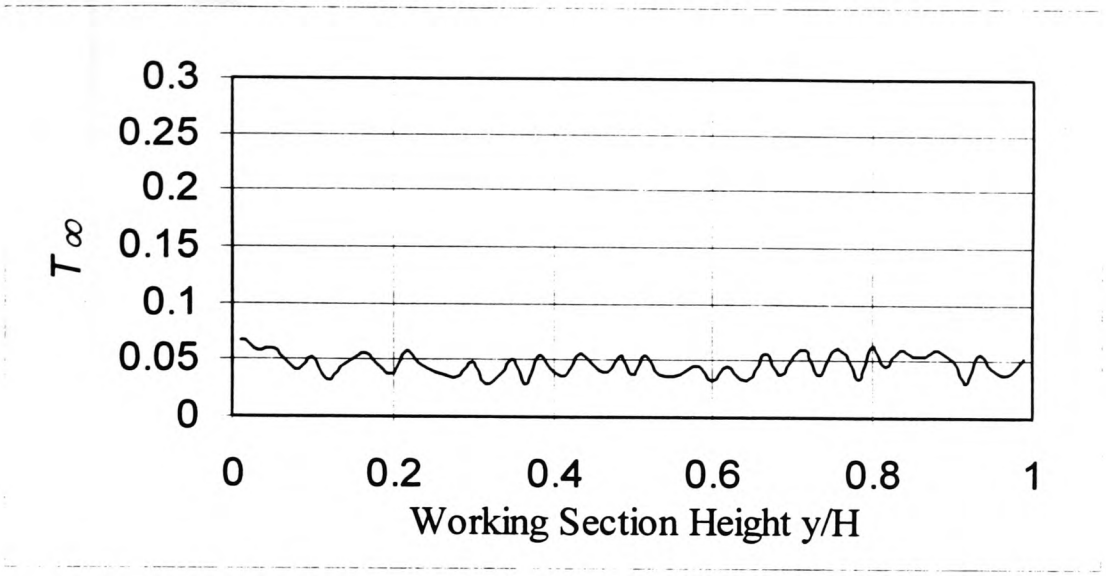

Figure 3-5 Turbulence Intensity Along the Height of the Test Section

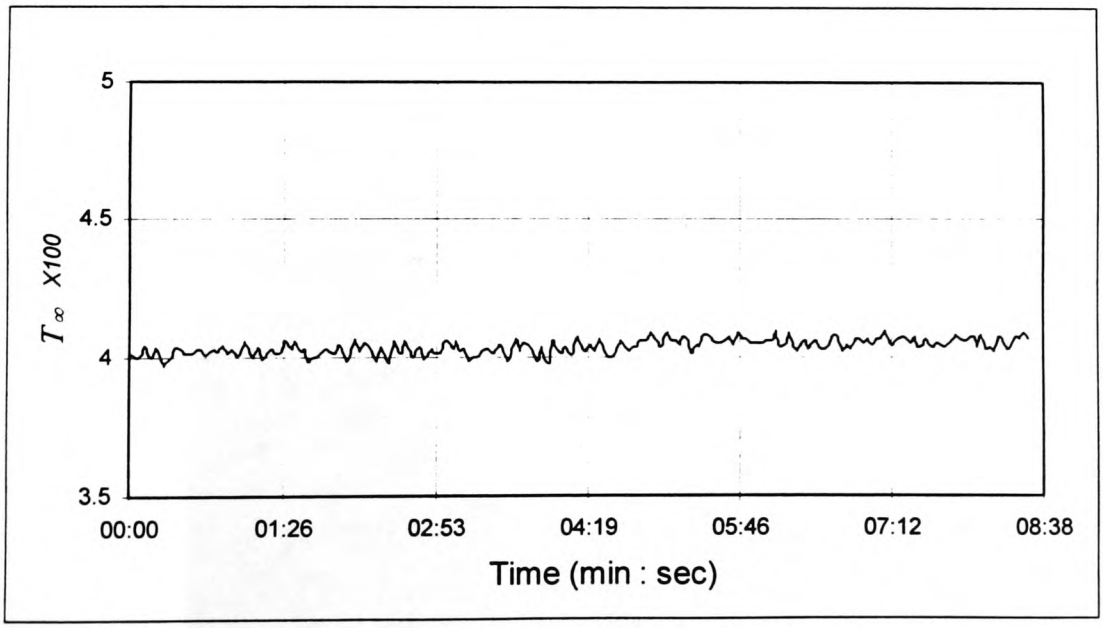

Figure 3-6 Turbulence Intensity Inside the Wind Tunnel

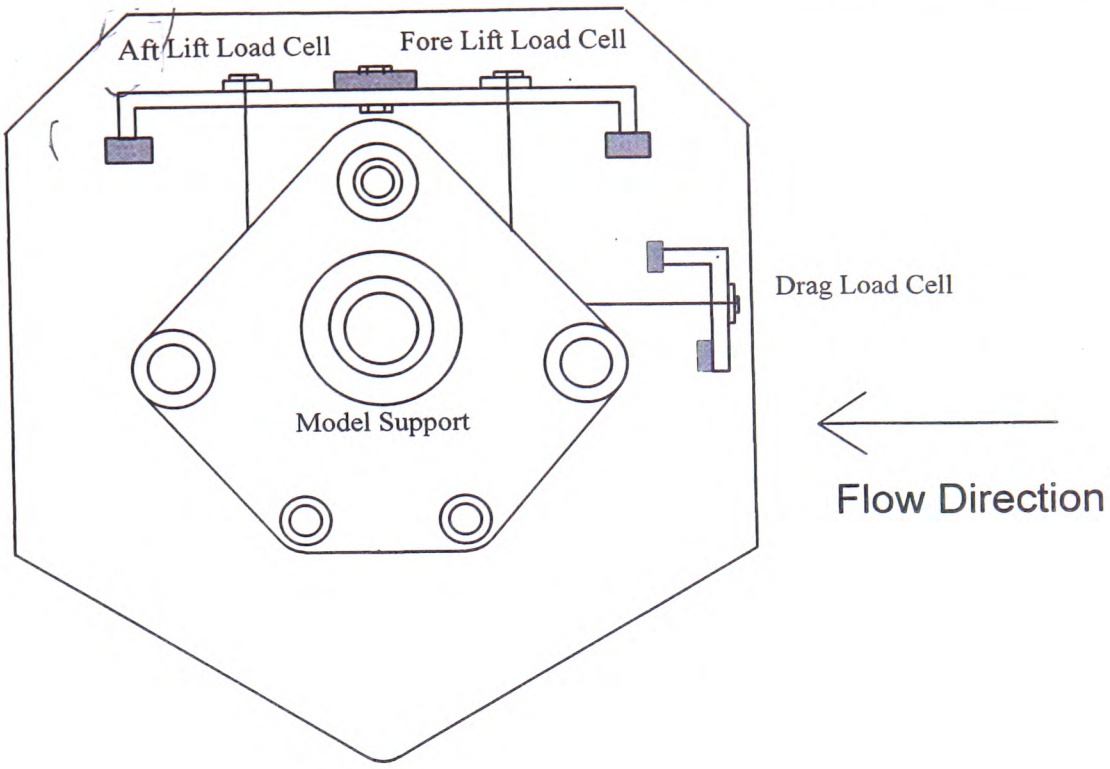

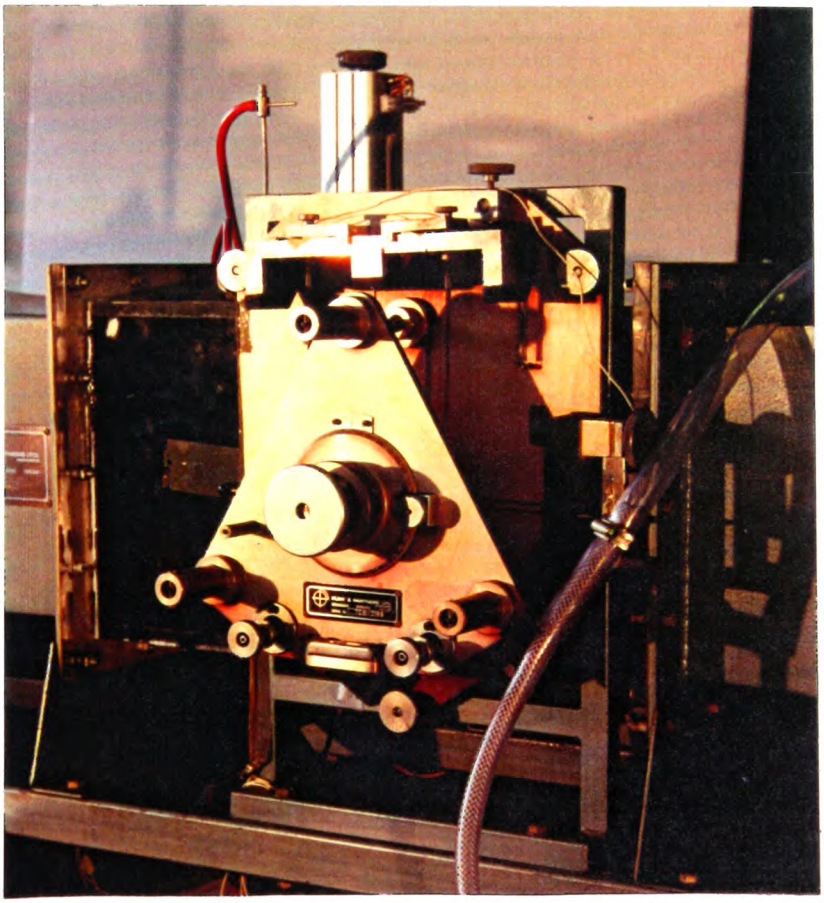

Figure 3-7 Three component balance

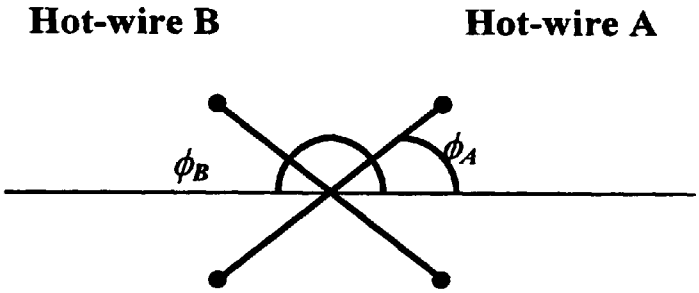

Figure 3-8 Orientation of X Hot-wire. Flow Direction is Perpendicular to the Plane of Paper

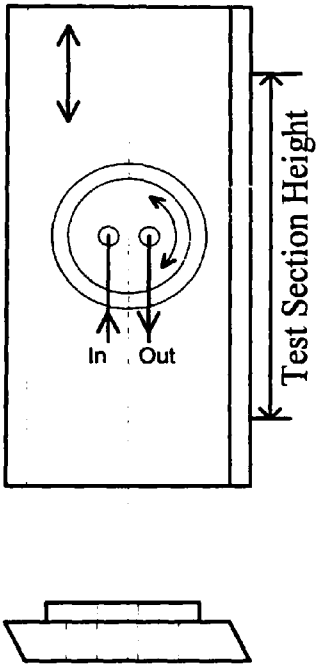

Figure 3-9a Aerofoil model support

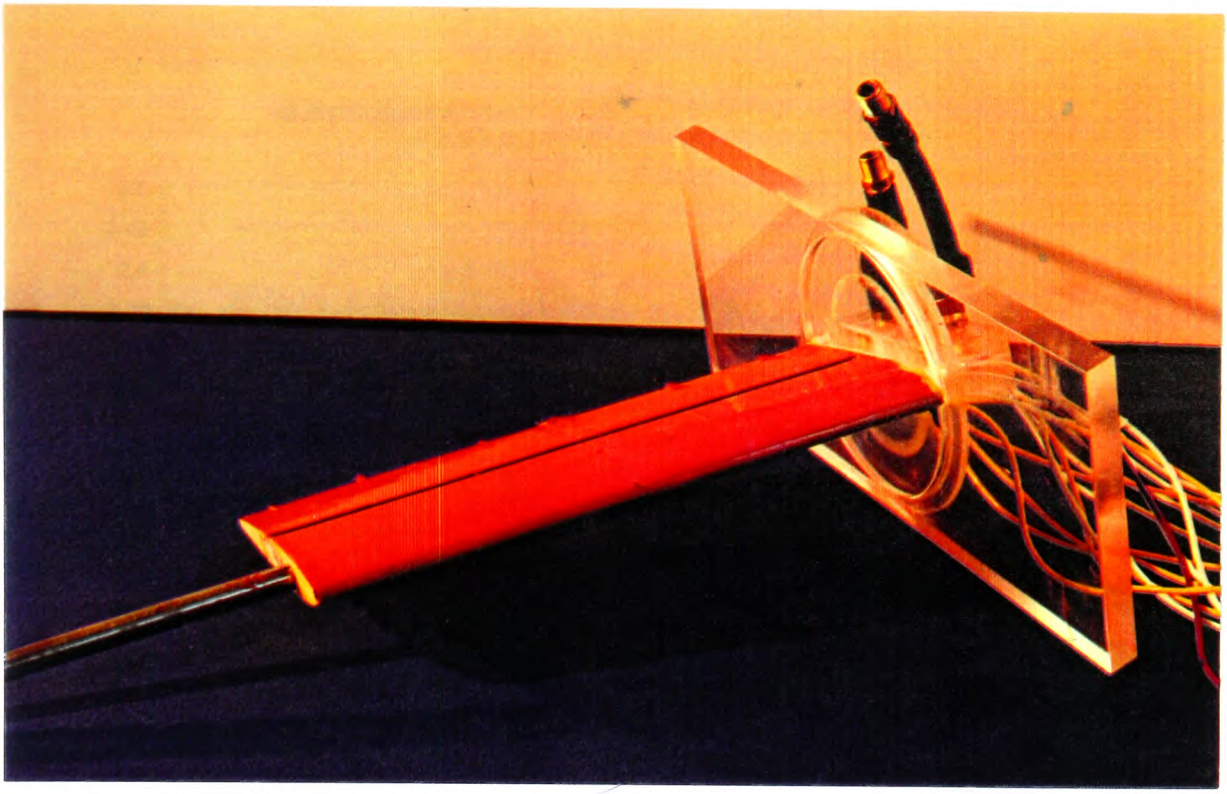

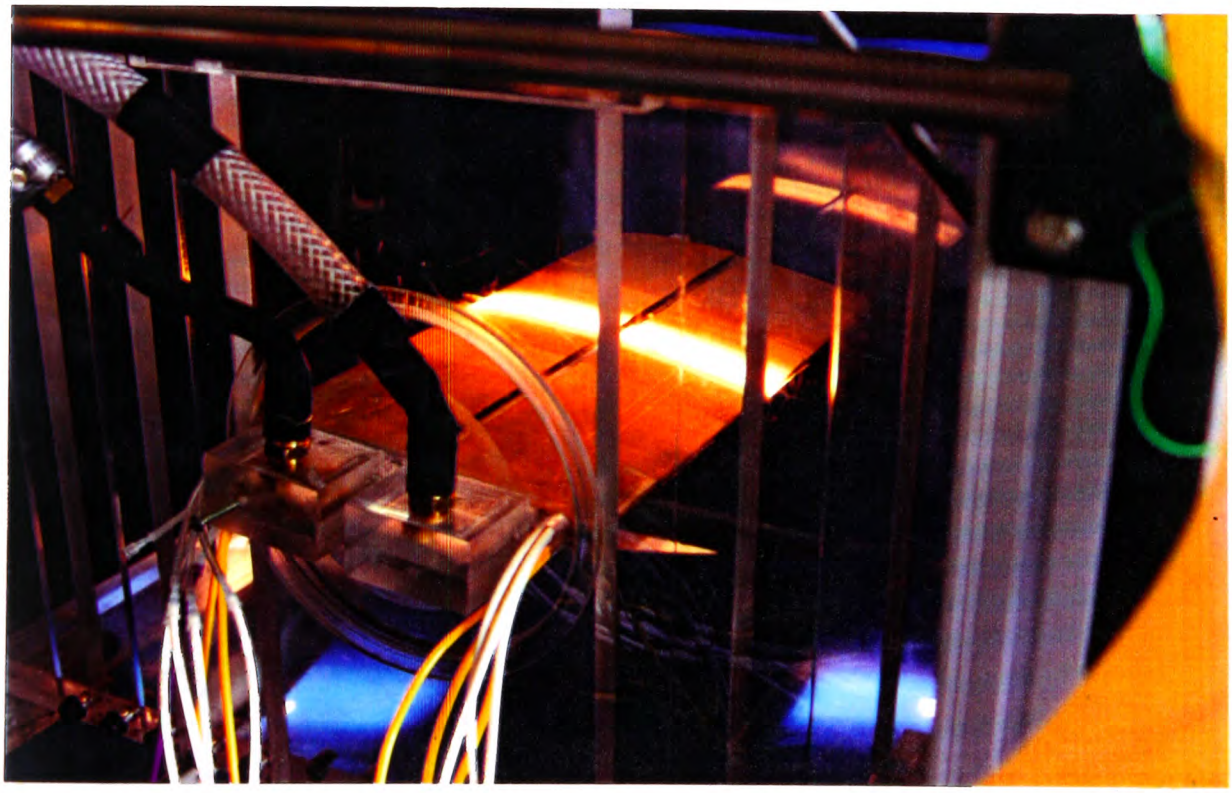

Figure 3-9b Aerofoil model support

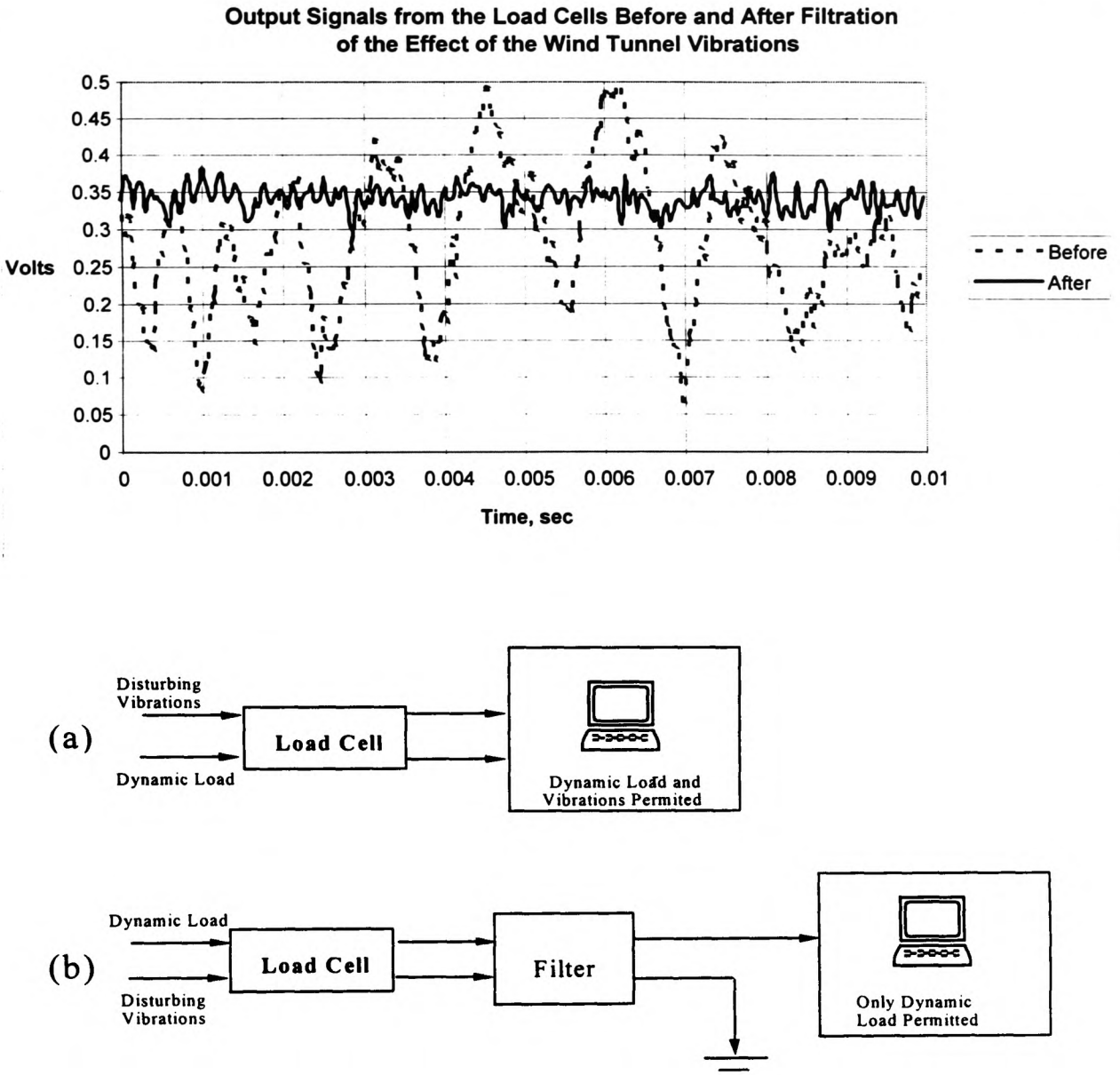

Figure 3-10 Load cells signals (a) before and (b)after filtration

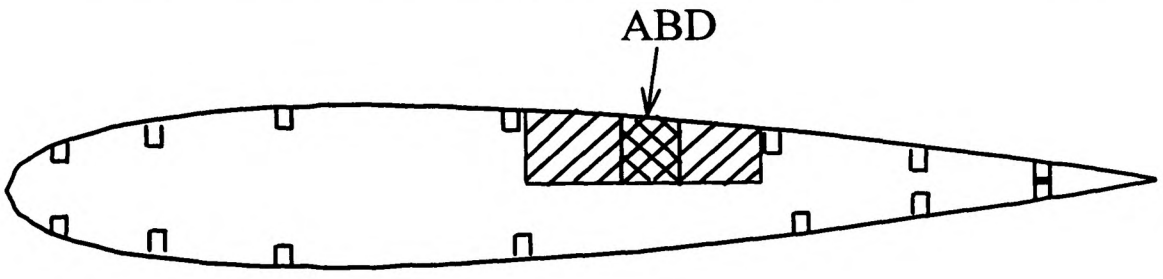

Figure 3-11 Schematic Diagram of Pressure tappings over an aerofoil surface with fitted ABD

Figure 3-12 Flow over the wing in flight test (Surface tuft method)

(Nakayama, 1988)

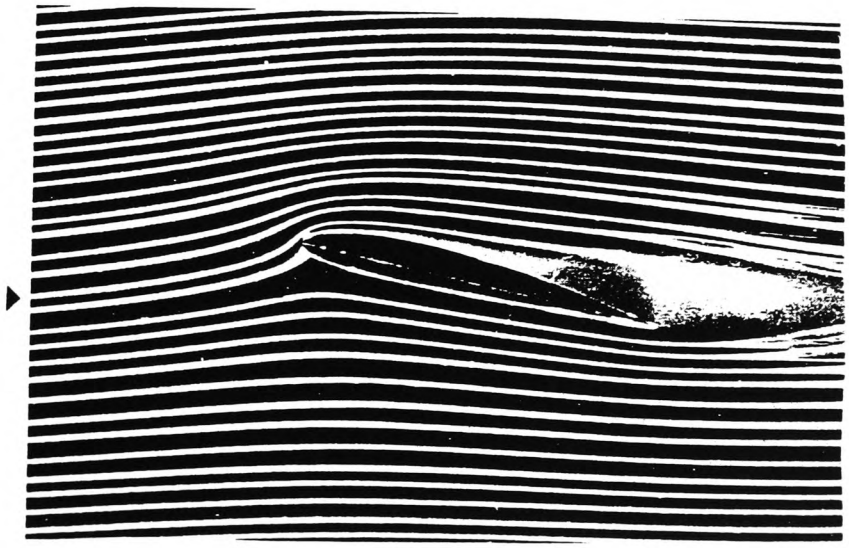

Figure 3-13 Smoke visualisation of flow around an aerofoil. α=15°

(Nakayama, 1988)

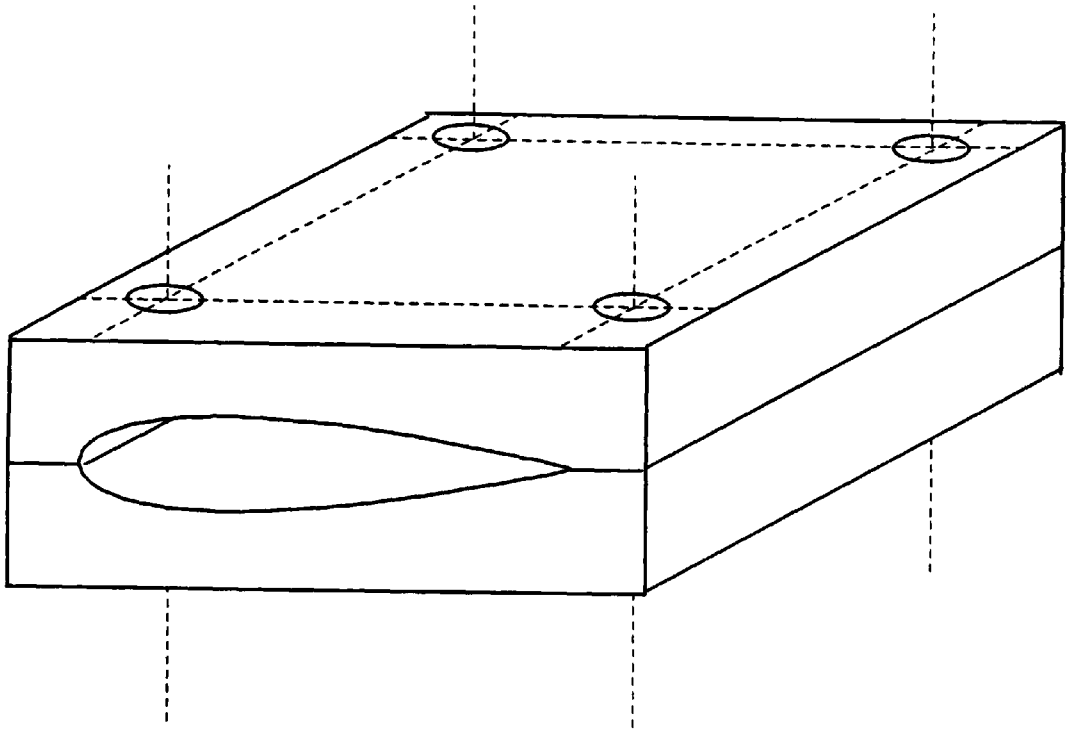

Figure 3-14 Die used in casting the aerofoil model

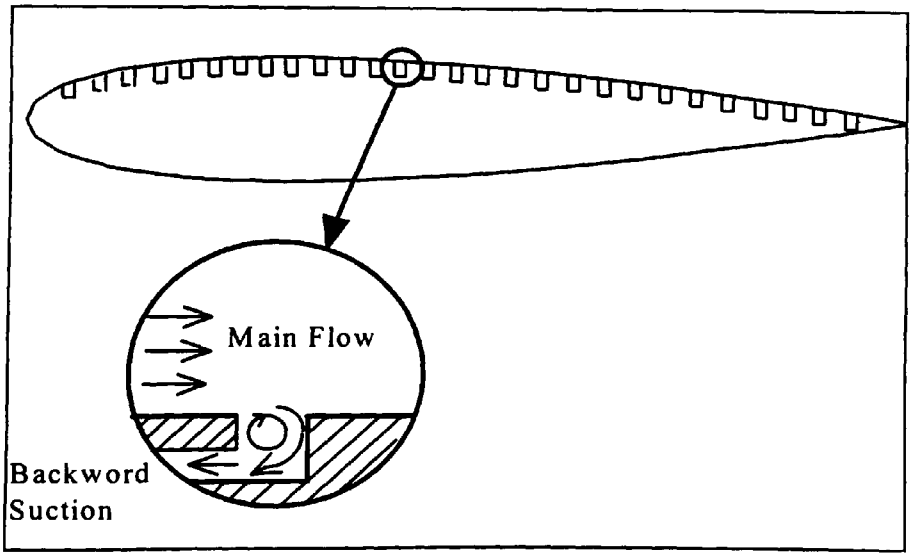

Figure 3-15 Schematic Diagram of Backward holes suggested for suction arrangement on transverse grooves

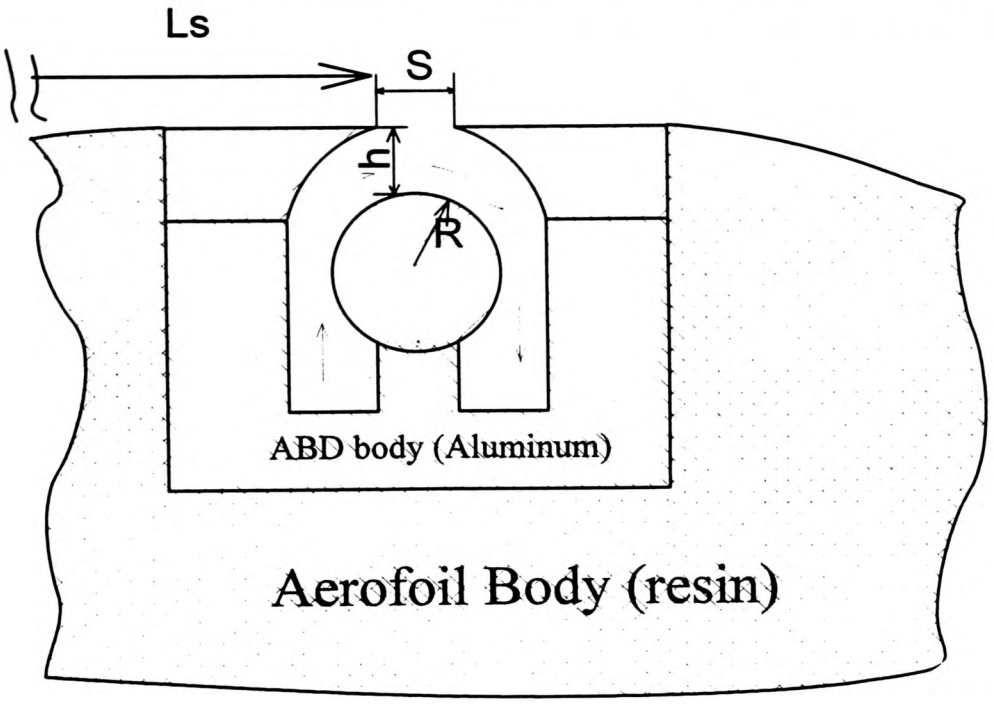

Figure 3-16 Model 1 of the assembled ABD

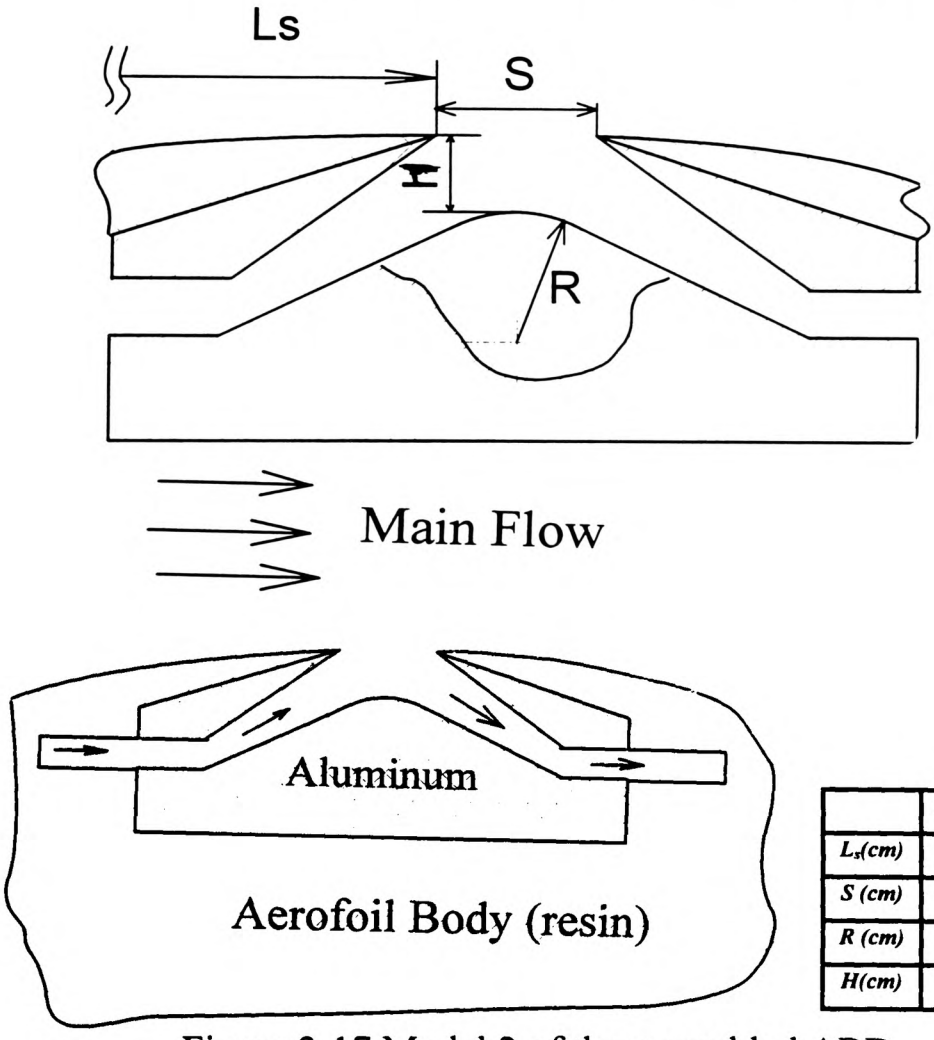

	Model 1	Model 2
L_s(cm)	5.7	5.7
S (cm)	.5	.6
R (cm)	.5	2
H(cm)	.5	.6

Figure 3-17 Model 2 of the assembled ABD

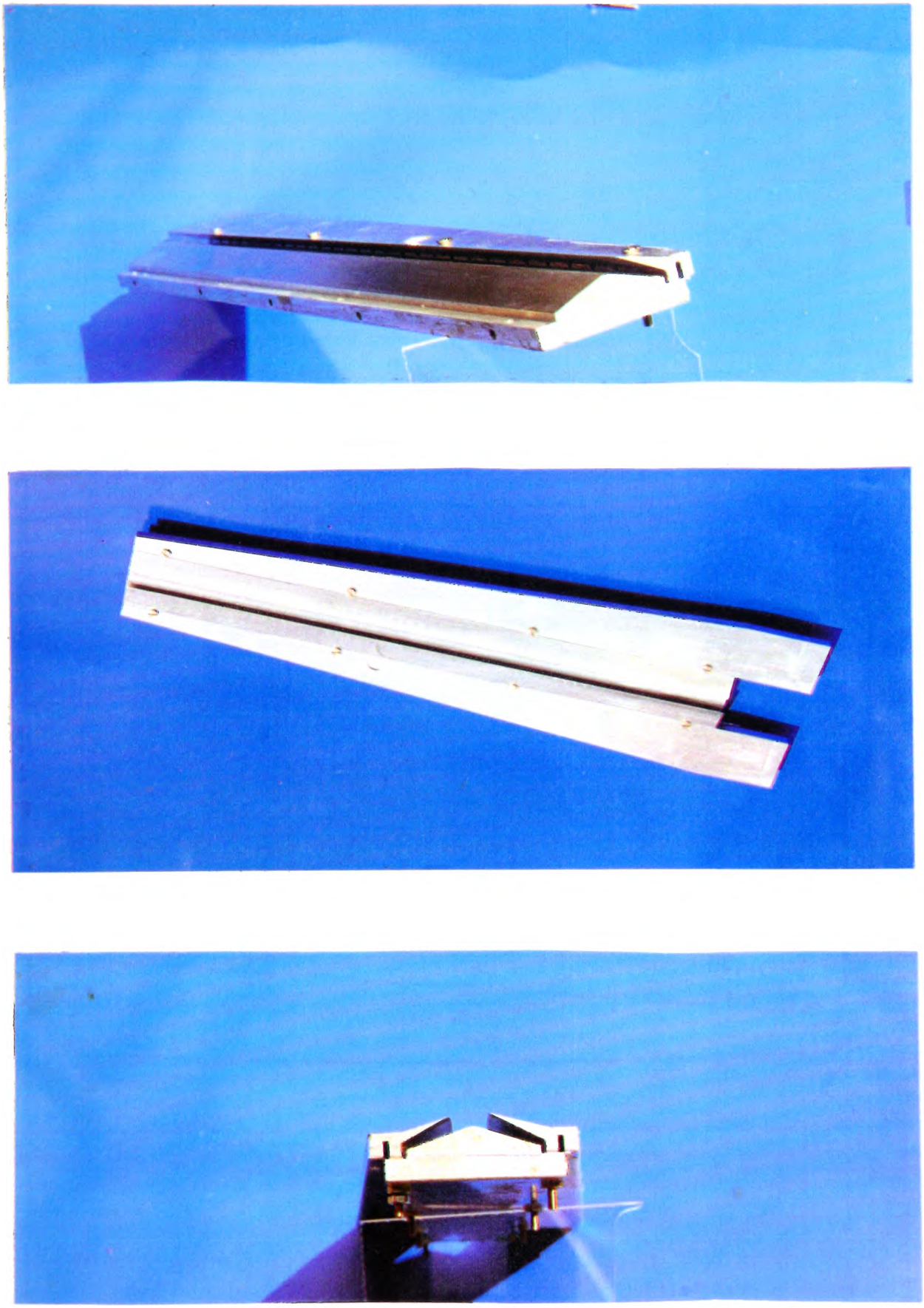

Figure 3-18 Assembled ABD - Model 2

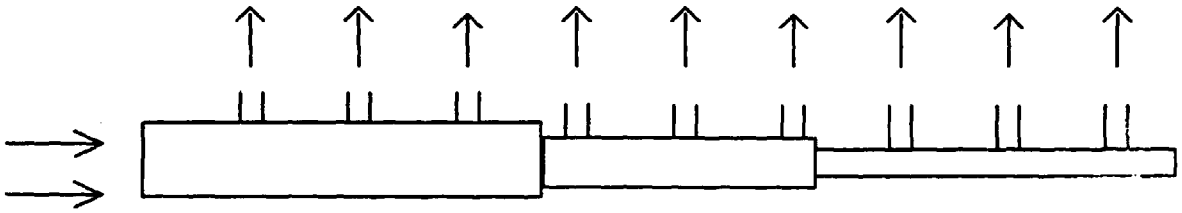

Figure 3-19 Telescopic Pipe with holes and slot.

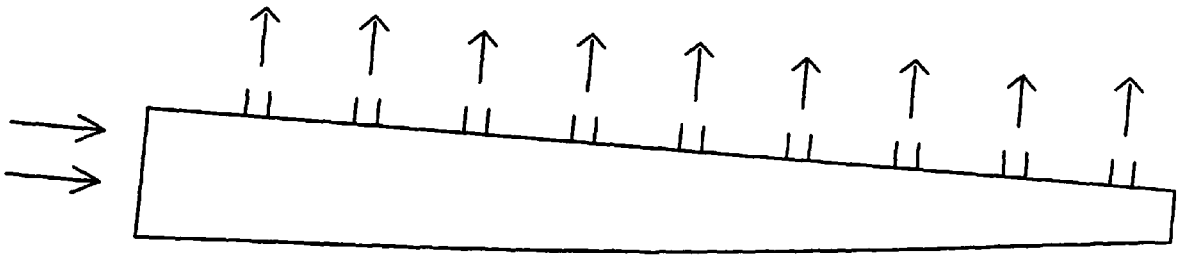

Figure 3-20 Tapered chamber with large number of holes.

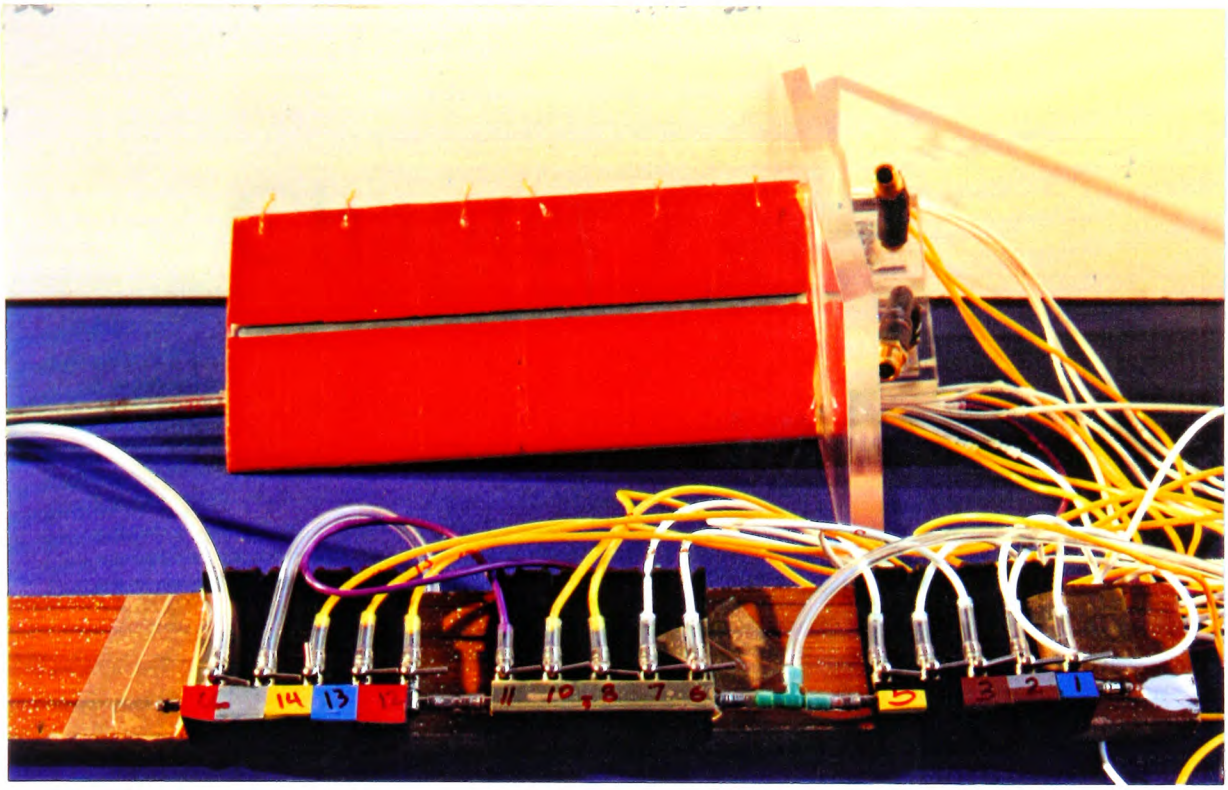

Figure 3-21 Assembled aerofoil with ABD Model-2

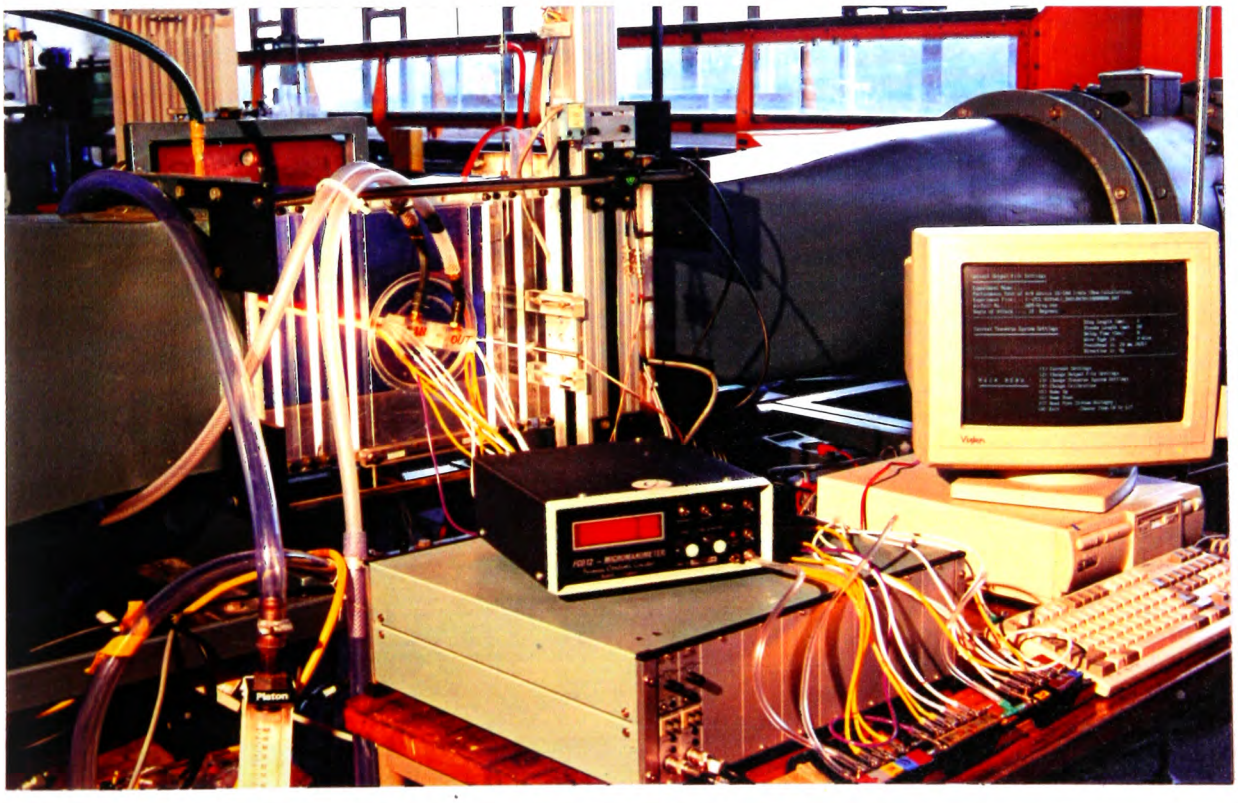

Figure 3-22 Piping system for the ABD.

Chapter Four

Experimental Results and Discussion

4.1 Introduction
4.2 Lift and Drag Force Measurements
4.3 Hot Wire Results
4.4 Pressure Distribution
4.5 Flow Visualisation
4.6 Experimental Results

Chapter Four

Experimental Results and Discussion

4.1 Introduction

The experimental study was aimed at investigating the effect of the ABD on the flow over an aerofoil. It should be noted that the experiments which were performed in this research were limited by the size of the model aerofoil and the test section of the wind tunnel. In particular the choice of location and dimensions of the ABD were restricted. It is, therefore important to carry out a further extended experimental programme with a larger model aerofoil as part of future work. These larger models will allow proper optimisation of the ABD parameters. Although the choice of the ABD location and the size were dictated by the aerofoil size, the results which were obtained are very promising.

The experimental programme was discussed in Chapter 3, and the following sections present some of the results.

4.2 Lift and Drag Force Measurements

The experimental measurements of lift and drag forces and consequently C_l and C_d were performed by means of the load cells on the balance system. The load cell signals were triggered at a frequency of 5 kHz, at a rate of 3000 samples per point; and each experiment was repeated at least 5 times at each angle of incidence. The choice of these values was made after a series of preliminary experiments that were conducted to determine the conditions under which the readings were independent of frequency and the number of samples. It is worth mentioning that the low frequencies caused by the vibration of the test section of the wind tunnel were measured and, hence, isolated from the final readings. This point was discussed in Chapter 3.

The smooth aerofoil, cast in the laboratory, was tested in the wind tunnel and the results

were compared with the characteristics of the NACA0012 aerofoil published in (Thibert, 1979); Figures 4-1 and 4-2 show this comparison. For the present aerofoil it was found that 12° is the angle of maximum lift (α_{max}), while the corresponding value in AGARD-AR-138 report is 14°,(Thibert, 1979). This difference may be related to the higher level of flow turbulence and to the higher level of vibrations in the current test section. These factors are thought to promote trailing edge separation at lower values of α_{max}. Generally there is reasonable agreement up to an angle of incidence of 10° although the performance of the present aerofoil deteriorates substantially at higher angles.

Despite these differences the present smooth aerofoil results were used as a comparison. In other words, the results obtained in the present tests were used to compare the cases with and without the ABD. Therefore the effect of the difference in behaviour from the standard NACA aerofoil will not affect the comparison.

The rest of the figures presented in this section show the C_l, C_d and C_l/C_d curves for the smooth aerofoil (with no ABD fitted) and for the aerofoil fitted with the ABD. Two models of the ABD were tested, Model-1 and Model-2. The specifications of both these models were presented in Chapter 3.

Figures 4-3 through 4-6 show the effect of the ABD on the top surface of the aerofoil *without* any "air bearing flow" for Model-1 and Model-2 respectively. The drag was found to increase by up to 17% at some locations and the lift decreased by 13%. This result is not unexpected since the ABD with no-flow behaves as a cavity and this is known to cause some interruption to the main flow as a result of the loss of some fluid energy due to the induced circulation in the ABD. Figures 4-5 and 4-6 show the effect of the ABD under no flow conditions on the C_l/C_d ratio of the aerofoil. The reduction in this ratio is generally within 20%. However, it can be seen from the figures shown that the deterioration in the performance of the no-flow ABD is not sufficiently large to lead to stall of the aerofoil especially at low to moderate angles of incidence. This is an important feature in practice and means that if the flow inside the ABD is ceases for any reason the aerofoil will still produce a sufficient amount of lift.

Figures 4-7 through 4-10 show the effect of C_i on both C_l and C_d for the Model-1 and Model-2 cases, respectively. In these figures C_l is clearly enhanced by increasing C_i. An

Increase in lift of up to 35% was obtained and the drag coefficient, in general, decreases especially at higher angles of incidence, α. This reduction in drag at higher angles of incidence means that the stall point is postponed and gives the aerofoil a wider range of operation. Figures 4-11 through 4-14 show the effect of C_i on the C_l/C_d ratio. Good enhancement of this ratio can be seen over most of the operating range of the aerofoil. This enhancement increases to some extent with increasing C_i. Generally, the ratio C_l/C_d is an important parameter which indicates the performance of the aerofoil by combining the individual changes in C_l and C_d. It is important to note that improving either of these two parameters, C_l or C_d, is a valuable advantage for the ABD technique. Fortunately, both parameters were improved for most of the range of operation of the aerofoil.

The performance of Model-2 was, in general, found to be better than that of Model-1. This is may be due to the larger value of the width of the ABD, *S*, in Model-2 which results in greater interaction between the main flow and the flow inside the ABD. From the geometry of the two models, (Chapter 3), it is clear that the flow inside the ABD is "smoother" in the case of Model-2 than that of Model-1. In Model-1 the flow has to change direction through an angle of almost 180° inside the ABD piping, whilst in the case of Model-2 the flow changes direction only slightly before it exits from the ABD. According to the above results it can be said that the "efficiency" of Model-2 is better than the Model-1.

4.3 Hot Wire Results

Using the traverse system, it was possible to scan the wake region downstream of the aerofoil with a X-hot wire probe to measure the velocity profile. The effect of the ABD can be shown from the velocity profile inside the wake region. The width of the wake as well as the minimum value of the wake velocity both determine the "amount" of loss in momentum of the flow caused by the presence of the aerofoil. Consequently, reducing the width of the wake and/or increasing the value of the minimum wake velocity means that the flow is enhanced and the drag is reduced.

The readings from the X-hot wire were taken from 3000 samples at every point at a frequency of 10kHz. The average readings are then considered. The experiments were repeated at least 5 times to check the repeatability. As a checking procedure, different frequencies were tested and it was found that the frequency of 10 kHz gives almost the

same results as measurements undertaken at higher frequencies (up to 40 kHz) over the same period.

Figures 4-15 through 4-22 present the velocity profiles behind the aerofoil with a Model-2 ABD for different ABD velocities and angles of incidence. The higher the value of C_i the greater the enhancement in the wake region. It is also clear that for lower values of C_i, the wake width is increased although it is always narrower than the wake for the smooth profile system.

These figures seem to indicate that some of the momentum in the outer region of the wake is "pulled" in to the inner region. This may not necessarily reduce the drag coefficient, but the lift of the device will be increased due to the "higher" circulation around the aerofoil; and, more importantly, the flow on the top surface will be more capable of resisting separation. The "pulling" of the higher momentum flow to the wake region can be seen particularly in Figure 4-17 where the velocity at the outer region of the wake (i.e. for y/C <-0.1 and y/C > 0.0) is lower in the case of the aerofoil with the ABD than that of the smooth aerofoil.

It is worth mentioning here that, the experimental results were in reasonable agreement with the CFD analysis, see Chapter 5. However, it is believed that with more careful design the performance of the ABD can be improved. The rolling action of air inside the ABD should be uniform over the whole of the span, and also the degree of protrusion of the ABD on the surface should be carefully adjusted. To a certain extent these requirements were incorporated in the design of Model-1 and Model-2.

4.4 Pressure Distribution

It was possible to measure the pressure distribution over the aerofoil of Model-2 with and without the ABD fitted to its top surface using the pressure tappings described in Chapter 3. Figures 4-23 and 4-24 show that the ABD had a favourable effect on the pressure distribution over the aerofoil. In these figures it is clear that the ABD was able to "absorb" some of the adverse pressure over the top surface of the aerofoil which gave high suction. This is thought to be due the drop in pressure associated with the relatively high speed in the rolling flow inside the ABD. This drop in pressure is "sensed" in the region upstream of the ABD. It is this improvement in pressure distribution which is

responsible for increasing the lift of the aerofoil since the lift is proportional to the area under the curve of C_p. It was not possible to measure the pressure in the region of the ABD, and therefore, the curves do not show any details about the pressure in the region of the ABD. However, it was possible to predict the change in pressure inside the region of the ABD by theoretical simulation as will be discussed in Chapter 5. Both studies show that the pressure distribution after the location of the ABD is better than that of the case of smooth aerofoil.

The improvement in pressure distribution increases with an increase in C_i. These results are also in good agreement with the theoretical calculations.

4.5 Flow Visualisation

It was intended to perform flow visualisation using two methods: smoke lines and tufts. The photographs for the smoke-lines over an aerofoil are presented in Figures 4-25 and 4-26. It is difficult, however, to conclude precise information from these two photographs and therefore photographs of tufts appear to give a more accurate representation about the effect of the ABD on the main flow Figures 4-27 through 4-38 show photographs taken for the tufts over an aerofoil fitted with an ABD. It can be seen from those figures that the flow is attached to the surface of the aerofoil for the cases at which the ABD is off up to 8°. This is clear evidence that the main flow is not significantly interrupted by the existence of the ABD especially at moderate angles of incidence. When the ABD is on, the attachment of the flow to the surface is ensured as can be seen from the figures. The aerofoil is found to experience a separation as the angle of incidence exceeds 12°. Separation occurs at the trailing edge as is clear from the tufts pattern in Figure 4-35. In this figure some of the tufts beside the trailing edge were moved backward (which indicated a *S* reversed separated flow) while the tufts on the other line stay almost straight. In the cases with the ABD the separation can be delayed and the tufts show that the flow is still attached even at higher angles. In Figures 4-35 through 4-38 the aerofoil is working in the stall condition and the tufts are almost reversed when the ABD is off. When the device is on, the tufts in the case of 14° were kept straight with the attached flow showing that the separation is almost prevented by the effect of the ABD. In the case of 16° the adverse pressure is so large that the ABD could not prevent separation and therefore the tufts were reversed. It was not possible to test experimen-

tally more than one ABD, but in the theoretical study (Chapter 5) it was found that using two devices can prevent separation even at the high angle of incidence of 16°.

Figures

4.6 Experimental Results

4.6.1 Lift and Drag Force Measurement

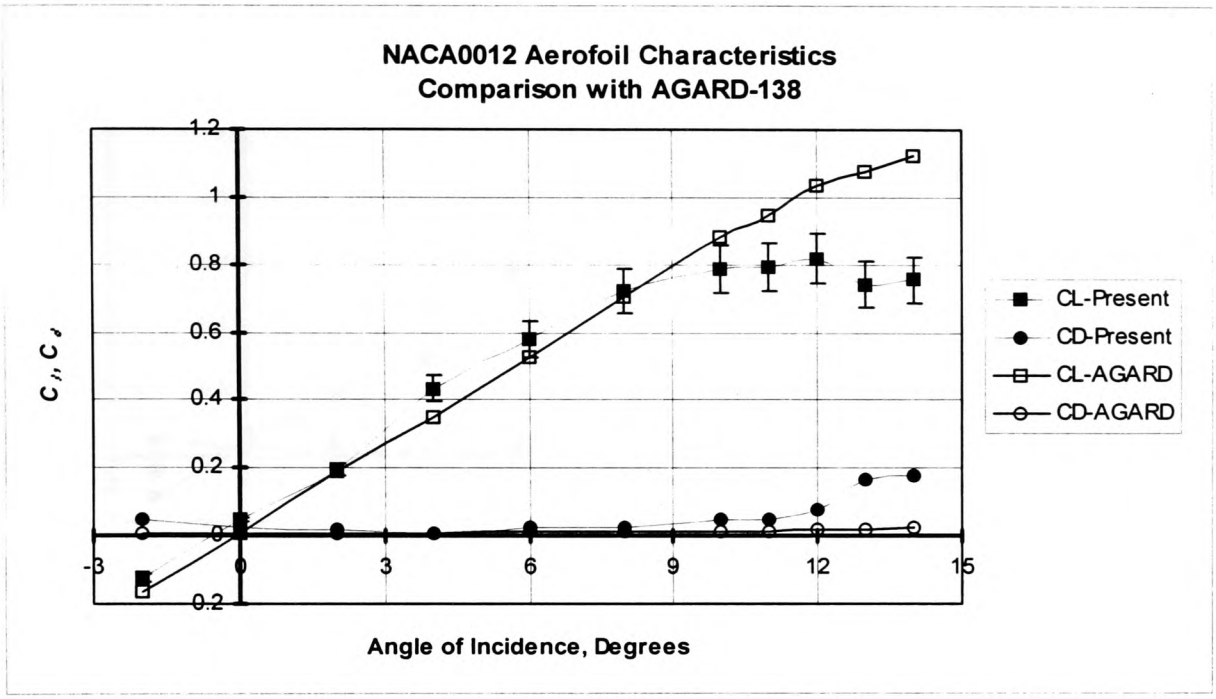

Figure 4-1

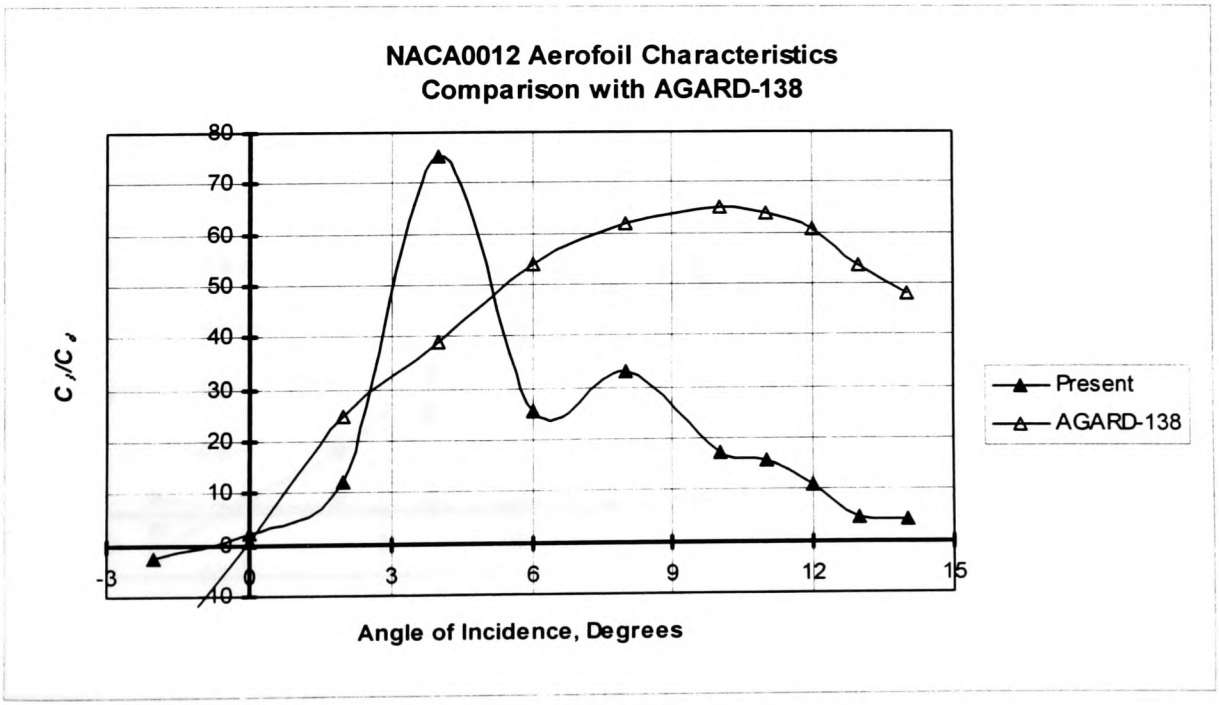

Figure 4-2

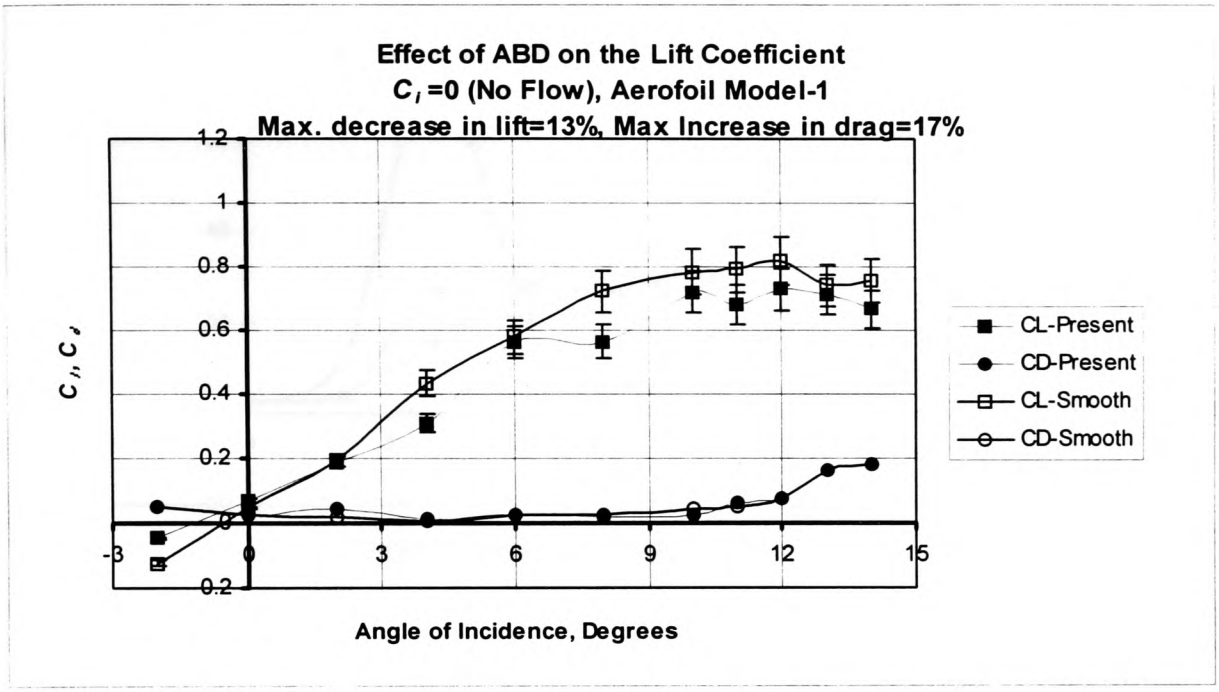

Figure 4-3

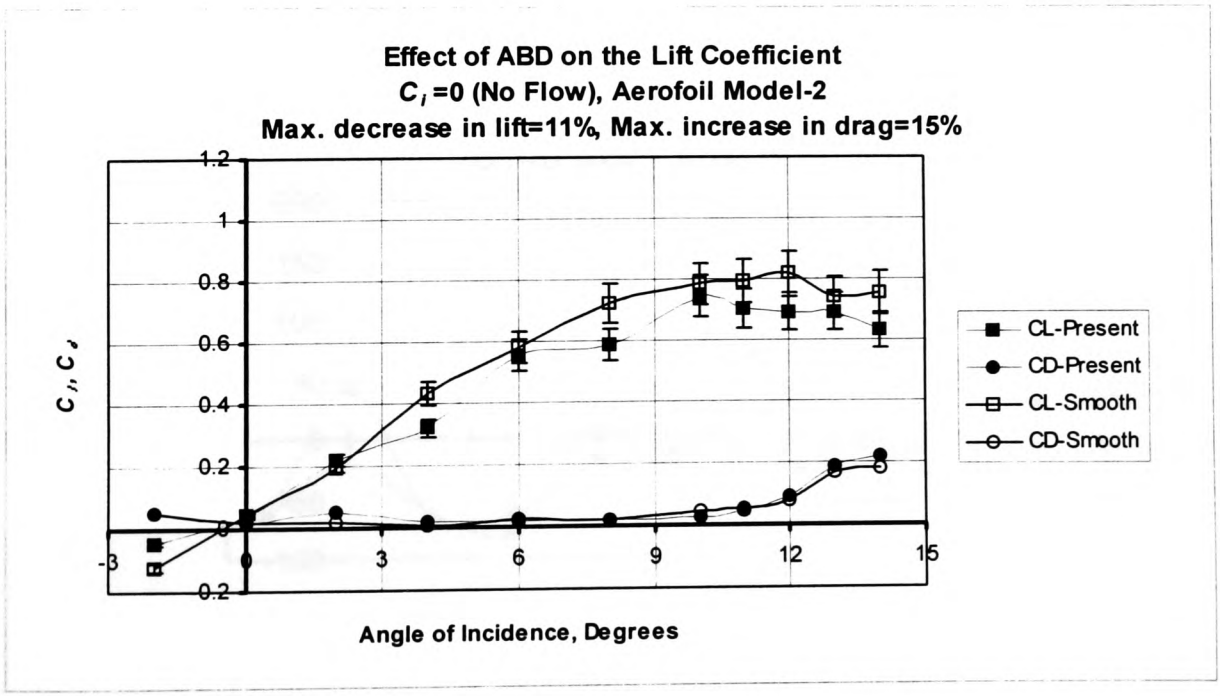

Figure 4-4

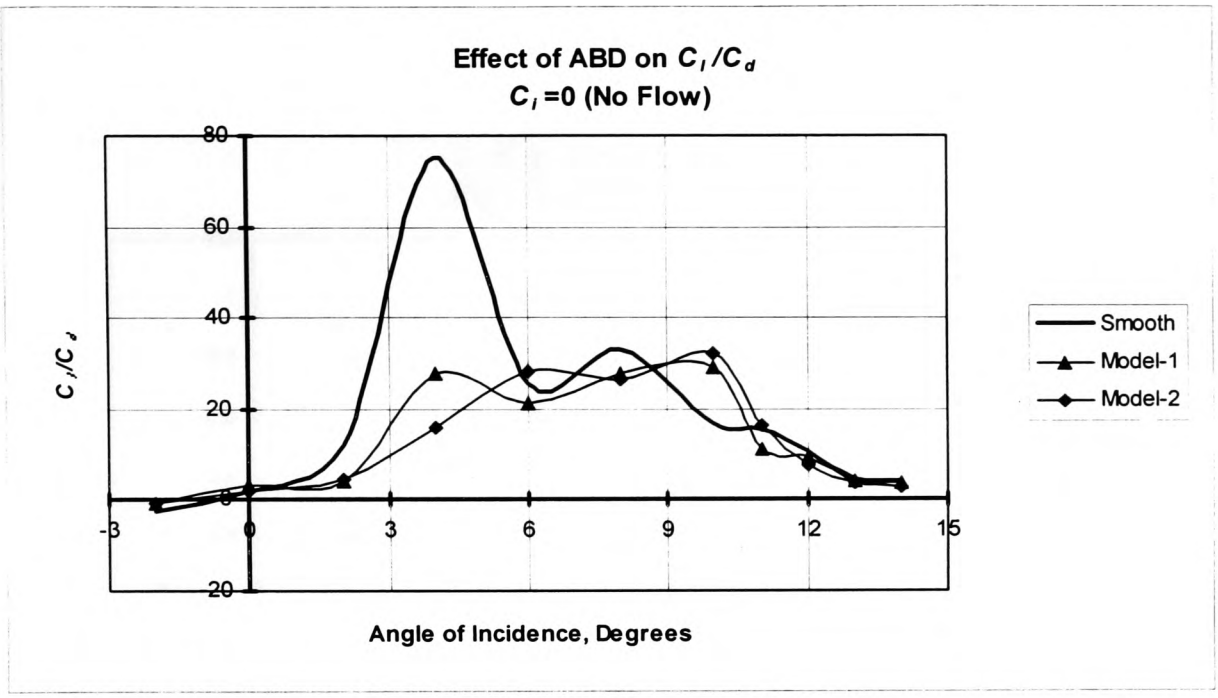

Figure 4-5

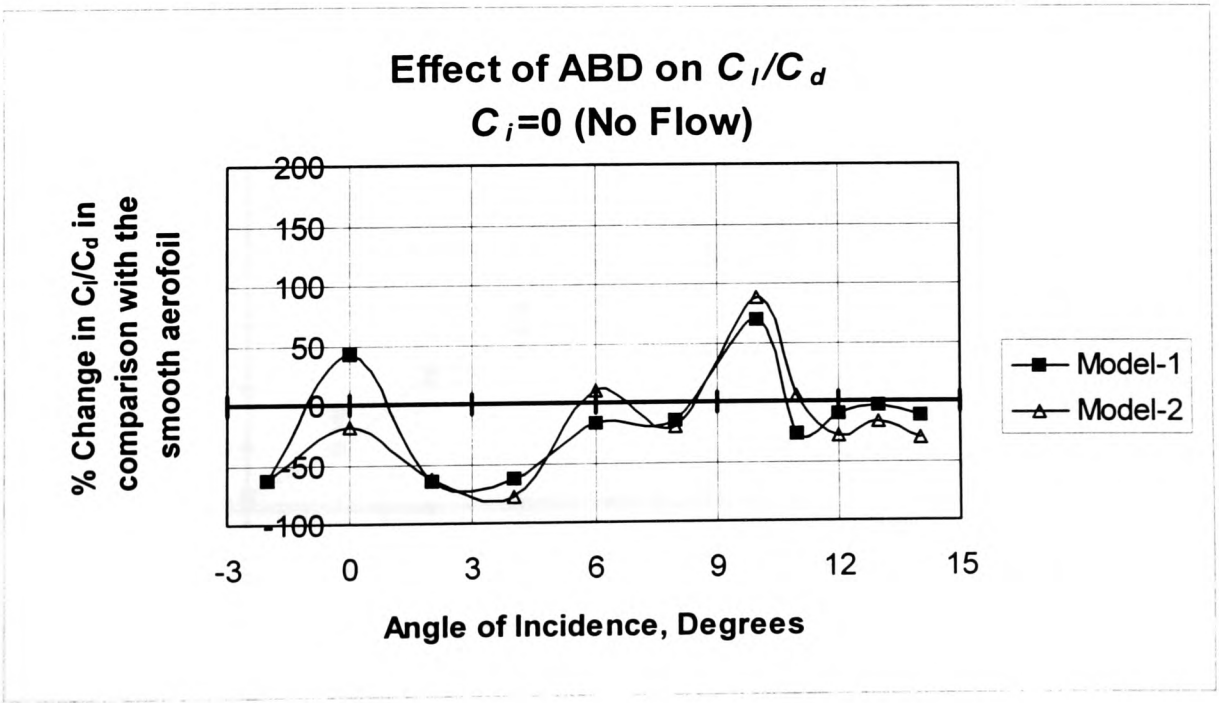

Figure 4-6

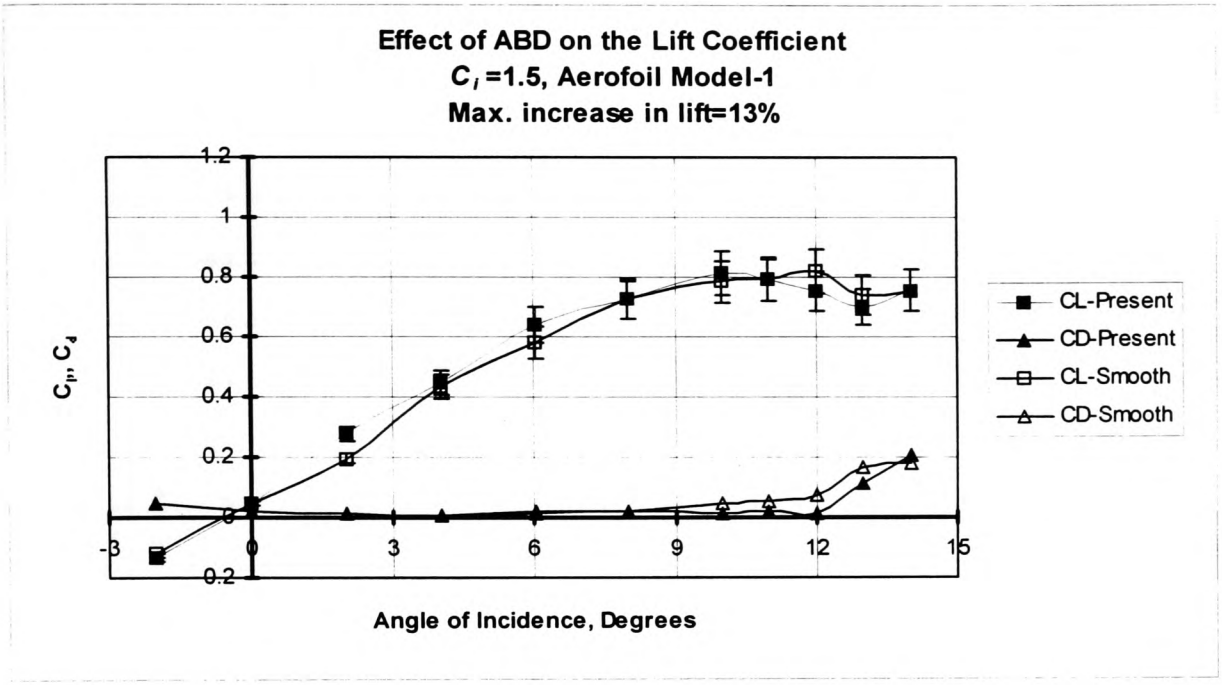

Figure 4-7

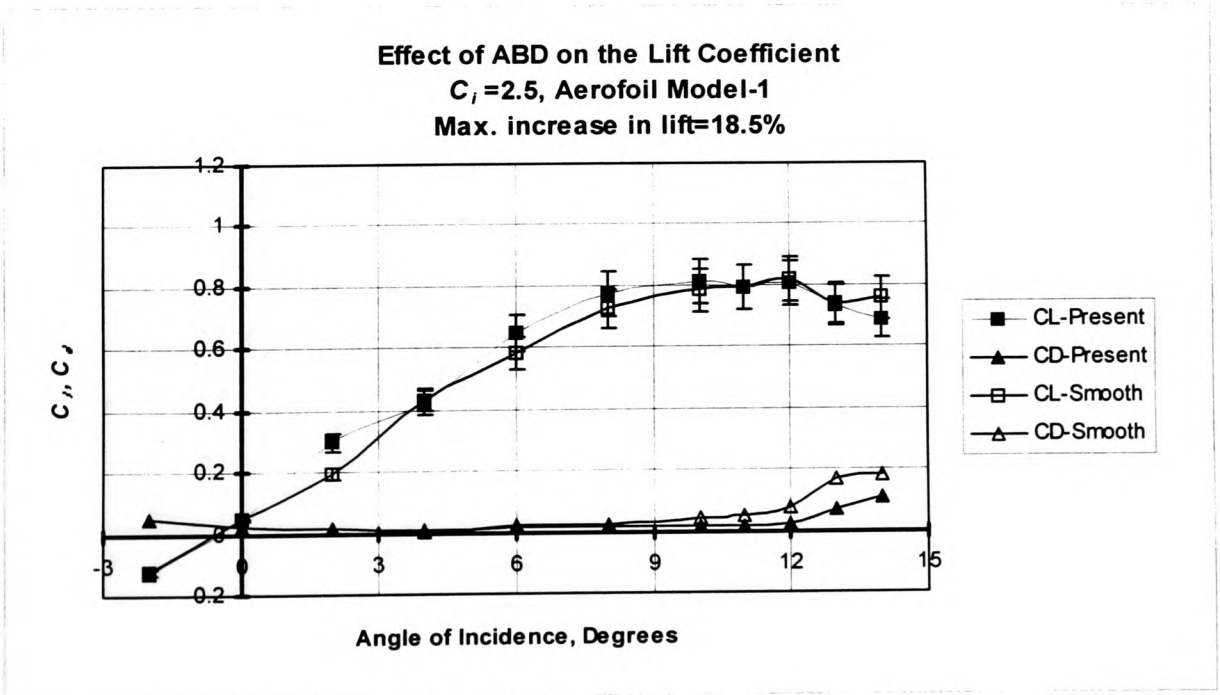

Figure 4-8

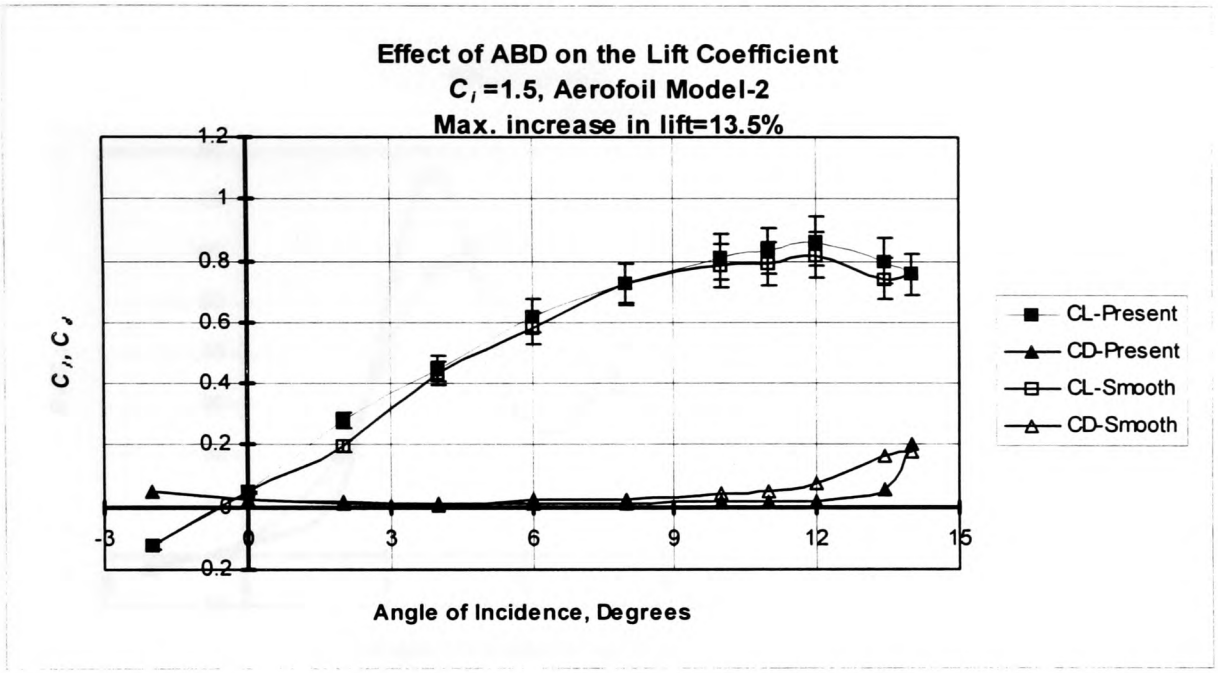

Figure 4-9

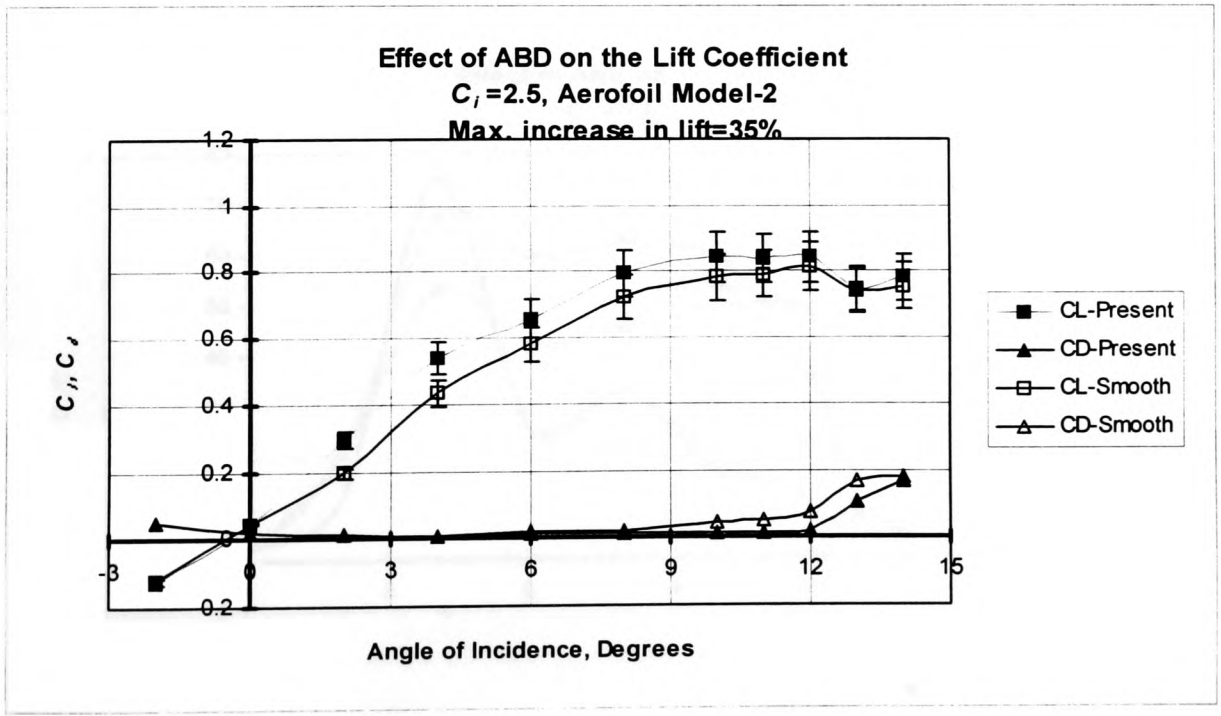

Figure 4-10

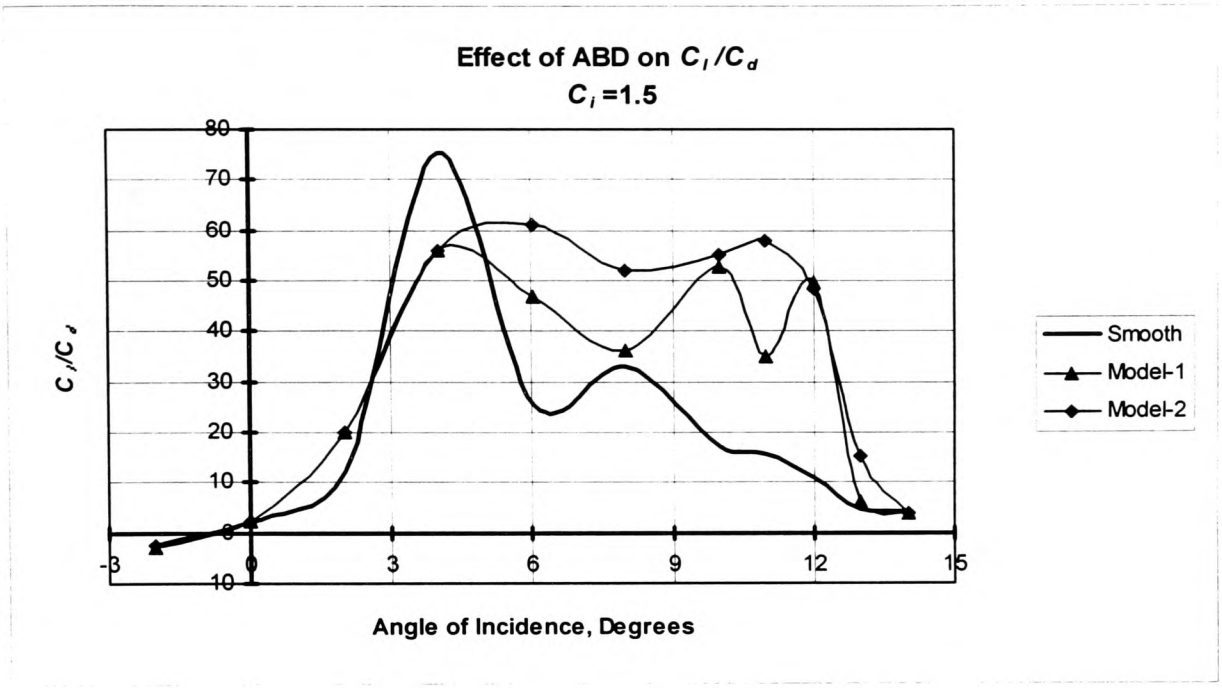

Figure 4-11

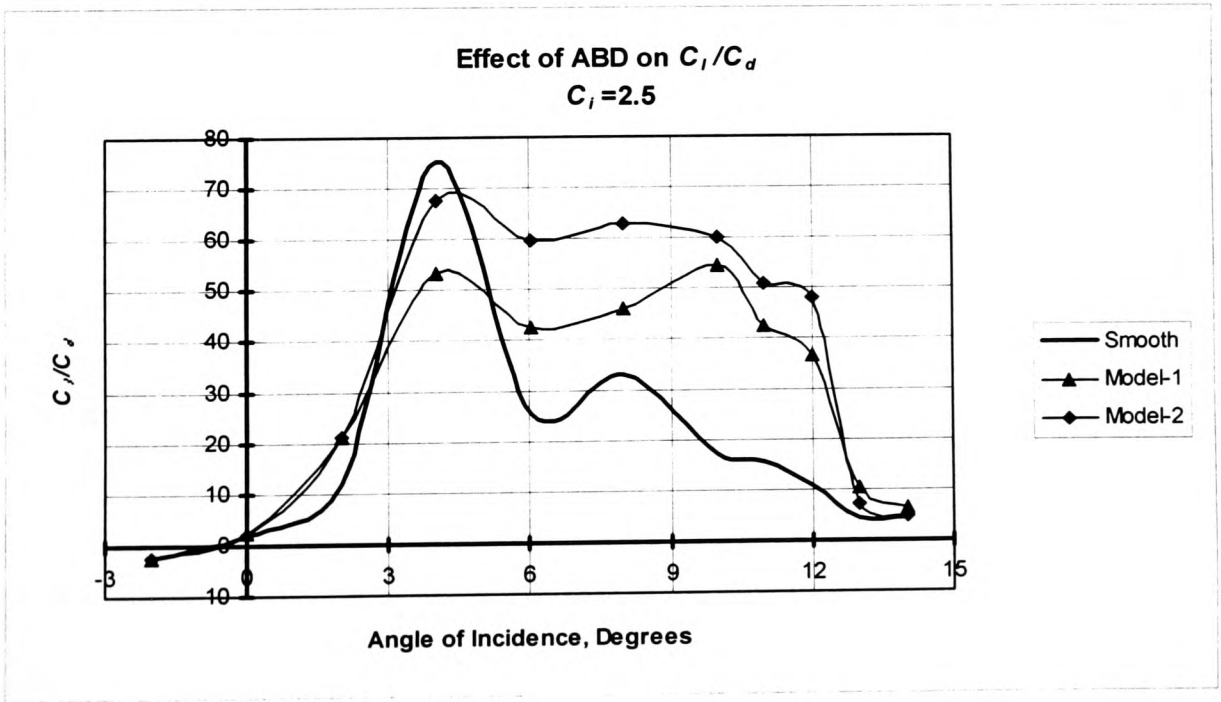

Figure 4-12

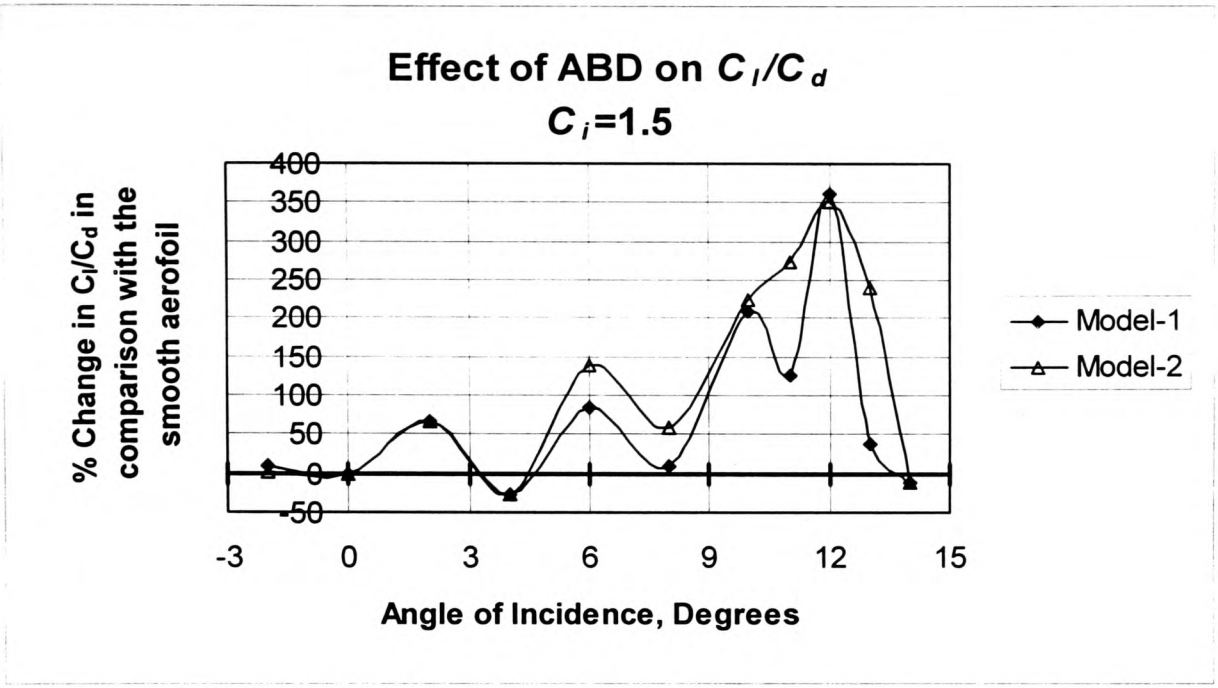

Figure 4-13

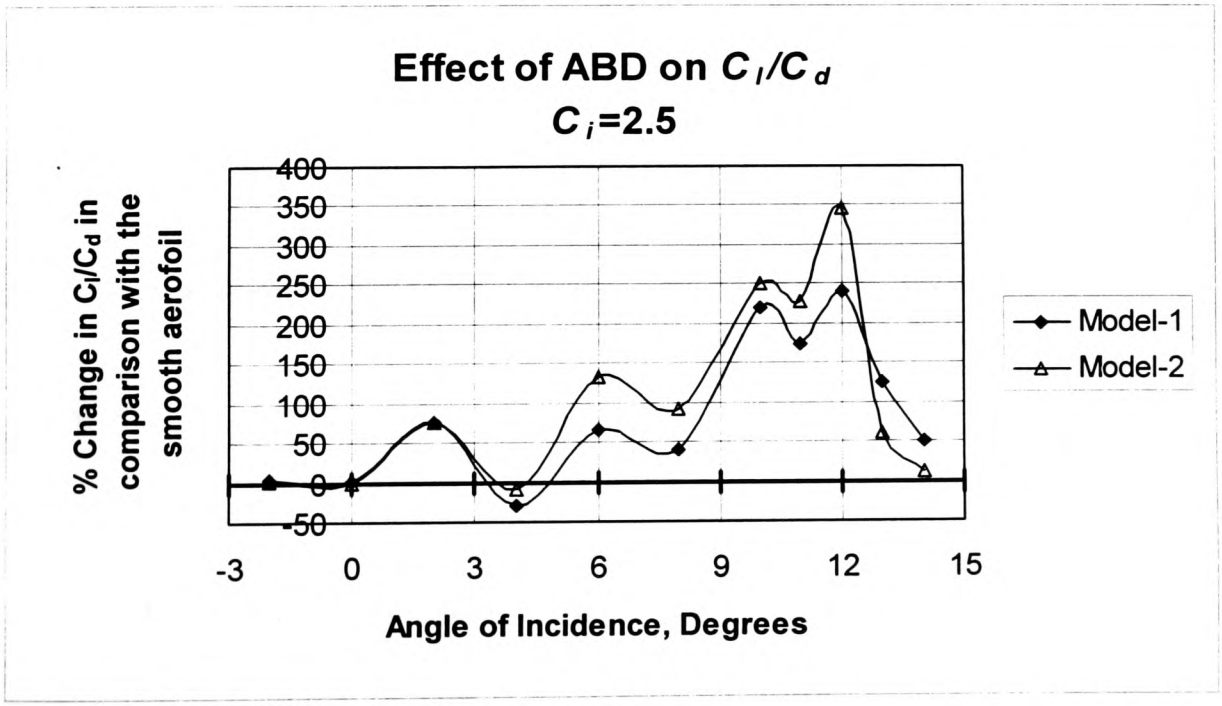

Figure 4-14

4.6.2 X-Hot Wire Results

In Figure 4-15 to Figure 4-22 the definition of y is as shown in this diagram:

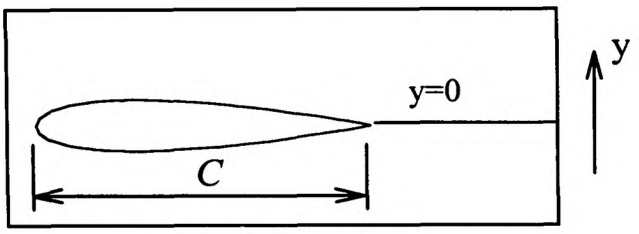

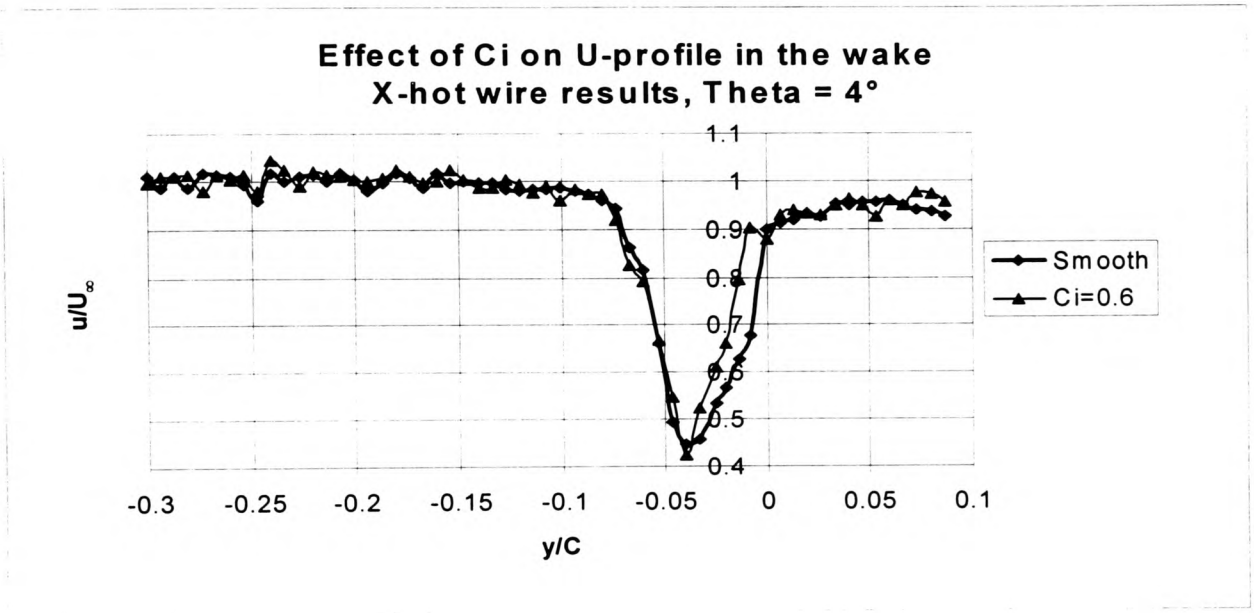

Figure 4-15

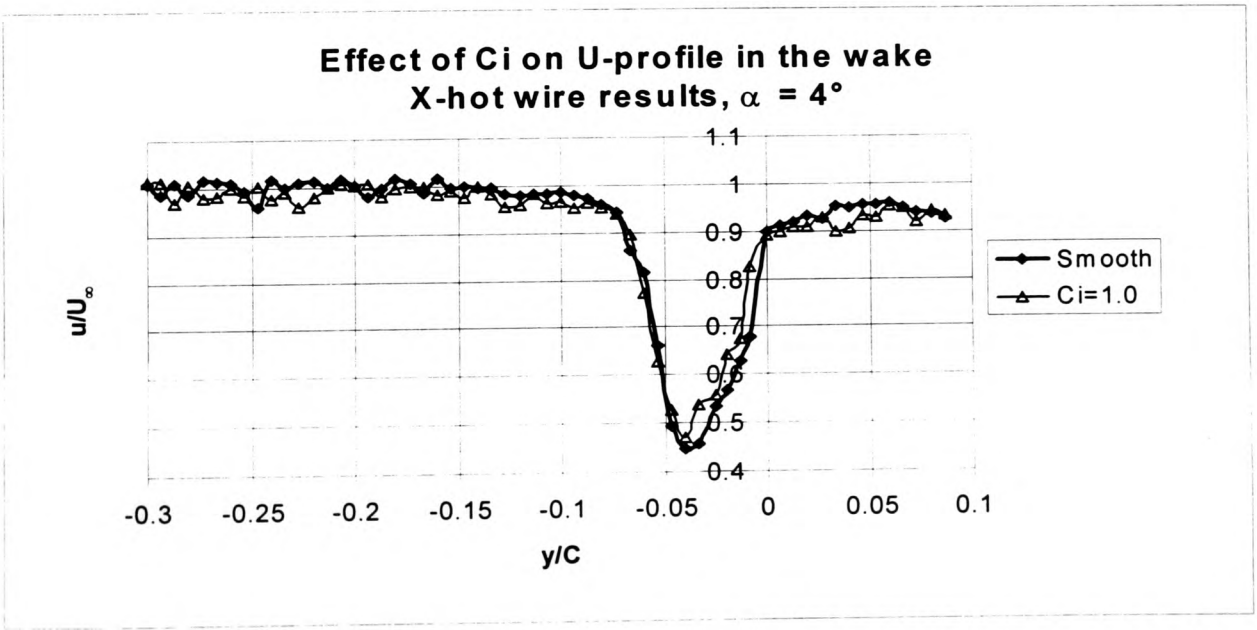

Figure 4-16

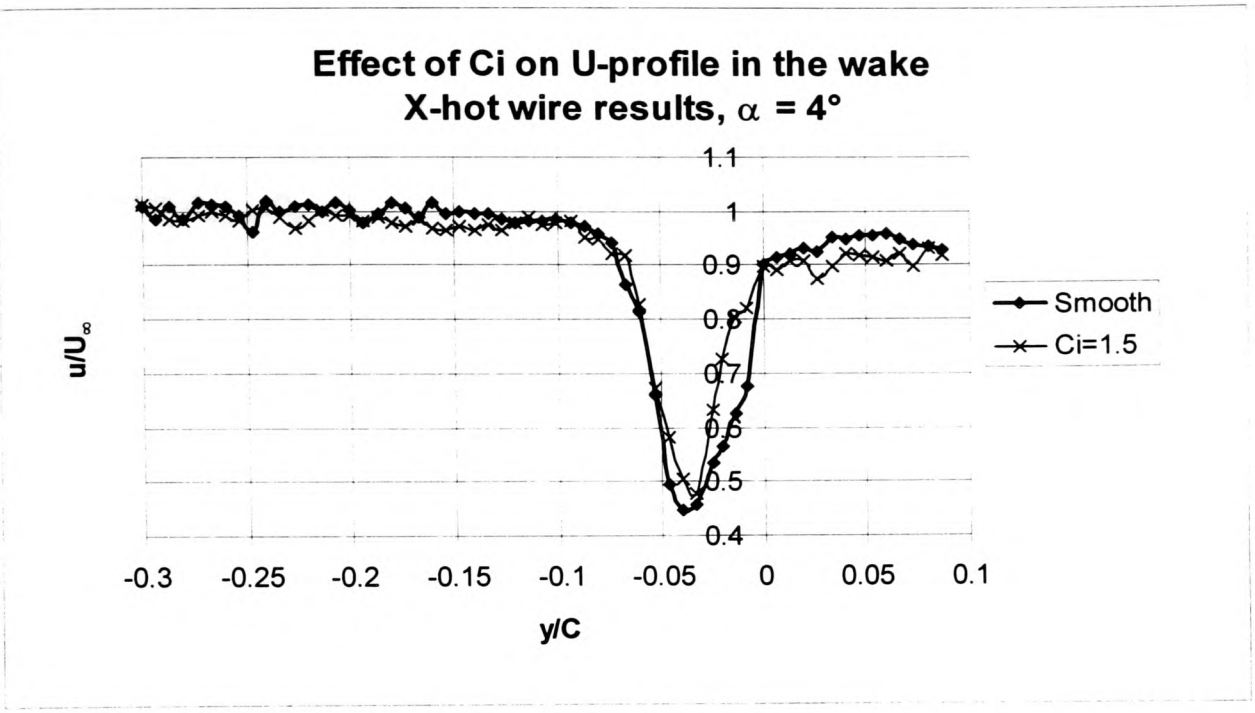

Figure 4-17

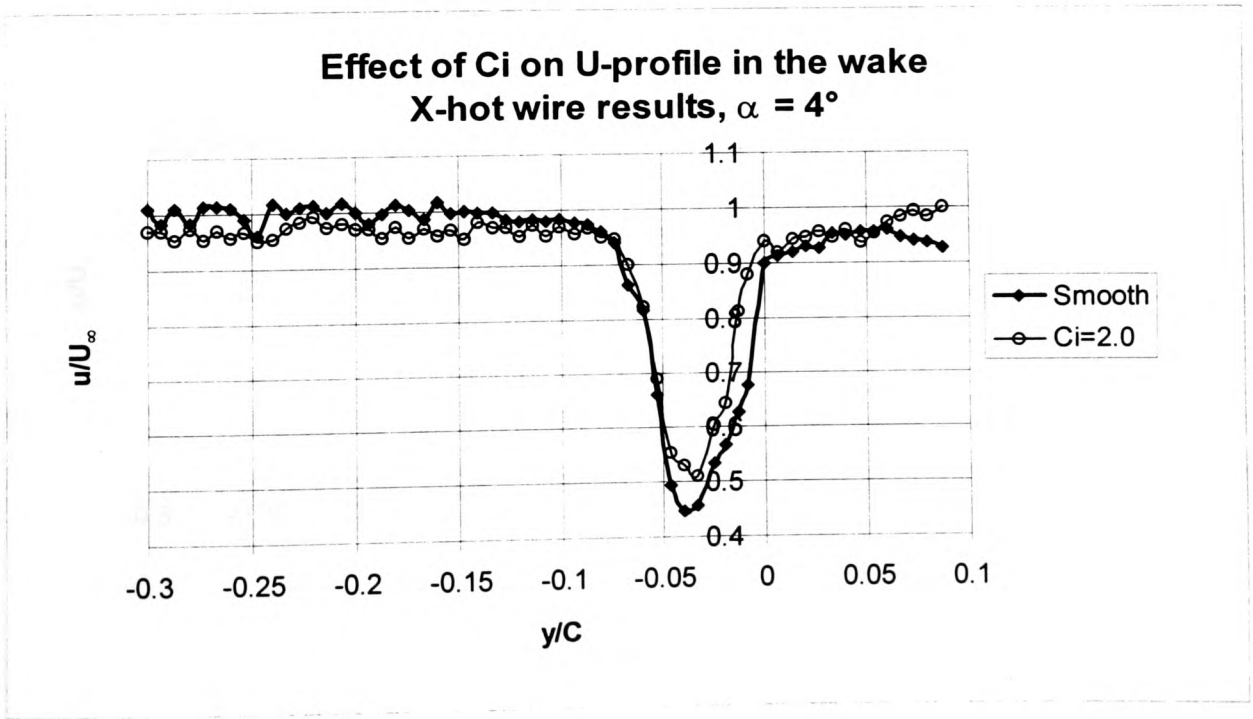

Figure 4-18

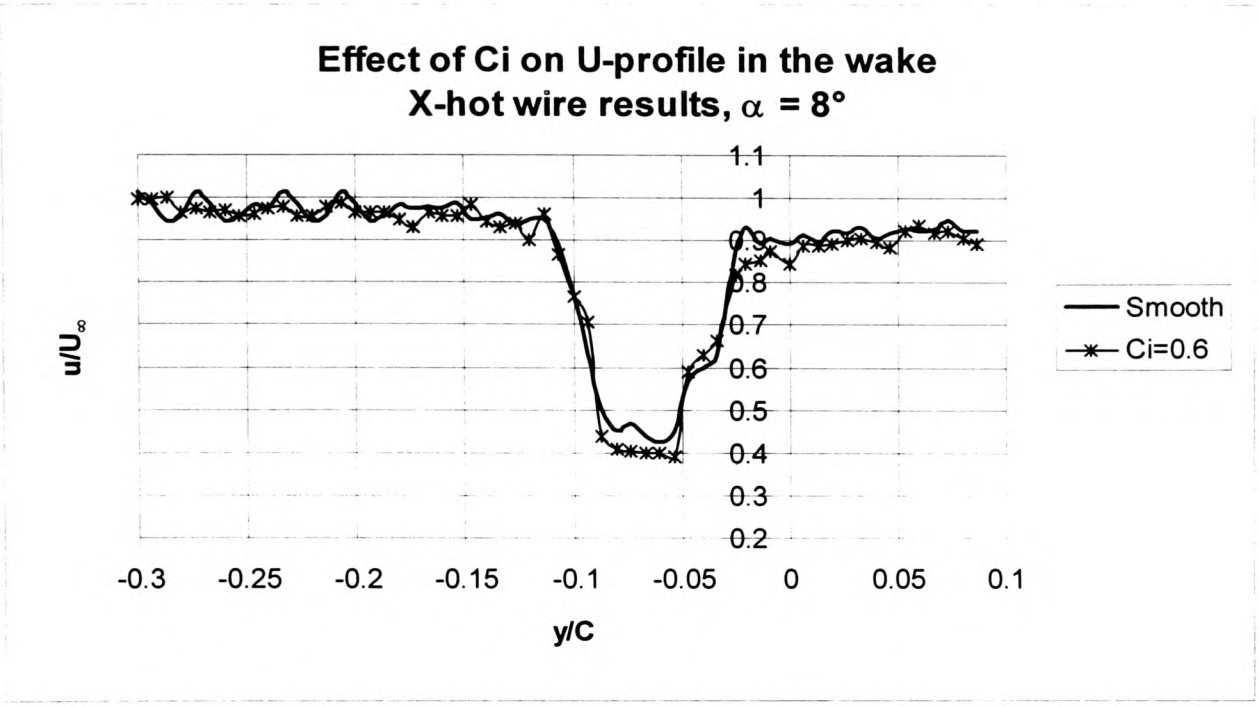

Figure 4-19

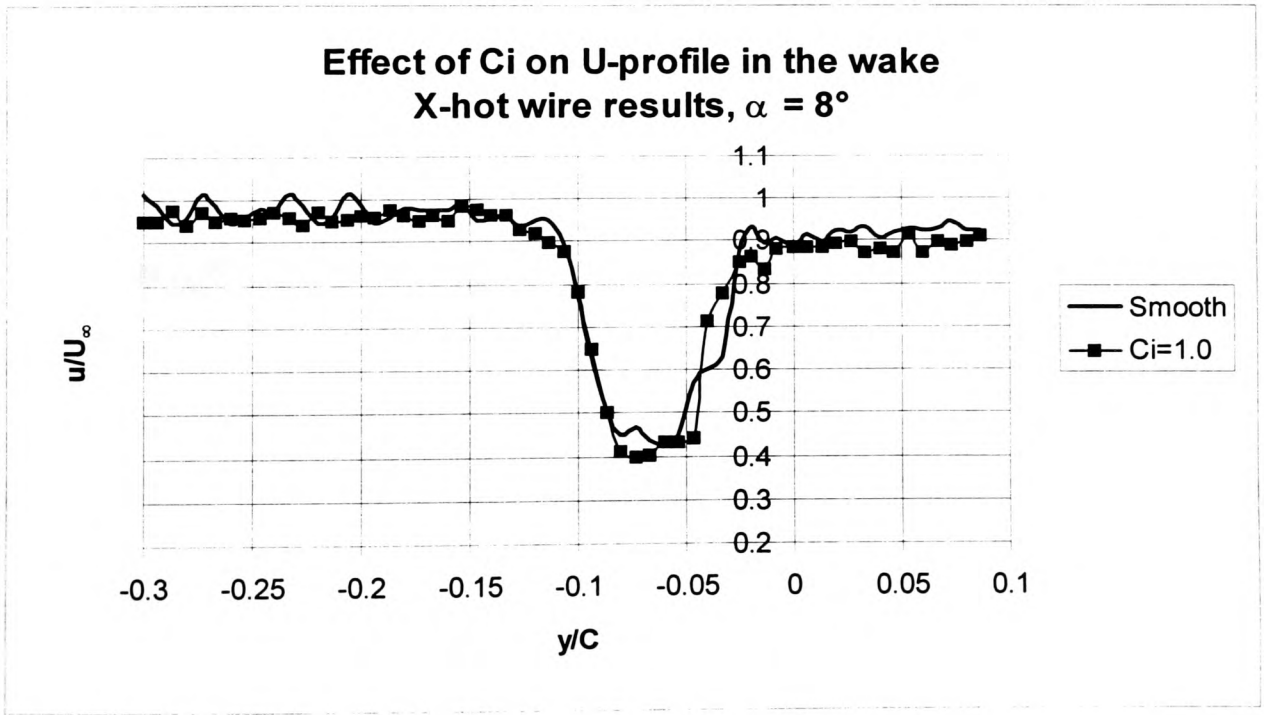

Figure 4-20

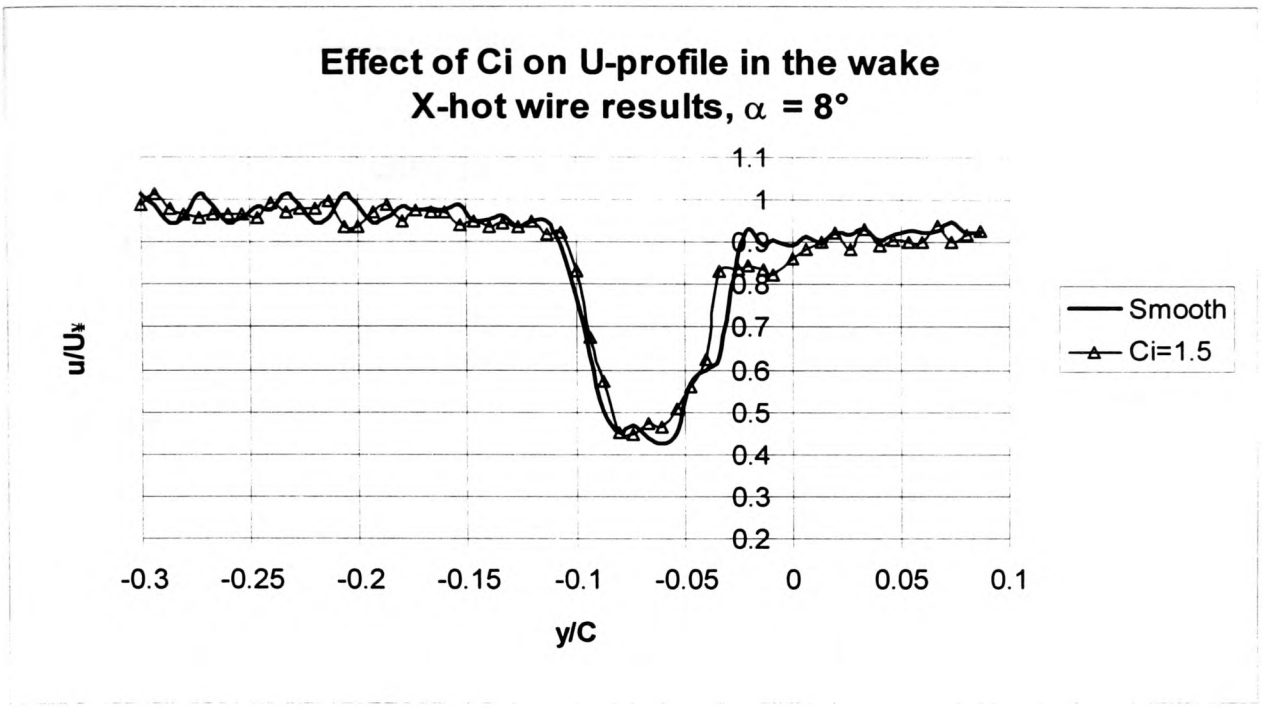

Figure 4-21

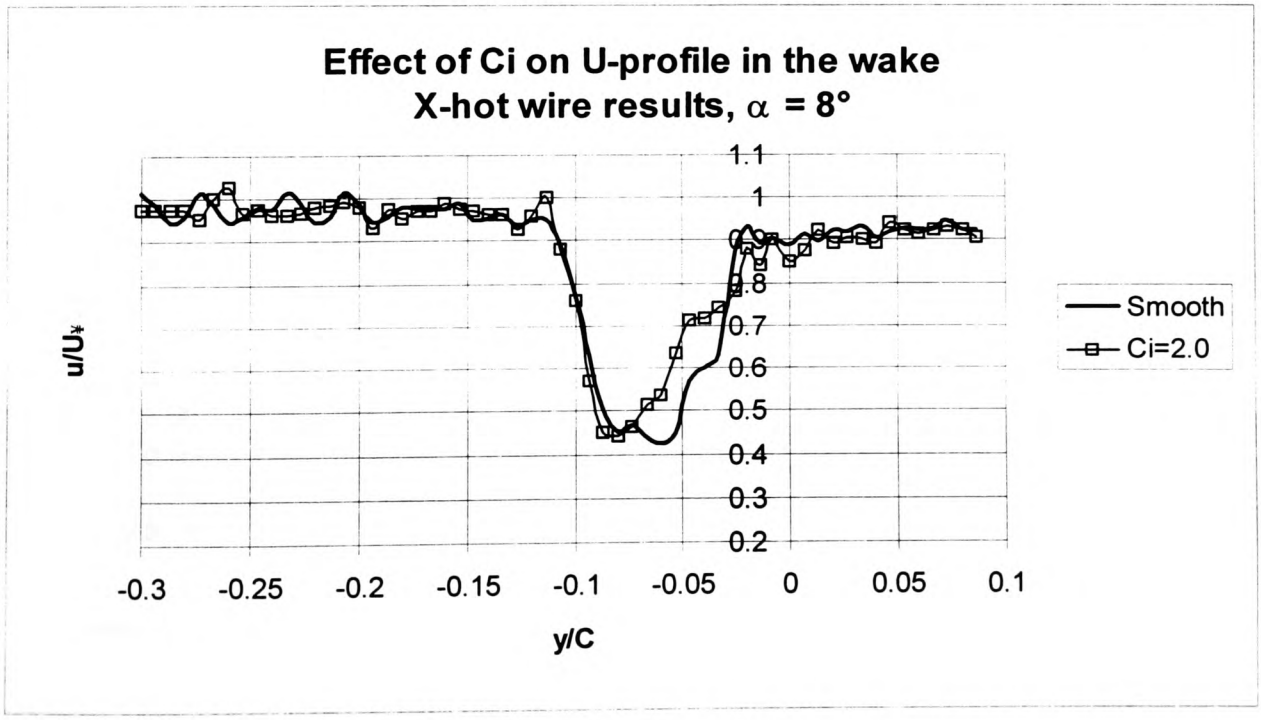

Figure 4-22

4.6.3 Pressure Distribution Results

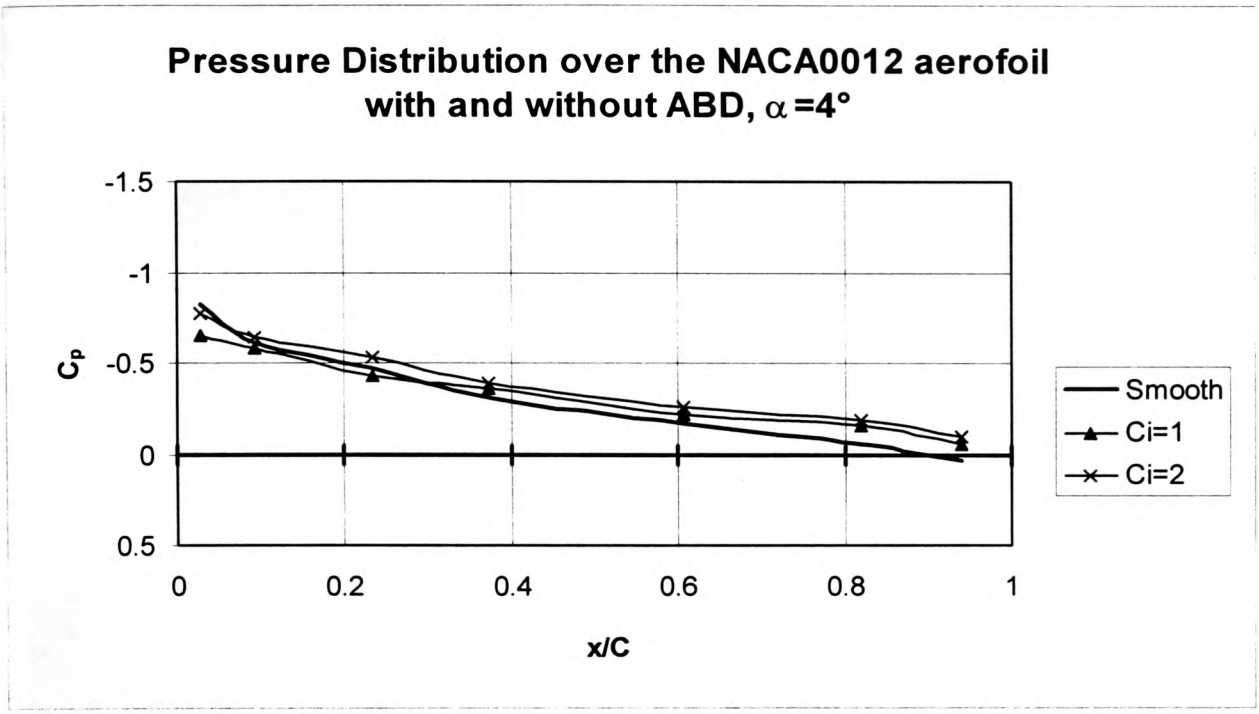

Figure 4-23 Pressure distribution over an aerofoil with and without ABD fitted on its top surface, α=4°

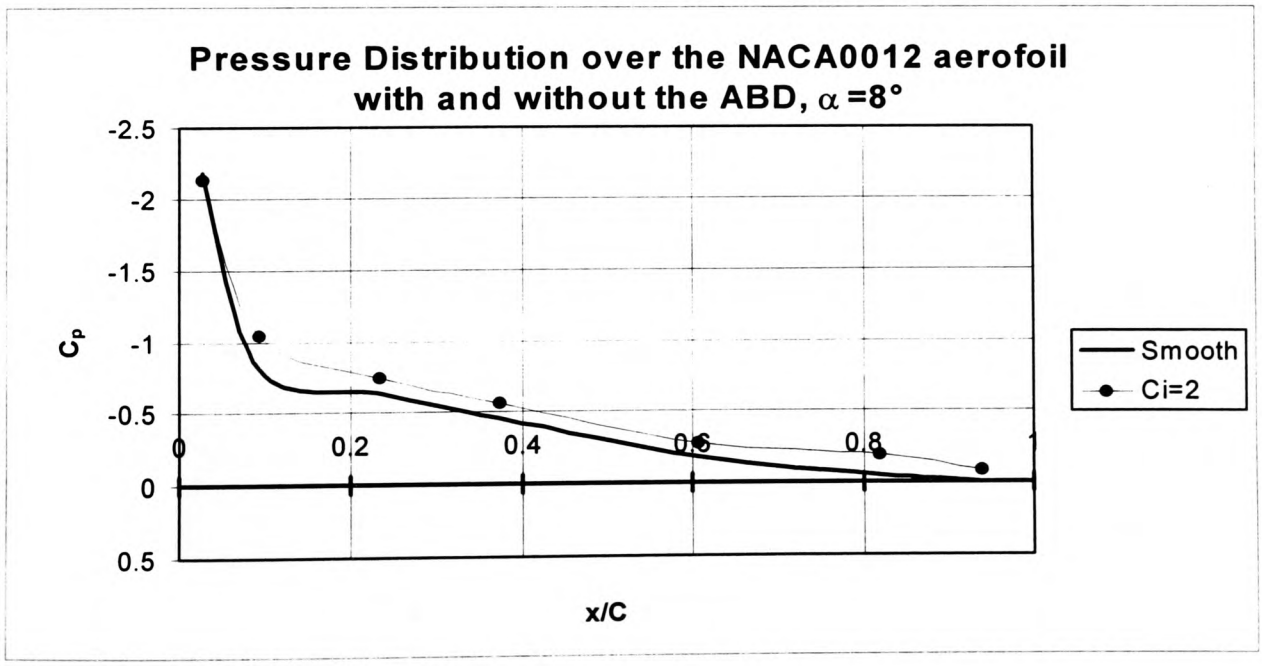

Figure 4-24 Pressure distribution over an aerofoil with and without ABD fitted on its top surface, α=8°

4.6.4 Flow Visualisation

Figure 4-25 Smoke lines over the aerofoil, α=4°, ABD is on

Figure 4-26 Smoke lines over the aerofoil, α=8°, ABD is on

Figure 4-27 Flow visualisation using tufts over an aerofoil, α=2°.

The ABD is off, tufts still attached with the aerofoil surface.

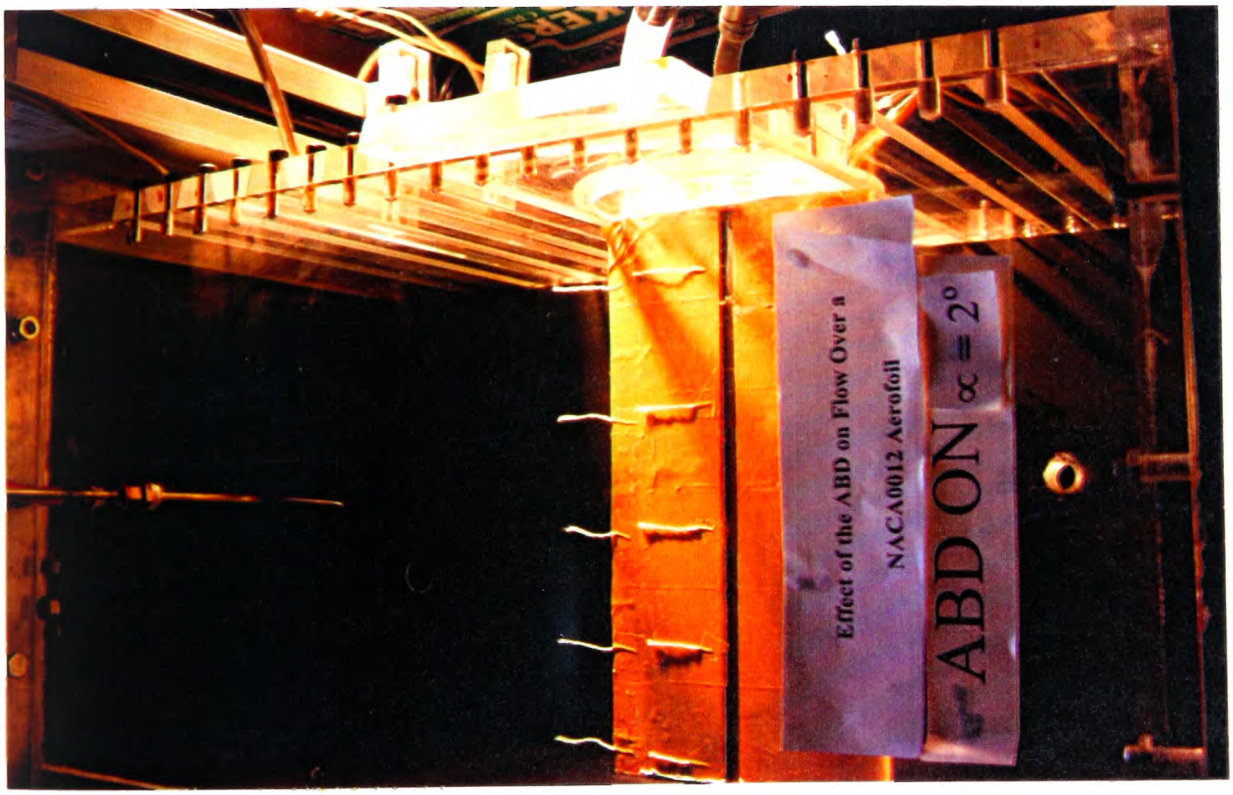

Figure 4-28 Flow visualisation using tufts over an aerofoil, α=2°.

The ABD is on.

Figure 4-29 Flow visualisation using tufts over an aerofoil, α=4°.

The ABD is off, tufts still attached with the aerofoil surface.

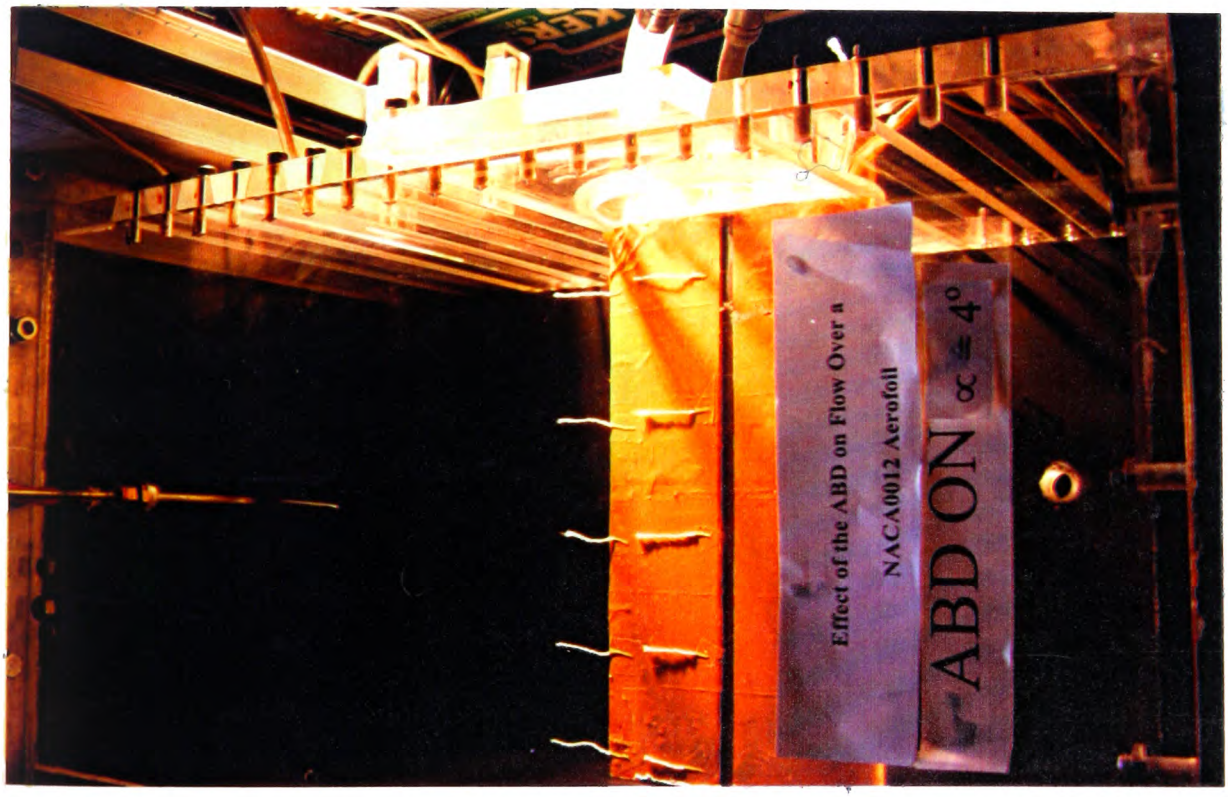

Figure 4-30 Flow visualisation using tufts over an aerofoil, α=4°.

The ABD is on.

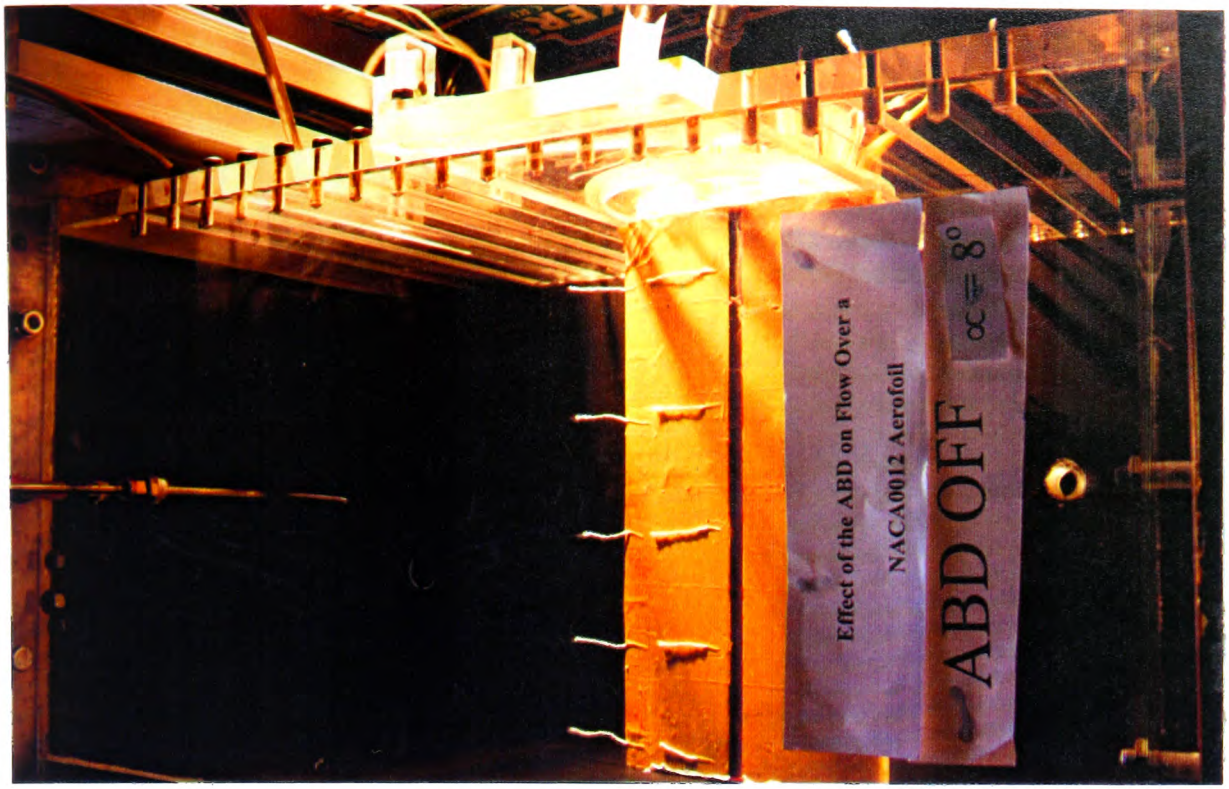

Figure 4-31 Flow visualisation using tufts over an aerofoil, α=8°.

The ABD is off, tufts still attached with the aerofoil surface.

Figure 4-32 Flow visualisation using tufts over an aerofoil, α=8°.

The ABD is on

Figure 4-33 Flow visualisation using tufts over an aerofoil, α=12°.

The ABD is off, tufts still attached with the aerofoil surface.

Figure 4-34 Flow visualisation using tufts over an aerofoil, α=12°.

The ABD is on

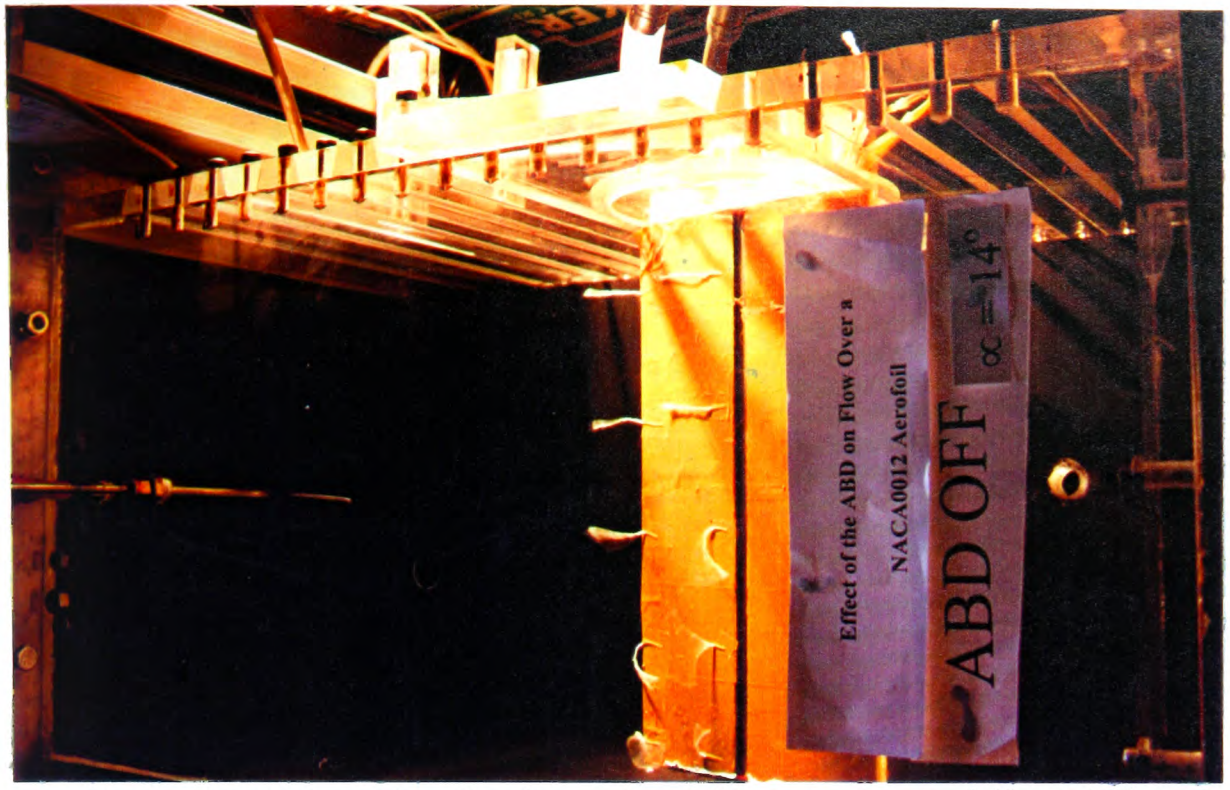

Figure 4-35 Flow visualisation using tufts over an aerofoil, α=14°.

The ABD is off, tufts still attached with the aerofoil surface.

Figure 4-36 Flow visualisation using tufts over an aerofoil, α=14°.

The ABD is on

Figure 4-37 Flow visualisation using tufts over an aerofoil, α=16°.

The ABD is off, tufts still attached with the aerofoil surface.

Figure 4-38 Flow visualisation using tufts over an aerofoil, α=16°.

The ABD is on

Chapter Five

Theoretical Results and Discussion

Chapter Five

Theoretical Results and Discussion

5.1 Introduction

One of the main objectives of the present study was to investigate theoretically the design parameters that influence the effect of the ABD on the flow.

This chapter presents the numerical results obtained by using computational fluid dynamics (CFD) techniques for the cases of the ABD which were studied in this research.

5.2 Justification for the Theoretical Study

The CFD simulation of the fluid-flow problem under investigation was compared with the experimental data in order to justify the CFD study. Two cases of a smooth aerofoil and an aerofoil fitted with the ABD were tested both theoretically and experimentally. The CFD results were found to be in reasonably good agreement with the limited experimental data as shown in Figure 5-1 through Figure 5-6. It should be noted that the general trend of the effect of the ABD on the performance of the aerofoil is similar in both the theoretical and experimental results which are presented in Chapter 4 and 5.

This general agreement which was obtained between theoretical and experimental results provides confidence in the validity of the CFD simulation of the problem under investigation. Consequently, the detailed CFD study of the ABD parameters which follows in this chapter can be accepted as a relative indication of the effect of each of these parameters on the performance of the ABD.

5.3 Theoretical Investigation of The Effect of Different ABD Parameters on the Main Flow

5.3.1 Introduction

The number of parameters that can determine the characteristics of the ABD include (see Figure 2-6):

- The location of the ABD (L_s) ,
- The width of the ABD (S),
- The height of the ABD (H),
- The relative height of the curved base of the ABD (h), and
- The relative flow rolling speed inside the ABD (C_i)

The effect of these parameters on the flow over a flat plate as well as on the flow over an aerofoil is discussed in the following sections.

It should be noted that the optimisation of the performance of the ABD is *not* the main objective of this theoretical study. Instead it is intended to create a clear picture concerning the main factors affecting the performance of the ABD. Optimisation of the ABD performance is a considerable area of research due to the large number of parameters involved and the strong interaction between them. Since the idea of an ABD was introduced for the first time in the present study, the general "behaviour" of the device was clarified before taking a further step towards optimisation. However, the results and their discussion presented in this section can be used as a starting point in the optimisation process.

In the following sections, the discussion is linked to the figures presented at the end of the chapter. In this theoretical study the geometry of the ABD, its location, the angle of attack of the aerofoil, and the flow characteristics inside the ABD are all varied according to Table (5-1) which was also initially presented in Chapter (2).

5.4 Effect of the ABD on the Flow Over a Flat Plate

In this section the case of a flat plate fitted with an ABD is studied, and the effect of the various parameters of the ABD is analysed.

The flat plate cases were tested at a Reynolds number of 4×10^5 based on the total length of the flat plate. This Reynolds number is the same as that in the case of the aerofoil experiments. The dimensions of the flat plate and the ABD used in these cases are presented in Table 2-1.

The results of the flat plate cases are presented in Figure 5-7 through Figure 5-10. These figures present the velocity profiles within the boundary layer at the trailing edge of the flat plate and illustrate the differences in these profiles between a smooth flat plate and one fitted with an ABD.

These figures show the effect of the location of the ABD, L_s, the effect of the width, S, the effect of height, H, and the rolling speed C_i.

In general, these figures show that the ABD has a substantial effect on the boundary layer over a flat plate surface, and by choosing appropriate characteristics for the ABD a significant enhancement of the main flow can be achieved.

The location of the ABD relative to the leading edge, L_s, is an important parameter and Figure 5-7 shows that, in general, reducing L_s provides improved enhancement of the main flow. More discussion of this point will be undertaken in section 5.5.2.

The effect of the width of the ABD, S, is shown in Figure 5-8. The general conclusion of this figure is that increasing S gives greater enhancement to the main flow. This is thought to be due to the larger distance of interaction between the ABD flow and the main stream. Accordingly, for flow over flat plates (or similar applications) it is recommended that S should be increased in order to obtain more enhancement of the main flow. However, for flows over curved bodies, such as an aerofoil, increasing the width "S" beyond certain limits may actually lead to a deterioration in performance. This particular point will be discussed in more detail in section, 5.5.3.

The height of the ABD, H, also has an important effect on the performance of the ABD. This is clear from Figure 5-9. The conclusion of this figure is that increasing H provides greater enhancement to the main flow. This is thought to be due to the higher flow rate associated with the greater height H. For flows over a curved body, it was found that there is an optimum range of H for best performance of the ABD. More discussion of this point will follow in section 5.5.4.

Figure 5-10 shows the effect of the rolling speed of the ABD, C_i. It is clear that increasing C_i can substantially enhance the performance of the ABD and provide greater controlling effect on the main flow.

Overall, it appears that the performance of an ABD on a flat plate may differ from its performance on an aerofoil. This is thought to be due to the existence of an adverse pressure over the surface of the aerofoil. Accordingly, it is likely that the optimum "combination" of ABD parameters for a flat plate will not necessarily provide the best performance with curved bodies. Nevertheless this initial flat plate study indicates that the geometry and flow characteristics of the ABD can markedly affect the performance of the device.

5.5 Effect of the ABD on the Flow Over an Aerofoil

5.5.1 Effect of the Velocity Inside the ABD on the Wake Velocity Profile

In an ABD the injection flow rate should be equal to the suction flow rate so that the flow acts as "roller". The speed of the injected/sucked air inside the ABD is related to the main flow speed U_∞ via the coefficient $C_i=u_i / U_\infty$. As may be expected, it was found that increasing the relative ABD flow speed, C_i, enhances the main stream flow directly. This result can be clearly seen in Figure 5-11 through Figure 5-28. In these figures, the wake velocity profiles were calculated at a distance of $0.13C$ downstream of the trailing edge of the aerofoil. These figures show how the magnitude of the minimum velocity in the wake is shifted to higher values as the relative "rolling" speed increases. This means that the "tired" flow in the wake region is energised so that wake recovery occurs over a shorter distance behind the aerofoil. Integration of the areas under the wake-velocity profiles indicate that the energy supplied to the "most tired" flow is re-distributed from the free stream flow (i.e. the flow outside the wake region). This can be observed in the figures where the velocities in the free stream away from the relatively narrow, low speed wake region are decreased as the wake recovery is enhanced due to the application of the ABD.

It is clear that installing the ABD on the top surface of an aerofoil without any flow (i.e. $C_i=0$) results in a cavity in the surface. A circulation of part of the main flow will be induced inside the cavity so that the main stream flow will loose part of its energy. This effect will also occur in an ABD so that the presence of the ABD geometry leads to

some loss in the energy of the main stream flow. To overcome this effect, C_i must be high enough so that it energises the main flow not only to compensate for the loss in energy but also to provide an enhancement to the main flow. According to this simple discussion it would be expected that a flow of C_i=1 will lead to some loss of flow energy. It appears that with C_i=1 the gain from the ABD is less than the loss associated with the presence of it. On the other hand, at higher values of C_i the gain from the ABD is sufficiently high enough not only to overcome the loss but also to enhance the main stream flow substantially.

By inspection of Figure 5-11 through Figure 5-28, it is clear that the same value of C_i gives different results depending on other parameters which differ from geometry to geometry. However, as a general conclusion, increasing the value of C_i leads to greater enhancement of the main stream flow. Increasing the value of C_i means that more energy is required to maintain the flow "injected" into the ABD, and therefore, the overall benefit from using the ABD should be compared with the cost of providing the energy to the "rolling" flow. This comparison be necessary to determine the applicability of the ABD technique in a particular application.

It can be concluded from comparing the data for the same geometry at different angles of incidence that whilst the ABD enhances the flow at high incidence it gives greater enhancement at lower angles. However, the flow is enhanced at almost all angles of attack except at an angle of 14° where separation of flow occurred even when using the ABD. It should be kept in mind that an angle of 14° is well within the stall region for the particular aerofoil section used in the tests. Beneficial effects were obtained even at this high angle of attack by fitting more than one ABD on the top surface of the aerofoil since their effects are approximately additive. This will be discussed in a later section dealing with twin ABDs at high angles of attack.

It is apparent that the main stream flow can be controlled by changing C_i and therefore this feature can be used in practice in order to increase the lift during departure and landing. This will enhance the role of flaps and/or slats.

5.5.2 Effect of the Location (L_s) of the ABD on the Wake Velocity Profile

The ABD was located on the top surface of the aerofoil at a distance L_s from the leading edge. This distance was found to have a limited effect on wake recovery, see Figure 5-

29 through Figure 5-64. The general trend from these figures is that the cases with smaller L_s often provided better performance than the system with high L_s since the minimum speed in the wake region is frequently higher for the cases of low L_s. This is again due to "re-distribution" of momentum from the outer region of the wake to the minimum-speed region as illustrated by the reduction in the speed in the outer region.

It is not clear why the location L_s affects the behaviour of the ABD. In an attempt to explain this effect, it should be noted that the boundary layer thickness increases with downstream distance from the leading edge. The flow associated with the larger boundary layer looses more energy than the flow at smaller thicknesses. However, the growth of the boundary layer is interrupted by the presence of the ABD and a new boundary layer will reform. By reducing the value of L_s the ABD will be located in the region in which the boundary layer is relatively thin. The flow is then enhanced and it will have a thinner boundary layer than in the smooth case. This will ensure that the energy loss due to friction is lower and consequently the main stream flow will have more momentum. Overall, however, over the range simulated in this present study the position of the ABD has relatively little general effect.

An important consequence of this result is that the ABD can be installed near a thick section of the aerofoil. This will provide more space for installation of the device and associated piping for the injection/suction air especially if this technique is applied to small sections.

Over the leading part of the aerofoil the pressure gradient is favourable and an adverse pressure only ensures further along the section. Thus whatever the optimal location it should be noted that the ABD *must* be located downstream of the point of minimum pressure. This usually occurs after the point of maximum thickness when an aerofoil is at 0° angle of incidence. As the angle of incidence increases the point of minimum pressure advances towards the leading edge.

5.5.3 Effect of the Width of the ABD (S) on the Wake Velocity Profile

Figure 5-65 to Figure 5-88 show the effect of the width of the ABD on the wake flow. In these figures it is clear that the influence of the ABD is strongly affected by this parameter. The near-wall fluid flows tangential to the flow inside the ABD and consequently becomes the part of the main flow which is most energised by the ABD. The transfer of

energy from the ABD to this near-wall flow takes place through the interaction between the two flows. Accordingly; it can be said that as the area of interaction between the ABD and the main flow increases the energy transferred to the main flow will increase. This can be translated directly into a preference for higher values of *S*. This effect is clear with high values of C_i (i.e. high relative rolling speeds) where an increase in the width *S* leads to larger minimum velocities in the wake, see for example Figure 5-67 and Figure 5-68.

On the other hand, the larger the width of the ABD the greater the interruption which will be caused to the main flow unless C_i is high enough. As discussed in the previous sections, it is necessary for the ABD to compensate for the geometry-obstruction to the main flow and also enhance this flow. When *S* is large the compensation for the geometry-obstruction becomes more demanding. This may explain the behaviour illustrated in the figures for low C_i, for example Figure 5-70 and Figure 5-73. In these figures, the curves for large values of *S* show poor performance when compared with the cases for small *S*.

In practice, there may be some scope for optimising the value of *S* to minimise C_i. Another reason for using smaller widths is that the flow inside the cavity may depart from the ABD region and interrupt the main stream flow if the width is too large. If this occurs, one of the main criteria for the ABD, (i.e. the device should not interrupt the main flow), will be lost and the ABD may promote separation. This will be similar to the case of injection, where promotion of separation is one of the main disadvantages.

It is also apparent from Figure 5-65 through Figure 5-79 that the behaviour of the ABD depends on both of these parameters so that any optimisation process will need to consider not only the individual values of these parameters but also their interaction.

5.5.4 Effect of the Height of the ABD (*H*) on the Wake Velocity Profile

The Height of the ABD (*H*) is a very important parameter since it determines the amount of the flow that should be injected into and removed from the ABD. For a given value of C_i, a large height results in higher flow rate and consequently higher power is required to drive the ABD. For a small values of height less power is required to provide the same value of C_i. However below a minimum value of *H* the injected air will be

choked so that the power consumption will increase with no corresponding increase in C_i.

From another point of view, it is preferable to keep H as small as possible to reduce the geometrical obstruction to the main flow and to extend the applicability of the technique to small-size aerofoils. Nevertheless, the injection holes or slots must be manufactured so that the upper tip is as small as possible. The best configuration of the ABD is one in which the flow virtually occupies all the height on both the injection and suction sides. The problem of minimising the influence of the tip of the ABD is similar to problems found in the injection technique, (Henfer and Bushnell, 1990).

Whilst Figure 5-89 and Figure 5-90 indicate that slightly better performance is obtained with H=0.027 it is clear that over the range simulated in the present project that changes in H have little effect on the minimum wake velocity. This result indicates that the volumetric-flow rate inside the ABD is relatively unimportant and it is the rolling speed (i.e. C_i) which is the dominant factor. More detailed study may well be necessary to clarify the effect of the H on the performance of the device.

5.5.5 Effect of the Relative Height of the Curved Base of the ABD (h) on the Wake Velocity Profile

One of the parameters which was found to be of a particular interest and can play an important role in the influence of the ABD on the main flow is the relative height of the base, h, see figure 2-6. Most of the cases examined in the theoretical study were for a flat base. However, the interaction between the main flow and the flow inside the ABD was found to be affected by the shape of the base of the ABD. If this base has a convex shape, the flow inside the ABD is "forced" to interact with the main flow more strongly so that more energy is transferred to this main flow. However, if the curvature is too high then the angle of injection will be increased to such an extent that the main flow may be badly interrupted and separation may occur as a result at the location of the ABD. Another problem associated with high convex radius of curvature of the base of the ABD is that all the injected flow may not be entrained into the suction side, i.e. the rolling action of the device will no longer be satisfied. This is due to the high inertia of the injected flow. This effect is likely to promote separation since this is usually associated with the normal injection technique, (Merkle and Deutsch, 1990). In the light of the

above discussion it would appear that optimisation of the relative height is necessary to balance the two conflicting effects. It is likely that there is a certain range of curvature which can provide a strong interaction between the two flows inside and outside the ABD without adversely interrupting the main flow.

Figure 5-91 and Figure 5-92 appear to support this argument to certain extent. At an angle of incidence of 4° it was found that the optimal relative height h=0.0007. However, the effect of changing h is less clear at a higher angle of incidence of 8°. However, a convex base was used in the experimental cases to attempt to get better performance from the ABD. Once again further work is probably necessary to clarify the optimal effect.

5.5.6 Effect of C_i on the Drag Coefficient C_d

Since the drag coefficient depends solely on the velocity profile in the wake region, the arguments in section 5.5.1 on the effect of C_i is applicable in this section. However, the relationship between wake velocity profiles and drag coefficient is not always clear since whilst velocity recovery in the centre of the wake may be improved there is often lower velocity in the major part of the wake region. Thus it was necessary to examine the effect of the ABD on drag coefficients directly. Figure 5-93 through Figure 5-110 presents the effect of C_i on C_d. Generally as C_i is increased C_d decreases. However, for lower values of C_i (e.g. C_i=1) there is an initial increase in the drag so that value of C_d is often higher than that in the smooth case. As discussed previously, the reason for the poor performance of the ABD at C_i=1 is that the ABD at this speed ratio is not able to compensate for the geometrical-drag penalty. This result of an initial increase in drag agrees with the effect of C_i on the velocity profile in the wake region as discussed in section (5.4). It can also be said that the reason for the decrease of C_d with increasing C_i is most likely because of the extra energy given to the main flow. This replaces part of the energy lost by the effect of friction, and also reduces the adverse pressure gradient as will be seen in later sections.

5.5.7 Effect of the Width of the ABD (S) on the Drag Coefficient

Figure 5-111 through Figure 5-122 show the effect of the width of "S" and location of the ABD "L_s" on C_d. In all these figures, the negative values are better since it means that C_d with an ABD is lower than C_d for the smooth case. Although the number of cases

examined theoretically is quite large, it was difficult to fully cover all of the parameters so that the above figures contain only two points for the location of the ABD, L_s.

It can be deduced from these figures that a larger width S generally results in a lower C_d .In virtually all cases the greater drag reduction is obtained with S=1.0 although in a few cases S=0.8 give slightly better performance. As already explained in section (5.5.3) this may be due to the larger distance over which the two flows interact with each other so that more energy is transferred to the main flow. The effect of changing S can be more clearly seen in these drag coefficient curves than from the velocity profile data.

Choosing an appropriate value of the width "S" of the ABD can markedly affect the efficiency of the device. As an example, in Figure 5-119 changing the value of S from 0.04 to .067 can increase the reduction in drag coefficient from 4 to % 22% of the smooth case value.

It is also clear from the figures that lower values of L_s generally results in greater reductions in drag coefficient although as mentioned earlier the range of ABD positions which were simulated is very limited at present.

5.5.8 Effect of the Height of the ABD (H) on the Drag Coefficient

Figure 5-123 and Figure 5-124 present the effect of changing the height of the ABD on the values of C_d. These two figures show more clearly than the velocity profile data that there is an optimum value of H within the range tested at which the ABD has the best efficiency. However for a given value of C_i the flow rate and hence the power consumption will also increase as the height is increased.

5.5.9 Effect of the Relative Height of the Curved Base of the ABD on the Drag Coefficient

Figure 5-125 and Figure 5-126 show the effect of changing the curvature of the base of the ABD on the drag coefficient. It is clear from these two figures that changing the geometry of the base of the ABD has a significant effect on the performance of the system. The effect of changing the radius of the base is somewhat different at different angles of incidence. For example, the reduction in drag at h=0.0013 dropped from about 20% at α=4° to around 10% at α=8°. In both cases it was found that larger values of relative height appeared to be beneficial.

In practice, the parameter, h, could be dynamically changed according to the flow circumstances by using a flexible material for the base of the ABD which can be adjusted through a simple mechanism.

5.5.10 Effect of C_i on the Pressure Distribution

In previous sections, the velocity profile at the wake region was used to study the effect of the important parameters of the ABD on its performance. In order to complete the study of the aerofoil fitted with an ABD, the pressure distribution should be considered. In fact, pressure distribution is one of the most important means of distinguishing the performance of wing sections. From the pressure distribution, the lift force and pitching moment can be calculated. The importance of the pressure distribution can be gauged from the application of a new CFD technique called "the reverse method" which is widely used nowadays (Rubbert, 1994). This technique uses the pressure distribution as an input to the program and the output is the geometry of the aerofoil which will give that pressure distribution.

This section presents the effect of various designs of ABD on the pressure distribution over an aerofoil and on the lift coefficient. Figure 5-127 through Figure 5-138 show the pressure distribution C_p over the aerofoil.

The presence of the ABD on the top surface of the aerofoil causes the pressure to decrease initially at the beginning of the ABD due to the high velocity in the injection side. At the suction side, particularly at the corner, the flow is obstructed when it reaches the edge of the ABD causing the pressure to increase. To a certain extent, the shape of the pressure distribution inside the ABD is not important; the important quantity is the *average* pressure distribution over the aerofoil. If the average pressure is less than the smooth case it means that the ABD contributes to a reduction of the pressure over the top surface of the aerofoil; whilst if the average pressure is more than the smooth case it means the opposite. As any increase in pressure is undesirable, part of the enhancement of the main flow will be *consumed* in compensation for this increase. However, it was found that as C_i increases the average pressure over the ABD decreases.

The general tendency of the pressure distribution curves shows that the pressure over the upper surface is lower, in all cases examined, than its value for the smooth cases. This translates to larger differences between the pressure on the two sides of the aerofoil and,

consequently, higher lift. As the value of C_i increases this pressure difference increases. This is true for all the cases tested although it should be noted that the geometry of the ABD determines the amount of enhancement given to the pressure distribution and hence to the lift coefficient.

It is important to note that the enhancement in pressure distribution (and consequently the lift) results from two effects. The first one is a decrease in boundary-layer thickness over the aerofoil (since an increased boundary layer thickness decreases the lift and increases the profile drag). The second effect is the pressure drop caused by the ABD itself especially at high values of C_i. Both effects combine together to produce the positive outcome from the ABD.

The ABD only affects the velocity profile just after its location whereas the effect on the pressure distribution occurs virtually over the whole chord length. This leads to significantly enhanced lift but, at the same time, may change the pitching moment characteristics of the aerofoil.

5.5.11 Effect of the Location of the ABD, L_s, on the Pressure Distribution over an Aerofoil

Examination of the pressure distribution gives more details about the "history" of the flow over the surface of an aerofoil. In fact the interaction of the flow inside the ABD with the main flow and hence transfer of energy to the main flow can be noted from the pressure distribution curves. Figure 5-139 through Figure 5-162 presents the effect of L_s on the pressure distribution over an aerofoil. Two values of L_s were used, L_s =0.413 and L_s =0.58, and comparisons were made at different values of C_i, α, and S.

It can be seen from these figures that the lower value of L_s (0.413) generally gives better performance. This results from the increase of the negative value of pressure distribution and from the size of the interaction of the ABD. This interaction can be determined from the change in pressure inside the ABD itself. This can be understood as the main flow "sensing" the flow inside the ABD when L_s is short more than in the case of the longer L_s. The pressure distributions indicate that locating the ABD closer to the leading edge increases its efficiency; particularly with lower values of C_i, see for example Figure 5-139 to Figure 5-141 for α=4° and Figure 5-151 to Figure 5-154 for α=8°. Whatever the

best value of L_s, it should be noted that the ABD *must* be located downstream of the point of minimum pressure.

It is clear that the pressure distribution is improved both upstream and downstream of the ABD. In general, the upstream improvement is more significant particularly in the case of the lower L_s. This change in pressure distribution will be important in calculating the bending moment. As already discussed in section 5.5.2 it is thought that the reason for this enhancement at low L_s is that the flow loses more of its energy due to the growth of the boundary layer and hence early interruption of this layer and subsequent restarting of a new layer leads to greater reduction in energy losses. Since the adverse pressure is higher at large angles of incidence, the growth of the boundary layer is much faster over the top surface. Accordingly, an ABD located at the same distance L_s, gives less improvement at higher angles. This is clear from comparing Figure 5-139 to Figure 5-150 with the corresponding Figure 5-151 to Figure 5-162. It should be noted that at a high angles of incidence (e.g. 14°) the adverse pressure gradient is so high that separation is unavoidable despite the presence of the ABD. The solution to this problem may well be fitting more than one ABD as will be discussed in a later section.

5.5.12 Effect of Width of the ABD, *S*, on the Pressure Distribution over an Aerofoil

As discussed previously in section 5.5.3 two conflicting effects exist with regard to the width of the ABD, S. Higher values of S enable more interaction between the main flow and the flow inside the ABD, and consequently leads to a higher efficiency for the system. However, higher values of S can lead to greater interference with the main flow. This is clear, again, from consideration of the pressure distributions in Figure 5-163 to Figure 5-178. The greater improvements in the pressure distribution are noted for the cases associated with higher values of S. At the same time, at these high S values there are maximum interruptions to the main flow as can be seen from the large changes in pressure distribution inside the ABD. This disadvantage associated with large values of S is thought to be more significant at higher angles of incidence, α, where the flow is more "ready-to-separate". In these cases separation of the main flow may be promoted by the interference caused by the ABD. Moreover, the enhancement offered by the ABD

is not large enough to "draw back" the flow and promote reattachment at the surface. Accordingly, a compromise value of S should be found.

5.5.13 Effect of the Height of the ABD, H, on the Pressure Distribution over an Aerofoil

Figure 5-179 and Figure 5-180 show the effect of the height of the ABD, H, on the pressure distributions. The higher values of H lead to greater disturbances of the flow inside the ABD whilst there is little significant effect on the pressure distribution over the aerofoil. Hence it can be said that the pressure distribution over an aerofoil is relatively insensitive to the height H. The effect of changing H is essentially confined to the region of the ABD. As a conclusion, it can be said that using a small values of H produce relatively little interruption to the main flow, and a low flow rate and hence power consumption inside the ABD

5.5.14 Effect of the Relative Height of the base of the ABD, h, on the Pressure Distribution

The effect of h on the performance of the ABD has already been discussed when describing its influence on the wake velocity profiles and on the drag coefficient. The effect of h on the pressure distribution is significant as can be seen from Figure 5-181 and Figure 5-182. Choosing a correct value of the relative height h leads to strong interaction between the flow inside the ABD and the main flow and, at the same time, avoids the large interruption to the main flow caused by injecting the flow to the ABD at a high injection angle. From the three cases tested, h=0.007, 0.013, and 0.20, the value of h=0.013 was found to produce the best performance. Changing h has less influence as the incidence angle, α, increases. This can be shown by comparing Figure 5-181 (at α=4°) with Figure 5-182 (at α=8°). This confirms the existence of a strong interrelation between the different parameters of the ABD and the flow characteristics.

5.5.15 Effect of C_j on the Lift Coefficient, C_l

The lift coefficient C_l describes the ability of the aerofoil to create lift force, which is the main function of the these devices. The lift can be improved through proper choice of the section-geometry of the lifting device (i.e. the thickness, camber...etc.); or by controlling the flow. Controlling the main flow by using an ABD shows substantial promise

in terms of increasing the C_l of an aerofoil. The use of the ABD appears to be an effective flow-control technique which can increase the value of C_l substantially.

Figure 5-183 through Figure 5-194 shows that C_l can be increased significantly by increasing C_i. When C_i=1, however, the lift coefficient is lower than that of the smooth case. However, increasing C_i up to a value of 2.5 can increase C_l by up to 30% depending on the geometry of the ABD and its location. Since the pressure distribution over an aerofoil was improved by increasing C_i, as already discussed in a previous section, the lift coefficient was expected to be improved accordingly. However, the existence of the ABD on the top surface (suction side of the aerofoil) is associated with a considerable change of the pressure distribution over the region of the ABD. In this region, the pressure changes its value from a large negative value to a large positive value before returning back to its value at the surface. The difference between these two values is significant compared with the difference between the two surfaces of the aerofoil. In fact, only integration of the pressure over the whole surface of an aerofoil can show the net effect of the ABD on lift; this is because the integration will include all the values over both sides of the aerofoil. The lift coefficient is the result of this integration, and, therefore, can be considered as an accurate measure of the net influence of the ABD on the main flow.

The lift coefficient was calculated by integrating the pressure coefficient C_p over the chord of the aerofoil as discussed in Chapter 2.

5.5.16 Effect of the Width, S, and Location of the ABD, L_s, on the Lift Coefficient, C_l

Changes in the lift coefficient, C_l, provide more details about the effect of the location of the ABD, L_s, on the flow-control process. In a previous section 5.5.7 it was found that the lower values of the L_s gave greater reductions in drag coefficient, C_d. However, in Figure 5-195 to Figure 5-204 it is clear that the optimal position of the location L_s depends on the values of S. For small values of S, the lower value of L_s provides better performance, while for some of the larger values of S, it appears that higher values of L_s are better. There is a certain value of S=0.058, in the middle of the values tested, at which changing L_s has very little effect.

C_l / C_d is the ratio which is used to describe the overall lift-performance of an aerofoil. Accordingly, any improvement in lift only or drag only does not necessarily mean improvement in the performance of the aerofoil. However, if the ABD is fitted to a surface of a non-lifting device, such as wind tunnel wall, reduction in drag coefficient may be sufficient criterion to measure the improvement of the performance of the ABD.

5.5.17 Effect of Height, *H*, and Relative Height, *h*, of ABD on Lift Coefficient C_l

The discussion of the effect of these two parameters, H and h, on the pressure distribution in the previous section, (5.5.14), is also applicable here too. Figure 5-205 to Figure 5-208 show the effect of changing the values of H and h. In these figures, it is clear that there is an optimum range of the values of these two parameters from the values tested, (i.e. h =0.013 and H=0.20). Optimisation of these values as well as studying their inter-relation with other parameters is a field for further research.

5.6 Flow Visualisation

Drawing the stream function contours can provide a clear view about the flow pattern around an aerofoil. Therefore, it was important to draw these contours over the aerofoil which was simulated in the present study with and without the ABD. Figure 5-209 through Figure 5-220 show the stream function contours over an aerofoil at α=4°, 8°, 12°, and 16°. In the figures for the low angles α=4° and 8° the flow is fully attached to the surface of the two cases of an aerofoil. Since the effect of the ABD in this range of α is to enhance the "already attached" flow, the significant enhancement is not apparent from the stream line contours. As the angle α increases, it can be shown that the ABD "pulls" the main stream flow towards the aerofoil surface and that the effect of this "pulling" continues from the location of the ABD until the trailing edge. This translates in prevention (or delay) of trailing edge separation. Comparison of the smooth cases with the corresponding ABD-cases shows the effect of the ABD on the distribution of streamlines at the trailing edge. For the case of α=12° the flow over a smooth aerofoil is "ready to separate" due to the large adverse pressure. Putting only one ABD on the aerofoil can clearly remove the tendency to separation and keep the flow attached to the aerofoil surface. It was found, however, that it was necessary to fit two ABDs in order to ensure full attachment of the flow at higher angles of incidence α=14° and 16°. For the

case of α=14° and α=16°, (well beyond the onset of stall for this aerofoil section), twin ABDs were able to keep the flow attached to the surface of the aerofoil. Accordingly, it can be said that using the ABD technique it was possible to postpone the onset of the stall from 12° to 16°.

It is important to note, however, that in all these figures the ABD did not interrupt the main flow and the injected air to the ABD was completely removed from the suction side. This can be seen from the patterns of the stream lines and velocity vectors (see Figure 5-219 and Figure 5-220 where no interference occurred between the stream lines inside and outside the region of the ABD. It can be said, therefore, that the ABD flow is essentially isolated from the main flow.

5.7 More than one ABD

At high angles of attack, aerofoils experience a stall condition at which the drag increases substantially and the ratio C_l / C_d decreases significantly. This type of stall is usually caused by massive trailing-edge separation at higher angles of attack. Introducing a single ABD has been shown to successfully enhance the performance of an aerofoil by increasing the lift and decreasing the drag. These two benefits are useful also in extending the operating range of the aerofoil by postponing the stall to higher angles. Beyond certain angles, however, separation occurs on the trailing edge of an aerofoil even when the ABD is fitted. In this situation it is useful to fit more than one ABD. This idea was tested theoretically and appeared to work efficiently. Beyond 14° the NACA0012 aerofoil definitely enters the stall region. However, introducing two ABD's can reattach the flow to the aerofoil and produce a high ratio of C_l / C_d. This is clear by comparing the stream lines in Figure 5-215 through Figure 5-218.

5.8 Power Consumption of the Air Bearing Device (ABD)

The injection and removal of air within the ABD will require provision of auxiliary power. This additional power requirement will reduce the benefits of any reduction in drag and improvements in lift. Consequently it is important to estimate this additional power consumption.

The air injected through the injection side of the ABD is withdrawn from the suction side. Due to the similarity in geometry between the two sides, the power consumption by each of the two processes can be assumed to be the same. Therefore;

$$P^*_{suc} = P^*_{inj} = P^* \qquad (5\text{-}1)$$

But

$$P^* = P_{total} * \dot{m}/\rho \qquad (N/m^2\ kg/sec\ m^3/kg = W) \qquad (5\text{-}2)$$

Where P_{total} is the total pressure required to overcome the flow resistance in the ABD and $\dot{m}$ is the mass flow rate. At the exit of the injection side the total pressure provided by the pump is converted solely to a dynamic head equal to $u_i^2/2$. Thus;

$$P^* = P_{total} * \dot{m}/\rho \quad (N/m^2\ kg/sec\ m^3/kg = W)$$

$$P_{total} = \rho\, u_i^2/2 \qquad (5\text{-}3)$$

$$\therefore P^* = \dot{m} \times u_i^2/2 \qquad (5\text{-}4)$$

Since this calculation is only intended to provide an estimate of the power consumption it has neglected pressure losses in the ABD itself.

5.8.1 Calculations of the Power Required in the Laboratory Experiment

From the dimensions of the injection throat for

$U_\infty = 30$ m/sec,

for $C_i = 1.5$, $u_i = 45$ m/sec

and for a slot area of 60 mm^2

$\dot{m} = 60\times10^{-6}\times45 \times 1.21 = 0.00327$ Kg/sec. Therefore, from (5-4)

$P^* = 2025*.00327 / 2 = 3.3$ W

$\therefore P^*_{total} = 6.6$ W

The drag force over the aerofoil was measured by the direct balance system and was found to be equal 2.51 N.

The power (P^*_{gross}) required to operate the flow around the aerofoil is:

P^*_{gross} = Drag force × U_∞ = 2.51×30 = 75.3 W

The ratio of the ABD power consumption to the power required to overcome the aerofoil drag is 6.6/75.3 ≈ 9%

The u_i in the above equations is the difference between the velocity of the air at the ABD fan inlet (assumed zero in the laboratory experiment) and the discharge velocity. This is quite a large power consumption. It will however be less significant at higher velocities.

If the ABD flow is withdrawn from point (1) at high-pressure region(e.g. in the pressure side of the aerofoil) and injected at point (2) inside the ABD then by applying Bernoulli's equation between these two points (1) and (2):

$$\frac{1}{2}\rho V_1^2 + p_1 = \frac{1}{2}\rho V_2^2 + p_2$$

$$\text{or, } V_2^2 - V_1^2 = \frac{p_1 - p_2}{2\rho} \qquad (5\text{-}5)$$

But using the definition of C_p, ΔC_p can be written as:

$$p_1 - p_2 = \Delta C_p \bullet \frac{1}{2}\rho V_\infty^2, \qquad \text{where } V_\infty \neq 0 \qquad (5\text{-}6)$$

From (5-5) and (5-6)

$V_2^2 - V_1^2 = \Delta C_p \bullet V_\infty^2$; and from the definition of $C_i = \frac{V_2}{V_\infty}$;

$$C_i^2 = \Delta C_p + \frac{V_1^2}{V_\infty^2} \qquad \text{or} \quad C_i = \sqrt{\Delta C_p + \frac{V_1^2}{V_\infty^2}} \qquad (5\text{-}7)$$

Knowing that ΔC_p almost exceeds the value of 1 (some times up to 6); and the second term $\frac{V_1^2}{V_\infty^2}$ is always positive, it can be said that achieving a value of C_l=1.5 is possible without additional power.

For the suction side of the ABD, the addition of the thrust obtained from (throwing) the air into the wake of the aeroplane should be considered. This thrust is almost equal to the value of the power required to drive the suction fan. Therefore, the thrust power required from the engines will be reduced by an amount equal to the suction fan power.

However, from these preliminary calculations it is clear that a large saving in power can overcome most of the power needed to operate the ABD; this is true for low amount of losses due to the friction in ducts which likely is the case in practice. In order to calculate the exact amount of power required to operate the ABD and to compare it with the savings in engines power, the calculations should consider the following facts:

- The improvement in the lift, (about 10%), which can indirectly reduce the skin friction by reducing the wing area.
- Injected air can be taken from a high pressure zone at the front of aeroplane.
- Removed air will be discharged in a relatively low pressure zone in the wake of the aeroplane.
- The momentum of the discharged air will contribute to the thrust of the engines. It is expected that this contribution weighs a substantial part of the total power required to operate the ABD.

The benefits obtained by the ABD should be added to the possibility of increasing the manoeuvrability of the aircraft by postponing the stall point.

5.9 Practicality of the ABD Technique

The method of the ABD which was invented in this research is proved to be efficient, practical, and economical method of flow control. Practicality of this technique can be seen from different aspects such as:

- relative simplicity of its geometry, which means that manufacturing of this device does not involve much complications provided that the overall dimensions of the aerodynamic / hydrodynamic device are large enough.
- relatively lower cost of maintenance since there is no moving parts but the pump.
- The large amount of savings which the ABD can provide comparing to its fixed and running costs.
- The relative simplicity of controlling its performance (by controlling the rolling-speed flow).
- The relatively small adverse effect when the rolling flow is unable to be injected (i.e. C_i=0). This effect, however, could be erased by putting a simple moving cover on the top of the ABD.

Comparing this technique with many other active techniques which are suggested in the literature and still under investigation makes it clear that the use of the ABD is far practical and effective. If the ABD technique is compared, for example, with the moving surface technique (MST), (Modi et al. 1994) and (Arain, 1991), means that the need for the relatively complex, vibration-free mechanical design as well as costly maintenance does not exist in the ABD. The active wall technique, Thomas, (1990), requires a much more complicated mechanism with a high level control of the surface. It is clearly far more complicated than the requirements of the ABD. The suction technique, (Braslow et al., 1990; Wagner et al., 1989; Wagner and Fischer, 1984), has proved its practicality and efficiency as a flow control method but the substantial loss of lift associated with a higher amounts of suction determines the maximum gain from this technique, while in the ABD technique this maximum gain can be increased. Injection techniques, (Fontaine and Deutsch, 1992; Merkle and Deutsch, 1990), have a disadvantage of separation promotion which makes them unsuitable for the ready-to-separate flows, whilst using the ABD technique appears to postpone the separation and to help strong attachment of the flow to the wall.

The noise level associated with the ABD should be, however, considered and careful design of the ABD (especially the geometry of the tips) may be necessary so that the noise level is less than that produced by engines and other sources of noise. This may require a real flight test of the ABD if it is to be used over a wing of an aeroplane.

Geometry	File Name	U_∞	C_i	S (cm)	L_s(cm)	H(cm)	h(cm)
10	AB*-10	40	1	0.6	8.7	0.5	0
	AB*-13		1.5				
	AB*-15		2				
	AB*-16		2.5				
20	AB*-20		1	0.8			
	AB*-23		1.5				
	AB*-25		2				
	AB*-26		2.5				
30	AB*-30		1	1.0			
	AB*-33		1.5				
	AB*-35		2				
	AB*-36		2.5				
40	AB*-40		1	0.6	6.2		
	AB*-43		1.5				
	AB*-45		2				
	AB*-46		2.5				
50	AB*-50		1	0.8			
	AB*-53		1.5				
	AB*-55		2				
	AB*-56		2.5				
60	AB*-60		1	1.0			
	AB*-63		1.5				
	AB*-65		2				
	AB*-66		2.5				
80	AB*-80		1.5	0.6	8.7		0.1
81	AB*-81						0.2
82	AB*-82						0.3
83	AB*-83					0.4	0
84	AB*-84					0.3	0
85	AB*-85					0.2	0

Table (5-1)ABD Parameters for Different Modelled Cases

Repeated at angles 4°,8°,12°,14°,16°

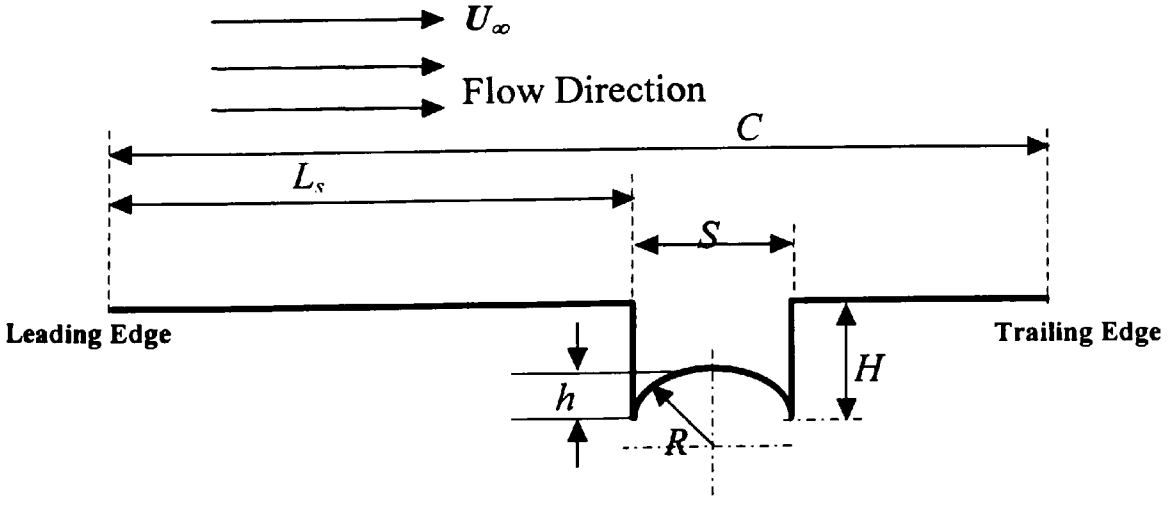

Figures

5.9.1 Comparison Between CFD and Experimental Results

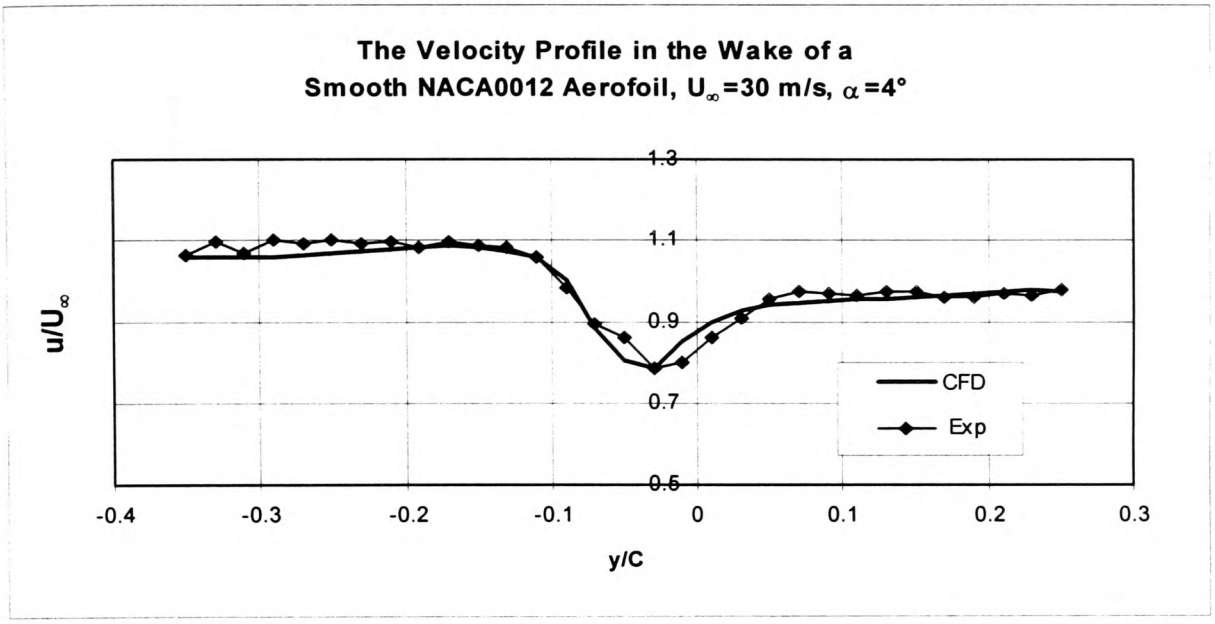

Figure 5-1

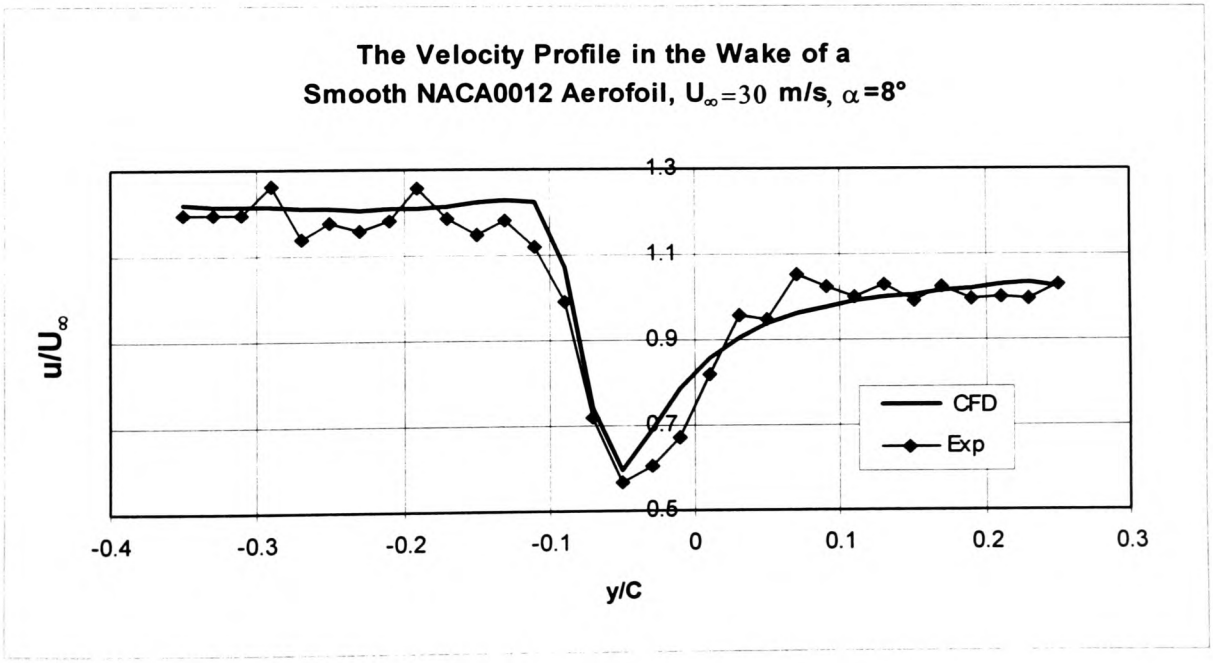

Figure 5-2

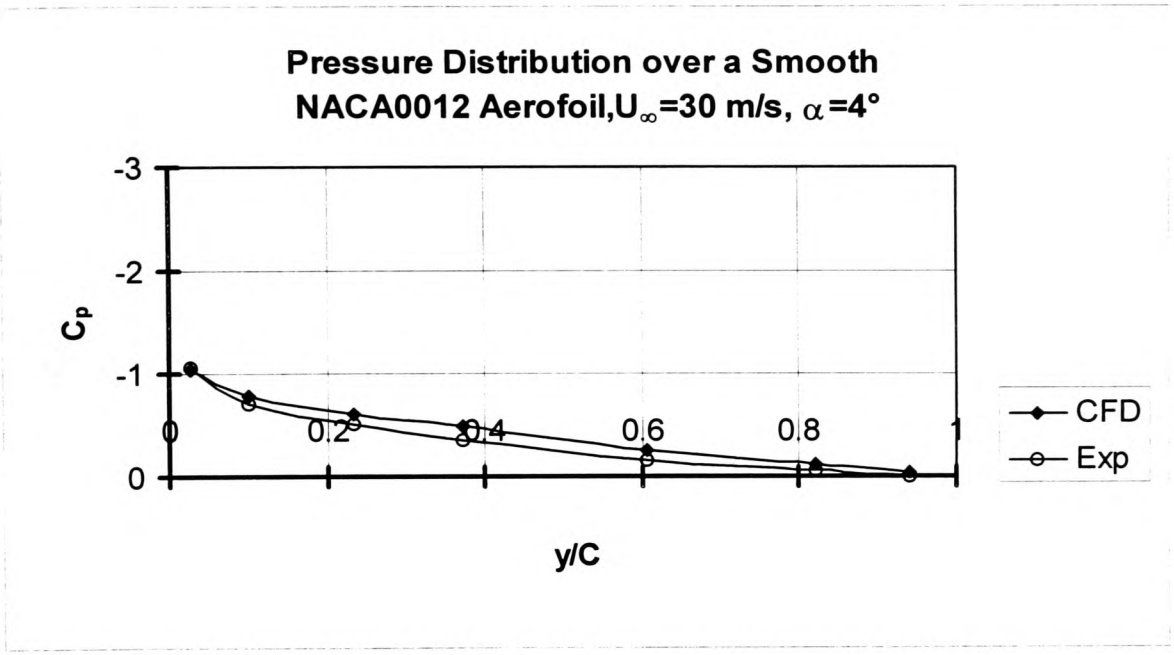

Figure 5-3

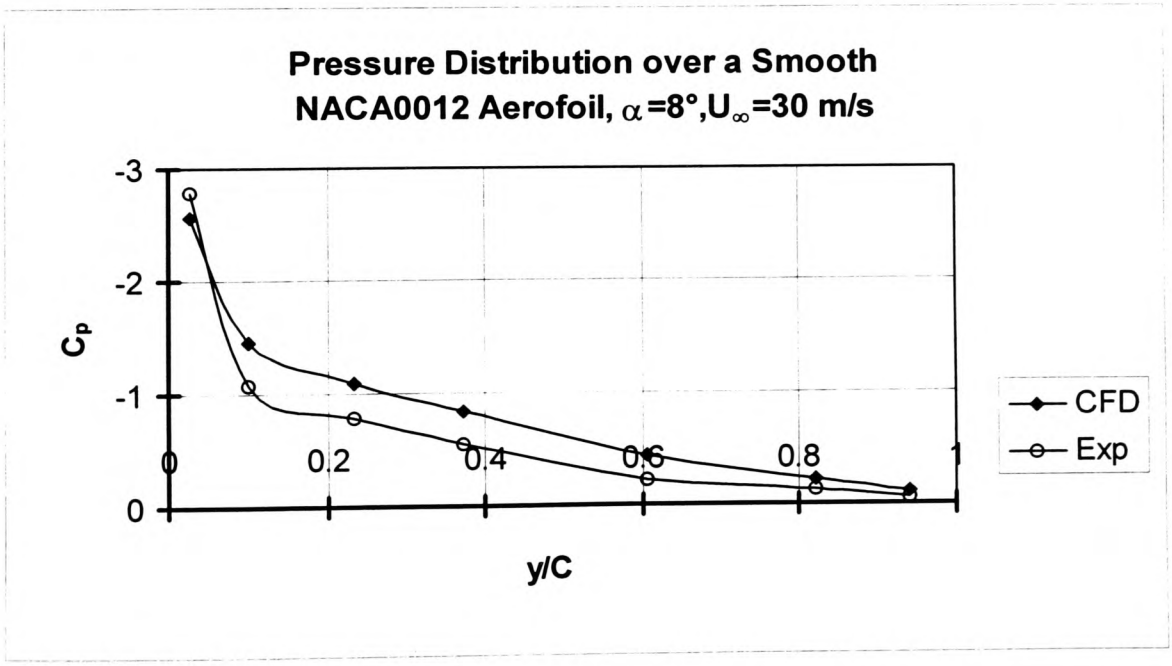

Figure 5-4

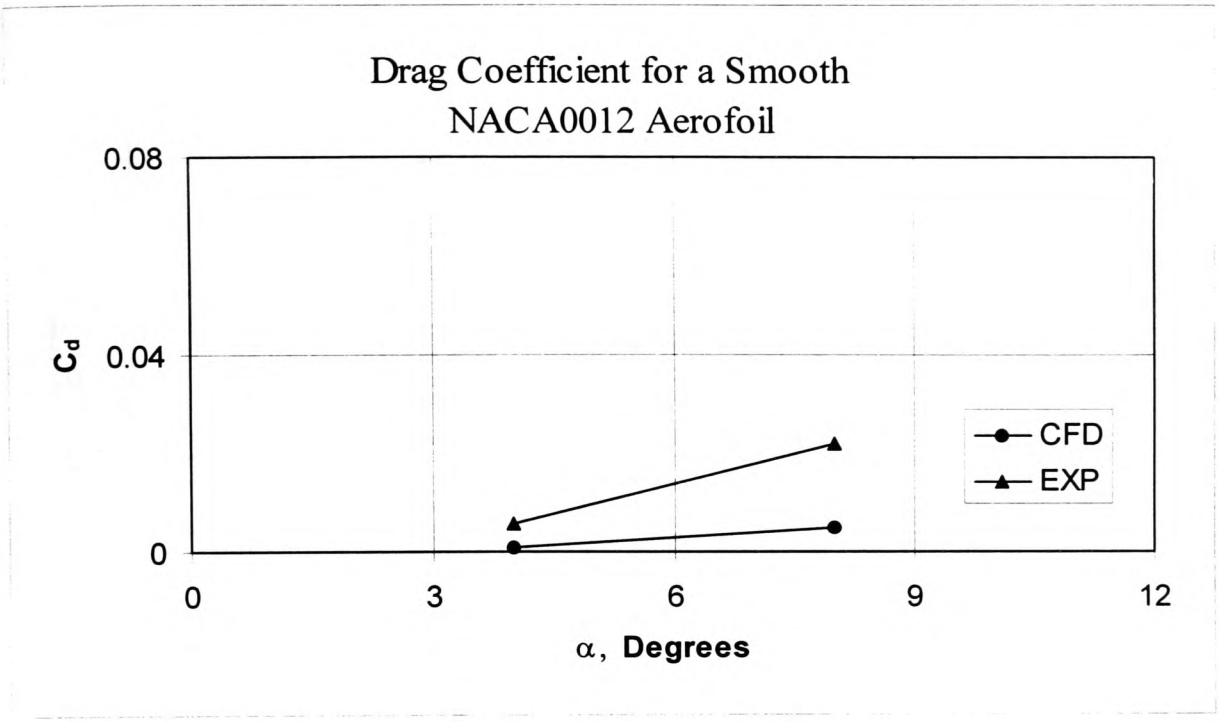

Figure 5-5 (a)

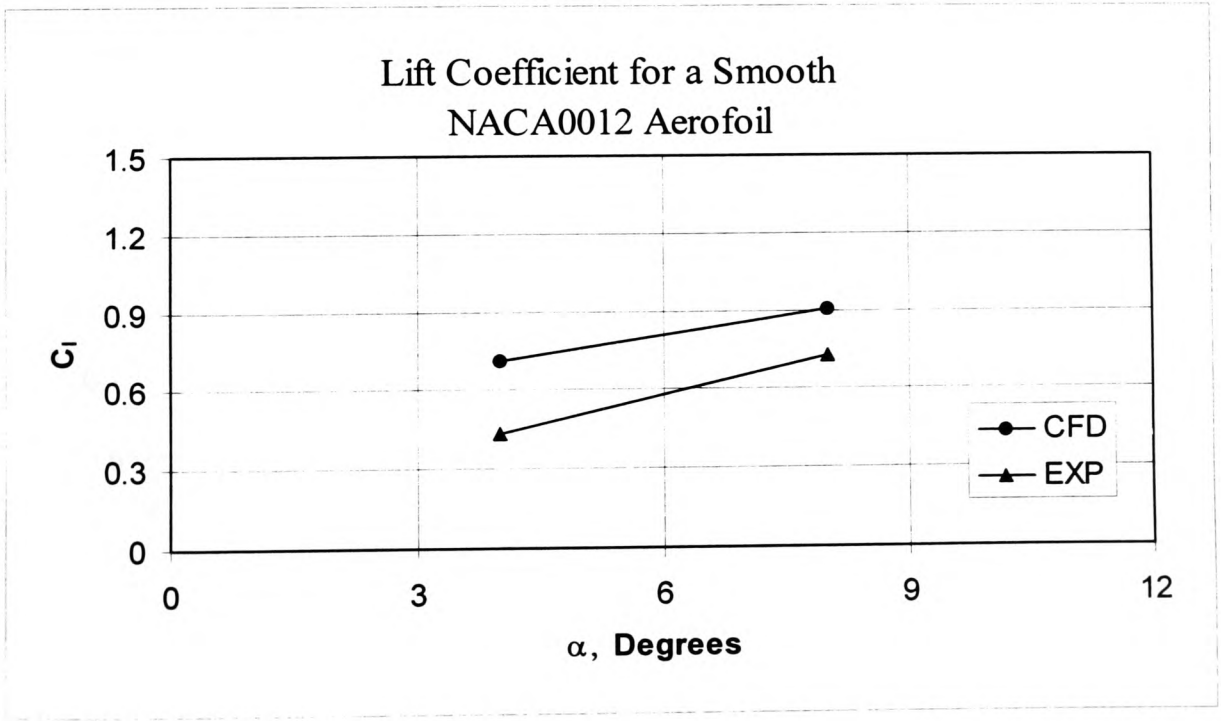

Figure 5-5 (b)

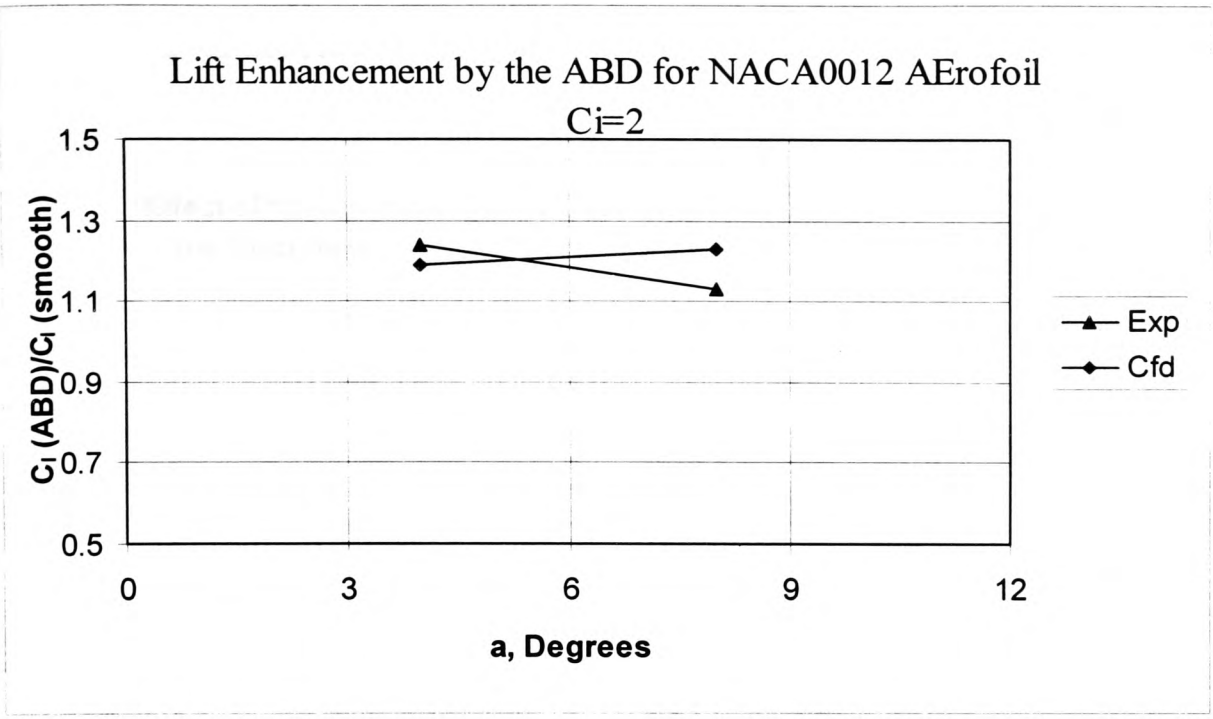

Figure 5-6 (a)

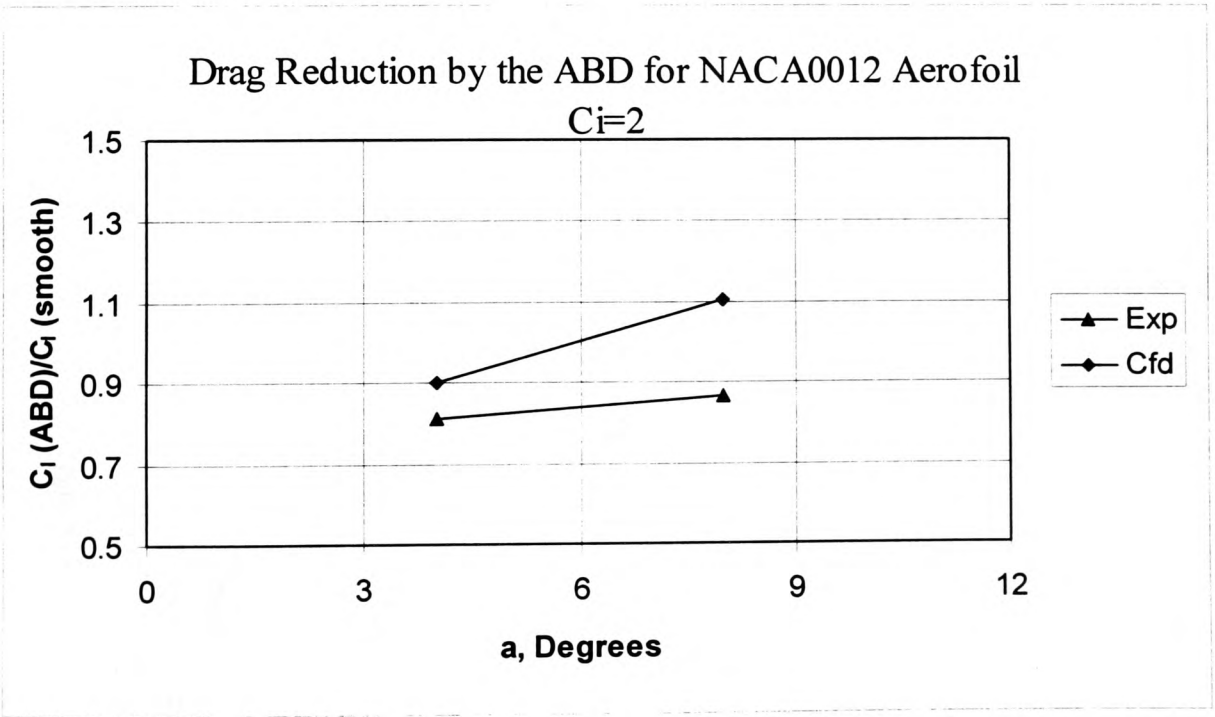

Figure 5-6 (b)

5.9.2 Effect of the ABD on the Flow over a Flat Plate

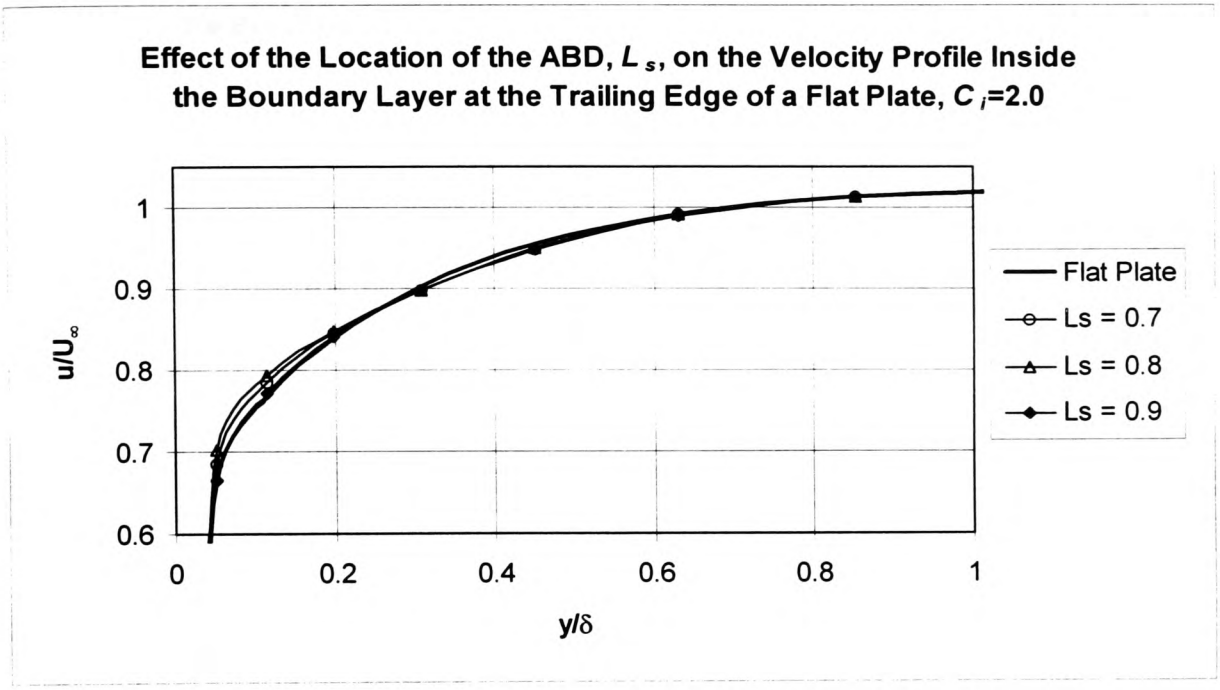

Figure 5-7

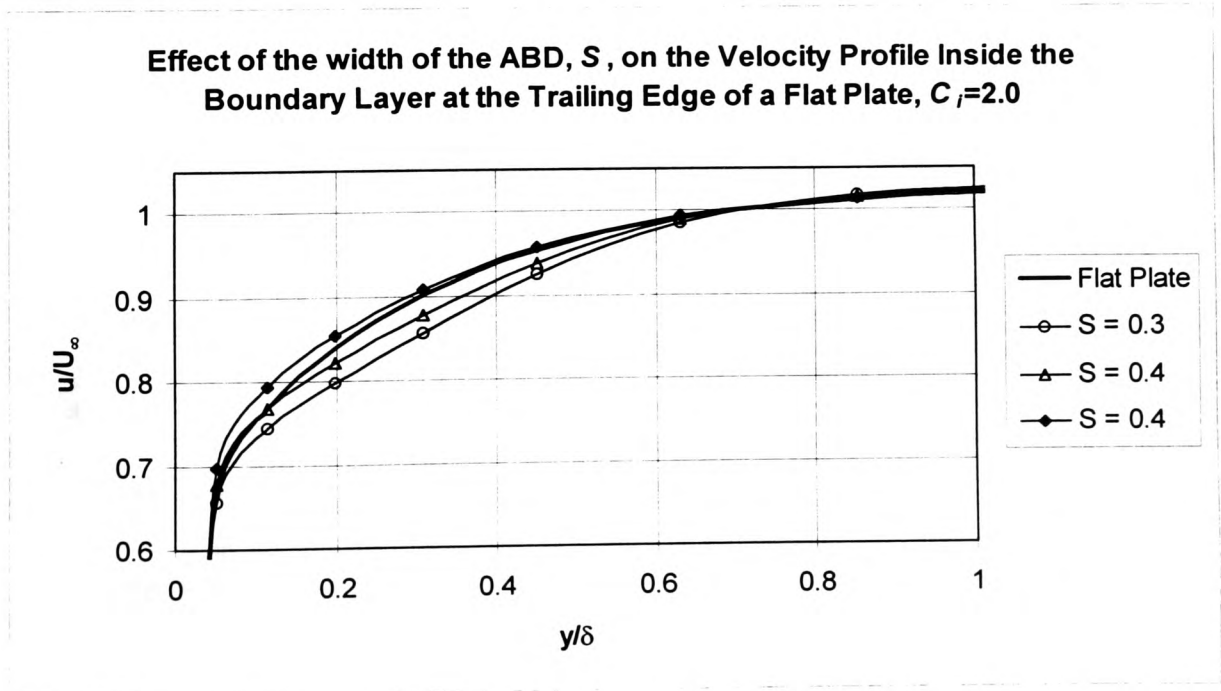

Figure 5-8

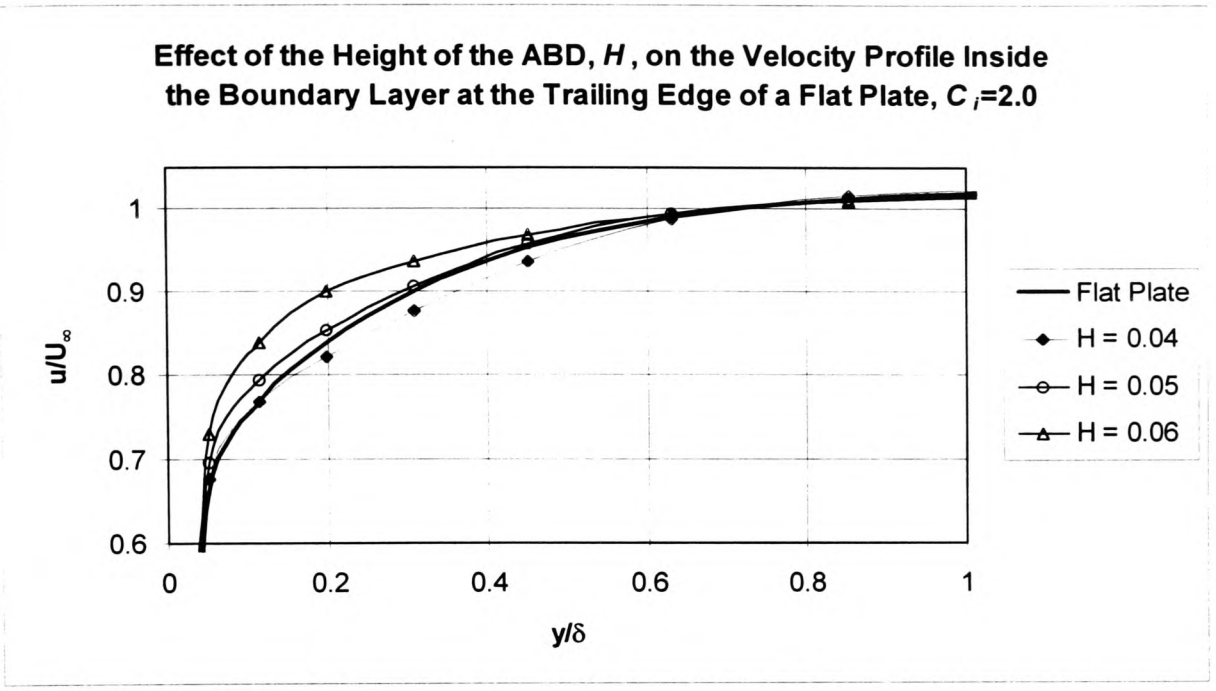

Figure 5-9

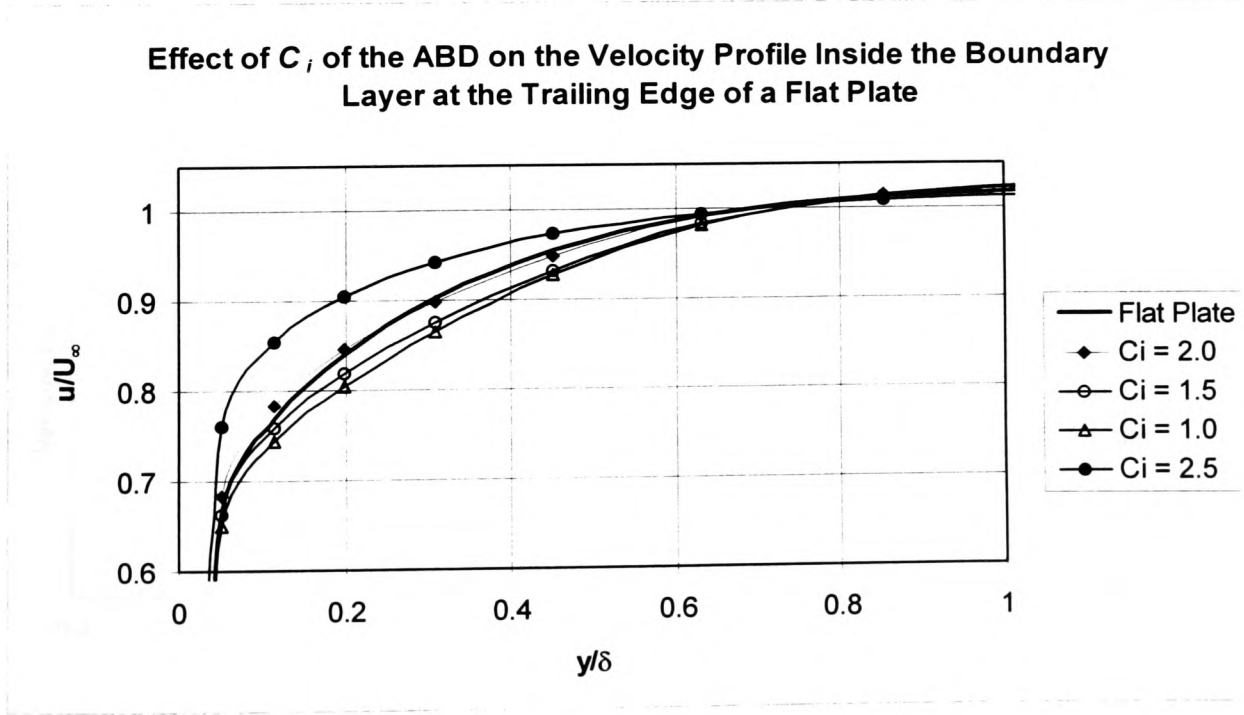

Figure 5-10

5.9.3 Effect of Velocity inside ABD on the Wake Velocity Profile

5.9.3.1 Alpha = 4 Degrees

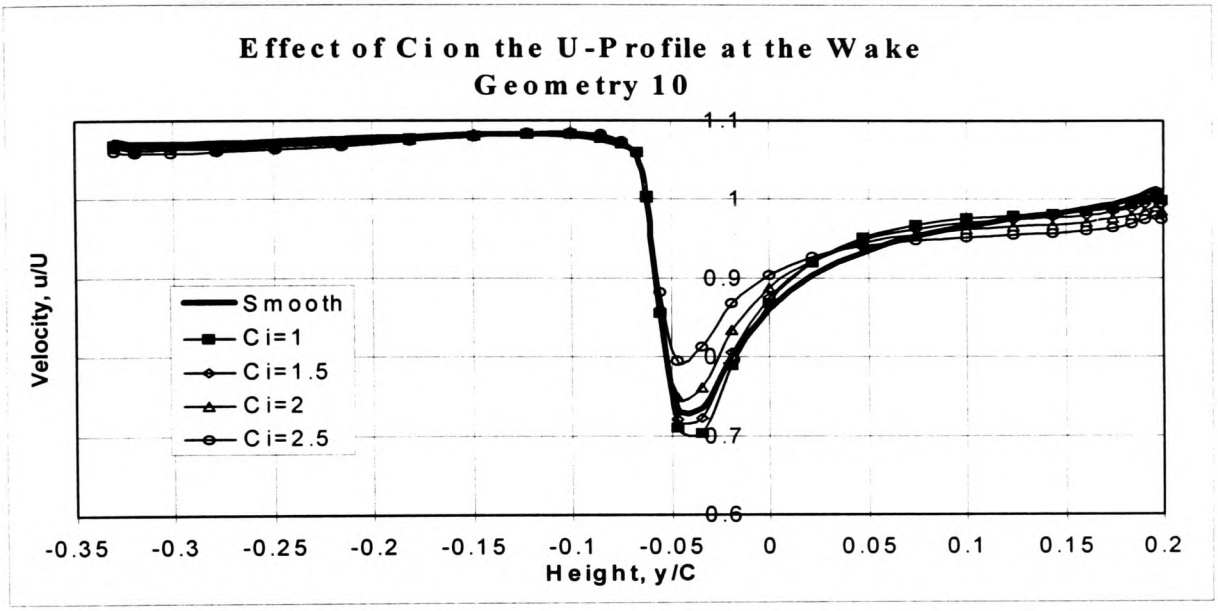

Figure 5-11

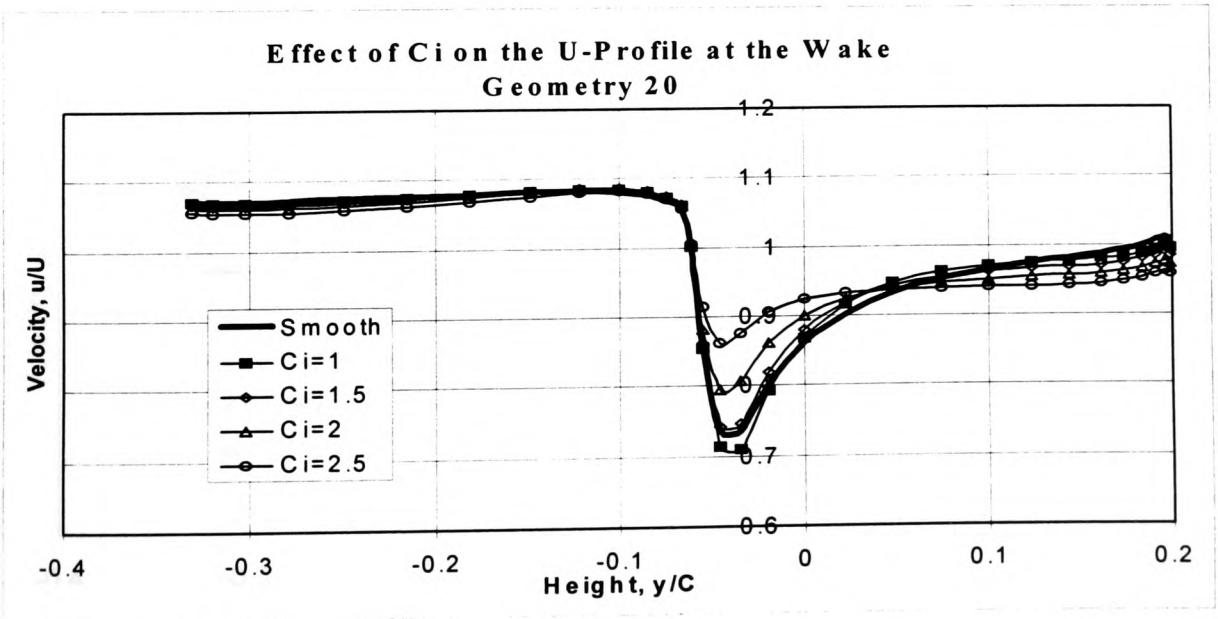

Figure 5-12

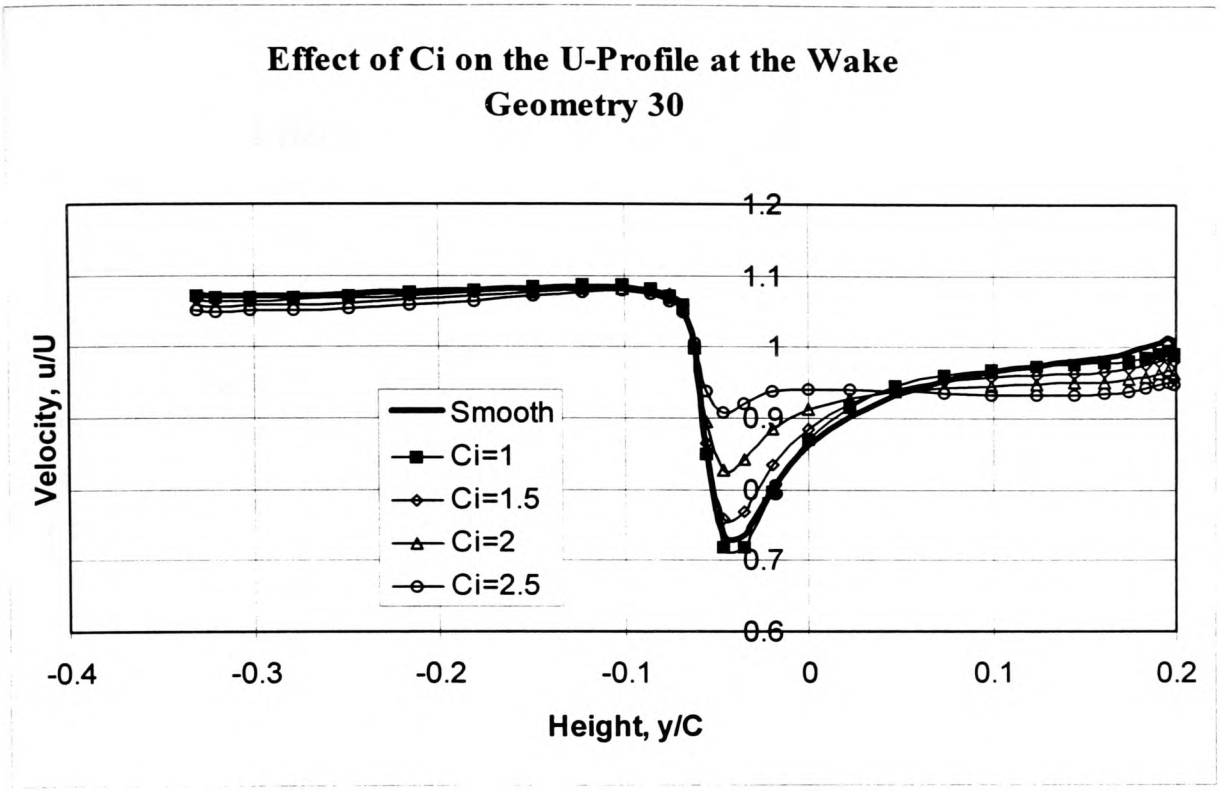

Figure 5-13

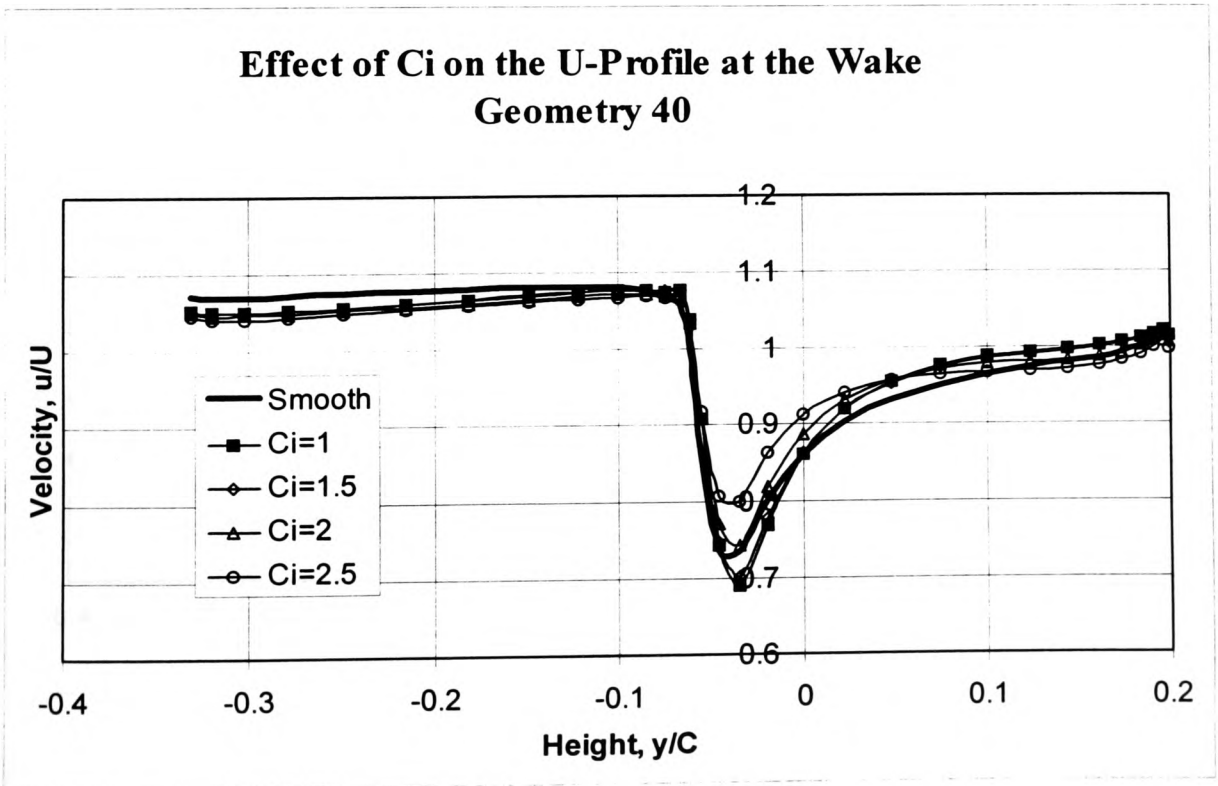

Figure 5-14

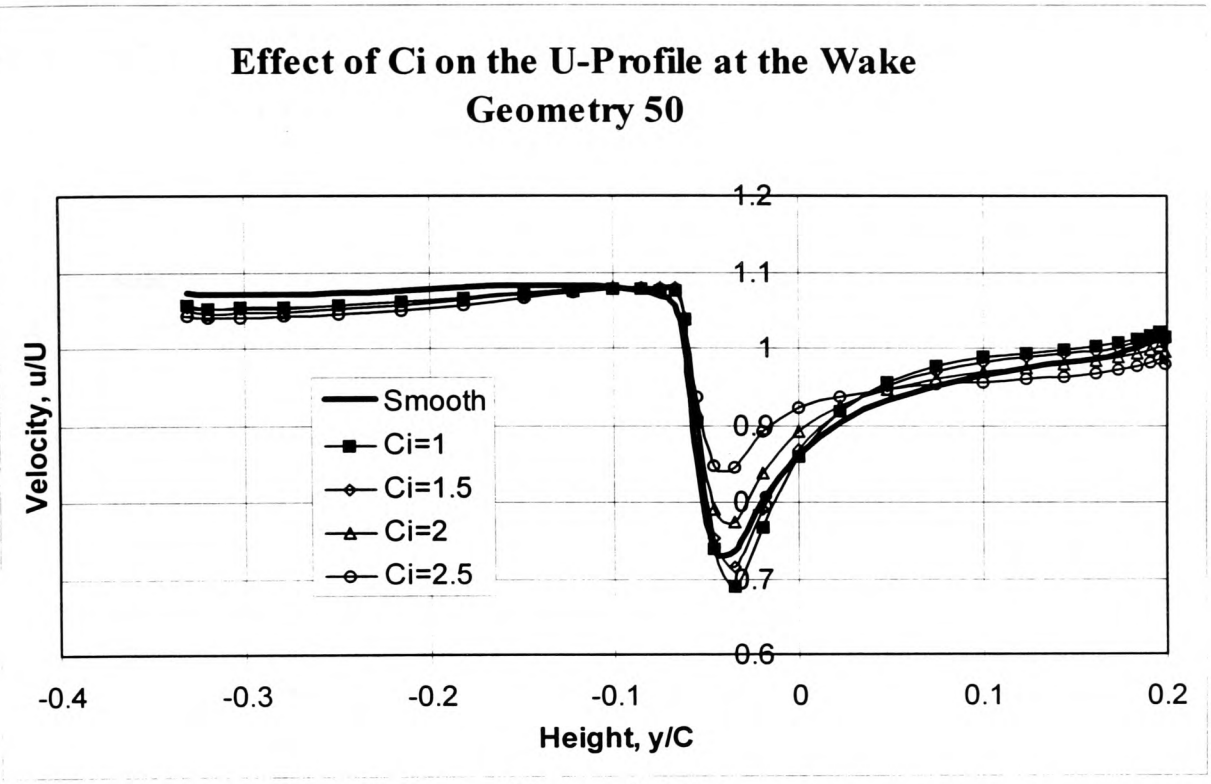

Figure 5-15

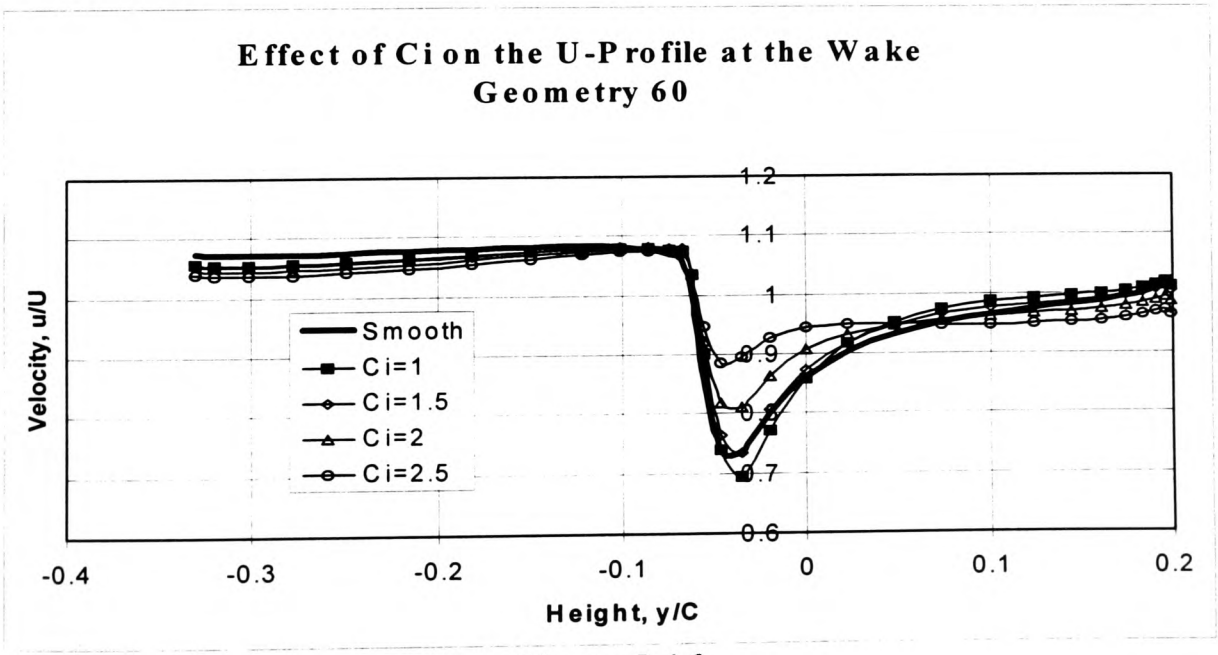

Figure 5-16

5.9.3.2 Alpha = 8 Degrees

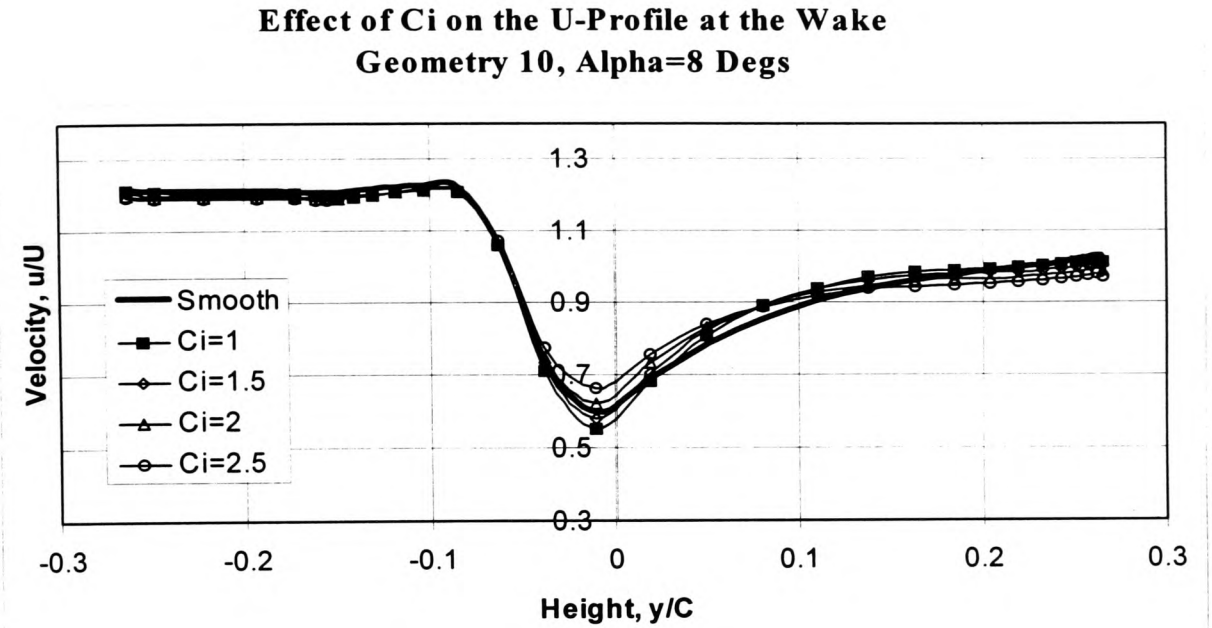

Figure 5-17

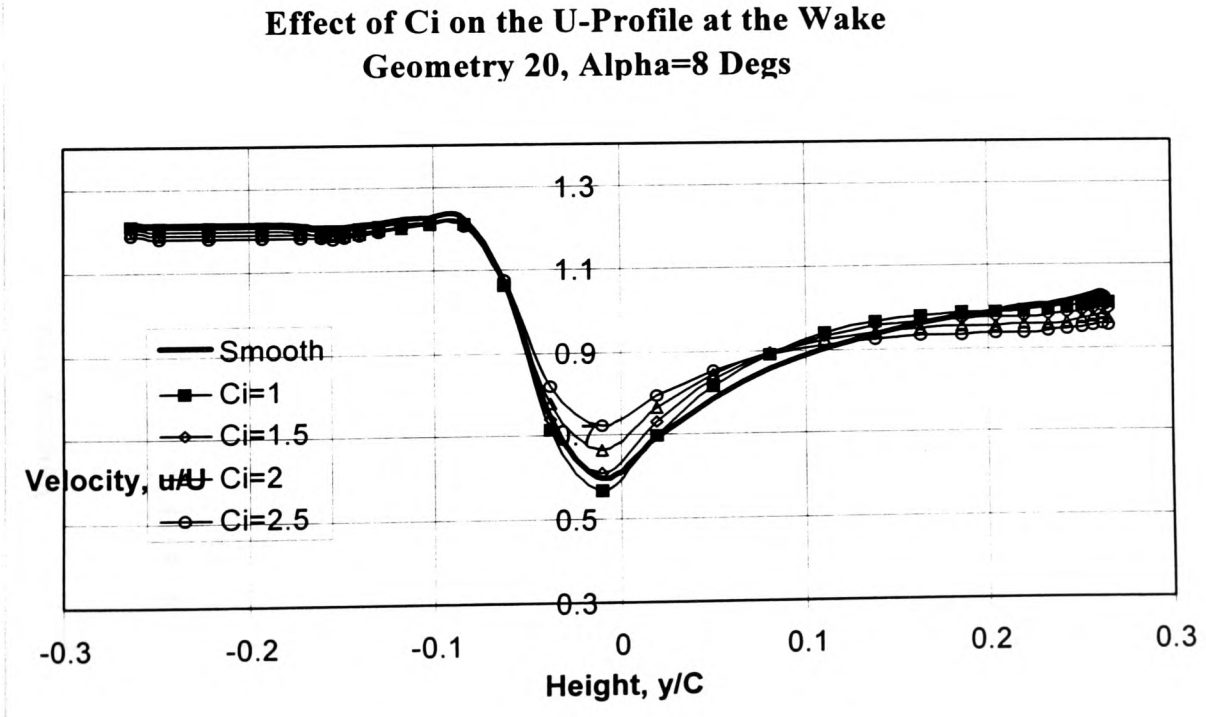

Figure 5-18

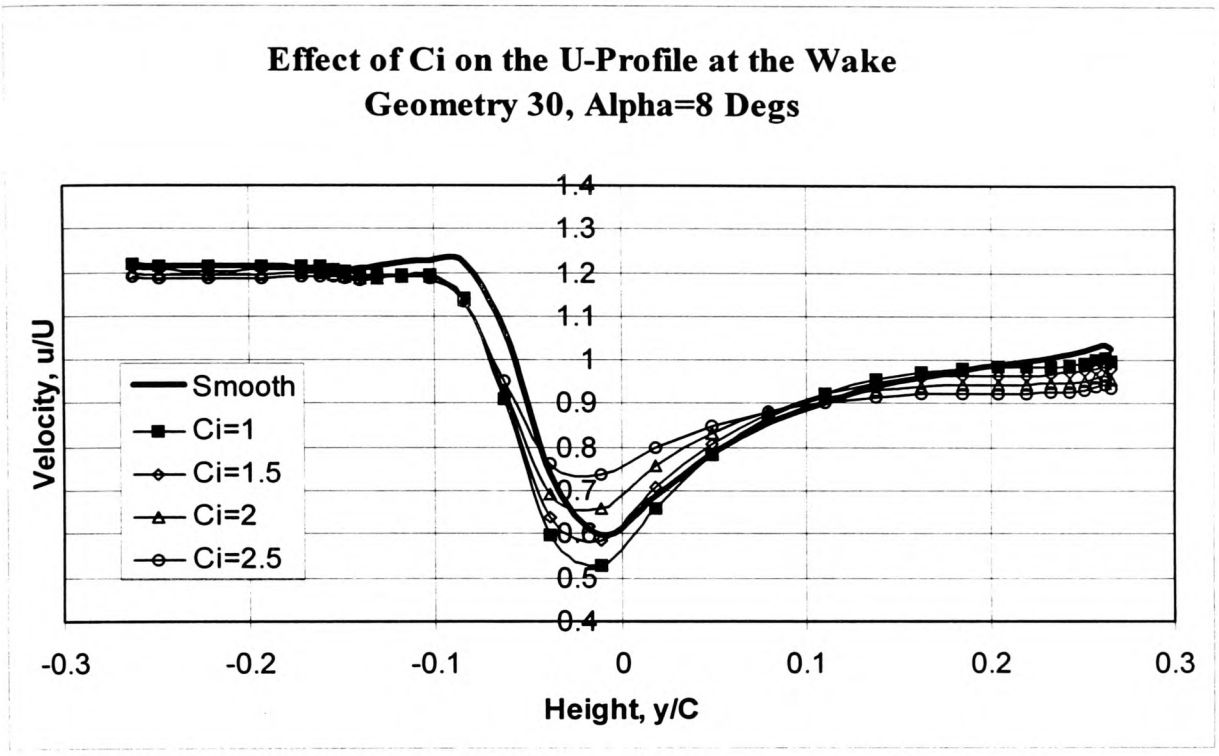

Figure 5-19

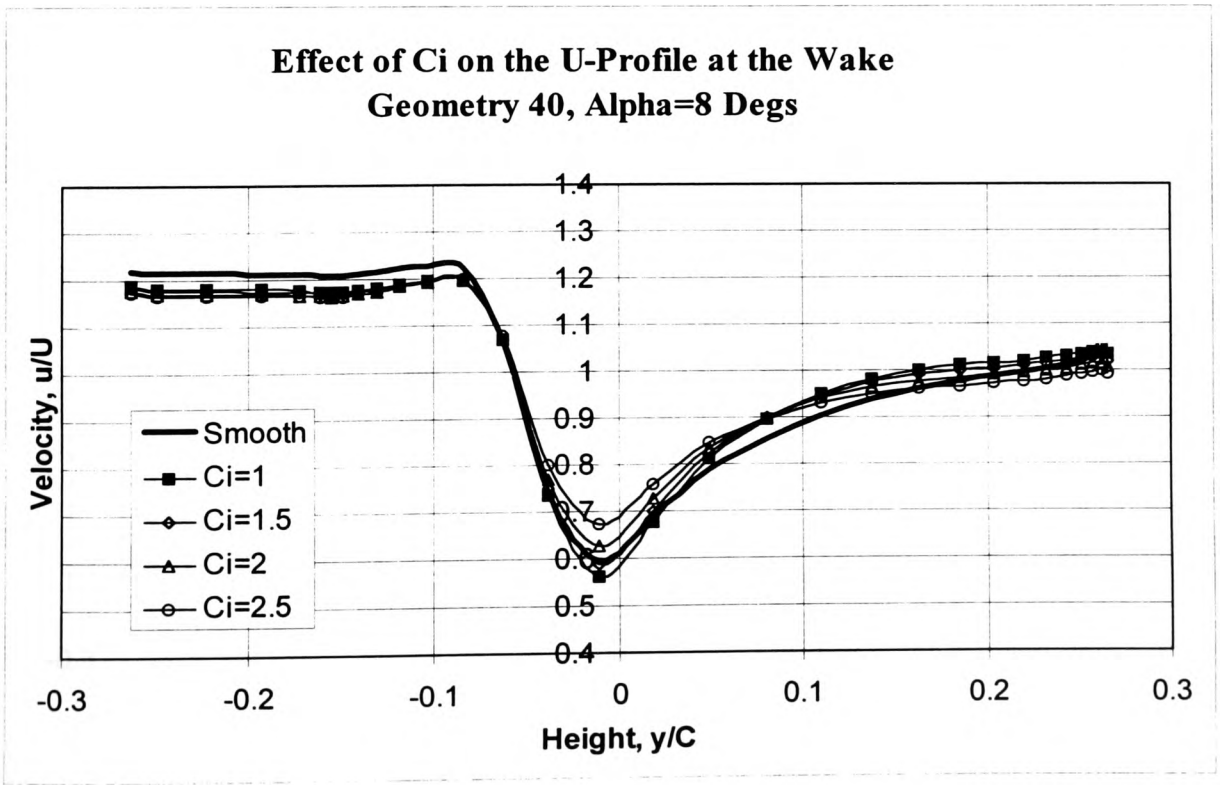

Figure 5-20

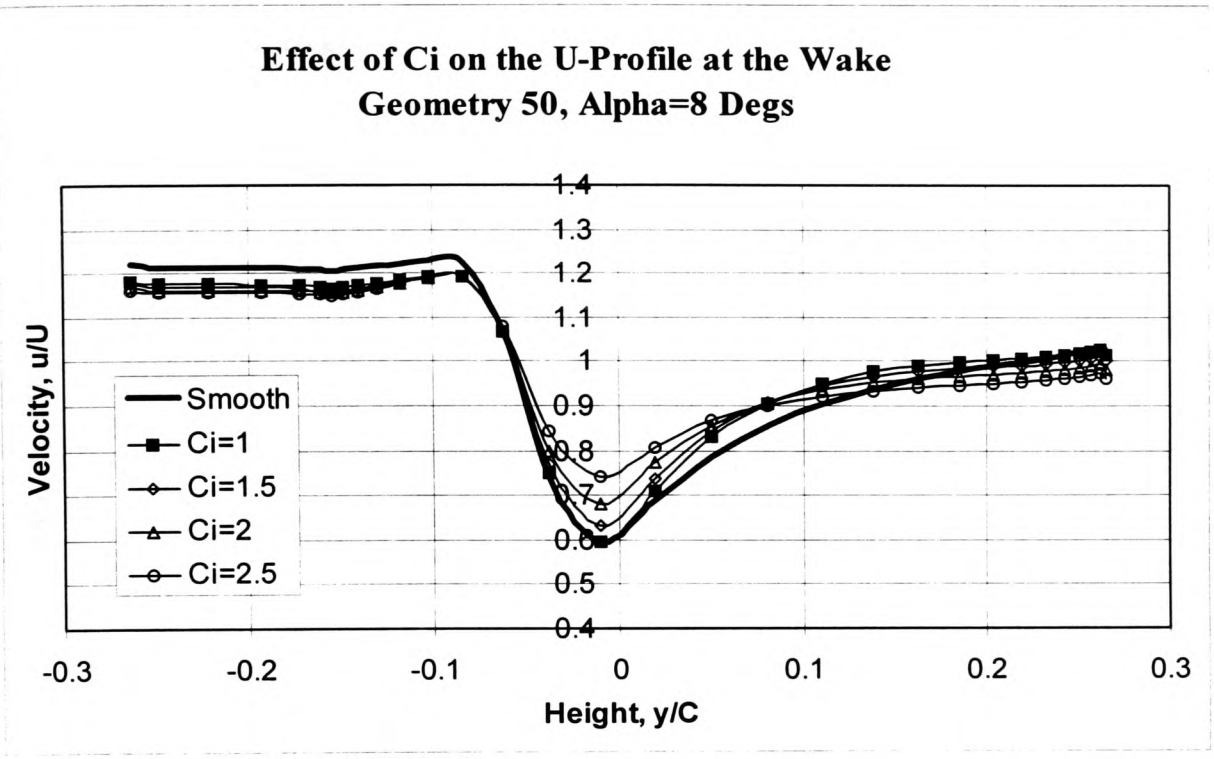

Figure 5-21

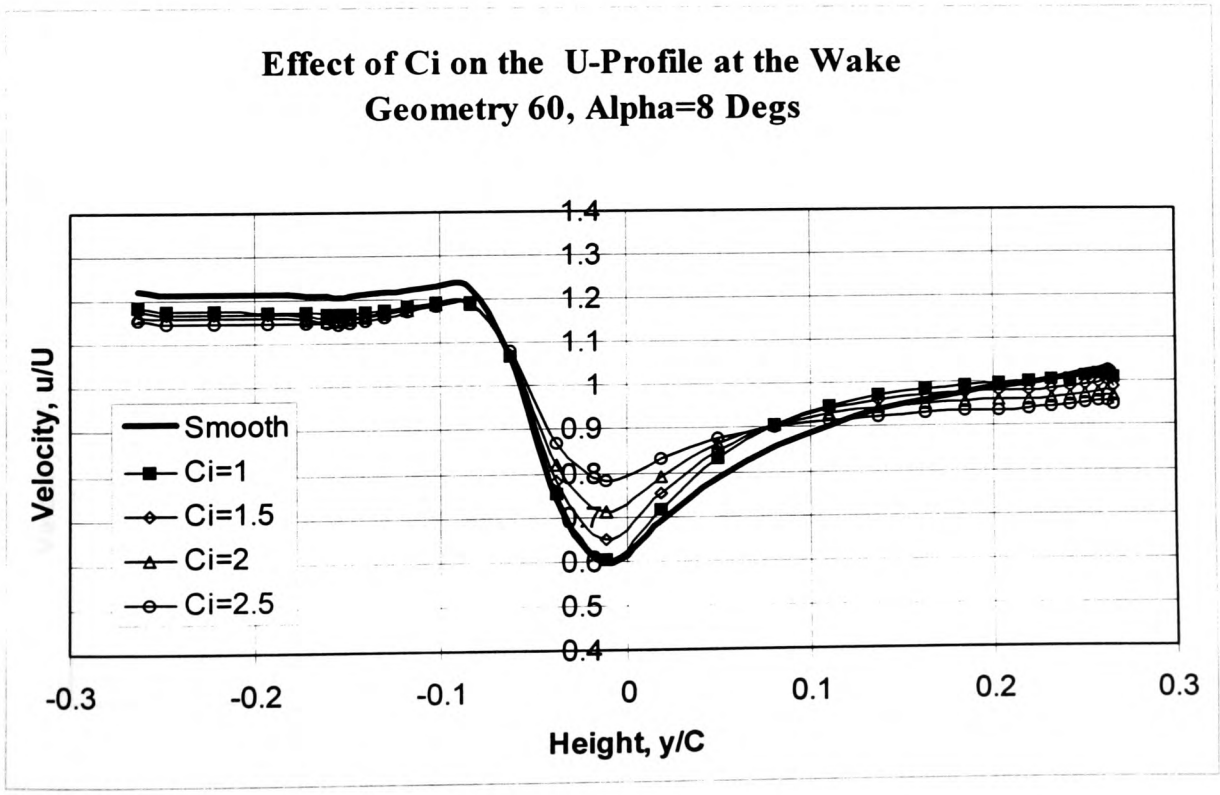

Figure 5-22

5.9.3.3 Alpha = 12 Degrees

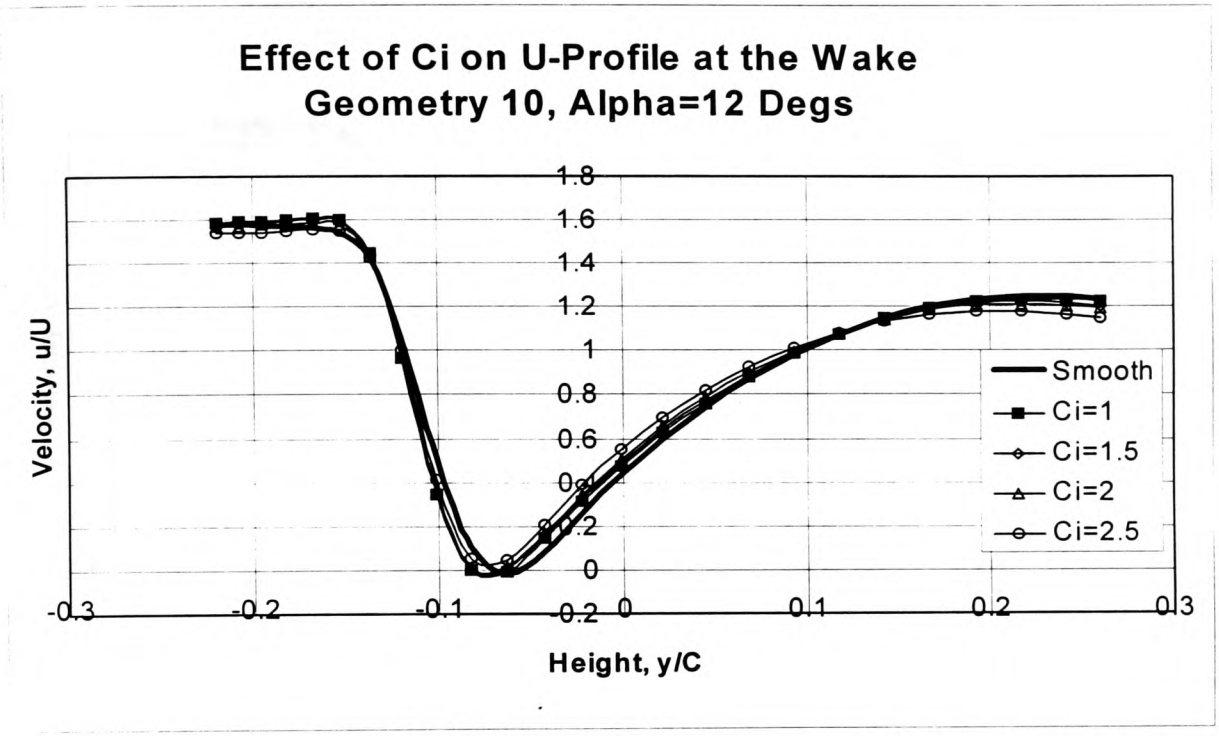

Figure 5-23

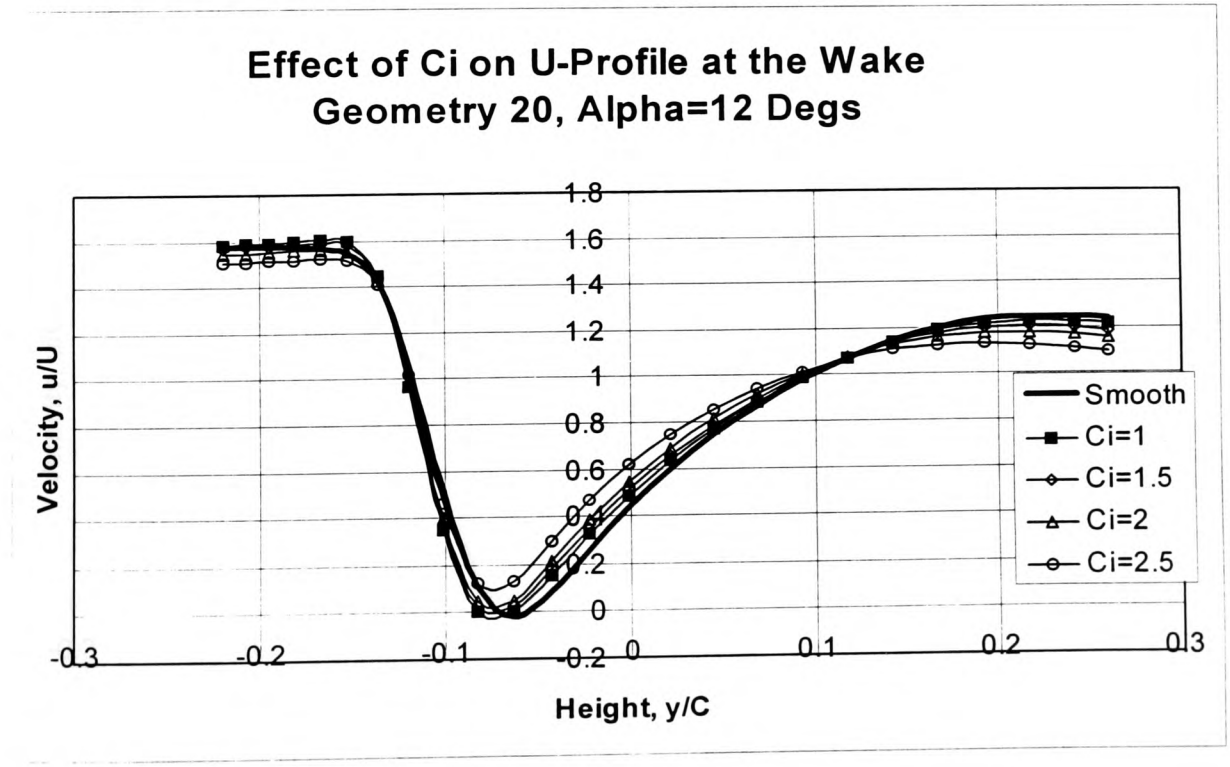

Figure 5-24

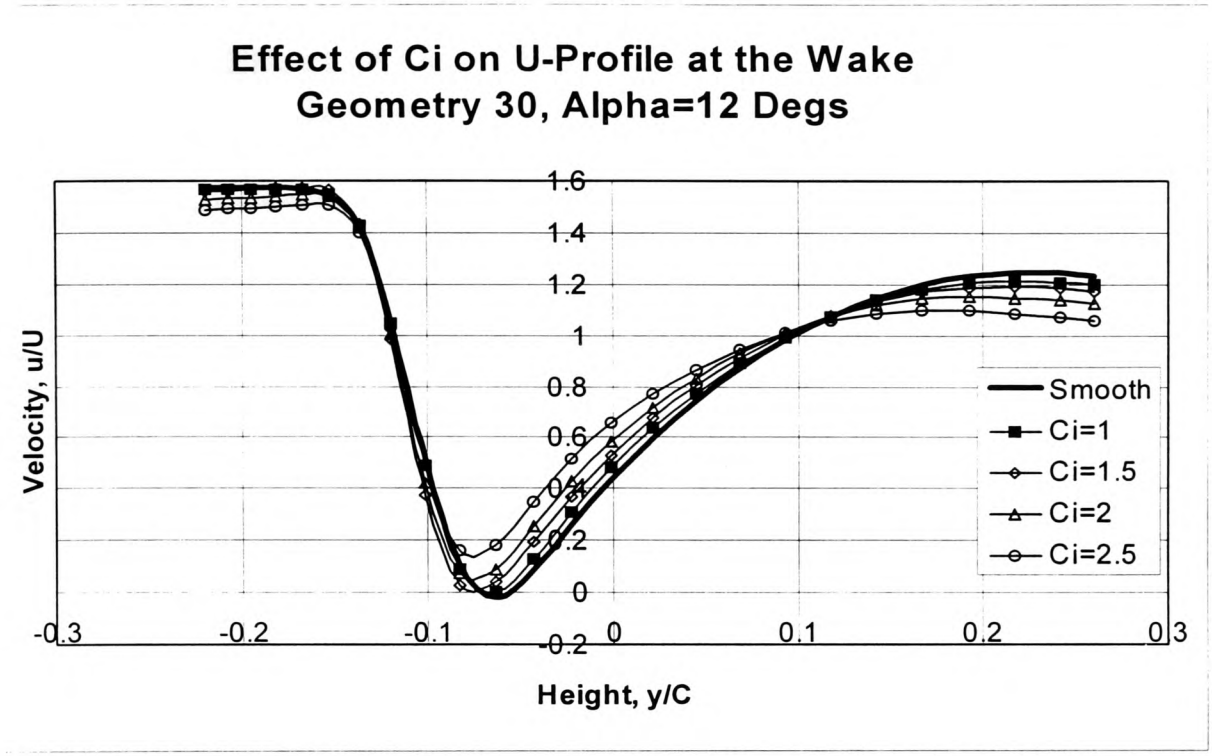

Figure 5-25

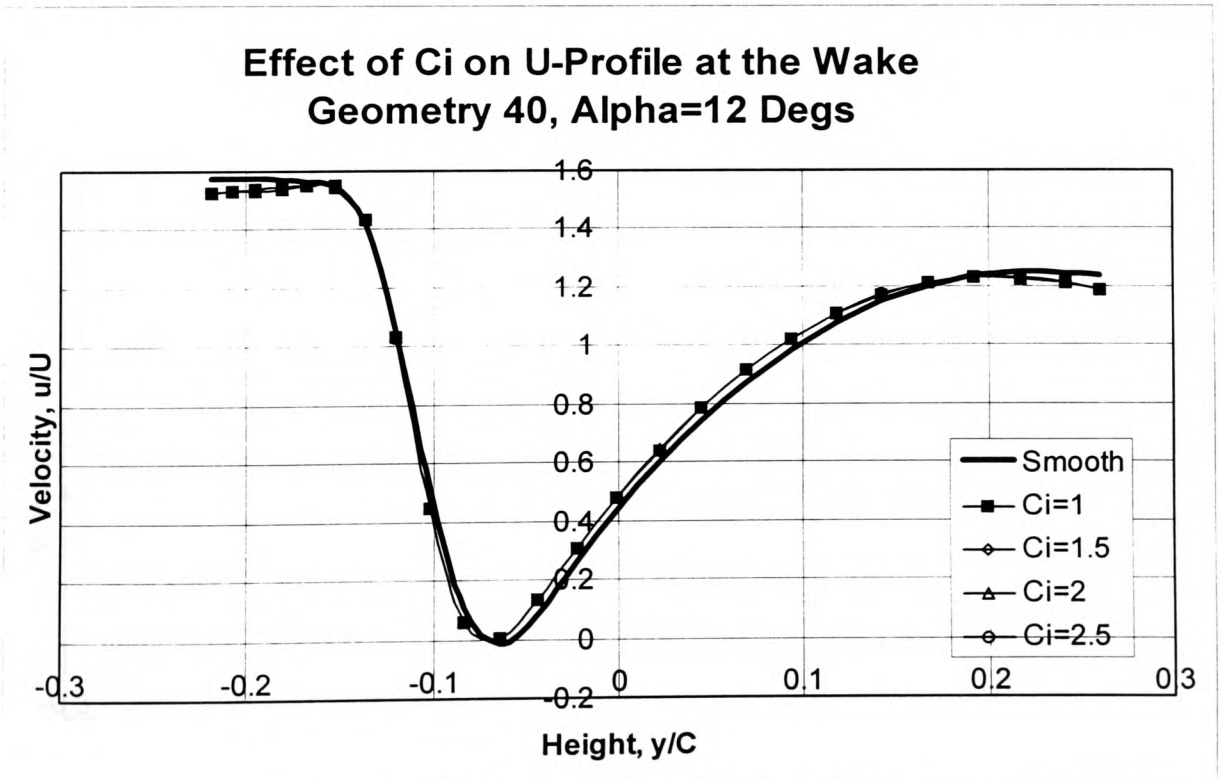

Figure 5-26

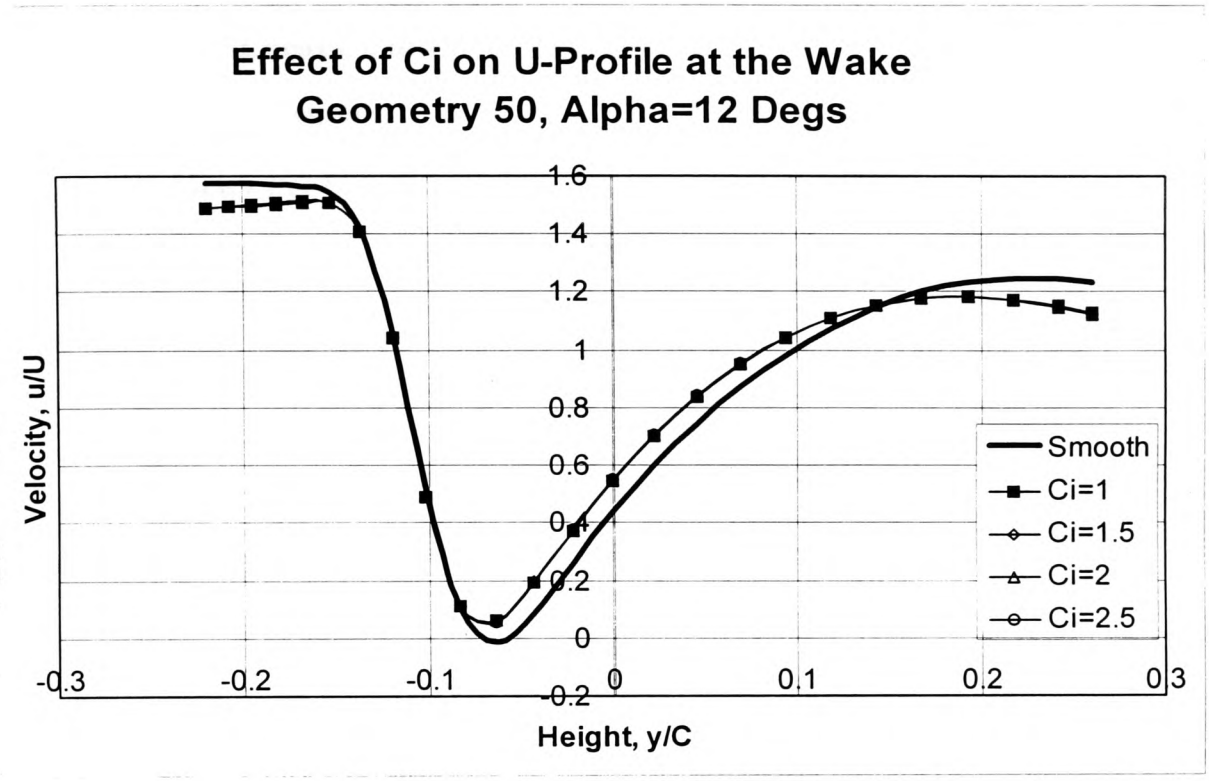

Figure 5-27

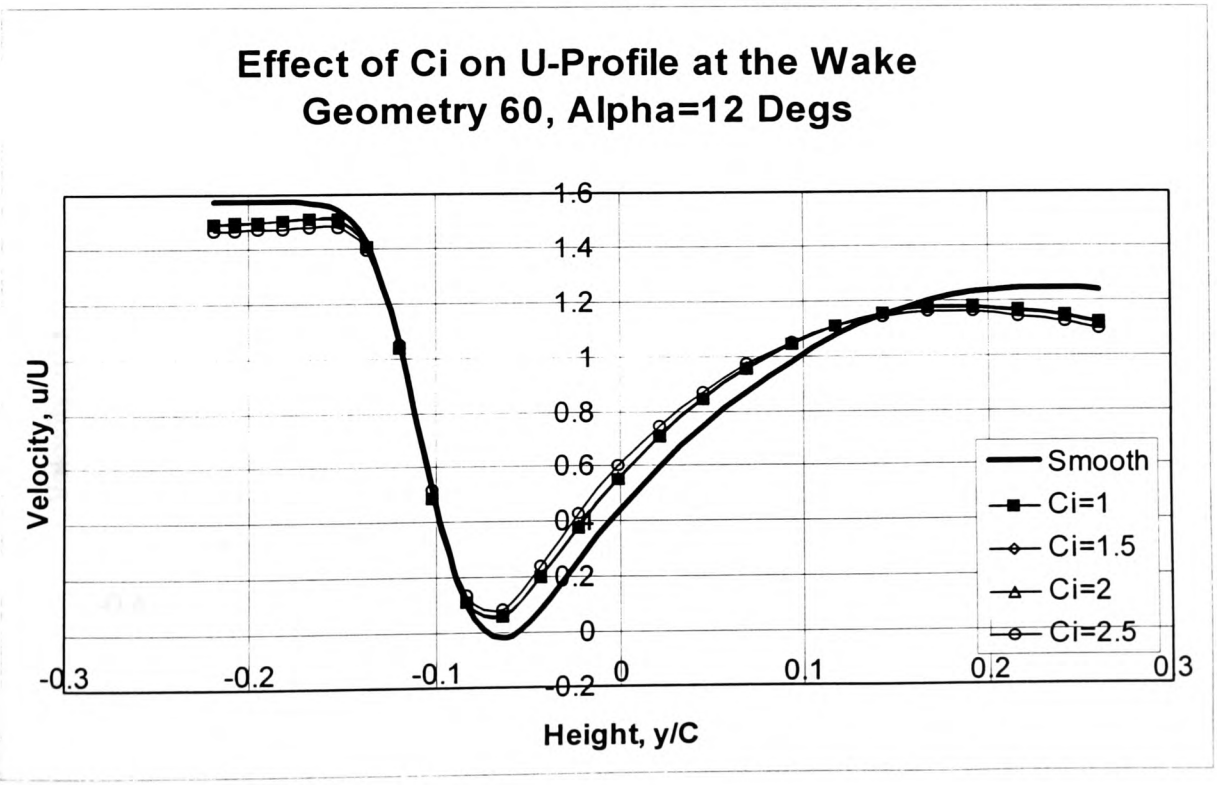

Figure 5-28

5.9.4 Effect of Location of the ABD on the Wake Velocity Profile

5.9.4.1 Alpha = 4 Degrees

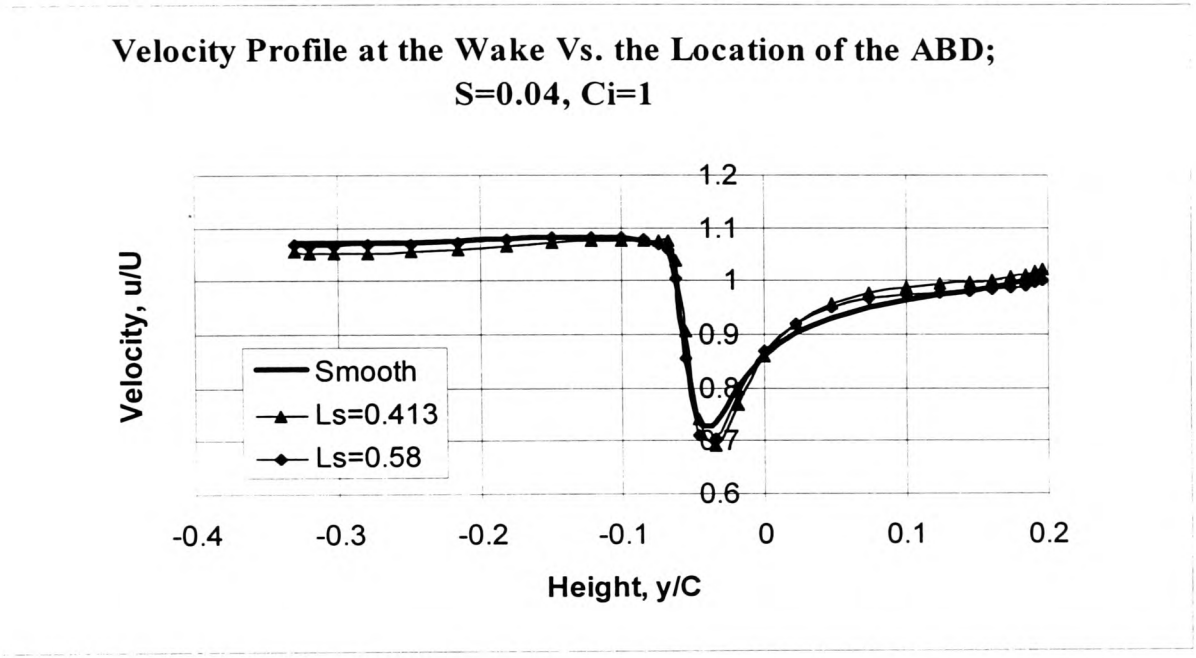

Figure 5-29

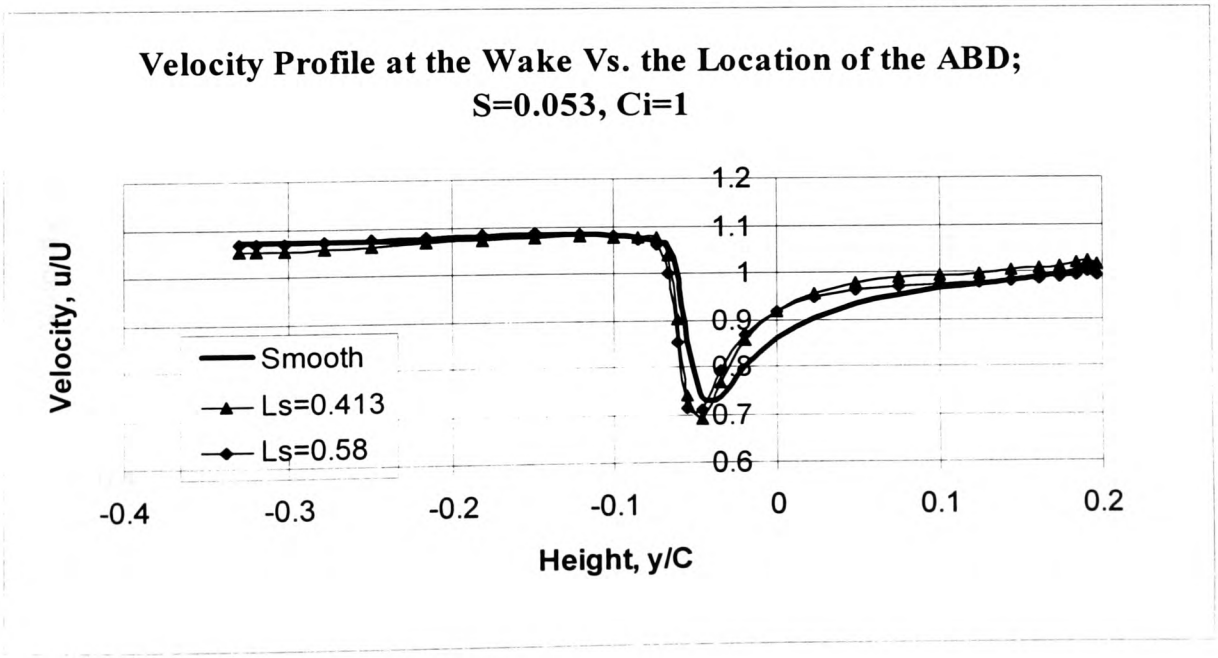

Figure 5-30

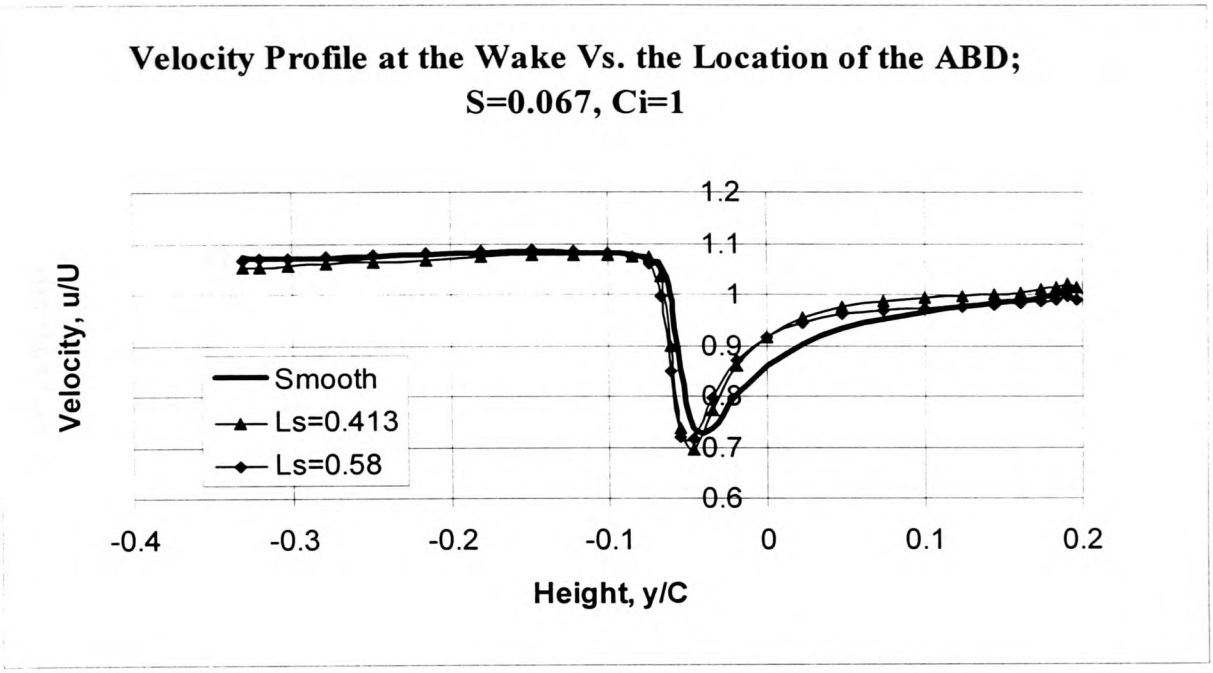

Figure 5-31

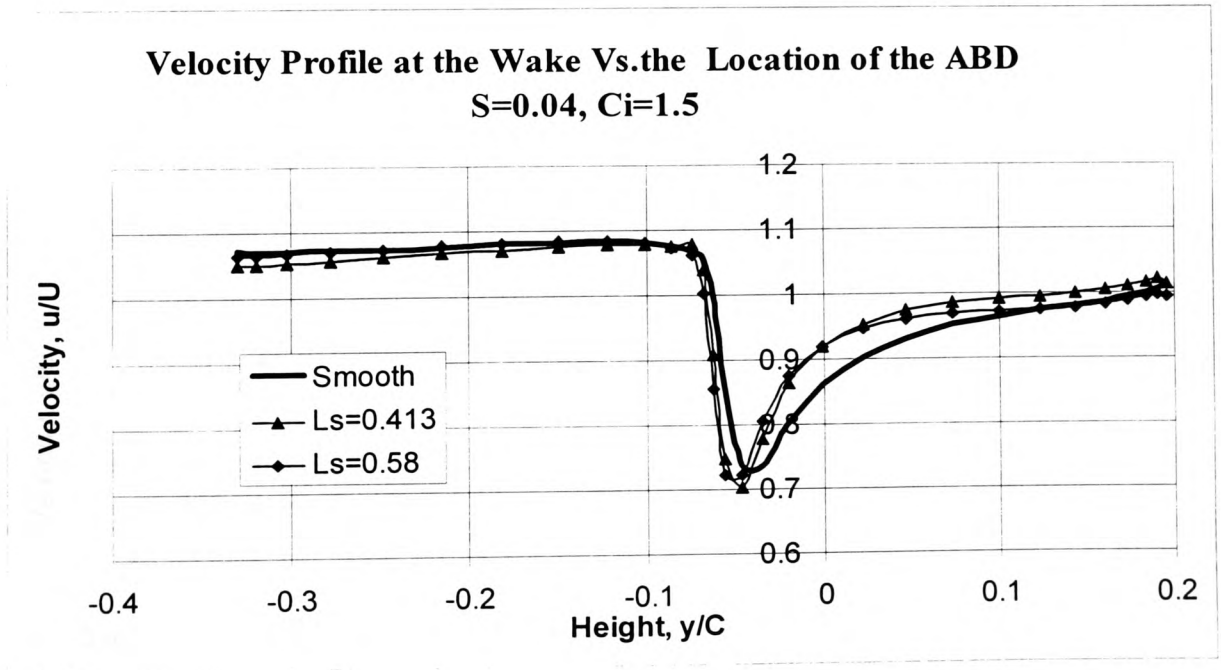

Figure 5-32

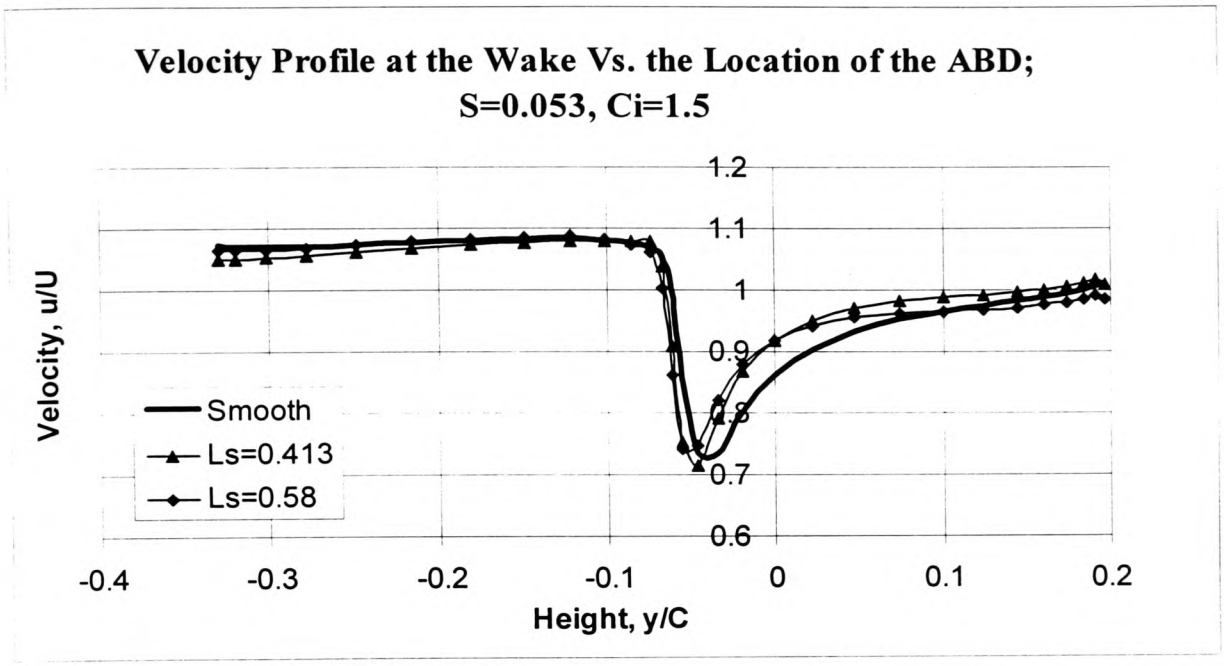

Figure 5-33

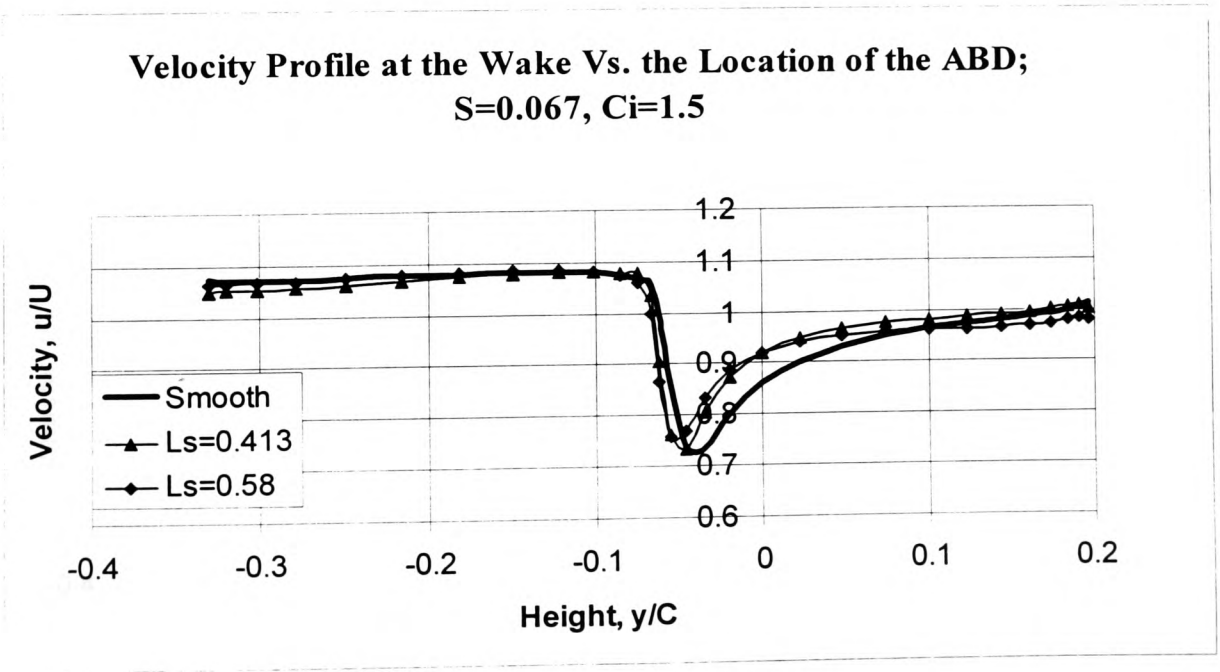

Figure 5-34

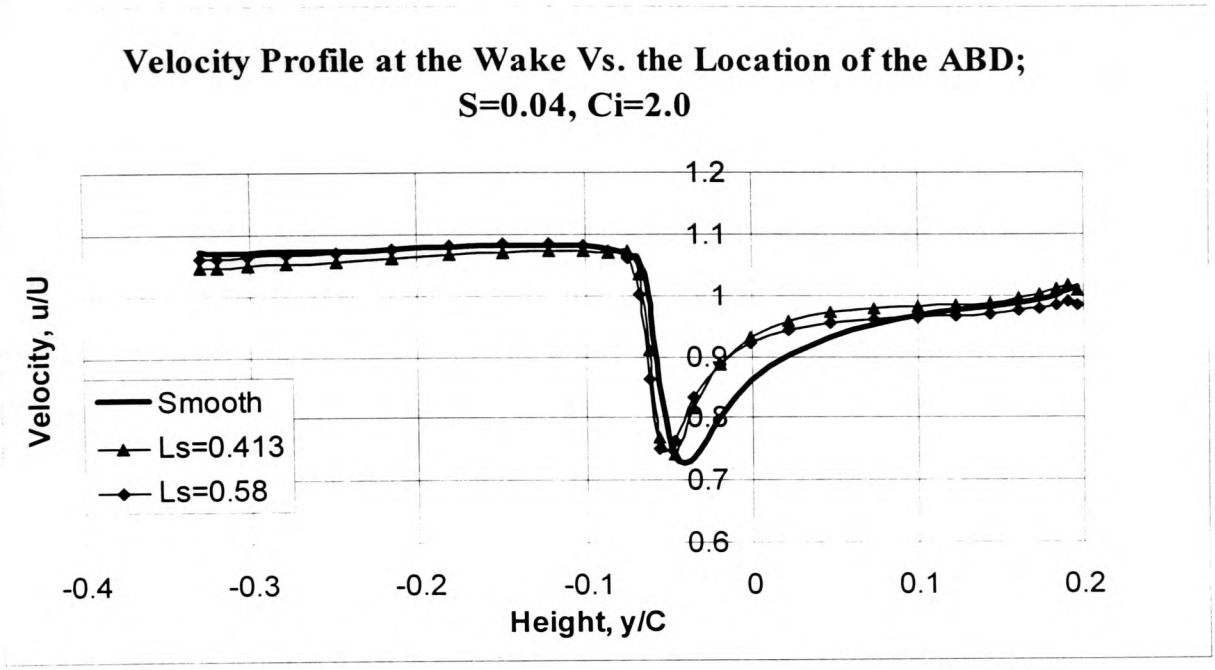

Figure 5-35

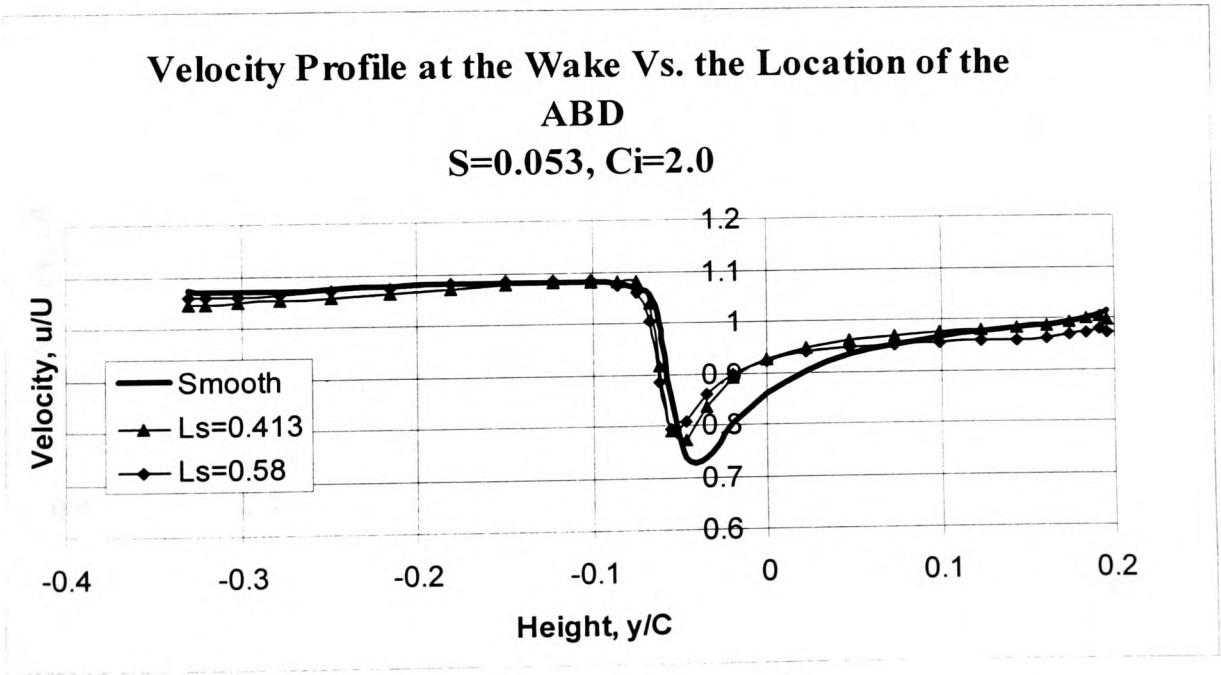

Figure 5-36

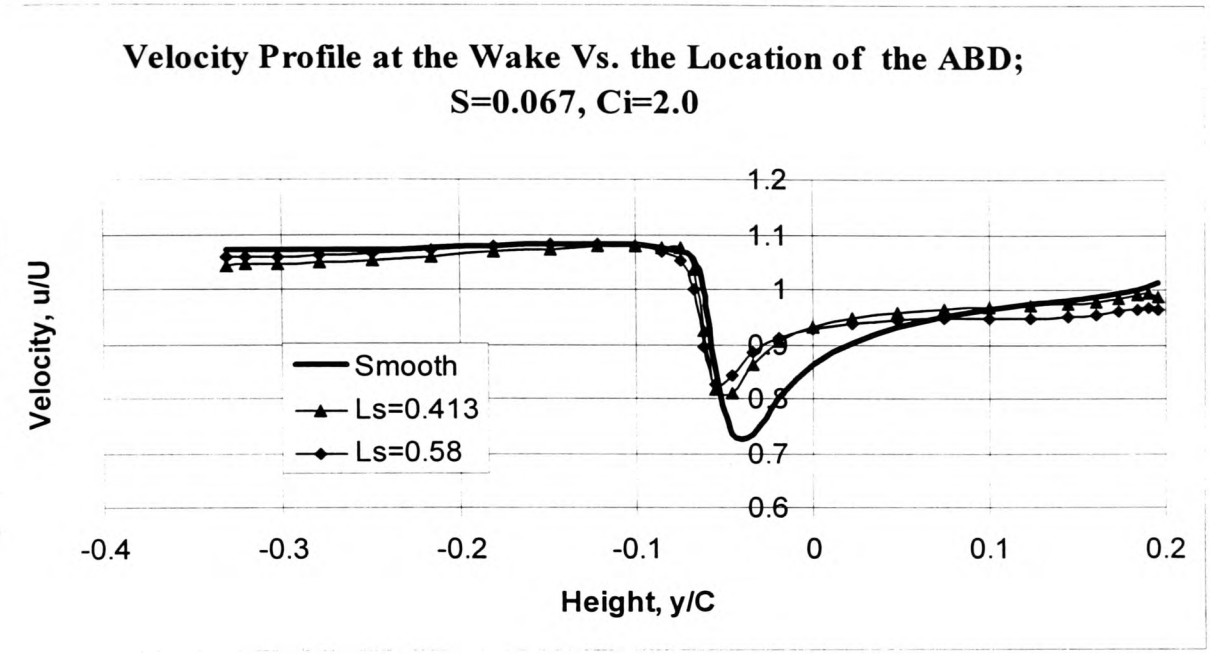

Figure 5-37

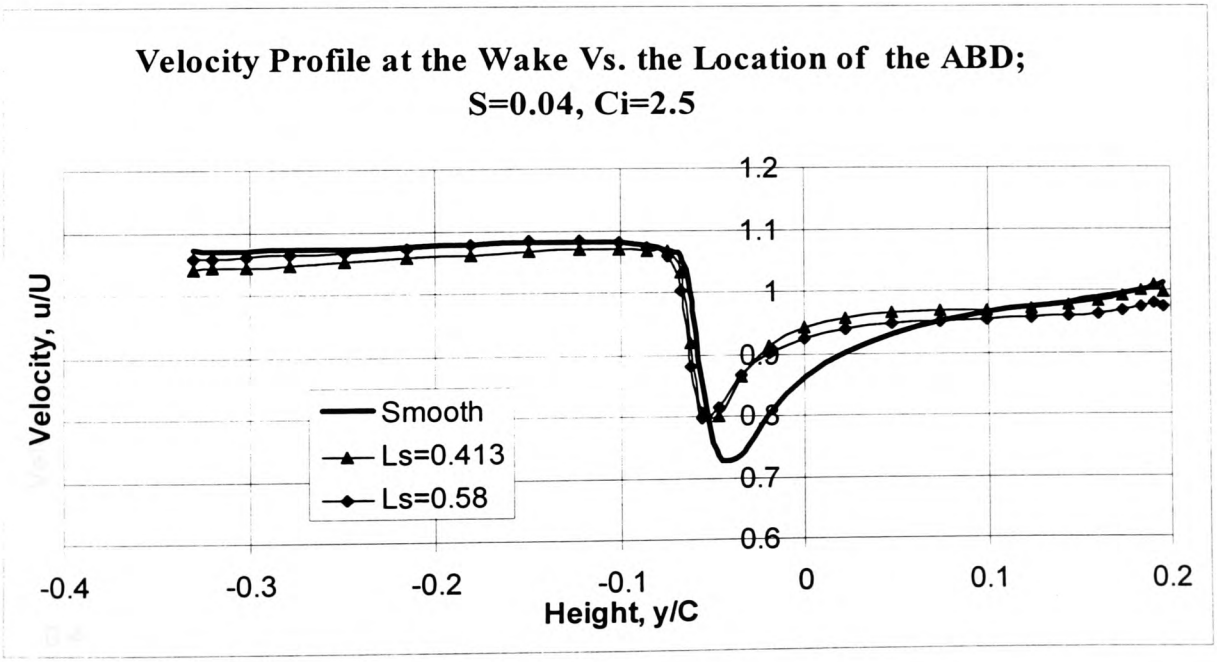

Figure 5-38

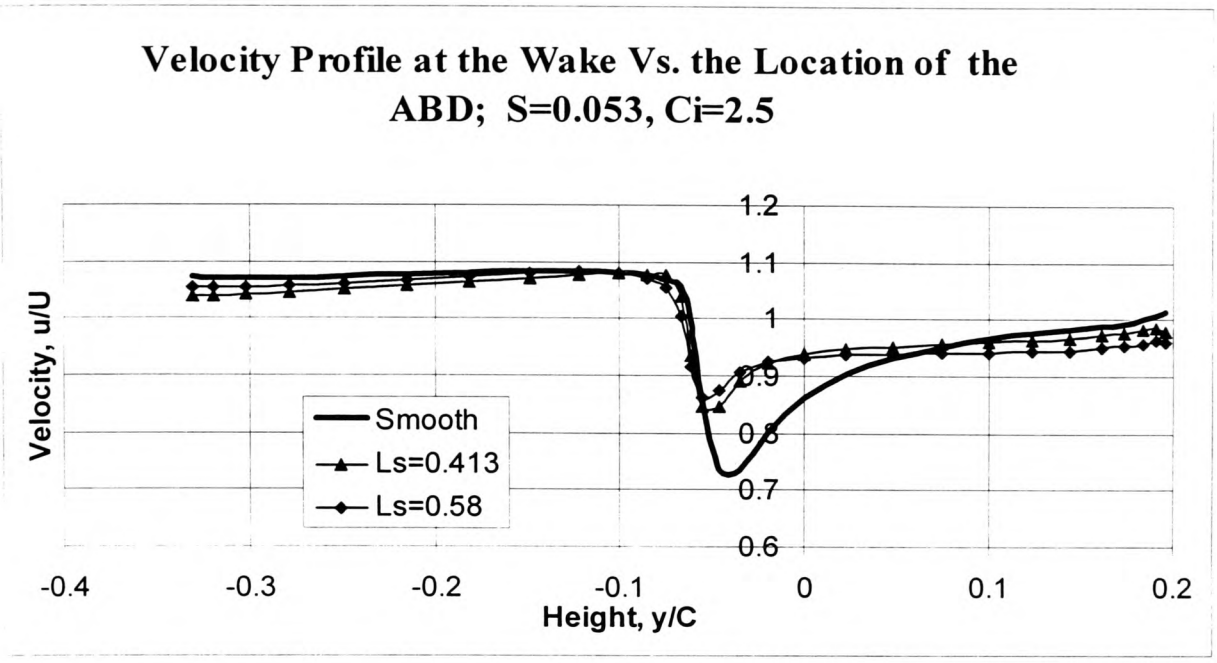

Figure 5-39

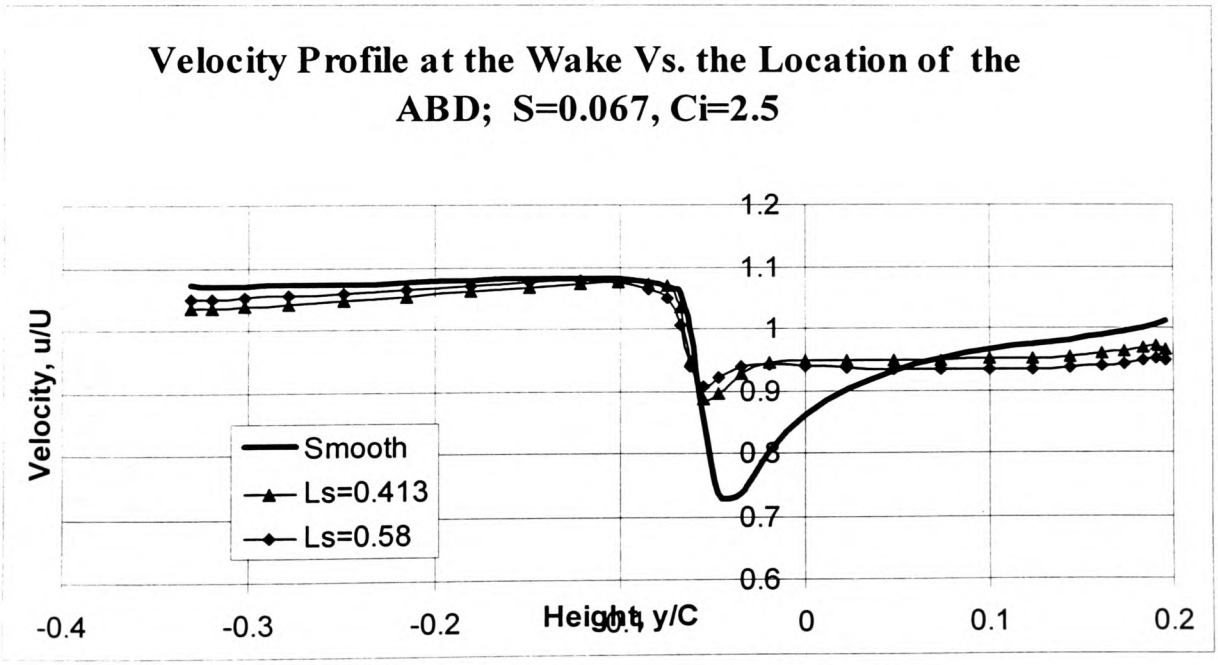

Figure 5-40

5.9.4.2 Alpha = 8 Degrees

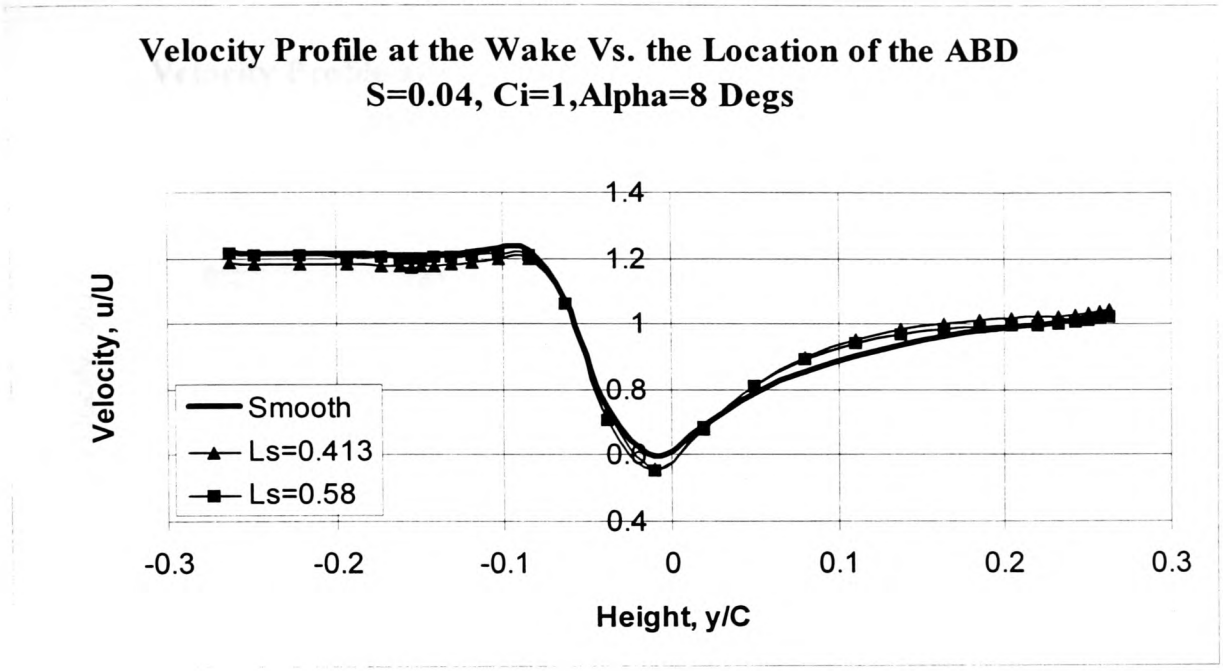

Figure 5-41

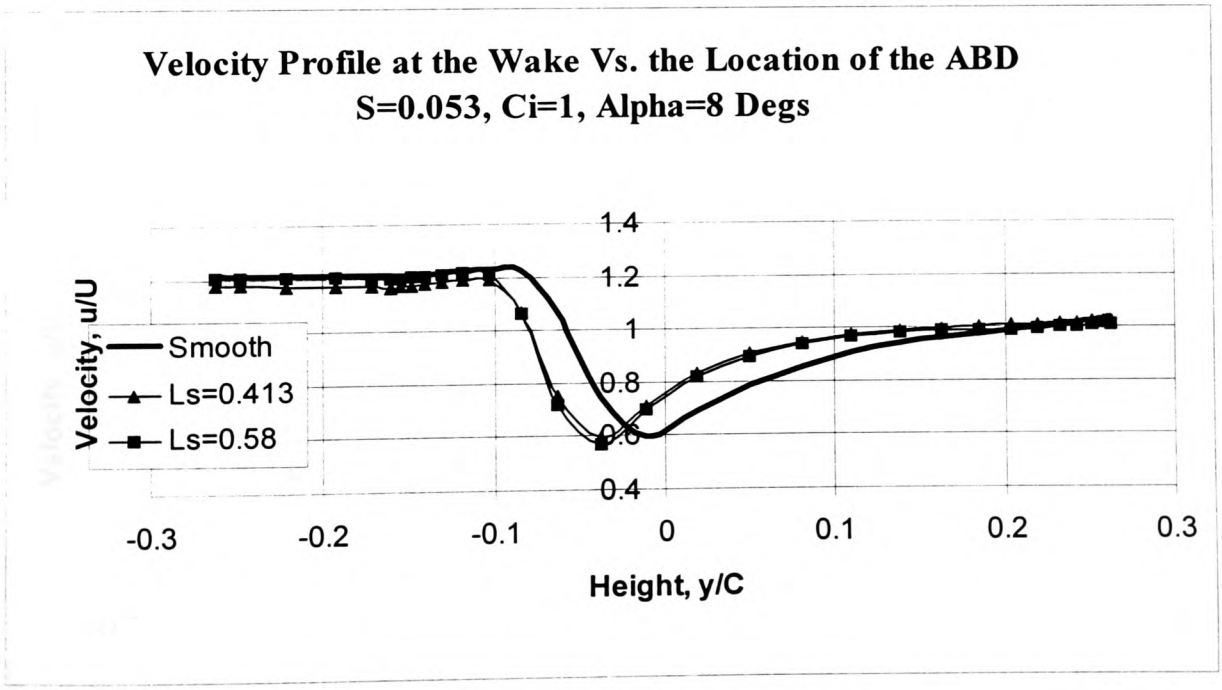

Figure 5-42

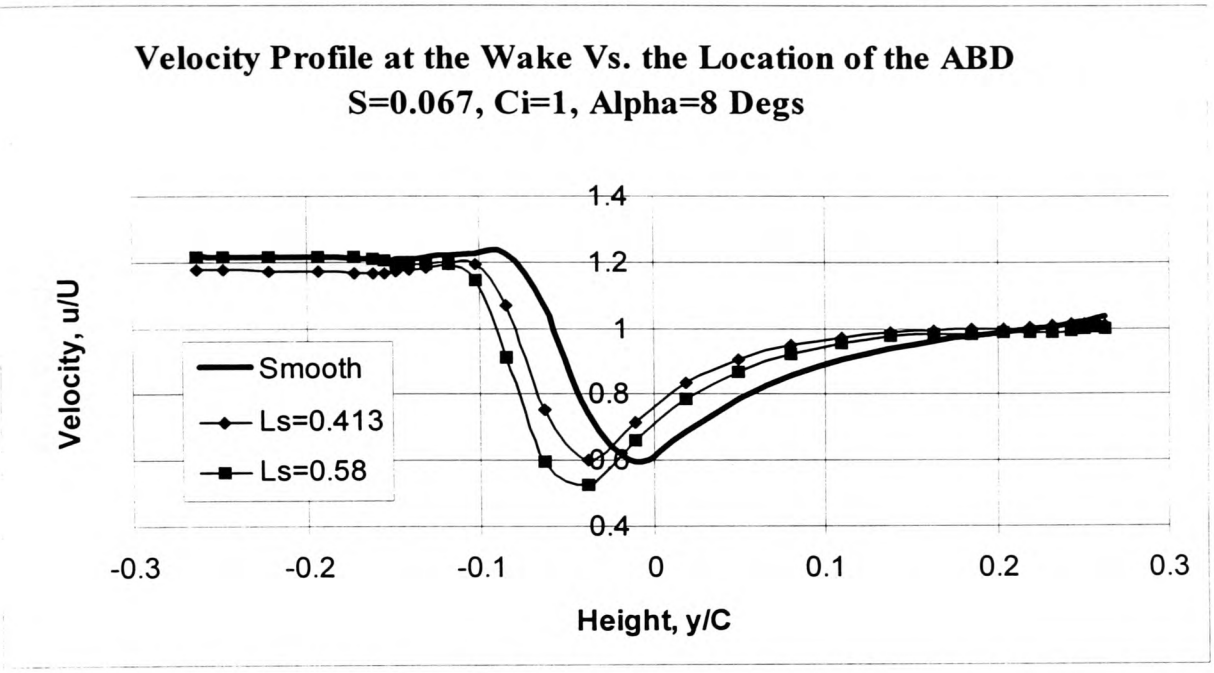

Figure 5-43

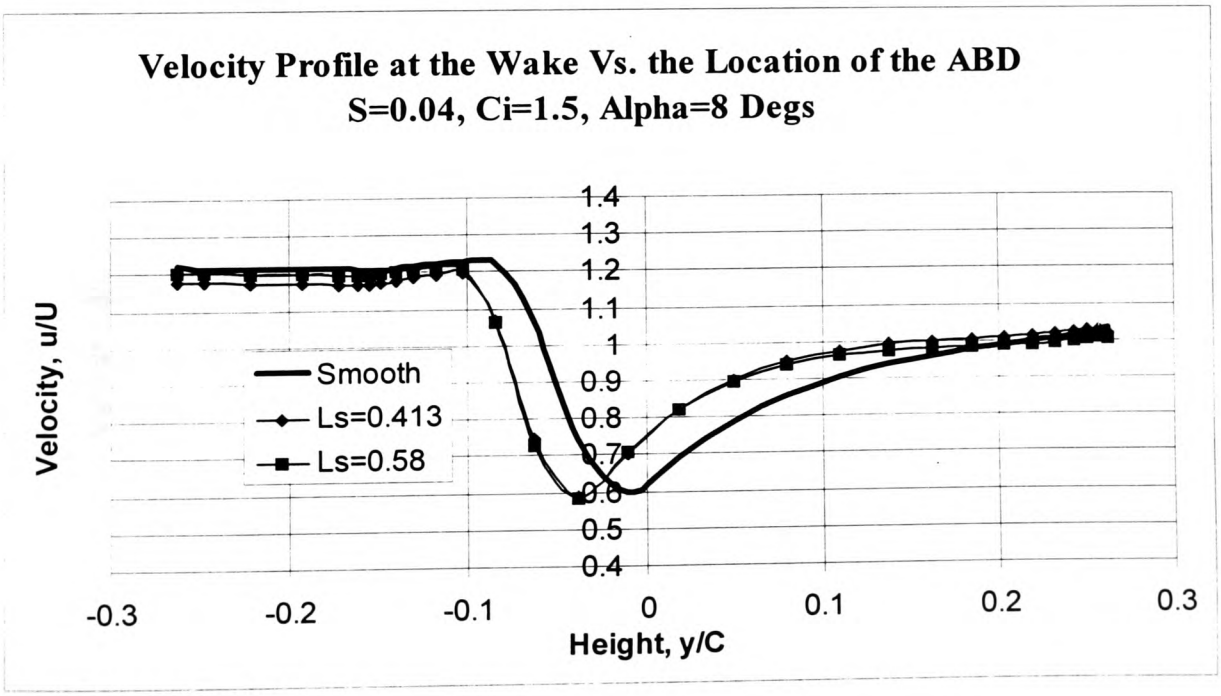

Figure 5-44

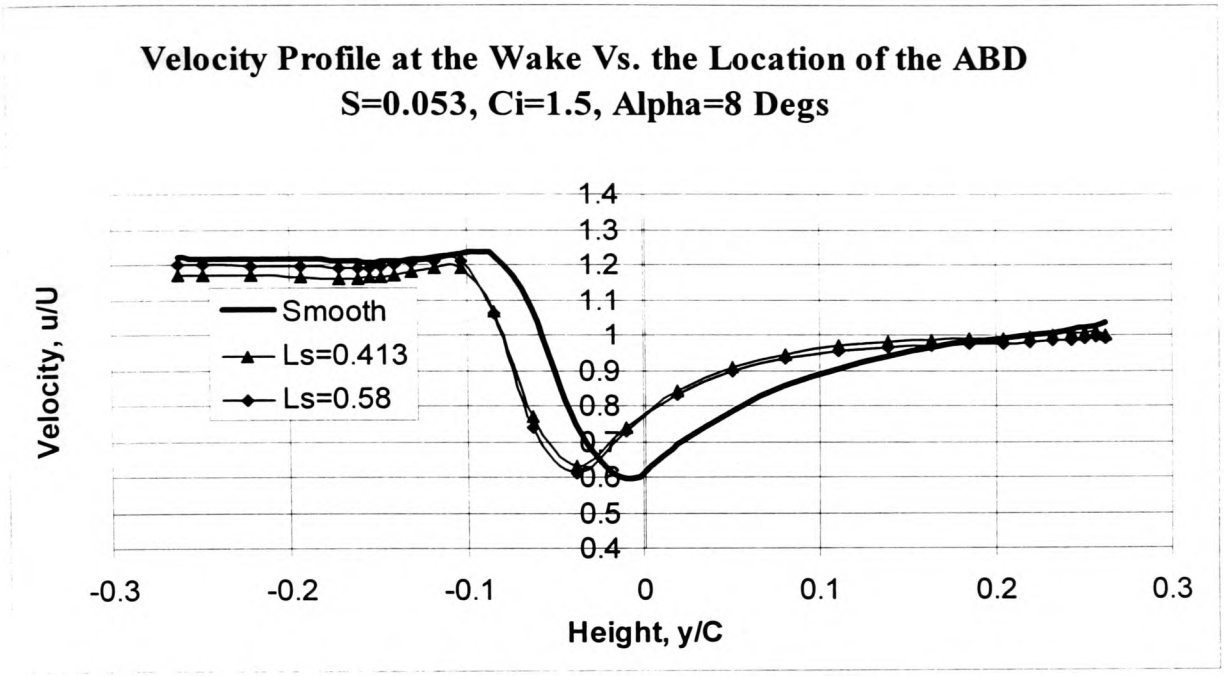

Figure 5-45

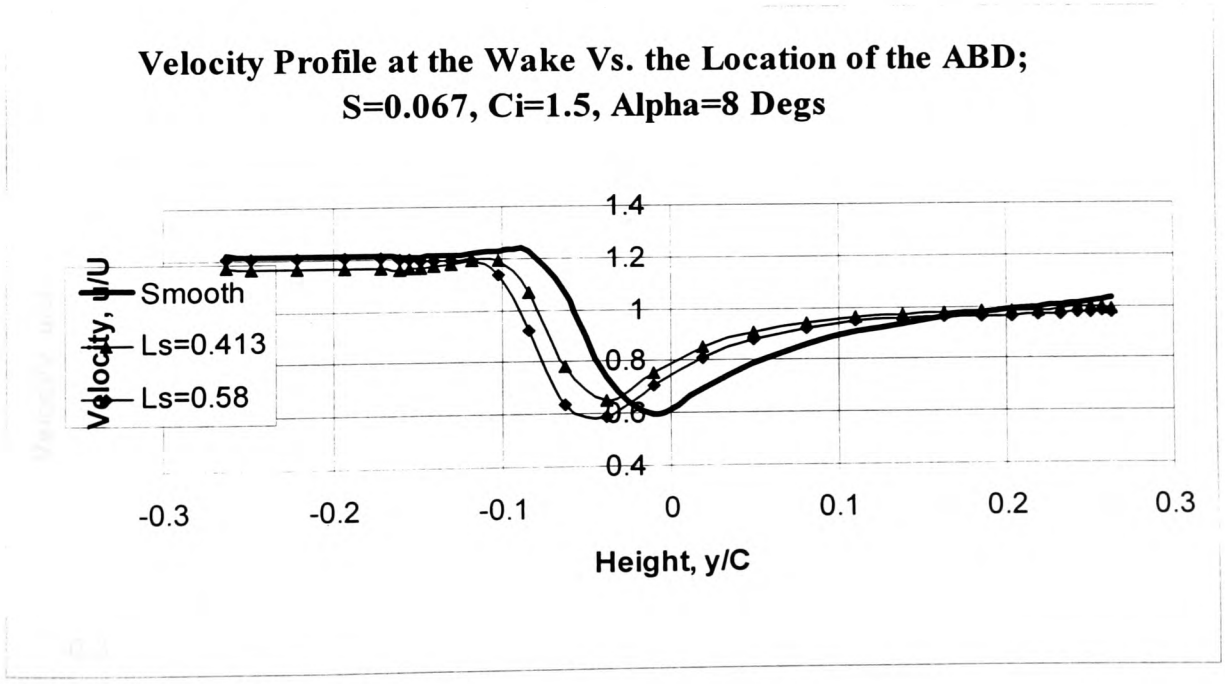

Figure 5-46

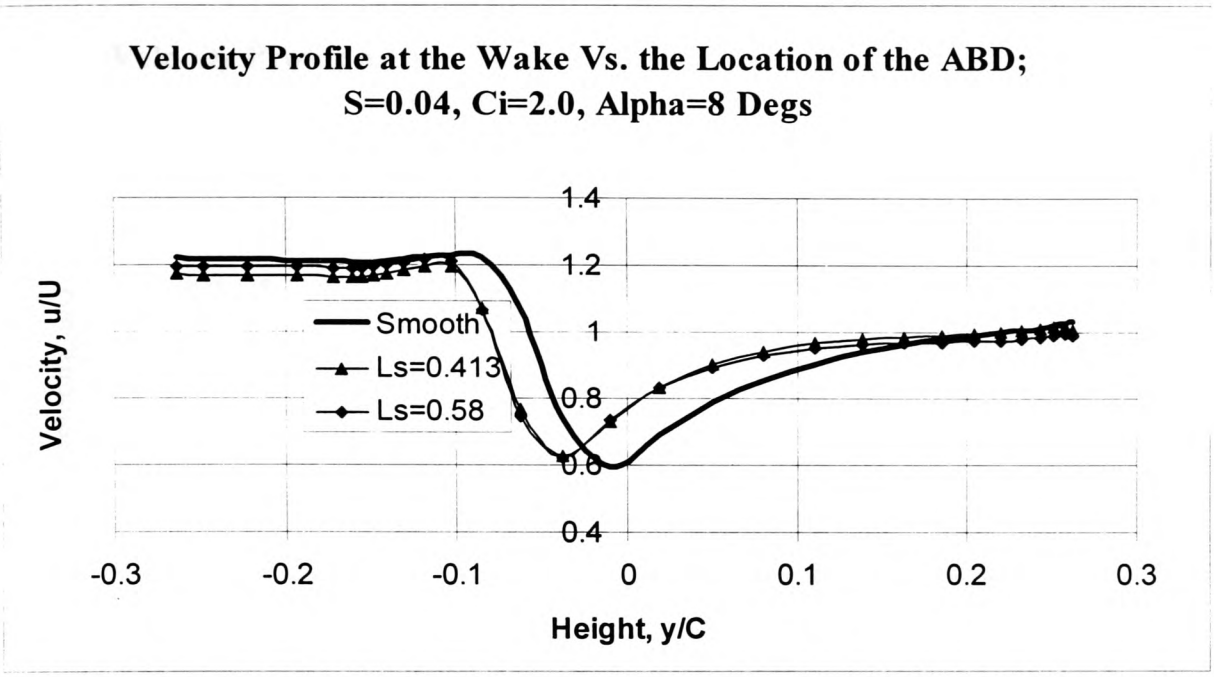

Figure 5-47

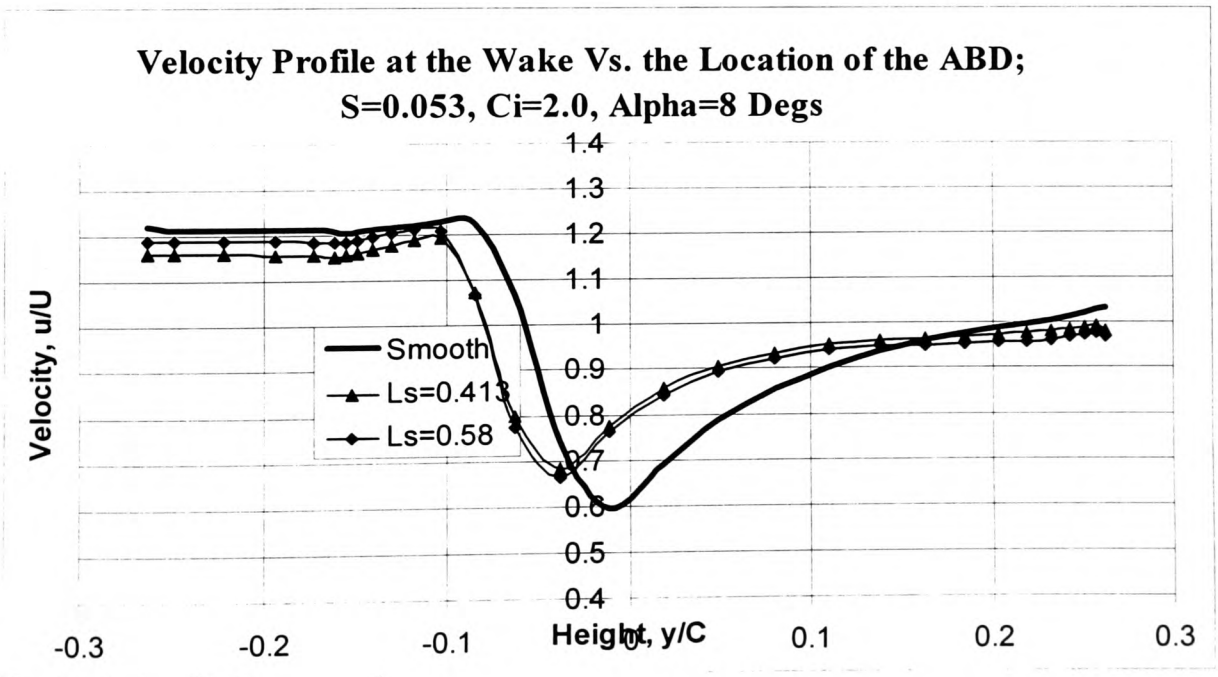

Figure 5-48

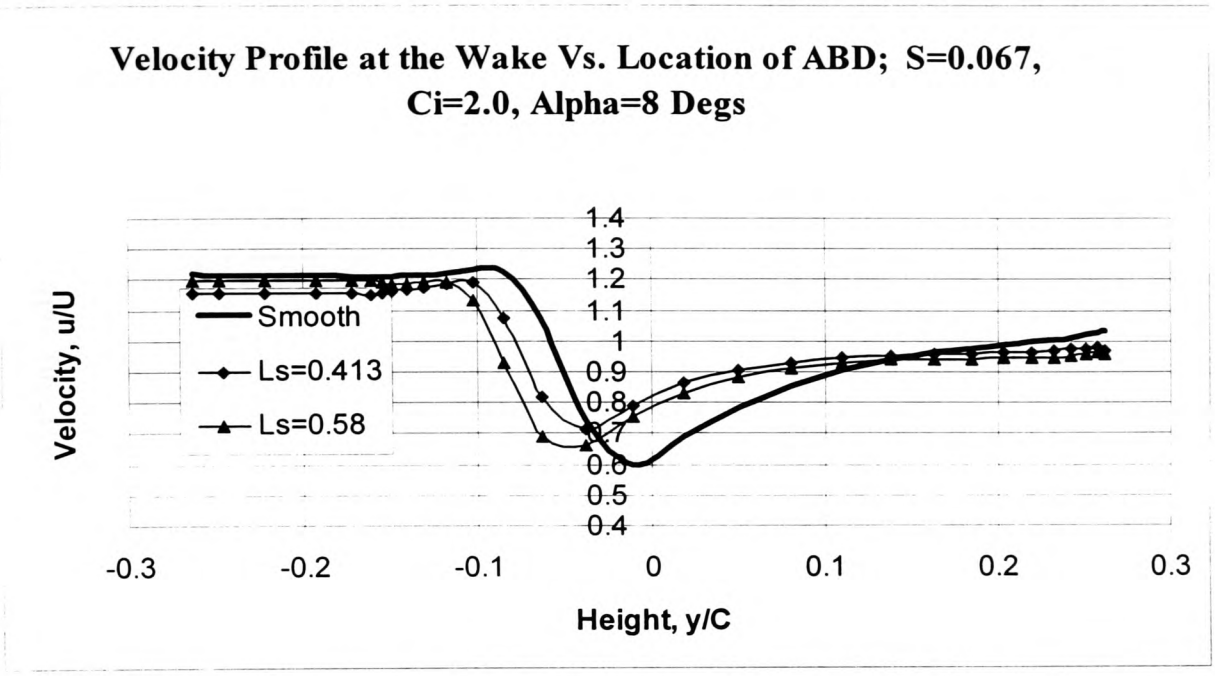

Figure 5-49

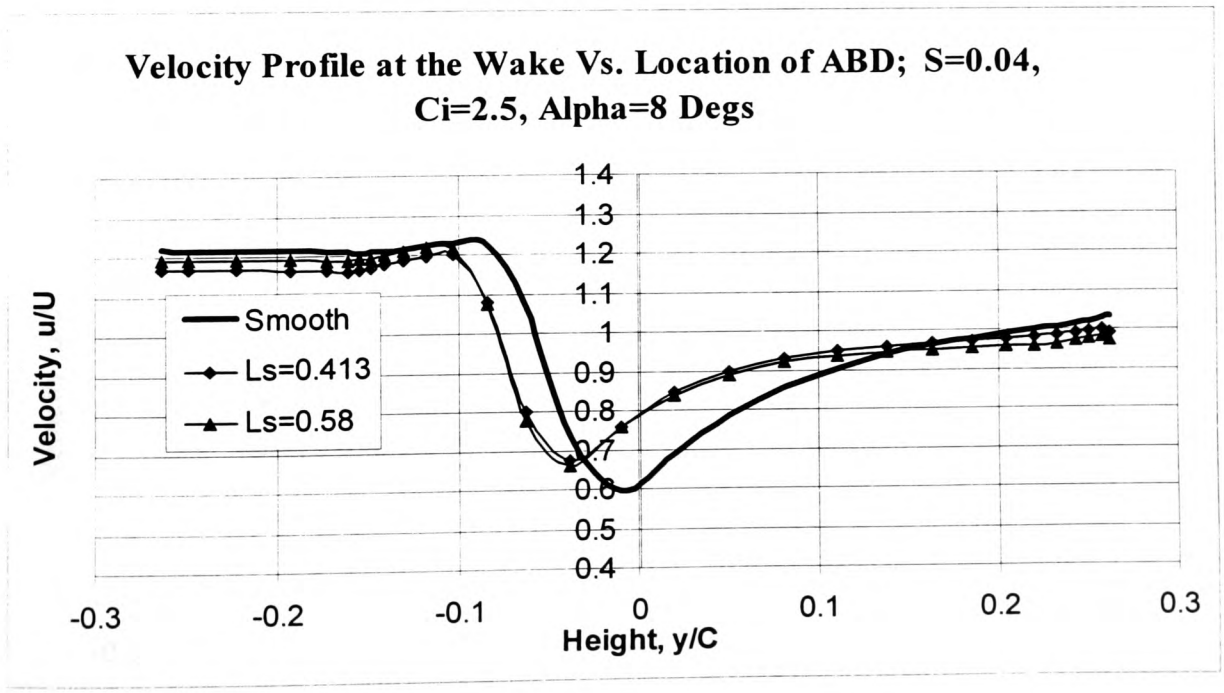

Figure 5-50

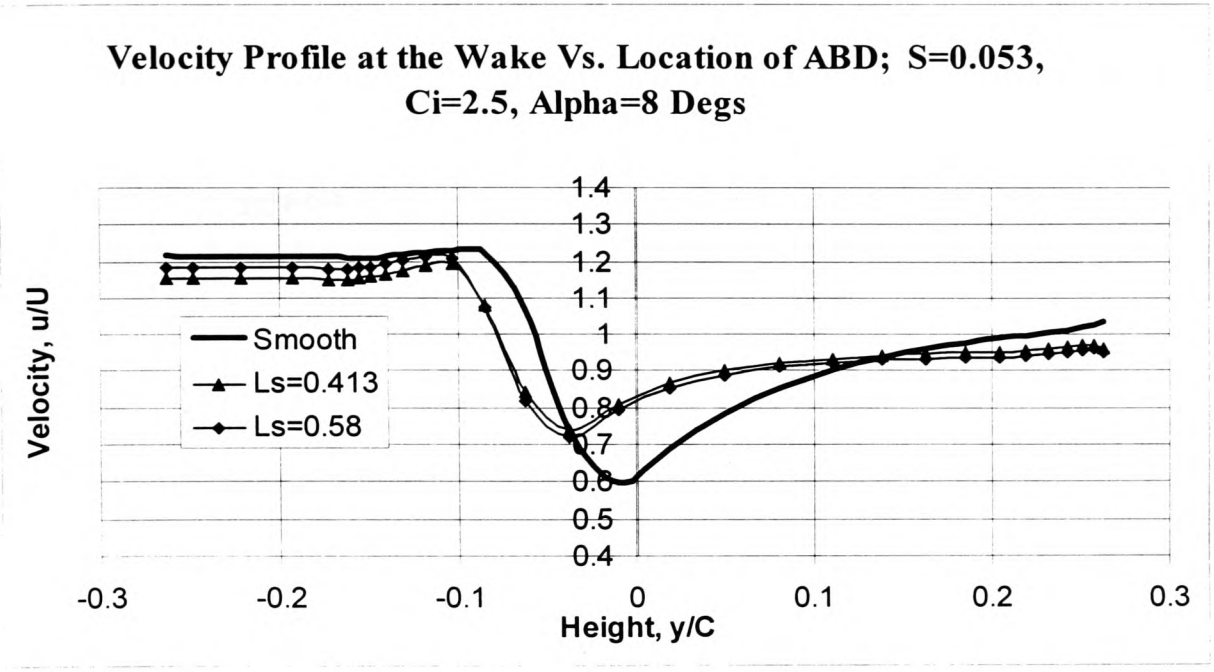

Figure 5-51

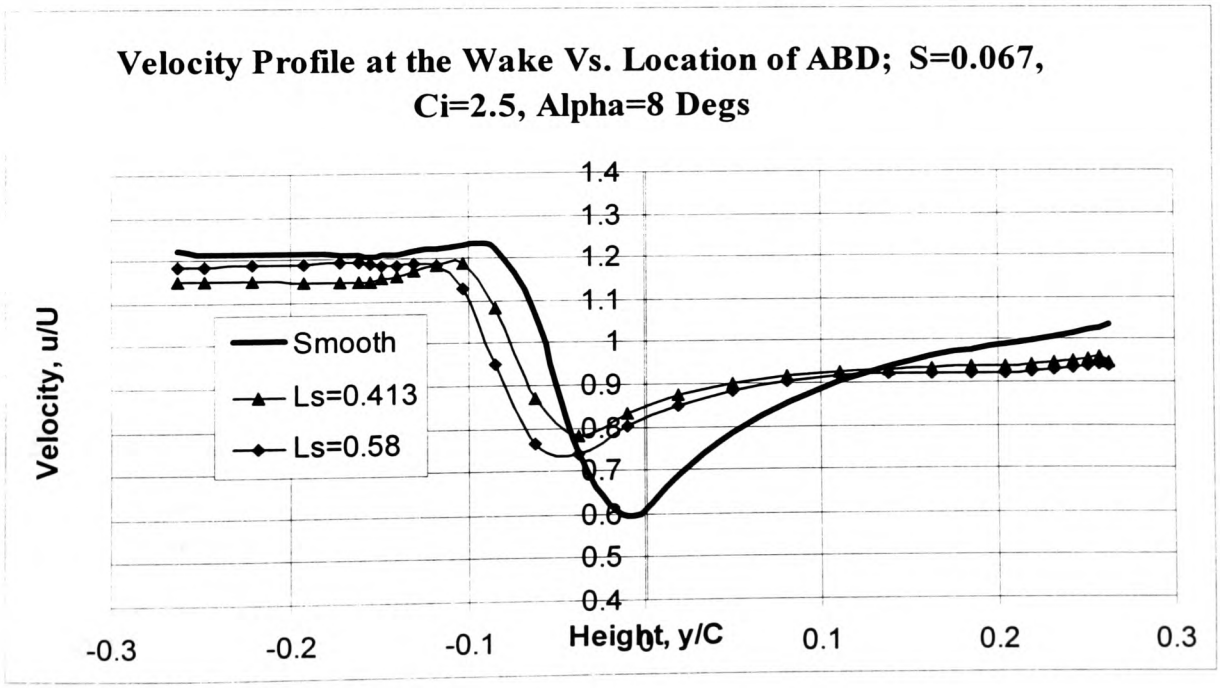

Figure 5-52

5.9.4.3 Alpha = 12 Degrees

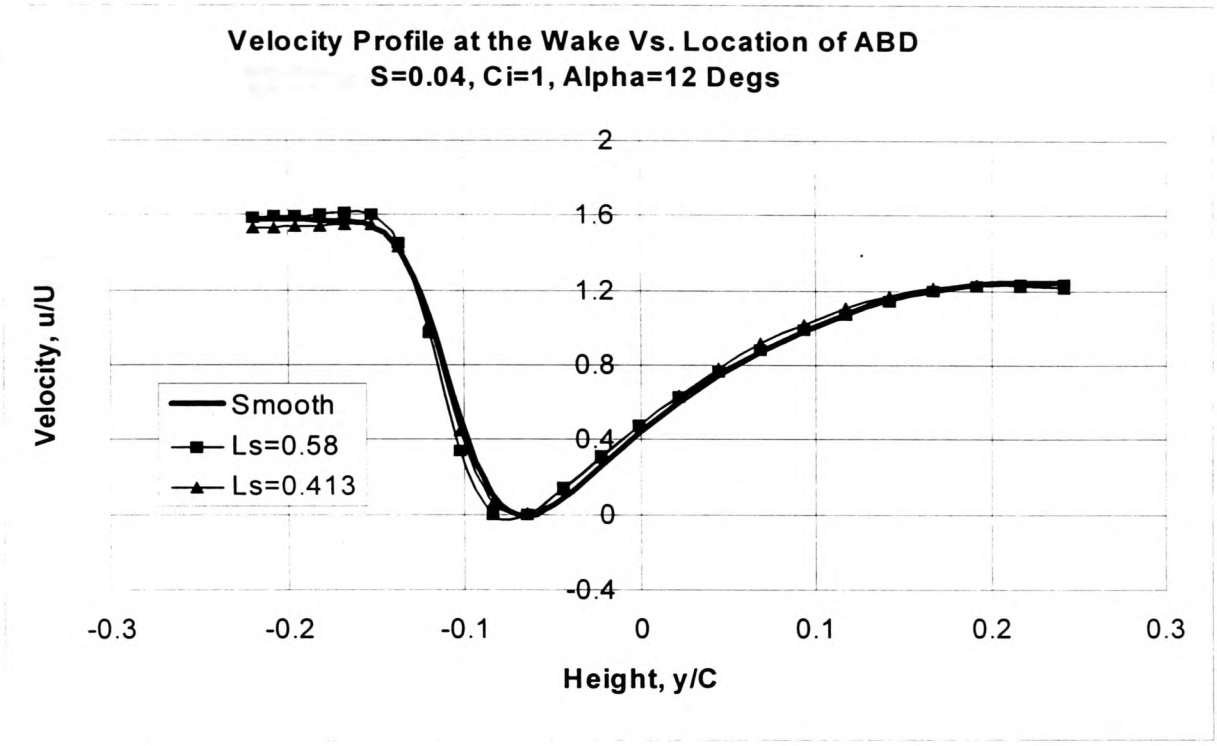

Figure 5-53

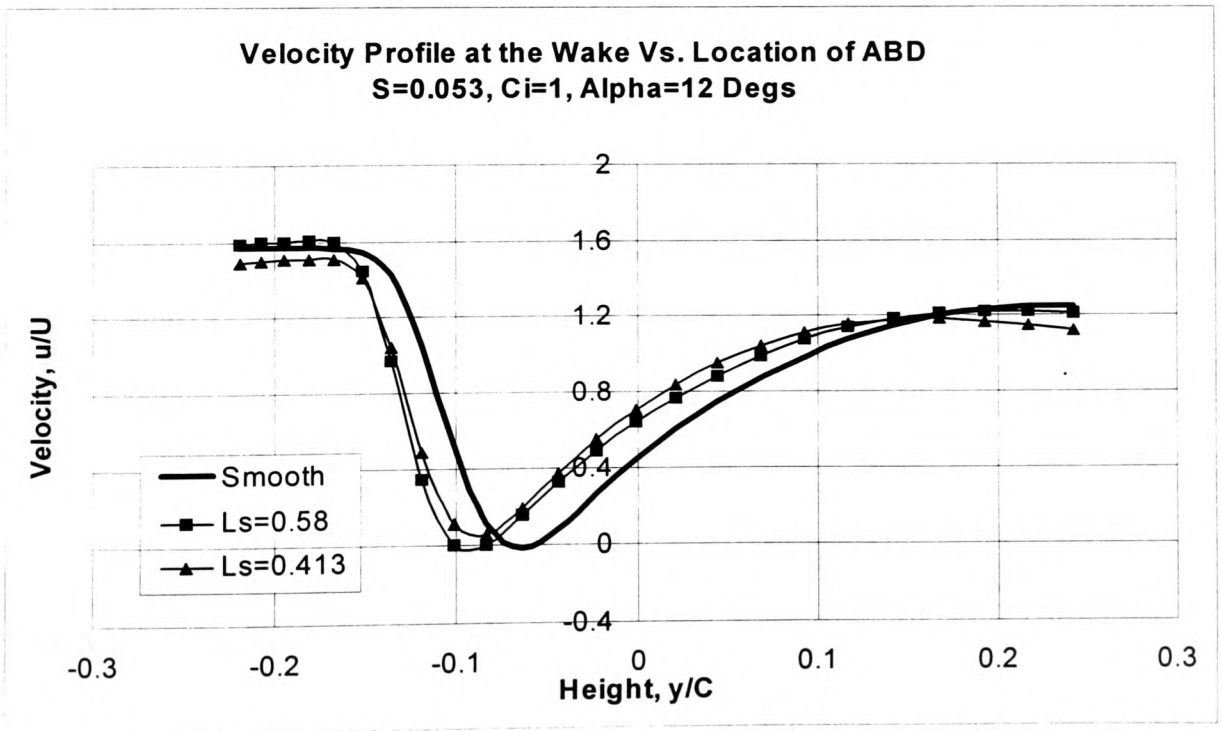

Figure 5-54

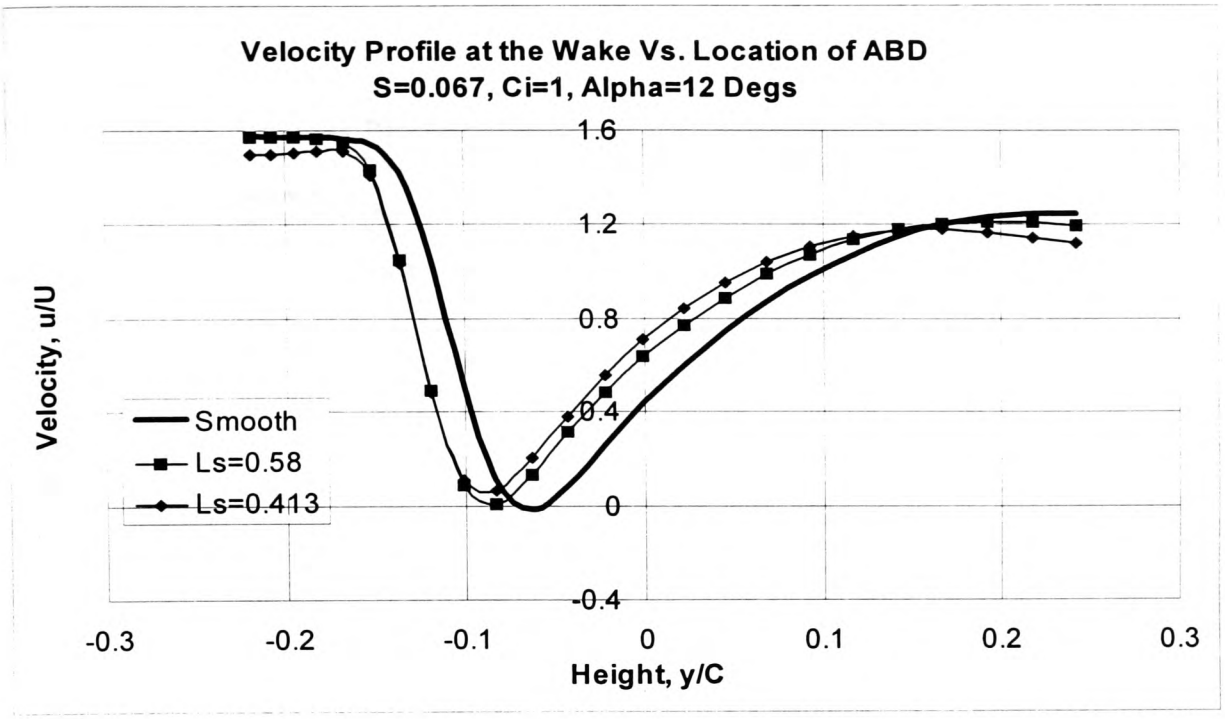

Figure 5-55

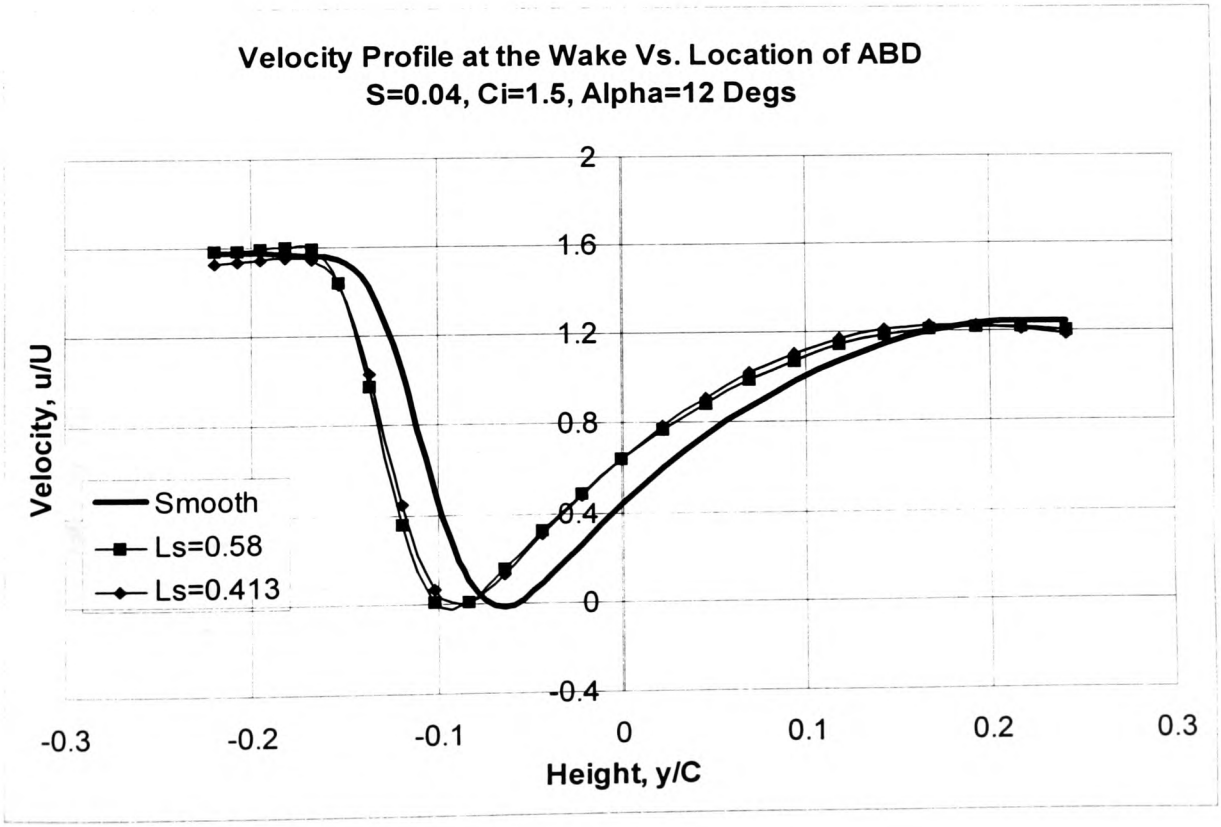

Figure 5-56

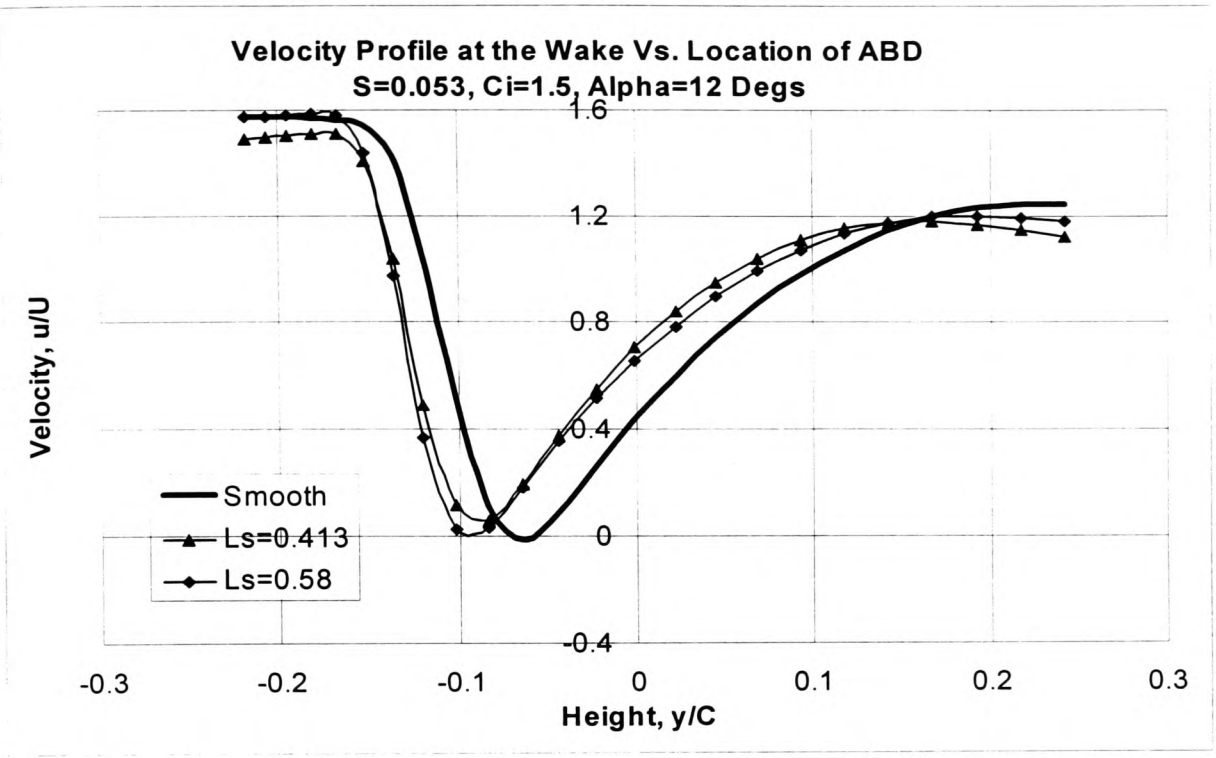

Figure 5-57

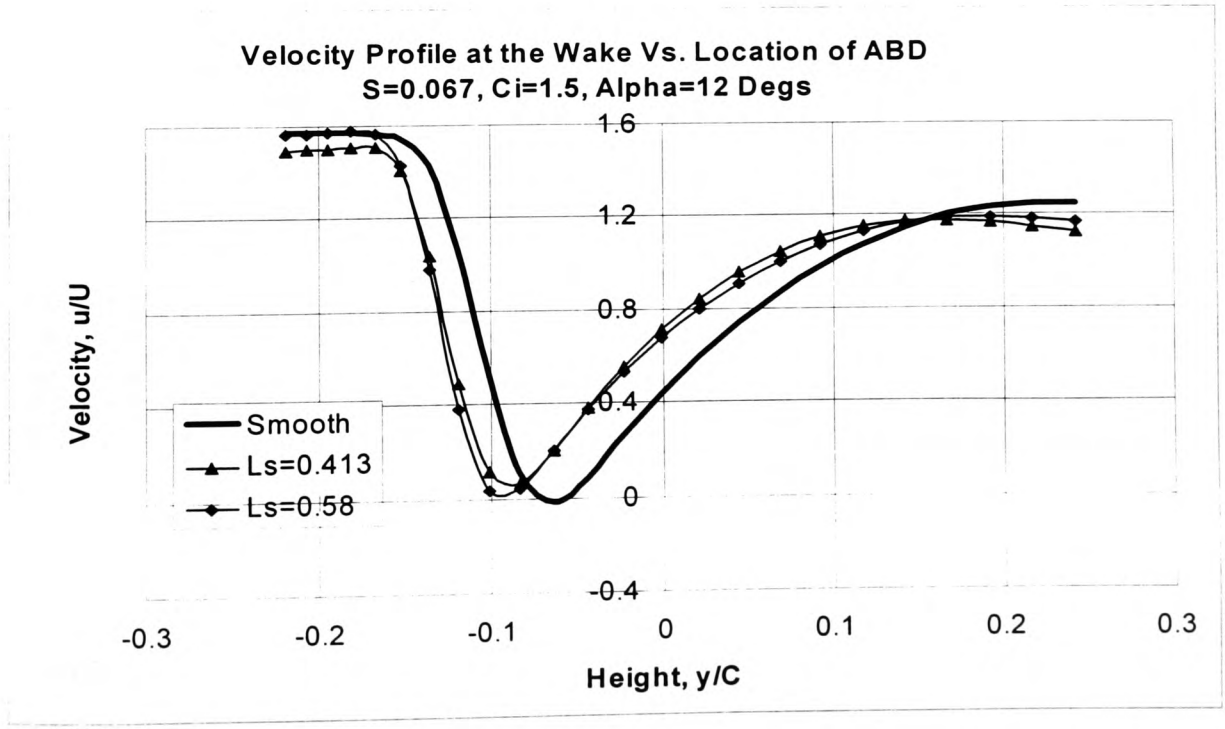

Figure 5-58

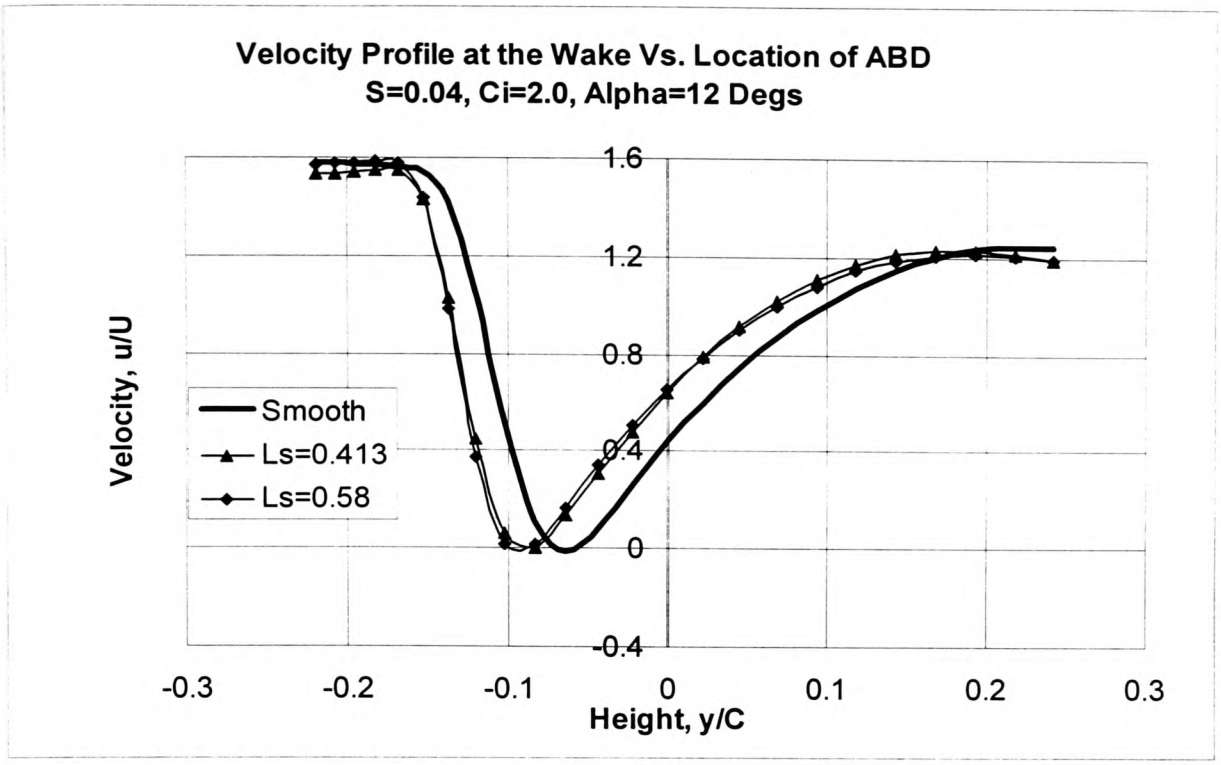

Figure 5-59

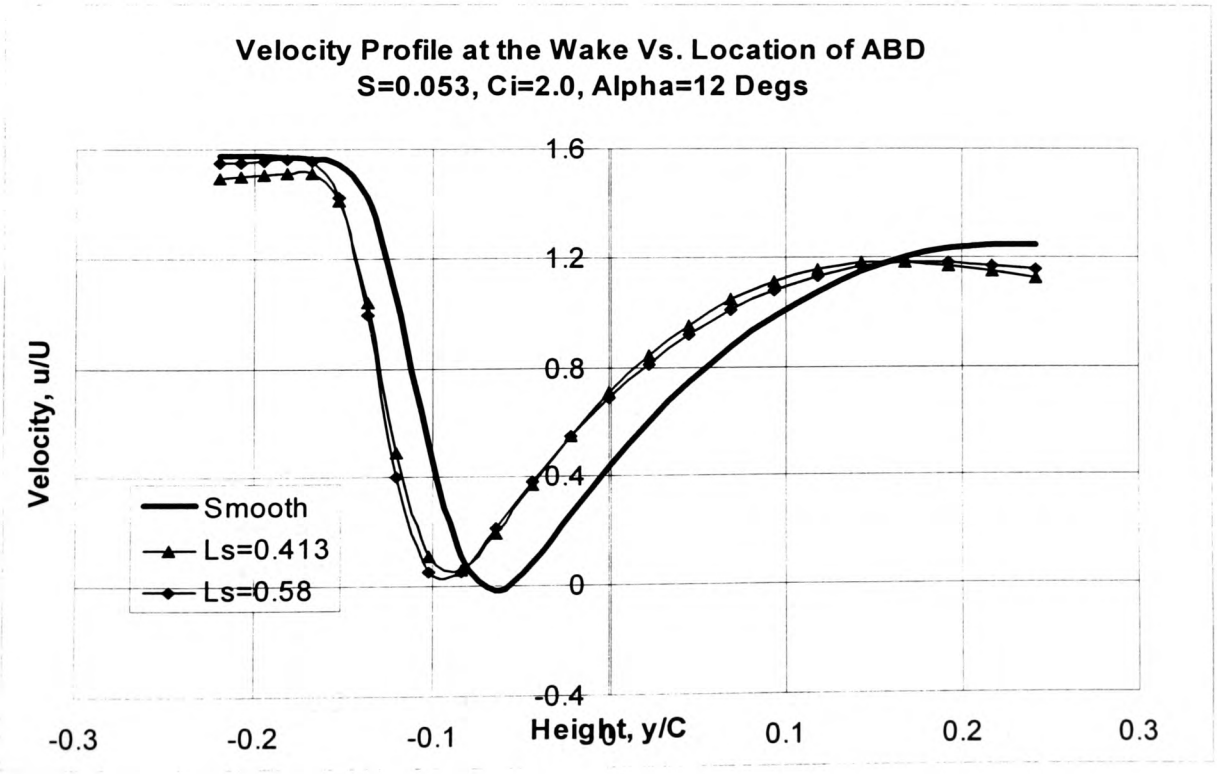

Figure 5-60

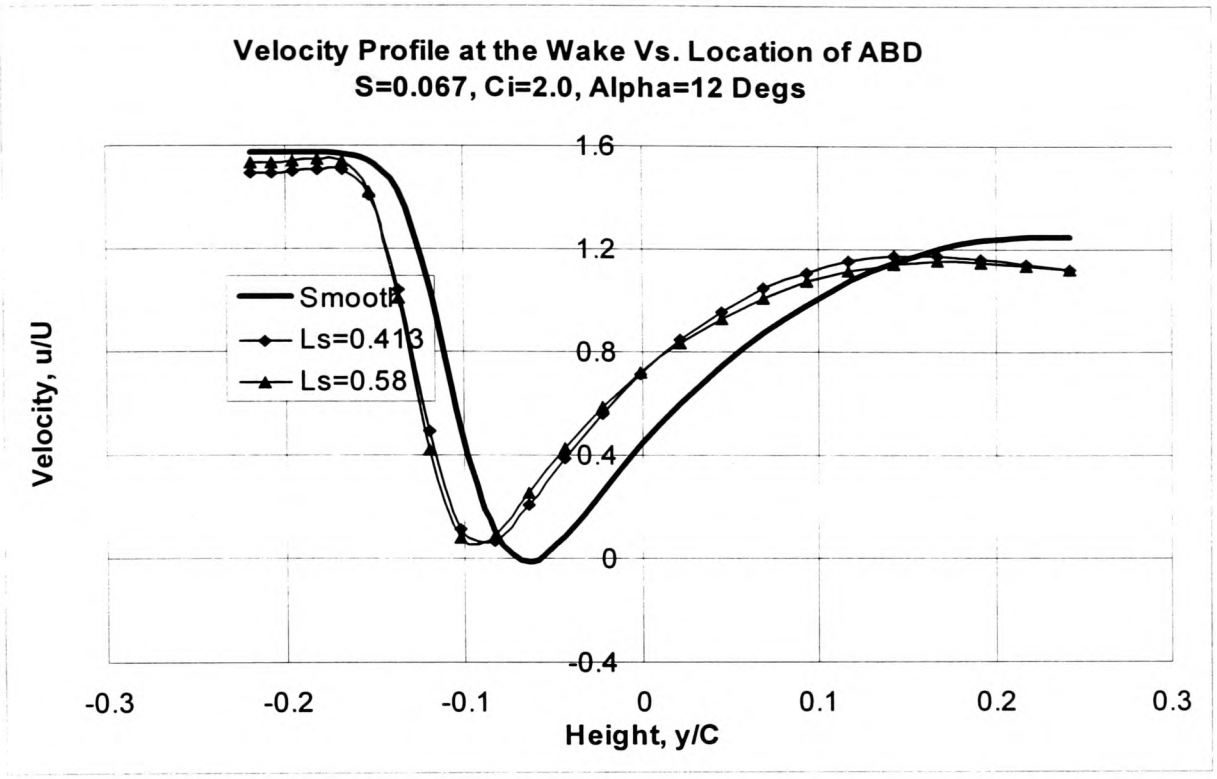

Figure 5-61

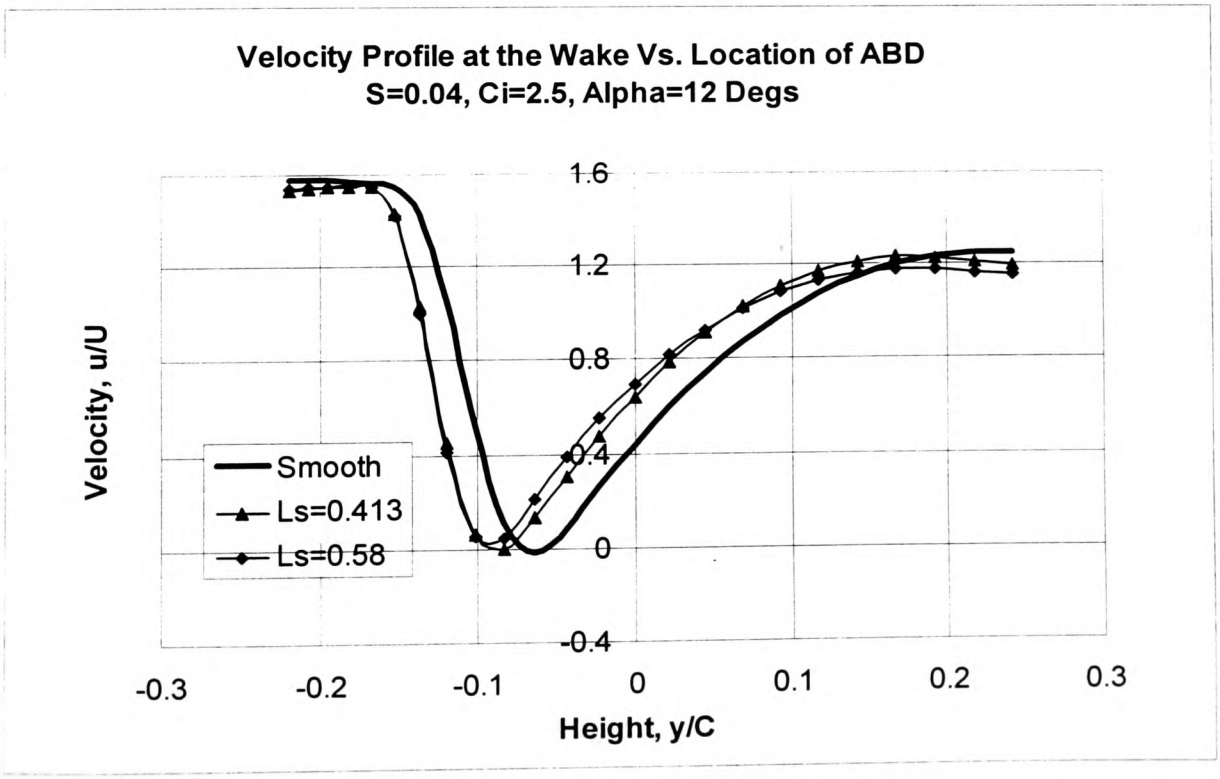

Figure 5-62

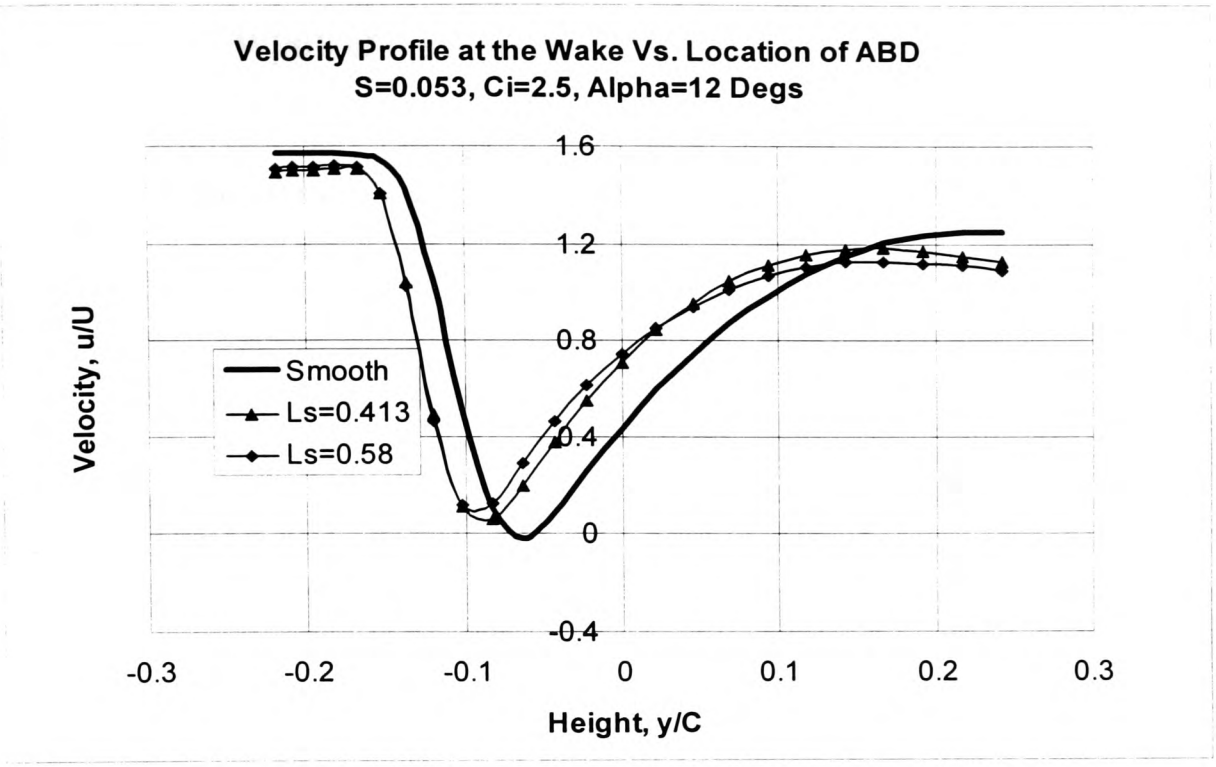

Figure 5-63

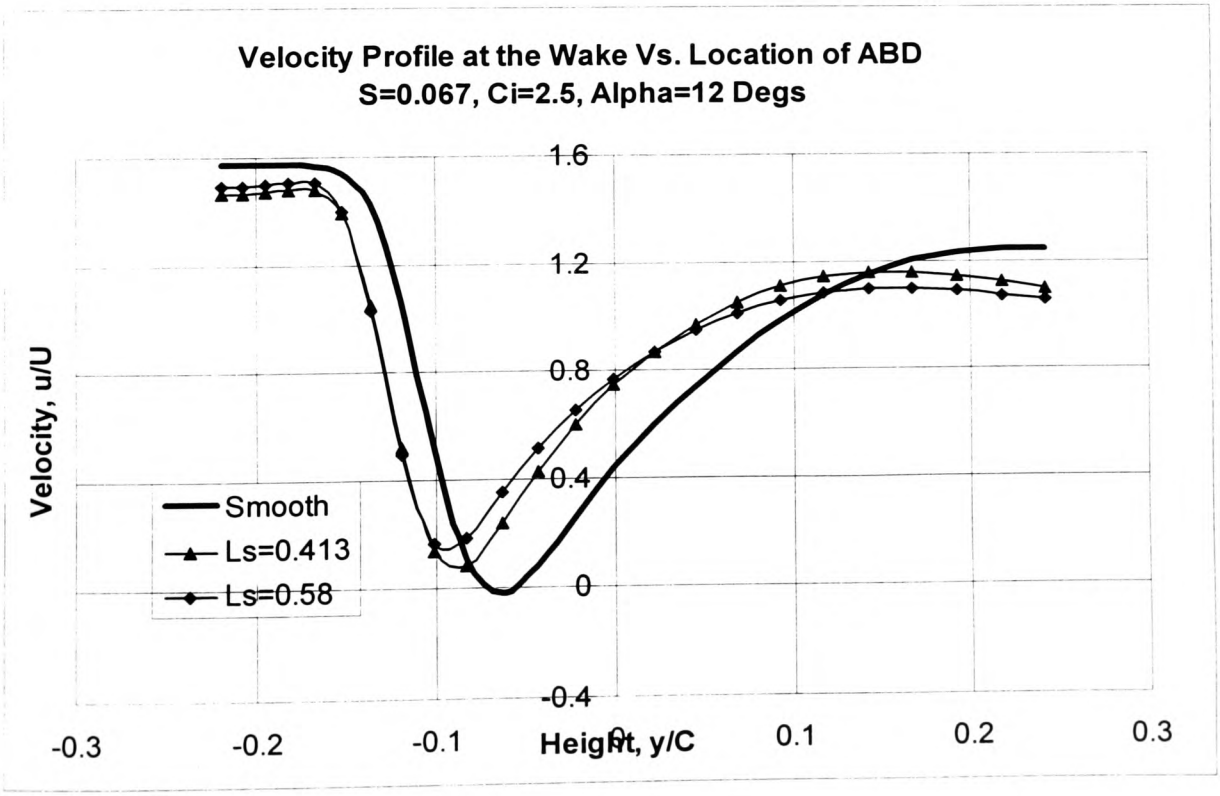

Figure 5-64

5.9.5 Effect of Width of the ABD on the Wake Velocity Profile

5.9.5.1 Alpha = 4 Degrees

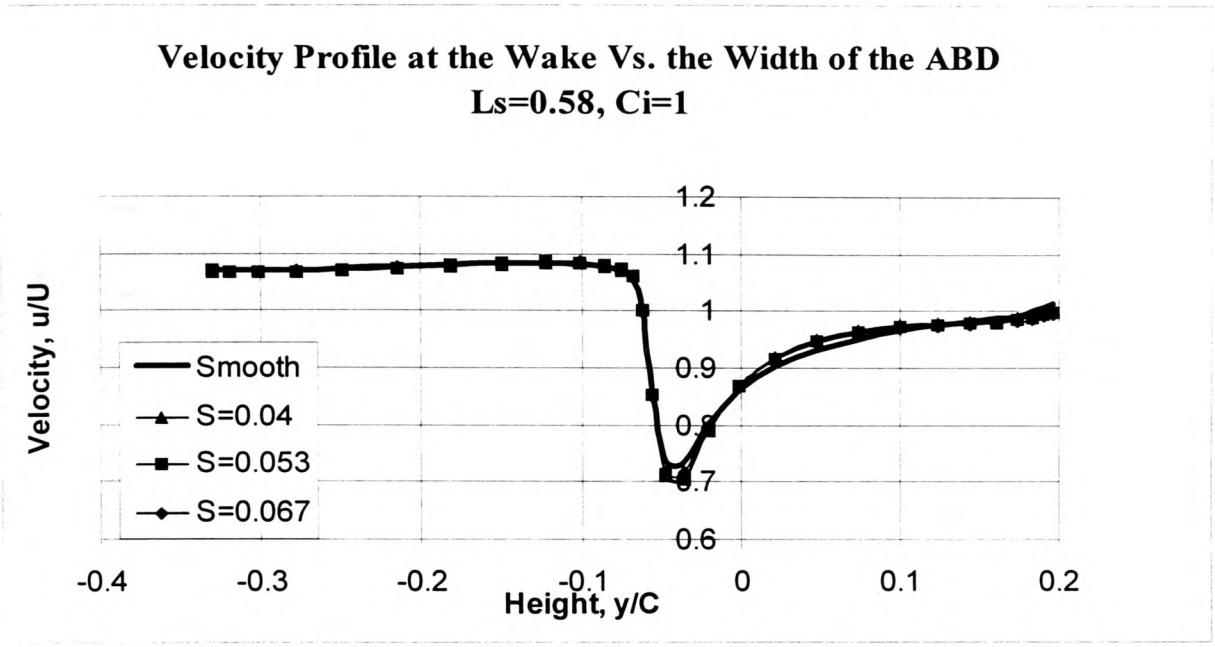

Figure 5-65

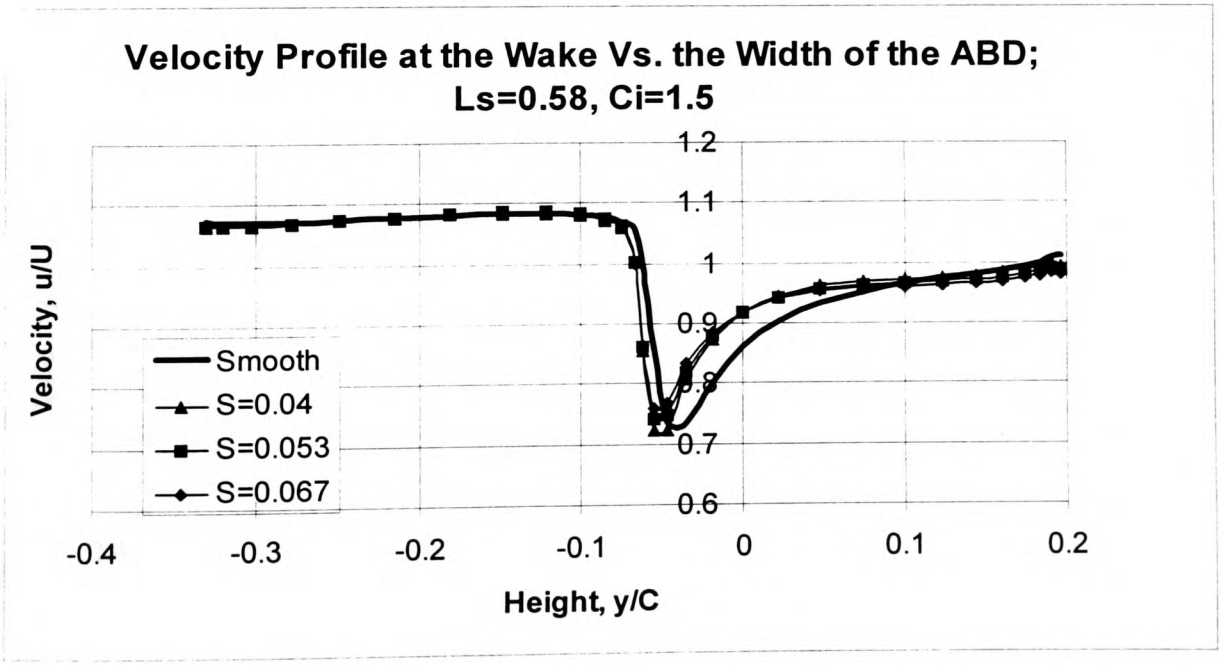

Figure 5-66

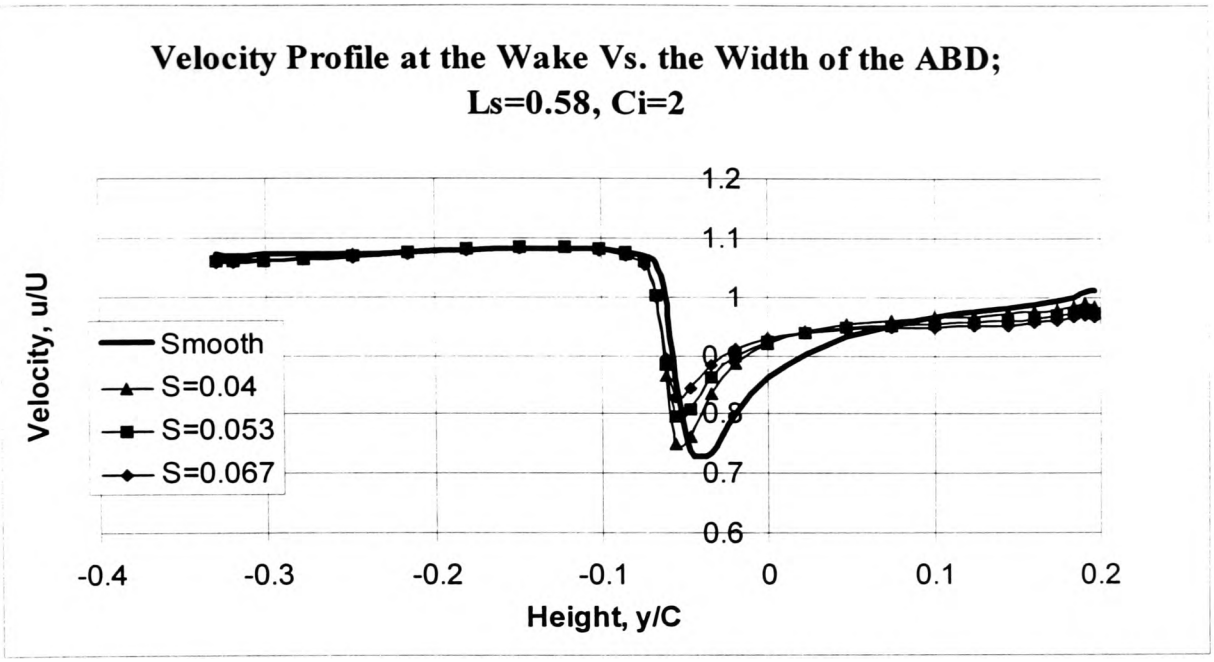

Figure 5-67

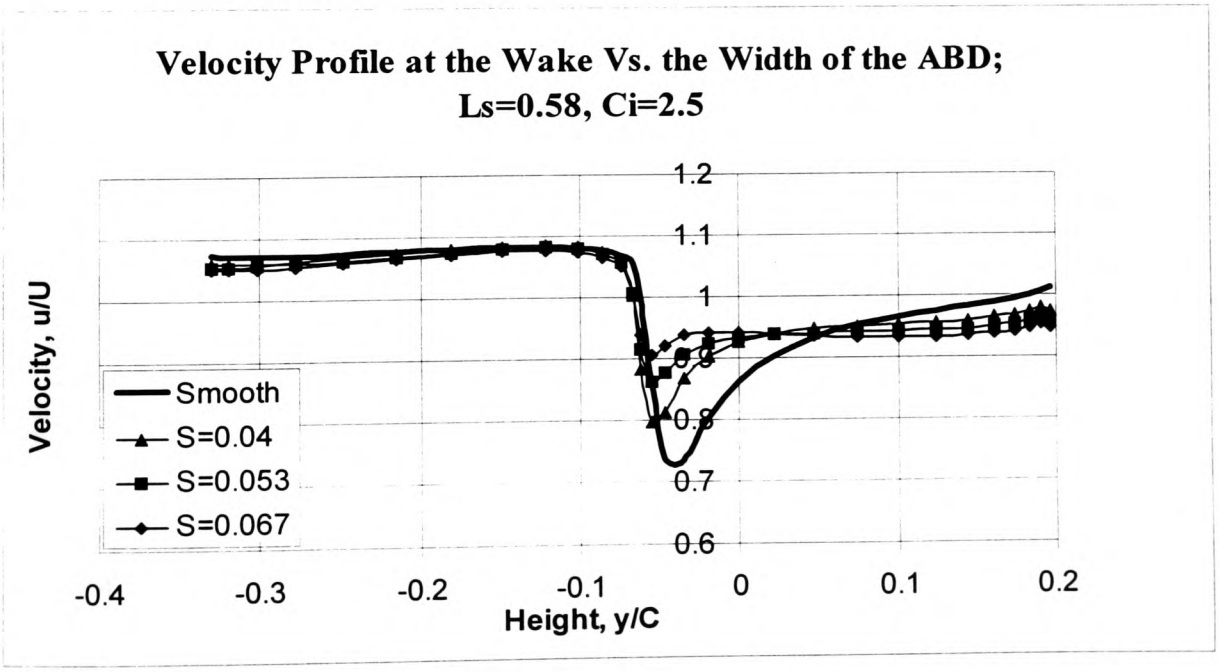

Figure 5-68

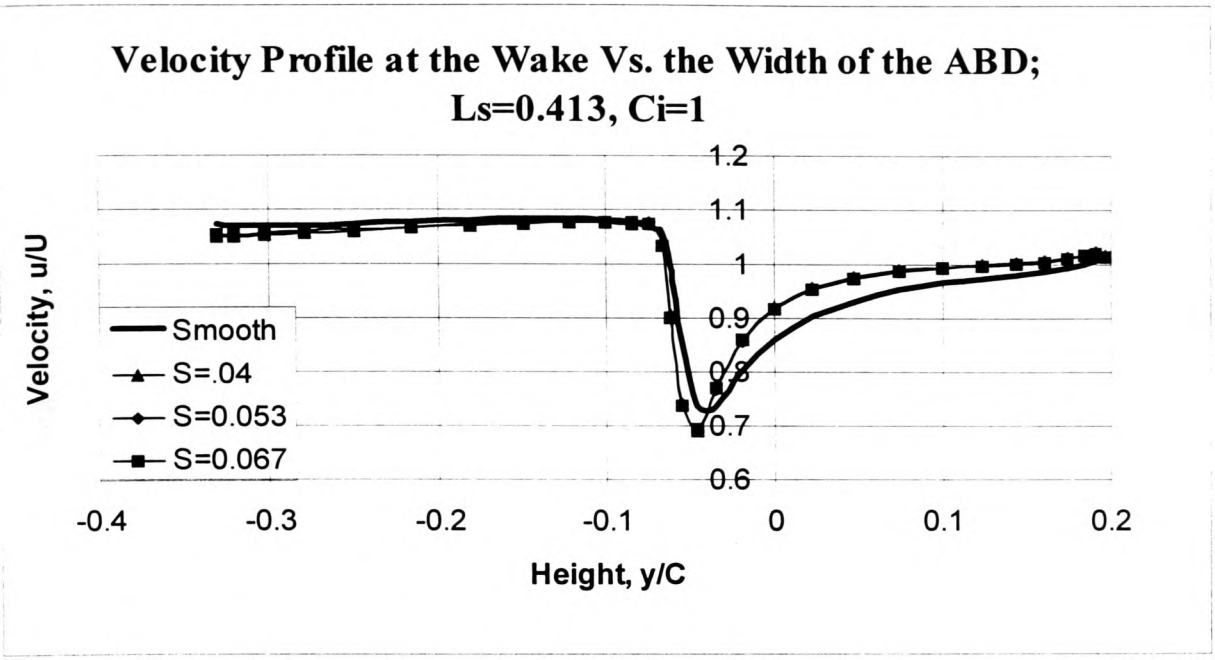

Figure 5-69

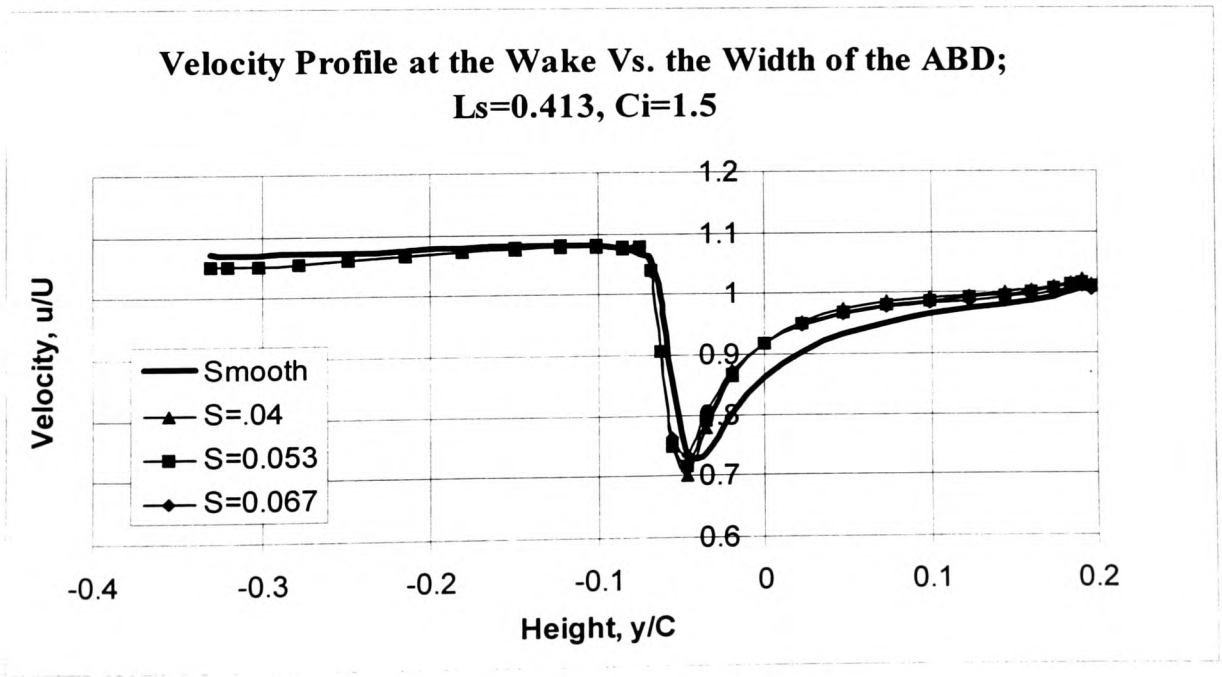

Figure 5-70

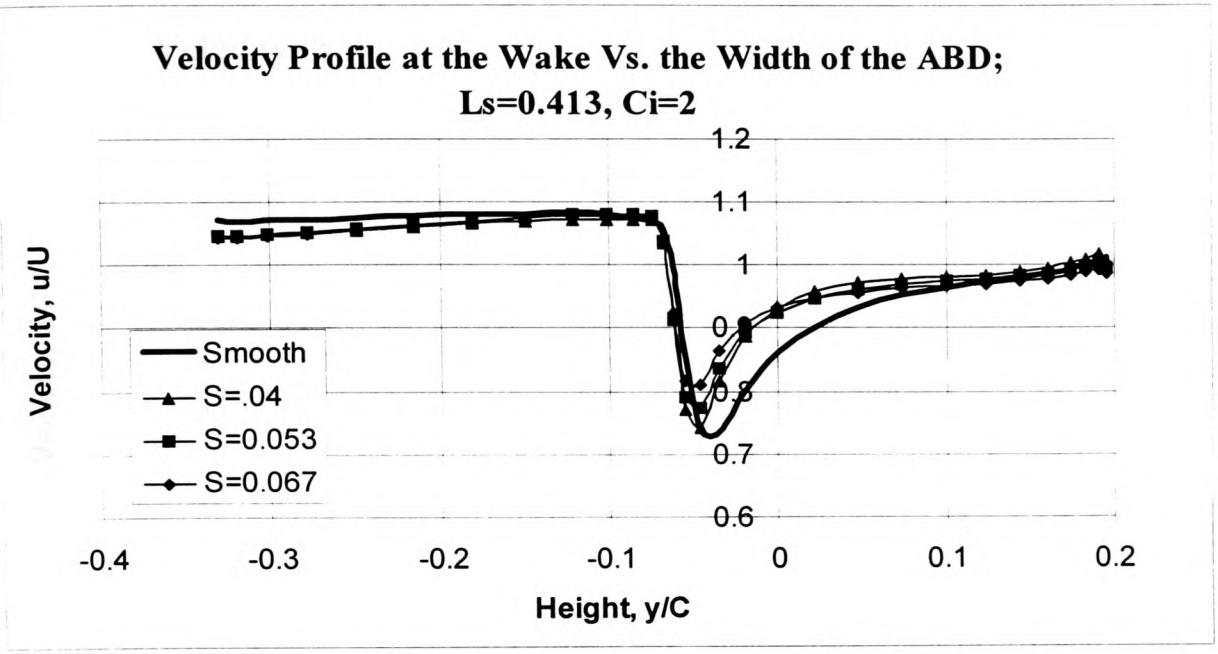

Figure 5-71

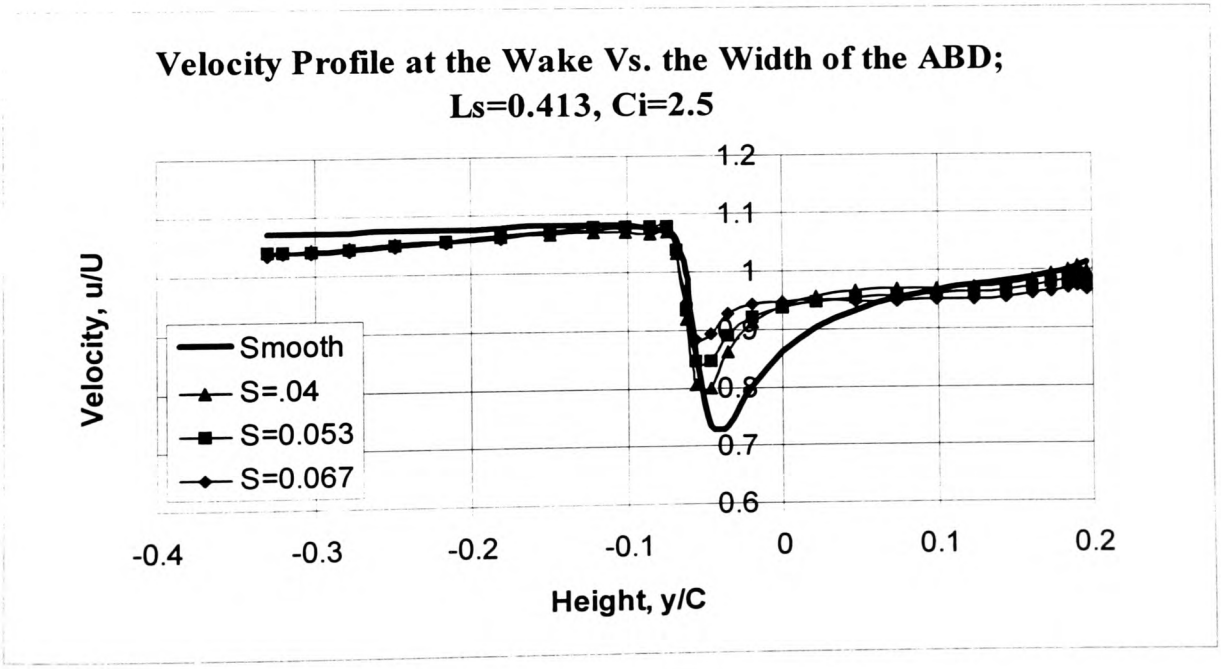

Figure 5-72

5.9.5.2 Alpha = 8 Degrees

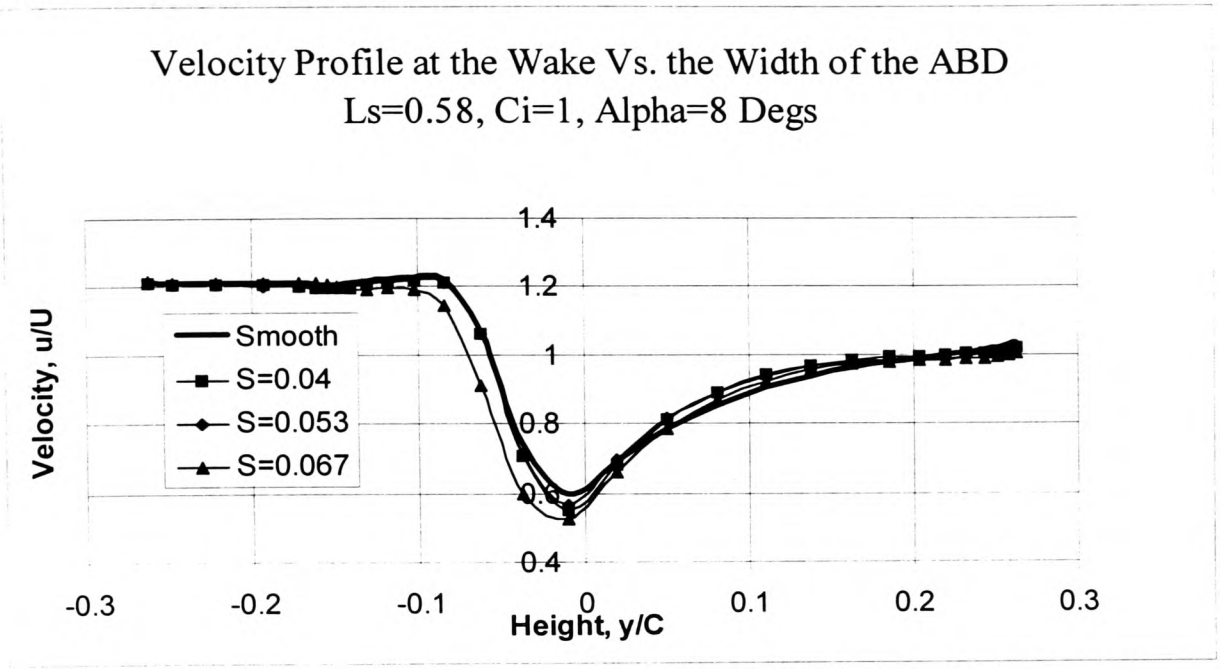

Figure 5-73

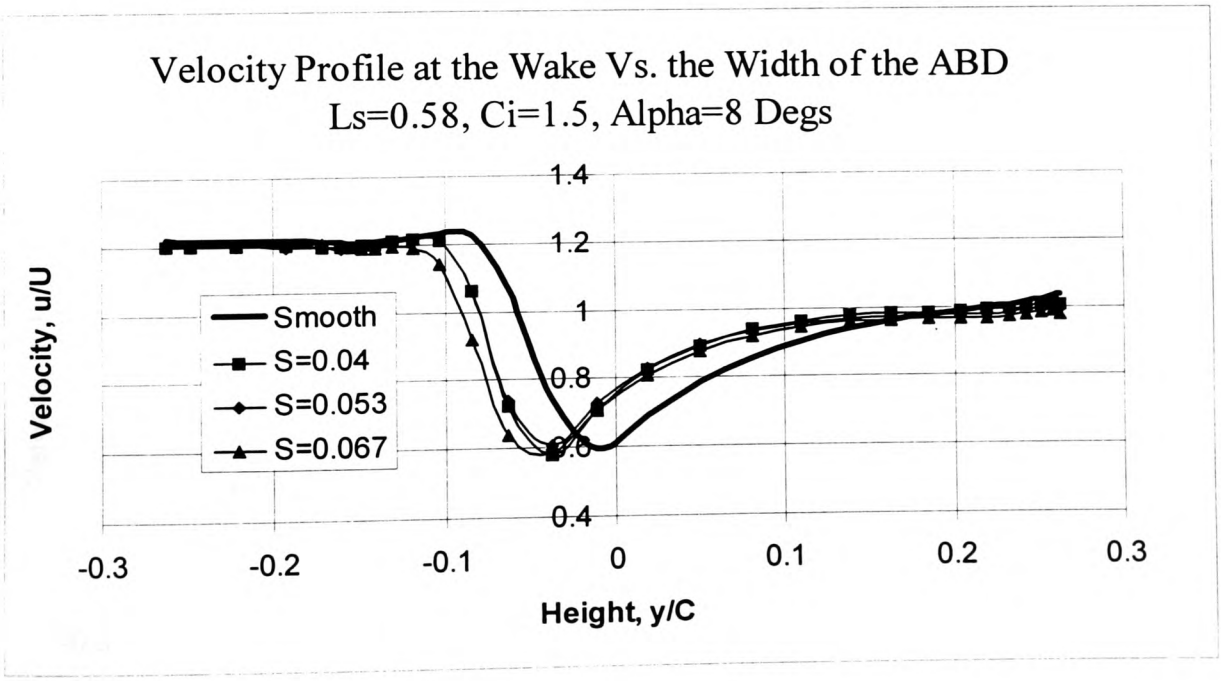

Figure 5-74

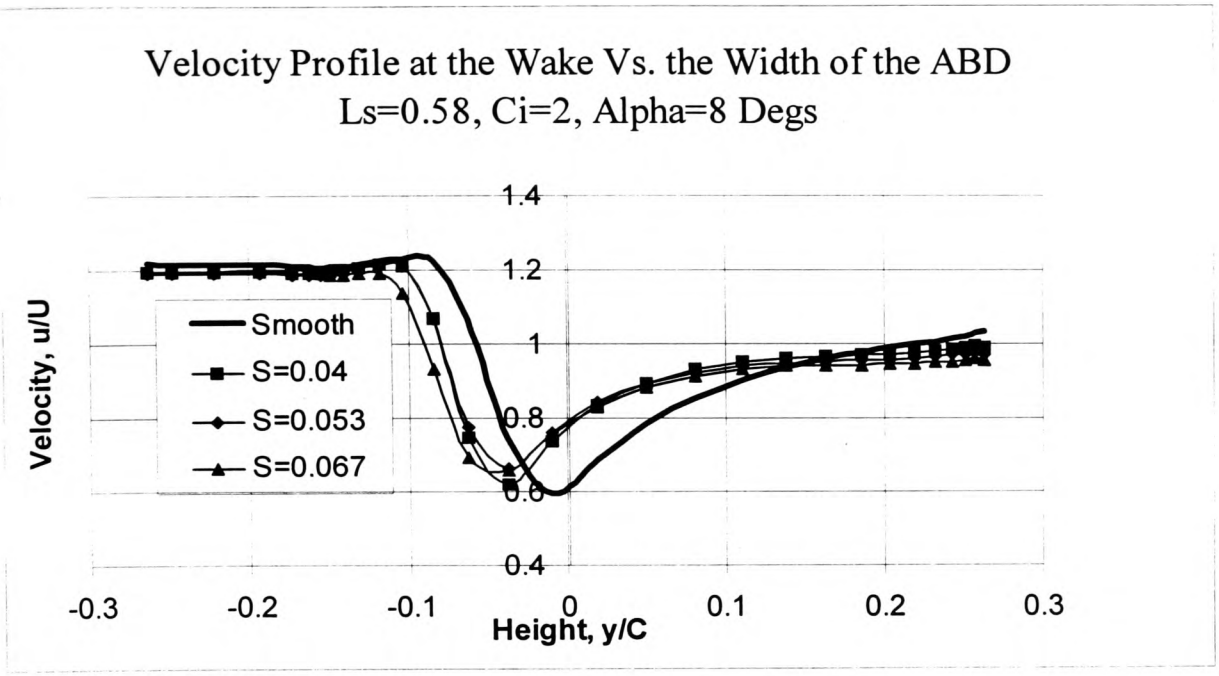

Figure 5-75

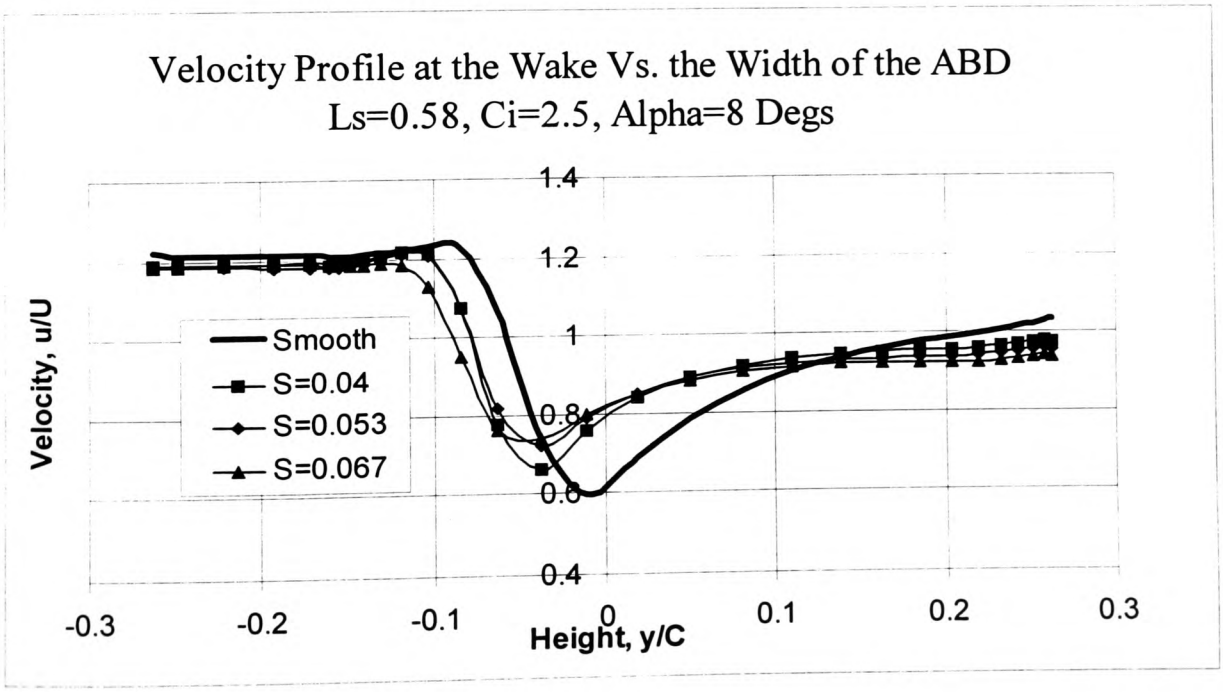

Figure 5-76

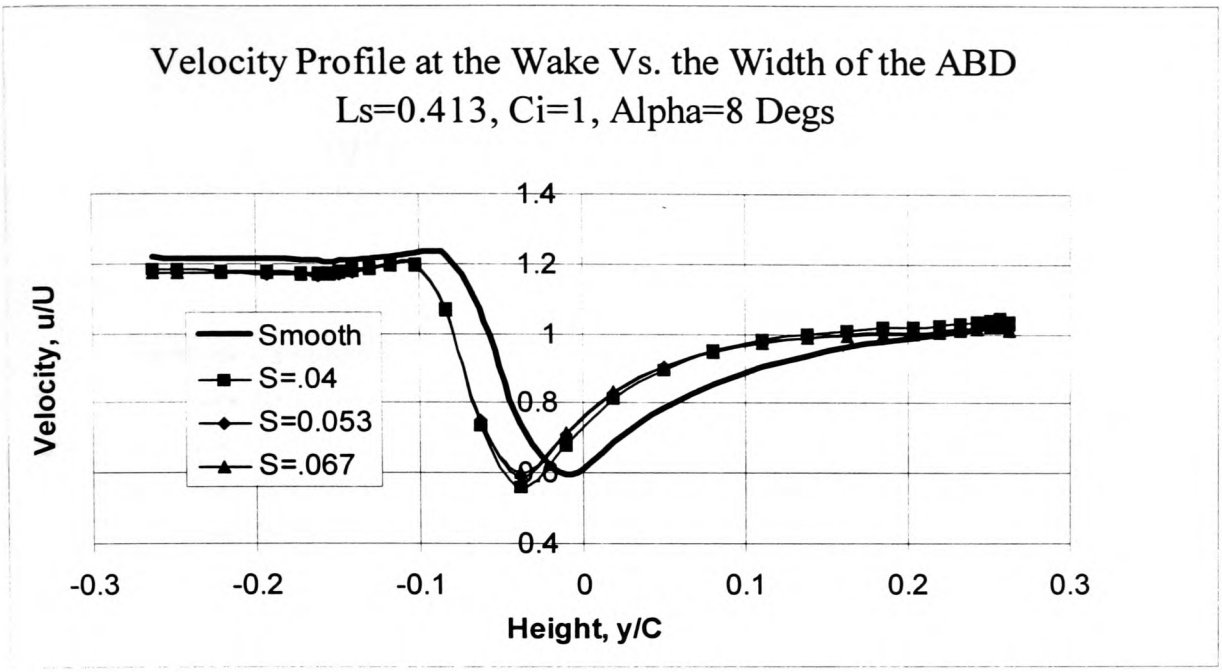

Figure 5-77

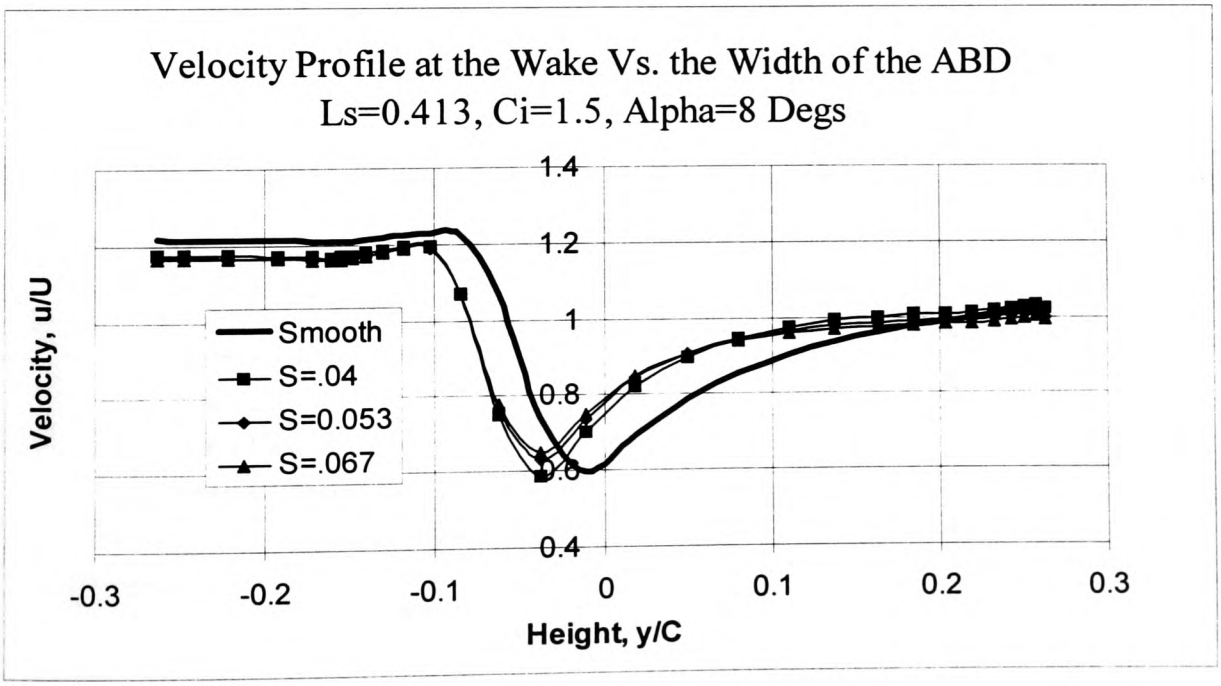

Figure 5-78

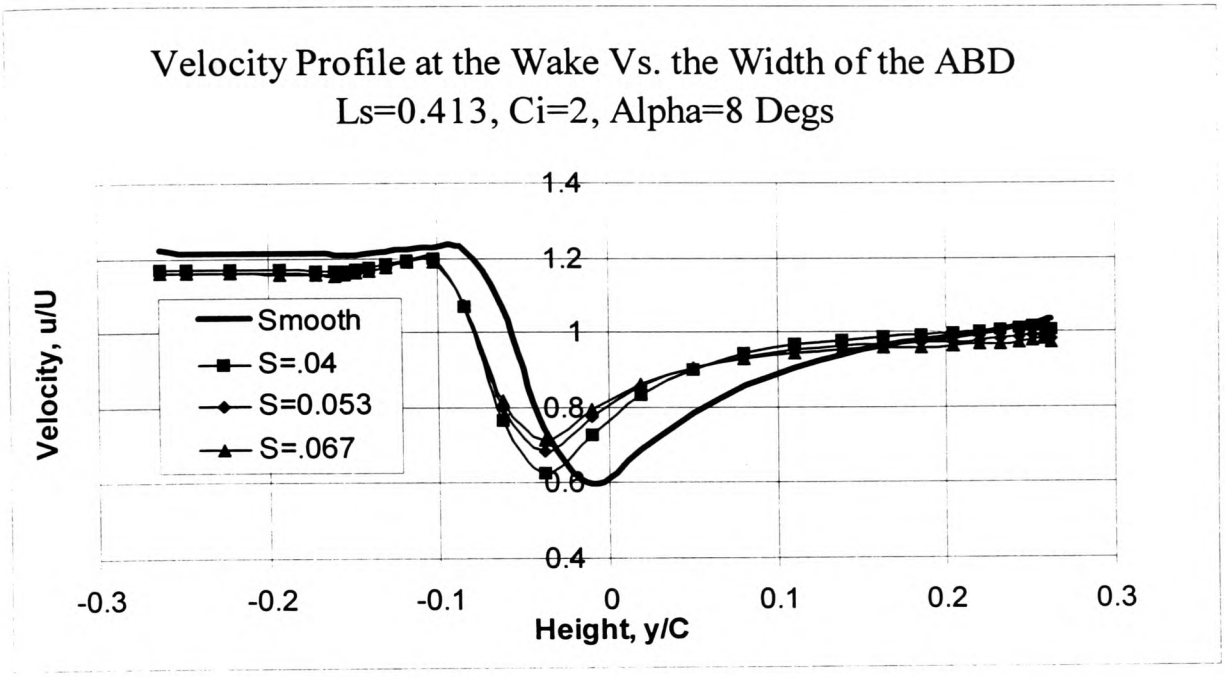

Figure 5-79

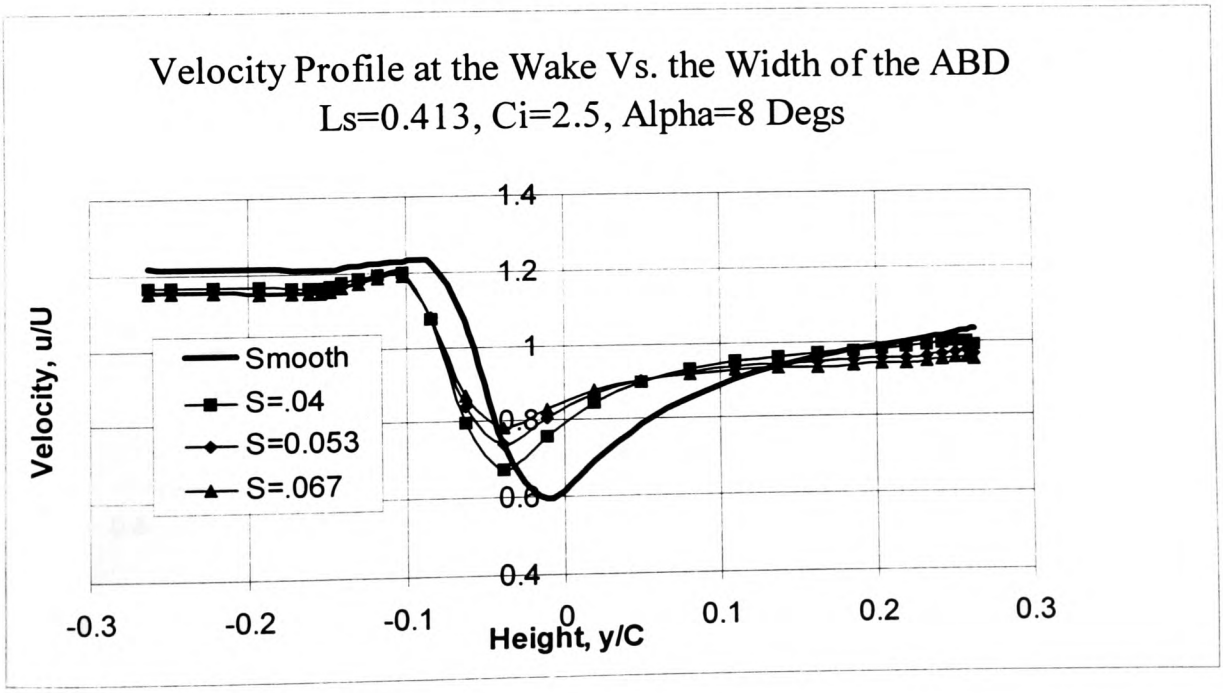

Figure 5-80

5.9.5.3 Alpha = 12 Degrees

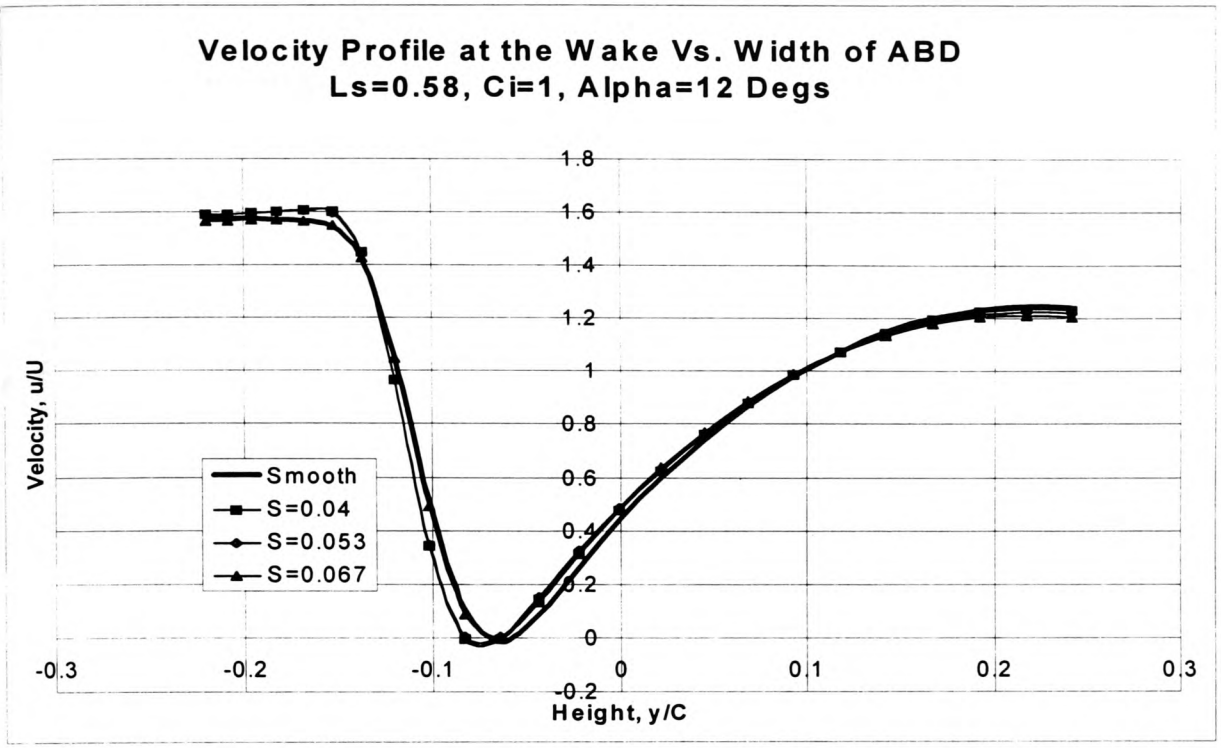

Figure 5-81

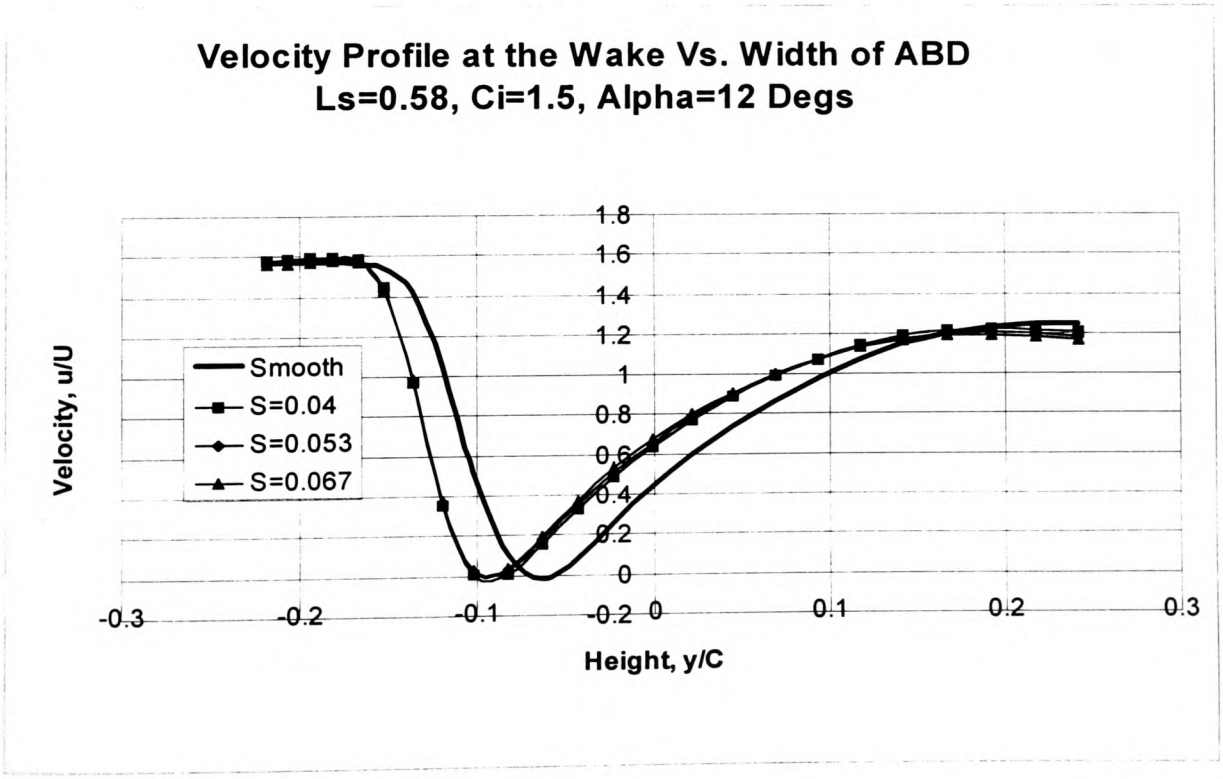

Figure 5-82

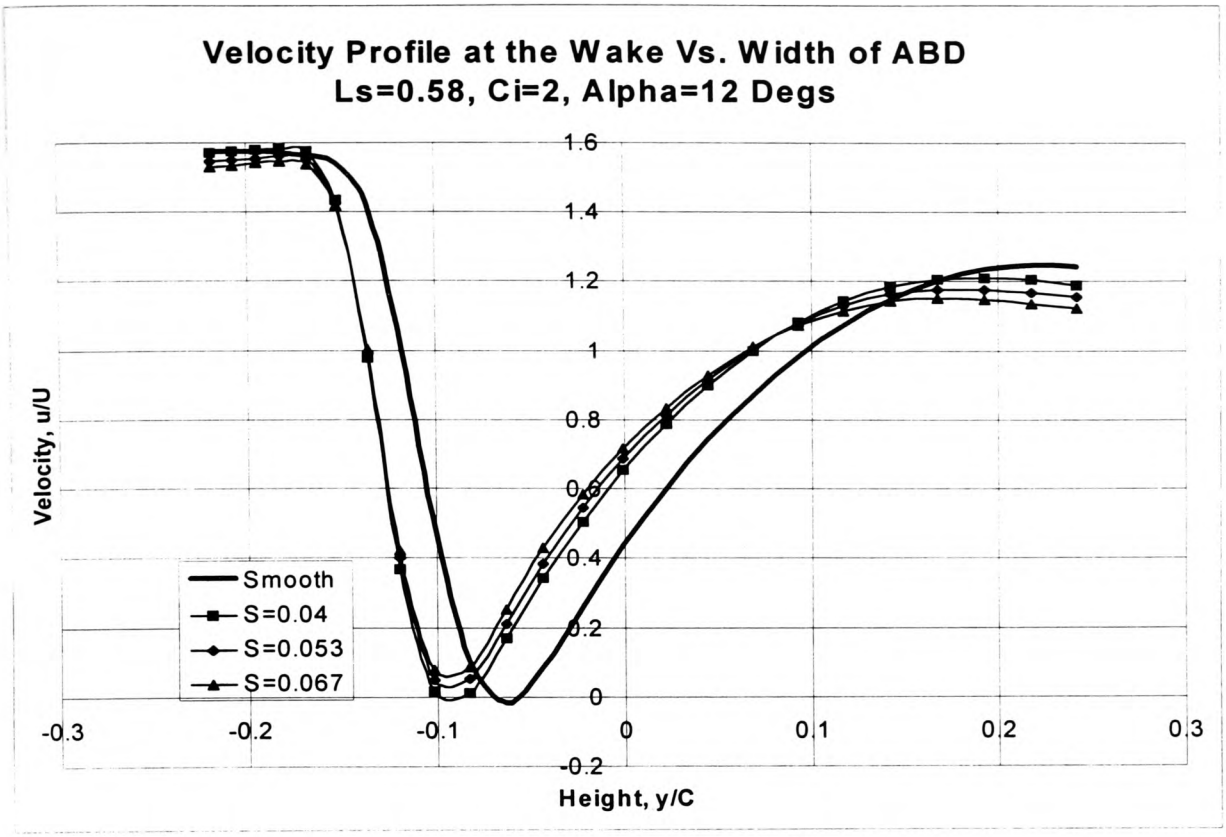

Figure 5-83

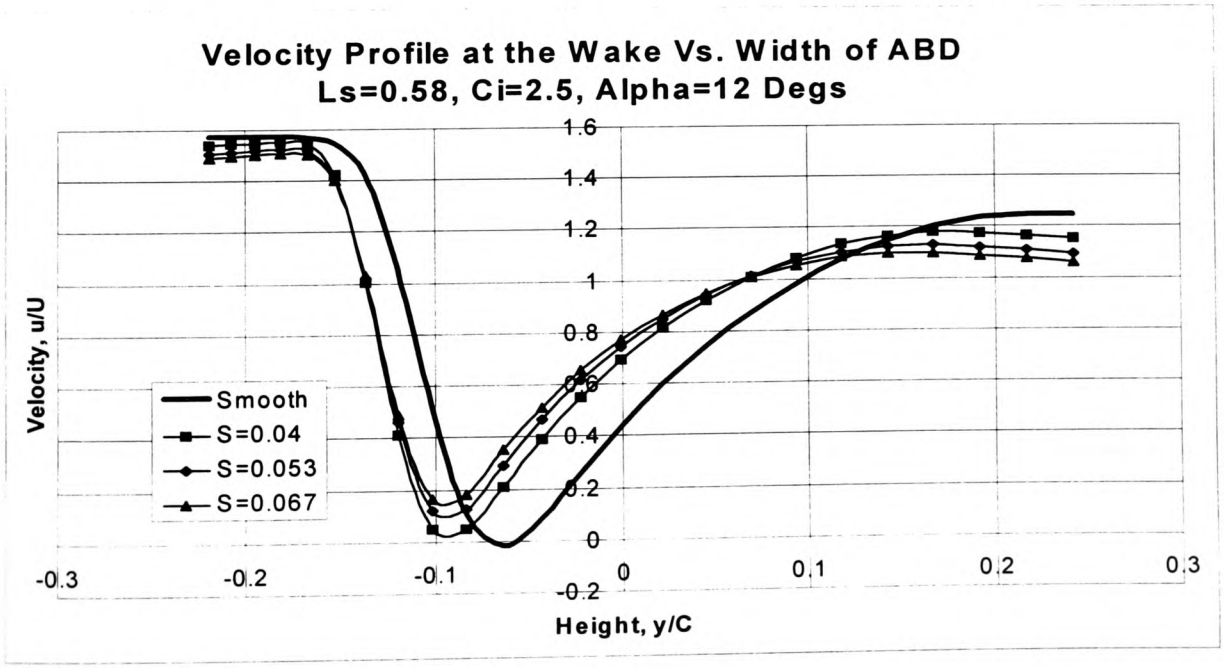

Figure 5-84

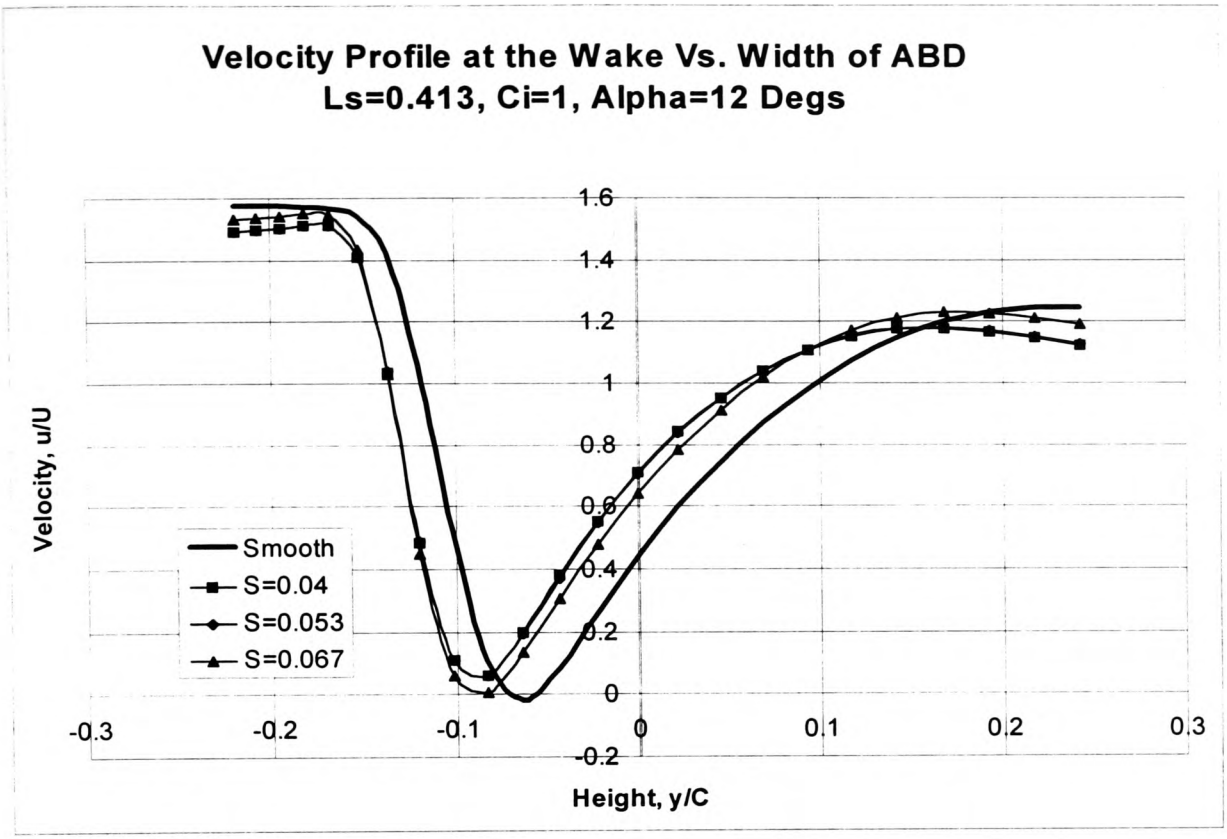

Figure 5-85

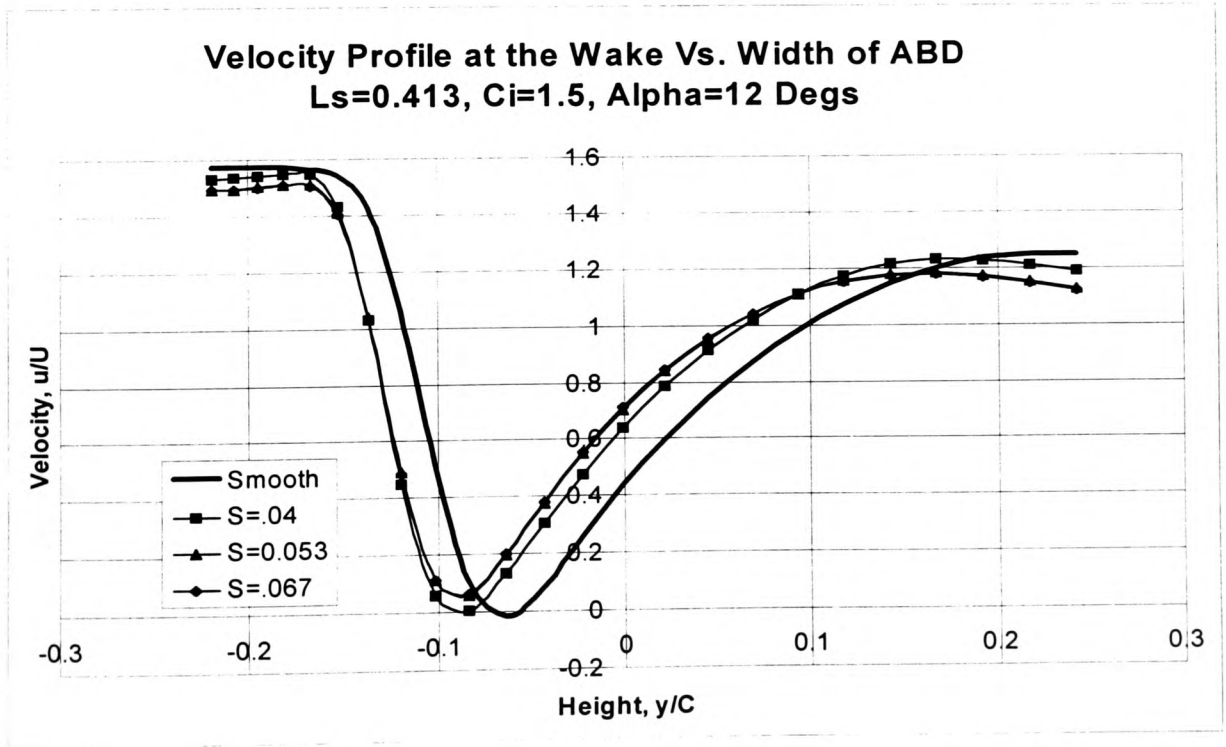

Figure 5-86

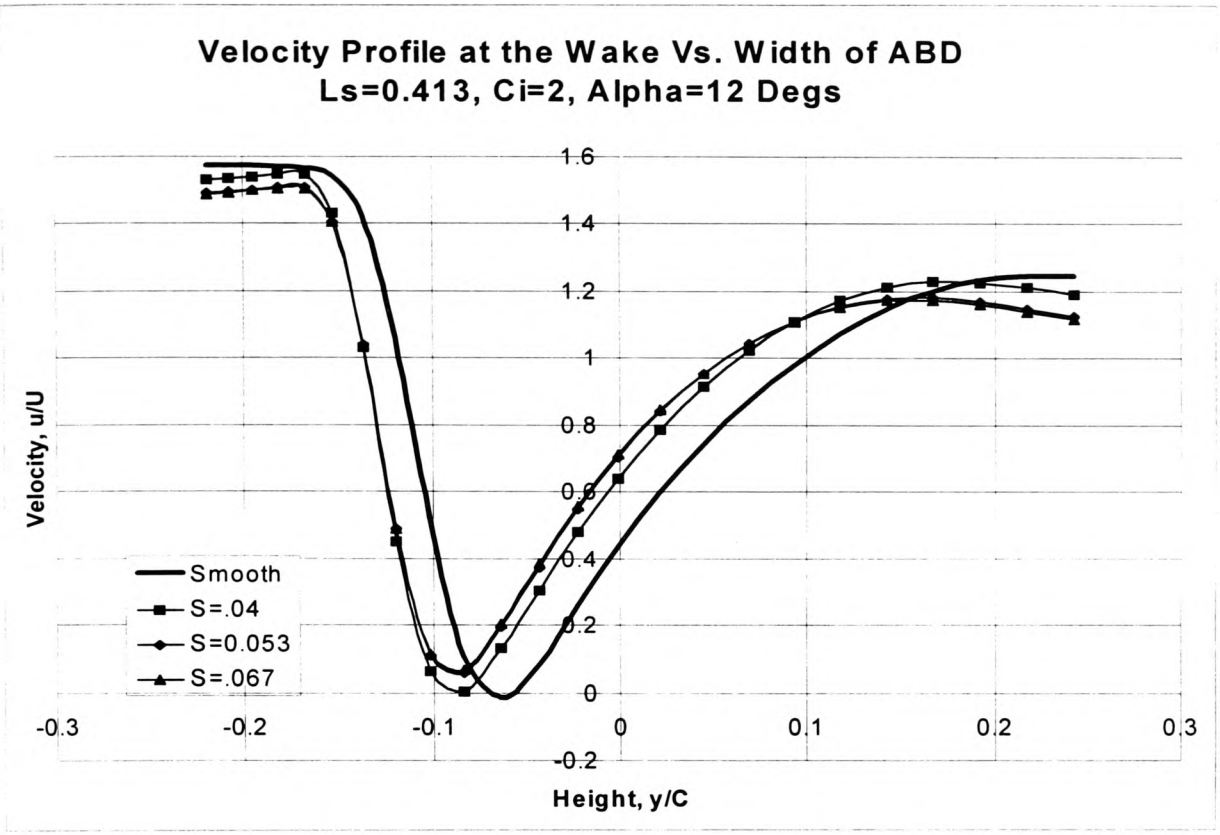

Figure 5-87

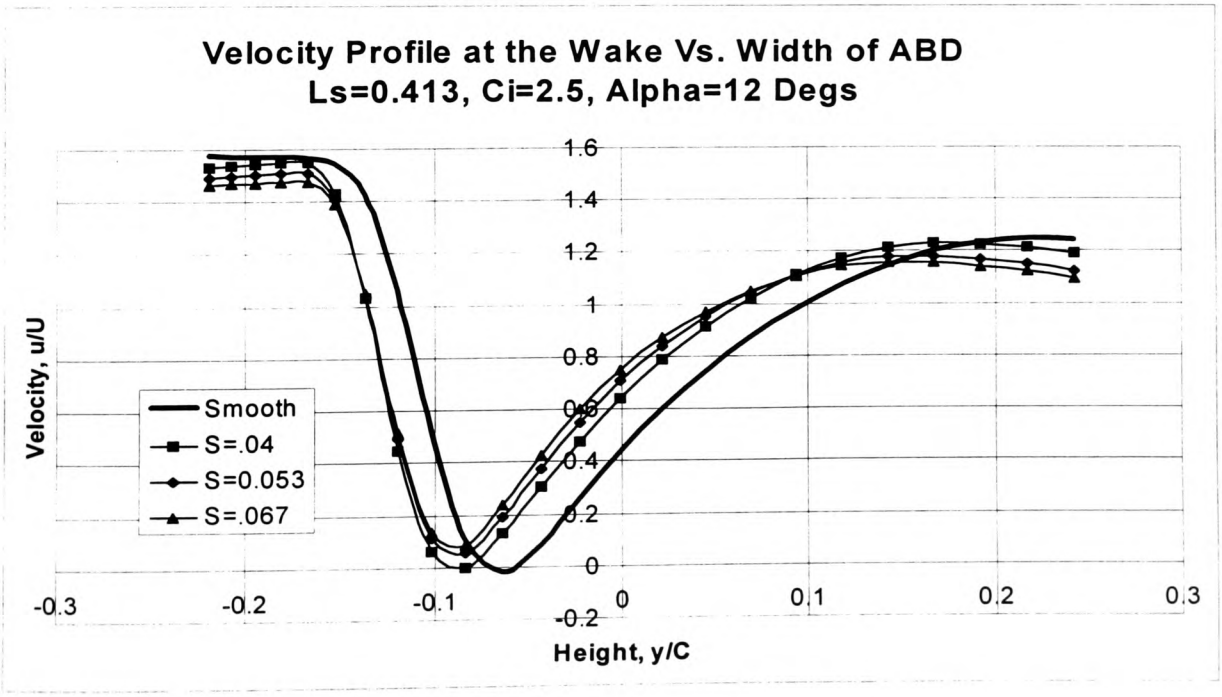

Figure 5-88

5.9.6 Effect of the Height of the ABD on the Velocity Profile at the Wake

5.9.6.1 Alpha = 4 Degrees

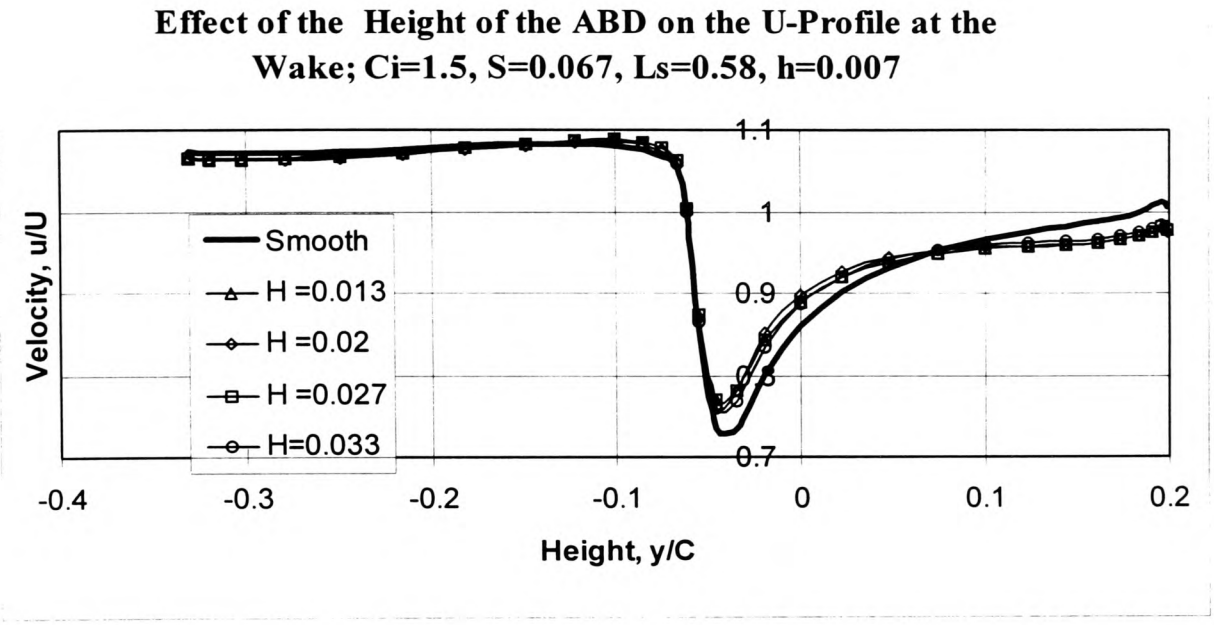

Figure 5-89

5.9.6.2 Alpha=8Degrees

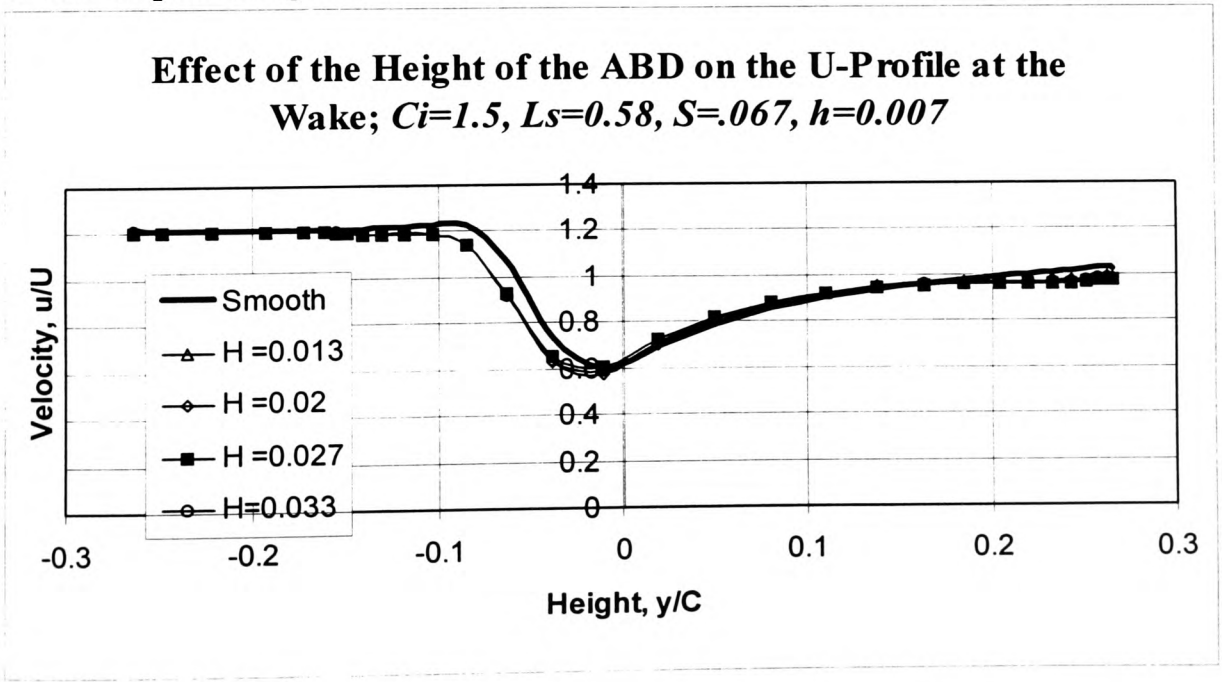

Figure 5-90

5.9.7 Effect of the Relative Height of the ABD Base, *h*, on the Velocity Profile at the Wake

5.9.7.1 Alpha = 4 Degrees

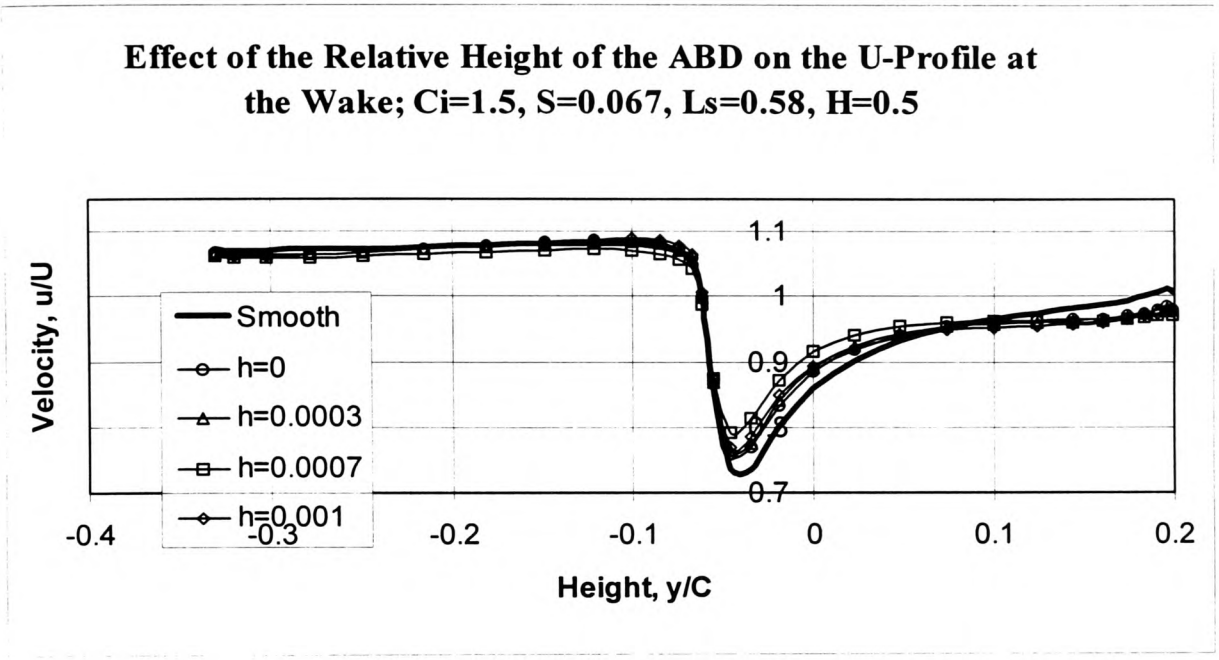

Figure 5-91

5.9.7.2 Alpha = 8 Degrees

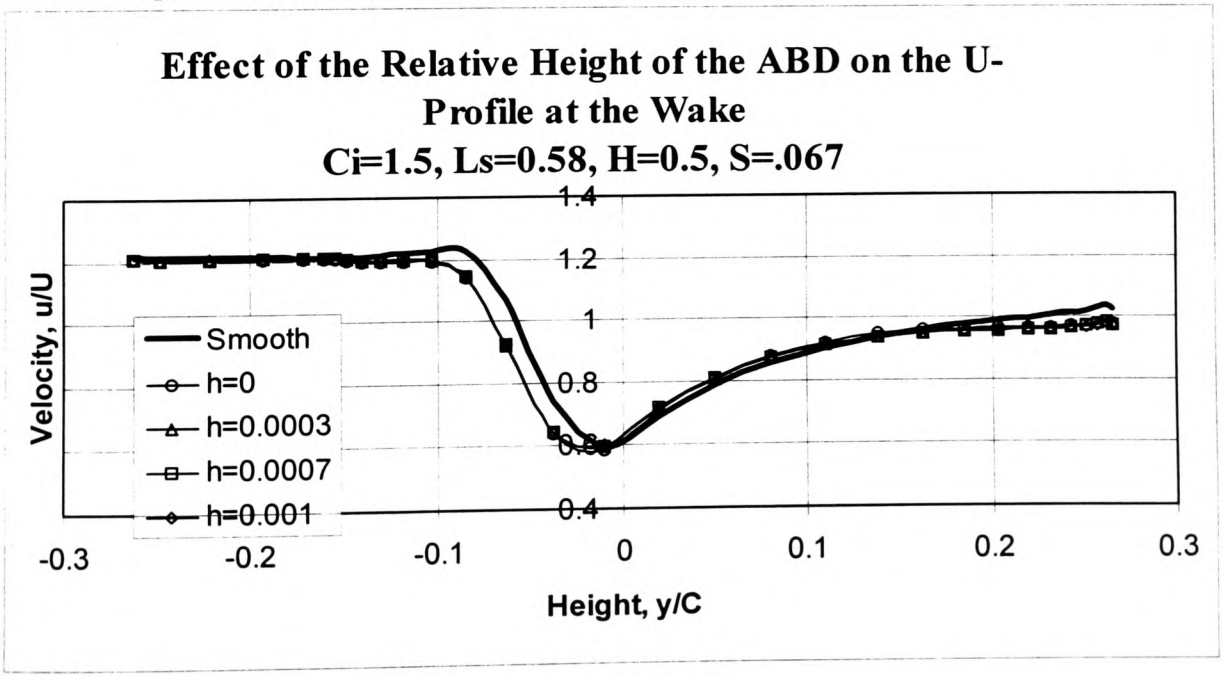

Figure 5-92

5.9.8 Effect of the Relative Velocity Inside the ABD on the Drag Coefficient (C_d)

5.9.8.1 Alpha = 4 Degrees

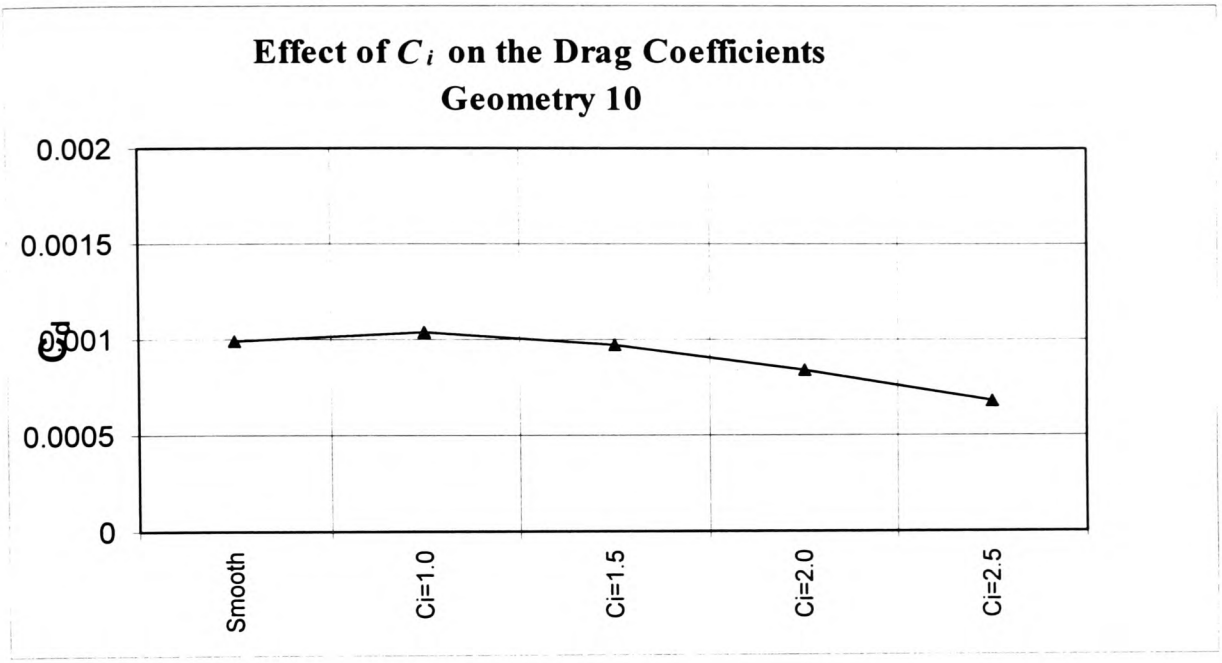

Figure 5-93

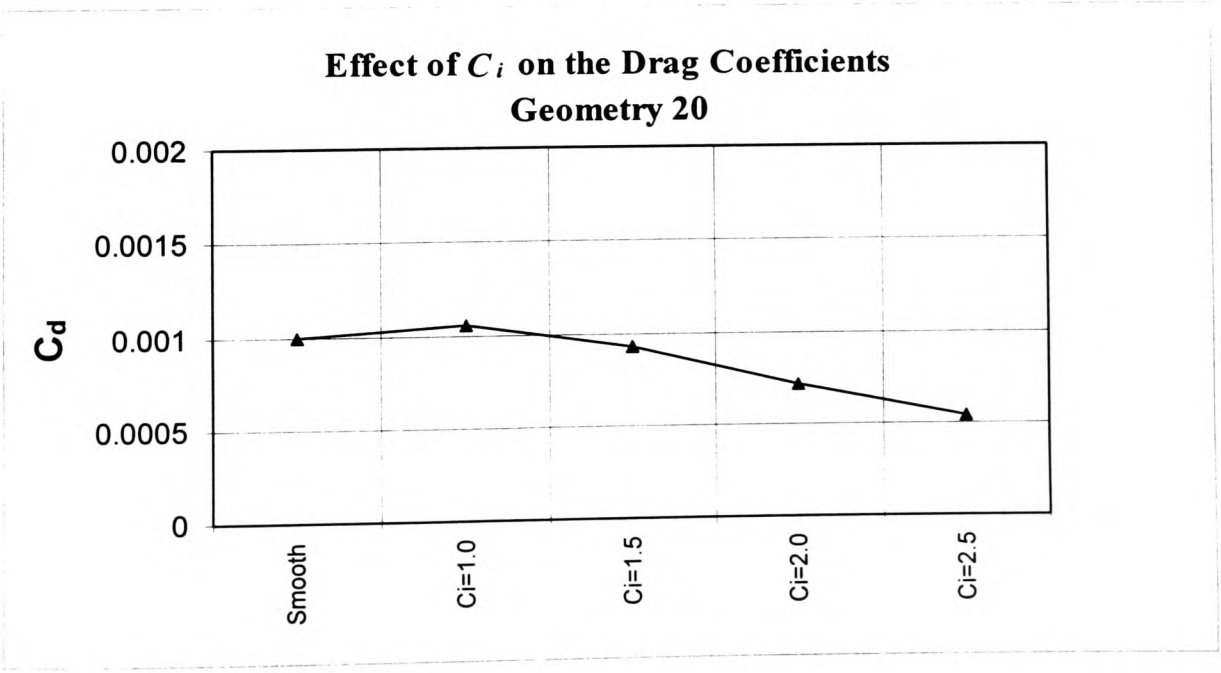

Figure 5-94

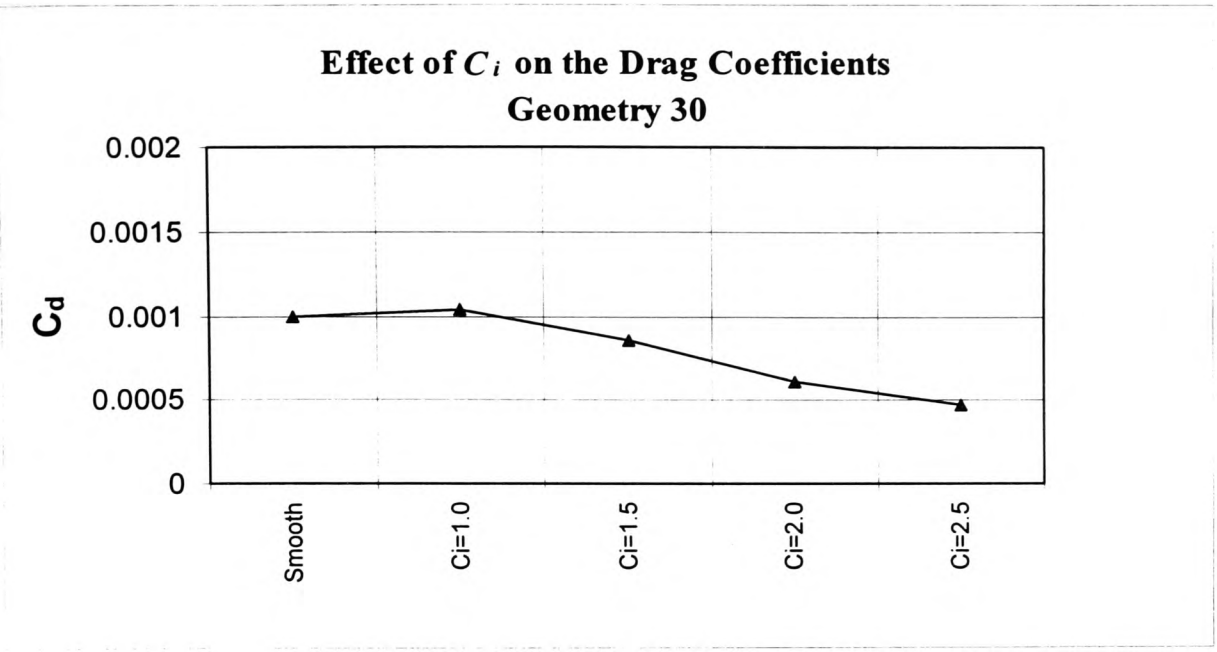

Figure 5-95

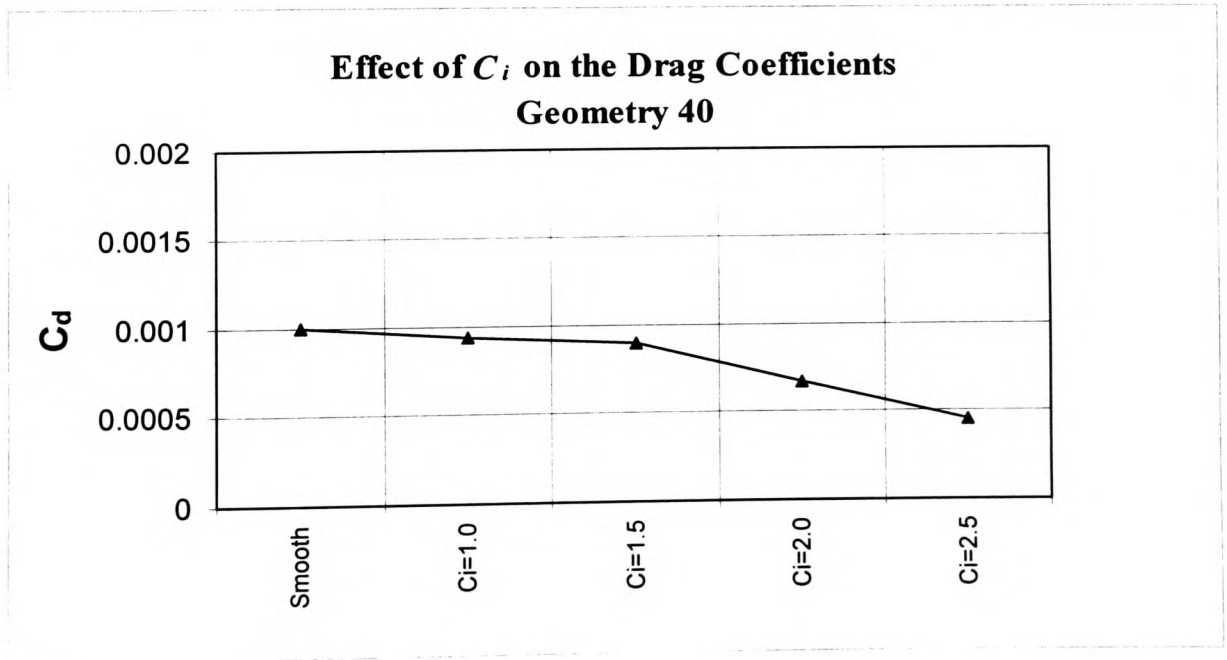

Figure 5-96

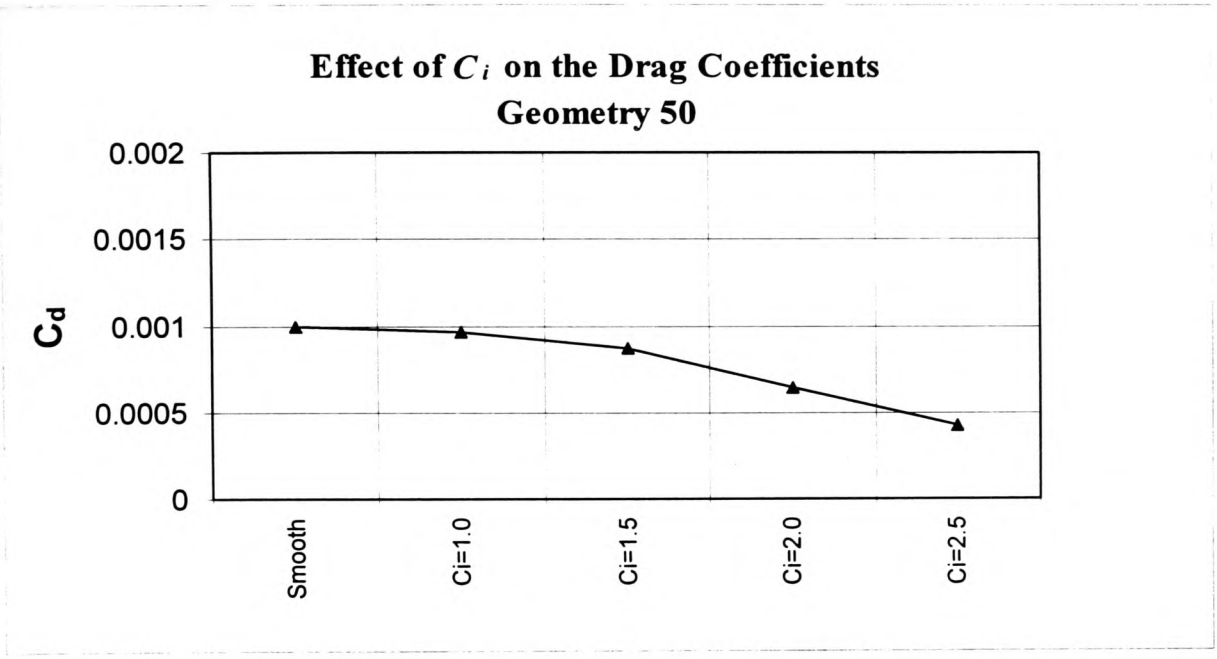

Figure 5-97

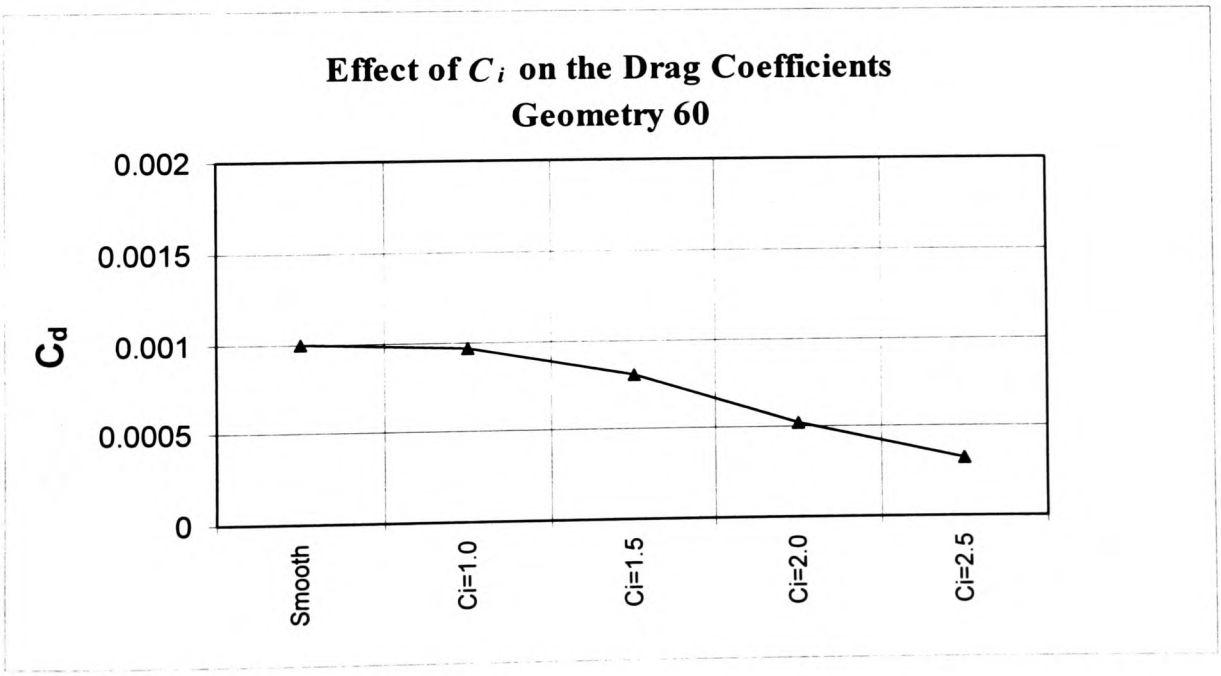

Figure 5-98

Alpha = 8 Degrees

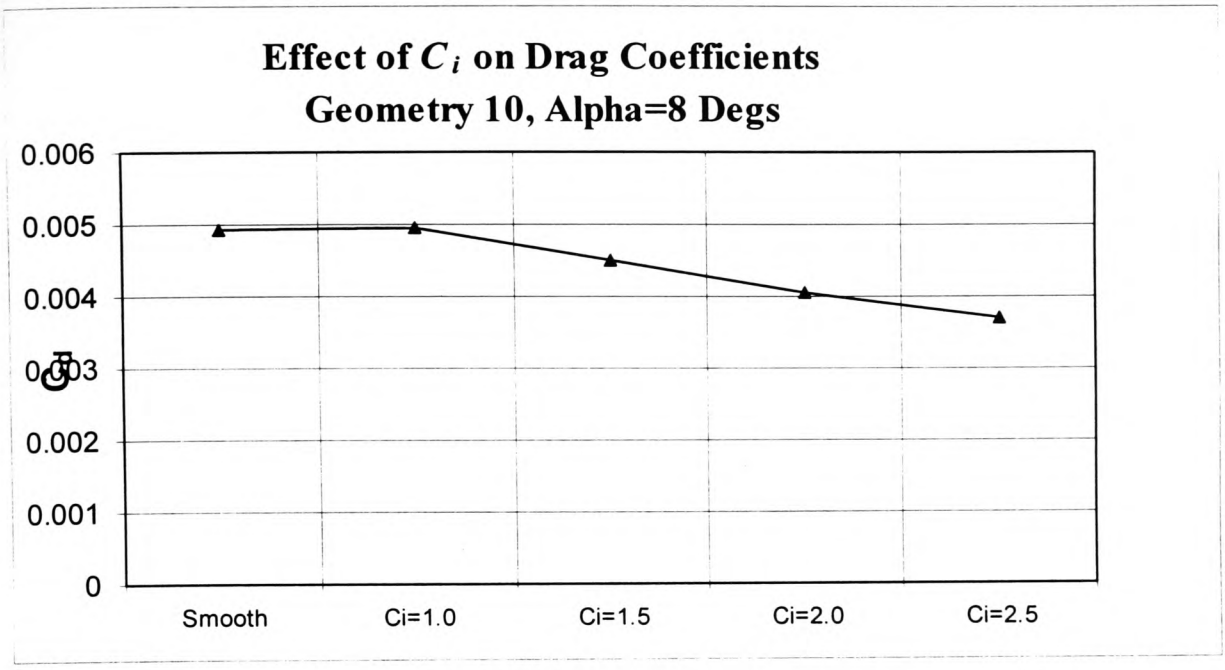

Figure 5-99

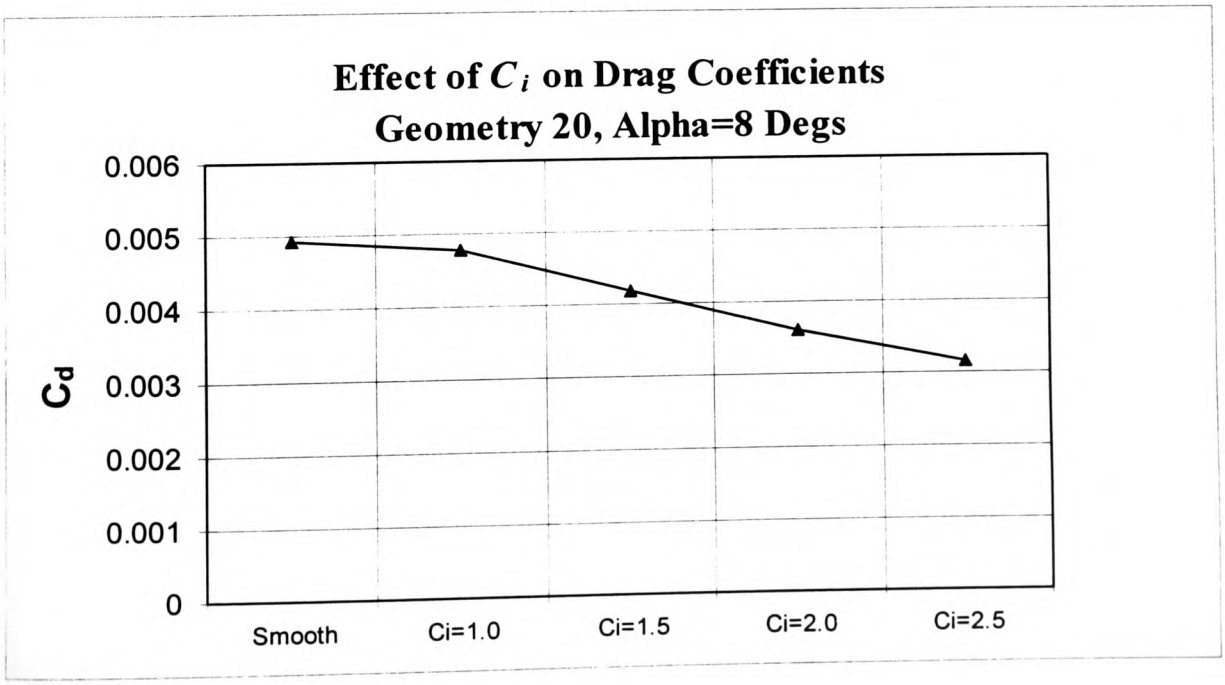

Figure 5-100

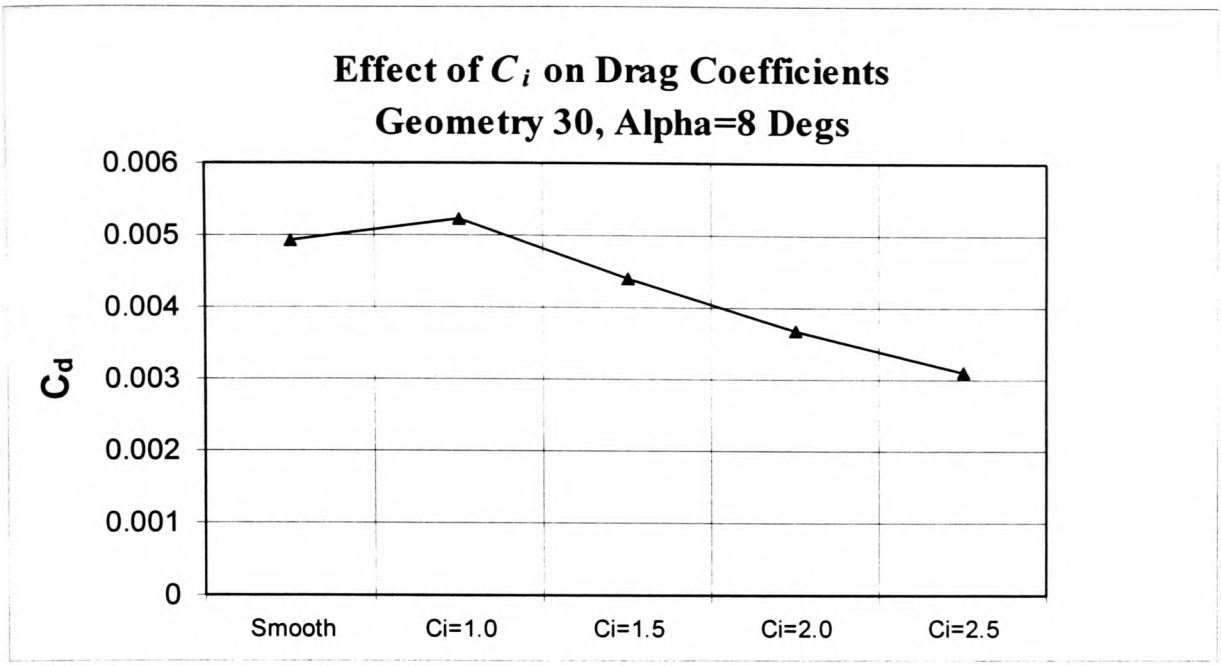

Figure 5-101

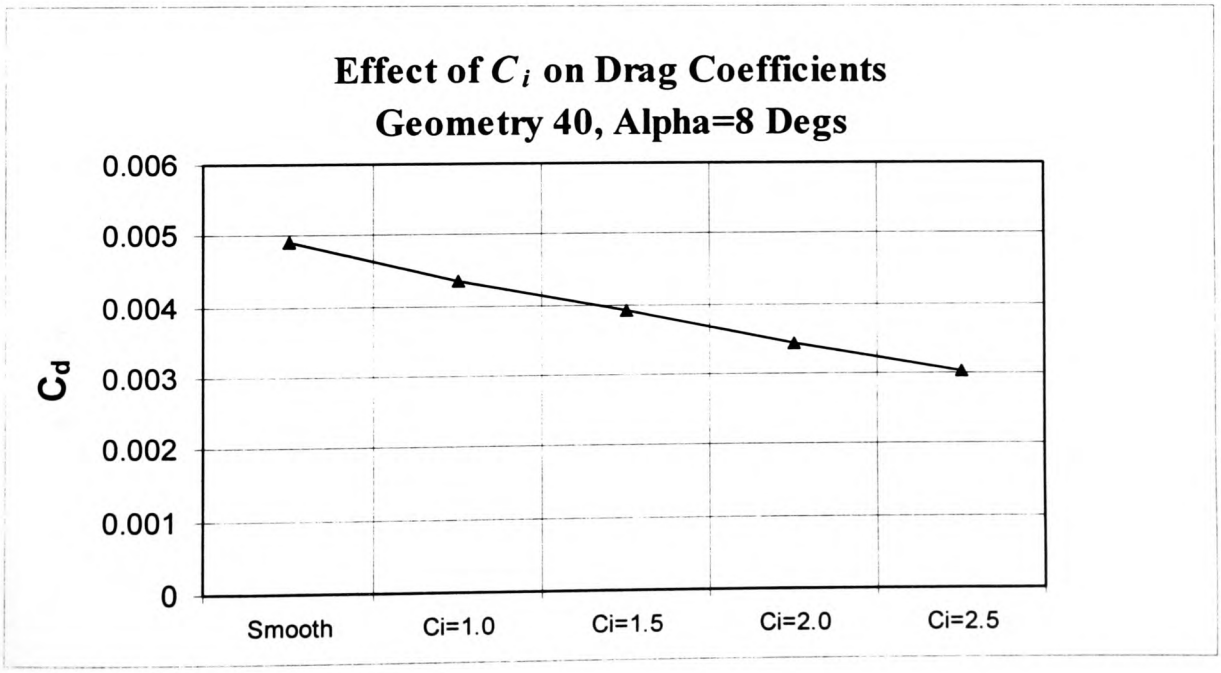

Figure 5-102

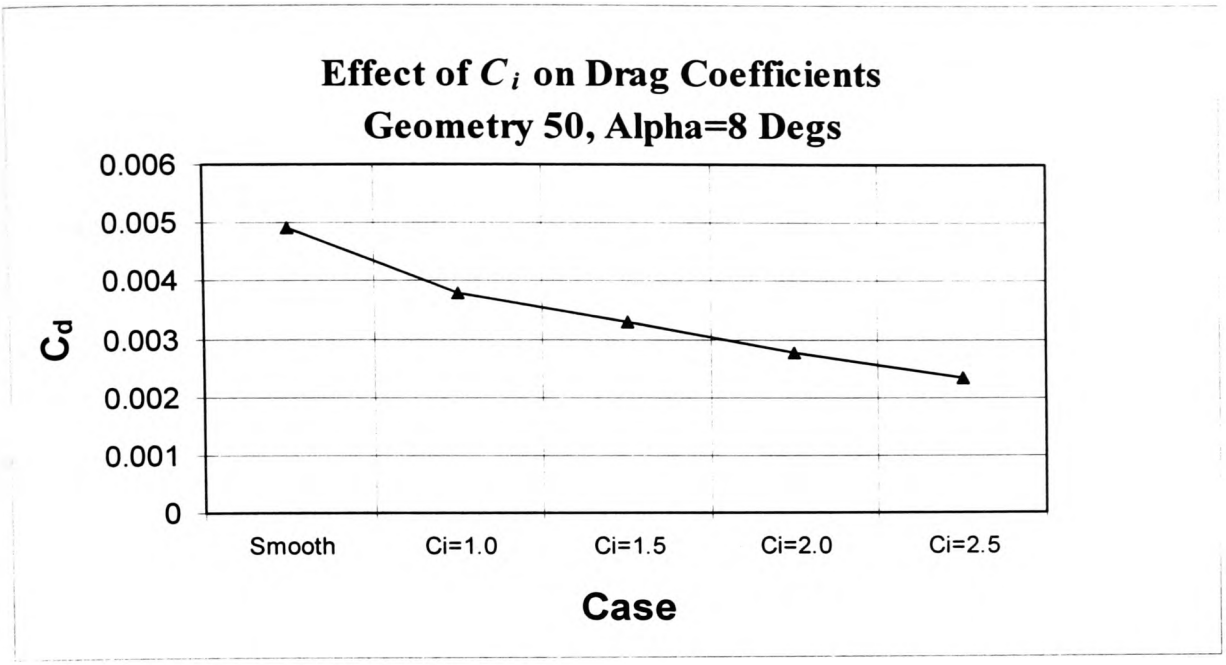

Figure 5-103

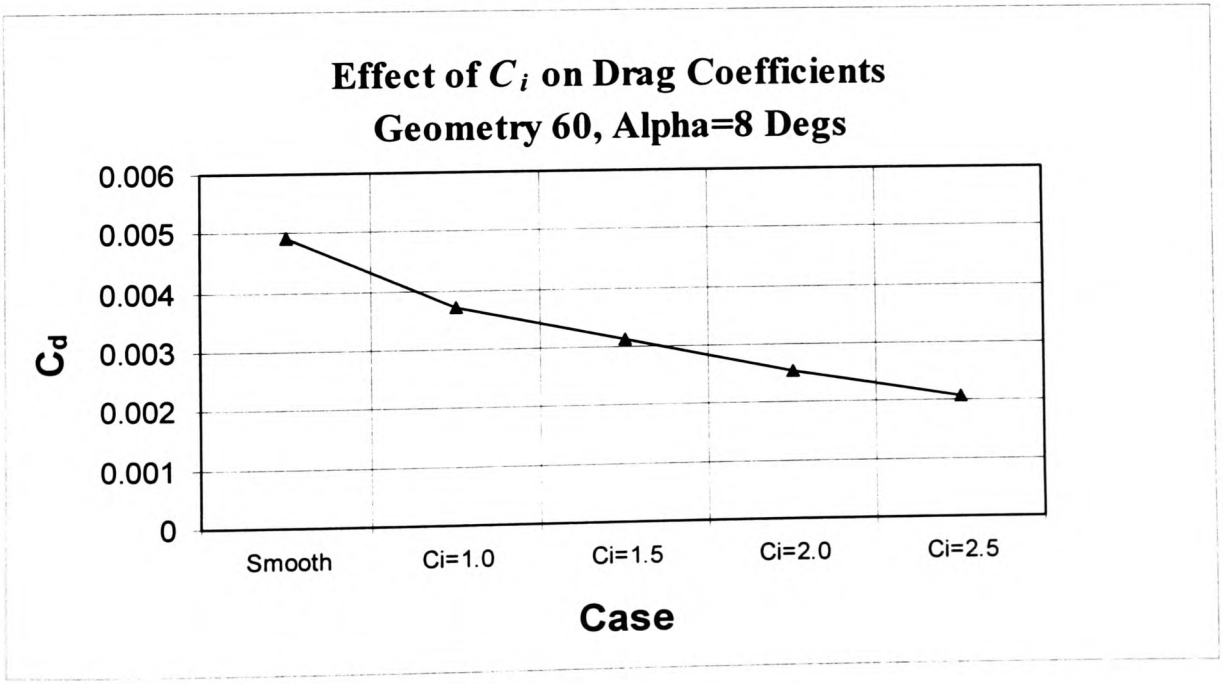

Figure 5-104

Alpha = 12 Degrees

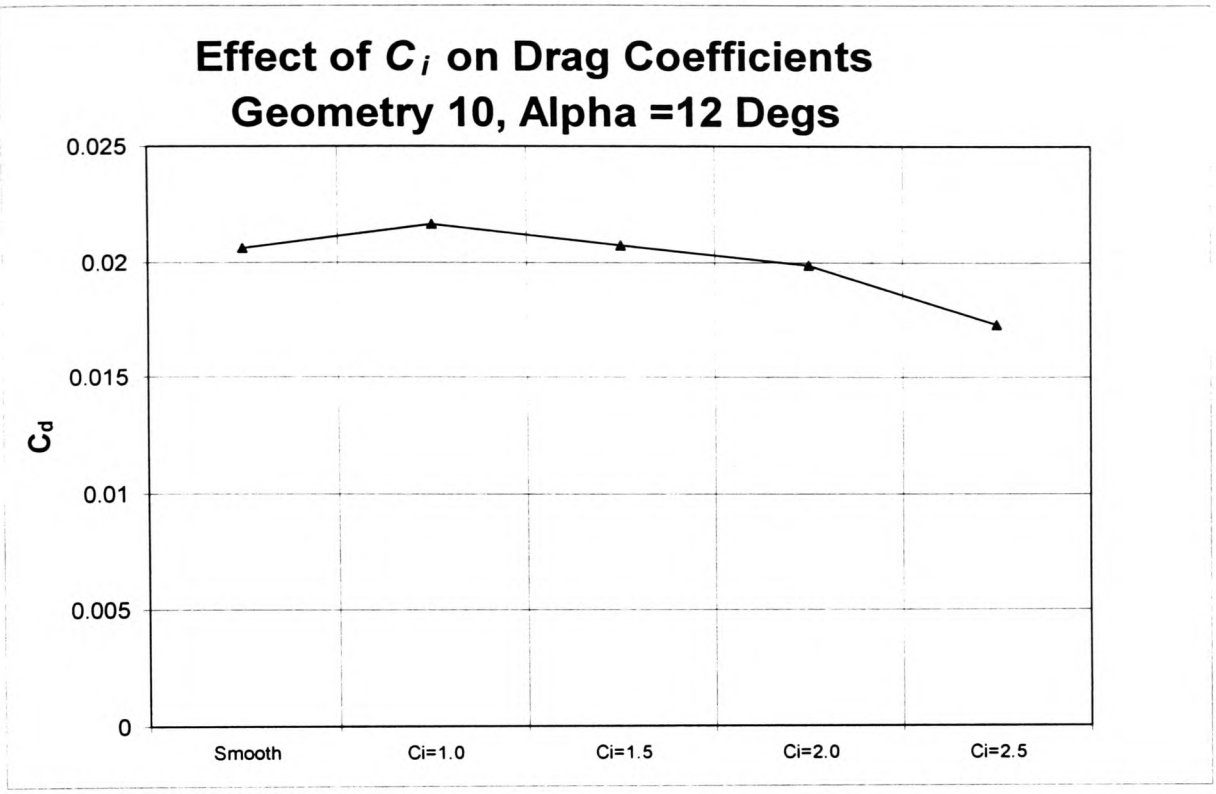

Figure 5-105

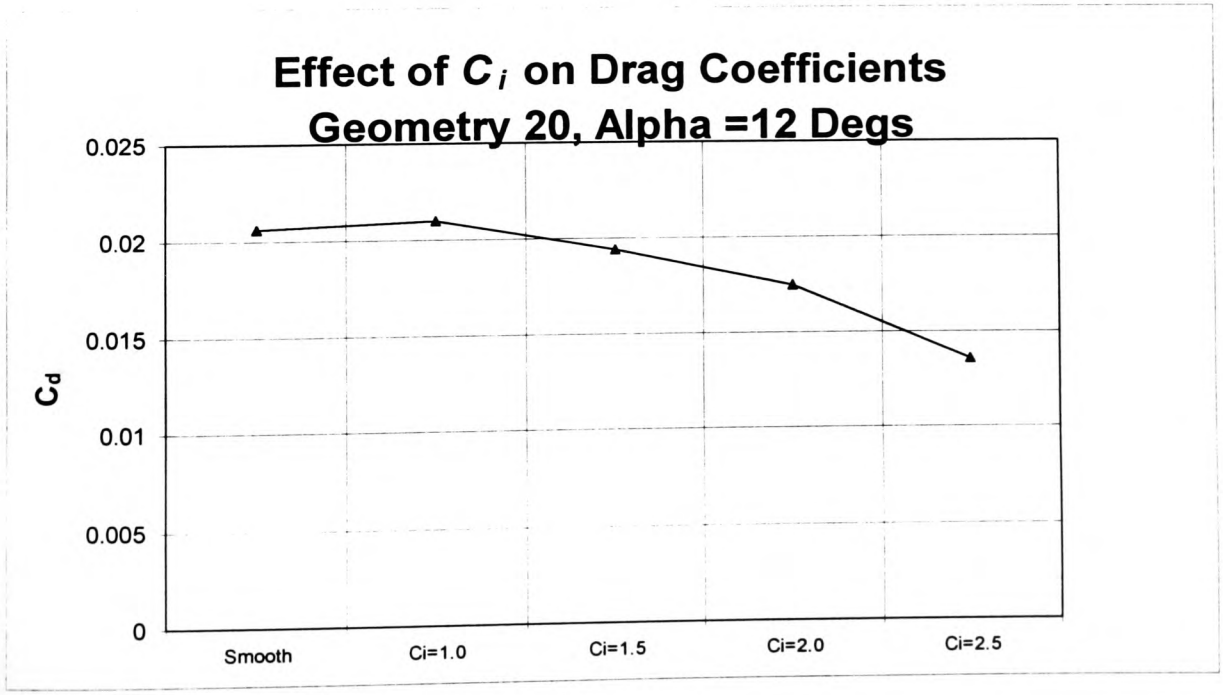

Figure 5-106

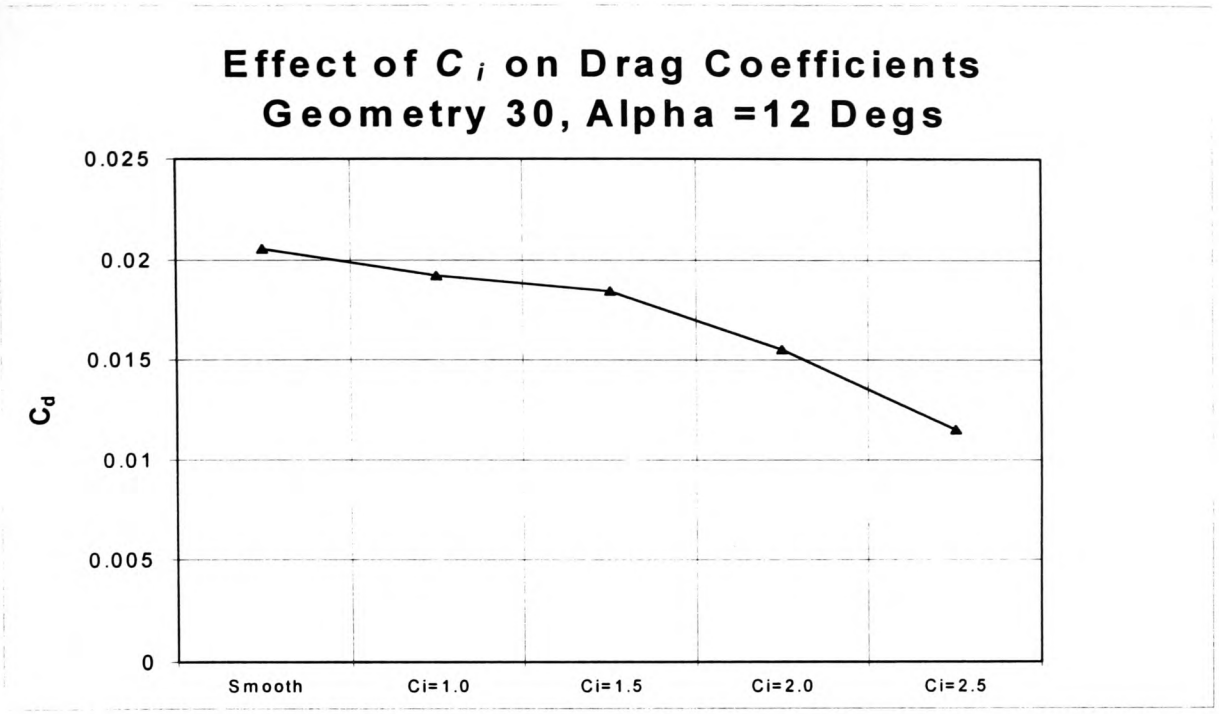

Figure 5-107

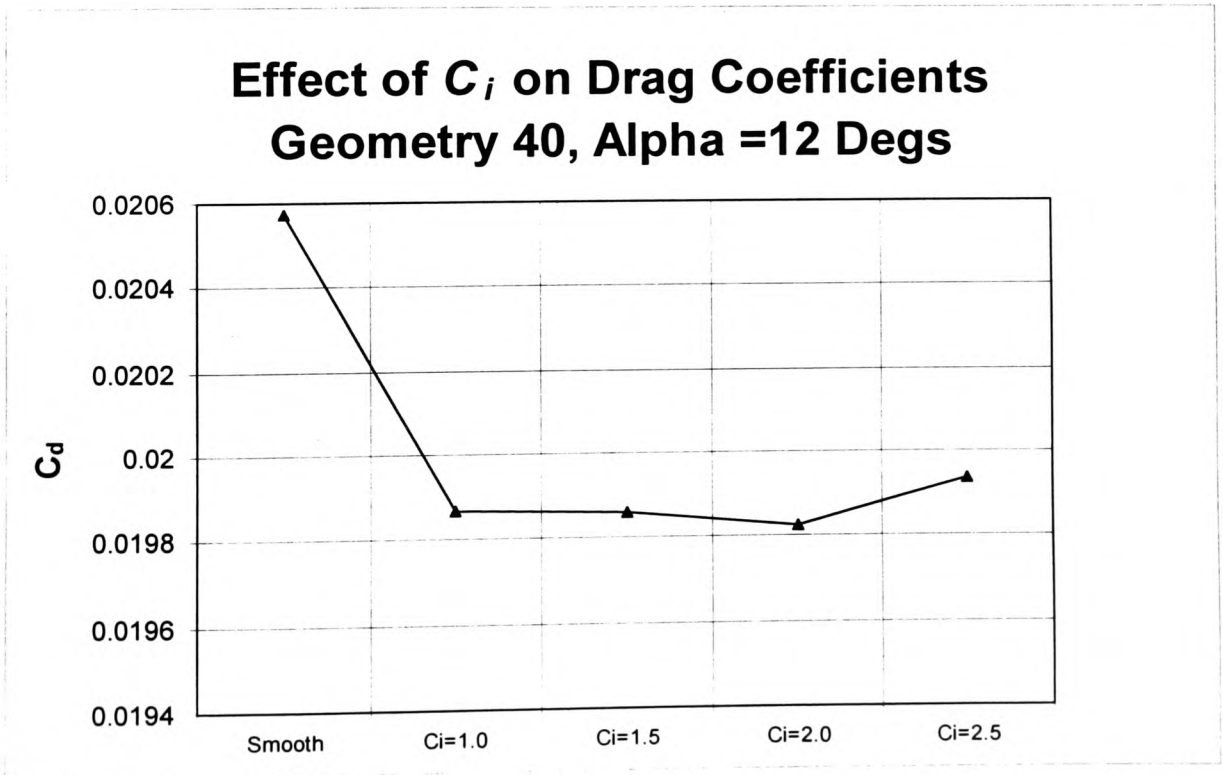

Figure 5-108

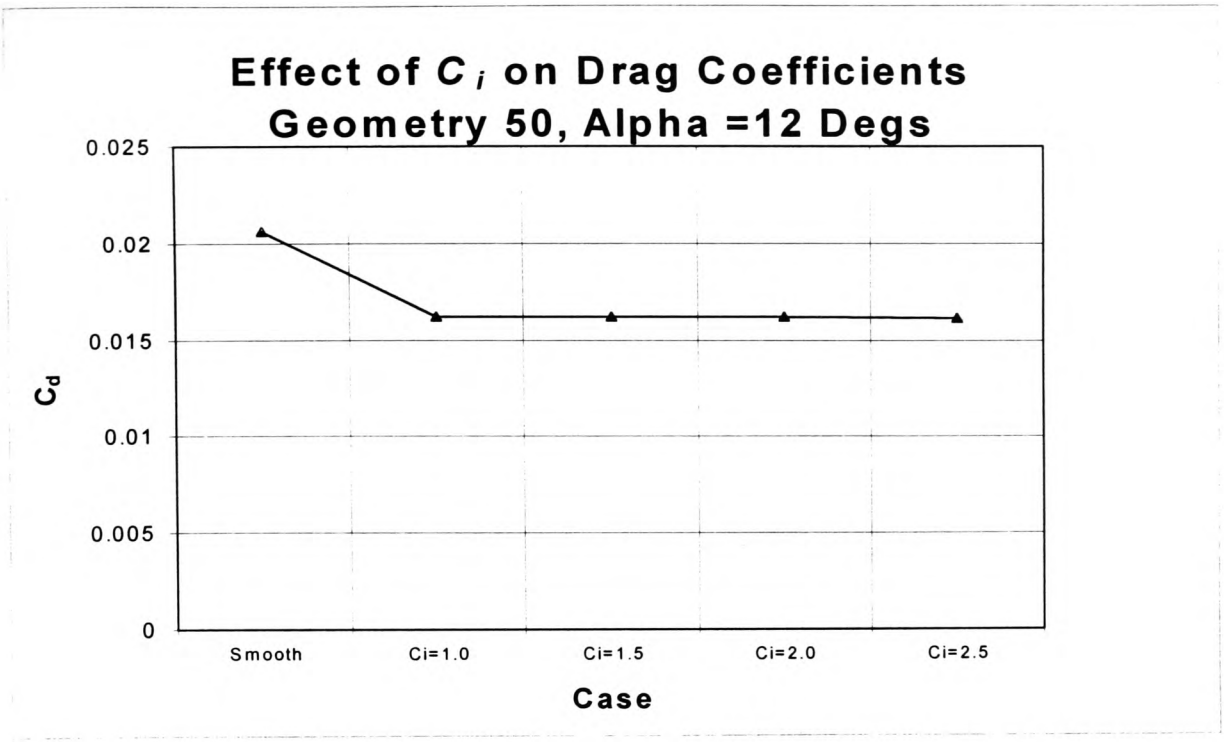

Figure 5-109

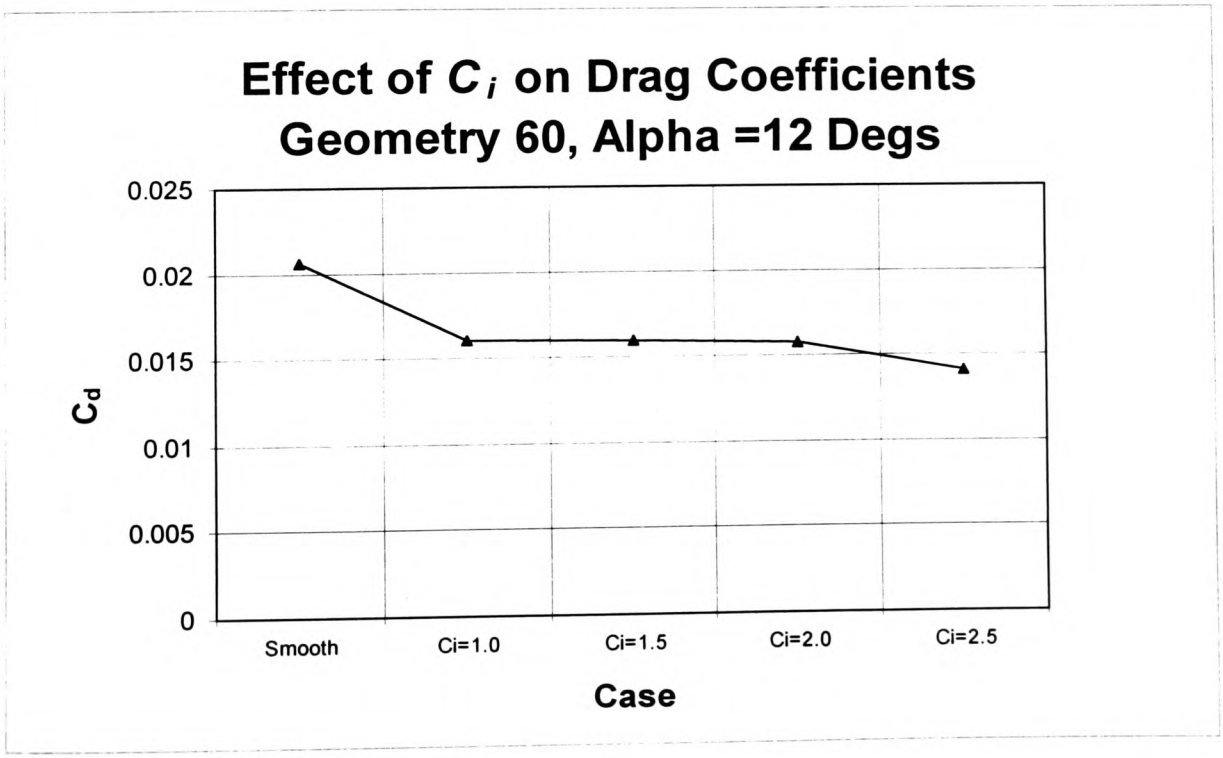

Figure 5-110

5.9.9 Effect of the Width and Location of the ABD on Drag Coefficient (C_d)

5.9.9.1 Alpha = 4 Degrees

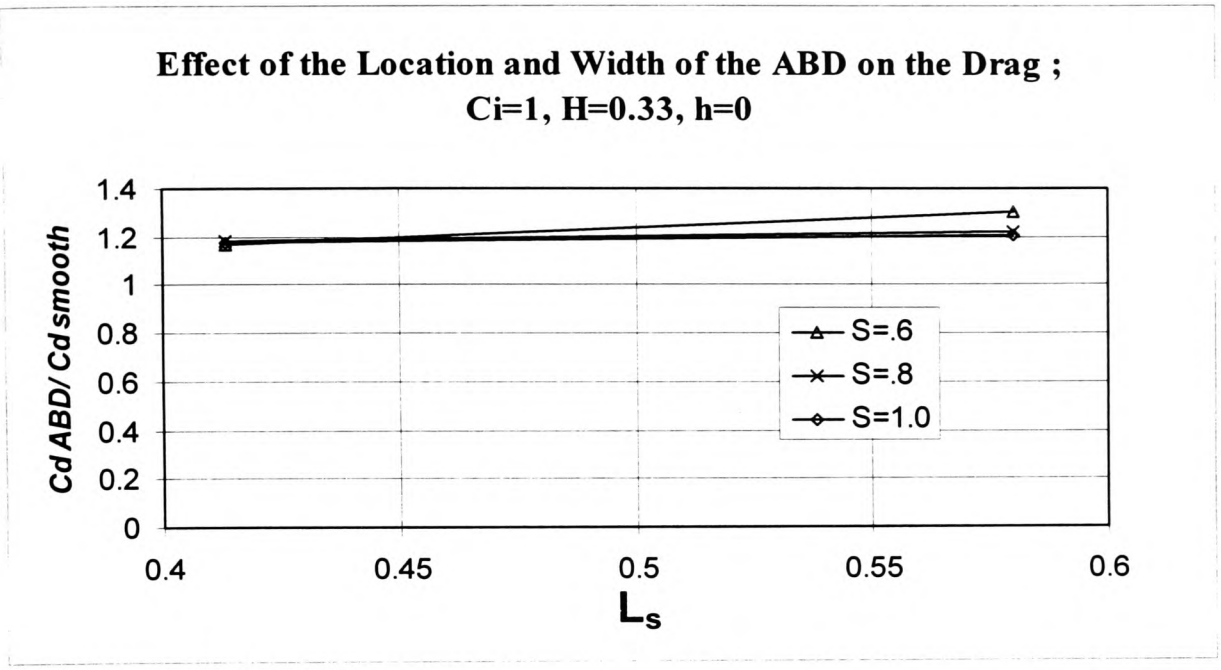

Figure 5-111

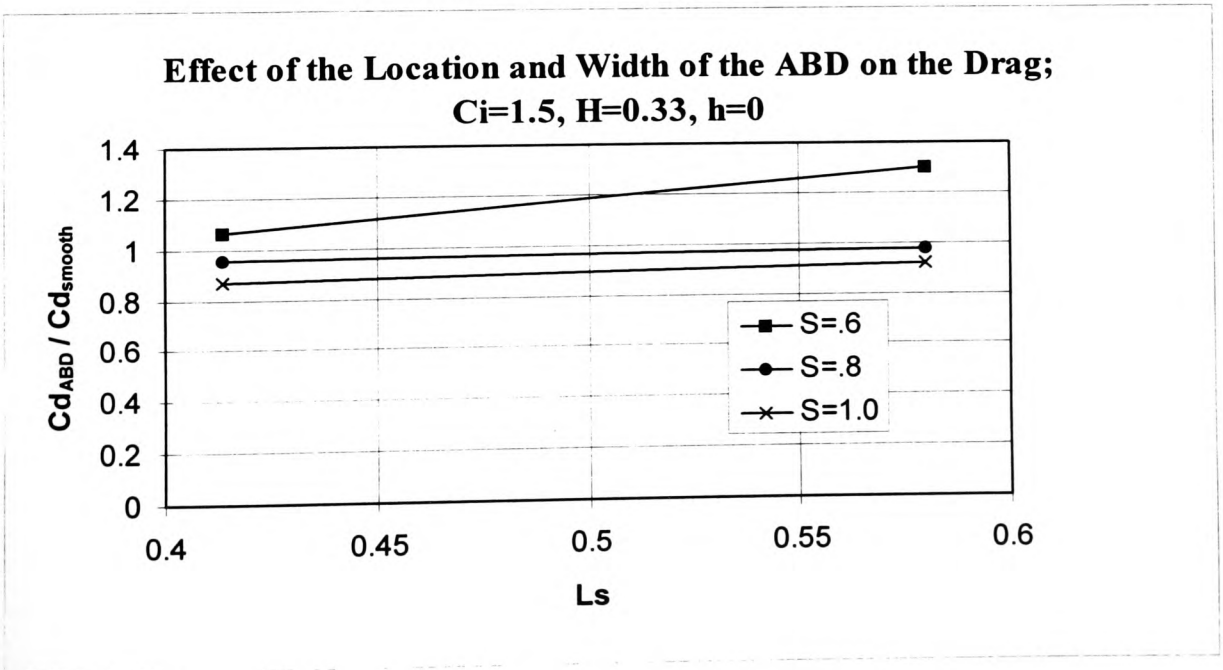

Figure 5-112

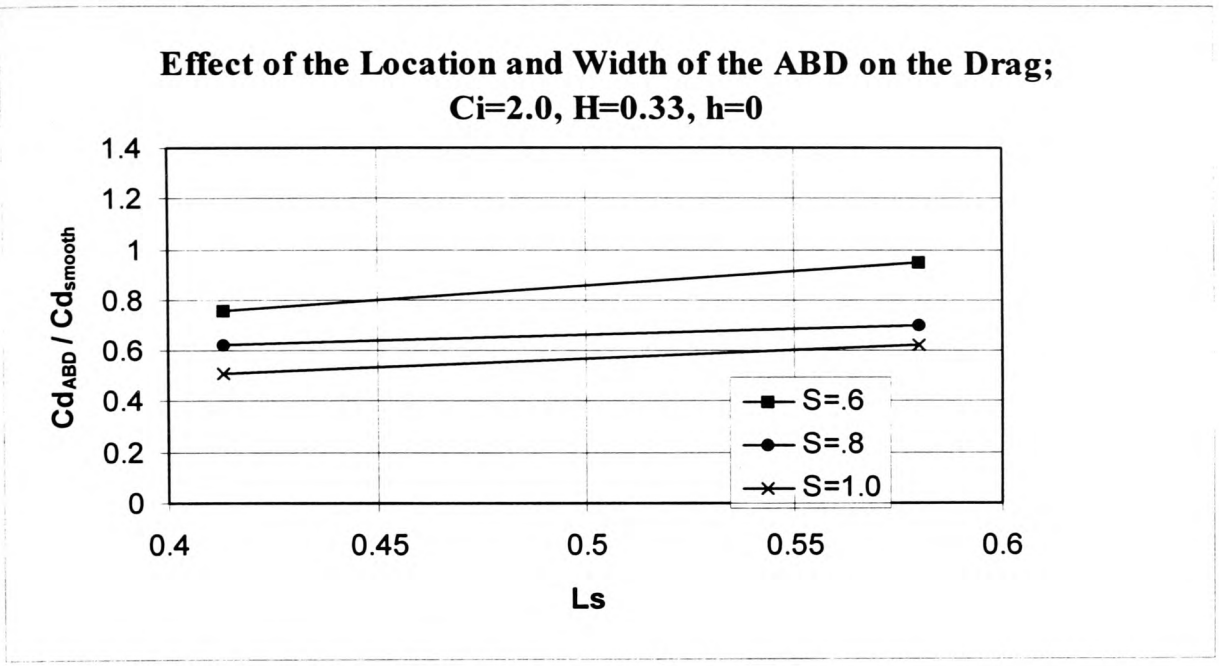

Figure 5-113

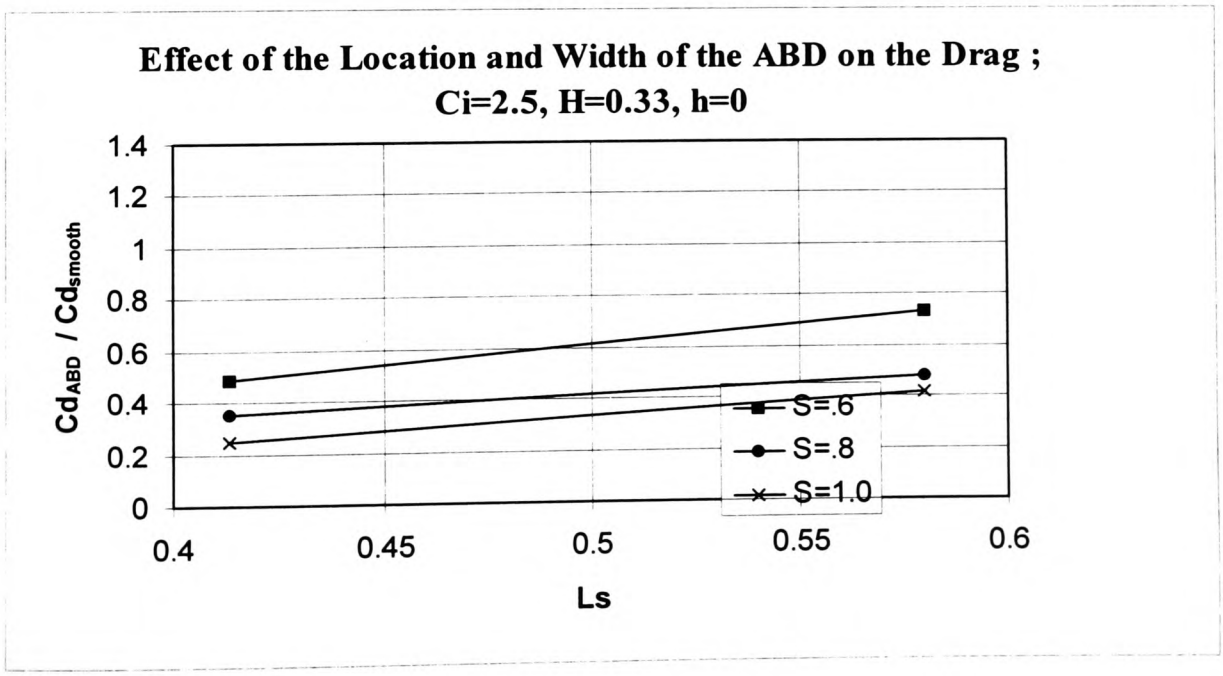

Figure 5-114

Alpha = 8 Degrees

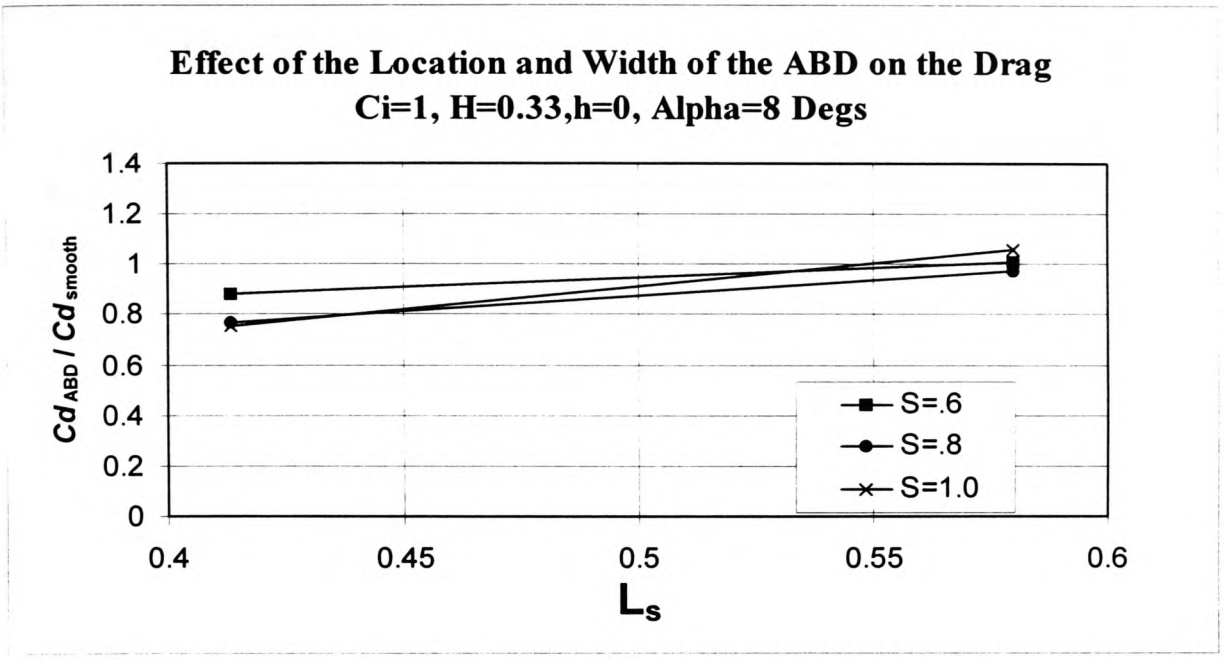

Figure 5-115

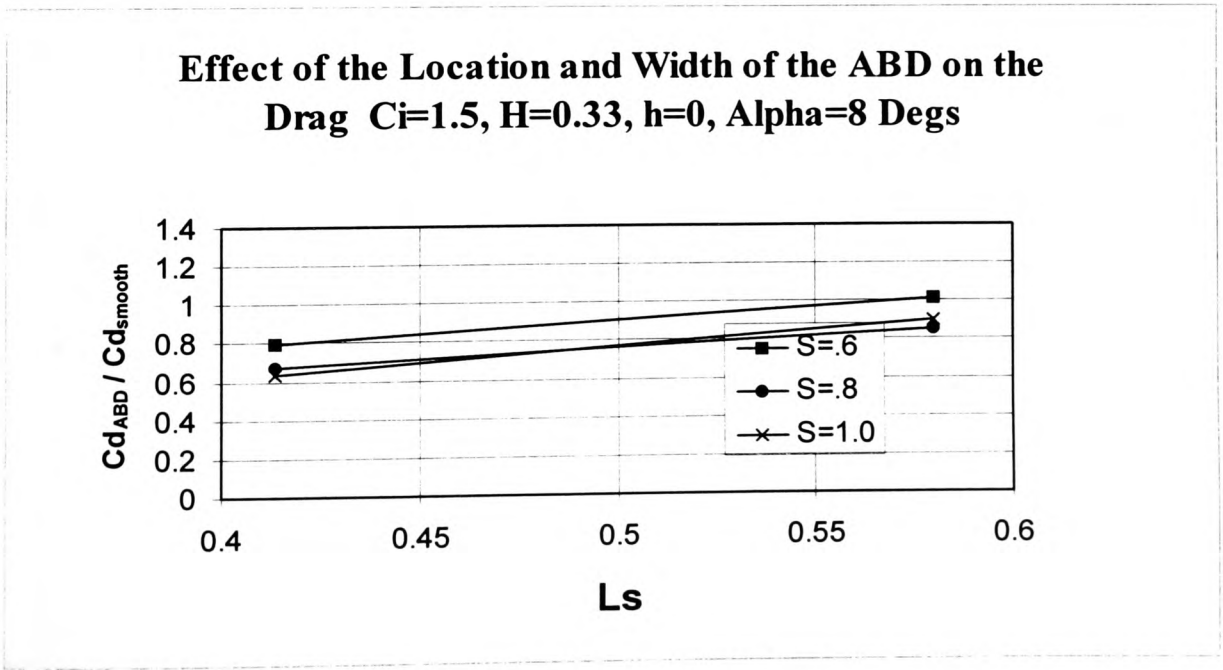

Figure 5-116

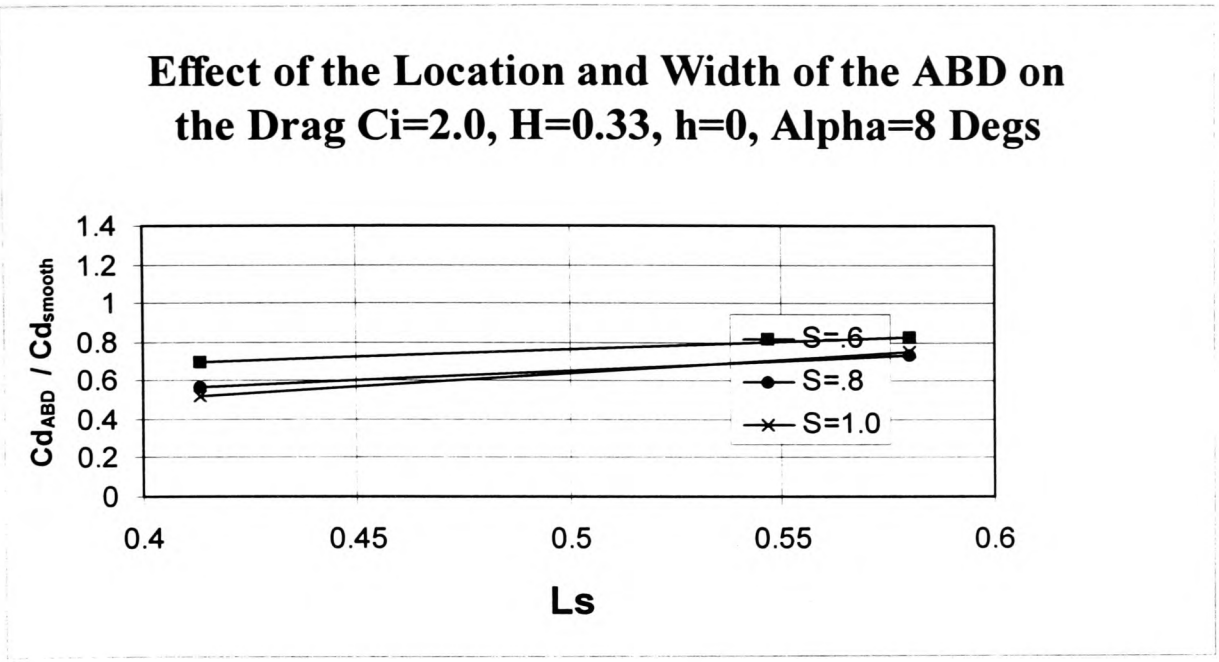

Figure 5-117

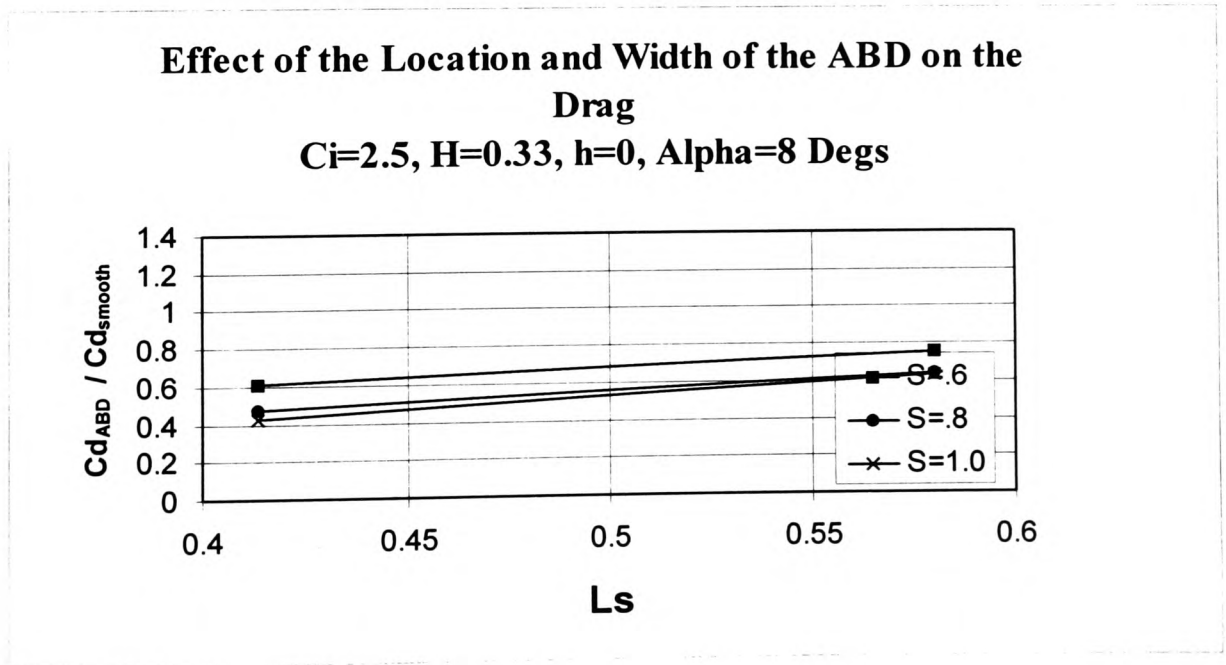

Figure 5-118

Alpha = 12 Degrees

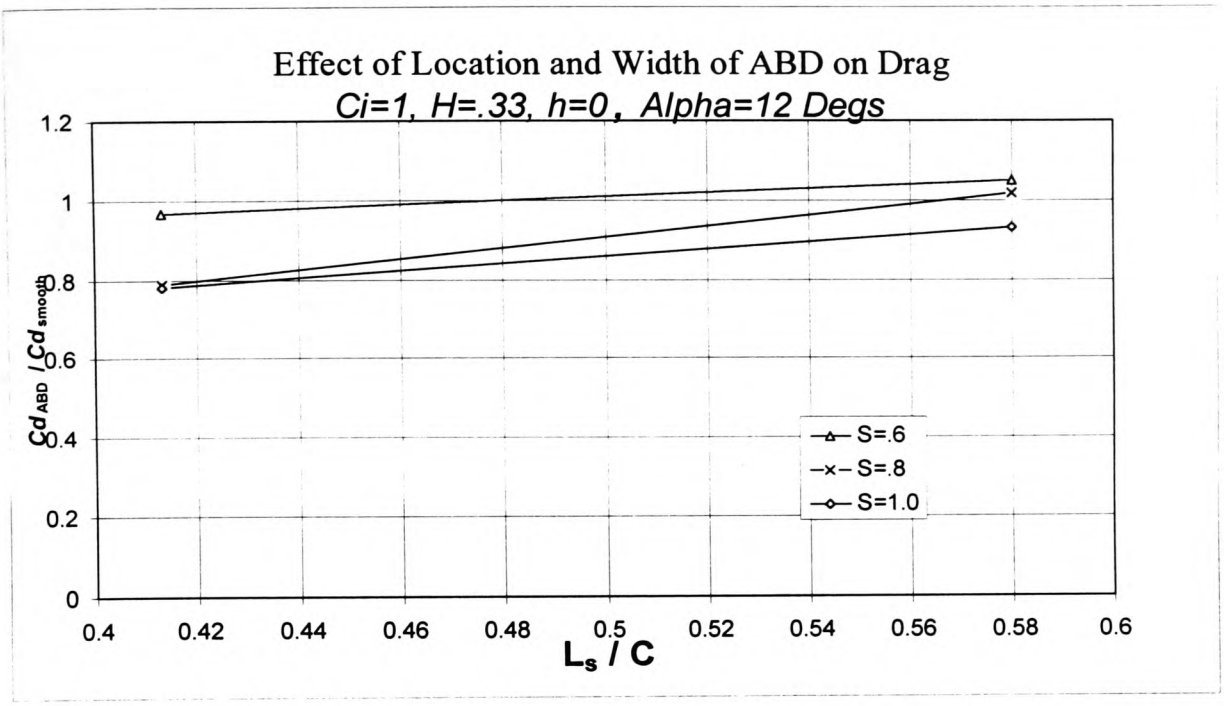

Figure 5-119

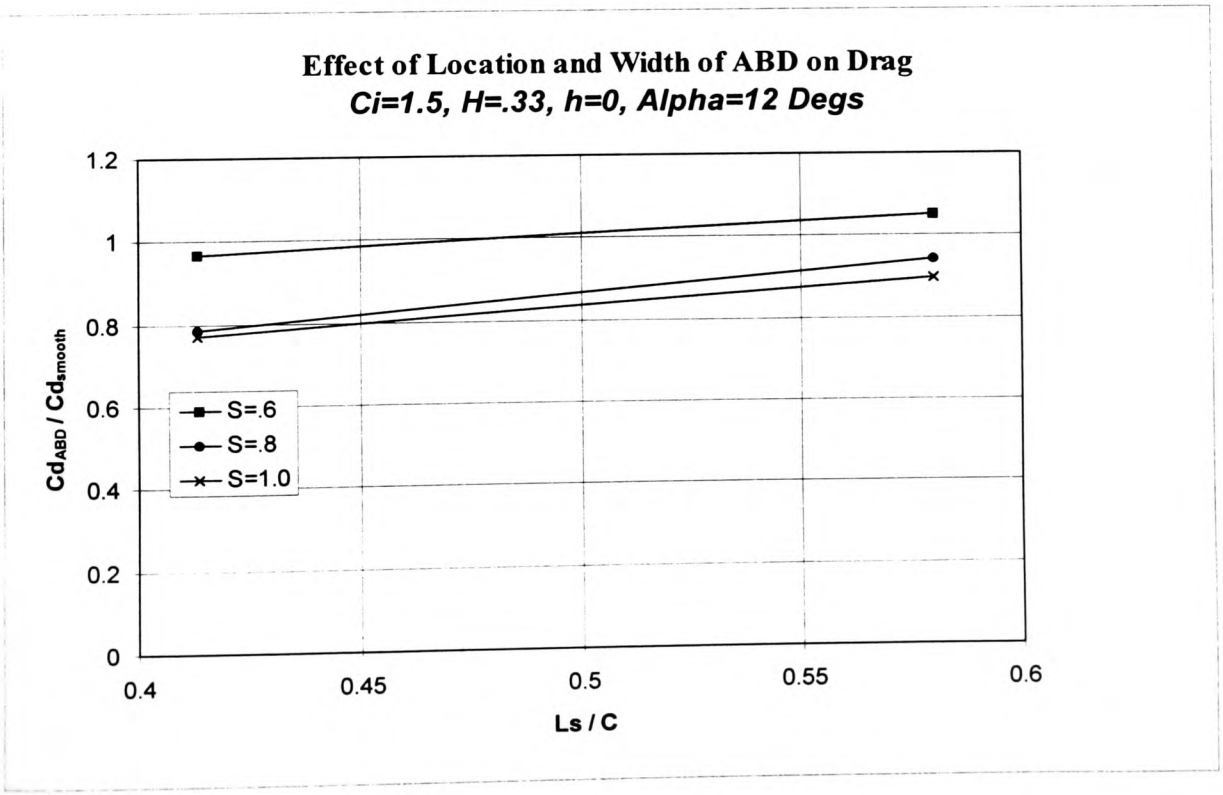

Figure 5-120

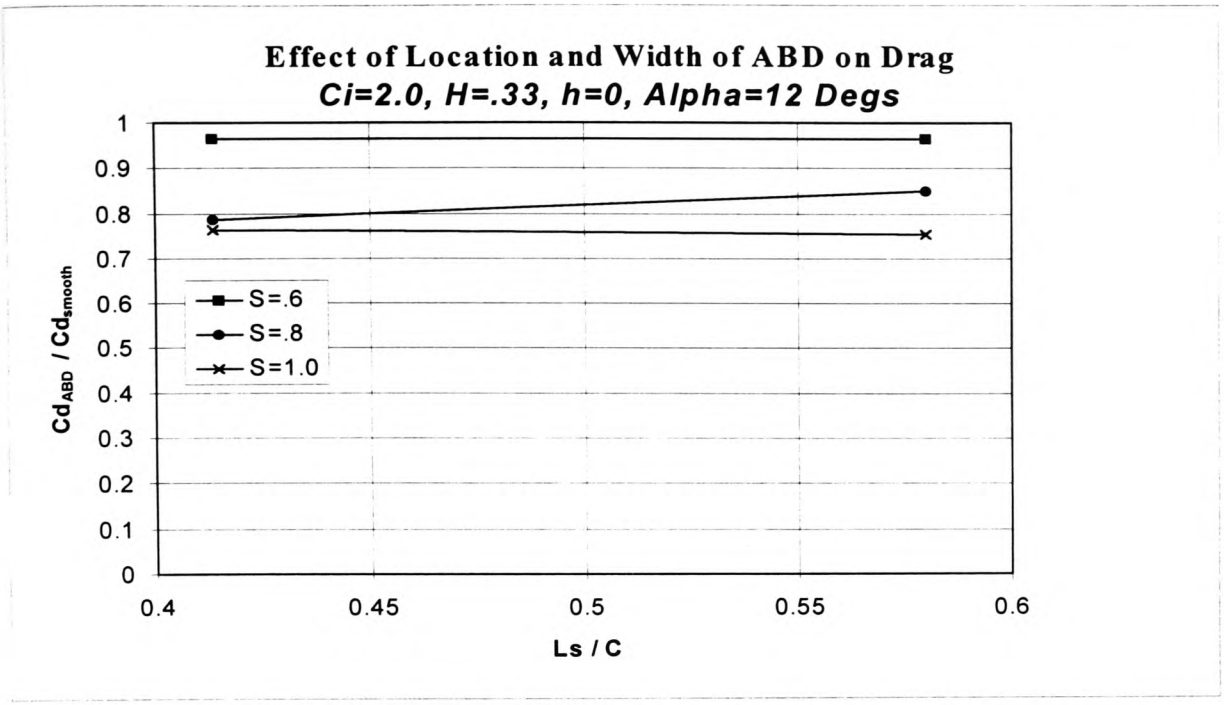

Figure 5-121

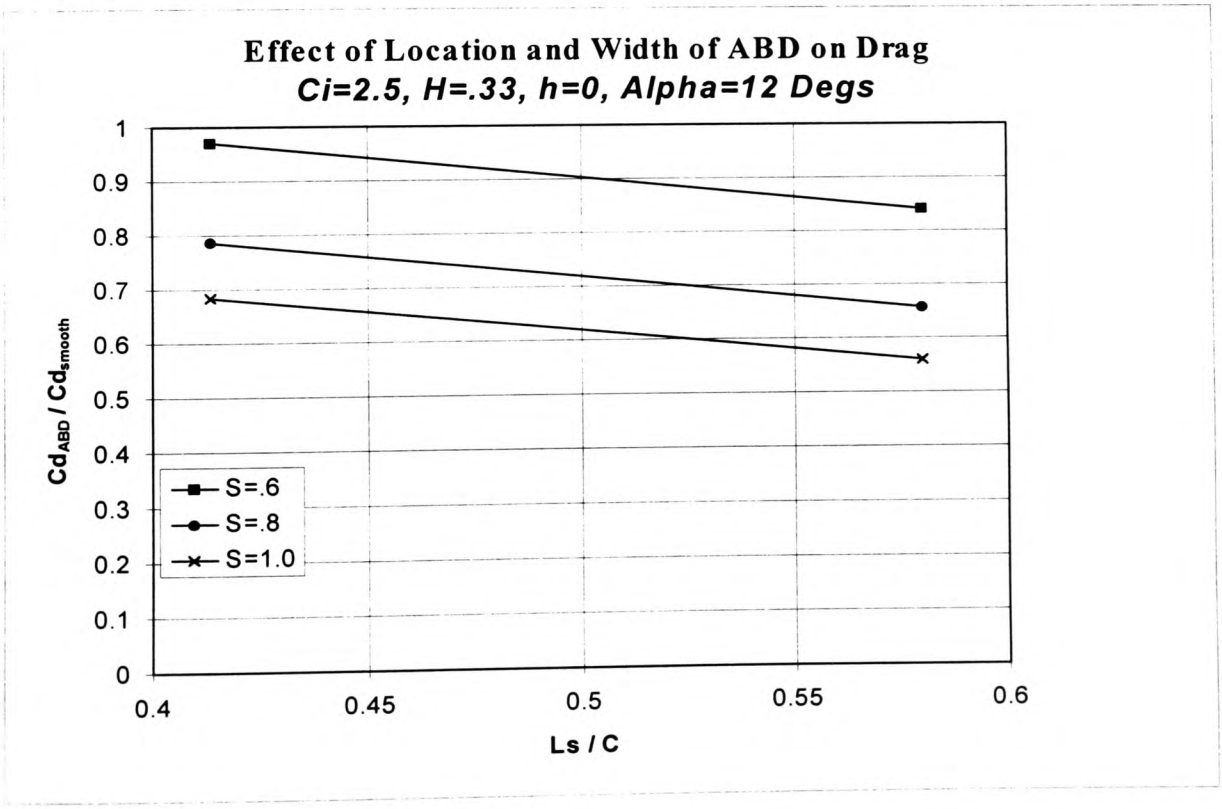

Figure 5-122

5.9.10 Effect of the Height of the ABD on Drag Coefficient (C_d)

5.9.10.1 Alpha = 4 Degrees

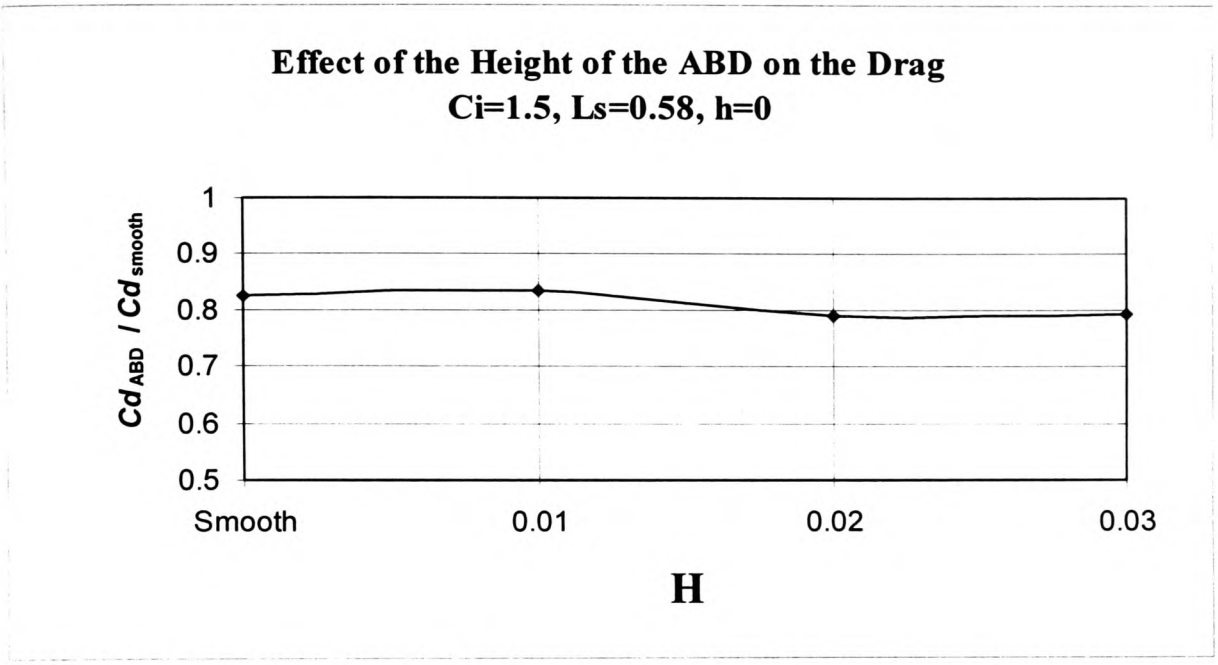

Figure 5-123

5.9.10.2 Alpha = 8 Degrees

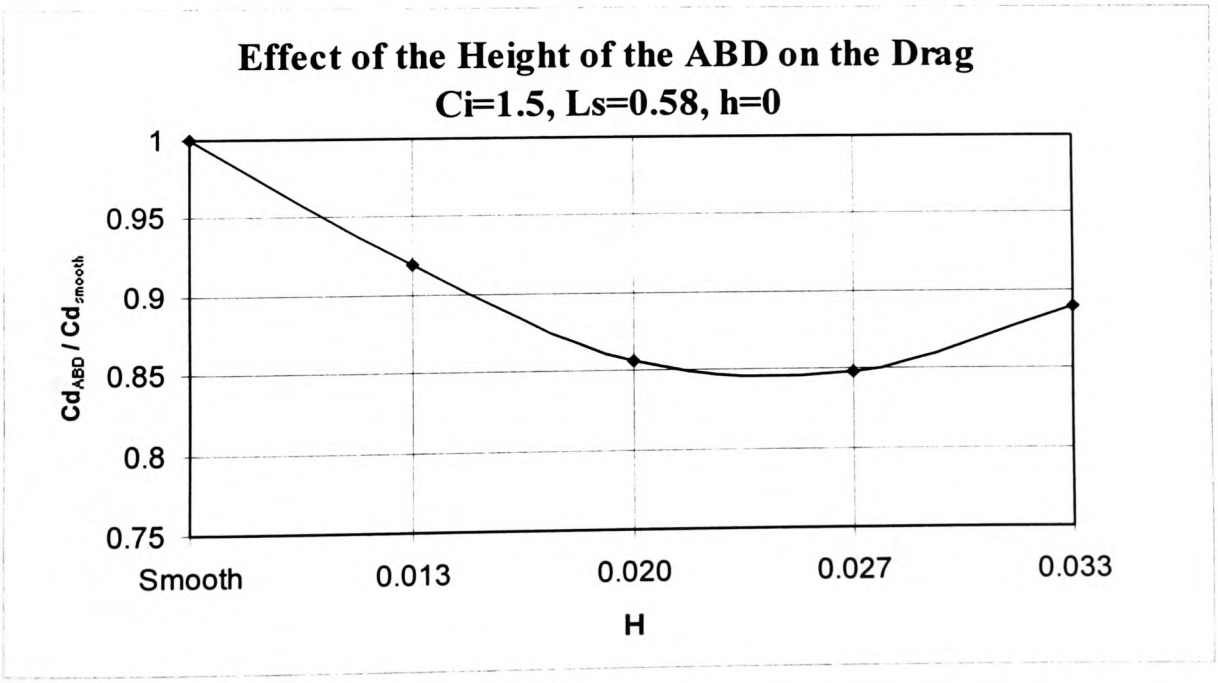

Figure 5-124

5.9.11 Effect of the Relative Height of the base of the ABD on Drag Coefficient (C_d)

5.9.11.1 Alpha = 4 Degrees

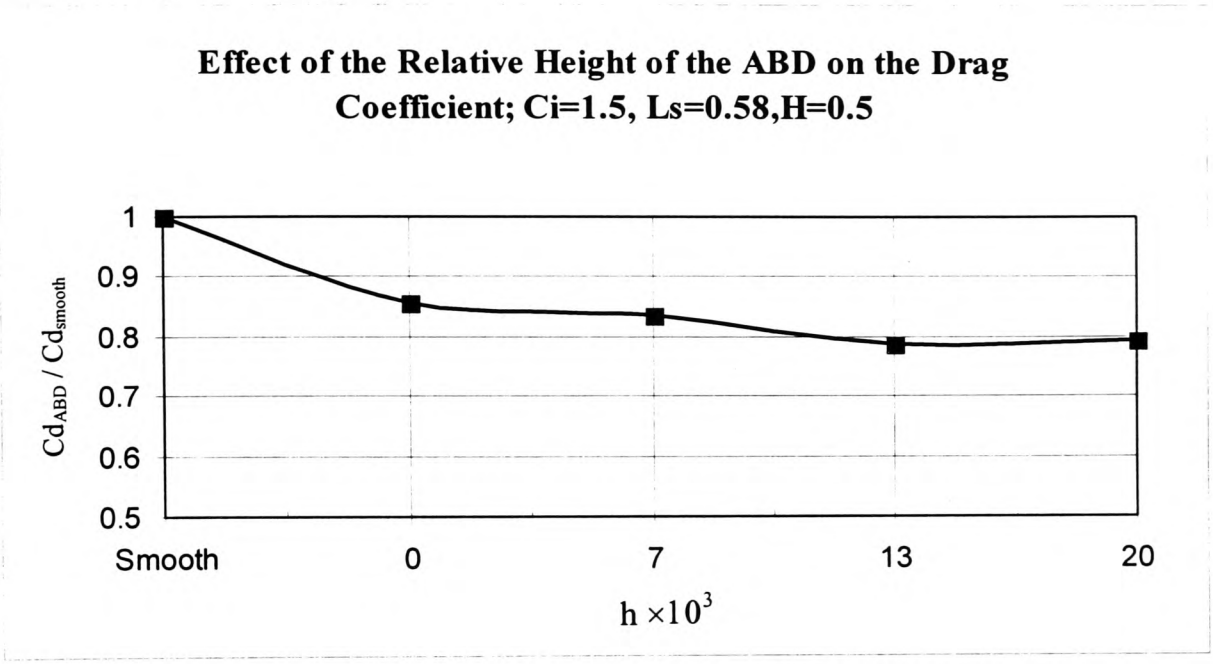

Figure 5-125

5.9.11.2 Alpha = 8 Degrees

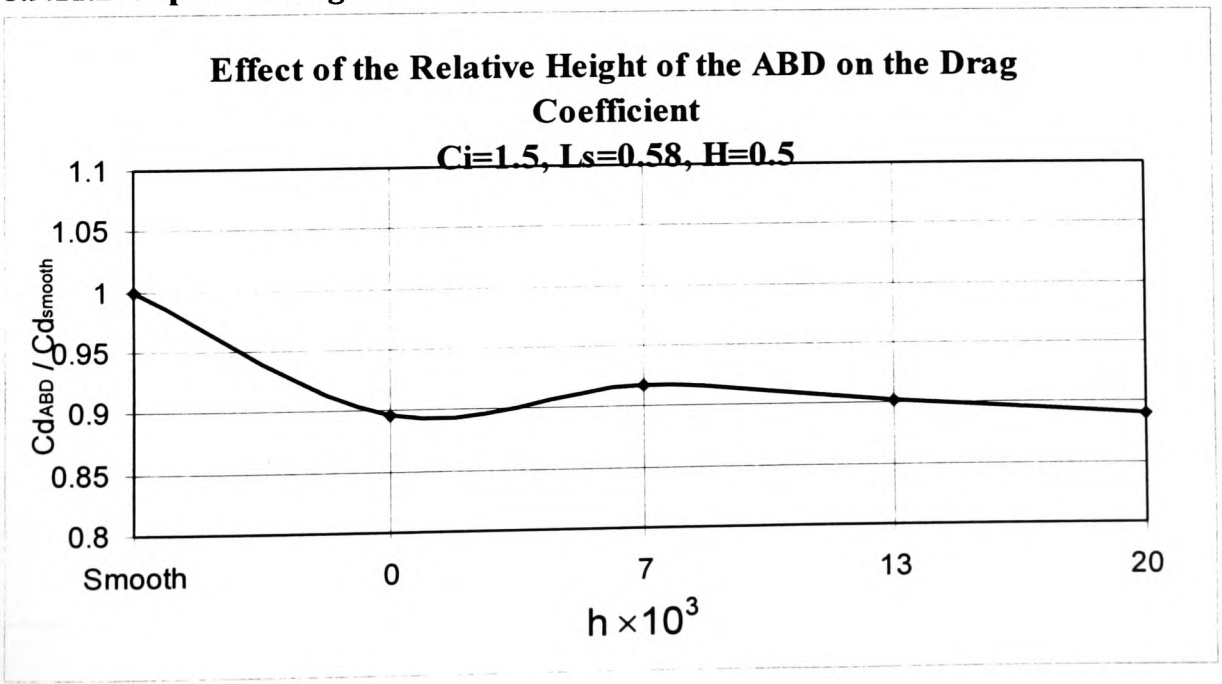

Figure 5-126

5.9.12 Effect of the Relative Velocity Inside the ABD on the Pressure Distribution over an Aerofoil

5.9.12.1 Alpha = 4 Degrees

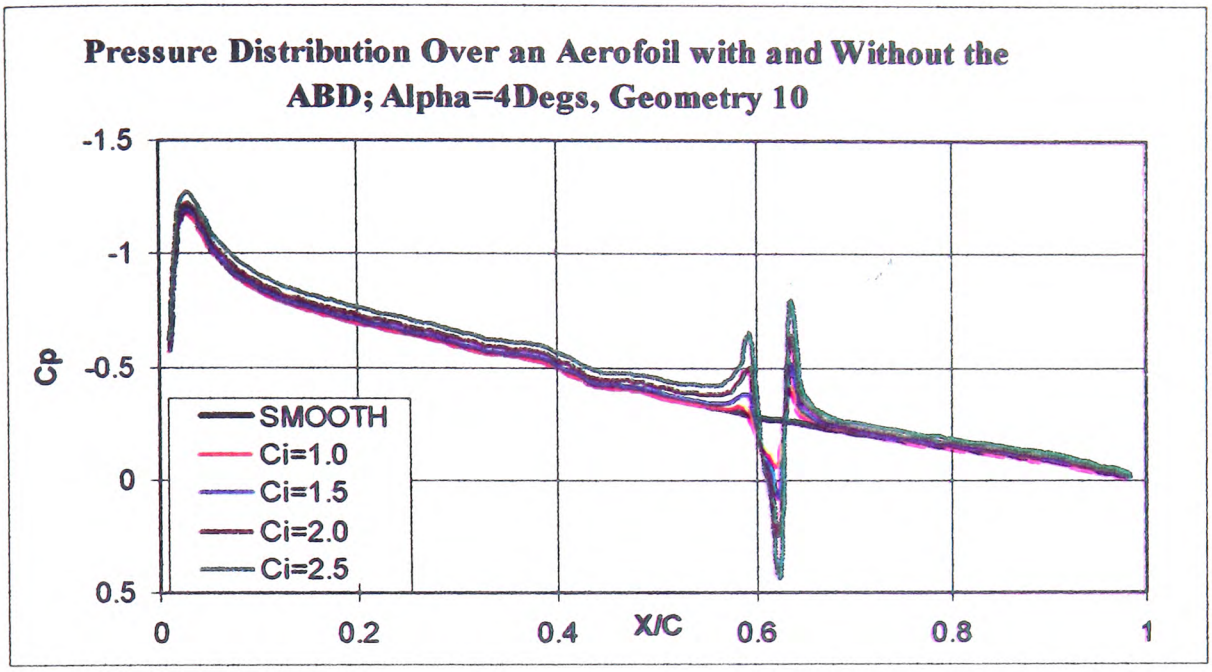

Figure 5-127

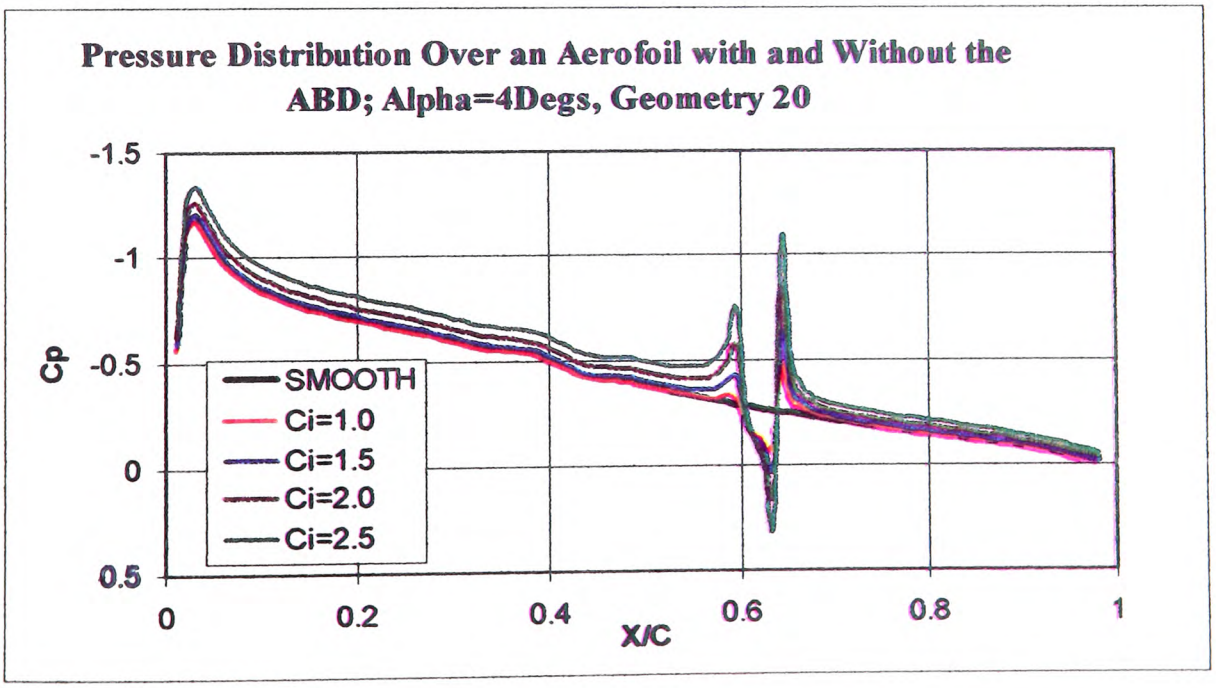

Figure 5-128

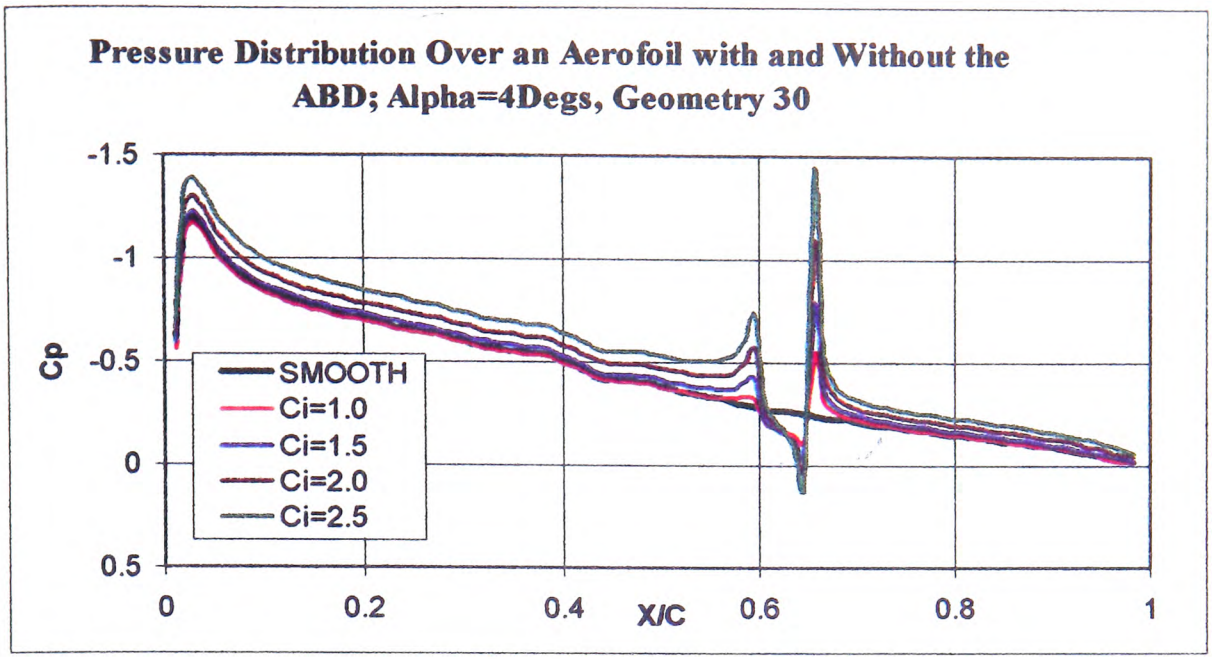

Figure 5-129

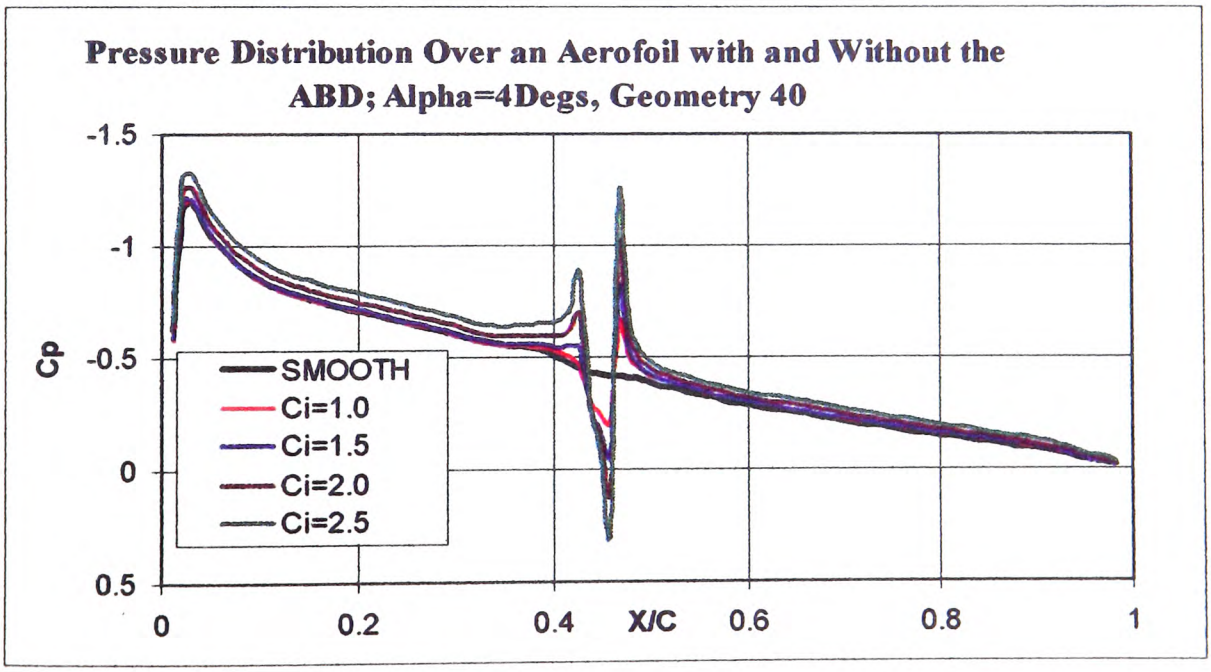

Figure 5-130

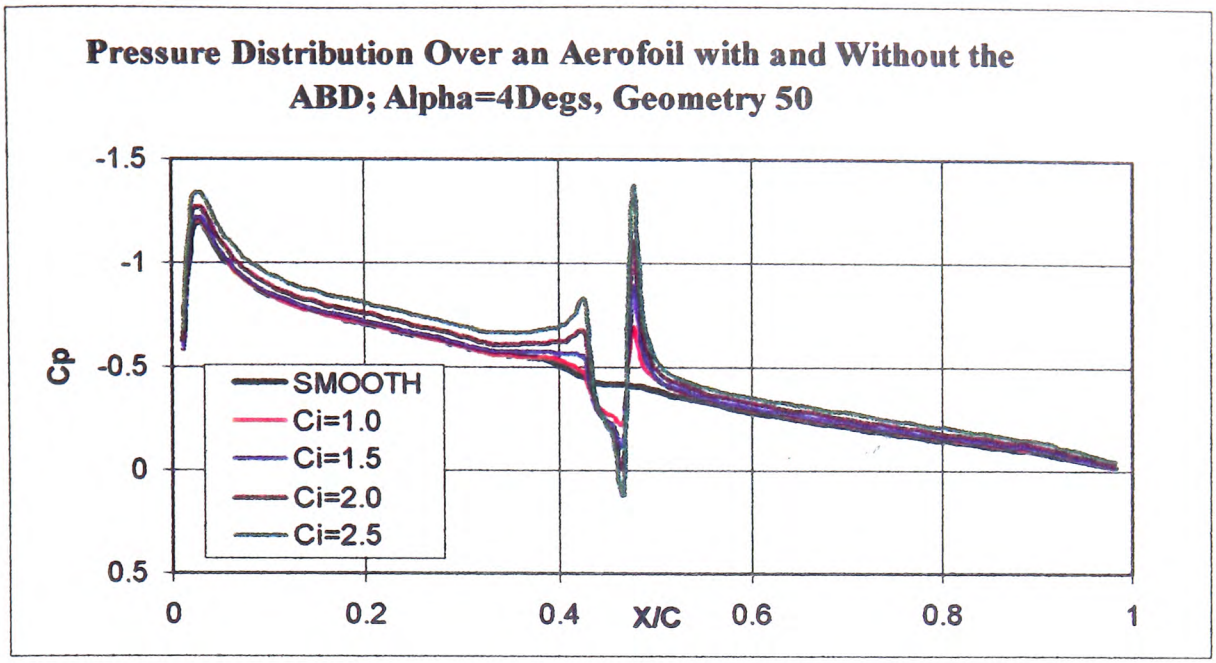

Figure 5-131

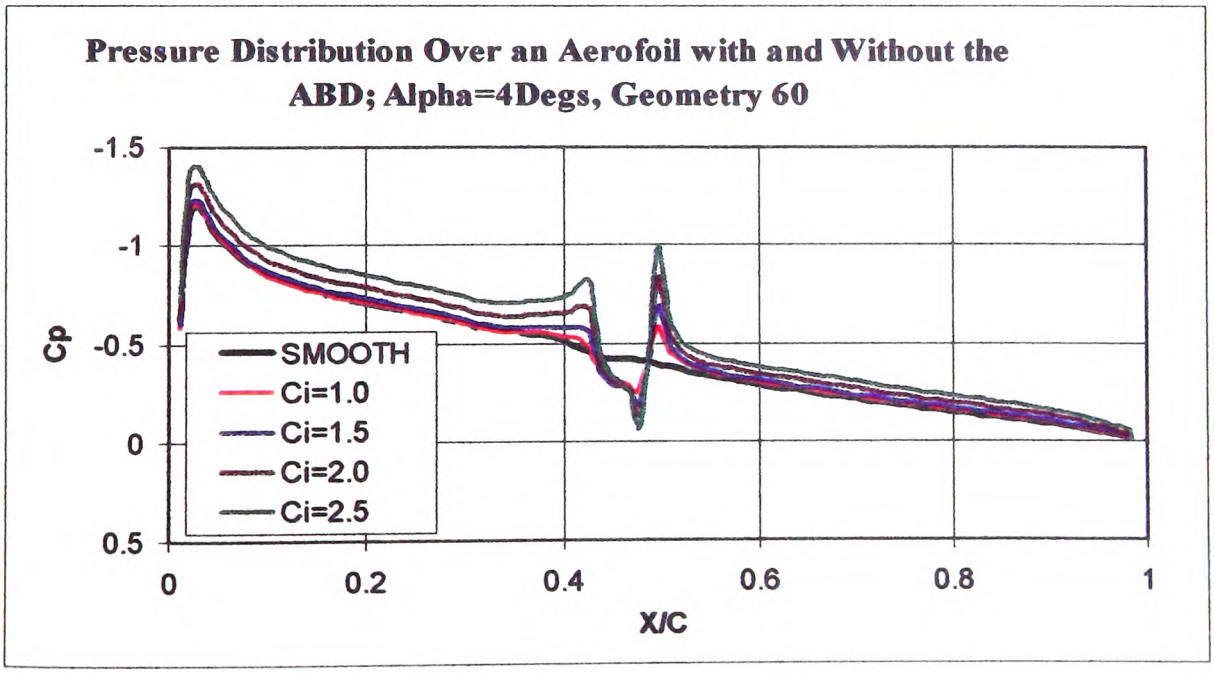

Figure 5-132

Alpha = 8 Degrees

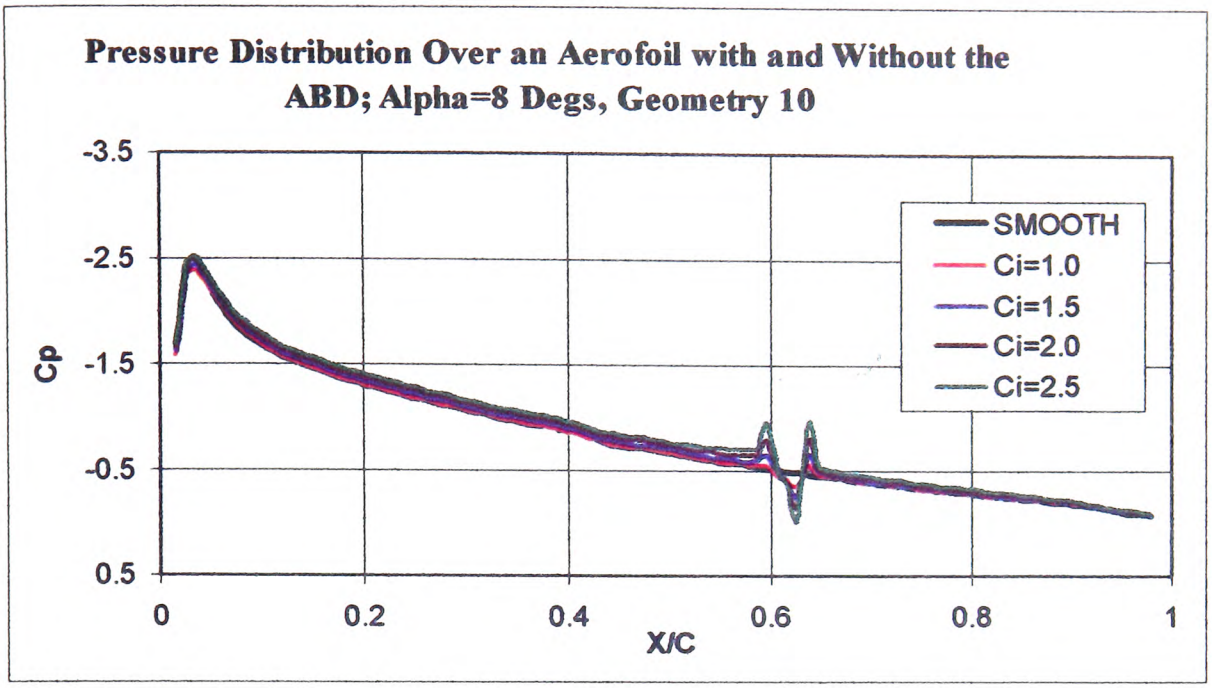

Figure 5-133

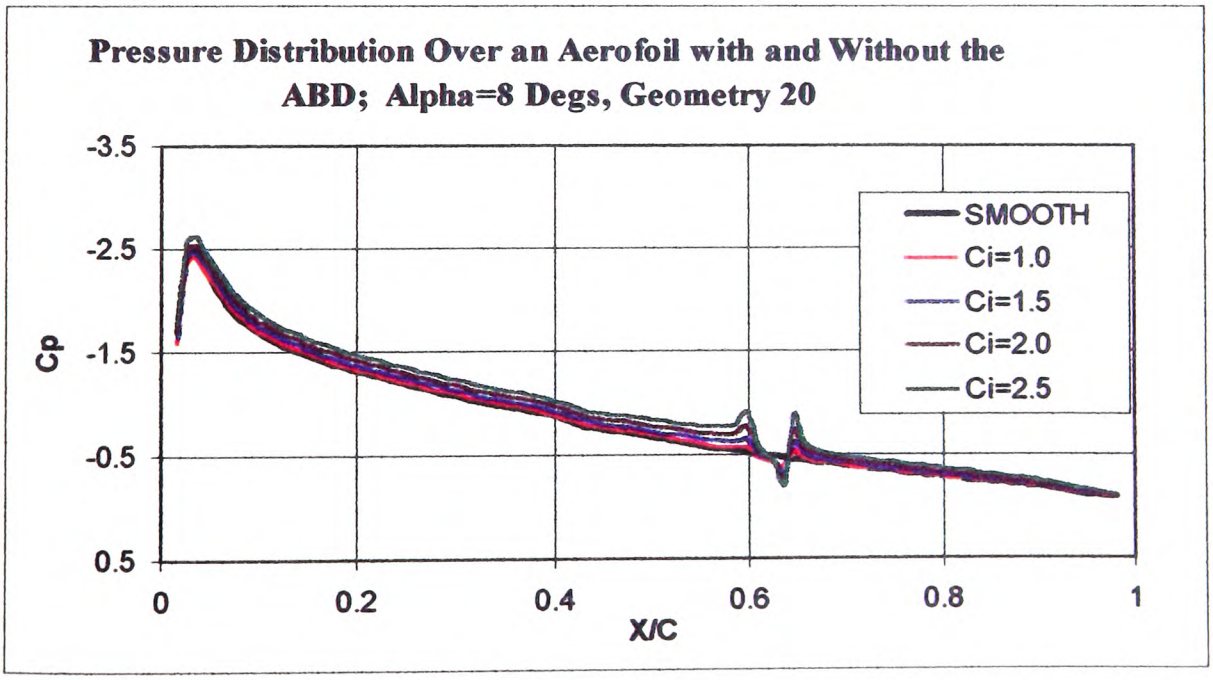

Figure 5-134

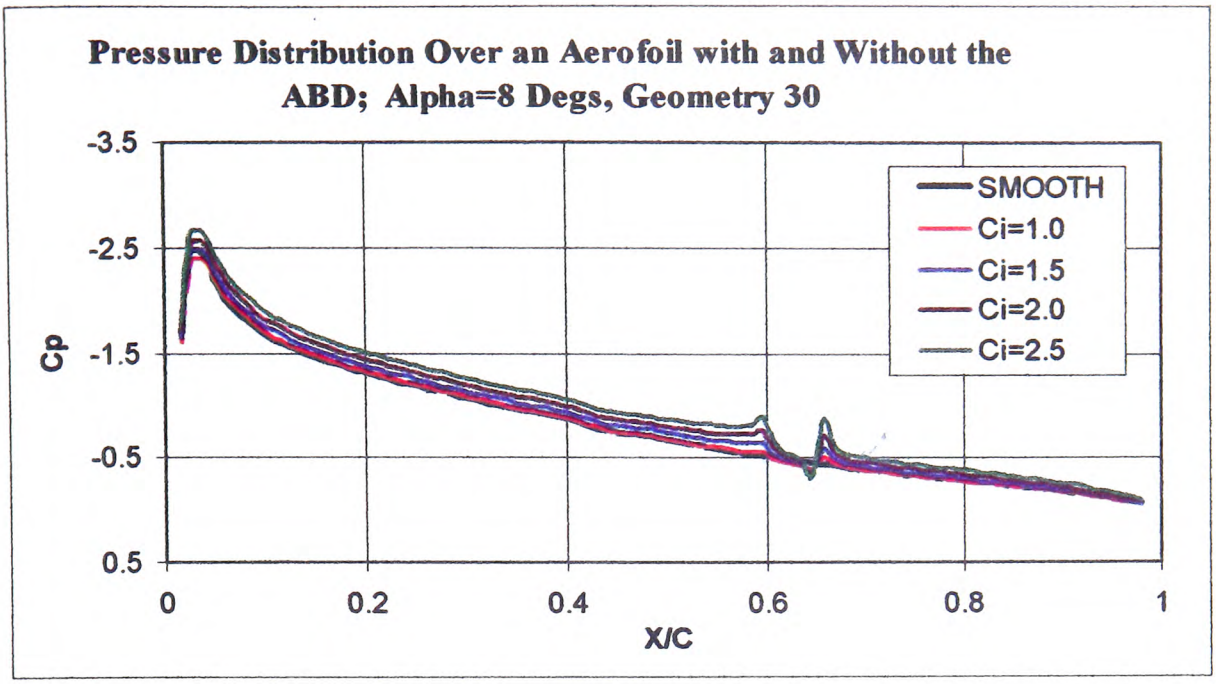

Figure 5-135

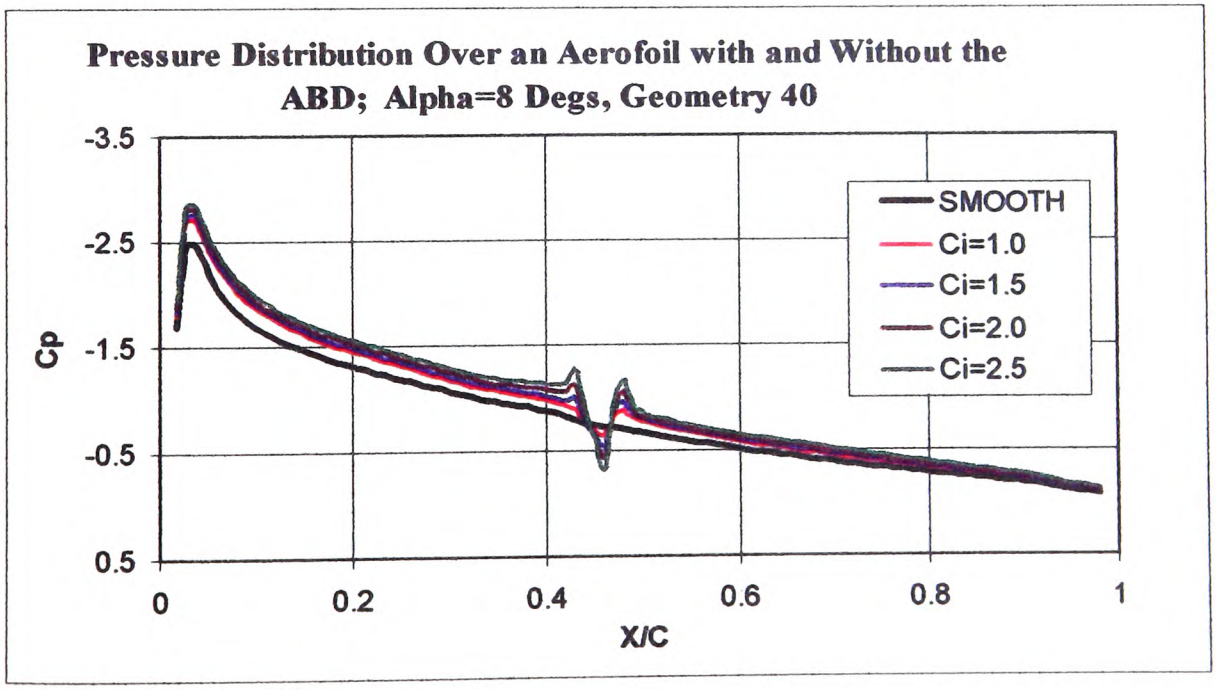

Figure 5-136

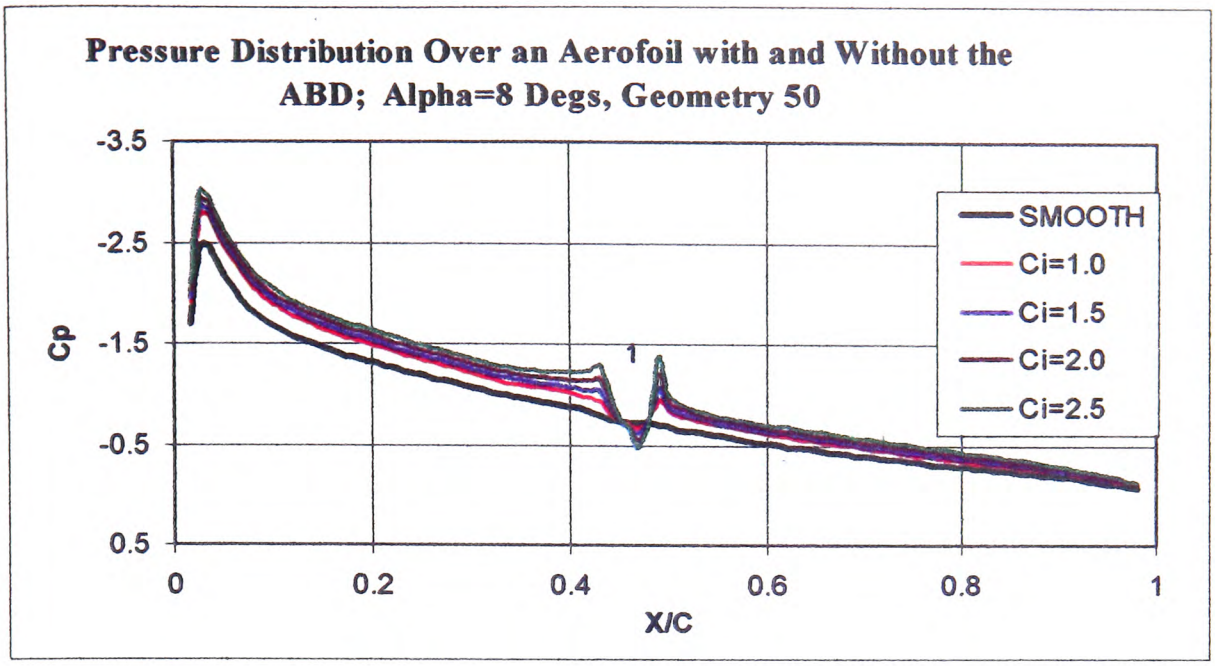

Figure 5-137

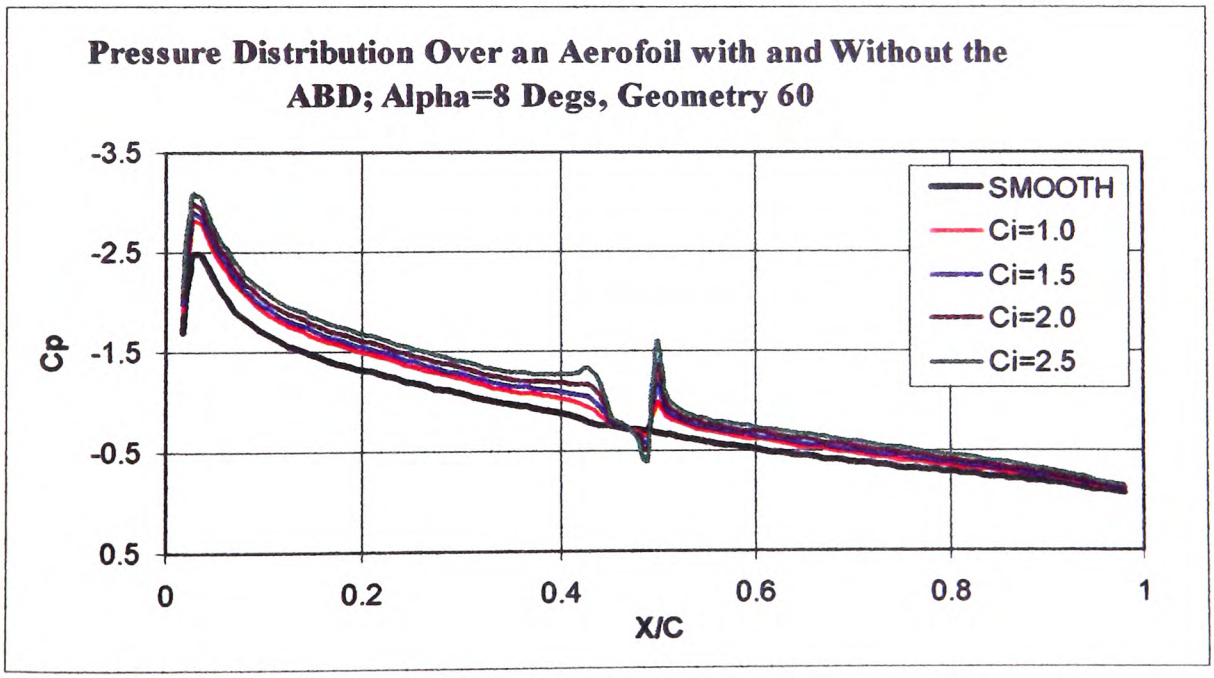

Figure 5-138

5.9.13 Effect of the Location of the ABD on the Pressure Distribution over an Aerofoil

5.9.13.1 Alpha = 4 Degrees

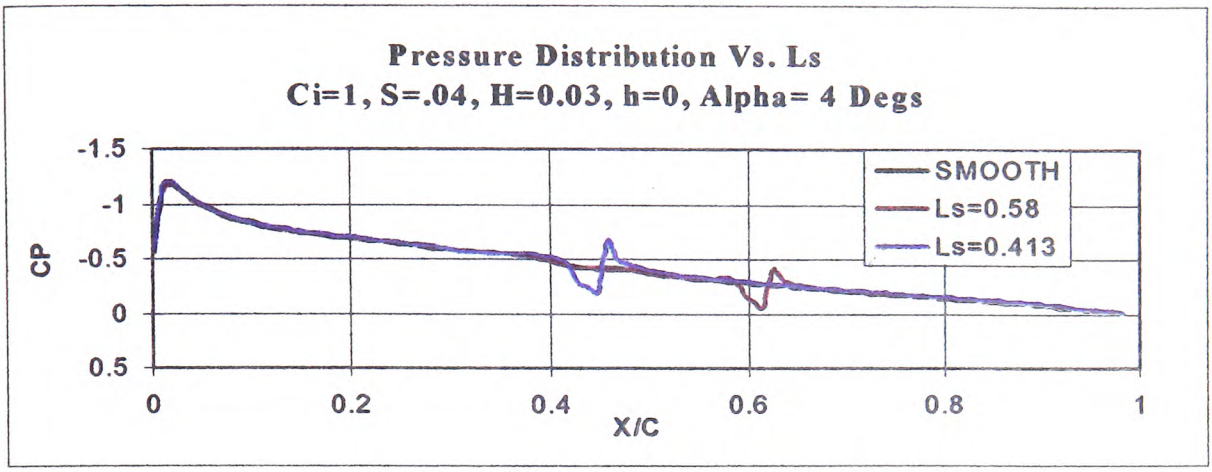

Figure 5-139

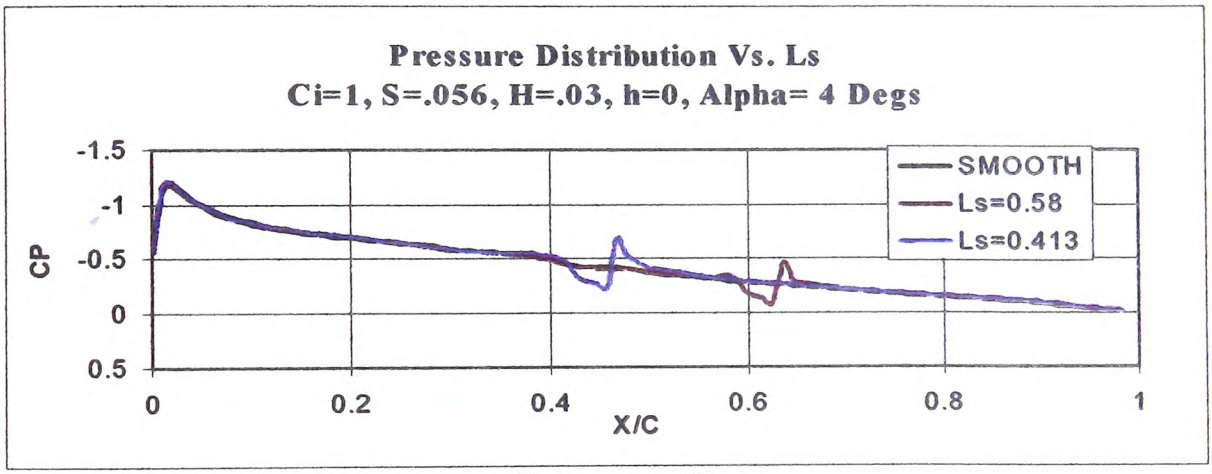

Figure 5-140

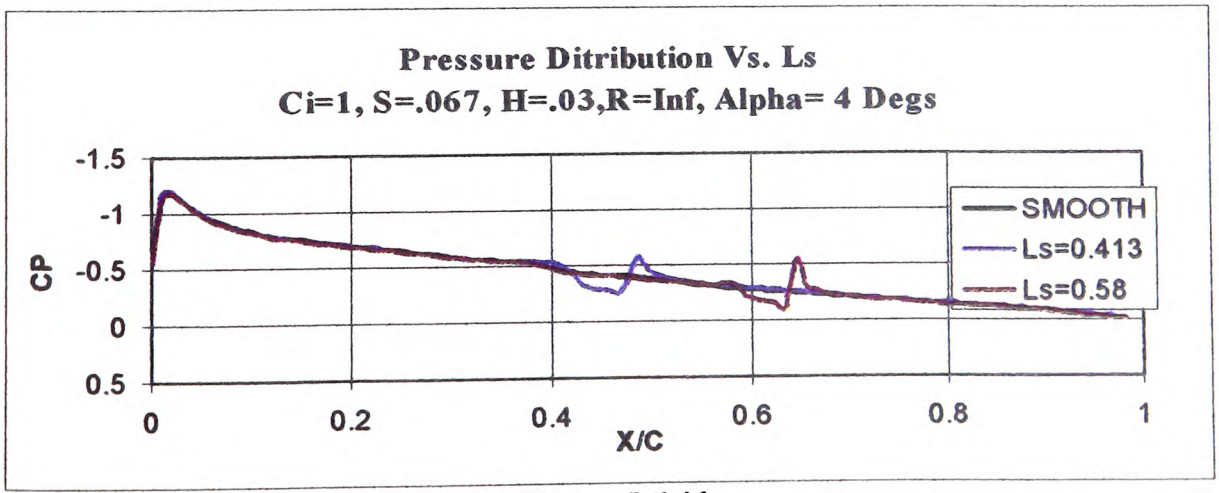

Figure 5-141

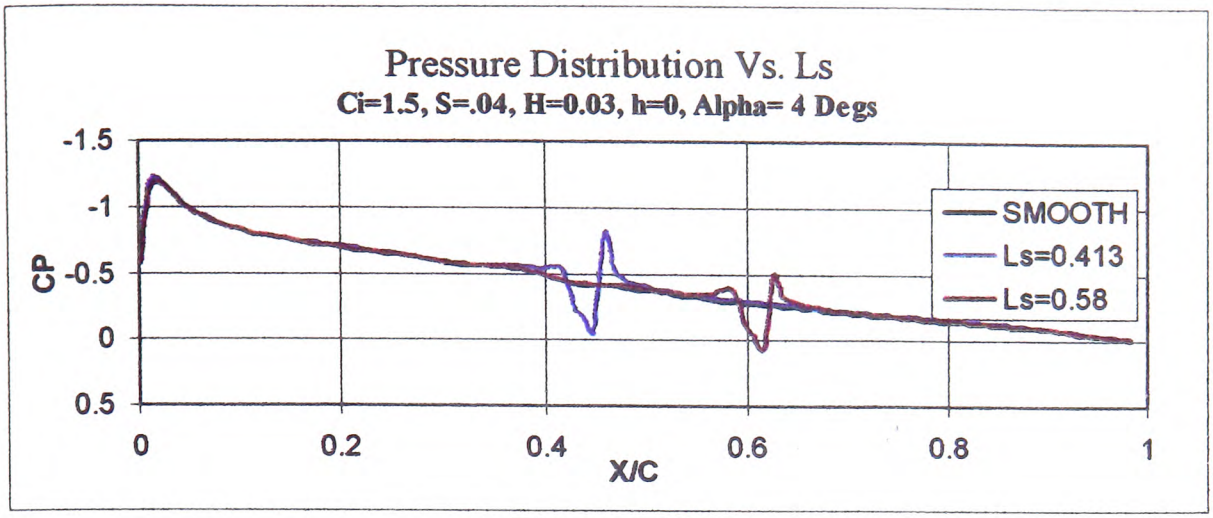

Figure 5-142

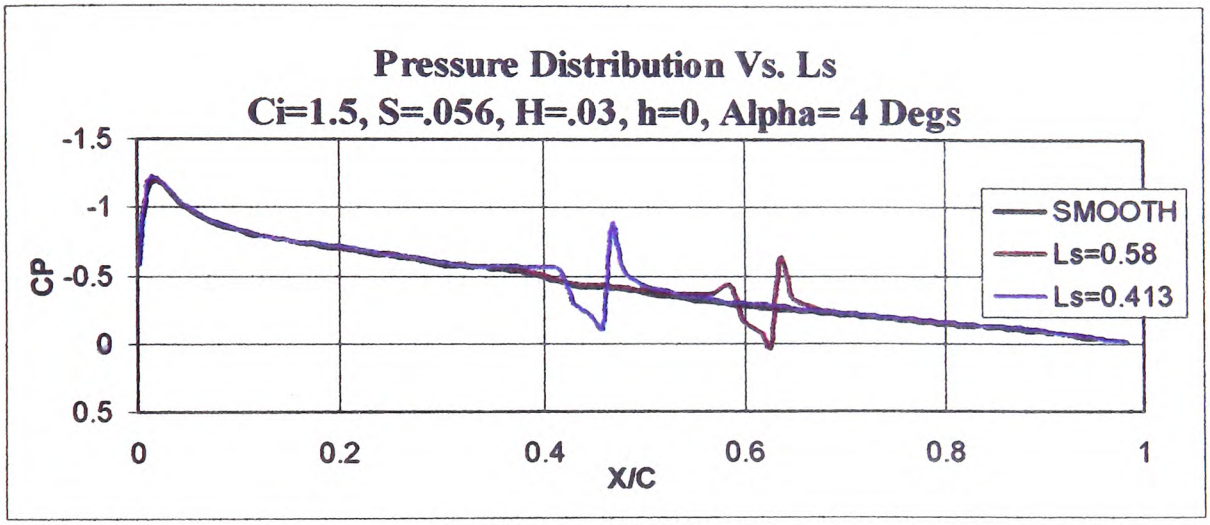

Figure 5-143

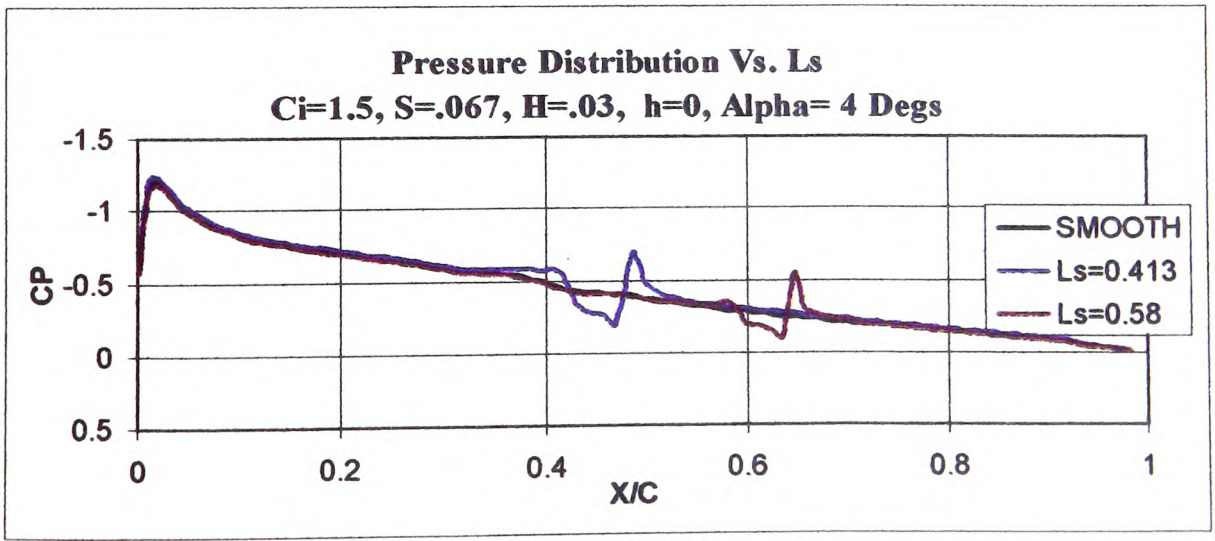

Figure 5-144

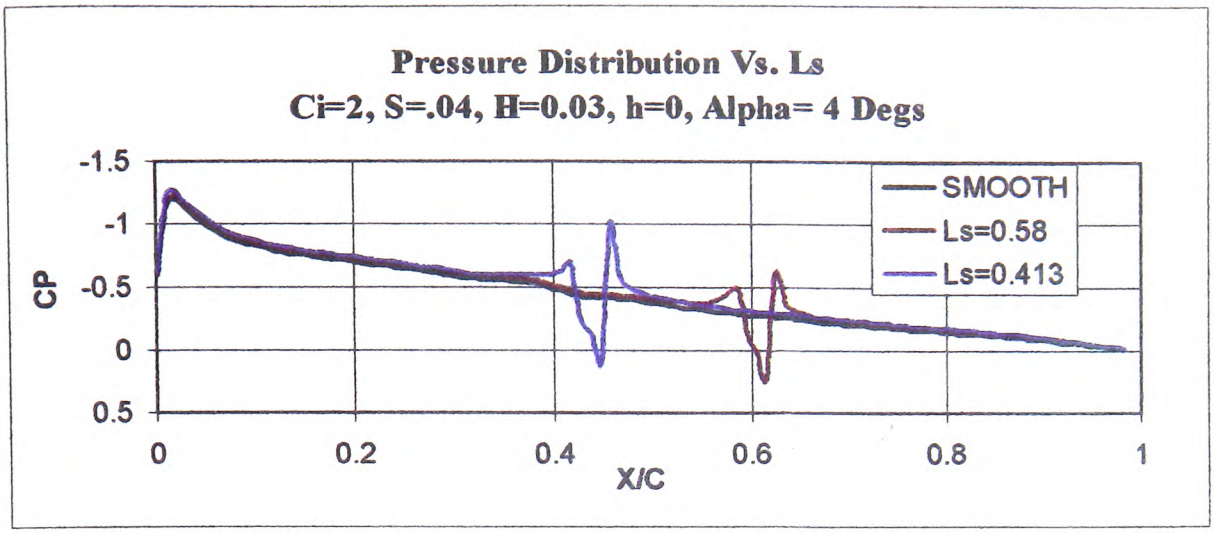

Figure 5-145

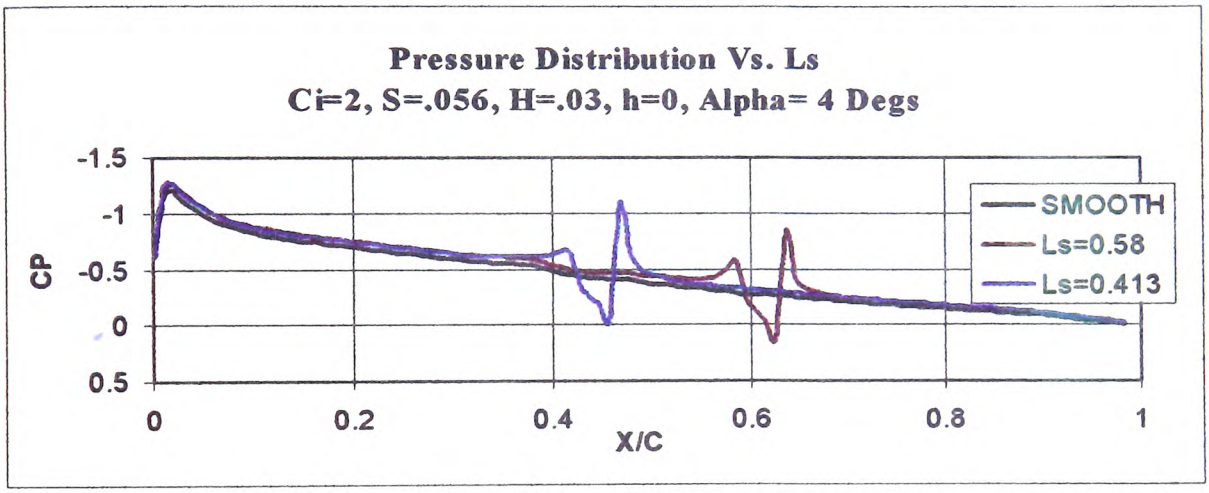

Figure 5-146

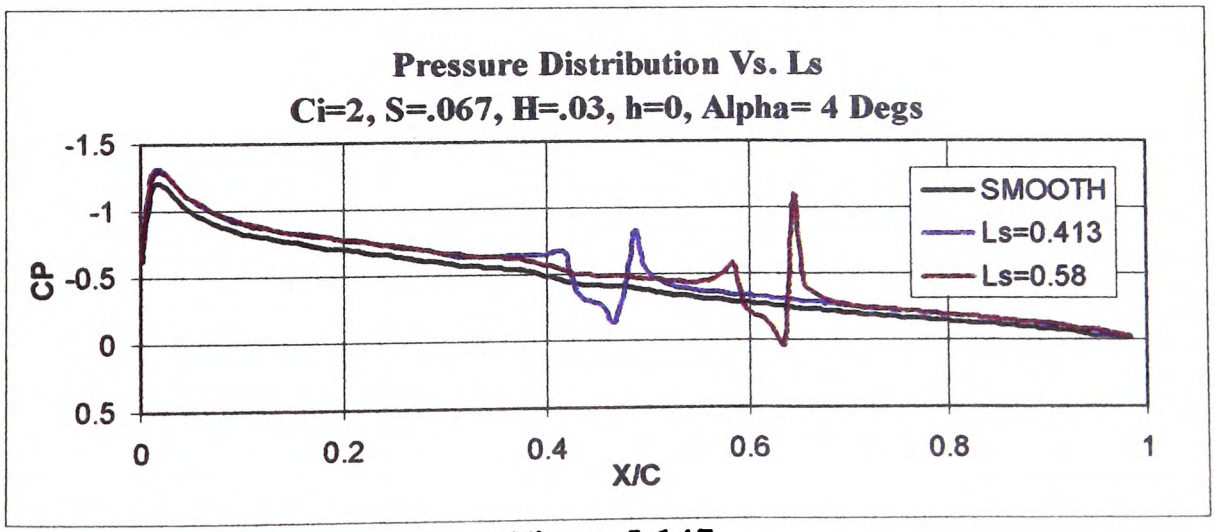

Figure 5-147

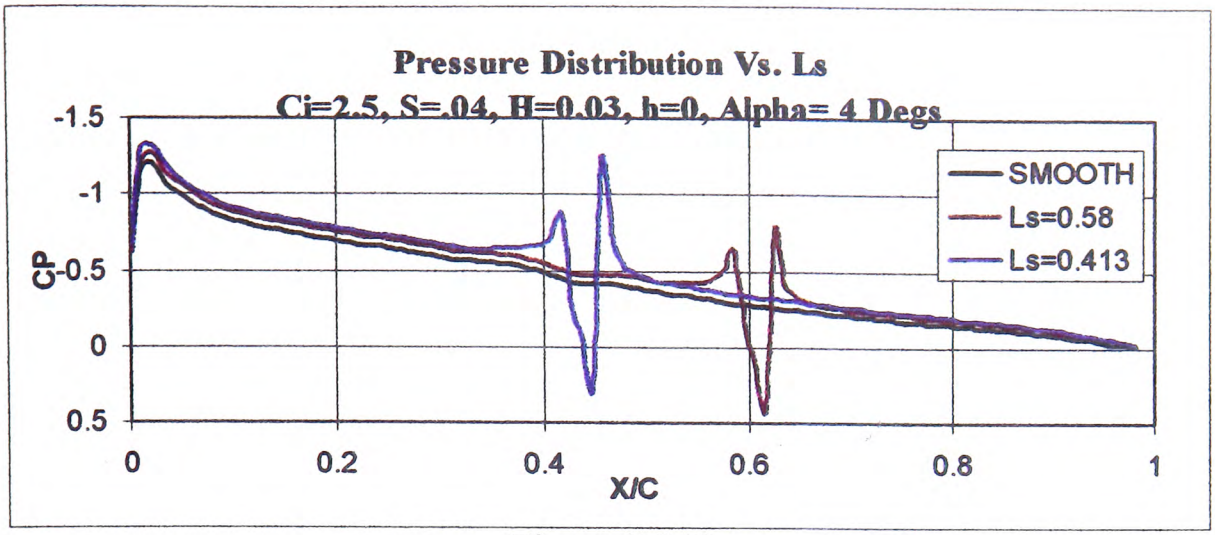

Figure 5-148

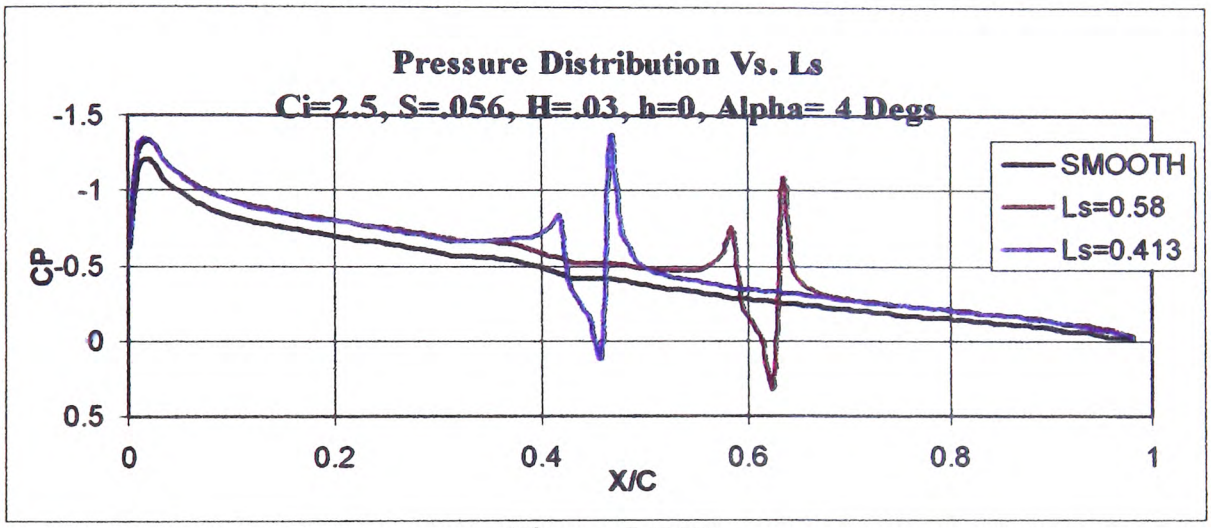

Figure 5-149

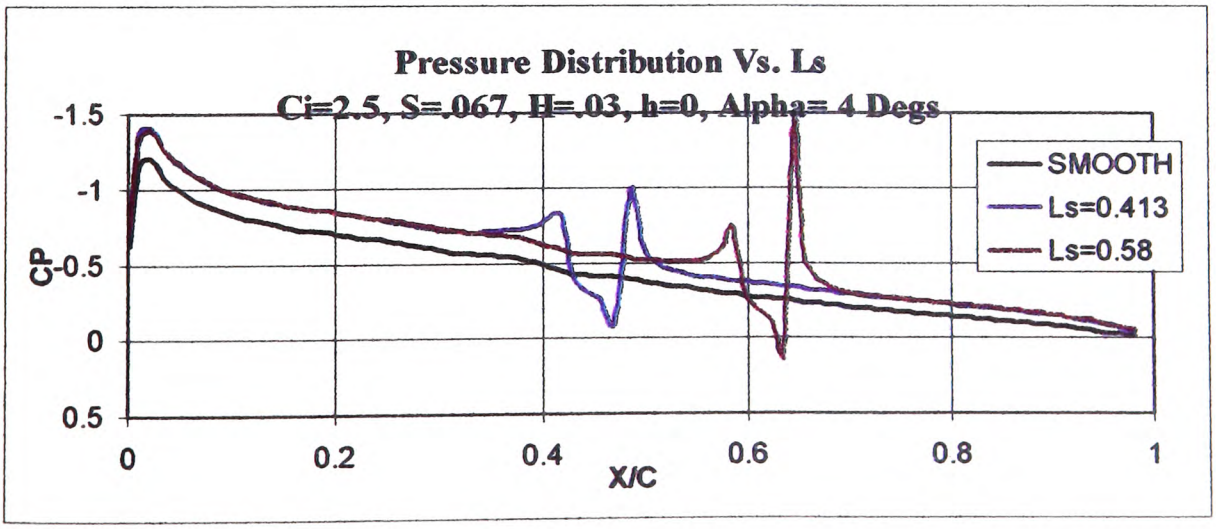

Figure 5-150

5.9.13.2 Alpha = 8 Degrees

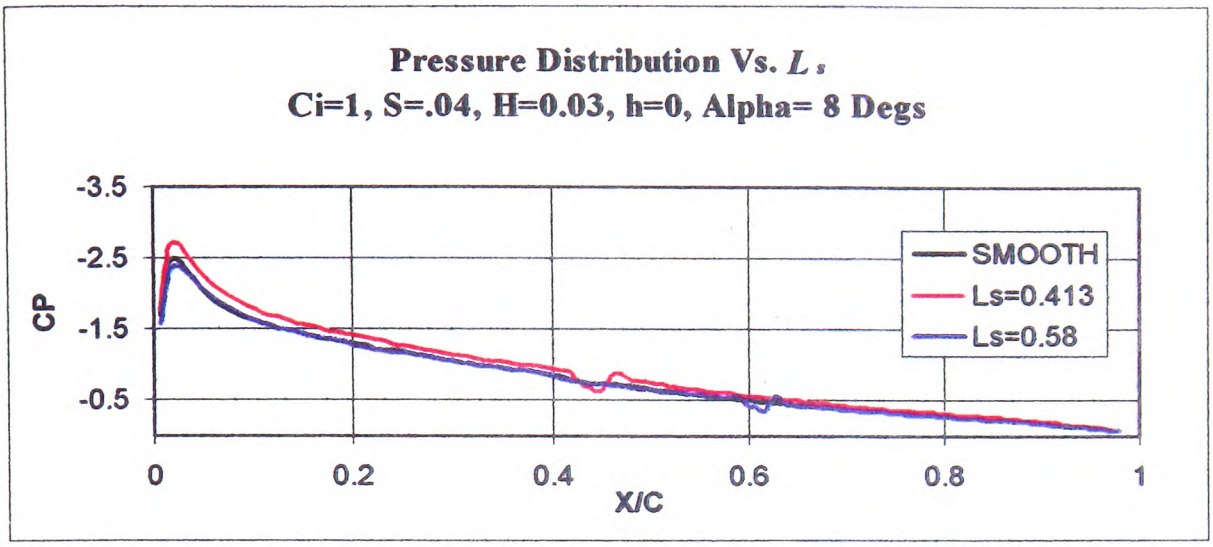

Figure 5-151

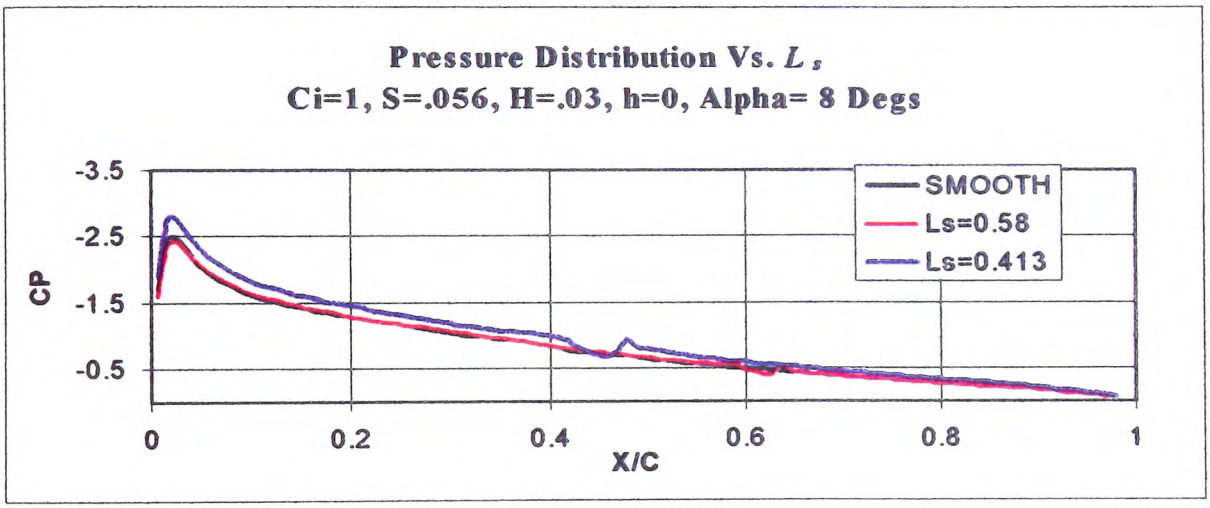

Figure 5-152

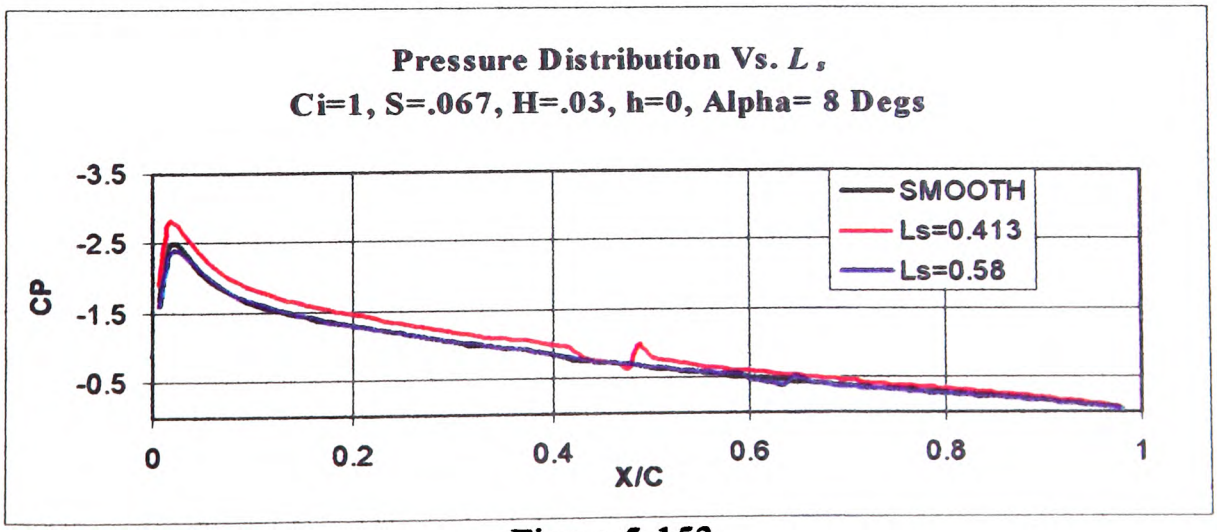

Figure 5-153

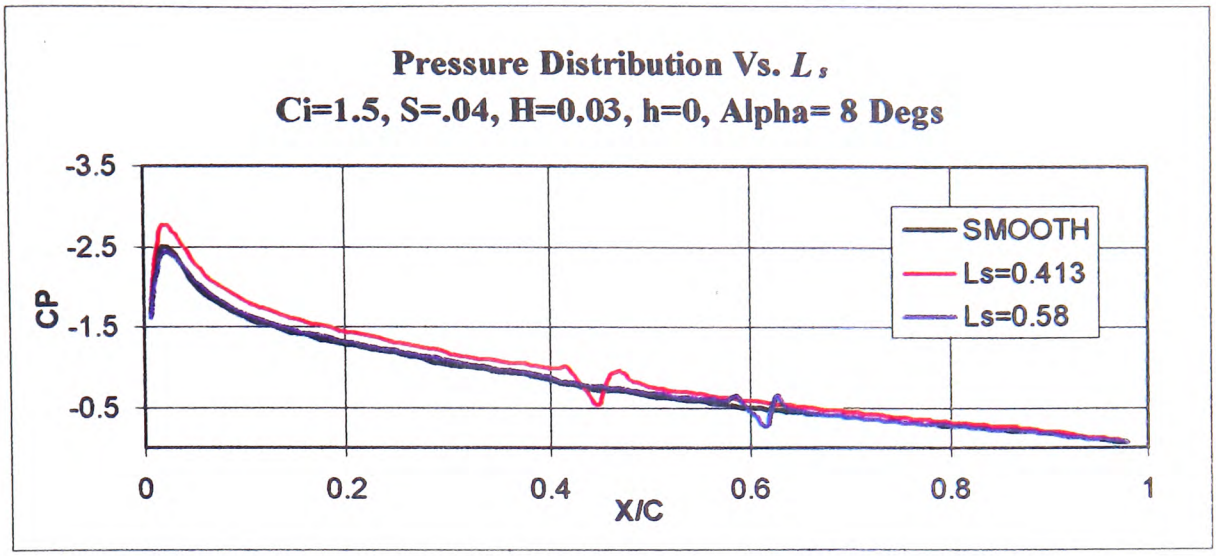

Figure 5-154

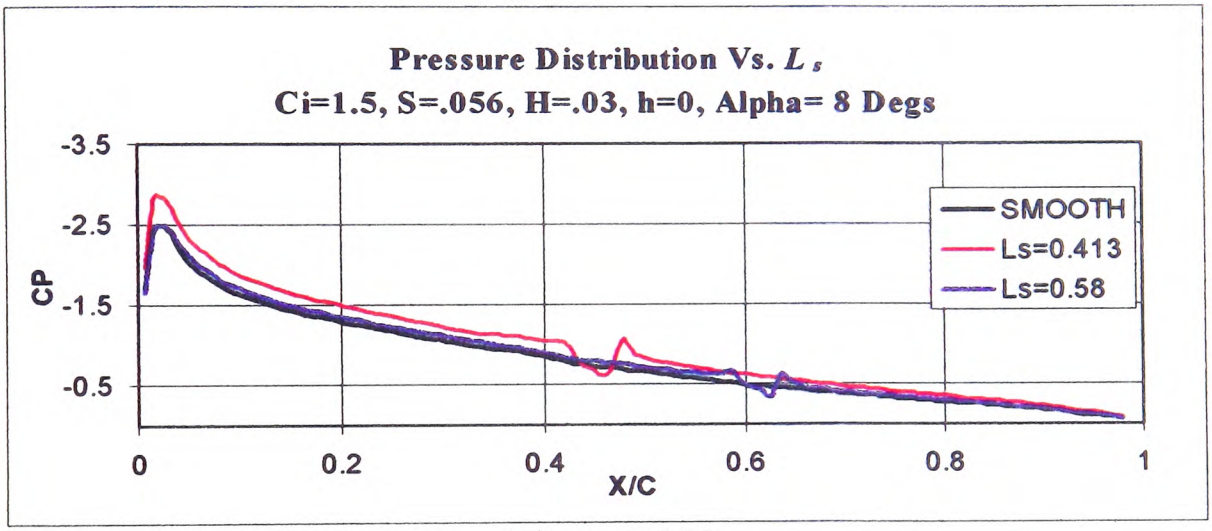

Figure 5-155

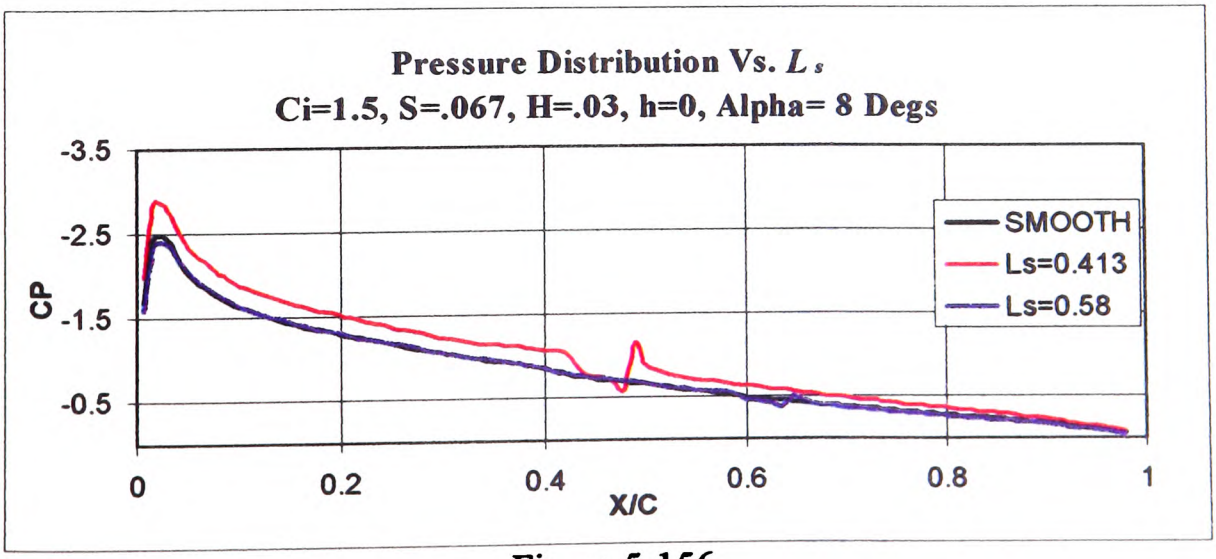

Figure 5-156

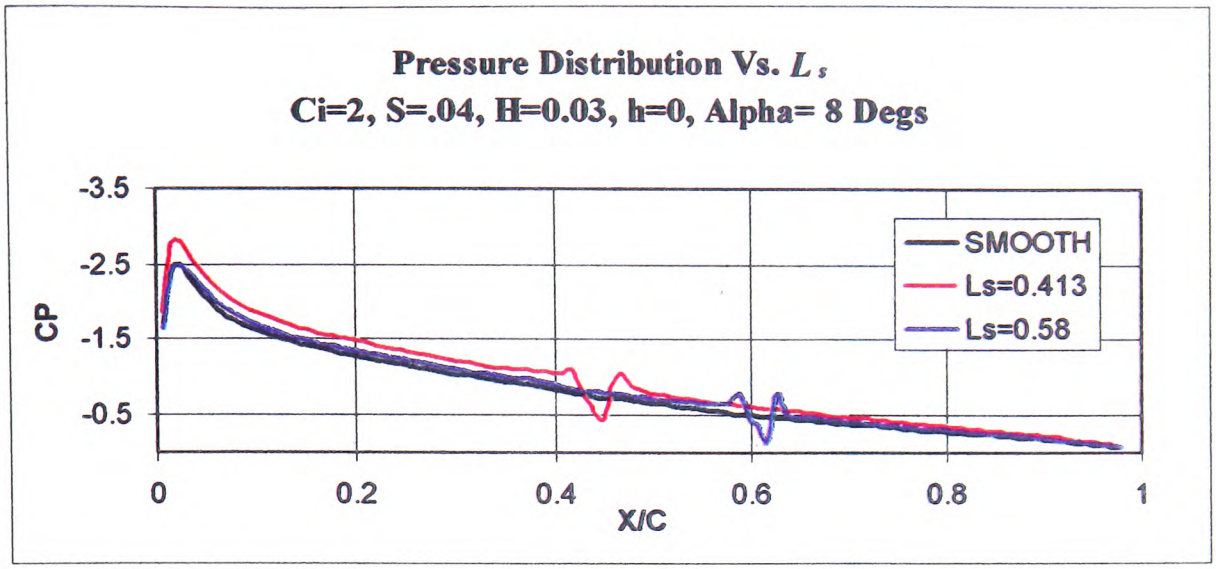

Figure 5-157

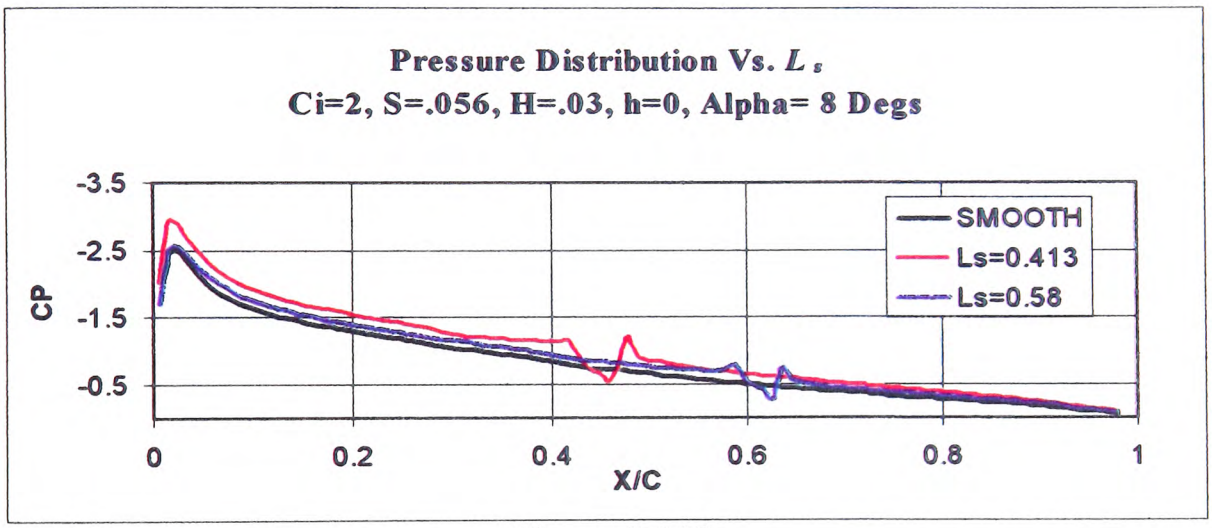

Figure 5-158

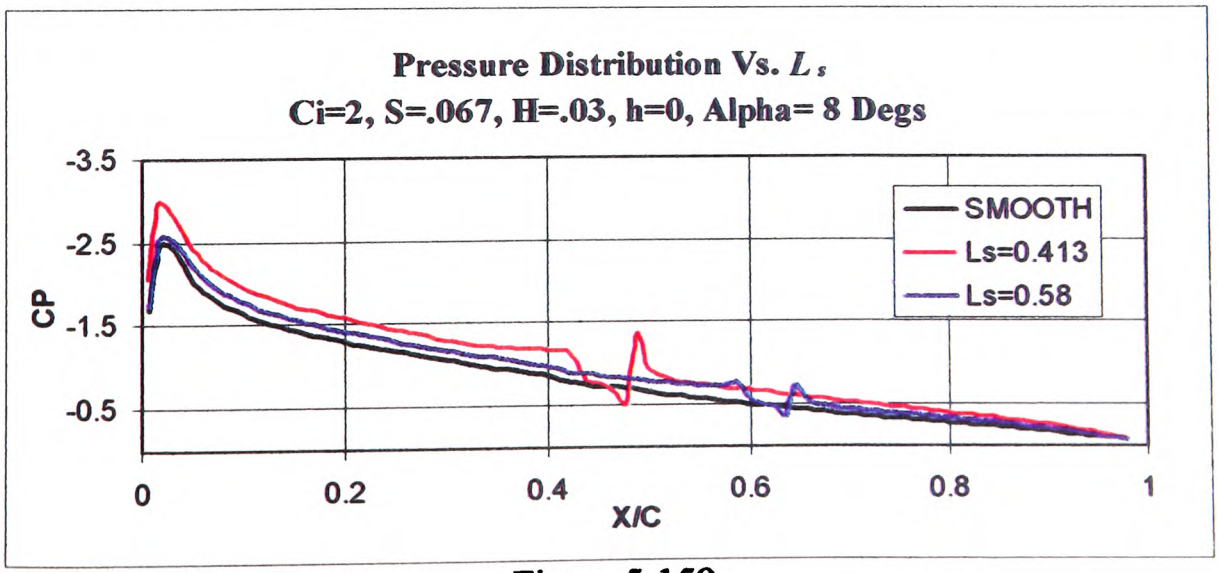

Figure 5-159

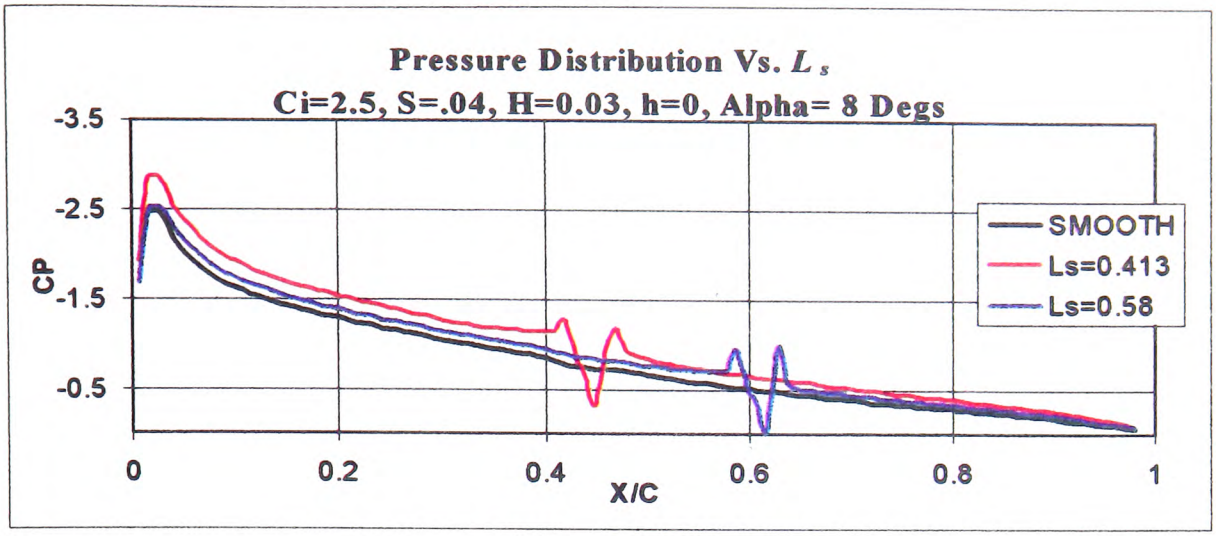

Figure 5-160

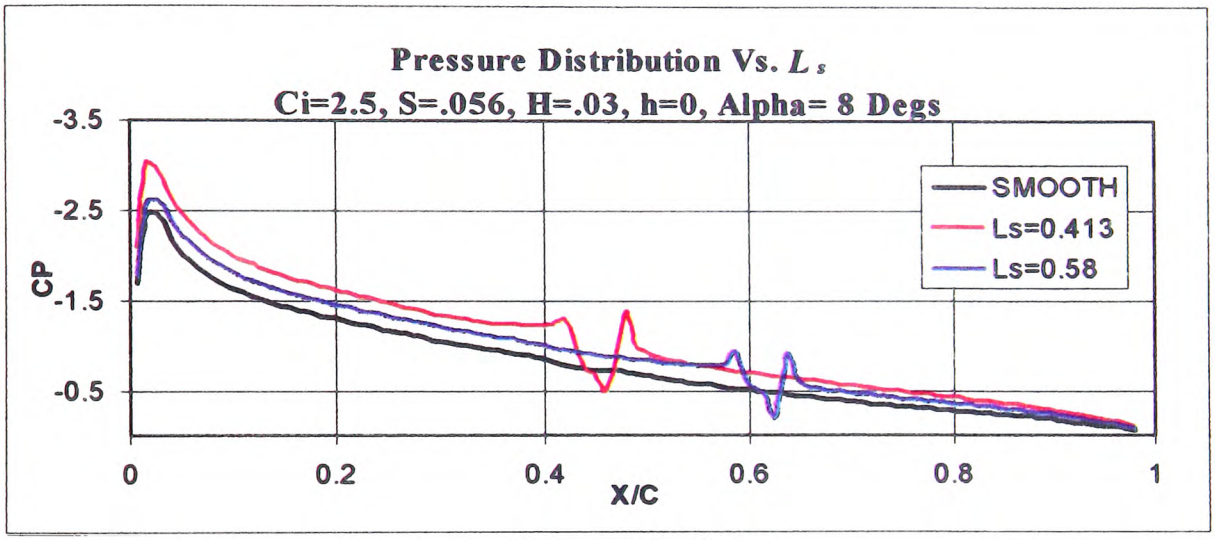

Figure 5-161

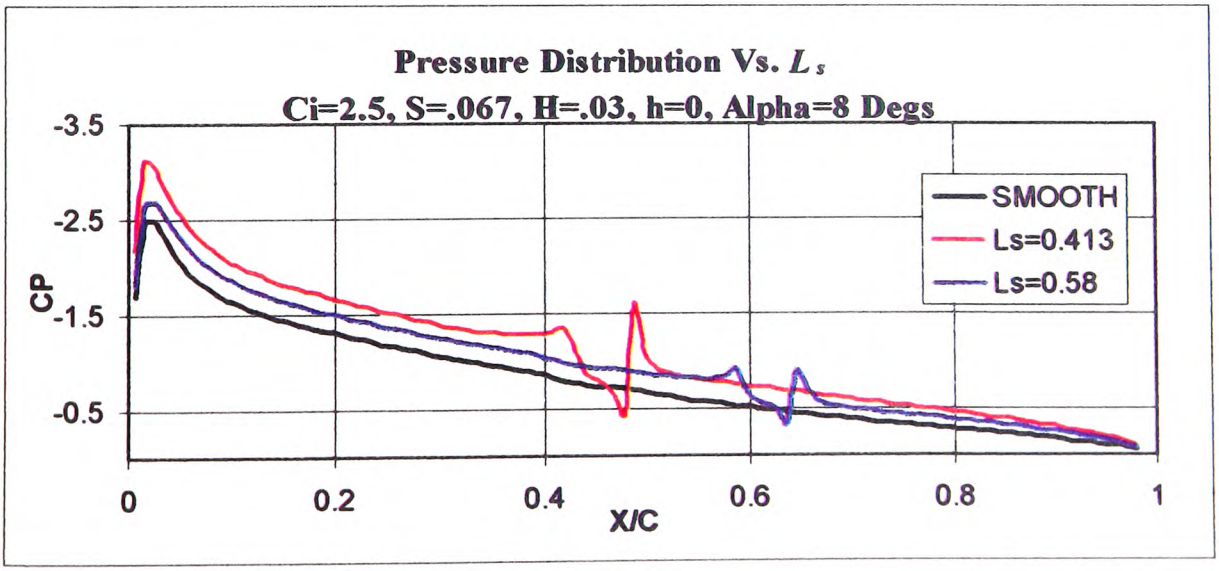

Figure 5-162

5.9.14 Effect of the Width of the ABD on the Pressure Distribution over an Aerofoil

5.9.14.1 Alpha = 4 Degrees

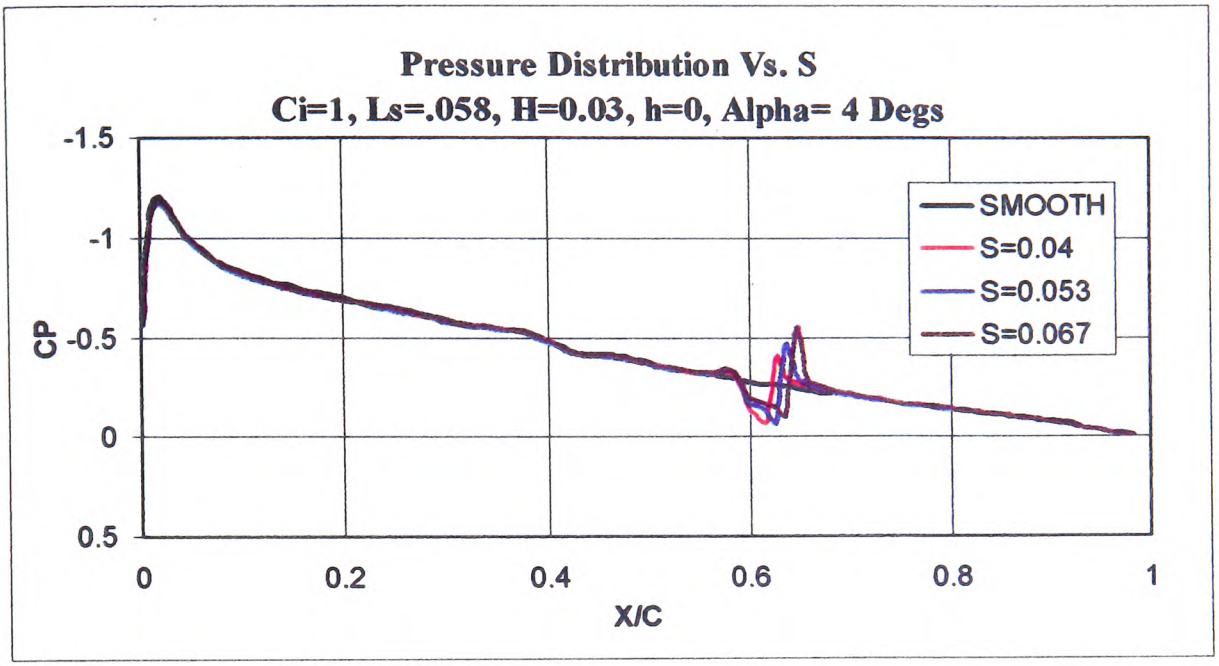

Figure 5-163

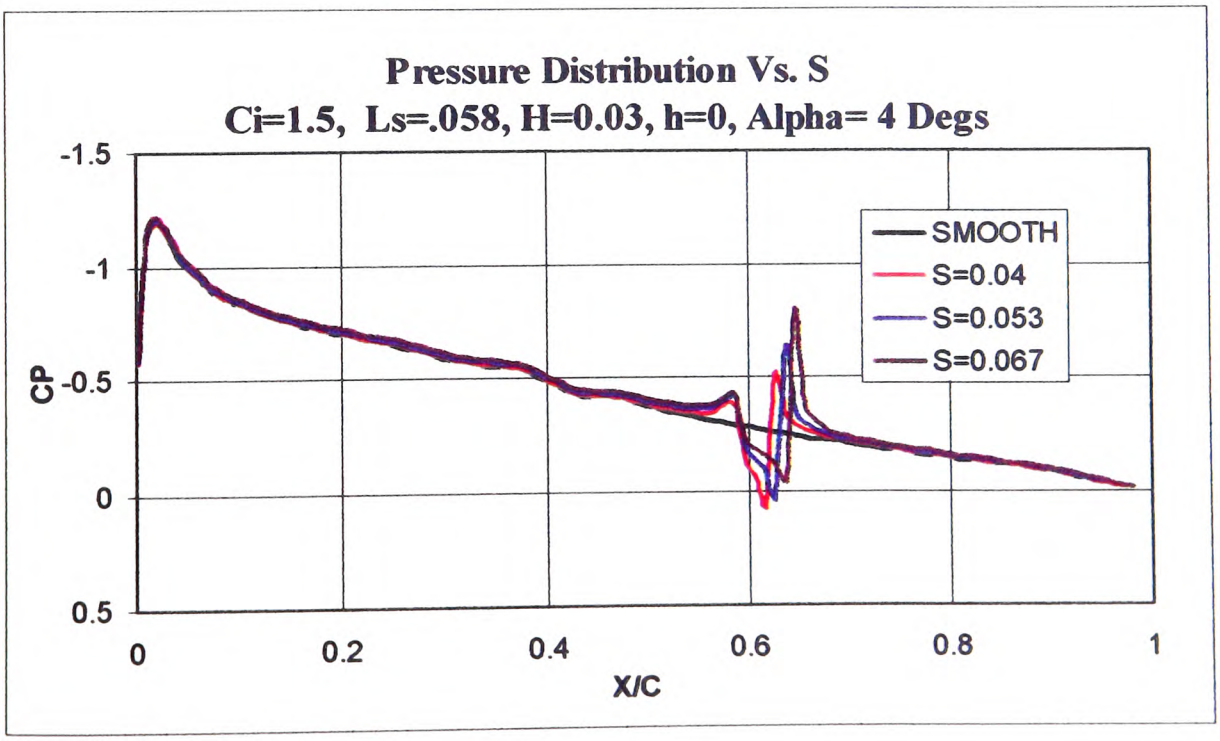

Figure 5-164

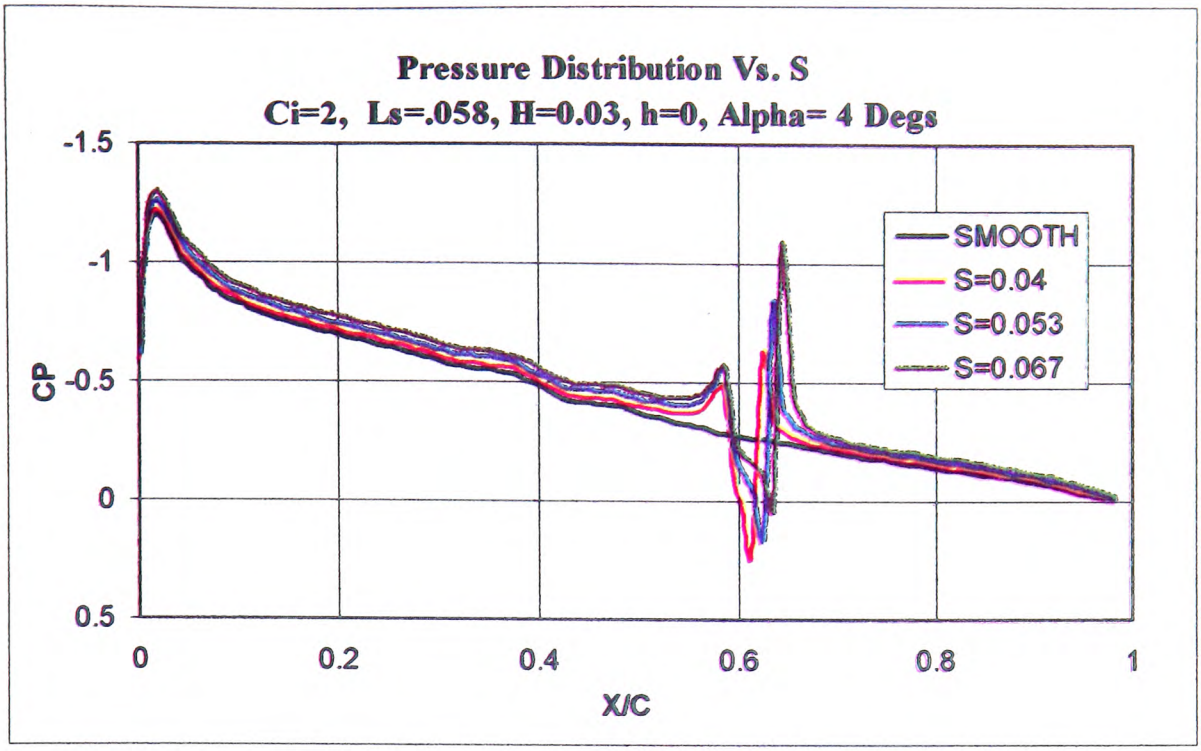

Figure 5-165

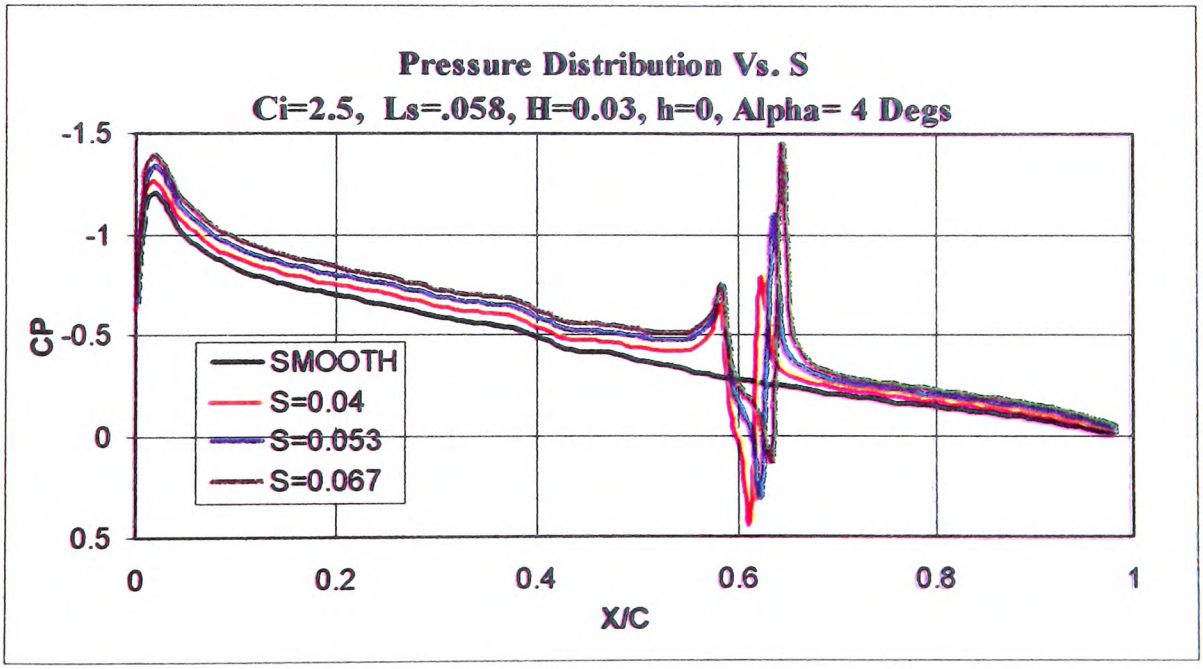

Figure 5-166

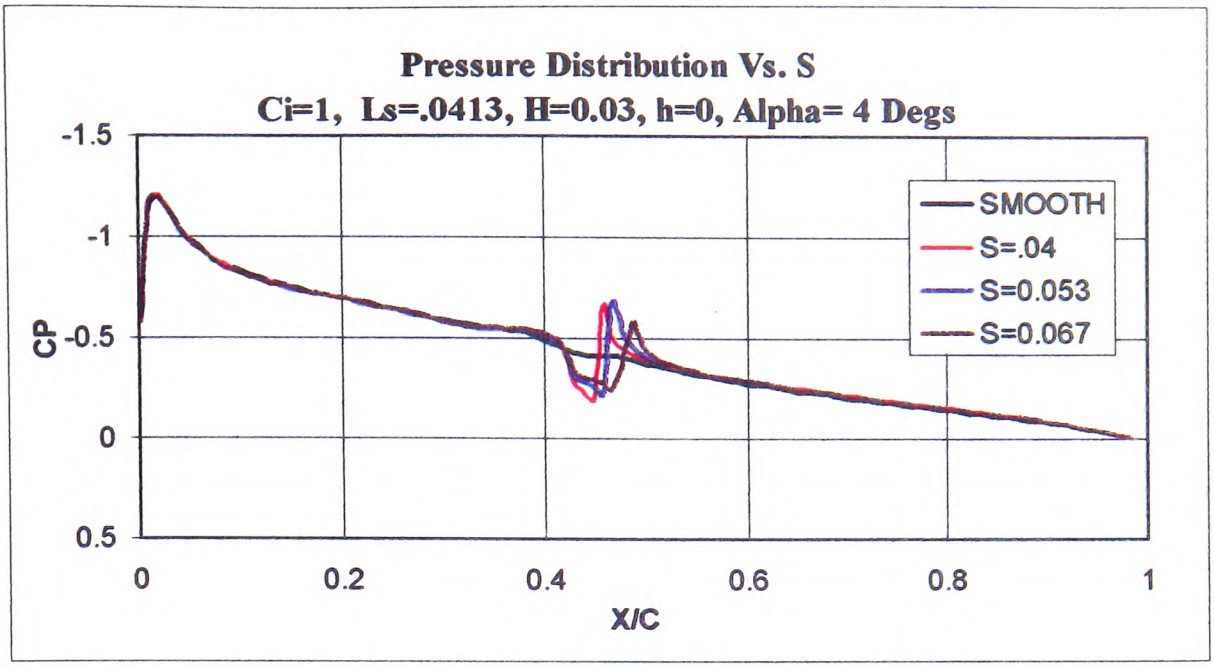

Figure 5-167

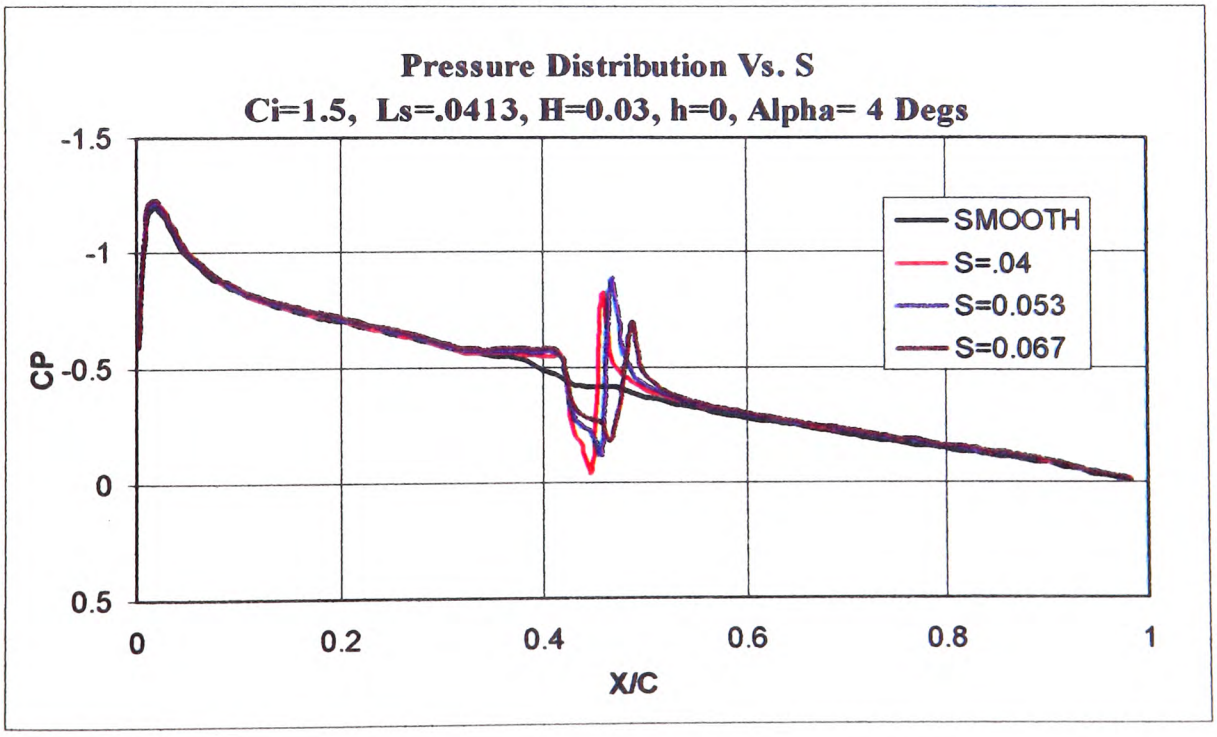

Figure 5-168

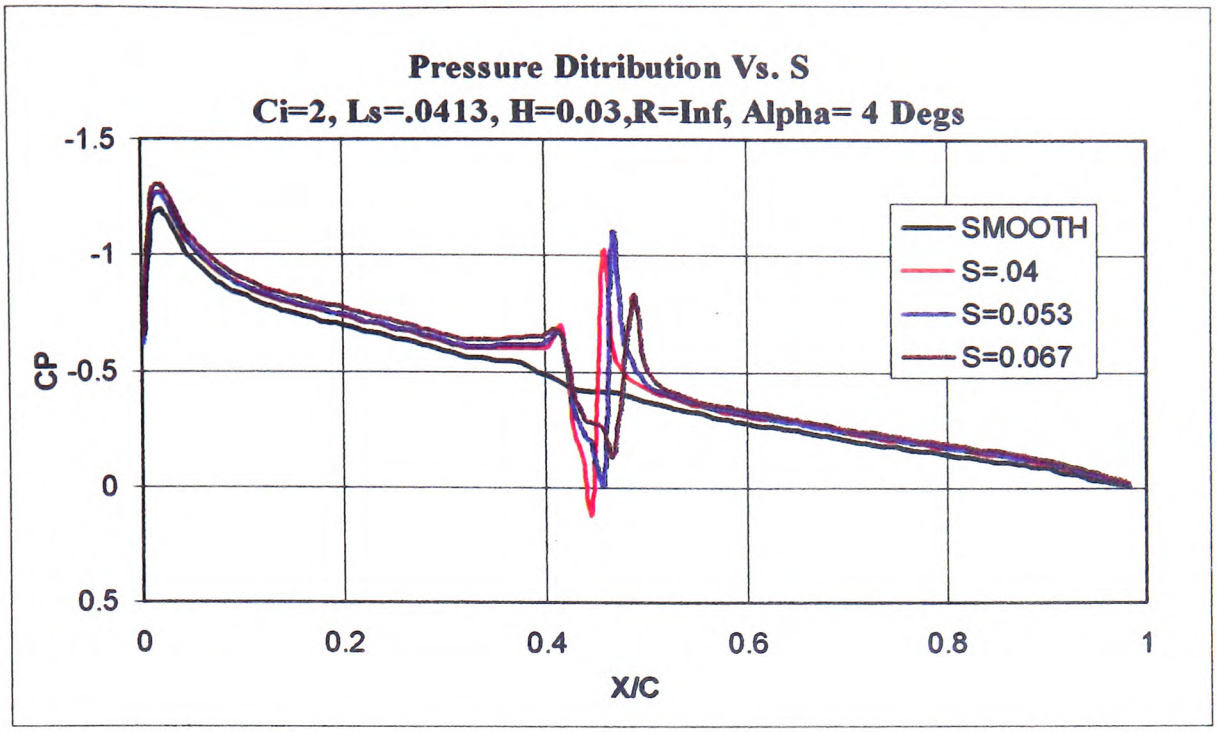

Figure 5-169

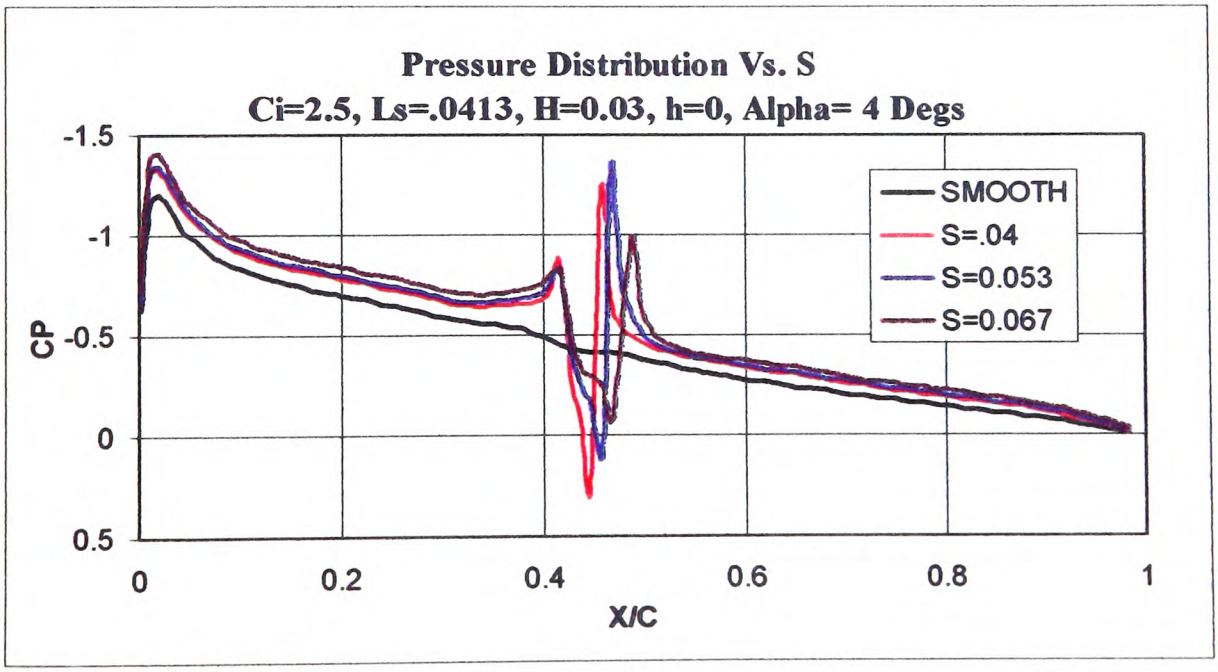

Figure 5-170

5.9.14.2 Alpha = 8 Degrees

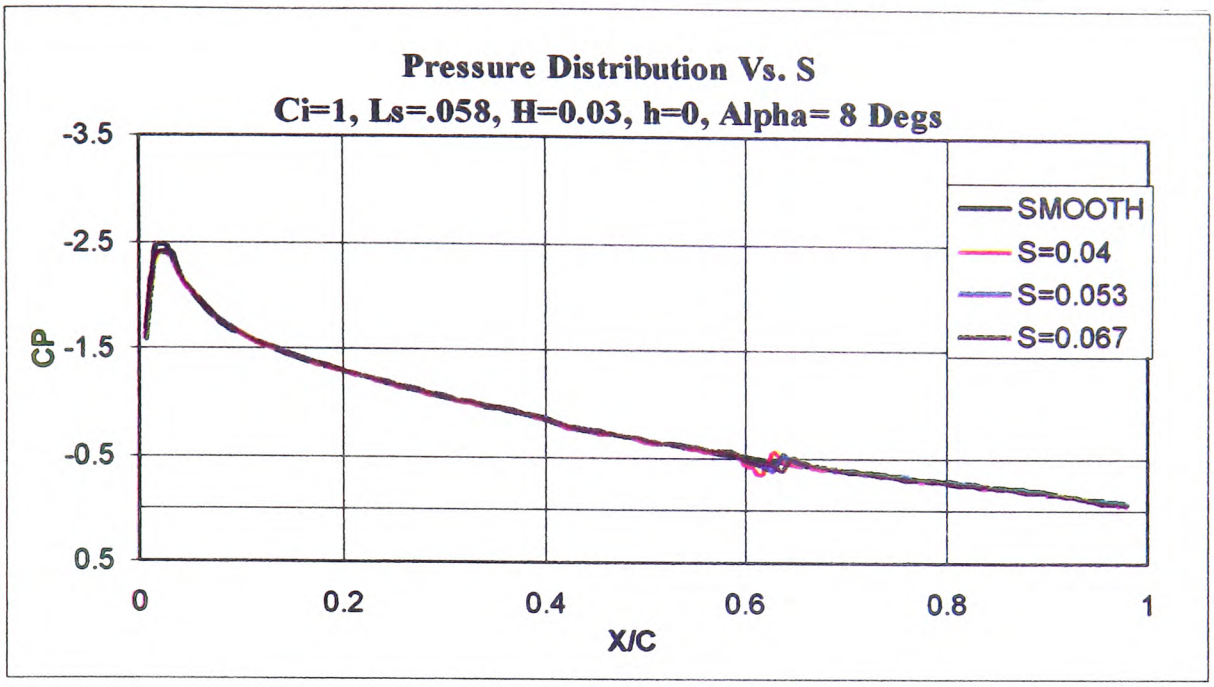

Figure 5-171

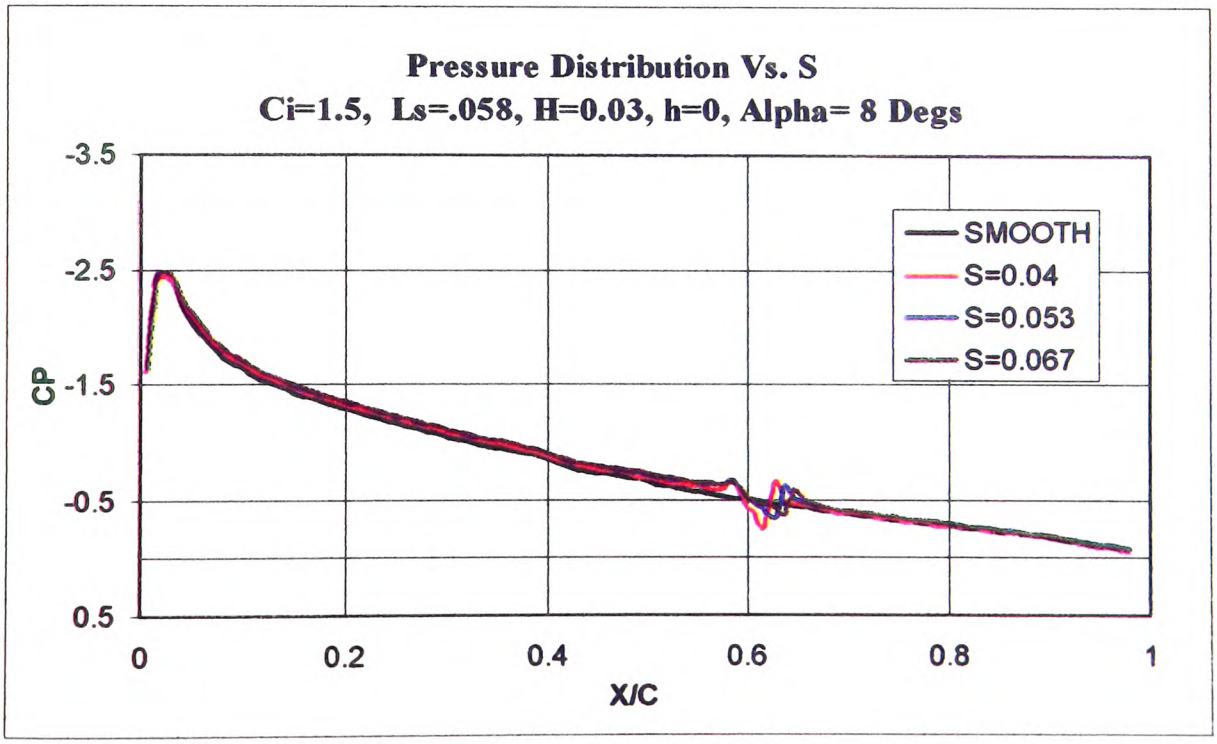

Figure 5-172

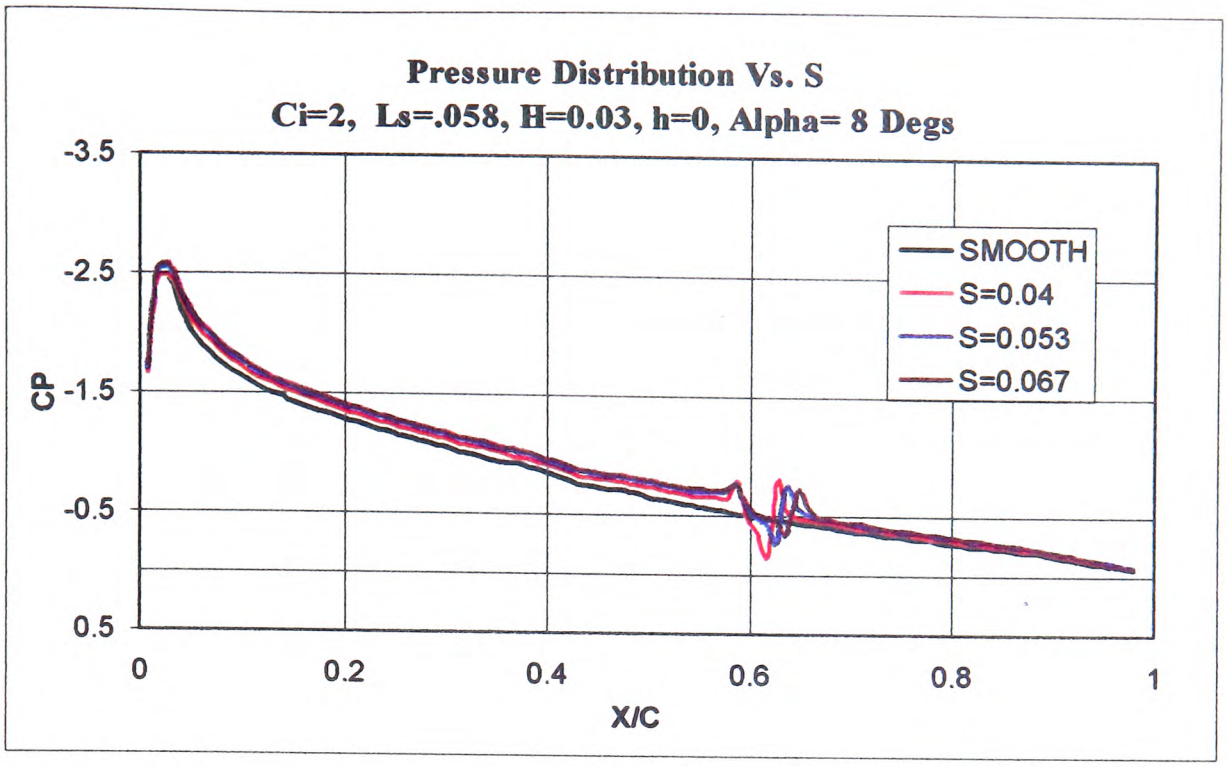

Figure 5-173

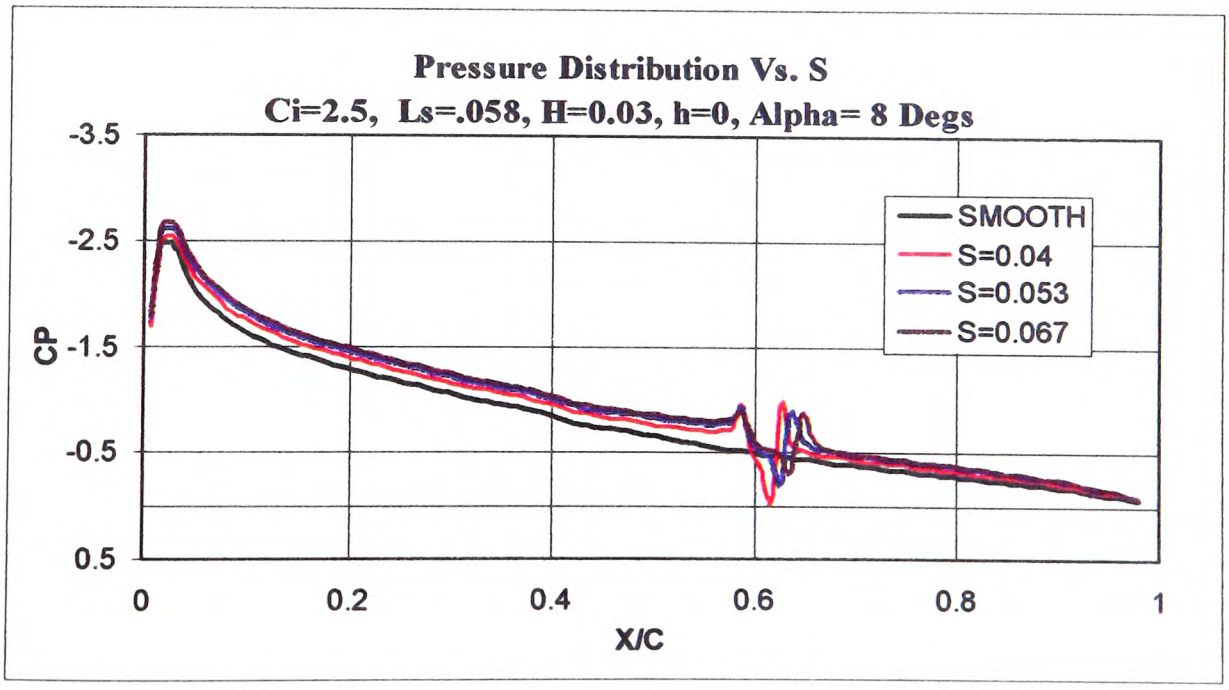

Figure 5-174

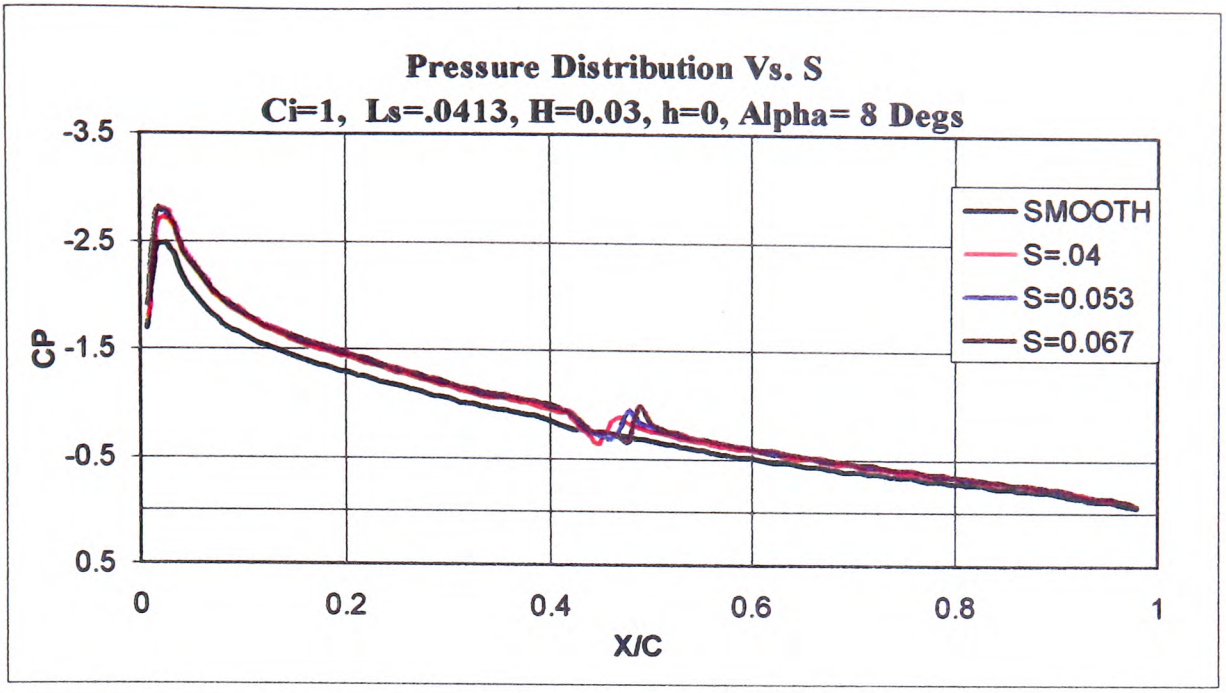

Figure 5-175

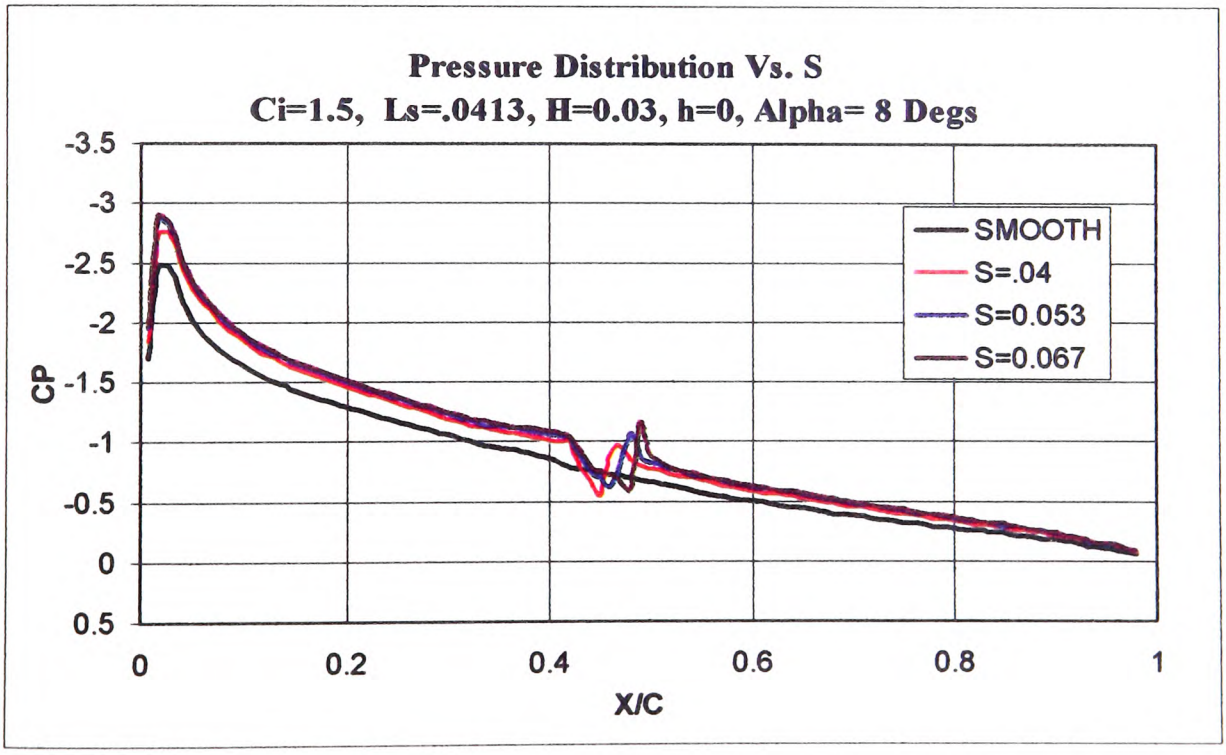

Figure 5-176

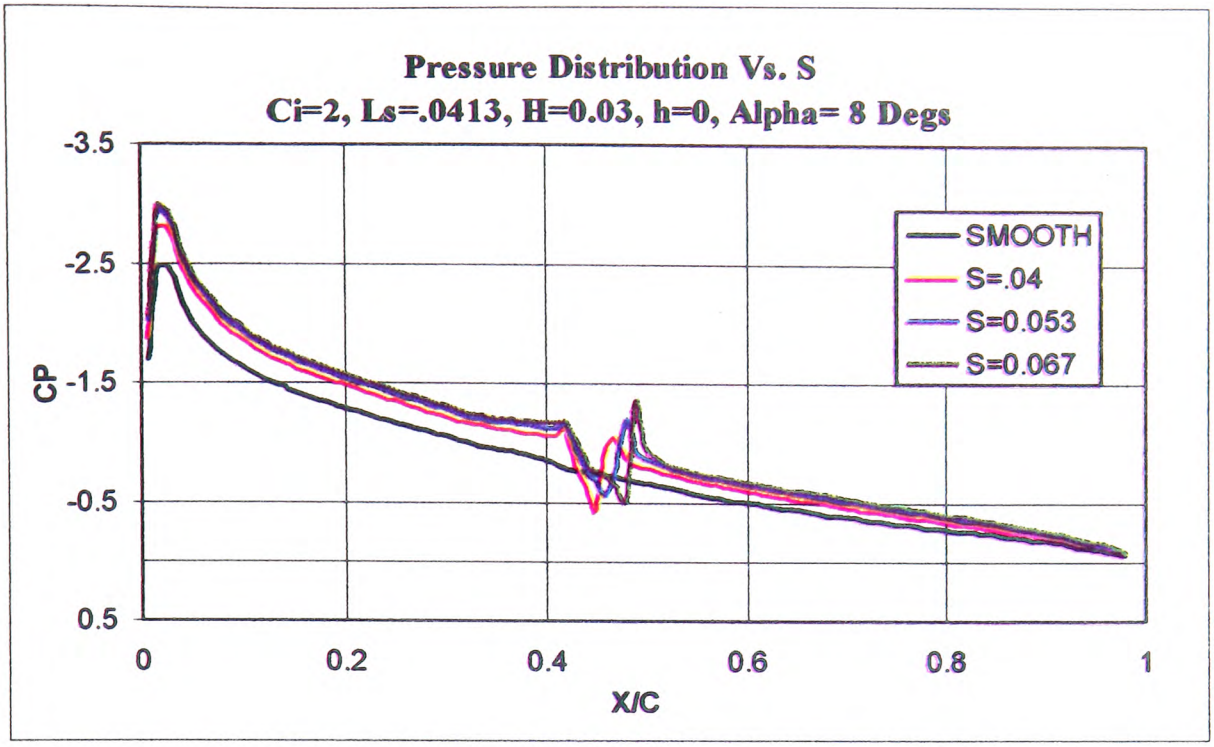

Figure 5-177

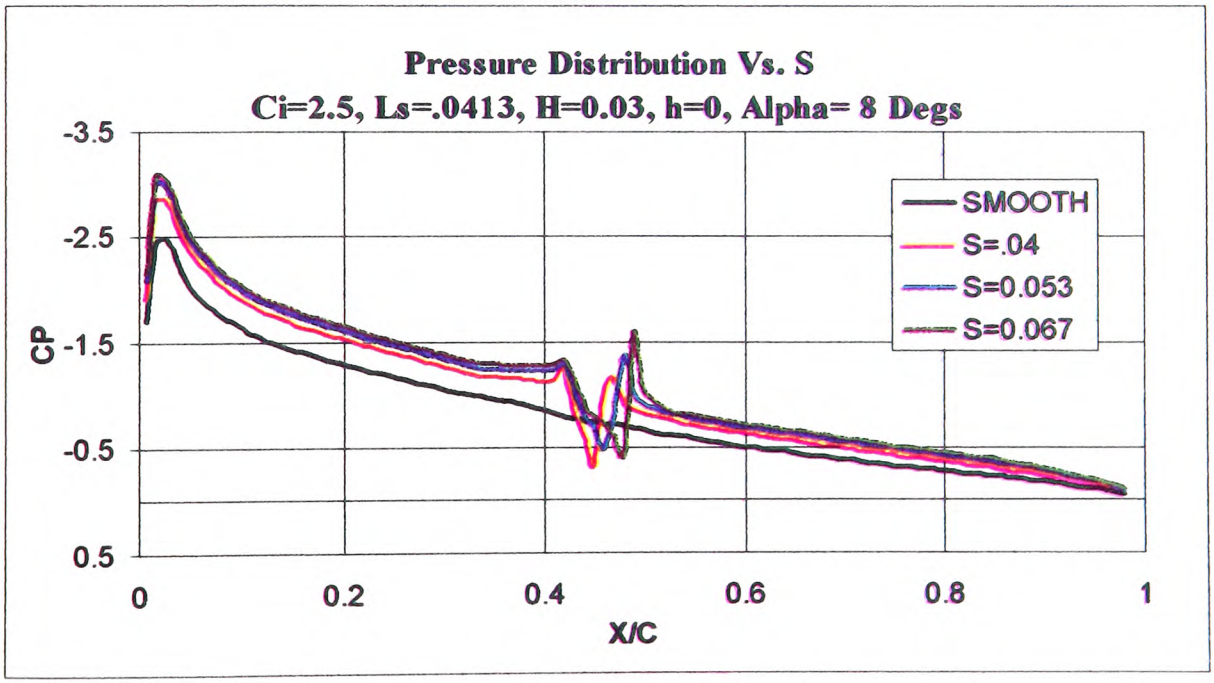

Figure 5-178

5.9.15 Effect of the Height of the ABD on the Pressure Distribution over an Aerofoil

5.9.15.1 Alpha = 4 Degrees

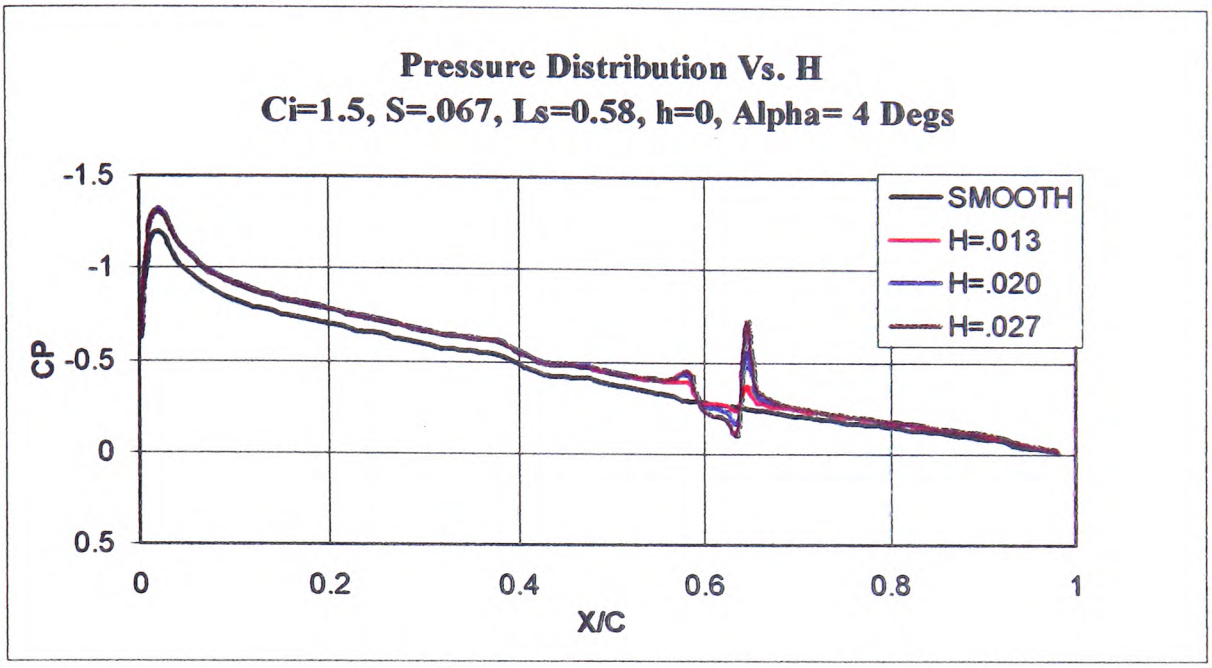

Figure 5-179

5.9.15.2 Alpha = 8 Degrees

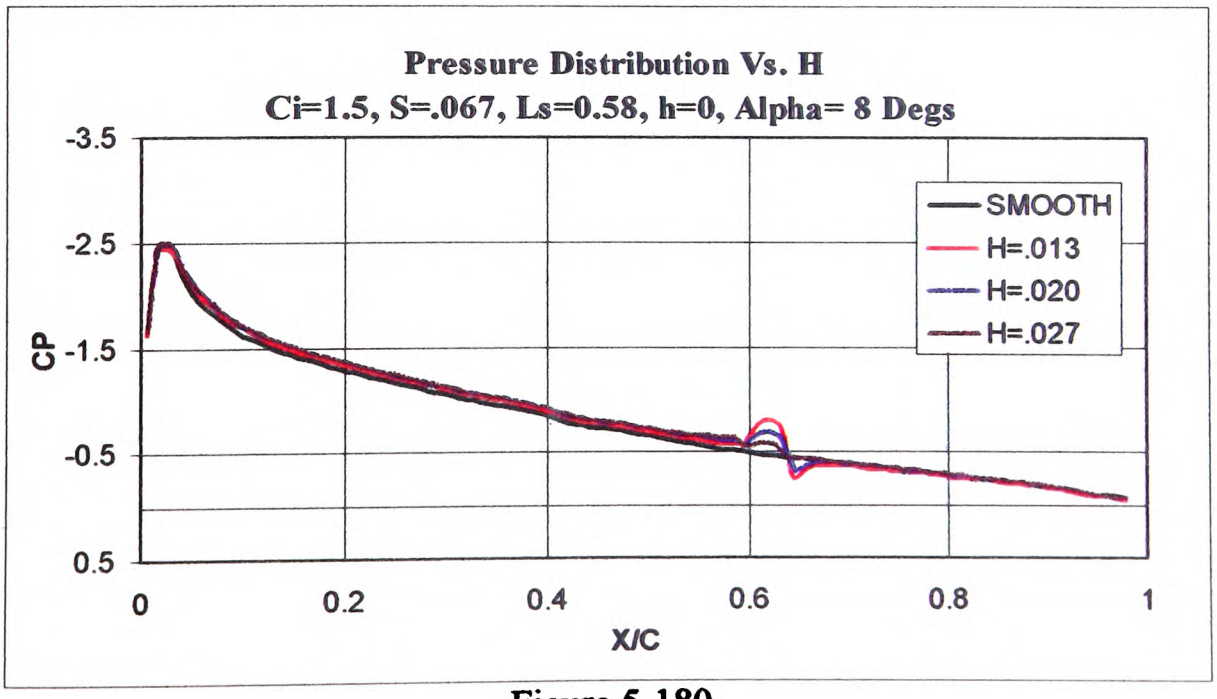

Figure 5-180

5.9.16 Effect of the Relative Height of the Base of the ABD, *h*

5.9.16.1 Alpha = 4 Degrees

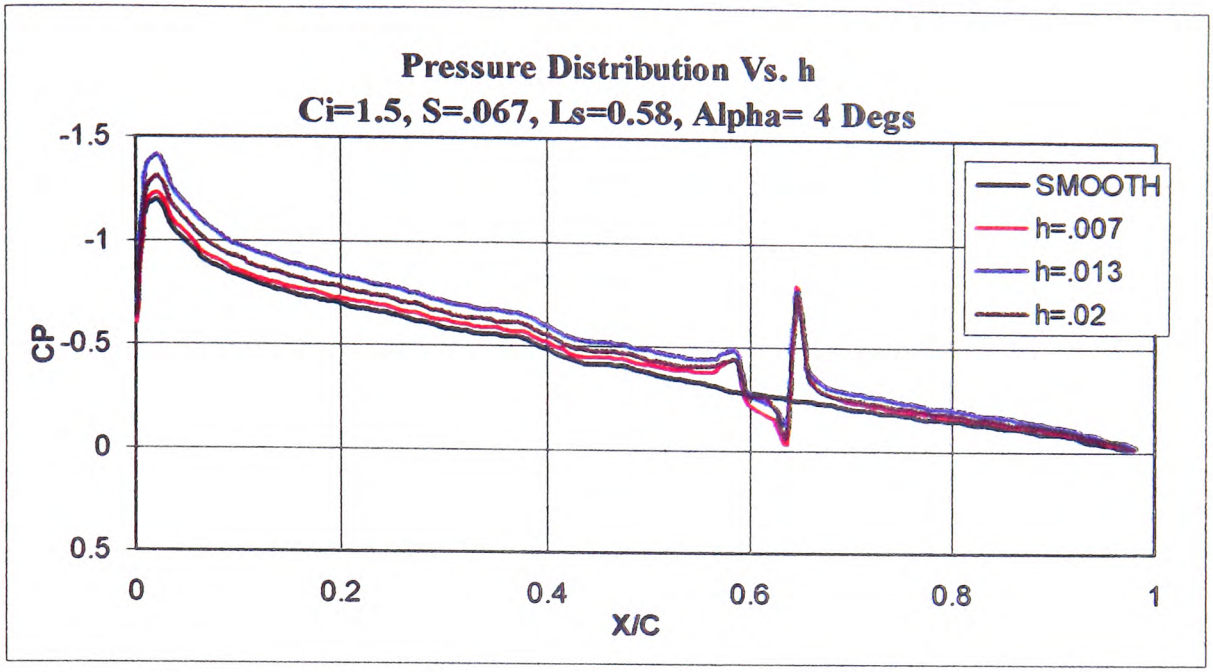

Figure 5-181

5.9.16.2 Alpha = 8 Degrees

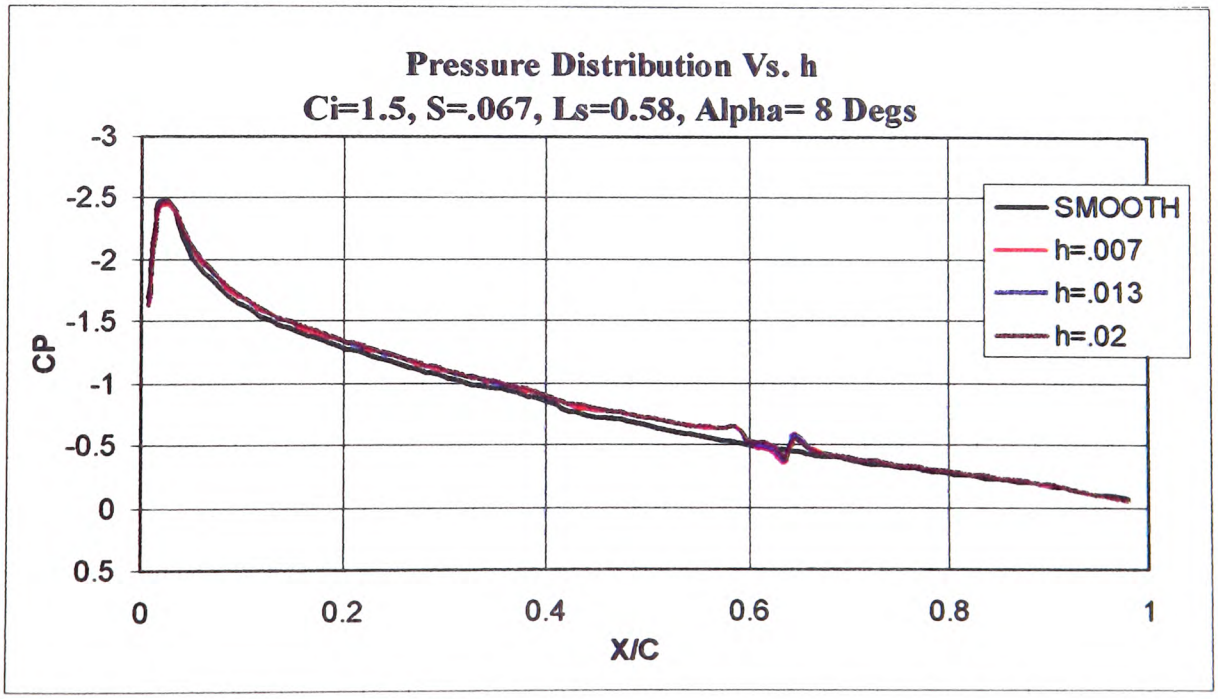

Figure 5-182

5.9.17 Effect of the Relative Velocity Inside the ABD on the Lift Coefficient (C_l)

5.9.17.1 Alpha = 4 Degrees

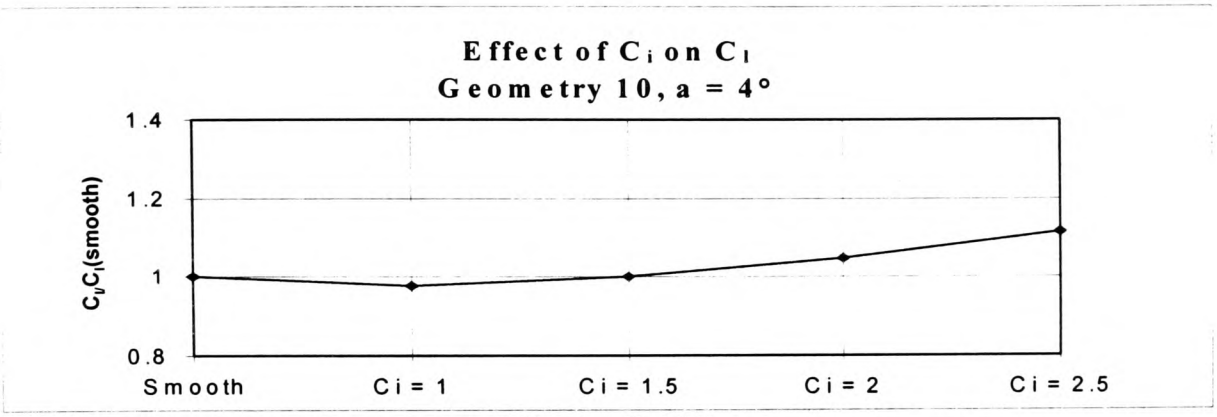

Figure 5-183

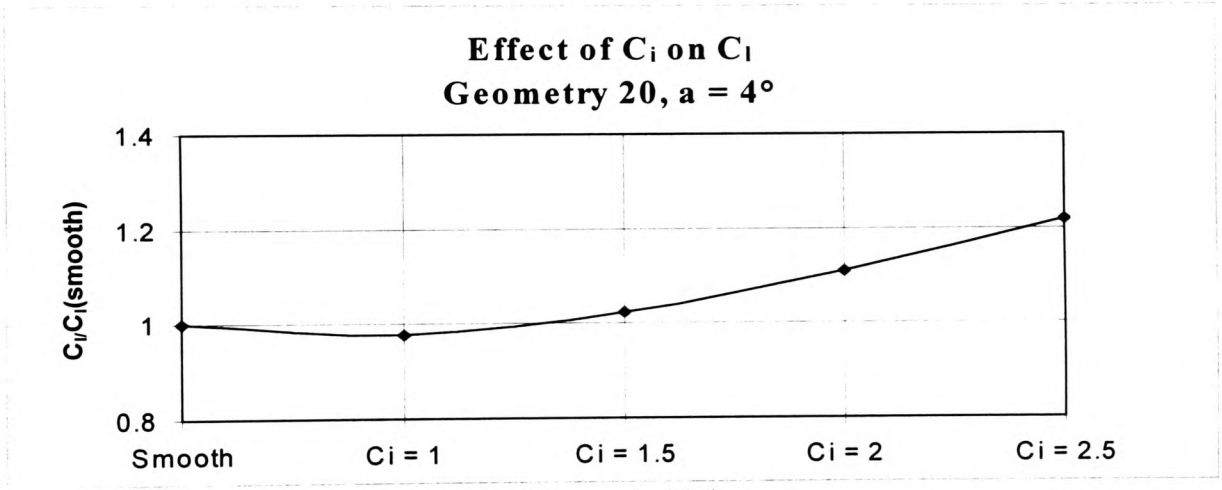

Figure 5-184

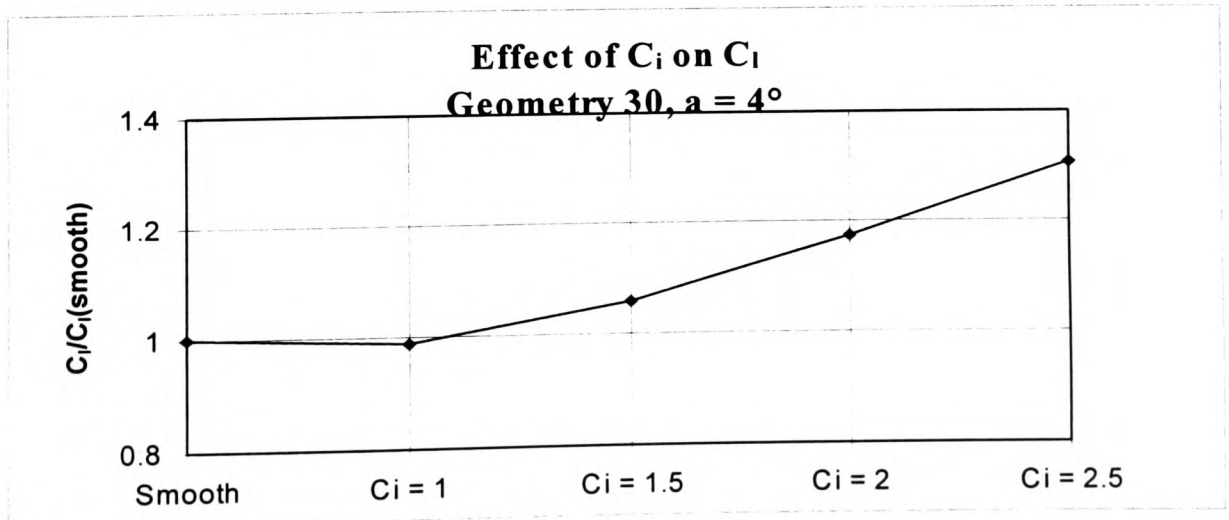

Figure 5-185

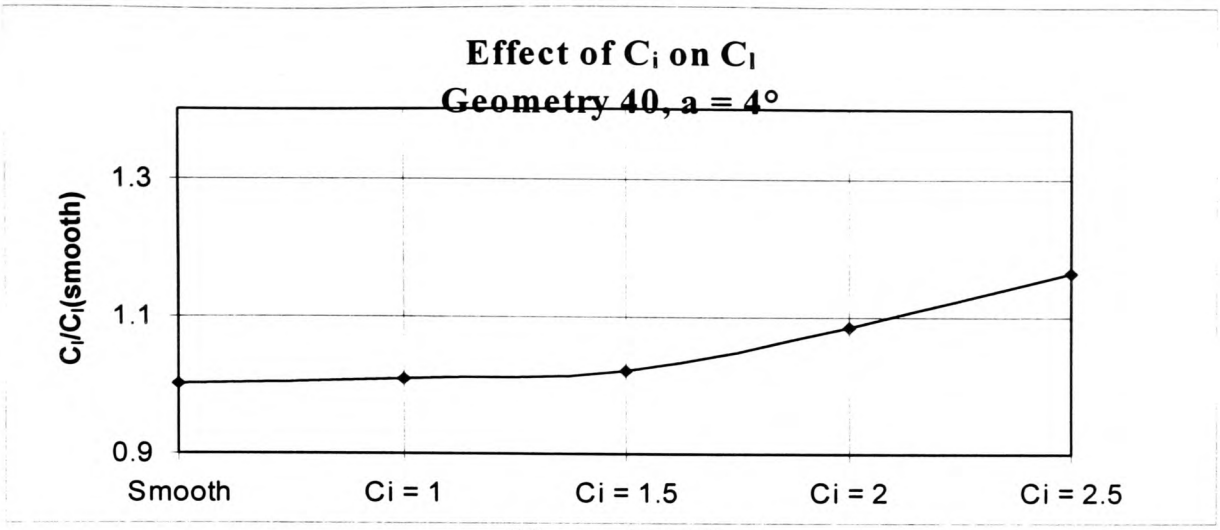

Figure 5-186

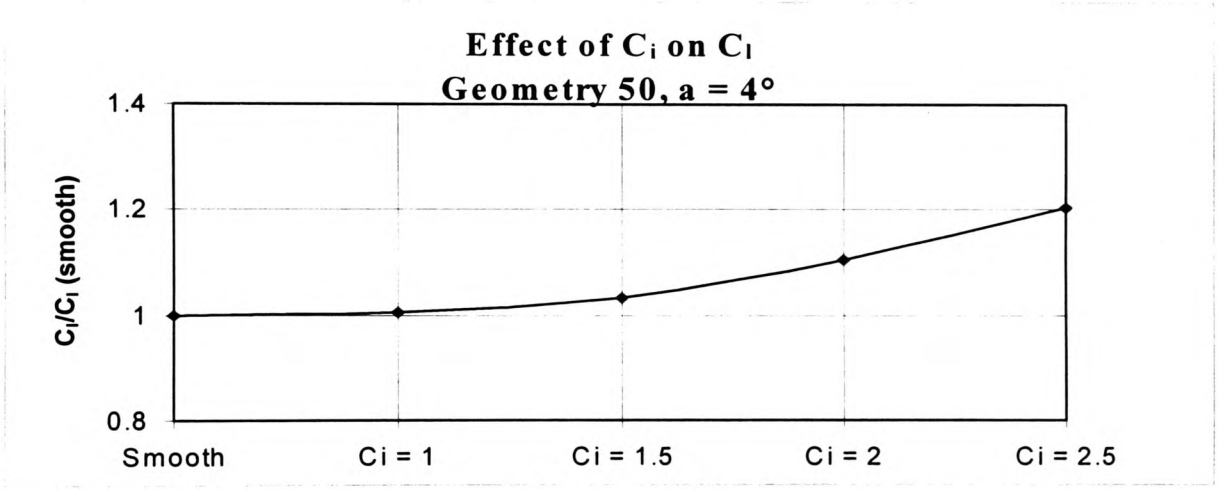

Figure 5-187

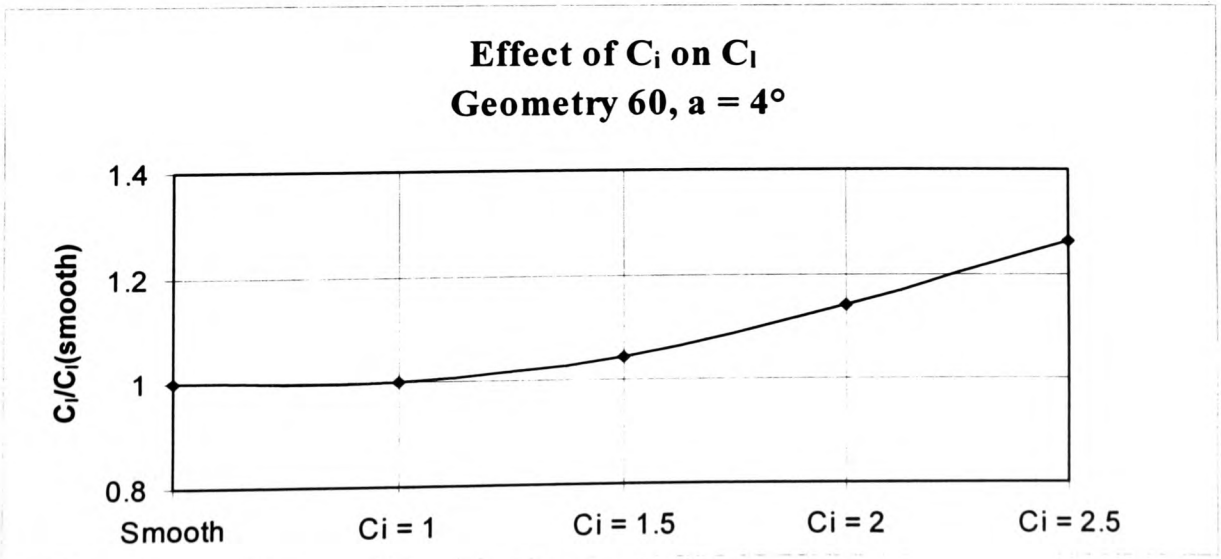

Figure 5-188

5.9.17.2 Alpha = 8 Degrees

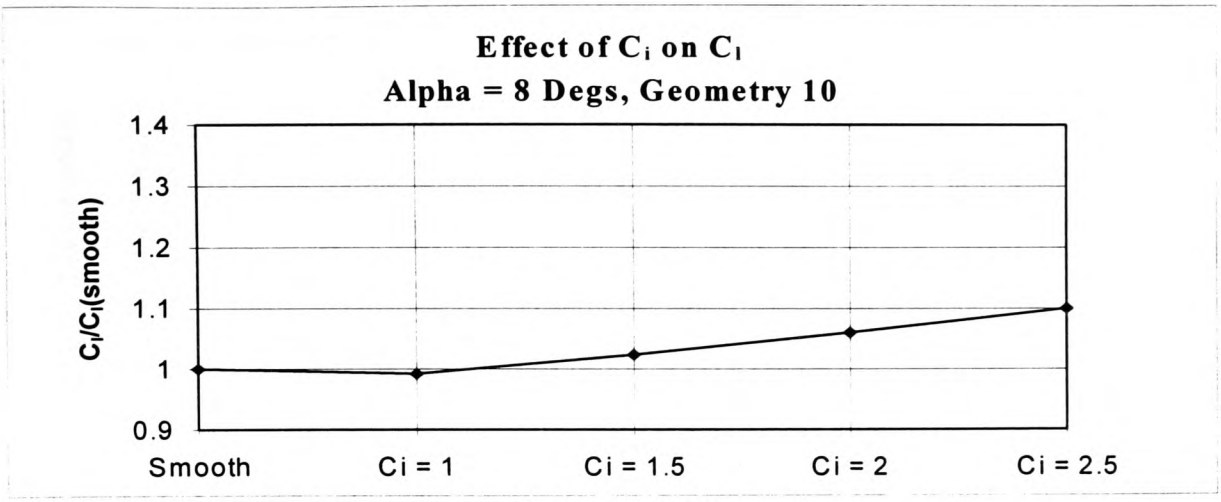

Figure 5-189

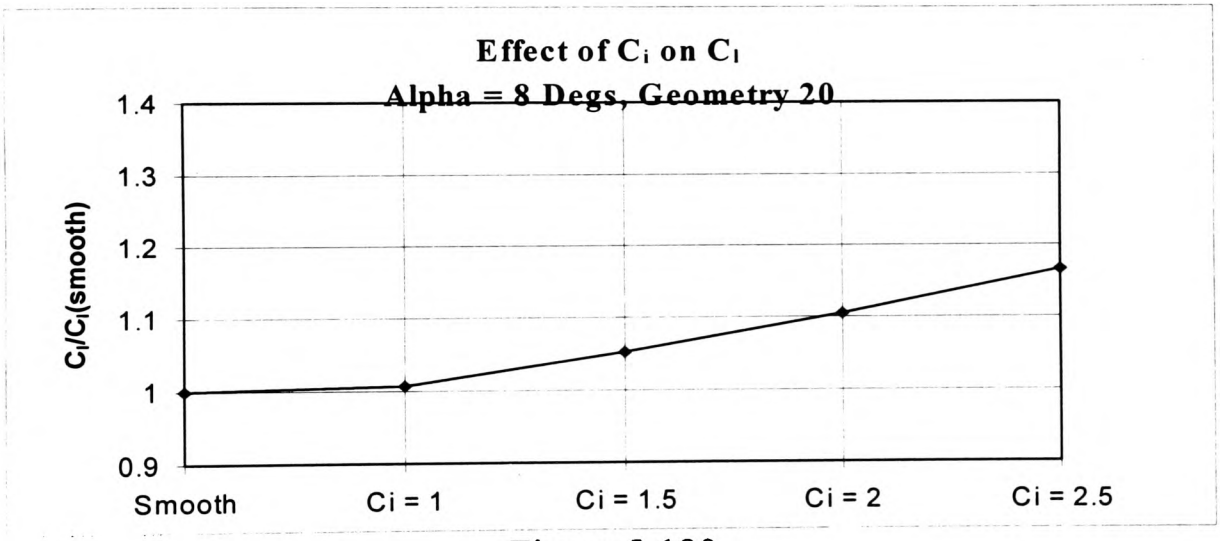

Figure 5-190

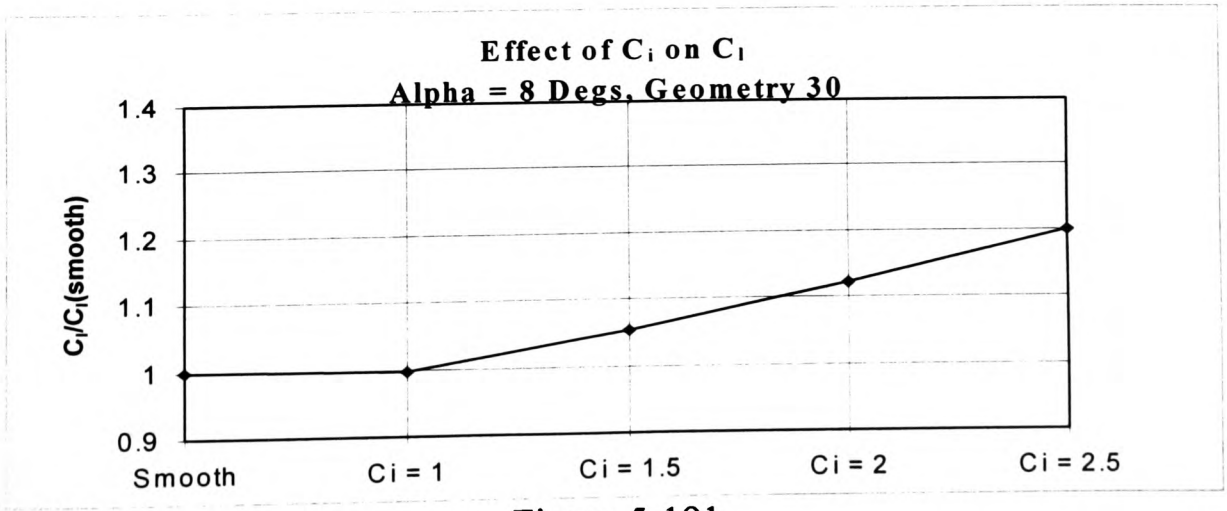

Figure 5-191

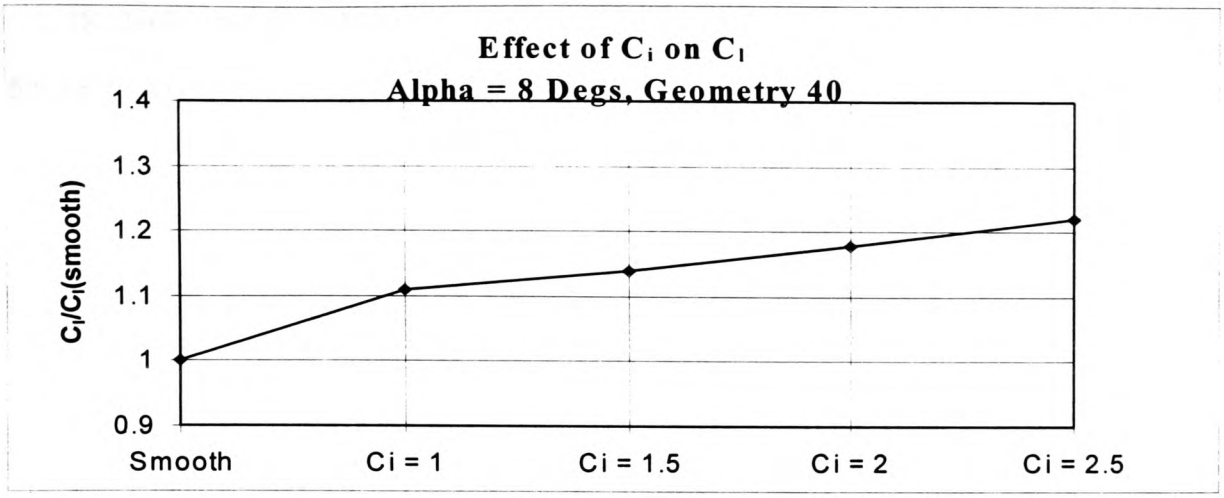

Figure 5-192

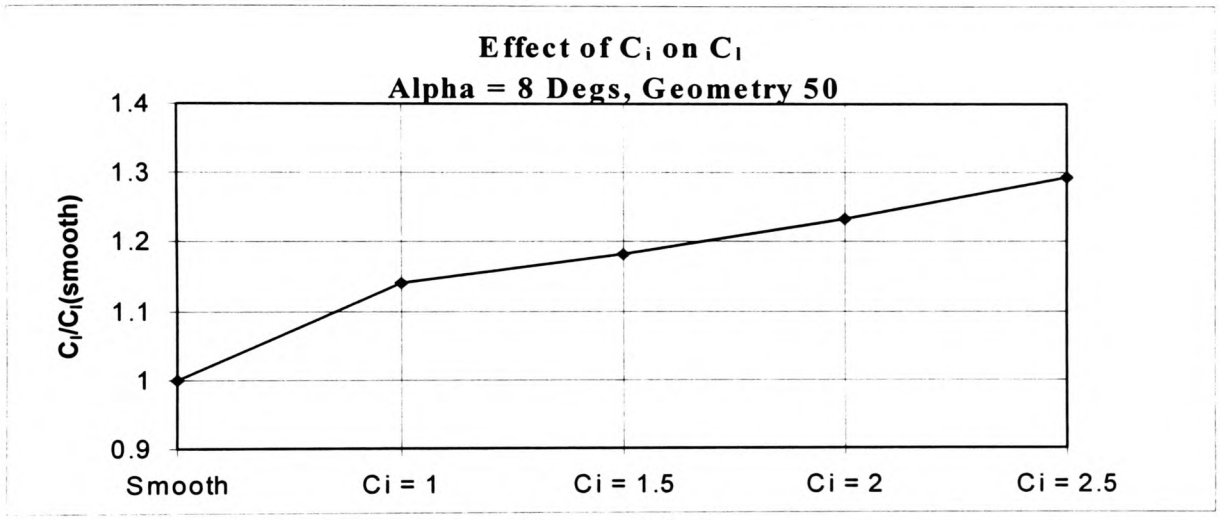

Figure 5-193

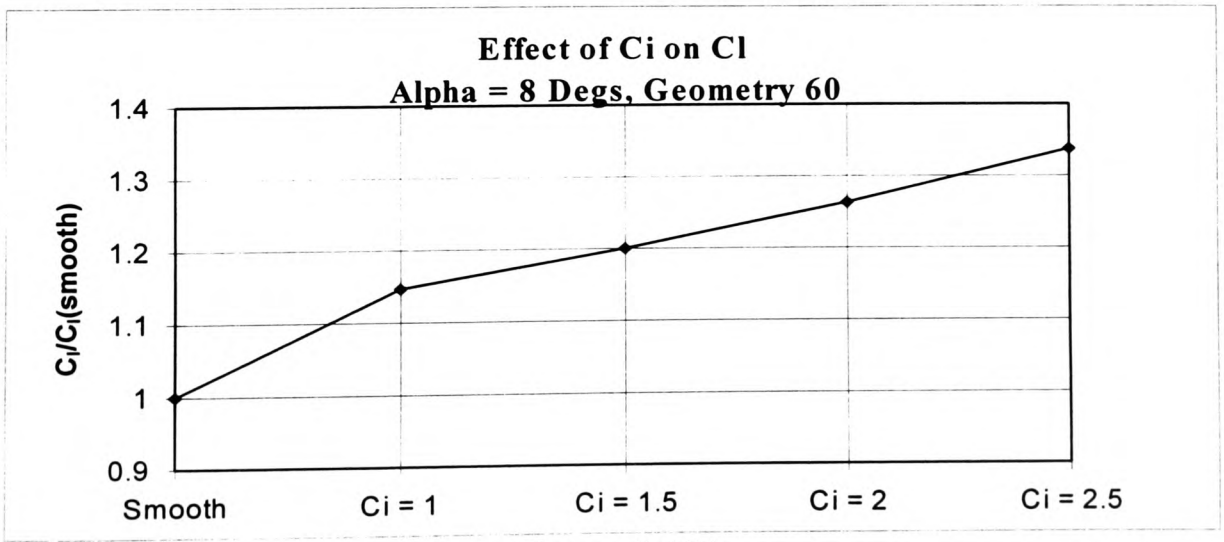

Figure 5-194

5.9.18 Effect of the Width and Location of the ABD on C_l

5.9.18.1 Alpha = 4 Degrees

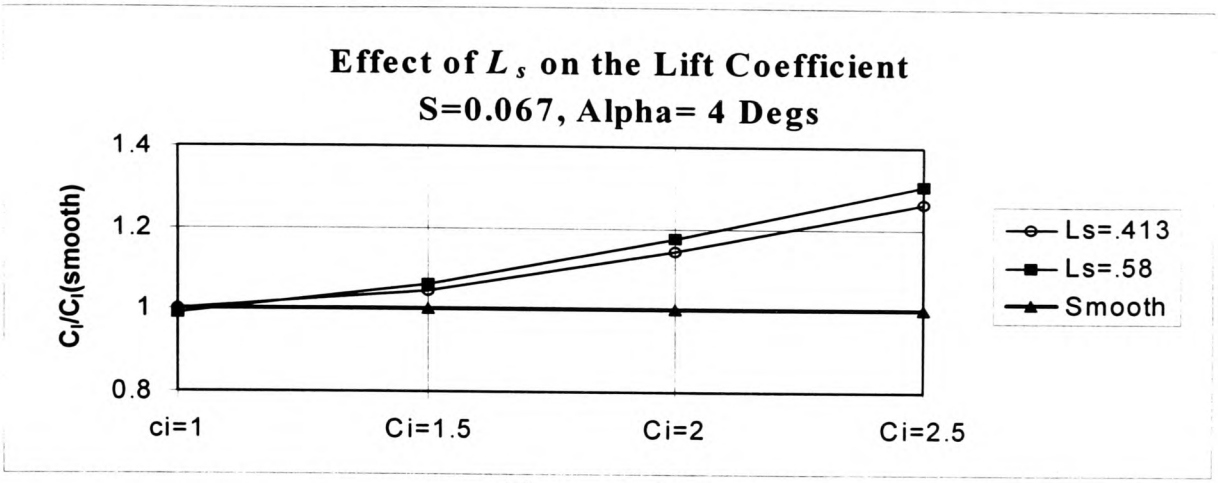

Figure 5-195

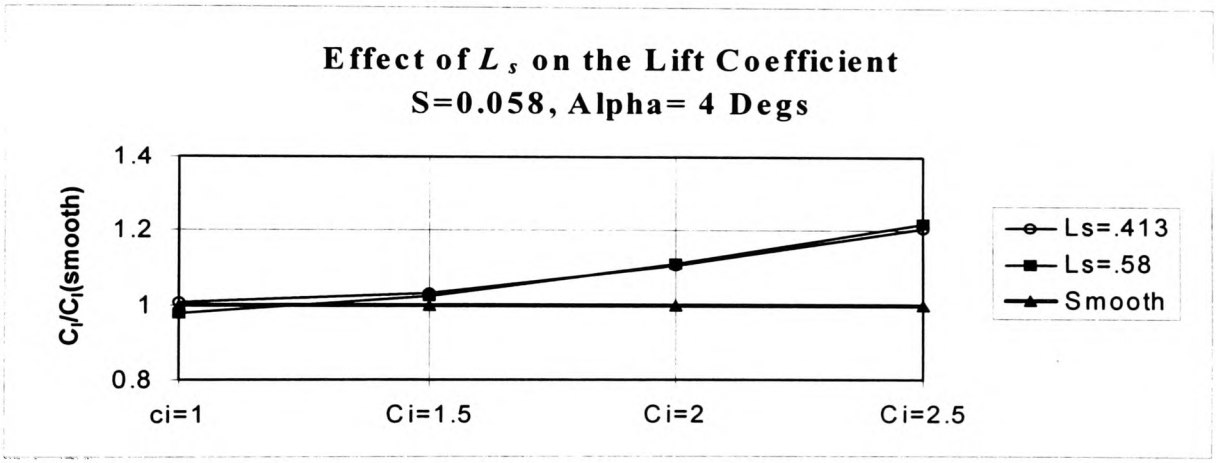

Figure 5-196

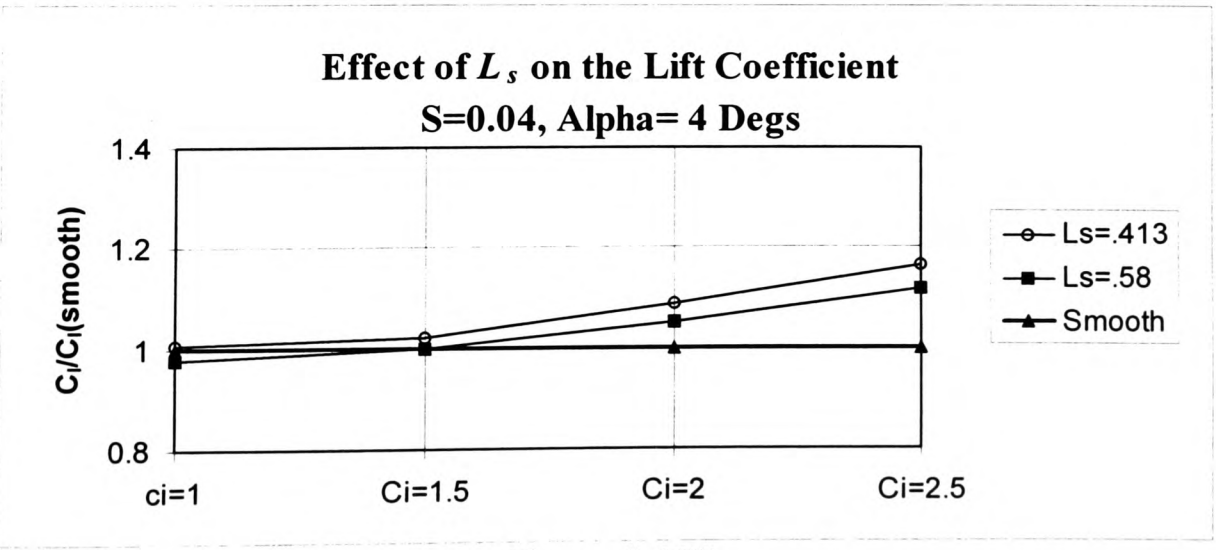

Figure 5-197

5.9.18.2 Alpha = 8 Degrees

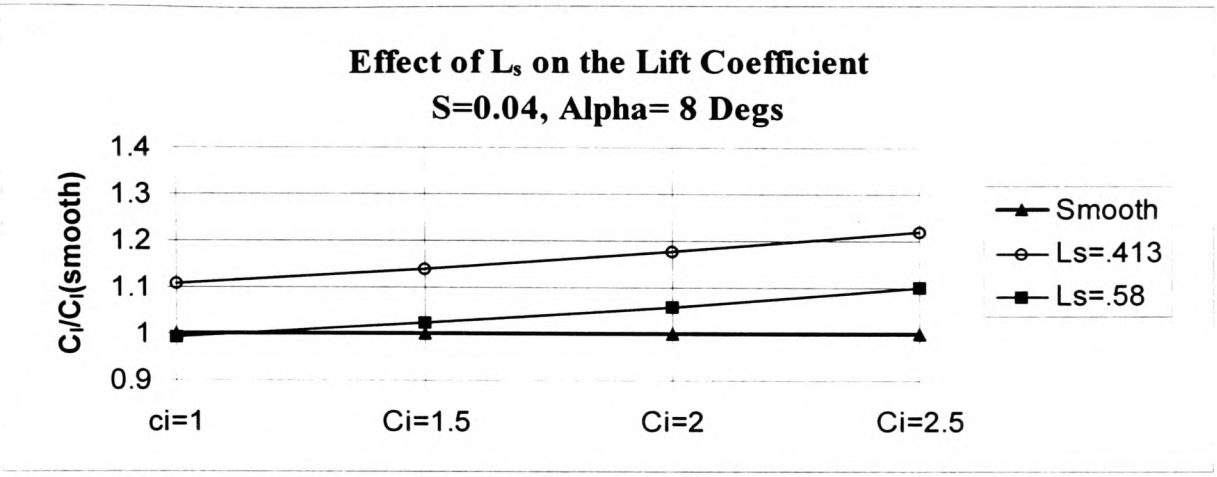

Figure 5-198

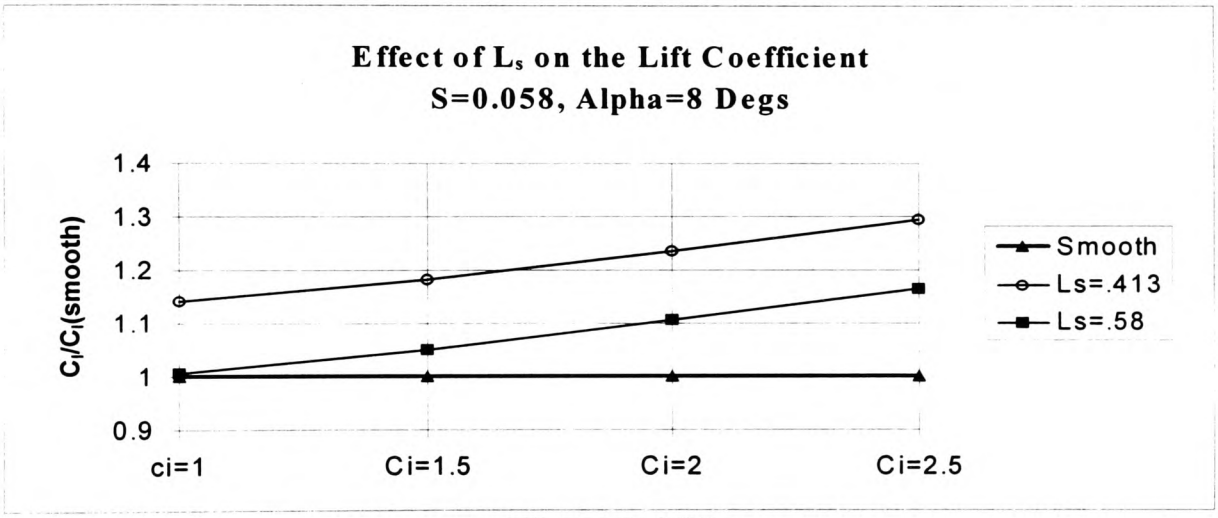

Figure 5-199

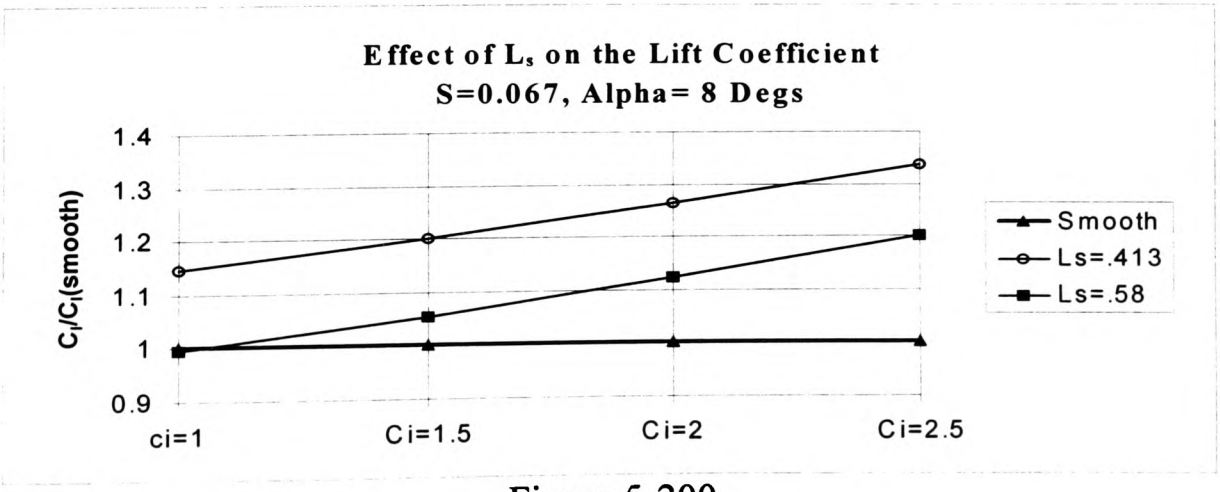

Figure 5-200

5.9.19 Effect of the Width of the ABD on the Lift Coefficient (C_l)

5.9.19.1 Alpha = 4 Degrees

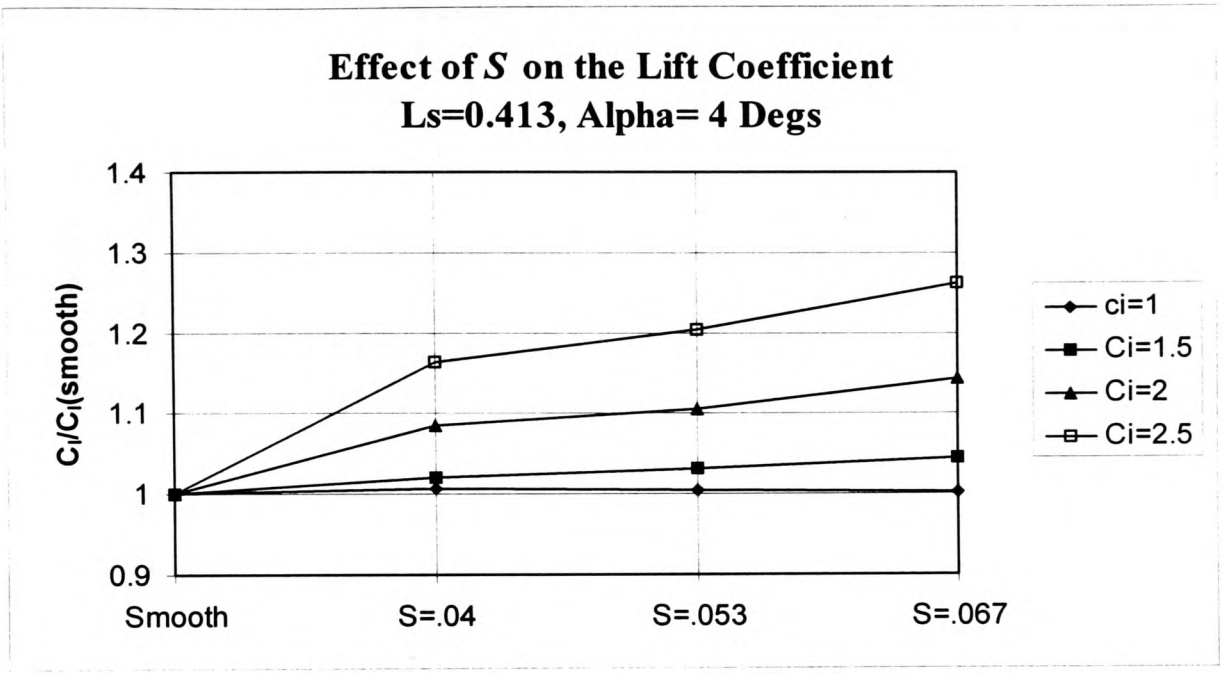

Figure 5-201

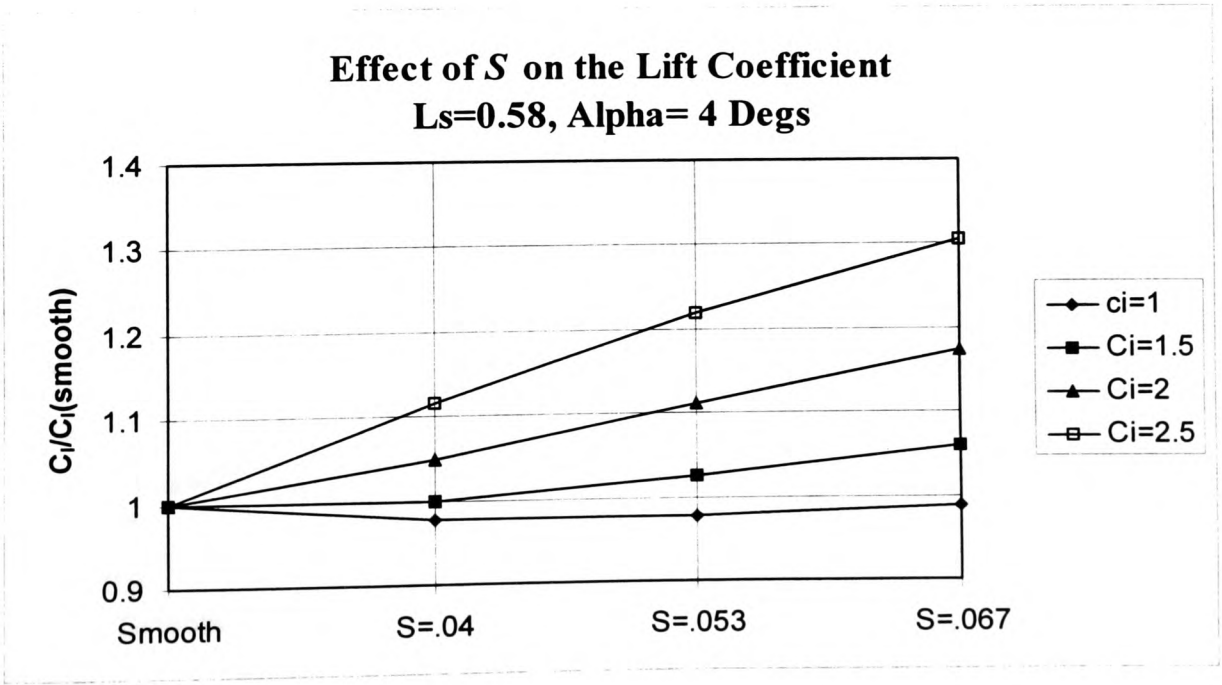

Figure 5-202

5.9.19.2 Alpha = 8 Degrees

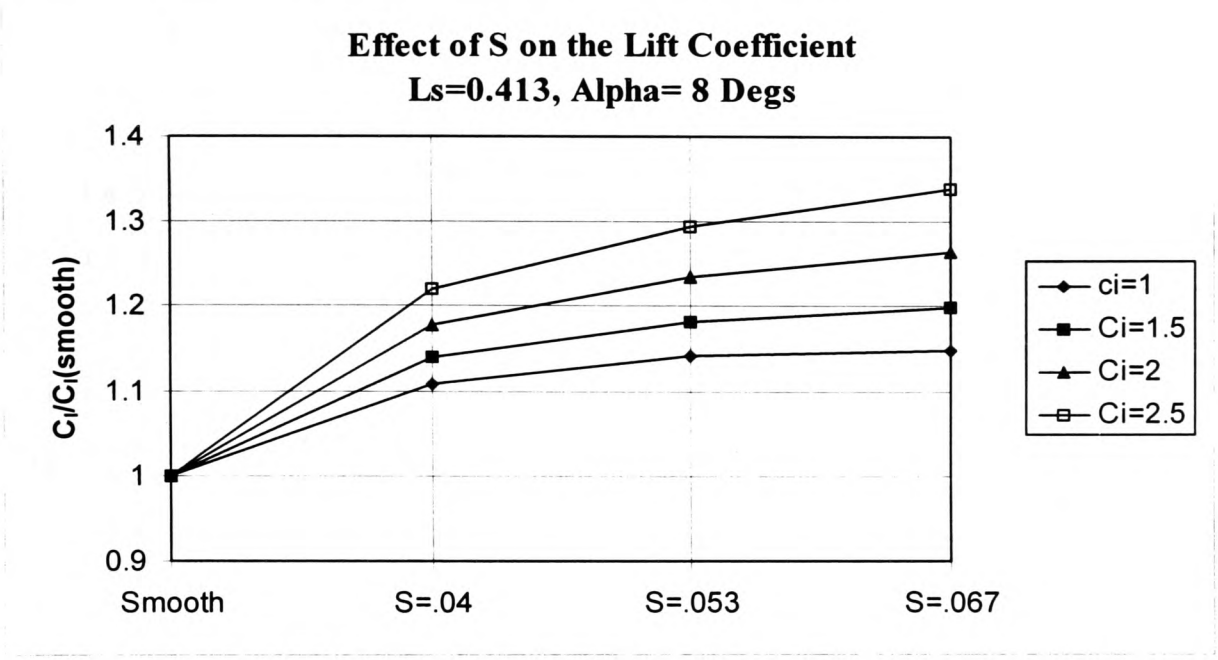

Figure 5-203

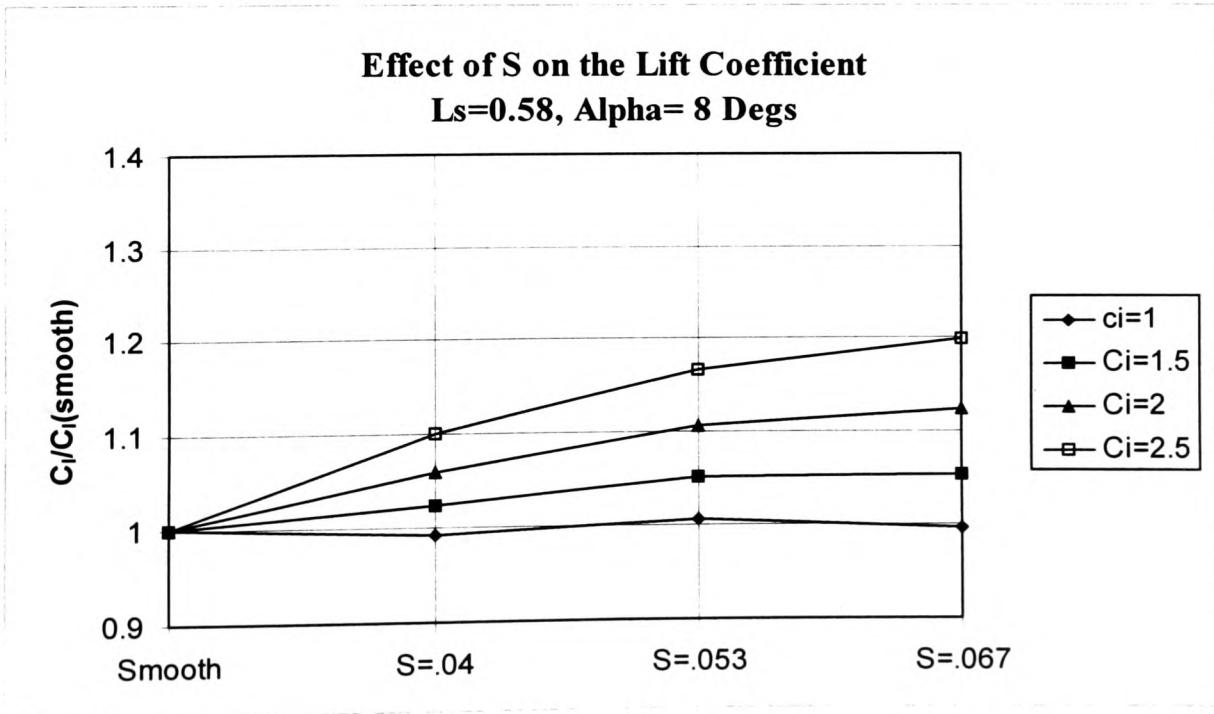

Figure 5-204

5.9.20 Effect of the Height (*H*) of the ABD on the Lift Coefficient (C_l)

5.9.20.1 Alpha = 4 Degrees

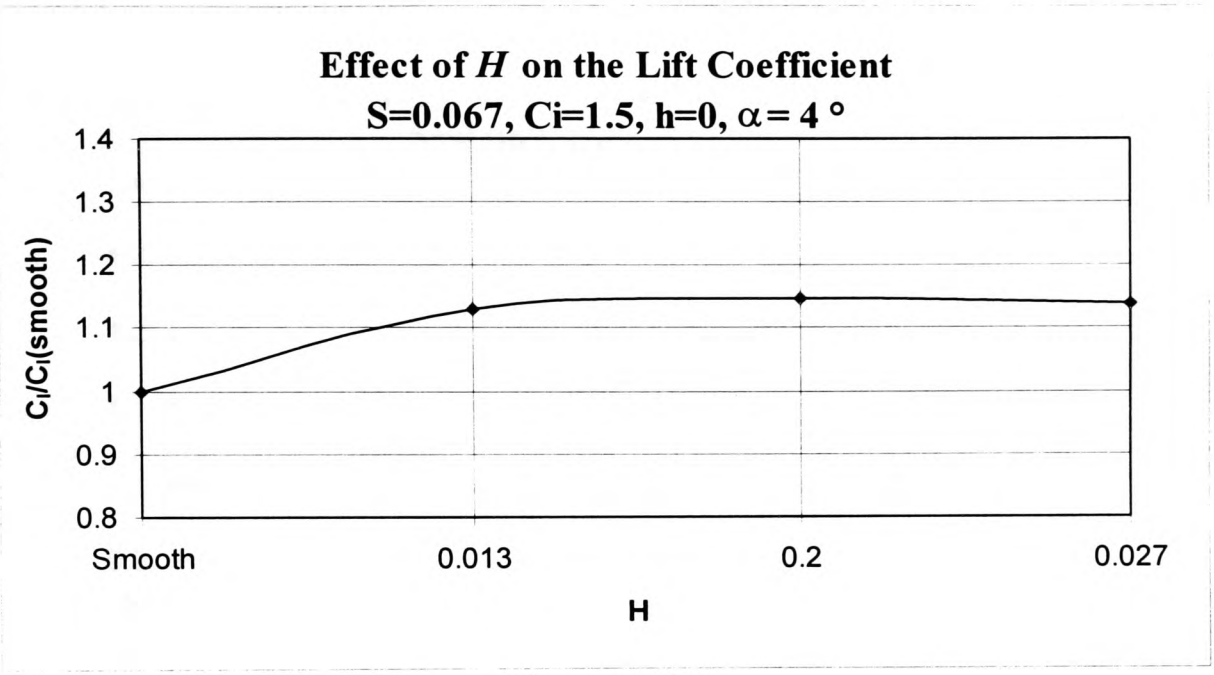

Figure 5-205

5.9.20.2 Alpha = 8 Degrees

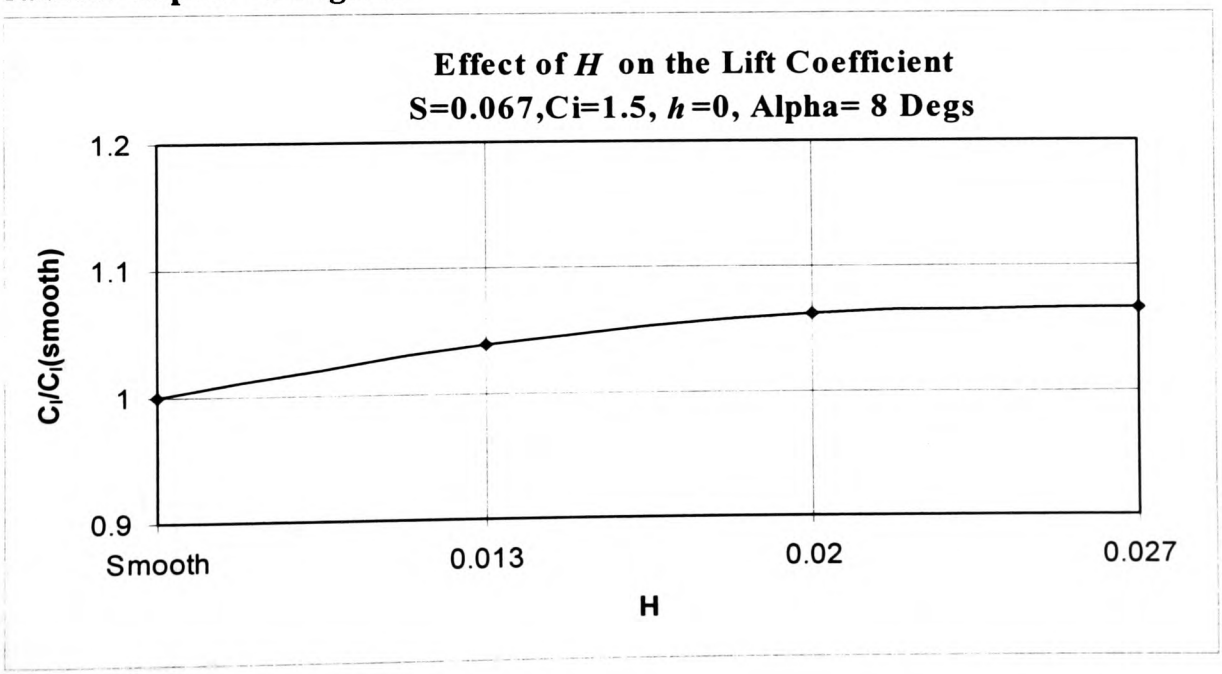

Figure 5-206

5.9.21 Effect of the Relative Height (*h*) of the Base of the ABD on the Lift Coefficient (C_l)

5.9.21.1 Alpha = 4 Degrees

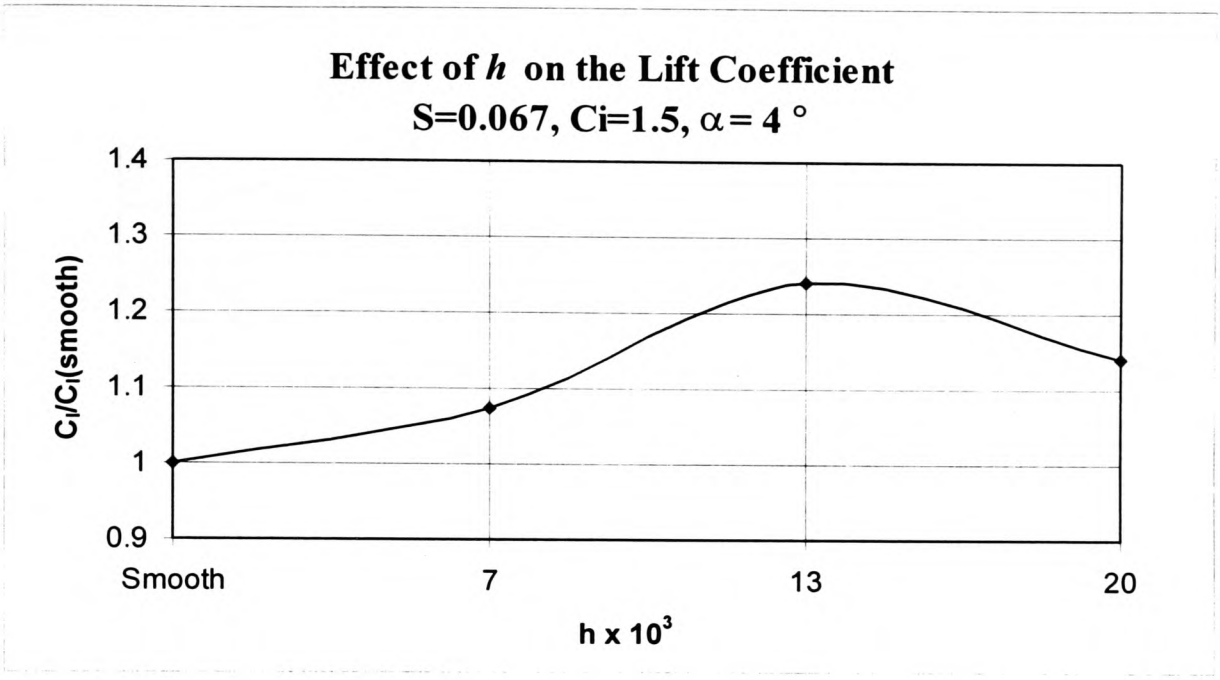

Figure 5-207

5.9.21.2 Alpha = 8 Degrees

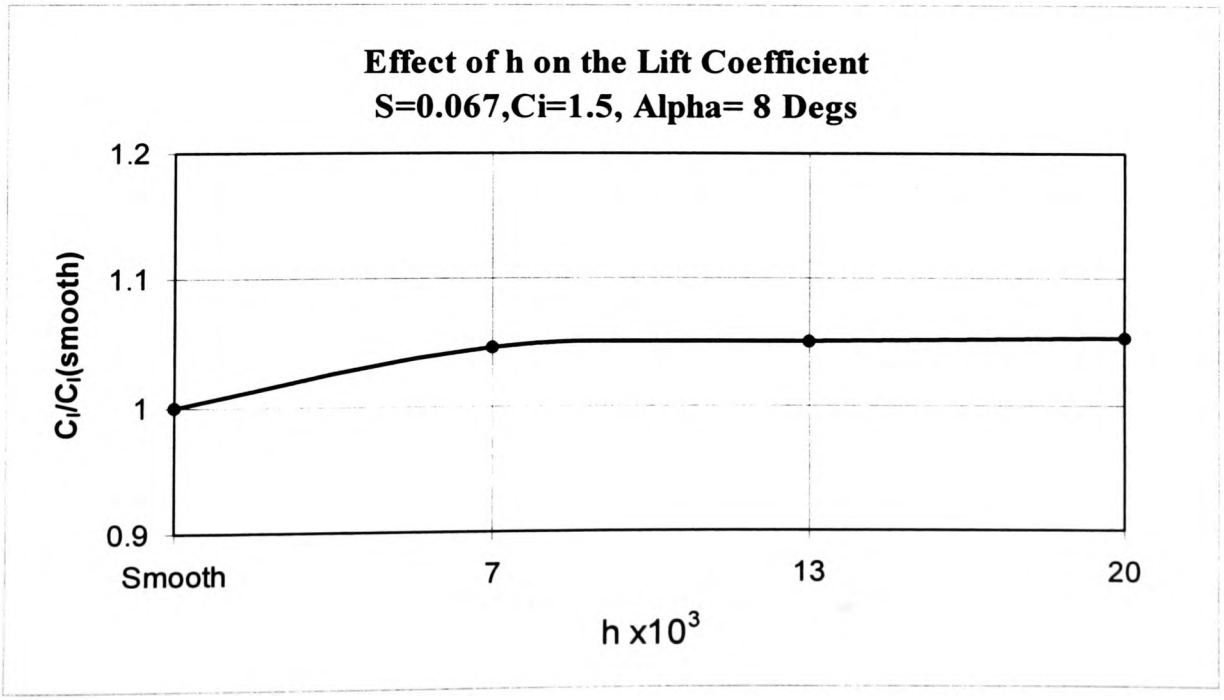

Figure 5-208

5.9.22 Flow Visualisation

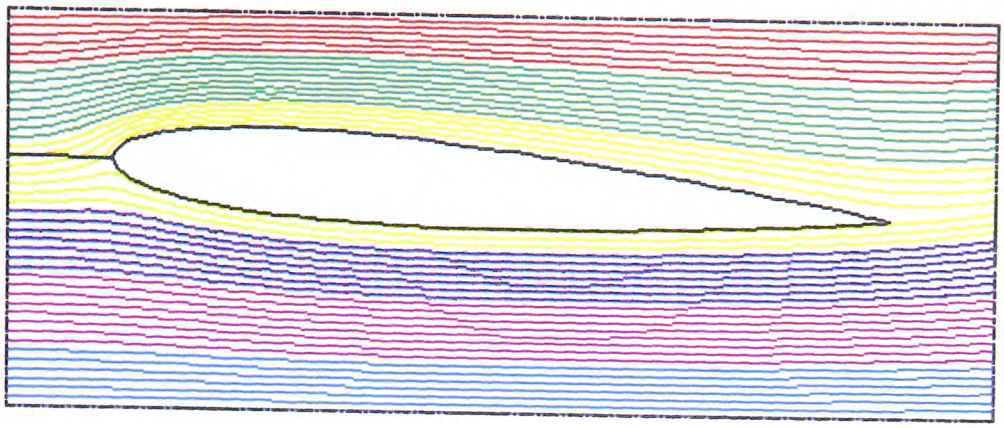

Figure 5-209 Streamlines contours over a smooth aerofoil at α=4°.

Figure 5-210 Streamlines contours over an ABD-fitted aerofoil at α=4°.

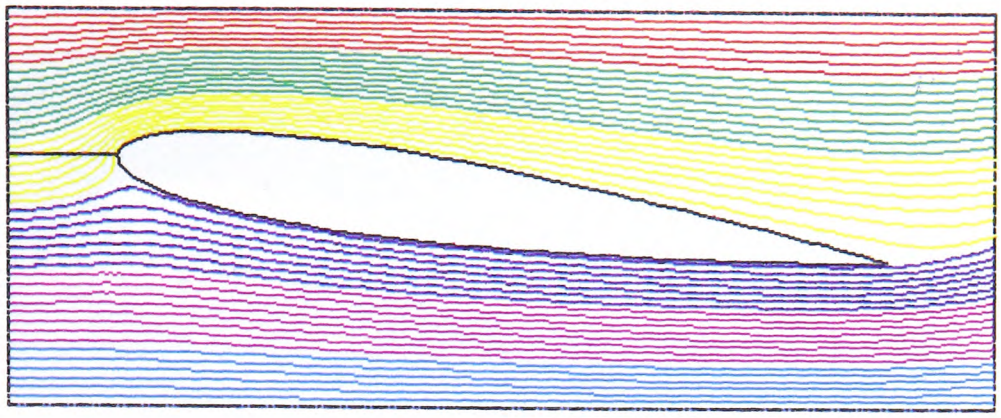

Figure 5-211 Streamlines contours over a smooth aerofoil at α=8°.

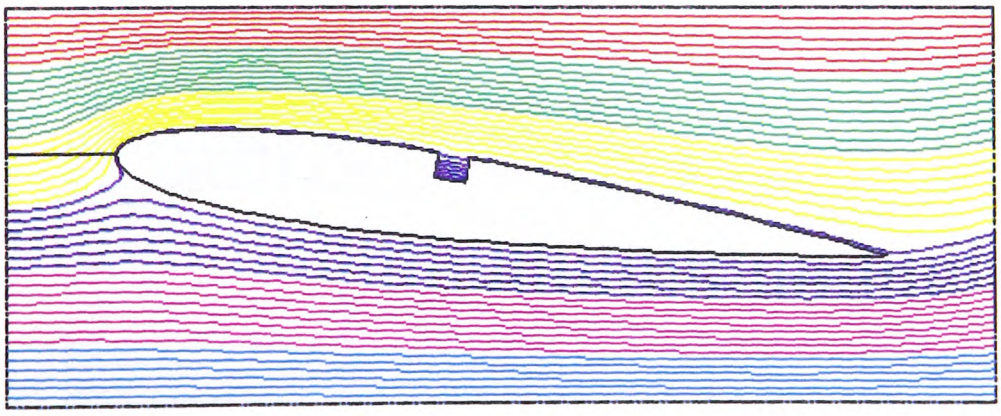

Figure 5-212 Streamlines contours over an ABD-fitted aerofoil at α=8°.

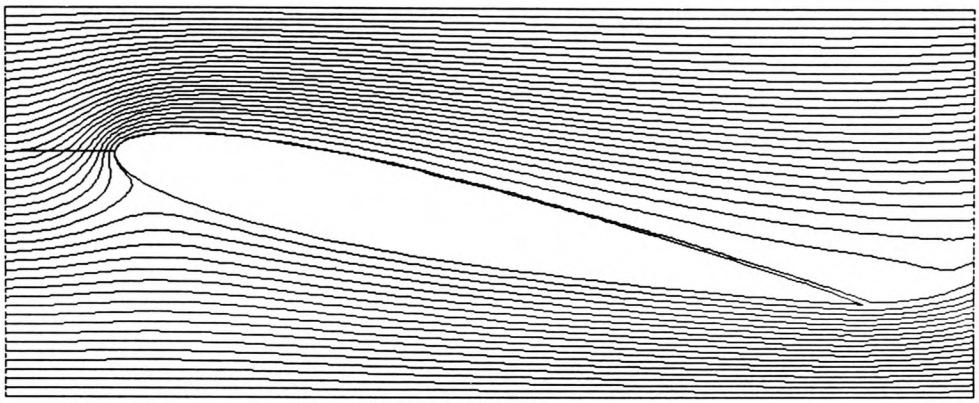

Figure 5-213 Streamlines contours over a smooth aerofoil at α=12°.

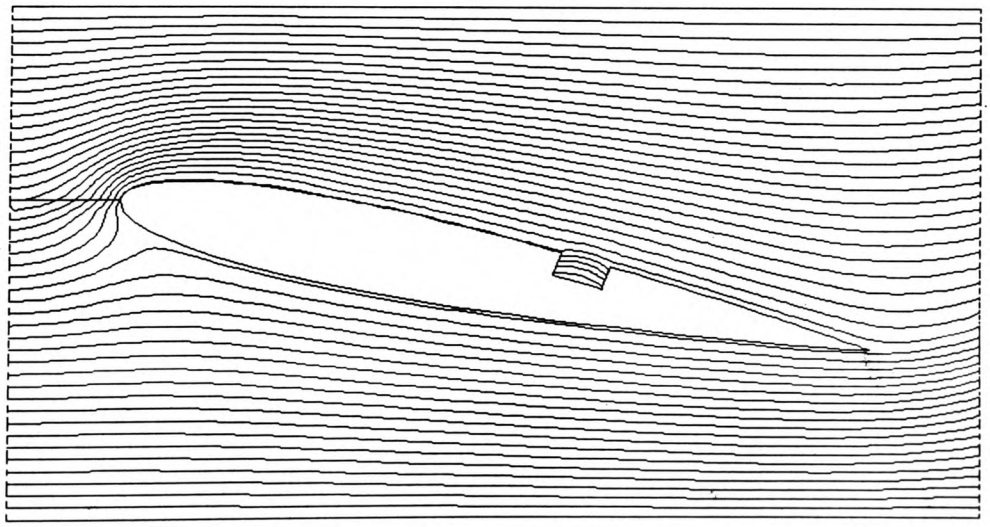

Figure 5-214 Streamlines contours over an ABD-fitted aerofoil at α=12°.

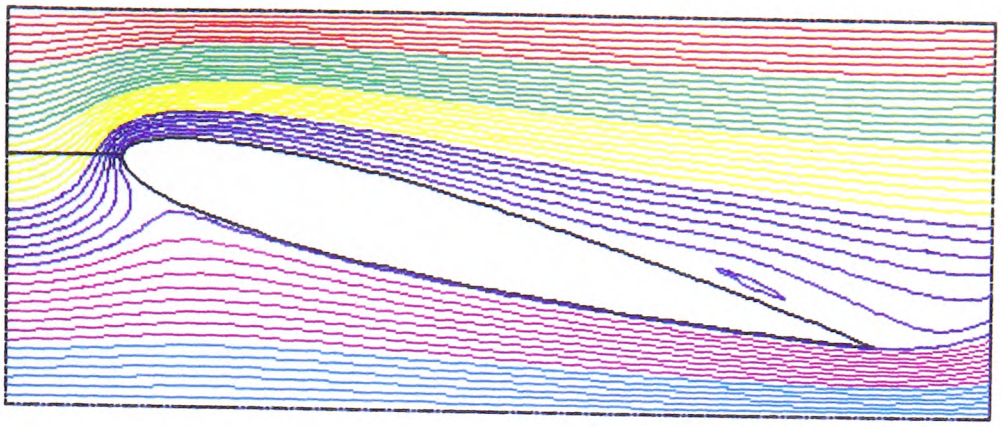

Figure 5-215 Streamlines contours over a smooth aerofoil at α=14°.

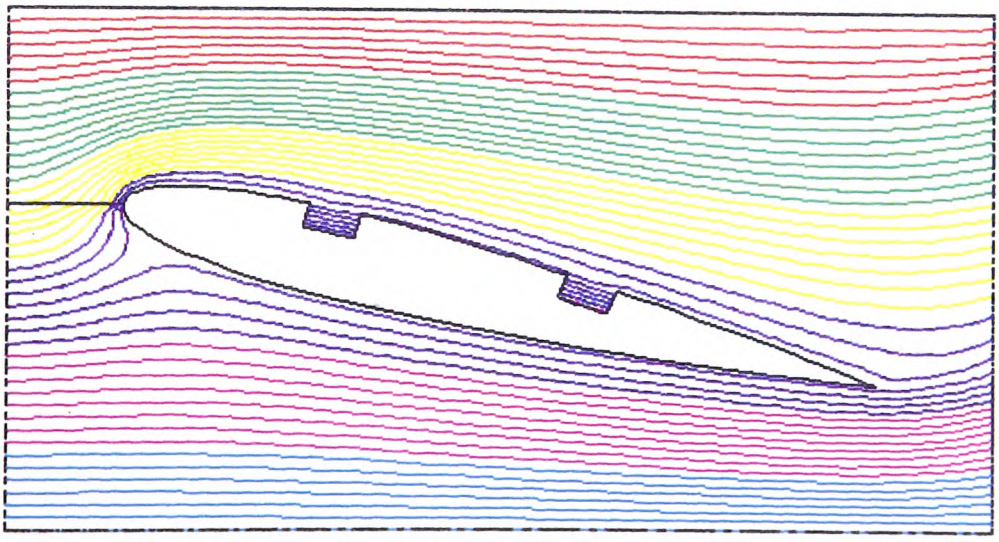

Figure 5-216 Streamlines contours over a twin ABD-fitted aerofoil at α=14°.

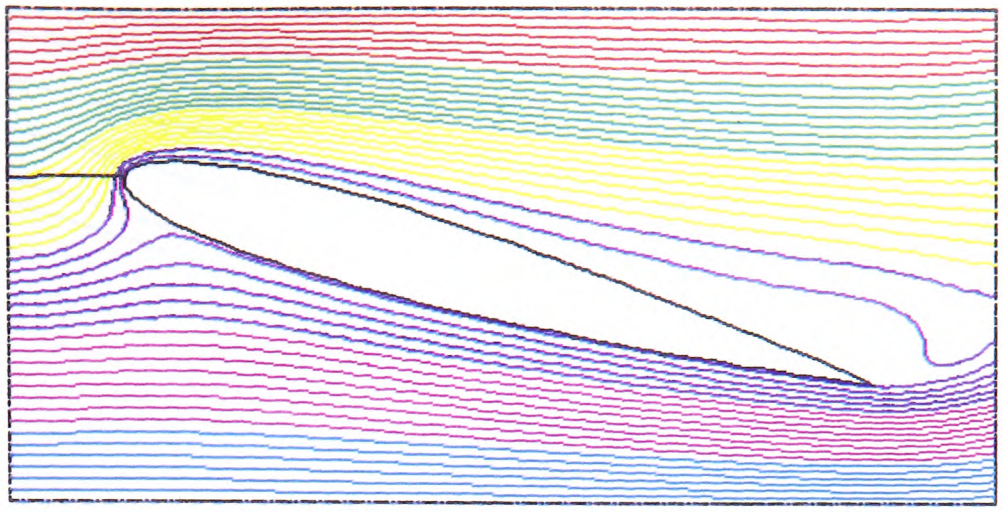

Figure 5-217 Streamlines contours over a smooth aerofoil at α=16°.

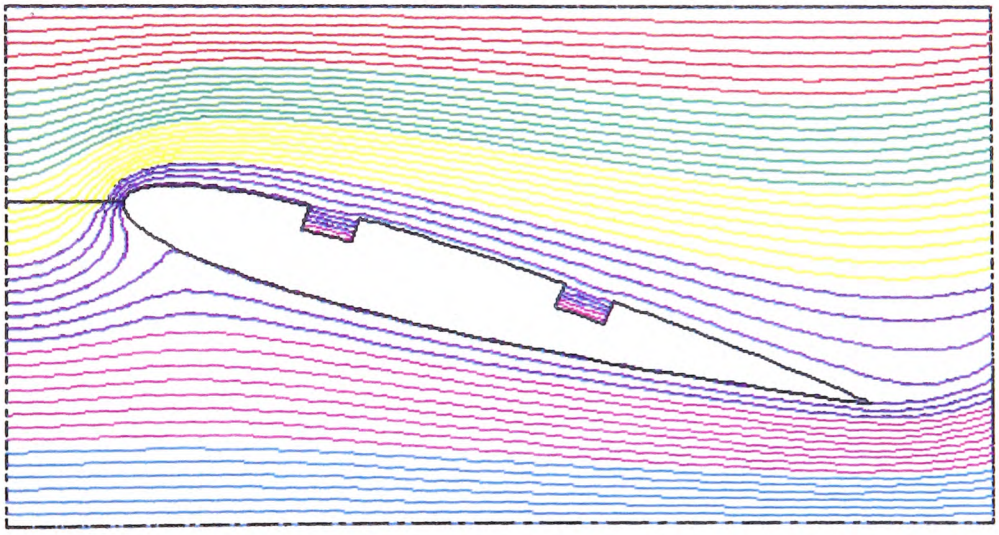

Figure 5-218 Streamlines contours over a twin ABD-fitted aerofoil at α=16°.

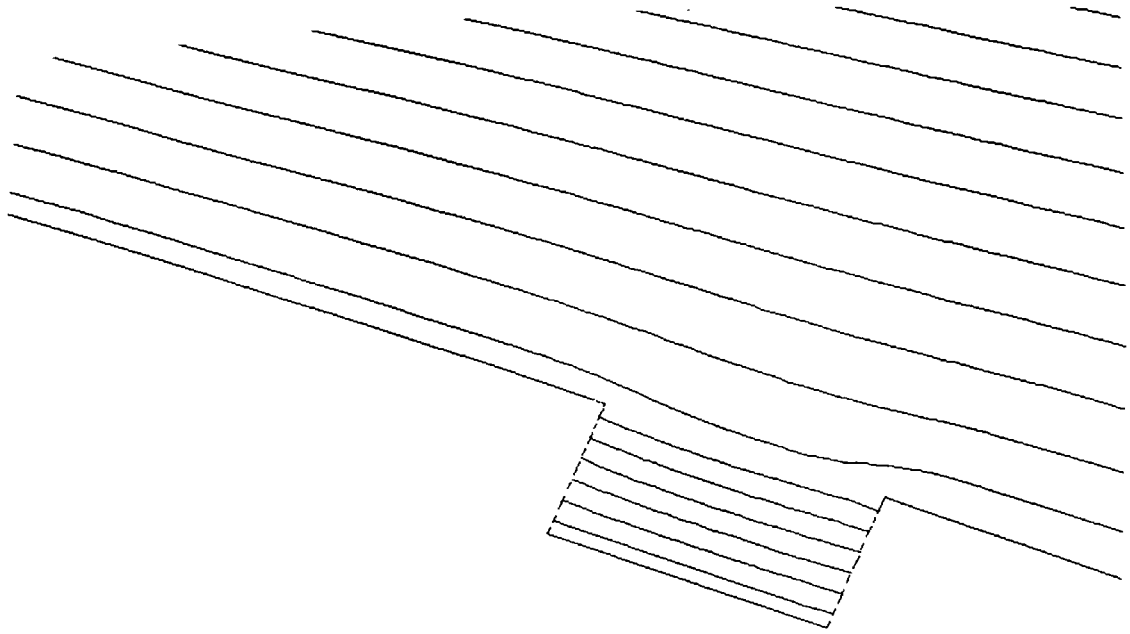

Figure 5-219 Expanded view of the stream lines inside the ABD.

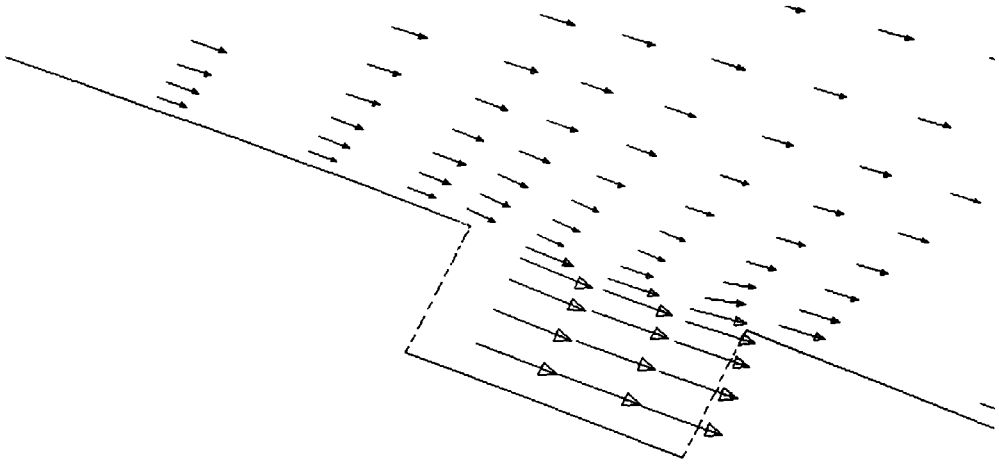

Figure 5-220 Velocity vectors inside the ABD.

Chapter Six

Conclusions and Recommendations for Further Studies

Chapter Six

Conclusions and Recommendations for Further Studies

6.1 Conclusions

This research project has introduced the idea and the use of a new active technique to control the flow over aerodynamic devices. This technique has been termed an "air bearing device" ABD.

In recent times, the subject of flow control has become more important due to the expansion of the aviation industry and rises in the cost of fuel. Reducing the drag, maintaining flow attachment to the surface and enhancing the lift of aerodynamic surfaces are the main goals of flow control methods. A large number of methods have been proposed for flow control, and these were classified in the literature review according to their effect on the different terms of the equations of motion. The advantages and disadvantages of each method are discussed in this review.

Following this review a *novel* method to control the flow over an aerofoil was introduced in this research by attempting to create an "air roller" underneath the fluid near the surface of the aerofoil. Originally transverse grooves were machined over the upper surface for this purpose. These had relatively little effect since the induced circulation was insufficiently strong. Subsequently, a device (the ABD) in which air was injected and removed was found to provide improved performance and this technique has been patented.

The performance of the ABD was tested theoretically and experimentally. The theoretical section used computational fluid dynamics CFD to model the flow. An accurate model of an aerofoil with the ABD fitted on its top surface was formulated. It was thus possible to calculate the pressure distribution, wake velocity profile, the lift coefficient , the drag coefficient and the other flow parameters in the computational domain.

The theoretical results were found to be very promising and, furthermore, were in good agreement with the experimental data.

The ABD was tested using a NACA0012 aerofoil section which was manufactured and tested in a low speed wind tunnel. The experimental programme included X-hot wire measurements of the flow velocity, direct measurement of the aerodynamic forces (lift and drag) and pressure distribution, and also flow visualisation using tufts.

The effect of each parameter of the ABD was studied and the overall effect on the "behaviour" of the ABD was identified.

By analysing the results which were obtained from both the theoretical and experimental programmes, it is clearly possible to conclude that using the ABD as a flow-control technique proved to be an efficient, practical and economical method of enhancing the performance of an aerofoil wing section. Reduction in profile drag (up to 19%) was achieved and, therefore, the operating cost will be expected to reduce accordingly. Lift was also enhanced (up to 30% for higher C_i) which means achieving a higher lift at lower angles of incidence. This, in turn, will again decrease the operating cost. The on-set of the stall point can be delayed due to delay of the trailing edge flow separation at high angles of attack. This was accomplished by using more than one ABD.

The effects of the different parameters of the ABD and their effects on the main flow were studied. It was found for instance that increasing the value of the rolling speed of the ABD, C_i, above a value of 1 can substantially enhance the main flow. Thus C_i is one of the most important parameters of the ABD in controlling the main flow. The performance of the aerofoil was found to deteriorate when the ABD had no flow inside it. The decrease in lift and increase in drag in this situation is thought to be within the range in which the aerofoil continues to provide an effective performance. Moreover this problem may be avoided by introducing a moving surface to cover the ABD in the no-flow condition. The width of the ABD, S, was also found to be an important parameter. In general it can be concluded that it is preferable to increase S (up to 5% of the chord) to provide more enhancement to the main flow. It was found, however, that beyond a certain limit increasing S may promote flow separation at the region of the ABD. The effects of the height of the ABD, H, and of the relative height of the base, h, were studied as well. Optimum values (among the cases tested) were found to be H=0.013

and h=0.007. The performance of the ABD appears not to depend on the total flow rate inside the device but, instead, on the rolling speed coefficient C_i. The location of the ABD relative to the leading edge of an aerofoil was found to have little effect on the device performance and relatively lower values of L_s are preferable.

The power consumption required to drive the ABD was estimated and it was found that the enhancement of the flow obtained from using the ABD justifies this power consumption.

Development of an effective tool to enhance the performance of lift devices is not an easy task since the subject has been very extensively studied for the last 70 years. Therefore the attractiveness of this technique lies in its surprising simplicity and ease of application.

Using the ABD in real flight conditions is predicted to be an efficient and practical method of enhancing performance. The ABD can also be used in many other applications where reducing the boundary layer thickness, δ, and drag coefficient, C_d, is required.

6.2 Recommendations for further study

Since the proposed ABD is novel and appears to have been studied for the first time in this research, much more work should be done in order to obtain a complete understanding about its performance in different applications. Thus a more comprehensive study should be undertaken both theoretically (using CFD) and experimentally.

On the theoretical side, as well as optimisation of the geometry of the ABD different applications can be studied such as: compressor blades, helicopter rotors, and flipped aerofoils on racing cars. The different boundary conditions for each of these applications is expected to require different designs and characteristics for the ABD, but the improvements are expected to be significant.

On the experimental side, more research on large-scale models of aerofoils with an ABD fitted on their top surface should be conducted particularly at higher speeds. This will extend the range of the results obtained in the present research . In particular it will then be possible to obtain more comprehensive validation of the theoretical studies. This was not possible due to experimental limitations arising from the small scale of the

model. Flow measurements and visualisation using laser sheets should also provide clarification of the effect of the ABD on the streamlines of the main flow.

Performing a real flight test with an aircraft equipped with an ABD fitted on its wings should eventually be considered. This experiment will give a real estimate of the power required to operate the ABD, the savings in operational costs and the noise level associated with the existence of the ABD.

References

- Abbott, I.H. and von Doenhoff, A.E. (1959) *Theory of wing sections*, 2nd Edition, New York: Dover Publications, Inc.
- Al-Shihry, A. M. (1989) Solution of Thin Navier-Stokes Equations for Viscous Flows, Ms.C. Thesis, Mech. Eng. Dept., King Saud University, Riyadh.
- Anders, J.B. (1990) Outer-Layer Manipulators for Turbulent Drag Reduction. *AIAA Progress in Astronautics and Aeronautics*, Washington DC, Vol 123, pp. 263-284.
- Anders J.B. and Watson R.D. (1985) Airfoil Large-Eddy Break-Up Devices for Turbulent Drag Reduction. AIAA Shear Flow Control Conference, Boulder, Co, USA, March 12-14.
- Anderson, G.W., Rohr, J.J. and Stanley, S.D. (1993) The Combined Drag Effects of Riblets and Polymers in Pipes. *Journal of Fluid Engineering*, Vol 115 pp. 213-221.
- Arain, A.A. (1991) Investigation of Surface control device for regulating an aero-generator, Ph.D. Thesis, Dept. of Mechanical, Materials and Manufacturing Engineering, University of Newcastle upon Tyne, England, June.
- Bandyopadhyay P.R.(1985) The Performance of Smooth-Wall Drag Reducing Outer-Layer Devices in Rough-Wall Boundary Layers. AIAA Shear Flow Control Conference, Boulder, Co, USA, March 12-14.
- Bandyopadhyay, P.R. (1986) Review-Main Flow in Turbulent Boundary Layers Disturbed to Alter Skin Friction. *Journal of Fluid Engineering*, June, Vol 108, pp. 127-140.
- Bandyopadhyay, P.R. (1990) Convex Curvature Concept of Viscous Drag Reduction. *AIAA Progress in Astronautics and Aeronautics*, Washington DC, Vol 123, pp. 285-324.
- Baron, A. and Quadrio, M. (1993) Some Preliminary Results on the Influence of Riblets on the Structure of a Turbulent Boundary Layer. *Int. J. Heat and Fluid Flow*, Vol 14(3) September, pp. 223-230.

- Beauchamp, C.H. and Philips, R.B. (1988) Riblets and Polymer Drag Reduction on an Axisymmetric Body. Presented at the Symposium on Hydrodynamic Performance Enhancement for Marine Applications. Newport, RI, USA, October 31-November 1, pp. 127-134.
- Bechert, D.W. and Hoppe, G. (1990) Turbulent Drag Reduction by Non- planar Surfaces - A Survey on the Research at TU/DLR Berlin. Presented at the IUTAM Symposium on Structure of Turbulence and Drag Reduction, Zurich, Switzerland, 1990. pp. 525-543.
- Beckwith, I.E. and Bushnell, D.M. (1971) Calculation by a Finite Difference Method of Super Sonic Turbulent Boundary Layers With Tangential Slot Injection. Report No. NASA TN D-6221, April.
- Bouis X., Bliek J.A., Harris G.L., and Hertrich H.A. (1994) The European transonic wind tunnel ETW -A break-through in international test facilities. Proceedings of the 19th Congress of the International Council of the Aeronautical Sciences, Anaheim, CA, USA, September 18-23, Vol. **1**, pp. LXXXIV -XCVI.
- Braslow, A.L., Maddalon, D.V., Bartlett, D.W., Wagner, R.D. and Collier, F.S. (1990) Applied Aspects of Laminar-Flow Technology. *AIAA Progress in Astronautics and Aeronautics*, Washington DC, Vol 123, pp. 47-78.
- Bushnell DM. (1983) Turbulent Drag Reduction for External Flows. Presented at the AIAA 21st Aerospace Sciences Meeting, Paper No. (AIAA-83-0227), Reno, Nevada, January12-13.
- Bushnell D.M. (1994)Viscous Drag Reduction in Aeronautics. Proceedings of the 19th Congress of the International Council of the Aeronautical Sciences, Anaheim, CA, USA, September 18-23, Vol. **1**, pp. XXXIII - LVI.
- Bushnell, D.M. and Waston, R.D. (1975) Mach and Reynolds Number Effect on Turbulent Skin Friction Reduction by Injection. *AIAA Journal of Spacecraft and Rockets*, Vol 12(8), August, pp. 506-508.
- Carmichael, B.H. (1981) Low Reynolds Number Airfoil Survey. Report No. NASA CR-165803, Washington DC.
- Carpenter, P.W. (1990) Status of Transition Delay Using Compliant Walls. *AIAA Progress in Astronautics and Aeronautics*, Washington DC, Vol 123, pp. 79-113.

Cary, A.M. and Henfer, J.N. (1970) Film Cooling Effectiveness in Hypersonic Turbulent Flow. *AIAA Journal*, Vol 8 (11) pp. 2090-2091.

Cary, A.M.C., Bushnell, D.M. and Henfer, J.N. (1977) Slot Injection for Skin Friction Drag Reduction. AGARD Report 654, Special Course on Concepts for Drag Reduction, Presented at von Karman Institute, Rhode-St-Genese, Belgium, March 28-April 1, pp. 5-1 - 5-11.

Cary, A. M., Weinstein M., and Bushnell D.M. (1979) Drag Reduction Characteristics of Small Amplitude Rigid Surface Waves. Presented at the Symposium on Viscous Drag Reduction, Dallas, Texas, USA, November 7-8, pp. 144-167.

Cebeci, T. (1989) Calculation of Flow Over Iced Airfoils. *AIAA Journal*, Vol 27, pp. 853-861.

Cebeci, T. (1990) Application of CFD to Reduction of Skin Friction Drag. *AIAA Progress in Astronautics and Aeronautics*, Washington DC, Vol 123, pp. 115-177.

Chang, P.K. (1976) *Control of Flow Separation*, Hemisphere, Washington DC.

Corke T.C., Guezennec Y., and Nagib H.M. (1979) Modification in Drag of Turbulent Boundary Layers Resulting From Manipulation of Large-Scale Structures. Presented at the AIAA Symposium on Viscous Drag Reduction. Dallas, Texas, November 7, pp. 128 -143.

Coustiex, J., Arnal, D. and Coustols, E. (1993) Reduction of Aerodynamic Skin-Friction Drag. *Novelle Revue d'Aeronautique et d'Astronautique* No. 1, April, pp. 23-31.

Coustols E., Cousteix J., and Belanger J. (1987) Drag Reduction Performance on Riblet Surfaces Through Outer Layer Manipulators. Proceedings of the International Conference on Turbulent Drag Reduction by Passive Means, Paper No. (A88-46227), Royal Aeronautical Society, London, England, September 15-17.

Davis, R.L., Carter, J.E. and Hafiz, M. (1989) Three-Dimensional Viscous Flow Solutions with a Vorticity-Stream Function Formation. *AIAA Journal* Vol 27(7) pp. 892-900.

Dougherty, N.S. and Fisher, D.F. (1980) Boundary Layer Transition on a 10-degree Cone. Paper No. AIAA 80-0154.

Dress, D.A. (1989) Drag measurements on laminar flow body of revolution. *AIAA Journal* Vol. **27**, pp. 1081-1082.

El-Seif, A., Zedan, M.F., Al-Shihry, A.M. (1990) Viscous Flow Solutions Using Thin Navier-Stokes Approximation. *Journal of Engineering Science,* King Saud University, Riyadh, Vol. **15**, Paper 11.

Ewald B. (1994) Advanced force testing technology for cryogenic and conventional wind tunnels. Proceedings of the 19th Congress of the International Council of the Aeronautical Sciences, Anaheim, CA, USA, September 18-23, Vol. **2** pp. 1597 -1609.

Fletcher, C.A. (1991) *Computational Techniques for Fluid Dynamics*, Springer-Verlag, Berlin.

Fontaine, A.A. and Deutsch, S. (1992) The Influence of the Type of Gas on the Reduction of Skin Friction Drag by Micro-bubbles Injection. *AIAA Journal*, Vol. 13**(2),** pp. 128-136.

Gad-el-hak, M. (1986) The Response of Elastic and Viscoelastic Surfaces to a Turbulent Boundary Layer. *Journal of Applied Mechanics* Vol. 53, March, pp. 206-212.

Gad-el-hak, M. (1989) Flow Control. *Applied Mechanics Review* Vol. 42(10) pp. 261-293.

Gad-el-hak, M. and Blackwelder, R.F. (1989) Selective Suction for Controlling Bursting Events in a Boundary Layer. *AIAA Journal* 27, pp. 308-314.

Gad-el-hak, M. (1990) Control of Low-Speed Aerofoil Aerodynamics. *AIAA Journal* Vol. 28, pp. 1537-1552.

Galbraith, R.A.M. and Head, M.R. (1975) Eddy viscosity and mixing-length from measured boundary layer developments. *Aero. Quart.* Vol. **26**, pp. 133-154.

Groth, E.E., Carmichael, B.H., Whites, R.C. and Pfenninger, W. (1957) Low Drag Boundary Layer Suction Experiments in Flight on the Wing Glove of a F94-A Aeroplane Phase II: Suction Through 69 Slots. NAI-57-318, BLC-94, Northrop Aircraft, Inc. February.

Hackett J.E. (1980) Vortex Drag Reduction by Aft-Mounted Diffusing Vanes. Proceedings of the 12th AIAA Congress of International Council of Aeronautics

Sciences, Paper No. (A81-11601) Munich, West Germany, October 12-17, pp. 542-553.

- Harris, R.V. and Henfer, H. (1987) NASA Laminar-Flow Program - Past, Present and Future. *Research in Natural Laminar Flow and Laminar-Flow Control*, Report No. NASA CP-2489, Paper 1.
- Henfer J.N., Weinstein M., and Bushnell D.M. (1979) Large-Eddy Break-Up Scheme for Turbulent Viscous Drag Reduction. Presented at the AIAA Symposium on Viscous Drag Reduction, Dallas, Texas, pp. 110 -127.
- Henfer, J.N. (1986) Overview of the Langley Viscous Drag Reduction Program. NASA Langley Research Centre, Hampton, VA, USA, December.
- Henfer, J.N. (1988) Dragging down fuel costs. *Aerospace America*, Vol. **26** pp.14-16.
- Henfer, J.N. and Bushnell, D.M. (1990) Viscous Drag Reduction Via Surface Mass Injection. *AIAA Progress in Astronautics and Aeronautics*, Washington DC, Vol. **123** pp. 457-476.
- Hill, D.C. (1994) *Drag Reduction Strategies*, Stanford University, CA, USA, December.
- Hinze, J.O. (1975) *Turbulence*, McGraw-Hill, New York, 2nd Edition, 1975.
- Houghton, E.L. and Carruthers, N.B. (1982) *Aerodynamics for Engineering Students*. 3rd Edition, Edward Arnold (Publishers) Ltd., London, England.
- Howard, F.G., Henfer, J.N. and Srowski, A.J. (1975) Multiple Slot Skin Friction Reduction. *J. Aircraft* Vol. 12, pp. 753-754.
- Howard, F.G. and Goodman, W.L. (1985) Axisymmetric Bluff-Body Drag Reduction Through Geometrical Modification. *J. Aircraft* Vol. 22, pp. 516-522.
- Howard, F.G. and Goodman, W.L. (1987) Drag Reduction on a Bluff Body at Yaw Angles to 30 Degrees. *Journal of Spacecraft*, Vol. 24(2) pp.179-181.
- Hoyt, J.W. (1990) Drag Reduction by Polymers and Surfactants. *AIAA Progress in Astronautics and Aeronautics*, Washington DC, Vol. 123, pp. 413-432.
- Johansoen, J.B. and Smith, C.R. (1986) The Effects Of Cylindrical Surface Modifications on Turbulent Boundary Layers. *AIAA Journal* Vol. 24 pp. 1081-1087.

- Jones, B.M. (1936) The measurement of profile drag by pitot traverse method. Report No. ARC RM 1688, 1936.
- Jones, M. and Head, M.R. (1951), The Reduction of Drag by Distributed Suction, 3rd Anglo-American Aeronautical Conference, September, Brighton, England, pp. 199-230.
- Jones, T., Oldfield, M.L.G., Ainsworth, R.W., Ireland, P.T., (1996) Fuel for Thought - Making jet-engines more efficient, Royal Society Esso Energy Award Lecture, London, England, November 21.
- Kalugin, V.N., Kononenko, O.V., Riutin, V.B. and Sliusarenko, V.I. (1982) Investigation of the Possibility of Reducing Aerodynamic Drag by a Mechanism of Initial Vortex Formation. *Vychislitel'naia i Prikladnaia Matematika* Vol. 48, pp. 114-119.
- Klatt, F. (1969) The X-Hot-Wire Probe in a Plane Flow Field. *DISA Information*, DISA Elektronik A/S, Herlev, Denmark, Vol. 8, July, pp. 3-12
- Kaname Sato (1994) *Use of Prediction Procedures to Model Swirl Burner/Furnace Flows*. Ph.D. Thesis, Division of Mech. Eng., University of Wales College of Cardiff, pp.32-70.
- Kane, R.S. (1990) Drag Reduction by Particle Addition. *AIAA Progress in Astronautics and Aeronautics*, Washington DC, Vol. 123, pp. 433-456.
- Khan M. (1986) A Numerical Investigation of Drag Reduction by Riblet-Surfaces. The 4th AIAA and ASME Fluid Mechanics, Plasma Dynamics and Lasers Conference, Lockheed Independent Research and Development, Atlanta, GA, USA, May 12-14.
- Konovalov, F., Lashkov, Y.A., Mikhailov, V.V., Fadeev, I.V. and Shapovalov, G.K. (1992) Effect of Longitudinal Riblets on Axisymmetric Body Drag. *Izvestiya Rossiiskoi Akademii Nauk, Mekhanika Zhidkosti i Gaza*, Vol. 2, March-April, pp. 174-178.
- Korner H. and Redeker G. (1994) The role of flight tests and wind tunnels in laminar flow research. Proceedings of the 19th Congress of the International Council of the Aeronautical Sciences, Anaheim, California, September 18-23, Vol. 1, pp. 46-56.

- Kreitinger, R.L. and Middleton, D.B. (1981) Aircraft Surface Coatings for Drag Reduction/Erosion Protection. SAE Report No. 811070, Presented at Aerospace Congress & Exposition, Anaheim, California, October 5-8, pp. 1-15.
- Lashkov, Y.A., Solova, I.N. and Shumikina (1992) Jet Flow Over Ribbed Curved Surfaces. *Izvestiya Rossiiskoi Akademii Nauk, Mekhanika Zhidkosti i Gaza*, Vol. 1, January-February, pp. 177-179.
- Lauchle, G.C. and Gurney, G.B. (1984) Laminar Boundary Layer Transition on a Heated Underwater Body. *J. Fluid Mech.* Vol. 144 pp. 79-101.
- Lazos, B. and Wilkinson, S.P. (1988) Turbulent Viscous Drag Reduction With Thin-Element Riblets. *AIAA Journal* Vol. 26, April, pp.496-498.
- Liepmann, H.W., Brown, G.L. and Nosenchuck, D.M. (1982) Control of Laminar Instability Waves Using a New Technique. *J. Fluid Mech.* Vol. 118 pp. 187-200.
- Lock, R.C. (1986) The Prediction of the Drag of Aerofoils and Wings at Subsonic Speeds. *Aeronautical Journal* Vol. 90, June-July, pp. 207-226.
- Luchini, P., Manzo, F. and Pozzi, A. (1991) Resistance of a Grooved Surface to Parallel Flow and Cross-Flow. *J. Fluid Mech.* Vol. 228, pp. 87-109.
- Madavan, N.K., Deutsch, S. and Merkle, C.L. (1984) Reduction of Turbulent Skin Friction by Micro bubbles. *Phys. Fluids* Vol. 27 pp. 356-363.
- Maksoud, T.M. and Al-Shihry, A.M. (1994) On The Drag Reduction of The Flow Over an Aerofoil. Proceedings of the 19th Congress of the International Council of the Aeronautical Sciences, Anaheim, CA, USA, September 18-23, pp. 104-108.
- Malik, R.M. (1990) Stability Theory for Laminar Flow Control Design. *AIAA Progress in Astronautics and Aeronautics*, Washington DC, Vol. 123, pp. 3-46.
- Manzalise, G. (1995) Theoretical Study of Flow over a Grooved-Surface Aerofoil, Final year project, Mechanical and Manufacturing Dept., University of Glamorgan.
- McLean J.D., George-Falvy D.N., and Sullivan P.P. (1987) Flight-Test of Turbulent Skin Friction Reduction by Riblets. Proceedings of the Royal Aeronautical Society International Conference on Turbulent Drag Reduction by Passive Means, RAeS, London, Vol. 2, September 15-17, pp. 408-424.

- McMasters, J.H. and Henderson, M.L. (1980) Low Speed Single Element Airfoil Synthesis. *Tech. Soaring* Vol. 6, pp.1-21.
- Merkle, C.L. and Deutsch, S. (1990) Drag Reduction in Liquid Boundary Layers by Gas Injection. *AIAA Progress in Astronautics and Aeronautics*, Washington DC, Vol. **123**, pp. 351-412.
- Modi, V.J., Munshi, S.R., Mokhtarian, F., Bandyopadhyay, G., and Tokomizo, T. (1994) Multielement Aerofoils With Moving Surface Boundary Layer Control: Wind Tunnel, Numerical and Flow Visualisation Studies. Proceedings of the 19th Congress of the International Council of the Aeronautical Sciences, Anaheim, CA, USA, September 18-23, Vol. **1**, pp. 80-103.
- Nakayama, Y. (1988) *Visualized Flow*, First English edition, , Pergamon Press, Oxford.
- Neubert, H.K.P. (1963) *Instrument Transducers*, Oxford Clarendon Press.
- Ower, E. and Pankhurst, R.C. (1965) *Measurement of air flow*, 4th Edition. Pergamon.
- Patankar, S.V. (1980) *Numerical Heat Transfer and Fluid Flow*, Hemisphere Publishing Corporation, Taylor & Francis Group, New York.
- Parthasrathy, K. and Zakkay, V. (1970) An Experimental Investigation of Turbulent Slot Injection at Mach 6. *AIAA Journal* Vol. 8, pp. 1302-1307.
- Perkins, W.F. and Rece, J.W. (1963) Reduction in Drag of Submerged Bodies by Partial Enclosure in Gaseous Cavities. Report No. B910062-4, United Aircraft Corporation Research Laboratories, East Hartford, CO, USA, pp.1-44.
- Pfenninger, W. and Bacon, J.W. (1965) Investigation of Methods for Re-Establishment of a Laminar Boundary Layer from Turbulent Flow. Northrop Norair Report No. 65-48 [Blc-161].
- Quass, B., Howard, F., Weinstein, L. and Bushnell, D.M. (1981) Longitudinal Grooves for Bluff Body Drag Reduction. *AIAA Journal* Vol. 19, April, pp. 535-537.
- Reidy, L.W. and Anderson, G.W. (1988) Drag Reduction for External and Internal Boundary Layers Using Riblets and Polymers. Proceedings of the 26th AIAA

Aerospace Sciences Meeting, Paper No. (AIAA 88-0138), Reno, NV, USA, January 11-14.

Reshotko E. (1979) Heated Boundary Layers. Proceedings of the 12th Symposium on Naval Hydrodynamics, National Academy of Sciences, Vol. 33.

Reshotko, E. (1979b) Drag Reduction by Cooling in Hydrogen-Fuelled Aircraft. *J. Aircraft* Vol. 16 pp. 584-590.

Roache, P.J. (1982) *Computational Fluid Dynamics*, 2nd Edition, Hermosa, Albuquerque, NM.

Rodi W. (1979) Influence of boundary and rotation on equations for the turbulent vortex flows. 2nd Symposium on Turbulent Flows, London.

Rubbert P.E. (1994) CFD and Changing World of Aeroplane Design. Proceedings of the 19th Congress of the International Council of the Aeronautical Sciences, Anaheim, CA, USA, 1994, September 18-23, Vol. **1**, pp. 80-103.

Schlichting, H. (1979) *Boundary-Layer Theory*, 7th Edition, McGraw-Hill, New York.

Smits, A.J., Young, S.T.B. and Bradshow, P. (1979) The Effect of Short Regions of High Surface Curvature on Turbulent Boundary Layers. *J. Fluid Mech.* Vol. 94(2) pp. 209-242.

Smith, G.D. (1985) *Numerical Solution of Partial Differential Equations: Finite Difference Methods*, 3d Edition, Clarendon Press, Oxford

Smith, A.M.O. and Murphy, J.S. (1955) Micromanometer for measuring boundary layer profile. *Rev. Sci. Instrum.*, Vol. **26**, pp. 775.

Thibert, J.J., Grandjacques, M. and Ohman, L.H. (1979) NACA0012 Airfoil, AGARD Advisory Report No. AGARD-AR-138, Neuily Sur Seine, France, pp.A1-1 ~ A1-36.

Thomas, A.S.W. (1990) Active Wave Control of Boundary-Layer Transition. *AIAA Progress in Astronautics and Aeronautics*, Washington DC, Vol. 123, pp. 179-199.

Toms, B.A. (1977) On the Early Experiments on Drag Reduction by Polymers. *Phys. Fluids* Vol. 20, No. 10 Part II, October, pp. 53-55.

- Vandam, C.P. and Hafiz, M. (1989) Comparison of Iterative and Direct Solution Methods for Viscous Flow Problems. *AIAA Journal* Vol. **27**, pp. 1459-1461.
- Versteeg, H.K. and Malalasekera, W. (1995) *An Introduction to Computational Fluid Dynamics. The Finite Volume Method*, Longman Group Ltd., 1st Edition, England.
- Vukoslavceic, P., Wallace, J.M. and Balint, J.L. (1991) Viscous Drag Reduction Using Stream Wise-Aligned Riblets. *AIAA Journal* Vol. 30(4) pp. 1119-1122.
- Wagner, R.D., Maddalon, D.V. and Fischer, M.C. (1989) Technology Developments for Laminar Boundary Layer Control On Subsonic Transport Aircraft. Report No. AGARD CP-365, Paper 16, pp. 1-13.
- Wagner, R.D. and Fischer, M.C. (1984) Fresh Attack on Laminar Flow. *Aerospace America* Vol. 22, pp. 72-76.
- Wallace J.M. and Balint J.L. (1988) Viscous Drag Reduction Using Stream Wise Aligned Riblets - Survey and New Results. Proceedings of the IUTAM Symposium on Turbulence Management and Relaminarization, Paper No. (A89-10154), Bangalore, India, January 19-23, pp. 01-34.
- Walsh, M.J. (1980) Drag Characteristics of V-Groove and Transverse Curvature Riblets. *AIAA Progress in Astronautics and Aeronautics*, Washington DC, Vol. 72 pp. 168-184.
- Walsh, M.J. (1983) Riblets as a Viscous Drag Reduction Technique. *AIAA Journal* Vol. 21, April, pp. 485-486.
- Walsh M.J., Sellers W.L., and McGinely C.B. (1988) Riblet Drag Reduction At Flight Conditions. Proceedings of the 6th AIAA Applied Aerodynamics Conference, Williamsburg, VA, USA, pp. 629-638.
- Walsh, M.J. (1990) Riblets. *AIAA Progress in Astronautics and Aeronautics*, Washington DC, Vol. 123, pp. 203-261.
- Walsh, M.J. and Lindemann, A.M. (1984) Optimisation and Application of Riblets for Turbulent Drag Reduction. Paper No. *AIAA* 84-0347.
- Walsh, M.J. and Weinstein, M. (1978) Drag and Heat Transfer on Surfaces with Small Longitudinal Fins. Paper No. AIAA 78-1161, Presented at the AIAA 11th Fluid and Plasma Dynamic Conference, Seattle, Washington, July, pp. 1-11.

- White, R.C., Sudderth, R.W. and Wheldan, W.G. (1966) Laminar Flow Control on the X-21. *Astronaut Aeronaut* Vol. 4 pp. 38-43.
- Whitehead, D.S., Kodz, M. and Hield, P.M. (1982) The Reduction of Drag by Corrugating Trailing Edges, Cambridge University, England.
- Wikoff, D., Cottrell, C., and Packard, J.D. (1987) An Examination of Controlled Vortex Drag Using Stepped After-Bodies from M=0.5 to 3.0. Proceedings of the 25th AIAA Aerospace Science Meeting, Reno, Nevada, January 12-15.
- Wilkinson, S.P. (1990) Interactive Wall Turbulence Control. *AIAA Progress in Astronautics and Aeronautics*, Washington DC, Vol. 123, pp. 479-509.
- Wilkinson S.P. and Lazos B.S. (1982) Direct Drag and Hot Wire Measurements on Thin-Element Arrays. Proceedings of the IUTAM Symposium on Turbulence Management and Relaminarization, Bangalore, India, January 19-23.
- Williams, D.R. and Amato, C.W. (1989) Unsteady Pulsing of Cylinder Wakes. in *Frontiers in Experimental Fluid Mechanics*, M Gad-el-Hak (Editor), Springer-Verlag, New York, pp. 337-364.
- Wood, C.J. (1967) Visualisation of an Incompressible Wake with Base Bleed. *J. Fluid Mech.* 29, pp. 259-272.
- Zaman KB, Panda J, and Rumsey C. (1993) Estimation of Unsteady Lift on a Pitching Aerofoil from Wake Velocity Surveys. Report No. NASA TM-105947, Presented at the 31st AIAA Aerospace Science Meeting and Exhibit, Reno, Nevada, January11-14.

Appendices

Appendix A

O-Grid Scheme

An aerofoil body which is located in a stream of fluid can be considered as an 'obstruction' to the main stream.. In regions with obstructions or blockages, it may be preferable to use a so-called O-grid scheme. Figure C-1 shows an O-grid used for an 'obstacle' which is represented by the circle ABCDA1. This circle may be any geometry such as an aerofoil or cylinder In this scheme a branch cut is introduced in the physical domain to generate a simply connected computational (I,J) domain. Thus grid points on A′E′ and A1′ E1′ in the computational domain coincide in the physical domain. The two lines AE and A′E′ are given a cyclic boundary condition.

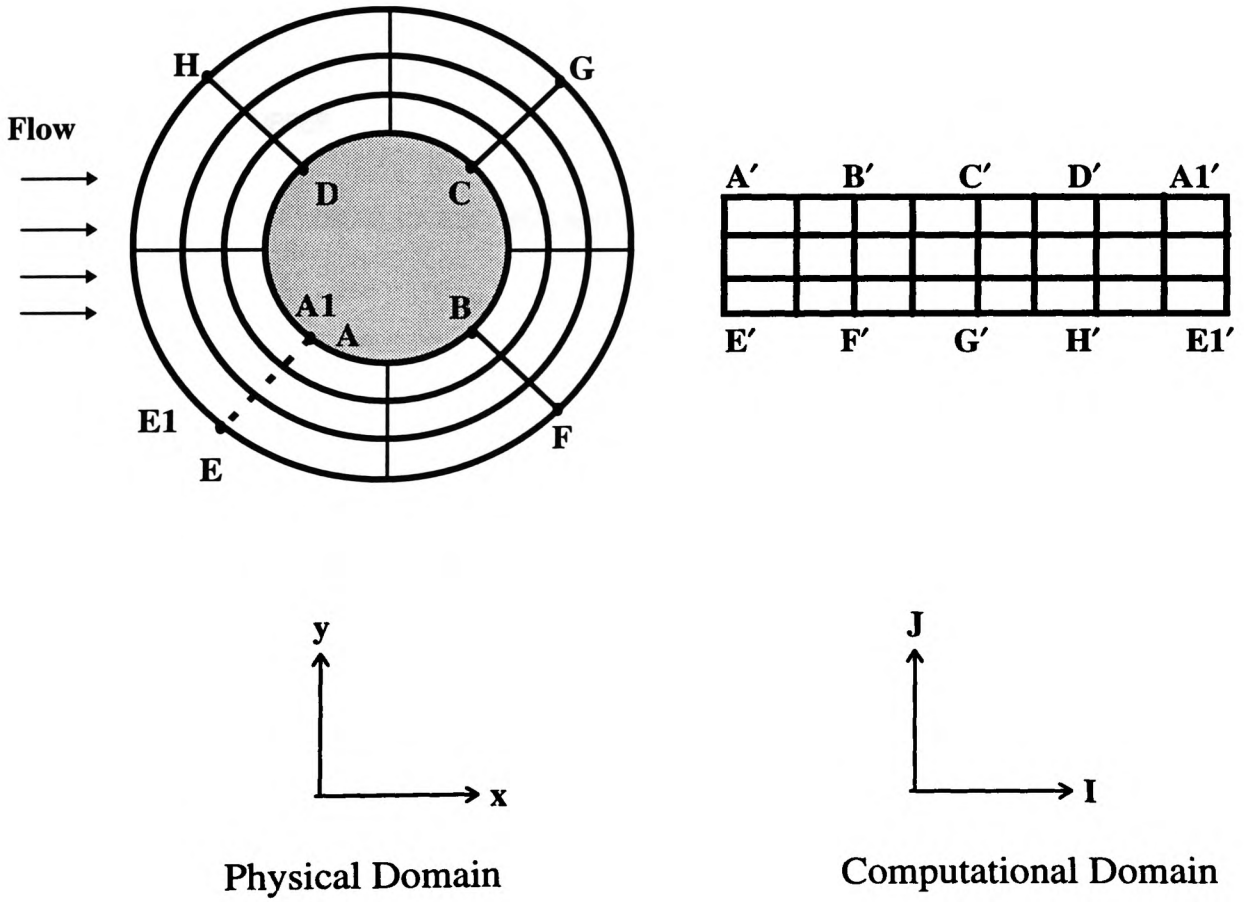

Figure A-1 Example of an O-Grid

Appendix B

FORTRAN Program to calculate the pressure distribution and pressure coefficient at an equal intervals. Input data are taken from FLUENT 4 output.

```
C    Interpolation Program To Calculate The Values of Pressure at an equi-spaced points from the output of FLUENT.
C    FLUENT output data are calculated at the locations of grid points which are not uniformally distributed.
C    Programmed by:  Ali M. Al-Shihry
C    Last Updated:  22/4/96
C
     DIMENSION XUPPER(140),XLOWER(140),PUPPER(140),PLOWER(140),CL(16)
     DIMENSION FUPPER(200),FLOWER(200),cp(16,100)
     INTEGER*2 NUPPER,NLOWER,NN
     CHARACTER*8  FILES(2)
     CHARACTER*12  DOMYC
     NFILES=16
     DATA (FILES(i), i=1,16) /'cp8-80','cp8-81','cp8-82','cp8-83',
    &'cp8-84','cp8-85','cp8-86','cp8-87','cp8-88','cp8-89',
    &'cp8-90','cp8-91','cp8-92','cp8-93','cp8-94','cp8-95'/
     DO 1001 K=1,16
c    PRINT *,FILES(K)
1001  CONTINUE
     NN=140
     NUPPER=105
     NLOWER=NN-NUPPER

     DO 130 kk=1,NFILES
        OPEN(1, FILE=FILES(kk),ACCESS='SEQUENTIAL', STATUS='OLD')
           DO 10 I=1,NN
          XUPPER(I)=0.0
          XLOWER(I)=0.0
          PUPPER(I)=0.0
          PLOWER(I)=0.0
10       CONTINUE
C        PRINT *,FILE1
        READ(1,1)DOMYC
1        FORMAT(/////////////,A12)
        DO 20 I=1 ,NUPPER
          READ (1,*)DOMY,XUPPER(I),PUPPER(I)
20       CONTINUE
        DO 30 J=NLOWER,1,-1
          READ (1,*)DOMY,XLOWER(J),PLOWER(J)
30       CONTINUE
c        PRINT *,7,NUPPER,NLOWER,NN
        XMIN=MAX(XUPPER(1),XLOWER(1))
        XMAX=MIN(XUPPER(NUPPER),XLOWER(NLOWER))
        DXPLOT = (XMAX-XMIN)/100
        XA  = XMIN
        IPLOT=1
100      DO 60 I=1,NUPPER
          IF (XUPPER(I) .LT. XA) THEN
c             print *,xa,xupper(i),i
            GOTO 60
          ELSE
            ILEFT  =I-1
            IRIGHT  =I
```

```
            GOTO 70
          ENDIF
60        CONTINUE
70        DELTAX=XUPPER(IRIGHT)-XUPPER(ILEFT)
          DX=XA-XUPPER(ILEFT)
          FUPPER(IPLOT)=(DX/DELTAX)*(PUPPER(IRIGHT)-PUPPER(ILEFT))
     &     +PUPPER(ILEFT)
          DO 80 I=1,NLOWER
            IF (XLOWER(I) .LT. XA)THEN
c             print *,i
              GOTO 80
            ELSE
              ILEFT  =I-1
              IRIGHT  =I
              GOTO 90
            ENDIF
80        CONTINUE
90        DELTAX=XLOWER(IRIGHT)-XLOWER(ILEFT)

          DX=XA-XLOWER(ILEFT)
          FLOWER(IPLOT)=(DX/DELTAX)*(PLOWER(IRIGHT)-PLOWER(ILEFT))
     &     +PLOWER(ILEFT)
C          PRINT *,FLOWER(IPLOT)-PLOWER(ILEFT),PLOWER(IRIGHT),
C     &     iplot,ileft,iright,xmax-xa
C     &     -FLOWER(IPLOT)
          XA=XA+DXPLOT
          IF (XA .GE. XMAX .OR. IPLOT .EQ. 100)THEN
           GOTO 110
          END IF
          IPLOT=IPLOT+1
          GOTO 100
110       NPLOT=IPLOT
C         PRINT *,NPLOT
          XA  = XMIN
          IPLOT=1
          DO 120 I=1,NPLOT
            cp(kk,I)= (FUPPER(I)- FLOWER(I))/(.5*1.21*40*40)
C             PRINT *,I,XA,FLOWER(I),FUPPER(I)
            XA=XA+DXPLOT
120       CONTINUE
C     print *,kk
130   CONTINUE
      DO 150 K=1,NFILES
        CL(K)=0.0
        DO 150 I=2,NPLOT
          CL(K)=CL(K)+(cp(K,I)+cp(K,I-1))*DXPLOT/2.0
C           PRINT *,CL(K)
150   CONTINUE

C     WRITE(6,*)(FILES(kk),kk=1,8)
C     WRITE(6,*)(FILES(K),K=9,16)
C     WRITE(6,*)(FILES(K),K=17,24)
C     WRITE(6,*)(FILES(K),K=25,32)
C     WRITE(6,*)(FILES(K),K=33,40)
C     WRITE(6,*)(FILES(15)
      XA=XMIN
      WRITE(6,2)(FILES(K),K=1,NFILES)
      DO 140 I=1,NPLOT
        WRITE(6,3)XA,(cp(K,I),K=1,NFILES)
        XA=XA+DXPLOT
140   CONTINUE
```

```
      DO 160 K=1, NFILES
        WRITE(6,5)FILES(K),CL(K)
160   CONTINUE
c     WRITE(6,2)(FILES(K),K=9,16)
c     DO 160 I=1,NPLOT
c       WRITE(6,4)(cp(K,I),K=9,16)
2     FORMAT(//,5x,9(A8,','))
3     FORMAT(F8.5,',',8(F12.8,','))
4     FORMAT(9(F12.8,','))
5     FORMAT(A8,'  ,Lift Coefficient : ,',F12.8)
      STOP
      END
```

Appendix C

BASIC Program to control the traverse system and acquire the hot wire readings.

```
'*************************************************************************
  '* Program    : CONTROL1.BAS
  '* Description : Program for PCL-818[1] acquisition card to move the traverse system,
  '* acquire and store hot-wire readings, perform calculations for some of the flow quantities
  '*  conversion on a block of channels with interrupt data transfer.
 '* Revision   : 3.0
  '* Date       : 2/10/95                Ali Al-Shihry
  '* Note SW4 Pin 3 Must be OFF to enable (0-10) Volts Input Range
 '*************************************************************************
    DECLARE SUB Acquire ()
    DECLARE SUB ReadFreeStream ()
    DECLARE SUB OutputFile ()
    DECLARE SUB HomeDown ()
    DECLARE SUB HomeUp ()
    DECLARE SUB switchs ()
    DECLARE SUB calc0 ()
    DECLARE SUB calc3 ()
    DECLARE SUB calibrateSingle ()
    DECLARE SUB showClbSingle ()
    DECLARE SUB showClbXwire ()
    DECLARE SUB calibrateXwire ()
    DECLARE SUB ShowSettings ()
    DECLARE SUB ReadSettings ()
    DECLARE SUB Settings ()
    DECLARE SUB KeyPressed ()

    COMMON SHARED E0, B, N, uPrime, Eainf, Ebinf
    COMMON SHARED E0a, Ba, Na, E0b, Bb, Nb, ea, eb, Eabar, EbBar, Alphaa, Alphab
    COMMON SHARED uMean, vMean, uRMS, vRMS, TrbU, TrbV, CorrCoeff, TurbShear
    COMMON SHARED WireType, TstFile$, StepsMm, StrokeLength, NoOfLoops
    COMMON SHARED AirFoil$, ExpName$, SwitchStatus, Alpha, PressureHead
    COMMON SHARED DelayUnits, Direction, DirFlag, StepRatio, StepPulses, CurrPosition
    COMMON SHARED Parm5, Parm6, Samples
    CLS
    DIM SHARED Data2(3000), Data3(3000), Dim1%, DAT%(3000), PARAM%(60)
    '*****************************************************************
    '* Assign PAARAM%() Table and Initialize the PCL-818 A/D Card  *
    '*****************************************************************
    Parm6 = 5
    GOSUB SETUP
    GOSUB INITIALIZE
    '*****************************
    '* Read User Parameters    *
    '*****************************

    yes = 0
    CALL ReadSettings
    IF WireType = 0 THEN 'Single Hot Wire
        DIM SHARED U(3000), uPrime(3000)
    ELSE
        DIM SHARED eaPrime(3000), ebPrime(3000)
```

[1]Although the control commands in this program was written for PCL-818 card, It can be changed to any other card using its own command and the rest of program can be used effectively.

```
    END IF
    FirstSweep = 0
    'PRINT DelayUnits
    CurrPosition = 0
    ScreenNo = 0
    FOR Nsweep = 1 TO NoOfLoops
        ScreenNo = ScreenNo + 1
        IF ScreenNo > 20 THEN
            ScreenNo = 0
            CALL ShowSettings
        END IF
        '*****************************
        '* Aquiring Hot-Wire Readings*
        '*****************************
        CALL Acquire
        IF WireType = 0 THEN
            CALL calc0              'calc0 for Single Hot Wire
        ELSEIF WireType = 1 THEN
            CALL calc3              'calc3 for X-Hot Wire
        END IF
        '************************************
        '* Move Traverse System One Step    *
        '************************************
        IF StepsMm <> 0 THEN
            GOSUB Move
            CurrPosition = CurrPosition + StepsMm
        END IF
        PRINT Nsweep;
        FOR IU = 1 TO DelayUnits * 21000: Domy = 10: NEXT   'Time Delay before Puls
        FirstSweep = 1
        '************************************
        '* Track the Last Key Pressed       *
        '************************************
        CALL KeyPressed
    NEXT

Finish:
    CLOSE #1
    CLOSE #2
    CLOSE #3
    PRINT Linkey$
    PRINT "ok....."
    GOTO 999
    PRINT
END
Move:
    'PRINT "move"
    '************************************
    '* Move Traverse System One Step    *
    '************************************
    'There are 16 channels comming out of the A/D card.
    'Channel 0 can be switched on (Binary 1) Using DAT%(0) = 1
    'Channel 1 can be switched on (Binary 1) Using DAT%(0) = 2
    'Channel 2 can be switched on (Binary 1) Using DAT%(0) = 4
    'Channel 3 can be switched on (Binary 1) Using DAT%(0) = 8
    'PRINT StepPulses
    FOR J% = 0 TO StepPulses + 0
        CALL KeyPressed
        CALL switchs
        'PRINT "Dir"; DirFlag, "Switch"; SwitchStatus
        IF DirFlag = 1 AND SwitchStatus = 2 THEN
```

```
            DirFlag = 0
        ELSEIF DirFlag = 0 AND SwitchStatus = 1 THEN
            DirFlag = 1
        END IF
        IF OldSwitch <> SwitchStatus THEN
            'CLS
            BEEP: BEEP: BEEP
            PRINT : PRINT : PRINT : PRINT
            PRINT "The Upper or Lower limit is reached..."
            PRINT "The data is saved...,and the program will stop.."
            GOTO Finish
            'Respond$ = " "
            'INPUT "Do you want to continue in the oppesite direction (Y/N) "; Respond$
            'IF Respond$ = "Y" OR Respond$ = "y" THEN
            '    OldSwitch = SwitchStatus
        '    ' ELSE
        '        GOTO Finish
        '    END IF
        END IF
        DAT%(0) = 2 + DirFlag          'Send either 0 for Up or 1 for Dwon
        'PRINT DirFlag
        FUN% = 29                  'FUNCTION 29
        CALL PCL818(FUN%, SEG PARAM%(0))  ' Func 29 : "N" times of digital output
        IF PARAM%(45) <> 0 THEN PRINT "DIGITAL OUTPUT FAILED !": STOP
        DAT%(0) = 0
        PulsDuration = 29
        FOR ip% = 1 TO PulsDuration
            CALL KeyPressed
        NEXT   'length of the pulse
        FUN% = 29                  ' FUNCTION 29 : To send pulses to move Traverse System
        CALL PCL818(FUN%, SEG PARAM%(0))  ' Func 29 : "N" times of digital output
        IF PARAM%(45) <> 0 THEN PRINT "DIGITAL OUTPUT FAILED !": STOP
    NEXT
RETURN
SETUP:
    PARAM%(1) = &H300          ' Base I/O address
    PARAM%(4) = 2              ' IRQ level : IRQ2
    PARAM%(5) = 200            ' Pacer rate = 1MHz / (PARAM%(5) * PARAM%(6))  Hz
    PARAM%(6) = 5
    PARAM%(7) = 0              ' Trigger mode, 0 : pacer trigger
    PARAM%(8) = 0              ' Non-cyclic
    PARAM%(10) = VARPTR(DAT%(0))  ' Offset of A/D data buffer A
    PARAM%(11) = VARSEG(DAT%(0))  ' Segment of A/D data buffer A
    PARAM%(12) = 0             ' Data buffer B address, if not used,
    PARAM%(13) = 0             ' must set to 0.
    PARAM%(14) = 3000          ' A/D conversion number
    PARAM%(15) = 0             ' A/D conversion start channel
    PARAM%(16) = 0             ' A/D conversion stop channel
    PARAM%(17) = 0             ' Overall gain code, 0 : +/- 5V
    PARAM%(20) = VARPTR(DAT%(0))  ' Offset of D/A output data buffer A
    PARAM%(21) = VARSEG(DAT%(0))  ' Segment of D/A output data buffer A
    PARAM%(22) = 0             ' Output data buffer B address, if not used,
    PARAM%(23) = 0             ' must set to 0.
    PARAM%(24) = 1             ' D/A conversion number
    PARAM%(25) = 0             ' D/A conversion start channel
    PARAM%(26) = 0             ' D/A conversion stop channel
    PARAM%(27) = VARPTR(DAT%(0))  ' Offset of digital input data buffer A
    PARAM%(28) = VARSEG(DAT%(0))  ' Segment of digital input data buffer A
    PARAM%(29) = 0             ' Data buffer B address, if not used,
    PARAM%(30) = 0             ' must set to 0.
    PARAM%(31) = 2             ' Digital input number
```

```
    PARAM%(32) = 0              ' Digital input port
    PARAM%(33) = VARPTR(DAT%(0))  ' Offset of digital output data buffer A
    PARAM%(34) = VARSEG(DAT%(0))  ' Segment of digital output data buffer A
    PARAM%(35) = 0              ' Data buffer B address, if not used,
    PARAM%(36) = 0              ' must set to 0.
    PARAM%(37) = 1              ' Digital output number
    PARAM%(38) = 0              ' Digital output port
    ' param%(45) : Error Code
    ' param%(46) : Return Value 0
    ' param%(47) : Return Value 1
    PARAM%(50) = 1              ' 1 : PCLD-779 daughter board type
    PARAM%(51) = 0              ' 0 : SoftWare, 2 : Interrupt trigger
    'PARAM%(52) = VARPTR(CJC%(0))  ' Offset of PCLD-779 CJC data buffer
    'PARAM%(53) = VARSEG(CJC%(0))  ' Segment of PCLD-779 CJC data buffer
RETURN
INITIALIZE:
    PRINT 1
    '*****************************
    '* Initialize PCL-818 Card  *
    '*****************************
    FUN% = 3                  ' FUNCTION 3
    CALL PCL818(FUN%, SEG PARAM%(0))  ' Func 3 : Hardware initialization
    IF PARAM%(45) <> 0 THEN PRINT "DRIVER INITIALIZATION FAILED !": STOP
    '
    FUN% = 4                  ' FUNCTION 4, See Program ADINT.BAS
    CALL PCL818(FUN%, SEG PARAM%(0))  ' Func 4 : A/D initialization
    IF PARAM%(45) <> 0 THEN PRINT "A/D INITIALIZATION FAILED !": STOP
    '
    FUN% = 12                 ' FUNCTION 12,See Program DAOUT.BAS
    CALL PCL818(FUN%, SEG PARAM%(0))  ' Func 12 : D/A initialization
    IF PARAM%(45) <> 0 THEN PRINT "D/A INITIALIZATION FAILED !": STOP
    '
    FUN% = 20                 ' FUNCTION 20, See Program DIGIN.BAS
    CALL PCL818(FUN%, SEG PARAM%(0))  ' Func 20 : Digital input initialization
    IF PARAM%(45) <> 0 THEN PRINT "DIGITAL INPUT INITIALIZATION FAILED !": STOP
    '
    FUN% = 28                 ' FUNCTION 28, See Program DIGOUT.BAS
    CALL PCL818(FUN%, SEG PARAM%(0))  ' Func 28 : Digital output initialization
    IF PARAM%(45) <> 0 THEN PRINT "DIGITAL OUTPUT INITIALIZATION FAILED !": STOP
    '
    FUN% = 96                 ' FUNCTION 96, See Program ADTHERM.BAS
    CALL PCL818(FUN%, SEG PARAM%(0))  ' Func 96  : A/D initialization
    IF PARAM%(45) <> 0 THEN PRINT "A/D INITIALIZATION FAILED !": STOP
    '

    FUN% = 100                ' FUNCTION 100, See Program ADBLOCK.BAS
    CALL PCL818(FUN%, SEG PARAM%(0))  ' Func 100  : A/D initialization
    IF PARAM%(45) <> 0 THEN PRINT "A/D INITIALIZATION FAILED !": STOP
RETURN
999   END

SUB Acquire
    '*****************************
    '* Aquiring Hot-Wire Readings*
    '*****************************
    '     See program ADBLOCK2.BAS
    ' Block channel scan function 100 is very similar to function 9.
    ' The only difference is block channel scan function 100 scans
    ' all input channels (specified by PARAM%(15) and PARAM%(16))
    ' on each trigger pulse, and the function 9 scans one channel
    ' on each trigger pulse.
```

```
    '
    '*************************************************************
    '*     Aquire for Single Hot Wire & Wire 1 in X-Hot Wire
    '*************************************************************
    FUN% = 105                  ' FUNCTION 105
    CALL PCL818(FUN%, SEG PARAM%(0))  ' Func 105 : Pacer trigger A/D
                        ' conversion with interrupt data transfer
    IF PARAM%(45) <> 0 THEN PRINT "A/D INTERRUPT DATA TRANSFER FAILED !": STOP
    '
600   FUN% = 106                    ' FUNCTION 106
    CALL PCL818(FUN%, SEG PARAM%(0))  ' Func 106: Check interrupt status
    CHK% = (PARAM%(46) AND 1)
    IF CHK% <> 0 THEN GOTO 600    ' 0 : Not active, 1 : Active
    FOR I = 0 TO PARAM%(14) - 1   ' Display data
        Data2(I) = (10! * DAT%(I) / 4096! + (-5!))
        'PRINT TIME$; USING "###.###### "; Data2(I)
    NEXT I

    '*************************************************************
    '*     Aquire Wire 2 in X-Hot Wire
    '*************************************************************
    IF WireType = 1 THEN
        PARAM%(15) = 1              ' A/D conversion start channel
        PARAM%(16) = 1              ' A/D conversion stop channel
        FUN% = 105                ' FUNCTION 105
        CALL PCL818(FUN%, SEG PARAM%(0))  ' Func 105 : Pacer trigger A/D
                            ' conversion with interrupt data transfer
        IF PARAM%(45) <> 0 THEN PRINT "A/D INTERRUPT DATA TRANSFER FAILED !": STOP
        '
610       FUN% = 106                      ' FUNCTION 106
        CALL PCL818(FUN%, SEG PARAM%(0))  ' Func 106: Check interrupt status
        CHK% = (PARAM%(46) AND 1)
        IF CHK% <> 0 THEN GOTO 610    ' 0 : Not active, 1 : Active
        '
        FOR I = 0 TO PARAM%(14) - 1   ' Display data
            Data3(I) = (10! * DAT%(I) / 4096! + (-5!))
            'PRINT TIME$; USING "###.###### "; Data3(I)
        NEXT I
        PARAM%(15) = 0              ' A/D conversion start channel
        PARAM%(16) = 0              ' A/D conversion stop channel
    END IF
    ' 10    : A/D input range (-5V to 5V) => 10 = 5 - (-5)
    ' DAT%(I) : A/D input data
    ' 4096   : Full scale 12 bit A/D data
    ' (-5)   : A/D input range "-5" V
END SUB

SUB calc0
    ' This Program is to calculate the values of:
    '     *) Mean Velocities, uMean,vMean
    '     *) RMS Velocity,uRMS
    '     *) Turbulance Intensities, TrbInt
    '     *) Correlation Coeffecient of Fluctuations, CorrCoeff
    '     *) Turbulant Shear Stress, TurbShear
    '  Refference of this program is :
    '
    ' The input data of this subroutine are :
    '     *) E0,B,N, King's Law of the single wire    (Common from calibration file)
    '     *) Values of the output voltages E from single Hot Wire
    '        acquired from the anemometer.
    ' *****************************************
```

```
    ' *     Calculation of uMean
    ' ****************************************
'
    'PRINT E0, B, N
    'INPUT rrr
'  Calculating the average Values of the output voltages
'
    Dim1% = PARAM%(14)
    Utotal = 0
    VoltageSum = 0
    PRINT
    FOR I = 0 TO Dim1% - 1    ' Display data
        IF Data2(I) ^ 2 < E0 ^ 2 THEN
            PRINT "The Input Voltage is Less Than the Minimum Calibration Value"
            BEEP
            EXIT SUB
        END IF

        'PRINT Data2(i) ^ 2 - E0 ^ 2
        VoltageSum = VoltageSum + Data2(I)
        U(I) = ((Data2(I) ^ 2 - E0 ^ 2) / B) ^ (1 / N)
        'PRINT U(i), Data2(i)
        Utotal = Utotal + U(I)

    NEXT I
    'INPUT yyyyy
    MeanVoltage = VoltageSum / Dim1%
    uMean = Utotal / Dim1%
'  Calculating the Root Mean Square Values for voltages
    Xtotal2 = 0
    FOR I = 0 TO Dim1% - 1    ' Display data
        uPrime(I) = U(I) - uMean
        'PRINT uPrime(i)
        Xtotal2 = Xtotal2 + uPrime(I) ^ 2
        'PRINT uPrime(i), Data2(i)
    NEXT I
    uPrimeSqBar = Xtotal2 / Dim1%          'Mean Square Values for uPrime
    uPrimeRMS = SQR(uPrimeSqBar)
    TrbU = uPrimeRMS / uMean
    uPrimeSqBar = Xtotal2 / Dim1%          'Mean Square Values for uPrime

    'INPUT CurrPosition

    PRINT #3, TIME$, CurrPosition, USING "###.###### "; MeanVoltage; uMean; TrbU; uPrimeRMS
'    PRINT TIME$, CurrPosition, USING "###.###### "; MeanVoltage; uMean; TrbU; uPrimeRMS
END SUB

SUB calc3
    'PRINT SIN(Alpha + Alphab)
    'PRINT COS(Alpha - Alphab)
    'INPUT xxxxxx

    'PRINT Na, Nb, Eainf, Ebinf
    IF Eainf = 0 OR Ebinf = 0 THEN
        CLS
        PRINT CHR$(7)
        PRINT : PRINT : PRINT : PRINT
        PRINT "Return to the Main Menu and run (7) in order to"
        PRINT "read the values of Eainf and Ebinf"
        END
    END IF
```

```
    ' This Program is to calculate the values of:
    '     *) Mean Velocities, uMean,vMean
    '     *) RMS Velocity,uRMS,vRMS
    '     *) Turbulance Intensities, TrbU, TrbV
    '     *) Correlation Coeffecient of Fluctuations, CorrCoeff
    '     *) Turbulant Shear Stress, TurbShear
    '  Refference of this program is :
    '  " The X Hot-Wire Probe in a Plane Flow Field" by F. Klatt,
    '   DISA Information, Volume No 8, July' 1969,pp 3-13.
    '
    ' The input data of this subroutine are :
    '     *) E0a,Ba,Na, King's Law of the wire a    (Common from calibration file)
    '     *) E0b,Bb,Nb, King's Law of the wire b    (Common from calibration file)
    '     *) Alphaa and Alphab, the angles between wires a and b (Common from calibration file)
    '     *) Values of the output voltages Ea and Eb from wires a and b
    '       acquired from the anemometer(s)
    ' ********************************************
    ' *     Calculation of uMean
    ' ********************************************
'
' Calculating the average Values of the output voltages
'
    Xtotal = 0
    FOR I = 0 TO PARAM%(14) - 1
        Xtotal = Xtotal + Data2(I)
    NEXT I
    Eabar = Xtotal / PARAM%(14)          'Time Average Value
    Xtotal = 0
    FOR I = 0 TO PARAM%(14) - 1
        Xtotal = Xtotal + Data3(I)
    NEXT I
    EbBar = Xtotal / PARAM%(14)          'Time Average Value
    'PRINT "Eabar "; Eabar, "EbBar "; Ebbar
' Calculating the Root Mean Square Values for voltages
    Xtotal2 = 0
    Xtotal3 = 0
    Xtotal4 = 0
    Xtotal5 = 0
    FOR I = 0 TO PARAM%(14) - 1
        'eaPrime(I) = (Data2(I) - Eabar)
        DeltaEa = (Data2(I) - Eabar)
        Xtotal2 = Xtotal2 + DeltaEa ^ 2

        'ebPrime(I) = (Data3(I) - EbBar)
        DeltaEb = (Data3(I) - EbBar)   'It was EaBar untill discovered at 23/9/96

        Xtotal3 = Xtotal3 + DeltaEb ^ 2

        'Xtotal4 = Xtotal4 + (eaPrime(J) + ebPrime(J)) ^ 2 'to calculate Kab(Eqn. 22)
        'Xtotal5 = Xtotal5 + (eaPrime(J) - ebPrime(J)) ^ 2 'to calculate Kab(Eqn. 22)
        'PRINT eaPrime(i), Data2(i), Eabar
    NEXT I
    eaPrimebar = Xtotal2 / PARAM%(14)          'Mean Square Values for ea
    ebPrimebar = Xtotal3 / PARAM%(14)          'Mean Square Values for eb

    'Upper = Xtotal4 / PARAM%(14)          'Mean Square Values for ea+eb to calculate Kab(Eqn. 22)
    'Lower = Xtotal5 / PARAM%(14)          'Mean Square Values for ea-eb to calculate Kab(Eqn. 22)
    'PRINT J
    'Kab = SQR((Upper / Lower))     'to calculate Kab(Eqn. 22)
            'PRINT Eabar, E0a, Eainf, E0a, Na
            'PRINT Ebbar, E0b, Ebinf, E0b, Nb
```

```
    Terma1 = (Eabar ^ 2 - E0a ^ 1)
    Terma2 = (Eainf ^ 2 - E0a ^ 1)
            'PRINT Terma1, Terma2
    IF Terma1 < 0 OR Terma2 < 0 THEN
        PRINT CHR$(7)
        PRINT "The Wind Tunnel May be OFF, OR The Hot Wire A is NOT responding.."
        END
    END IF
    Terma = (Terma1 / Terma2) ^ (1 / Na)
            'Terma = ((Eabar ^ 2 - E0a ^ 2) / (Eainf ^ 2 - E0a ^ 2)) ^ (1 / Na)

    Termb1 = (EbBar ^ 2 - E0b ^ 1)
    Termb2 = (Ebinf ^ 2 - E0b ^ 1)
            'PRINT Termb1, Termb2
    IF Termb1 < 0 OR Termb2 < 0 THEN
        PRINT CHR$(7)
        PRINT "The Wind Tunnel May be OFF, OR The Hot Wire B is NOT responding.."
        END
    END IF

    Termb = (Termb1 / Termb2) ^ (1 / Nb)
        'ermb = ((Ebbar ^ 2 - E0b ^ 2) / (Ebinf ^ 2 - E0b ^ 2)) ^ (1 / Nb)

        'uInfBar = 40
        'uMean = (1! / uInfBar) * .5 * (Terma + Termb) + .5 * SIN(Alphaa + Alphab) * (Terma - Termb)
'Eqn 12
        'vMean = (1! / uInfBar) * .5 * (1! + COS(Alphaa - Alphab)) * (Terma - Termb)                ' Eqn
13
    uMean = .5 * (Terma + Termb)              'Eqn 12
    vMean = .5 * (Terma - Termb)              'Eqn 13
    PRINT "uMean= "; uMean, "vMean= "; vMean
            'Ha = Eabar / (Na * (Eabar ^ 2 - E0a ^ 2)) * Terma    'Eqn 18
            'Hb = EbBar / (Nb * (EbBar ^ 2 - E0b ^ 2)) * Termb    'Eqn 18 too
            '
            'Turbulance Intensities Calculation
            '
            'Term1 = Ha ^ 2 * eaPrimeBar
            'Term2 = Hb ^ 2 * ebPrimeBar
            'Term3 = Ha * Hb * ((Kab ^ 2 - 1) / (Kab ^ 2 + 1)) * (eaPrimeBar + ebPrimeBar)
            'TuInf = SQR(Term1 + Term3 + Term2 + 2 * SIN(Alphaa + Alphab) * (Term1 - Termb))
            'Tvinf = (1 + COS(Alphaa - Alphab)) * SQR(Term1 - Term3 + Term2)
            'TrbShear = (1 + COS(Alphaa - Alphab)) * (Term1 - Term2) + SIN(Alphaa + Alphab) * Tvinf
^2
            'PRINT #3, TuInf, Tvinf, uMean, vMean, Eabar, EbBar, eaPrime, ebPrime
    PRINT #3, uMean; vMean; ","; Eabar; ","; EbBar; ","; eaPrimebar; ","; ebPrimebar
            'PRINT Eabar, EbBar, TuInf, Tvinf, uMean, vMean, eaPrime, ebPrime
            'PRINT Alphaa * 180 / 3.141593, Alphab * 180 / 3.141593, COS(Alphaa), COS(Alphab)



            'PRINT Ebar, Xtotal2, uMeanSq, u, TurbInt
'
'  Calculating the Skewness and Peakedness Values for U-Velocity
'
    'Xtotal3 = 0
    'Xtotal4 = 0
    'IF U > .00001 THEN
    '    FOR I = 0 TO PARAM%(14) - 1    ' Display data
    '        Diff = (Data2(I) - EBar)
```

```
'            Xtotal3 = Xtotal3 + Diff * Diff * Diff / U ^ 3
'            Xtotal4 = Xtotal4 + Diff * Diff * Diff * Diff / U ^ 4
'        NEXT I
    'END IF
    'Skewness = Xtotal3 / PARAM%(14)
    'Peakedness = Xtotal4 / PARAM%(14)
    'uBar  = SQR(uBarAverage) / Ebar
    'PRINT #3, "  uAv        uBar        uMean       uMeanSq     u        TurbInt     Skew        Peak"
    'PRINT #3,  uMean; vMean; TurbInt; Skewness; Peakedness
    'PRINT #3, USING "####.##########"; Ebar; uBar; uMean; uMeanSq; u; TurbInt; Skewness; Peaked-
ness
    'PRINT Ebar, uBar

END SUB

SUB calibrateSingle
    CalibFile$ = "CALIBS.DAT"
    OPEN CalibFile$ FOR INPUT AS #2  ' Calibration Data File
    INPUT #2, E0a, Ba, Na

    CALL showClbSingle
    KeyPress = 9
    DO WHILE KeyPress <> 1 AND KeyPress <> 2
        'CLS
        PRINT : PRINT : PRINT
        PRINT "Input the following data..."
        INPUT "E0 for single wire A....:"; E0a
        INPUT "B for single wire A.....:"; Ba
        INPUT "n for single wire A.....:"; Na
        CALL showClbSingle
        PRINT : PRINT : BEEP
        PRINT "(1) to Accept New Values"
        PRINT "(2) to Retain Old Values"
        INPUT "Enter Your Choice  ", KeyPress
        IF KeyPress = 1 THEN
            '"CalibFile$ = "CALIBS.DAT"
            CLOSE #2
            OPEN CalibFile$ FOR OUTPUT AS #2  ' Calibration Data File
            PRINT #2, E0a, Ba, Na
        ELSEIF KeyPress = 2 THEN
            EXIT DO
        END IF
    LOOP
END
CLOSE #2
END SUB

SUB calibrateXwire
    CalibFile$ = "CALIBX.DAT"
    OPEN CalibFile$ FOR INPUT AS #2  ' Calibration Data File
    INPUT #2, E0a, Ba, Na
    INPUT #2, E0b, Bb, Nb
    INPUT #2, Alphaa, Alphab

    CALL showClbXwire
    KeyPress = 9
    DO WHILE KeyPress <> 1 AND KeyPress <> 2
        'CLS
        PRINT : PRINT : PRINT
        PRINT "Input the following data..."
        INPUT "E0 for wire A....:"; E0a
```

```
        INPUT "B for wire A.....:"; Ba
        INPUT "n for wire A....:"; Na
        INPUT "Alpha for wire A....:"; Alphaa
        INPUT "E0 for wire B....:"; E0b
        INPUT "B for wire B.....:"; Bb
        INPUT "n for wire B....:"; Nb
        INPUT "Alpha for wire B....:"; Alphab
        Alphaa = 3.141593 * Alphaa / 180
        Alphab = 3.141593 * Alphab / 180
        CALL showClbXwire
        PRINT : PRINT : BEEP
        PRINT "(1) to Accept New Values"
        PRINT "(2) to Retain Old Values"
        INPUT "Enter Your Choice  ", KeyPress
        IF KeyPress = 1 THEN
            ""CalibFile$ = "CALIBX.DAT"
            CLOSE #2
            OPEN CalibFile$ FOR OUTPUT AS #2  ' Calibration Data File
            PRINT #2, E0a, Ba, Na
            PRINT #2, E0b, Bb, Nb
            PRINT #2, Alphaa, Alphab
            EXIT DO
        ELSEIF KeyPress = 2 THEN
            EXIT DO
        END IF
    LOOP
END
CLOSE #2
END SUB

SUB GenerateFile
END SUB

SUB HomeDown
    '    DirFlag= 0 for Up
    '    DirFlag= 1 for Down
    '    SwitchStatus=1 for Up
    '    SwitchStatus=2 for Down
    CLS : PRINT : PRINT : PRINT : PRINT
    PRINT "The Traverse System is Going Down... Press End to stop it"
    '************************************
    '* Move Traverse System to the Top  *
    '************************************
    'PRINT StepPulses
    'PRINT Parm5, Parm6
    Pm5 = Parm5
    Pm6 = Parm6
    Parm5 = 300
    Parm6 = 5
    PARAM%(5) = Parm5
    PARAM%(6) = Parm6

    'PARAM%(6) = 5
    FOR JJ% = 0 TO 1
        JJ% = 0        ' To keep running forever
        CALL switchs
        Linkey$ = INKEY$
        IF SwitchStatus = 1 OR MID$(Linkey$, 1, 2) = CHR$(0) + "O" THEN
            CALL ShowSettings
            BEEP
            Parm5 = Pm5
```

```
            Parm6 = Pm6
            PARAM%(5) = Parm5
            PARAM%(6) = Parm6
            EXIT SUB
        END IF

        DAT%(0) = 2 + 0         'Send 0 for Up
        FUN% = 29                'FUNCTION 29
        CALL PCL818(FUN%, SEG PARAM%(0))  ' Func 29 : "N" times of digital output
        IF PARAM%(45) <> 0 THEN PRINT "DIGITAL OUTPUT FAILED !": STOP
        DAT%(0) = 0
        FUN% = 29                'FUNCTION 29
        CALL PCL818(FUN%, SEG PARAM%(0))  ' Func 29 : "N" times of digital output
        IF PARAM%(45) <> 0 THEN PRINT "DIGITAL OUTPUT FAILED !": STOP
    NEXT
    Parm5 = Pm5
    Parm6 = Pm6
    PARAM%(5) = Parm5
    PARAM%(6) = Parm6
END SUB

SUB HomeUp
    '    DirFlag= 0 for Up
    '    DirFlag= 1 for Down
    '    SwitchStatus=1 for Up
    '    SwitchStatus=2 for Down
    CLS : PRINT : PRINT : PRINT : PRINT : PRINT
    PRINT "The Traverse System is Going UP... Press End to stop it      "
    'PRINT "HomeUp"
    '************************************
    '*  Move Traverse System to the Top  *
    '************************************
    'PRINT StepPulses
    Pm5 = Parm5
    Pm6 = Parm6

    Parm5 = 300
    Parm6 = 5
    PARAM%(5) = Parm5
    PARAM%(6) = Parm6

    FOR JJ% = 0 TO 1
        JJ% = 0        ' To keep running forever
        CALL switchs
        Linkey$ = INKEY$
        IF SwitchStatus = 2 OR MID$(Linkey$, 1, 2) = CHR$(0) + "O" THEN
            CALL ShowSettings
            BEEP
            Parm5 = Pm5
            Parm6 = Pm6
            PARAM%(5) = Parm5
            PARAM%(6) = Parm6
            EXIT SUB
        END IF
        'PRINT PARAM%(5), PARAM%(6)
        DAT%(0) = 2 + 1         'Send 0 for Up
        'PRINT DirFlag
        FUN% = 29                'FUNCTION 29
        CALL PCL818(FUN%, SEG PARAM%(0))  ' Func 29 : "N" times of digital output
        IF PARAM%(45) <> 0 THEN PRINT "DIGITAL OUTPUT FAILED !": STOP
        DAT%(0) = 0
```

```
        FUN% = 29                ' FUNCTION 29
        CALL PCL818(FUN%, SEG PARAM%(0))  ' Func 29 : "N" times of digital output
        IF PARAM%(45) <> 0 THEN PRINT "DIGITAL OUTPUT FAILED !": STOP
    NEXT
    Parm5 = Pm5
    Parm6 = Pm6
    PARAM%(5) = Parm5
    PARAM%(6) = Parm6
END SUB

SUB KeyPressed
    Linkey$ = INKEY$
    IF LEN(Linkey$) > 0 THEN
        'PRINT Linkey$
        'print domy
        SELECT CASE MID$(Linkey$, 1, 2)
        CASE IS = CHR$(0) + "O"       'End Key is pressed
            CLOSE #1
            CLOSE #2
            CLOSE #3
            PRINT "ok....."
            PRINT "Press any please"
            END
        CASE IS = CHR$(0) + "H"       'Up Arrow Key is pressed
            DirFlag = 1
            CALL ShowSettings
            PRINT
            PRINT
            PRINT "          Press End To Stop Moving The Traverse System.."
            PRINT "          Press Arrows to change direction.."
            PRINT "No of Steps :", NoOfLoops
            PRINT "Current Step..."
        CASE IS = CHR$(0) + "P"       'Down Arrow Key is pressed
            DirFlag = 0
            CALL ShowSettings
            PRINT
            PRINT
            PRINT "          Press End To Stop Moving The Traverse System.."
            PRINT "          Press Arrows to change direction.."
            PRINT "No of Steps :", NoOfLoops
            PRINT "Current Step..."

        CASE IS = CHR$(0) + "I"       'PgUp Key is pressed
        END SELECT

    END IF
    'RETURN
END SUB

SUB OutputFile
    '****************************************
    '* Read User output file Parameters     *
    '****************************************
    TstFile$ = ""
    'WHILE LEN(TstFile$) < 1 OR LEN(TstFile$) > 8 OR AirFoil$ = "" OR ExpName$ = ""
    AirFoil$ = ""
    ExpName$ = ""
    WHILE AirFoil$ = "" OR ExpName$ = ""
        CLS
        'INPUT "Experiment File....."; TstFile$
        INPUT "AirFoil No....."; AirFoil$
```

```
        INPUT "Experiment Name.....", ExpName$
        INPUT "Angle of Attack Degs"; Alpha
        'IF LEN(TstFile$) < 1 OR LEN(TstFile$) > 8 OR AirFoil$ = "" OR ExpName$ = "" THEN
        IF AirFoil$ = "" OR ExpName$ = "" THEN
            BEEP
            PRINT
            PRINT
            PRINT
            PRINT
            PRINT
            INPUT "Invaled Input..Try again", Domy

        END IF
    WEND
    Directory$ = "C:\PCL-818\ALI_BAS\DATA\"
    Name1$ = MID$(DATE$, 1, 2) + MID$(DATE$, 4, 2) + MID$(TIME$, 1, 2) + MID$(TIME$, 4, 2) ' +
MID$(TIME$, 7, 1)
    PRINT Name1$
    TstFile$ = Directory$ + Name1$ + ".DAT"
    'TstFile$ = TstFile$ + ".DAT"
    CLOSE #1
    OPEN "system.set" FOR OUTPUT AS #1

    WRITE #1, WireType     'From Old Data
    WRITE #1, StepsMm
    WRITE #1, StrokeLength
    WRITE #1, DelayUnits
    WRITE #1, DirFlag
    WRITE #1, Parm5

    'WRITE #1, TstFile$     ' Form New Data
    WRITE #1, AirFoil$
    WRITE #1, ExpName$
    WRITE #1, Alpha
    WRITE #1, PressureHead
    WRITE #1, Samples
    CLOSE #1
    CALL ShowSettings
END SUB

    SUB PresHead
    ' This Program is to read the pressure(s) of
    ' the variuos points inside the wind tunnel
    PRINT #3, TIME$, CurrPosition, USING "###.###### "; MeanVoltage; uMean; TrbU; uRMS
END SUB

SUB ReadFreeStream
    CLS
    PRINT : PRINT : PRINT
    PRINT CHR$(7)
    PRINT "If The X-Hot Wire is located at the Free Stream Position, Press Enter"
    PRINT "Or Press 1 to return to the Main Menu and Move it."
    INPUT Domy
    IF Domy > 0 THEN
        CALL ShowSettings
        EXIT SUB
    END IF
    CALL Acquire
    VoltageSum = 0
    FOR I = 0 TO PARAM%(14) - 1    ' Display data
        VoltageSum = VoltageSum + Data2(I)
```

```
    NEXT I
    Eainf = VoltageSum / PARAM%(14)
    VoltageSum = 0
    FOR I = 0 TO PARAM%(14) - 1    ' Display data
        VoltageSum = VoltageSum + Data3(I)
    NEXT I
    Ebinf = VoltageSum / PARAM%(14)
    PRINT : PRINT
    PRINT "Eainf = "; Eainf
    PRINT "Ebinf = "; Ebinf
    PRINT : PRINT : PRINT : PRINT
    PRINT "Return The Wire To Starting Position..."
    PRINT "Press A Key When Ready.."
    PRINT CHR$(7)
    INPUT Domy
    CALL ShowSettings
END SUB

SUB ReadSettings

    OPEN "system.set" FOR INPUT AS #1

    INPUT #1, WireType     'From Old Data
    INPUT #1, StepsMm
    INPUT #1, StrokeLength
    INPUT #1, DelayUnits
    INPUT #1, DirFlag
    INPUT #1, Parm5
    INPUT #1, AirFoil$
    INPUT #1, ExpName$
    INPUT #1, Alpha
    INPUT #1, PressureHead
    INPUT #1, Samples

    Directory$ = "C:\PCL-818\ALI_BAS\DATA\"
    Name1$ = MID$(DATE$, 1, 2) + MID$(DATE$, 4, 2) + MID$(TIME$, 1, 2) + MID$(TIME$, 4, 2) ' +
MID$(TIME$, 7, 1)
    PRINT Name1$
    TstFile$ = Directory$ + Name1$ + ".DAT"
    VltFile$ = Directory$ + Name1$ + ".VLT"
    PARAM%(5) = Parm5
    PARAM%(6) = Parm6
    PARAM%(14) = Samples
    'PRINT Samples, PARAM%(14), PARAM%(6), PARAM%(5)
    'INPUT XXX

    CALL ShowSettings
    '*************************************************************
    '*    Read the calibration data for the hot wire(s)
    '*************************************************************
    IF WireType = 0 THEN
        'INPUT "  Calibration Filename....."; CalibFile$
        CalibFile$ = "CALIBS.DAT"
        OPEN CalibFile$ FOR INPUT AS #2  ' Calibration Data File
        INPUT #2, E0, B, N
        'PRINT E0, B, n
    ELSEIF WireType = 1 THEN
        'INPUT "  Calibration Filename....."; CalibFile$
        CalibFile$ = "CALIBX.DAT"
        OPEN CalibFile$ FOR INPUT AS #2  ' Calibration Data File
        INPUT #2, E0a, Ba, Na
```

```
    INPUT #2, E0b, Bb, Nb
    INPUT #2, Alphaa, Alphab
END IF
CLOSE #2

NewData = 0

WHILE NewData >= 0 AND NewData < 8
    PRINT
    PRINT "                (1) Current Settings"
    'PRINT
    PRINT "                (2) Change Output File Settings"
    PRINT " M A I N  M E N U    (3) Change Traverse System Settings"
    PRINT " ------------------  (4) Change Calibration"
    PRINT "                (5) Home Up"
    PRINT "                (6) Home Down"
    PRINT "                (7) Read Free Stream Voltages"
    INPUT "                (0) Exit      Choose Item (0 to 6)"; NewData
    IF NewData = 1 THEN
        NewData = 9    'To force exit from WHILE loop
    ELSEIF NewData = 2 THEN
        CALL OutputFile
    ELSEIF NewData = 3 THEN
        CALL Settings
        CALL ShowSettings
    ELSEIF NewData = 4 AND WireType = 0 THEN
        CALL calibrateSingle
    ELSEIF NewData = 4 AND WireType = 1 THEN
        CALL calibrateXwire
    ELSEIF NewData = 5 THEN
        CALL HomeUp
    ELSEIF NewData = 6 THEN
        CALL HomeDown
    ELSEIF NewData = 7 THEN
        CALL ReadFreeStream
    ELSEIF NewData = 0 THEN
        CLOSE #1
        CLOSE #2
        CLOSE #3
        END
    END IF
WEND
CALL ShowSettings

StepRatio = 40              ' 40 Pulses Per 1 Mm
StepPulses = StepsMm * StepRatio * .94
'DelayUnits = DelayUnits * 11000       '1100 units per Sec
'PRINT StepsMm, StepRatio, StepPulses, NoOfLoops
'INPUT dom
IF StepsMm = 0 THEN
    NoOfLoops = 1000000     'keep reading untill End key is pressed
    PRINT
    PRINT "            The Program now is running....."
    PRINT "            Press End Key To Stop the Program"
    PRINT : PRINT "Current Reading.."
ELSE
    NoOfLoops = INT(StrokeLength / StepsMm)
    PRINT
    PRINT
    PRINT "            Press End To Stop Moving The Traverse System.."
    PRINT "            Press Arrows to change direction.."
```

```
        PRINT "No of Steps :", NoOfLoops
        PRINT "Current Step..."
    END IF
    OPEN TstFile$ FOR OUTPUT AS #3        'Output Data File
    PRINT #3, "Airfoil No..... "; AirFoil$
    PRINT #3, "Experiment Name.... "; ExpName$
    PRINT #3, "Output data file... "; TstFile$
    PRINT #3, "Date ..... "; DATE$, "Time "; TIME$
    PRINT PARAM%(5), PARAM%(6)
    PRINT #3, "Frequency..... "; 1000000 / (PARAM%(5) * PARAM%(6)); "  Hz"
    PRINT #3, "No. Of Locations Acquired : "; NoOfLoops
    PRINT #3, "Samples Per Scan are:"; Samples; " Samples"
    PRINT #3, "Pressure Head is:"; PressureHead; "mm (H2O)"
    PRINT #3, "Angle of Attack is: "; Alpha; " Degs"
    PRINT #3, "Step Length (mm)...."; StepsMm
    PRINT #3, "Stroke Length (mm).."; StrokeLength
    PRINT #3, "Delay Time (Sec)...."; DelayUnits
    IF WireType = 0 THEN
        PRINT #3, "Wire Type is ..... Single"
    ELSEIF WireType = 1 THEN
        PRINT #3, "Wire Type is..... X-Wire"
    END IF
    IF DirFlag = 1 THEN
        PRINT #3, "Direction is  Up"
    ELSEIF DirFlag = 0 THEN
        PRINT #3, "Direction is  Dwon"
    END IF

    PRINT #3, : PRINT #3, : PRINT #3,
    IF WireType = 0 THEN
        PRINT #3, " Time      Position(mm)  Voltage  uMean    TurbInt    uRMS"          '" Skew;
Peak "
    ELSEIF WireType = 1 THEN
        PRINT #3, "uMean    ,  vMean      , Eabar       ,Ebbar       ,eaPrimebar    ,ebPrimebar"
    END IF
    'PRINT
    'OPEN VltFile$ FOR OUTPUT AS #4       'Output Volts Data File
END SUB

SUB Settings
    '*****************************
    '* Read User Parameters    *
    '*****************************
    WireType = 0
    CLS
    DO
       PRINT "X-Hot Wire(1), Single Hot Wire(0) "; WireType;
       INPUT WireType
       IF WireType = 0 OR WireType = 1 THEN 20
       LOOP
    END
20   PARAM%(15) = 0              ' A/D conversion start channel
    PARAM%(16) = WireType        ' A/D conversion stop channel

    '************************************************************
    '*     Ask for traverse information and output file
    '************************************************************
    StepsMm = 0
    StrokeLength = 0
    DirFlag = 0
    Looping$ = "YES"
```

```
    WHILE Looping$ = "YES"
        CLS
        Looping$ = "NO"
        PRINT "X-Hot Wire(1), Single Hot Wire(0) "; WireType
        PRINT "Hz      P5"
        PRINT "_____________"
        PRINT "10000    20"
        PRINT "12500    16"
        PRINT "16666    12"
        PRINT "20000    10"
        PRINT "33333    6"
        PRINT "40000    5"
        PRINT "50000    4"
        Action$ = "LOOP"
        WHILE Action$ = "LOOP"
            INPUT "To Choose the Acquisition Frequency, Choose from the above Table P5"; Parm5
            IF Parm5 <> 20 AND Parm5 <> 16 AND Parm5 <> 12 AND Parm5 <> 10 AND Parm5 <> 6
AND Parm5 <> 5 AND Parm5 <> 4 THEN
                Action$ = "LOOP"
            ELSE
                Action$ = "NOLOOP"
            END IF
        WEND
        PARAM%(5) = Parm5
        PARAM%(6) = Parm6
        PRINT "Frequency = "; 1000000 / (PARAM%(5) * PARAM%(6)); " Hz"
        INPUT "Samples Per Scan (3000 Max)", Samples
        IF Samples < 100 THEN
            Samples = 100
        END IF
        Action$ = "LOOP"
        PressureHead = 1
        WHILE Action$ = "LOOP"
            INPUT "Wind Tunel Speed (mm H2O at Front Tube)"; PressureHead
            IF PressureHead > 20 THEN
                Action$ = "LOOP"
            ELSE
                Action$ = "NOLOOP"
            END IF
        WEND

        PRINT "Pressure Head="; PressureHead

        INPUT ; "Step Length (mm)....."; StepsMm
        INPUT "  Stroke Length (mm)....."; StrokeLength
        INPUT "  Delay Time (Sec)....."; DelayUnits
        DirFlag = 0
        INPUT "  Direction (0 Down, 1 Up)....."; DirFlag
        FUN% = 29                ' FUNCTION 29
        CALL PCL818(FUN%, SEG PARAM%(0))  ' Func 29 : "N" times of digital output
        IF PARAM%(45) <> 0 THEN PRINT "DIGITAL OUTPUT FAILED !": STOP
        'DelayUnits = DelayUnits * 11000       '1100 units per Sec

        IF StepsMm = 0 OR StrokeLength = 0 THEN
            StepsMm = 0
            StrokeLength = 0
            BEEP
            INPUT "Do you want to keep traverse system on position (Y/N)"; Travers$
            IF Travers$ = "Y" OR Travers$ = "y" THEN
                Looping$ = "NO"
            ELSE
```

```
                Looping$ = "YES"
            END IF
        END IF

        IF DirFlag <> 0 AND DirFlag <> 1 THEN
            Looping$ = "YES"
            BEEP
            PRINT
            PRINT
            PRINT
            PRINT
            PRINT
            INPUT "Direction Flag should equal 1 or 2", Domy
        END IF
    WEND
    CLOSE #1
    OPEN "system.set" FOR OUTPUT AS #1
    WRITE #1, WireType
    WRITE #1, StepsMm
    WRITE #1, StrokeLength
    WRITE #1, DelayUnits
    WRITE #1, DirFlag
    WRITE #1, Parm5

    'WRITE #1, TstFile$     'From old data
    WRITE #1, AirFoil$
    WRITE #1, ExpName$
    WRITE #1, Alpha
    WRITE #1, PressureHead
    WRITE #1, Samples
    CLOSE #1
END SUB

SUB showClbSingle
    CLS
    PRINT "E0 for wire A....:"; E0a
    PRINT "B for wire A.....:"; Ba
    PRINT "n for wire A....:"; Na
END SUB

SUB showClbXwire
    CLS
    PRINT "E0 for wire A....:"; E0a
    PRINT "B for wire A.....:"; Ba
    PRINT "n for wire A....:"; Na
    PRINT "Alpha for wire A....:"; Alphaa * 180 / 3.141593
    PRINT "E0 for wire B....:"; E0b
    PRINT "B for wire B.....:"; Bb
    PRINT "n for wire B....:"; Nb
    PRINT "Alpha for wire B....:"; Alphab * 180 / 3.141593
END SUB

SUB ShowSettings
    CLS
    'PRINT
    'PRINT "Current Output File Settings          Current Traverse System Settings"; ""
    'PRINT "----------------------------          ---------------------------------"
    PRINT "Current Output File Settings"
    PRINT "----------------------------"

    PRINT "Experiment Name....."; ExpName$
```

```
    IF StepsMm <> 0 THEN
        PRINT "Experiment File.... "; TstFile$
        PRINT "AirFoil No....."; AirFoil$
        PRINT "Angle of Attack....."; Alpha; " Degrees"
        PRINT

        PRINT "                              Step Length (mm)...."; StepsMm
        PRINT "Current Traverse System Settings      Stroke Length (mm).."; StrokeLength
    ELSE
        PRINT "Experiment File.... "; TstFile$, "No Motion in Traverse System"
        PRINT "AirFoil No....."; AirFoil$
    END IF
    'PRINT "Experiment Name....."; ExpName$
    PRINT "--------------------------------      Delay Time (Sec)...."; DelayUnits
    IF WireType = 0 THEN
        PRINT "                              Wire Type is ..... Single"
    ELSEIF WireType = 1 THEN
        PRINT "                              Wire Type is..... X-Wire"
    END IF
    'PRINT " Samples Per Scan is :"; Samples; "          Frequency is:"; 1000000 / (PARAM%(5) *
PARAM%(6)); "  Hz"
    PRINT "                          PressHead is:"; PressureHead; "mm (H2O)"

    IF DirFlag = 1 THEN
        PRINT "                              Direction is  Up"
    ELSEIF DirFlag = 0 THEN
        PRINT "                              Direction is  Dwon"
    END IF
    PRINT
END SUB

SUB switchs
    FUN% = 21               ' FUNCTION 21
    CALL PCL818(FUN%, SEG PARAM%(0))  ' Func 21 : "N" times of Digital input
    IF PARAM%(45) <> 0 THEN PRINT "DIGITAL INPUT FAILED !": STOP
    '
    'DirFlag= 0 for Up
    'DirFlag= 1 for Down
    'SwitchStatus=1 for Up
    'SwitchStatus=2 for Down
    'SwitchStatus = (65535! + DAT%(I)) \ 256 - 252
    SwitchStatus = 0
    'PRINT SwitchStatus
END SUB
```

Appendix D

Patent Certificate

Urquhart-Dykes & Lord

European Patent Attorneys
Chartered Patent Attorneys
Registered Trade Mark Attorneys

Three Trinity Court
21-27 Newport Road
CARDIFF
GB - CF2 1AA

Telephone 01222 487993
Facsimile 01222 488016
Telex 268210 (Patend)

Resident Partner: Stewart Gibson
Assisted by: Huw Evans
Mark Spittle

Mr. Gerry Rogers,
UGCS Limited,
Innovation House,
University of Glamorgan,
PONTYPRIDD,
Mid Glam. CF37 1DL.

Our ref: SHG/P74676

27th February 1997

Dear Gerry,

New U.K. Patent Application No. 9703303.9
Air roller bearing

I can now report that I filed this application on 18th February 1997 and I attach the official filing receipt showing the number given to it.

The next stage of this application must be carried out by **18th February 1998** and will involve preparing and filing claims and requesting the Patent Office to carry out its search to test the novelty of the invention. I shall write to remind you in good time before that date, but let me know if you wish to proceed with this next stage at an earlier date. Note that any corresponding overseas applications will also be due for filing by **18th February 1998**.

You are now free to disclose the invention to anyone you wish and I trust that you will be successful in commercially exploiting it. However, please note that if you make any significant modification or development of the invention during the months ahead, you should consult us before disclosing that modification or development, in case a follow-up application needs to be filed.

Finally, I attach our invoice for preparing and filing the application.

Yours sincerely,

STEWART GIBSON

enc.
jd

Partners
Fred (Steve) Walters, David Mere, Peter Wharton, Philip Archer, Anthony Wood, Laurence Ben-Nathan, Hedley Austin, Stewart Gibson, William Orr, Robin Browne, Simon Belcher, Mark Green

Associates
George Kelvie, Helen Johnstone, Julie Perry, David Watkins

Consultant
Guy Selby-Lowndes

London Office: 91 Wimpole Street, London W1M 8AH Telephone: 0171 629 1771 Facsimile: 0171 491 1216

Aberdeen, Blackburn, Bradford, Cardiff, Carlisle, Hull, Leeds, London, Manchester, Middlesbrough, Milton Keynes, Newcastle, Peterborough, Reading, Swansea, Warrington, Munich

The address for service for all partners is: Tower House, Merrion Way, Leeds GB-LS2 8PA